PACIFIC ENEWETAK ATOLL CRATER EXPLORATION (PEACE) PROGRAM,

ENEWETAK ATOLL, REPUBLIC OF THE MARSHALL ISLANDS

Part 4: Analysis of borehole gravity surveys and other geologic and bathymetric studies in vicinity of OAK and KOA craters

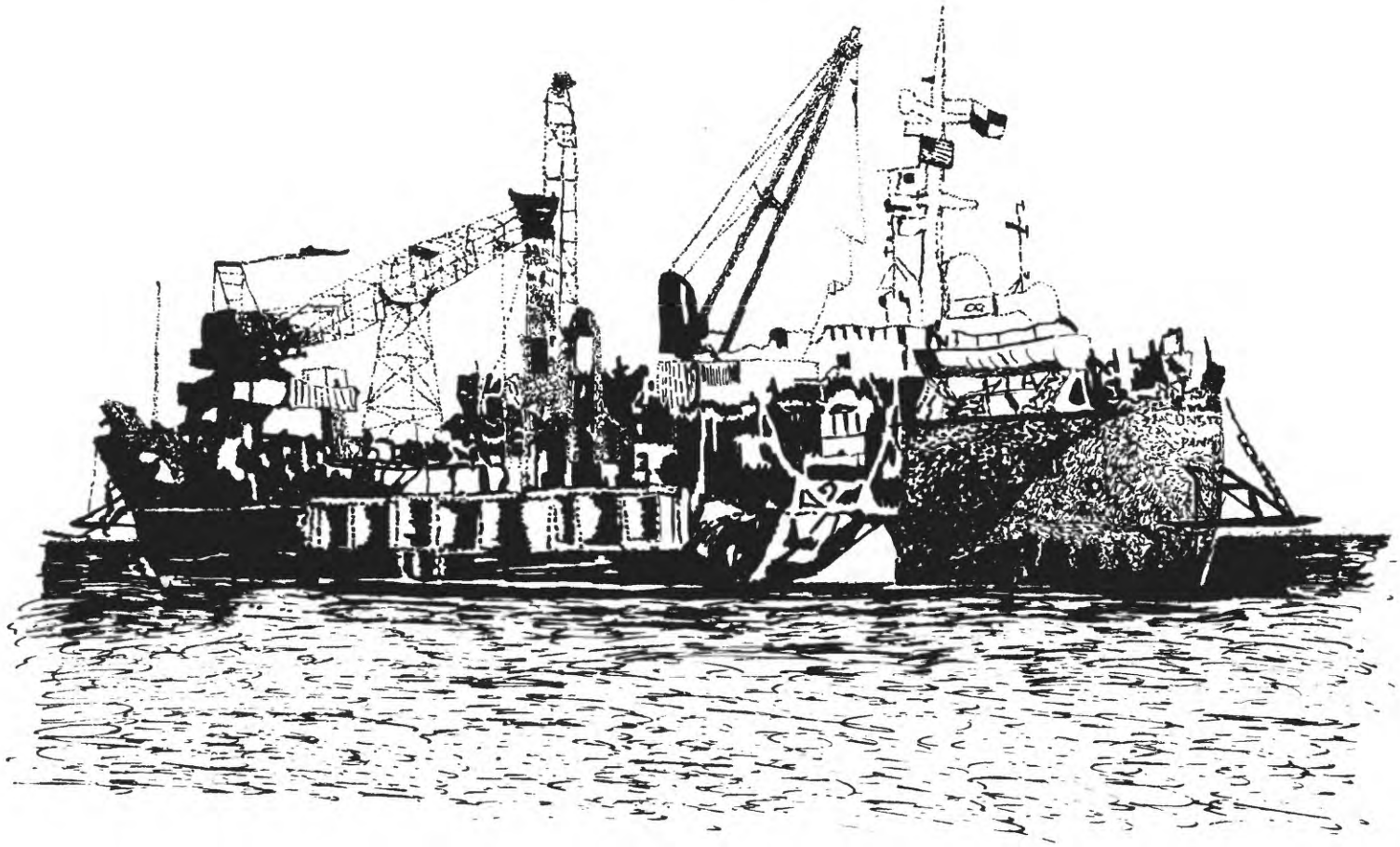

U.S. Geological Survey
Open-File Report 87-665
1987

UNITED STATES DEPARTMENT OF THE INTERIOR

GEOLOGICAL SURVEY

Pacific Enewetak Atoll Crater Exploration (PEACE) Program Enewetak Atoll, Republic of the Marshall Islands

Part 4: Analysis of borehole gravity surveys and other geologic and bathymetric studies in vicinity of OAK and KOA craters

edited by

Thomas W. Henry[1] and Bruce R. Wardlaw[2]

U.S. Geological Survey

Open File Report 87-665

Prepared in cooperation with the Defense Nuclear Agency

This report is preliminary and has not been reviewed for conformity with U.S. Geological Survey editorial standards and stratigraphic nomenclature

[1]Branch of Paleontology and Stratigraphy, Denver, CO 80225-0046
[2]Branch of Paleontology and Stratigraphy, Reston, VA 22092

1987

TABLE OF CONTENTS

(continued on next page)

TABLE OF CONTENTS (continued)

(continued on next page)

TABLE OF CONTENTS (continued)

(continued on next page)

TABLE OF CONTENTS (continued)

****

FIGURE INDEX

(continued on next page)

FIGURE INDEX (continued)

(continued on next page)

FIGURE INDEX (continued)

(continued on next page)

FIGURE INDEX (continued)

(continued on next page)

FIGURE INDEX (continued)

****

PLATE INDEX

(All plates in map pocket)

Plate No.	Description
CHAPTER 5: BATHYMETRIC STUDIES OF OAK CRATER	
5- 1	Digitized Holmes and Narver (1958a) Preshot Topographic and Hydrographic Map.
5- 2	Digitized Holmes and Narver (1958b) Postshot Topographic and Hydrographic Map.
5- 3	Digitized U.S. Geological Survey (1984) Postshot Bathymetric Map.
5- 4	Negative Δ-Relief Map, H&N Preshot and H&N Postshot Map Pair.
5- 5	Positive Δ-Relief Map, H&N Preshot and H&N Postshot Map Pair.
5- 6	Negative Δ-Relief Map, H&N Preshot and USGS Postshot Map Pair.
5- 7	Positive Δ-Relief Map, H&N Preshot and USGS Postshot Map Pair.
5- 8	Negative Δ-Relief Map, H&N Postshot and USGS Postshot Map Pair.
5- 9	Positive Δ-Relief Map, H&N Postshot and USGS Postshot Map Pair.

****

TABLE INDEX

(continued on next page)

TABLE INDEX (continued)

****

PACIFIC ENEWETAK ATOLL CRATER EXPLORATION (PEACE) PROGRAM
ENEWETAK ATOLL, REPUBLIC OF THE MARSHALL ISLANDS

Part 4: Analysis of borehole gravity survey and other geologic and bathymetric studies in vicinity of OAK and KOA craters

CHAPTER 1:

INTRODUCTION TO PART 4 OPEN-FILE REPORT

By

Thomas W. Henry[1/2] and Bruce R. Wardlaw[1/3]

GENERAL REMARKS

The Pacific Enewetak Atoll Crater Exploration (PEACE) Program was established and funded by the Defense Nuclear Agency (DNA) to resolve a number of questions for the Department of Defense (DOD) about the geologic and material-properties parameters of two craters (KOA and OAK), formed by near-surface bursts of high-yield thermonuclear devices on the northern margin of Enewetak Atoll (fig. 1-1), Marshall Islands, in 1958. The multidisciplinary studies conducted by the USGS in collaboration with the DNA, the Department of Energy (DOE), and other organizations during 1984 through 1987 were part of a much larger research initiative by the DNA to better understand the dynamic properties of strategic-scale nuclear bursts and the relevance of the Pacific Proving Grounds (PPG) craters to issues of strategic basing and targeting of nuclear weapons.

The reader is referred to the reports cited in the succeeding section for a detailed explanation of the events leading up to the PEACE Program and the collaborative roles of the USGS, other Federal agencies, and scientists and engineers from universities and private research laboratories.

---

[1] Branch of Paleontology and Stratigraphy, U.S. Geological Survey.

[2] Denver, CO 80225-0046. [3] Reston, VA 22092.

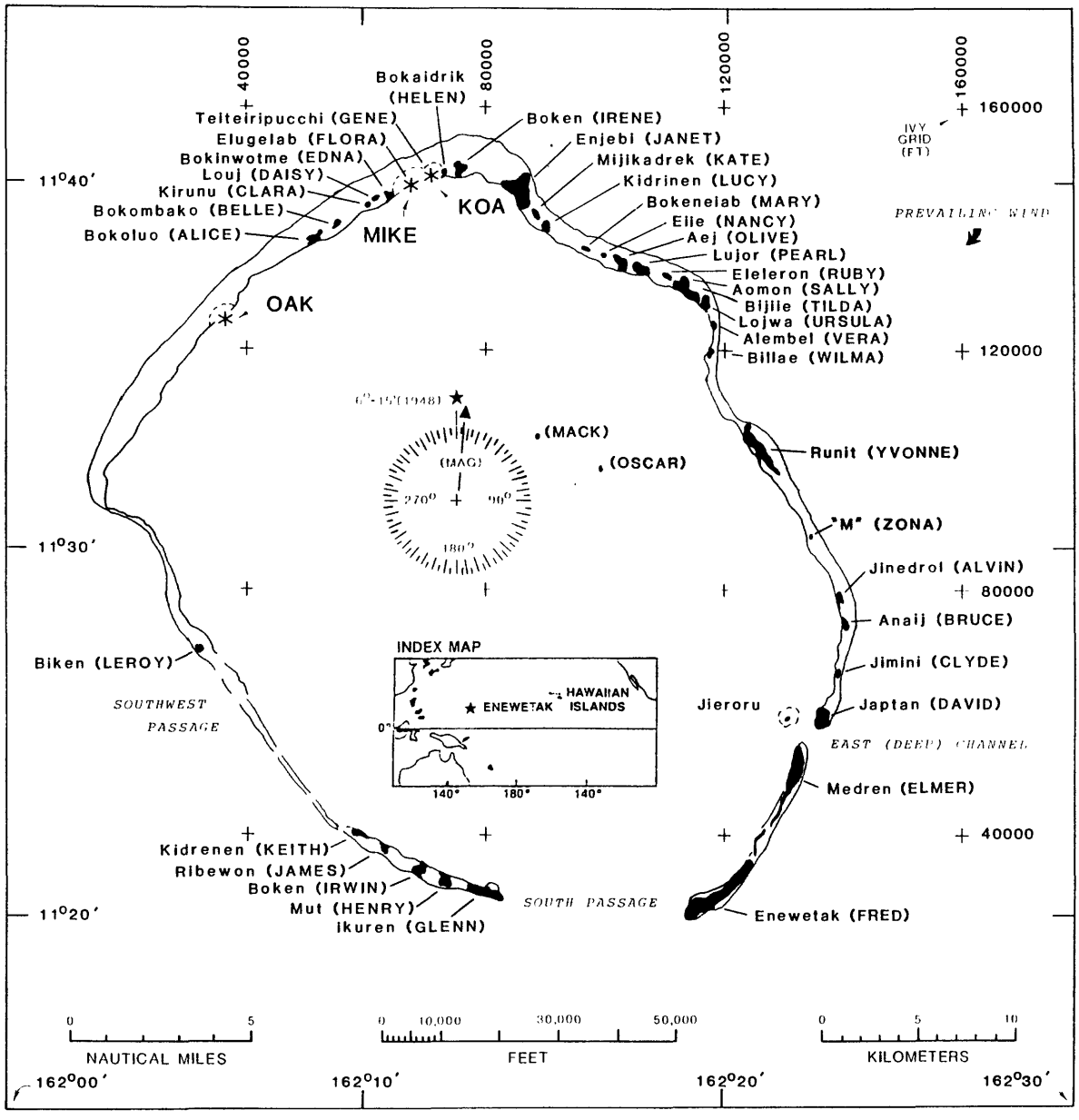

FIGURE 1-1. -- Map of Enewetak Atoll, Republic of the Marshall Islands (RMI), showing native names of principal islands and other features (military site name in parenthesis), and location of OAK, KOA, and MIKE craters. Inset map shows location of Enewetak within Pacific Ocean. Map from Henry, Wardlaw, and others (1986, p. 12, fig. 3).

PEACE PROGRAM REPORTS

This volume is the fifth and final volume of a series of four U.S. Geological Survey (USGS) Open-File Reports (Henry, Wardlaw, and others, 1986; Cronin, Brouwers, and others, 1986; and Henry and Wardlaw, 1986a) and one USGS Bulletin (Folger, 1986a) documenting geologic and geophysical data, analyses, and interpretations for the PEACE Program. Syntheses for the geologic and material-properties models for the craters are found in Wardlaw and Henry (1986, Ch. 14) and Wardlaw (1987, Ch. 7, this Report). The material-properties studies themselves, which provide quantitative parameters for computational modeling, for the most part were not conducted by USGS personnel and are published elsewhere for the DNA (e.g., Blouin and Timian, 1986a, 1986b; Borschel, Klauber, and Earley, 1986; McClelland Engineers, 1986; Mueller, 1987; Patti and Schatz, 1987 [1988], in preparation, Schatz, Patti, and Melzer, 1987 [1988], in preparation, and Simons and others, 1984).

DATA ACQUISITION AND BASES

The PEACE Program was truly a multidisciplinary endeavor. Field work for the program on Enewetak Atoll was done in two parts, the Marine Phase (mid- to late summer, 1984) and the Drilling Phase (late winter through mid-summer, 1985). The primary and derivative PEACE Program data bases and framework groups consist of the elements shown in Table 1-1. For general discussion of the fieldwork and data-acquisition procedures for the Marine Phase, the reader is referred to Folger (1986b), and, for the Drilling Phase, to Henry, Wardlaw, and others (1986, p. 29-97). For more detailed information about the field and laboratory procedures employed for a specific data set, refer to the individual Chapters or volumes (see tbl. 1-1). Many of the derivative data sets and framework groups from the Drilling Phase utilized samples from the 32 deep and intermediate boreholes drilled from the M/V Knut Constructor in the Enewetak lagoon. These boreholes (figs. 1-2 and 1-3) provide a data base upon which the subsurface geologic framework is grounded and upon which interpretations made from the geophysical and material-properties studies must be validated.

A wide array of pre-PEACE Program data from the PPG was re-examined, including (but not limited to) the following:

(1). Published accounts in USGS Professional Paper 260 series (see Emery, Tracey, and Ladd, 1954) from the initial geologic, geophysical, and oceanographic investigations in the Marshall Islands associated with the early phases of nuclear testing.

(2). Published reports and raw data from the geologic and geophysical studies of the PACE, EXPOE, and EASI Projects, sponsored by the DNA and conducted on Enewetak by the Air Force Weapons Laboratory (AFWL) (Couch, Fetzer, and others, 1975; Henny, Mercer, and Zbur, 1974; Ristvet, Tremba and others, 1978; Tremba, Jones, and Henny, 1981; Tremba, Couch, and Ristvet, 1982; and Tremba, 1987). For example, some of the multichannel-seismic lines lines from EASI were reprocessed by Grow, Lee, and others (1986), and selected PACE/EXPOE boreholes were redescribed and analyzed stratigraphically and isotopically before the Drilling Phase actually got underway (Henry, Wardlaw, and others, 1986;

TABLE 1-1. -- Matrix of data bases and analyses from PEACE Program. In heading, CH = Chapter; under heading PHASE, Marine or Drilling connotes which phase the samples were obtained originally. The pilot gravity survey in the old borehole on Medren (ELMER) Island was conducted in April 1984, hence the asterisk (*) in the appropriate column. The geologic and material-properties models for the craters are presented in Wardlaw and Henry (1986, Ch. 14) and in Wardlaw (1987, Ch. 8, this Report). U.S. Geological Survey Open-File Report 87-665 is the current volume.

DATA GROUP	PHASE	PUBLICATION	CH.	REFERENCE CITATION
Bathymetric Maps	Marine	Bull. 1678 OF-87- 665	A 5	Folger, Hampson, and others (1986); Peterson and Henry (1987*).
Side-Scan Sonar Imagery	Marine	Bull. 1678	B	Folger, Robb, and others (1986).
Single-Channel Seismic Reflection	Marine	Bull. 1678	C	Robb, Foster, and others (1986).
Multichannel-Seismic Reflection	Marine	Bull. 1678	D	Grow, Lee, and others (1986).
Seismic-Refraction	Marine	Bull. 1678	E	Ackermann, Grow, and Williams (1986).
Submersible Observations	Marine Both	Bull. 1678 OF-86- 555	F 13	Halley, Slater, and others (1986); Slater, Roddy, and others (1986).
Debris/Ejecta	Marine Marine Drilling	Bull. 1678 OF-86- 555 OF-87- 665*	G 3 4	Halley, Major, and others (1986); Ludvig, Halley, and others (1986); Polanskey and Ahrens (1987*).
Scuba Observations	Marine	Bull. 1678	H	Shinn, Kindinger, and others (1986).
Bottom Samples	Marine Mainly	OF-86- 555	10	Wardlaw, Henry, and Martin (1986).
Boreholes	Drilling	OF-86- 419	-	Henry, Wardlaw, and others (1986).
Lithostratigraphic Framework	Drilling	OF-86- 555	2	Wardlaw and Henry (1986a).
Biostratigraphic Framework & Mixing Studies	Drilling	OF-86- 159 OF-86- 555 OF-87- 665*	- 11 3	Cronin, Brouwers, and others (1986); Brouwers, Cronin, and Gibson (1986); Cronin and Gibson (1987*).
Geophysical Logs	Drilling	OF-86- 555 OF-87- 665*	7 6	Melzer (1986). Trullo (1987*).
Seismic Reference Survey	Drilling	OF-86- 555	9	Tremba and Ristvet (1986b).
Borehole Gravimetry	Drilling	OF-86- 555 OF-87- 665* OF-87- 665*	8 2 6	Beyer, Ristvet, and Oberste-Lehn (1986); Beyer (1987*). Trullo (1987*).
Sr-Isotope Framework	Marine Drilling	Bull. 1678 OF-86- 555	G 3	Halley, Ludwig, and others (1986). Ludwig, Halley, and Simmons (1986).
X-Ray Mineralogy	Drilling	OF-86- 555	4	Tremba and Ristvet (1986).
Organic Geochemistry	Drilling	OF-86- 555	5	Ristvet and Tremba (1986).
Insoluble Residues	Drilling	OF-86- 555	6	Ristvet and Tremba (1986).
Radiation Chemistry	Drilling	OF-86- 555	12	Ristvet and Tremba (1986).
Electron-Spin Resonanace	Drilling Mainly	OF-87- 665*	4	Polanskey and Ahrens (1987*).
Crater-Area Bottom Samples	Drilling	OF-86- 555 OF-86-555 ----	4 10 -	Tremba and Ristvet (1986). Wardlaw, Henry, and Martin (1986). Patti and Schatz (1987) [1988?].
Crater Synthesis	Marine Both Both	Bull. 1678 OF-86- 555 OF-87- 665*	A 14 7	Folger (1986b); Wardlaw and Henry (1986b); Wardlaw (1987*).

* OF-87-665 is the current report.

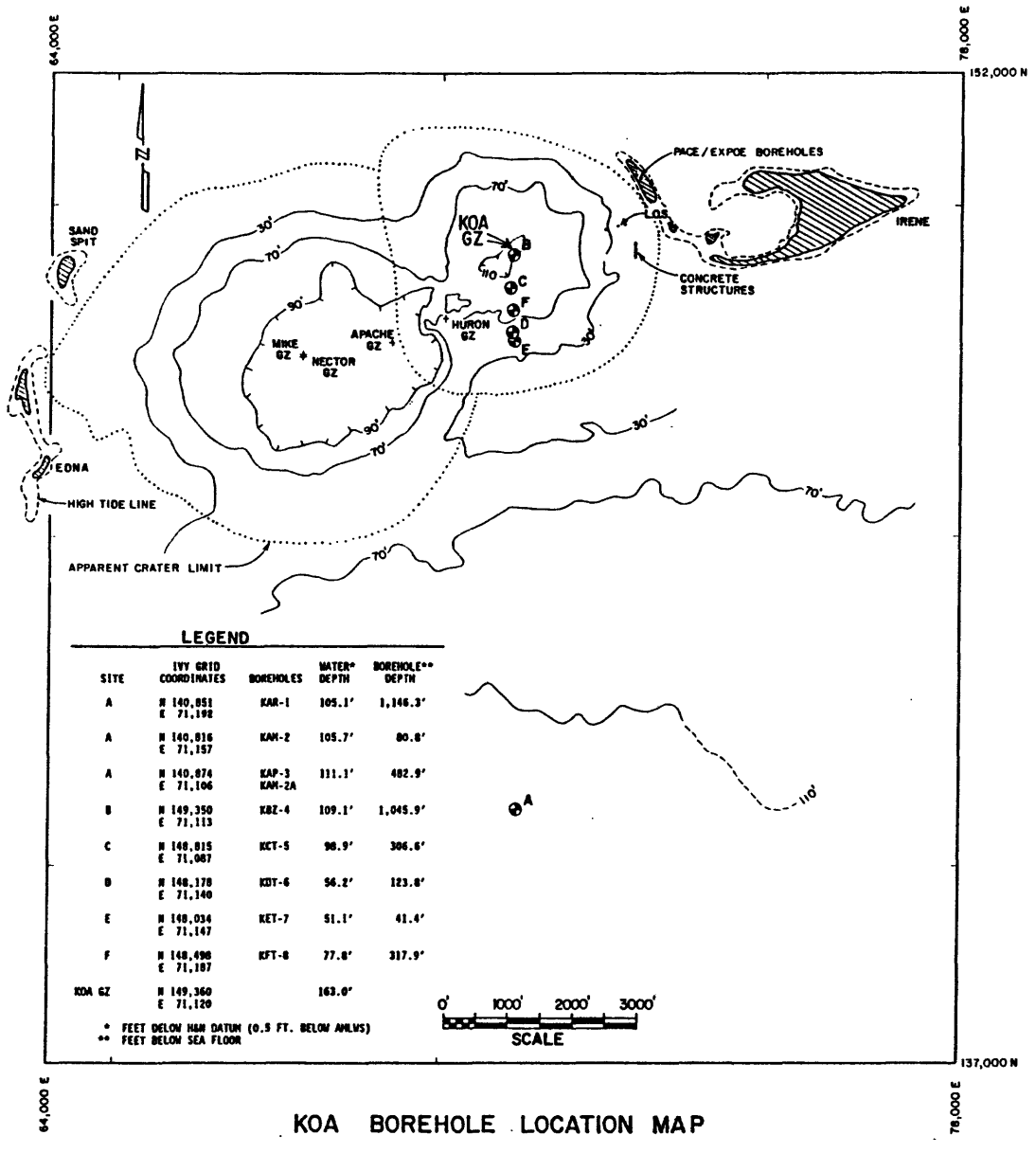

KOA BOREHOLE LOCATION MAP

FIGURE 1-2. -- Map of KOA crater area showing borehole sites (depicted by letters) and general bathymetric contours (contour interval in feet). Map modified from Henry and Wardlaw (1986b, fig. 1-2).

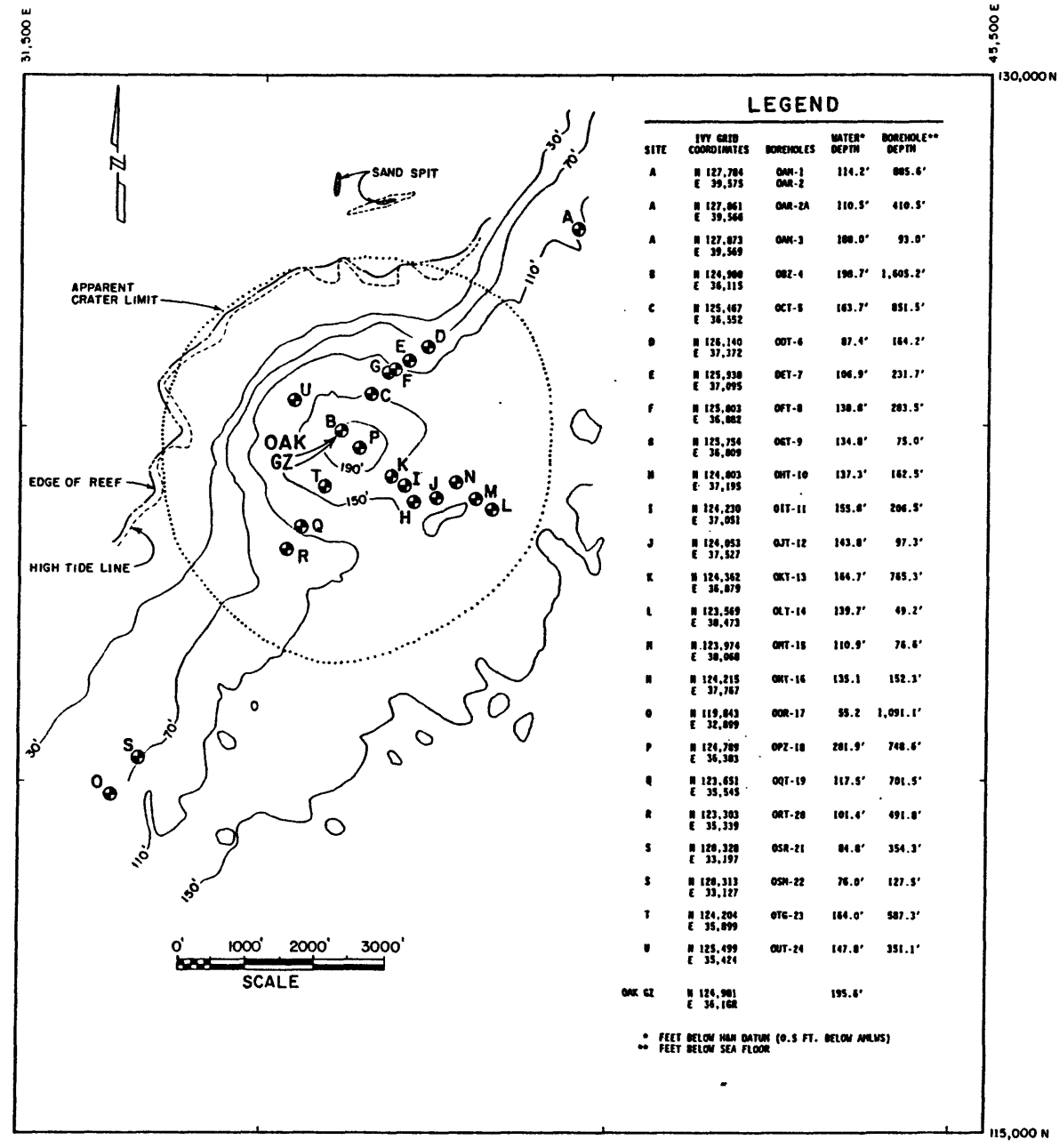

OAK BOREHOLE LOCATION MAP

FIGURE 1-3. -- Map of OAK crater area showing borehole sites (depicted by letters) and general bathymetric contours (contour interval in feet). Map modified from Henry and Wardlaw (1986b, fig. 1-3).

Cronin, Brouwers, and others, 1986; Halley, Major, Ludwig, and others, 1986).

(3). A broad spectrum of unpublished archival material from the PPG made freely available to us by the DNA and the DOE. These data include pre- and post-shot survey maps of the OAK and KOA crater areas, both black-and-white and color, stereographic aerial photographs, other kinds of aerial photographs, and pictures made (both pre- and post-testing) from ground-level of various crater features and man-made structures. The pre- and post-shot Holmes and Narver maps of OAK crater were digitized and form an essential part of the volumetric studies for the PEACE Program (Peterson and Henny, 1987, Chapter 5 of the current Report).

(4). Other published reports, too numerous to cite here.

SYNOPSIS OF CHAPTERS OF CURRENT VOLUME

This Open-File Report consists of seven Chapters. The interrelationship of each Chapter to the overall data base is depicted in Table 1-1. Salient points of each Chapter are summarized below.

Borehole Gravity (Ch. 2; Beyer)

The borehole gravity measurements from the southwest transect of OAK crater and in the Medren (ELMER) Island borehole provide a critical set of data for bulk density and porosity of both the undisturbed stratigraphic sequence and the sediments and rock that were affected by the OAK event.

Significant densification, porosity dimunition, and mass removal are indicated for discrete intervals within the boreholes in the central-crater region of OAK. Zones in which these phenomena are indicated correspond closely to the geologic crater zones and provide strong corroborative evidence for their integrity.

One of the primary goals of the gravimetry was to determine whether densification of the shallow substrate in the crater-flank region (or "wings") could account for the measured lowering of the sea floor. This is particularly critical because the bulk of the volume of the apparent crater lies within its flank region. Gravity analysis conducted in the upper parts of transition-zone boreholes (OQT-19 and ORT-20, see fig. 1-3) demonstrates conclusively that the materials (sediment, rock, and rock debris) are only slightly denser than comparable intervals of materials in reference boreholes OOR-17 and OSR-21. In fact, only perhaps about 15 percent of the documented lowering of the sea floor in the crater wings region can be explained by densification alone. Thus, for the wings region, processes other than densification clearly are also involved.

Paleontologic Evidence for Mixing (Ch. 3; Cronin, Gibson)

Paleontologic analysis of the upper 1,200 ft of strata on Enewetak established the division of the upper part of the carbonate cap into twelve discrete biostratigraphic zones (named zones AA, the youngest, through LL, the oldest -- see also Cronin, Brouwers, and others, 1986, and Brouwers, Cronin, and Gibson, 1986). For the current study, additional samples from stratigraphically undisturbed boreholes from the OAK crater area (i.e., from the reference boreholes) were examined to refine the local zonation and to more closely resolve key biostratigraphic boundaries. Several of these boundaries, combined with physical stratigraphic datums, form surfaces or marker horizons that are Lagrangian (see Chapter 6), permitting employment of a powerful tool in the analysis of crater evolution.

The microfossil studies of OAK reference-borehole plus crater samples provides significant new information about the timing and methods of emplacement[1] of materials from various biostratigraphic zones within the materials that partially infill the crater itself. This includes for the first time identification of sediments that were either at or within a few centimeters of the pre-event lagoon floor. These new data have furnished quantatative estimates of material from each zone (or group of zones) admixed in the crater fill. These estimates include volumes and percentages of materials originating from the deeper stratigraphic zones not involved in the excavation of the initial crater itself and from shallower geologic units as well. The editors emphasize that materials from stratigraphically shallower zones pose a real problem of differentiation. For example, how does one separate material that may have been emplaced from, say, zone CC from material within CC that has not moved? *Therefore, estimated volumes or percentages of material that may have been piped or otherwise moved from these shallow zones may be underestimated, perhaps grossly.*

Electron Paramagnetic Resonanace Studies (Ch. 4; Polanskey, Ahrens)

EPR spectrometry was applied to measure the peak-shock stress to which calcitic materials were subjected during the OAK event. Most of the samples analyzed can be characterized as either unshocked or very heavily shocked, with few samples showing intermediate states. Samples of the "transition sand" from OPZ-18 show the greatest concentration of very highly shocked material, interpreted as originating in the proximity of ground zero and plastered onto the walls of the excavational crater. Because of subsequent collapse of the excavational crater walls and dilution by mixing with less-shocked or unshocked materials, this lining, as a discrete stratigraphic unit, is identifiable only in the OPZ-18 borehole. Suprisingly, none of the 26 samples from the ground-zero borehole OBZ-4 showed significant shock damage. However, a zone containing less concentrated, very highly shocked material can be recognized in the three transition-zone boreholes studied (OCT-5, OET-7, and OFT-8), and its base occurs at progressively shallower depths away from ground zero.

---

[1] The term emplacement is used as a generic term to describe the deposition of material transported from one point to another without reference to the mechanism involved.

Bathymetric Studies of OAK Crater (Ch. 5; Peterson, Henny)

Three pertinent base maps were digitized and processed with a computer to facilitate analysis of the changes in the sea-floor bottom topography (bathymetry) and corresponding volumes in the area affected by the detonation of the OAK device (June 29, 1958) and by subsequent, longer term geologic processes. These maps are: (1) the pre-shot Holmes and Narver (H&N) survey, completed three days prior to the burst; (2) the post-shot H&N map, surveyed 47 to 67 days after the burst; and (3) the USGS map, made during the Marine Phase of the PEACE Program, 26 years after the burst.

The USGS map, in the format presented by Folger, Hampson, and others (1986), was not amenable for comparison with the two H&N maps (even undigitized) primarily because the USGS depth contours are given in meters rather than feet. The irregular area common to all three base maps is shown in Figure 5-1.

OAK is a strongly asymmetric crater; part of the asymmetry is a geologic function of the reef being on one side of surface ground zero and the atoll lagoon on the other. Many independent lines of evidence demonstrate that the excavational crater was appreciably smaller and more nearly circular than the current (or apparent) crater. Using the standardized digitized data for the common area of the base maps, three pairs[2] of vertical-difference contour maps were prepared. These maps show that: (1) the pre-shot topographic (geologic) features significantly influenced not only the evolution and final size/shape of the crater but also the initial distribution and subsequent reworking of debris from the OAK event; (2) the area of greatest downward displacement of the sea floor between the two post-shot base maps is that of the inner crater; and (3) the entire map area was lowered (and not uniformly) an average of 23 ft by 67 days after the burst and by another 12 ft during the next 26 years. As the surface of the lagoon and crater floor in this area was lowered, areas of positive-difference in relief (i.e., those areas that were higher post-shot than pre-shot) also decreased from about 27 percent by 67 days to about 14 percent 26 years later.

Two notes of caution must be clearly understood in using these maps for quantitative estimates for cratering calculations. The first is that there is no Lagrangian marker for the pre-event lagoon floor. The second is that the debris volumes estimated from these maps are understated simply because the apparent crater of OAK extends beyond the areas mapped, including the USGS map, which ecompasses the largest area.

---

[1] Following the glossary presented in Henry and Wardlaw (1986a), the apparent crater is defined as the locus of the zero-difference contour line surrounding a crater -- viz, the locus of points where the effects of an explosion can no longer be detected when the pre-event contours are compared with the post-event contours (fide, B.L. Ristvet.)

[2] A negative- and a positive-relief-difference (called Δ-relief) isopachous map was constructed for each combination of two base maps.

Constraints on Densification and Piping for OAK (Ch. 6; Trulio)

As mentioned previously, it is established from a wide array of data that the excavational crater of OAK had an appreciably smaller radius than that of the apparent crater. Because crater volume is a radius-squared function, it is evident that most of the volume of OAK is contained within its flank or "wing" area. What is (are) the significant mechanism(s) reponsible for forming the wings of the large apparent craters in the PPG? Trulio presents a number of different models dealing with the PEACE Program data bases and makes a number of inferences about these mechanisms based on these models.

Using the data base from the gravimetry (Chapter 2), Trulio applies mathematical analyses to the data, from a purely physical viewpoint, and verifies Beyer's conclusion that densification (or, in Trulio's terminology, "simple subsidence") accounts for just a small part of the formation of the wings of OAK crater. As a best estimate, only about 8 percent of the sea-floor drop on the wings can be attributed to density increases caused by the burst.

Another explanation for part of the observed sea-floor lowering phenomenon is piping, or movement (driven by gravity and density differences) of a sediment/water slurry through conduits (cracks, fissures, etc.) to generally shallower depths or to the surface through vents to form "sand volcanoes". That piping occurred associated with the OAK and KOA bursts, particularly in the central crater region, is supported by independent lines of evidence (see Chapter 7 for discussion). However, at issue are: (1) the role of piping relative to other mechanisms to account for the drop in the sea floor; and (2) the amount of material transported by this mechanism. Mean values for the density of material piped up to the sea floor from beneath OAK can be derived from the combination of sea-floor base maps and gravimetry profiles. If correct, this model poses limitations on the amount of material transported out of the crater by piping. The best estimate based on this model is that the piped and residual materials differed by only about 0.2 g/cc, a density difference that can drive piping, in Trulio's words, "but weakly". Trulio cautions that the sequence of events leading to the transport of piped material out of the crater is subject to interference at many points.[1]

It is suggested that plastic flow also should be considered as a plausible mechanism to account for most of the phenomenon of sea-floor lowering. Trulio points out, however, that little is known about the displacement field around a flow crater.

---

[1] See caveat in italics on page 1-8. The editors also emphasize that the observed "subsidence" or sea-floor lowering on the wings of the Enewetak craters studied is not reasonably attributable to one mechanism operating alone. The lowering was caused in part by densification, in part by piping (certainly upwardly and probably laterally as well), probably in part to plastic flow, and possibly to other mechanisms that may not have even been thought of yet.

Additional Studies of Geologic Crater Models (Ch. 7, Wardlaw)

The final Chapter provides an integration of the new information from the various studies presented in the current Open-File Report with the previously developed analyses of PEACE Program data. Of particular interest to the material-properties community is the formulation of a set of material-properties units for the normal stratigraphic (geologic) sequence and a discussion of the relationship of these units to the sedimentary packages presented in Wardlaw and Henry (1986a, 1986b).

Using available evidence, the pre-event geology beneath the OAK and KOA crater areas is reconstructed, including paleotopographic contour maps of several of the more significant subsurface datums. Wardlaw points out that topographic differences of the pre-event Holocene ground surfaces (i.e., the pre-1958 lagoon, reef, and island surface) between the KOA and OAK area produced differences in the surface configurations of the two craters. Differences in cementation and structural competency of key stratigraphic intervals beneath the surface ground zeros of KOA and OAK and the effects of these differences on the development of the two craters are summarized.

A study of the thinning of the stratigraphic units influenced by OAK and KOA is presented. A more comprehensive interpretation of the models for these two craters given in Wardlaw and Henry (1986b) is developed based primarily on the inferred pre-shot elevation of certain datums and thicknesses of stratigraphic intervals in contrast to their post-shot attributes. The case is ade that movement of material laterally ("lateral flow") may account for much of the "subsidence" and formation of the wings.

An idealized succession of cratering and depositional events is presented.

ACKNOWLEDGEMENTS

We, the editors, extend a special note f appreciation to the following people, without whom this program would have not been possible. Lt. Col. Robert F. Couch, Jr. (U.S. Air Force and DNA Program Manager for the PEACE Program) and Byron L. Ristvet and Edward L. Tremba (both of S-Cubed Division of Maxwell Laboratories), and Robert W. Henny (Air Force Weapons Laboratory) were full scientific collaborators with us during the PEACE Program. All four of these geologists logged extensive on-site experience in the PPG prior to the current program and were principal investigators in all of various phases of the earlier AFWL investigations on Enewetak. And, in a real sense, they represent a vital component of the record of cratering studies on Enewetak. Their expertise and geotechnical knowledge were invaluable to the current program, and we owe them a profound debt of gratitude. Couch, Ristvet, and Tremba served (alternatively) as Chief Scientists aboard the Knut Constructor during the Drilling Phase of the program, and all three were on-site during parts of the earlier Marine Phase.

We would like to thank also the authors of the Chapters of the current Open-File Report for their timely response to our needs in editing, compiling,

and finalizing this volume and for their input for synthesizing the diverse data bases.

We are indebted also to John F. Schatz and L. Stephen Melzer of SAIC for constructive exchange of scientific and technical information for this volume. Melzer was on-site with us as Chief Scientist during part of the Drilling Phase field work, and it was his observations along with that of the geologists and paleontologists studying the OAK ground-zero borehole aboard the drill ship that demonstrated the reality of piping of materials from zones from far below the excavational crater into the sediment forming part of the crater fill.

The plates for Chapter 2 were laid out by James MacCornack, S-Cubed, Albuquerque, and printed by the Defense Nuclear Agency Printing Plant, Kirtland AFB, New Mexico. We thank Leonard MacDonald, head printer, for his assistance.

REFERENCES CITED

Ackermann, H.D., Grow, J.A., and Williams, J.M., 1986, Chapter E: Seismic-refraction survey of OAK crater; 18 p., 19 figs., 1 tbl.; in Folger, D.W., editor, Sea-floor observations and subbottom seismic charac-teristics of OAK and KOA craters, Enewetak Atoll, Marshall Islands: U.S. Geological Survey Bulletin 1678.

Beyer, L.A., Ristvet, B.L., and Oberste-Lehn, D., 1986, Chapter 8: preliminary density and porosity data and field techniques of borehole gravity surveys, OAK crater; 28 p., 4 figs., 10 tbls., 2 appendices; in Henry, T.W., and Wardlaw, B.R., editors, Pacific Enewetak Atoll Crater Exploration (PEACE) Program, Enewetak Atoll, Republic of the Marshall Islands; Part 3: Stratigraphic analysis and other geologic and geophysical studies in vicinity of KOA and OAK craters: U.S. Geological Survey Open-File Report 86-555.

Blouin, S.E., and Timian, D.A., 1986a, Core description and ultrasonic logs from Enewetak Atoll: Defense Nuclear Agency, Washington, DC., Technical Report TR-86-198, 98 p., [released 3 February 1986, unclassified document].

Blouin, S.E., and Timian, D.A., 1986b, Material properties testing in support of PEACE Program, Enewetak Atoll: Defense Nuclear Agency, Washington, DC., Technical Report TR-86-197, 458 p., [released 4 June 1986, unclassified document].

Borshel, T.F., Klauber, W.P., and Earley, K.H., 1986, Lithological, physical, and mechanical characterization of geologic samples from Enewetak Atoll: TerraTek Research, Inc., Report TR-87-25, prepared for the Defense Nuclear Agency.

Brouwers, E.M., Cronin, T.M., and Gibson, T.G., 1986, Chapter 11: Additional paleontologic studies, OAK and KOA craters; 18 p., 5 figs., 5 tbls., 1 pl.; in Henry, T.W., and Wardlaw, B.R., editors, Pacific Enewetak Atoll Crater Exploration (PEACE) Program, Enewetak Atoll, Republic of the Marshall Islands; Part 3: Stratigraphic analysis and other geologic and geophysical studies in vicinity of KOA and OAK craters: U.S. Geological Survey Open-File Report 86-555.

Couch, R.F., Jr., Fetzer, J.A., Goter, E.R., Ristvet, B.L., Tremba, E.L., Walter, D.R., and Wendland, V.P., 1975, Drilling operations of Eniwetok Atoll during Project EXPOE: Air Force Weapons Laboratory Technical Report AFWL-TR-75-216, Kirtland Air Force Base, New Mexico, 270 p., 17 figs., 4 tbls. [unclassified document].

Cronin, T.M., Brouwers, E.M., Bybell, L.M., Edwards, E.E., Gibson, T.G., Margerum, R., and Poore, R.Z., 1986, Pacific Enewetak Atoll Crater Exploration (PEACE) Program, Enewetak Atoll, Republic of the Marshall Islands; Part 2: Paleontology and biostratigraphy, application to OAK and KOA Craters: U.S. Geological Survey Open-File Report 86-159, 39 p., 20 figs., 12 tbls., 3 appendices.

Emery, K.O., Tracey, J.I., Jr., and Ladd, H.S., 1954, Geology of Bikini and nearby atolls: U.S. Geological Survey Professional Paper 260-A, 265 p., 73 pls., 84 figs., 11 charts, 27 tbls.

Folger, D.W., editor, 1986a, Sea-floor observations and subbottom seismic characteristics of OAK and KOA craters, Enewetak Atoll, Marshall Islands: U.S. Geological Survey Bulletin 1678, 301 p., 112 figs., glossary, 2 appendices. [Chapters A - H, plus Introduction.]

Folger, D.W., 1986b, Introduction to the volume; 7 p., 2 figs., 2 tbls.; in Folger, D.W., editor, Sea-floor observations and subbottom seismic characteristics of OAK and KOA craters, Enewetak Atoll, Marshall Islands: U.S. Geological Survey Bulletin 1678.

Folger, D.W., Hampson, J.C., Robb, J.M., Woellner, R.A., Foster, D.S., and Tavares, L.A., 1986, Chapter A: Bathymetry of OAK and KOA craters; 35 p., 12 figs., 2 appendices; in Folger, D.W., editor, Sea-floor observations and subbottom seismic characteristics of OAK and KOA craters, Enewetak Atoll, Marshall Islands: U.S. Geological Survey Bulletin 1678.

Folger, D.W., Robb, J.M., Hampson, J.C., Davis, P.A., Bridges, P.M., and Roddy, D.J., 1986, Chapter B: Sidescan-sonar survey of OAK and KOA craters; 18 p., 6 figs.; in Folger, D.W., editor, Sea-floor observations and subbottom seismic characteristics of OAK and KOA craters, Enewetak Atoll, Marshall Islands: U.S. Geological Survey Bulletin 1678.

Grow, J.A., Lee, M.W., Miller, J.J. Agena, W.F., Hampson, J.C., Foster, D.S., and Woellner, R.A., 1986, Chapter D: Multichannel seismic-reflection survey of KOA and OAK craters; 46 p., 39 figs.; in Folger, D.W., editor, Sea-floor observations and subbottom seismic characteristics of OAK and KOA craters, Enewetak Atoll, Marshall Islands: U.S. Geological Survey Bulletin 1678.

Halley, R.B., Major, R.P., Ludwig, K.R., Peterman, Z.L., and Matthews, R.K., 1986, Chapter G: Preliminary analyses of OAK debris samples; 11 p., 6 figs., 4 tbls.; in Folger, D.W., editor, Sea-floor observations and subbottom seismic characteristics of OAK and KOA craters, Enewetak Atoll, Marshall Islands: U.S. Geological Survey Bulletin 1678.

Halley, R.B., Slater, R.A., Shinn, E.A., Folger, D.W., Hudson, J.H., Kindinger, J.L., and Roddy, D.J., 1986, Chapter F: Observations of OAK and KOA craters from the submersible; 32 p., 13 figs., 1 appendix; in Folger, D.W., editor, Sea-floor observations and subbottom seismic characteristics of OAK and KOA craters, Enewetak Atoll, Marshall Islands: U.S. Geological Survey Bulletin 1678.

Henny, R.W., Mercer, J.W., and Zbur, R.T., 1974, Near-surface geologic Investigations at Eniwetok Atoll: Air Force Weapons Laboratory Technical Report AFWL-TR-74-257, Kirtland Air Force Base, New Mexico, 367 p. [unclassified document].

Henry, T.W., and Wardlaw, B.R., editors, 1986a, Pacific Enewetak Atoll Crater Exploration (PEACE) Program, Enewetak Atoll, Republic of the Marshall Islands; Part 3: Stratigraphic analysis and other geologic and geophysical studies in vicinity of KOA and OAK craters: U.S. Geological Survey Open-File Report 86-555, 486 p., 92 figs., 90 tbls, 34 pls. [14 Chapters.]

Henry, T.W., and Wardlaw, B.R., 1986b, Chapter 1: Introduction: 13 p., 3 figs., 1 tbl., in Henry, T.W., and Wardlaw, B.R., editors, Pacific Enewetak Atoll Crater Exploration (PEACE) Program, Enewetak Atoll, Republic of the Marshall Islands; Part 3: Stratigraphic analysis and other geologic and geophysical studies in vicinity of KOA and OAK craters: U.S. Geological Survey Open-File Report 86-555.

Henry, T.W., Wardlaw, B.R., Skipp, B.A., Major, R.P., and Tracey, J.I., Jr., 1986, Pacific Enewetak Atoll Crater Exploration (PEACE) Program, Enewetak Atoll, Republic of the Marshall Islands; Part 1: Drilling operations and descriptions of boreholes in vicinity of KOA and OAK craters: U.S. Geological Survey Open-File Report 86-419, 497 p., 32 figs., 29 pls., 13 tbls., 3 appendices.

Ludwig, K.R., Halley, R.B., Simmons, K.R., and Peterman, Z.E., 1986, Chapter 3: Sr-isotope stratigraphy of disturbed and undisturbed carbonates; 23 p., 8 figs., 6 tbls.; in Henry, T.W., and Wardlaw, B.R., editors, Pacific Enewetak Atoll Crater Exploration (PEACE) Program, Enewetak Atoll, Republic of the Marshall Islands; Part 3: Stratigraphic analysis and other geologic and geophysical studies in vicinity of KOA and OAK craters: U.S. Geological Survey Open-File Report 86-555.

McClelland Engineers, Inc., 1986, Relative liquefaction for potential study for carbonate versus noncarbonate materials: Report No. 0186-1069, to Holmes and Narver, Inc., Honolulu, Hawaii; dated December 19, 1986; 37 p., 13 pls. [Signed by Ronald J. Ebehar, Project Supervisor, and Alan G. Young, Vice President, Marine Geosciences.]

Melzer, L.S., 1986, Chapter 7: Downhole geophysical logs; 32 p., 16 figs., 7 tbls.; in Henry, T.W., and Wardlaw, B.R., editors, Pacific Enewetak Atoll Crater Exploration (PEACE) Program, Enewetak Atoll, Republic of the Marshall Islands; Part 3: Stratigraphic analysis and other geologic and geophysical studies in vicinity of KOA and OAK craters: U.S. Geological Survey Open-File Report 86-555.

Mueller, C.M., 1987, Mechanical response of undisturbed cores and remolded coral sand from Enewetak Atoll: Department of the Army, Corps of Engineers, Waterways Experiment Station, Technical Report SL-87-14, Vicksburg, Mississippi, 361 p., 274 pls., 56 figs., 5 tbls. [unclassified document].

Patti, N., and Schatz, J.F., 1987 [1988?], in preparation, Material properties tests, material compaction on shot-similar stress/strain paths, and grain size distribution on Enewetak Atoll coral specimens: Science Applications International Corporation, Report SAIC-87/1158, prepared for the Defense Nuclear Agency.

Ristvet, B.L., and Tremba, E.L., 1986a, Chapter 5: Total organic content of lagoon benthic sediments and of subsurface samples from the PEACE drilling program; 9 p., 2 figs., 2 tbls.; in Henry, T.W., and Wardlaw, B.R., editors, Pacific Enewetak Atoll Crater Exploration (PEACE) Program, Enewetak Atoll, Republic of the Marshall Islands; Part 3: Stratigraphic analysis and other geologic and geophysical studies in vicinity of KOA and OAK craters: U.S. Geological Survey Open-File Report 86-555.

Ristvet, B.L., and Tremba, E.L., 1986b, Chapter 6: Insoluble residue analysis of carbonate sediments from the subsurface of Enewetak Atoll; 5 p., 1 tbl., ; in Henry, T.W., and Wardlaw, B.R., editors, Pacific Enewetak Atoll Crater Exploration (PEACE) Program, Enewetak Atoll, Republic of the Marshall Islands; Part 3: Stratigraphic analysis and other geologic and geophysical studies in vicinity of KOA and OAK craters: U.S. Geological Survey Open-File Report 86-555.

Ristvet, B.L., and Tremba, E.L., 1986c, Chapter 12: Radiation chemistry of the subsurface of OAK and KOA craters; 15 p., 5 figs., 5 tbls; in Henry, T.W., and Wardlaw, B.R., editors, Pacific Enewetak Atoll Crater Exploration (PEACE) Program, Enewetak Atoll, Republic of the Marshall Islands; Part 3: Stratigraphic analysis and other geologic and geophysical studies in vicinity of KOA and OAK craters: U.S. Geological Survey Open-File Report 86-555.

Ristvet, B.L., Tremba, E.L., Couch, R.F., Jr., Fetzer, J.A., Goter, E.R., Walter, D.R., and Wendland, V.P., 1978, Geologic and geophysical investigations of the Enewetak nuclear craters; Final reports: Air Force Weapons Laboratory Technical Report AFWL-TR-77-242, Kirtland Air Force Base, New Mexico, 298 p. [unclassified document].

Robb, J.M., Foster, D.S., Folger, D.W., Hampson, J.C., and Woellner, R.A., 1986, Chapter C: Single-channel seismic survey of OAK and KOA craters: 51 p., 24 figs.; in Folger, D.W., editor, Sea-floor observations and subbottom seismic charac-teristics of OAK and KOA craters, Enewetak Atoll, Marshall Islands: U.S. Geological Survey Bulletin 1678.

Schatz, J.F., Patti, N., and Melzer, L.S., 1987 [1988?], in preparation, Material properties at OAK/KOA -- Summary Report: Science Applications International Corporation, Report SAIC-87/1159, prepared for the Defense Nuclear Agency.

Simons, D., and others, 1984, Recommendations for laboratory material properties testing of core materials from the Pacific Proving Grounds: Research and Development Associates, Los Angeles, California; unnumbered report submitted to Defense Nuclear Agency.

Shinn, E.A., Kindinger, J.L., Halley, R.B., and Hudson, J.H., 1986, Chapter H: Scuba observations of OAK and KOA craters, 39 p., 38 figs., 1 tbl.; in Folger, D.W., editor, Sea-floor observations and subbottom seismic characteristics of OAK and KOA craters, Enewetak Atoll, Marshall Islands: U.S. Geological Survey Bulletin 1678.

Slater, R.A., Roddy, D.J., Folger, D.W., Halley, R.B., and Shinn, E.A., 1986, Chapter 13: Additional submersible studies; detailed observations of the seafloor of OAK, KOA, and MIKE craters; 153 p., 2 tbls., 4 pls.; in Henry, T.W., and Wardlaw, B.R., editors, Pacific Enewetak Atoll Crater Exploration (PEACE) Program, Enewetak Atoll, Republic of the Marshall Islands; Part 3: Stratigraphic analysis and other geologic and geophysical studies in vicinity of KOA and OAK craters: U.S. Geological Survey Open-File Report 86-555.

Tremba, E.L., 1987 [1984], Enewetak Atoll Seismic Investigation (EASI): Phase III; Final Report: Air Force Weapons Laboratory Technical Report 84-105, Air Force Systems Command, Kirtland Air Force Base, New Mexico, 87117-6008, 122 p., 36 figs., 11 tbls. [unclassified document].

Tremba, E.L., Couch, R.F., Jr., and Ristvet, B.L., 1982, Enewetak Atoll Seismic Investigation (EASI) Project; Phases I and II: Air Force Weapons Laboratory Technical Report AFWL-TR-82-20, Kirtland Air Force Base, New Mexico, 124 p., 38 figs., 3 tbls., 3 appendices [unclassified document].

Tremba, E.L., Jones, G.L., and Henny, R.W., 1981, Pacific atoll cratering experiments (Project PACE 2); Results and analysis of cratering and related effects: Air Force Weapons Laboratory Technical Report AFWL-TR-81-167, Air Force Systems Command, Kirtland Air Force Base, New Mexico, 334 p., 32 figs., 8 tbls., 8 appendices [unclassified document].

Tremba, E.L., and Ristvet, B.L., 1986a, Chapter 4: X-ray diffraction mineralogy; 49 p., 11 figs., 35 tbls., in Henry, T.W., and Wardlaw, B.R., editors, Pacific Enewetak Atoll Crater Exploration (PEACE) Program, Enewetak Atoll, Republic of the Marshall Islands; Part 3: Stratigraphic analysis and other geologic and geophysical studies in vicinity of KOA and OAK craters: U.S. Geological Survey Open-File Report 86-555.

Tremba, E.L., and Ristvet, B.L., 1986b, Chapter 9: Seismic reference surveys; 16 p., 1 fig., 12 tbls.; in Henry, T.W., and Wardlaw, B.R., editors, Pacific Enewetak Atoll Crater Exploration (PEACE) Program, Enewetak Atoll, Republic of the Marshall Islands; Part 3: Stratigraphic analysis and other geologic and geophysical studies in vicinity of KOA and OAK craters: U.S. Geological Survey Open-File Report 86-555.

Wardlaw, B.R., and Henry, T.W., 1986a, Chapter 2: Physical stratigraphic framework; 36 p., 10 figs., 2 tbls.; in Henry, T.W., and Wardlaw, B.R., editors, Pacific Enewetak Atoll Crater Exploration (PEACE) Program, Enewetak Atoll, Republic of the Marshall Islands; Part 3: Stratigraphic analysis and other geologic and geophysical studies in vicinity of KOA and OAK craters: U.S. Geological Survey Open-File Report 86-555.

Wardlaw, B.R., and Henry, T.W., 1986b, Chapter 14: Geologic interpretation of OAK and KOA craters; 39 p., 21 figs., 2 tbls.; in Henry, T.W., and Wardlaw, B.R., editors, Pacific Enewetak Atoll Crater Exploration (PEACE) Program, Enewetak Atoll, Republic of the Marshall Islands; Part 3: Stratigraphic analysis and other geologic and geophysical studies in vicinity of KOA and OAK craters: U.S. Geological Survey Open-File Report 86-555.

Wardlaw, B.R., Henry, T.W., and Martin, W.E., 1986, Chapter 10: Benthic samples from Enewetak Atoll; 50 p., 6 figs., 12 tbls., 29 pls.; in Henry, T.W., and Wardlaw, B.R., editors, Pacific Enewetak Atoll Crater Exploration (PEACE) Program, Enewetak Atoll, Republic of the Marshall Islands; Part 3: Stratigraphic analysis and other geologic and geophysical studies in vicinity of KOA and OAK craters: U.S. Geological Survey Open-File Report 86-555.

****

CHAPTER 2:

ANALYSIS OF BOREHOLE GRAVITY SURVEYS AT OAK CRATER

by

L. A. Beyerl

INTRODUCTION

Borehole gravity (BHG) surveys were made in selected PEACE Program boreholes at OAK crater on Enewetak Atoll because they provide the only means to directly and accurately measure in situ bulk density of large volumes of rock and sediment that surround the boreholes and to provide data to calculate the total porosity of these materials2. The differences between the density and porosity of undisturbed atoll materials and the sediment and rock involved in the excavational and apparent craters are crucial to understanding various cratering phenomena. In addition, accurate and representative density and porosity measurements of undisturbed atoll materials are important for nuclear-event calculations. The nature of BHG measurements, rationale for siting BHG boreholes, field techniques, and preliminary (apparent) BHG density data and calculated porosity values are given in Beyer, Ristvet, and Oberste-Lehn (1986).

This report presents the models used to correct the apparent (BHG) density and porosity data for large-scale lateral density changes across the reef margin (due to natural facies changes) and for smaller-scale lateral density changes due to cratering phenomena. Corrected BHG density data and calculated porosity values are described in terms of their modification due to cratering processes.

Ancillary topics include: (1) general results of the BHG survey in the E-1 borehole on Medren (ELMER) Island (Appendix 2-1), (2) brief comparison of estimates of density and porosity from BHG, gamma-gamma, and neutron logs, and (3) relationship between grain density and BHG porosity in undisturbed atoll materials. A short description of how average interval grain density was determined from the x-ray mineralogy and organic analyses studies of core samples is found in Appendix 2-2.

The locations of OAK crater and E-1 and F-1 deep boreholes referred to later in this chapter are shown in Figure 2-1. Locations of boreholes drilled at OAK crater during the PEACE Program are given in Figure 2-2, along with a table that summarizes pertinent information about the boreholes in which BHG surveys were made. Locations of two cross sections presented later in the chapter also are shown in Figure 2-2.

1Branch of Sedimentary Processes, U.S. Geological Survey, Menlo Park, CA.

2Bulk density and total porosity are abbreviated as density and porosity in this Chapter. Porosity is calculated from a combination of in situ density and grain-density data derived from x-ray mineralogic analyses.

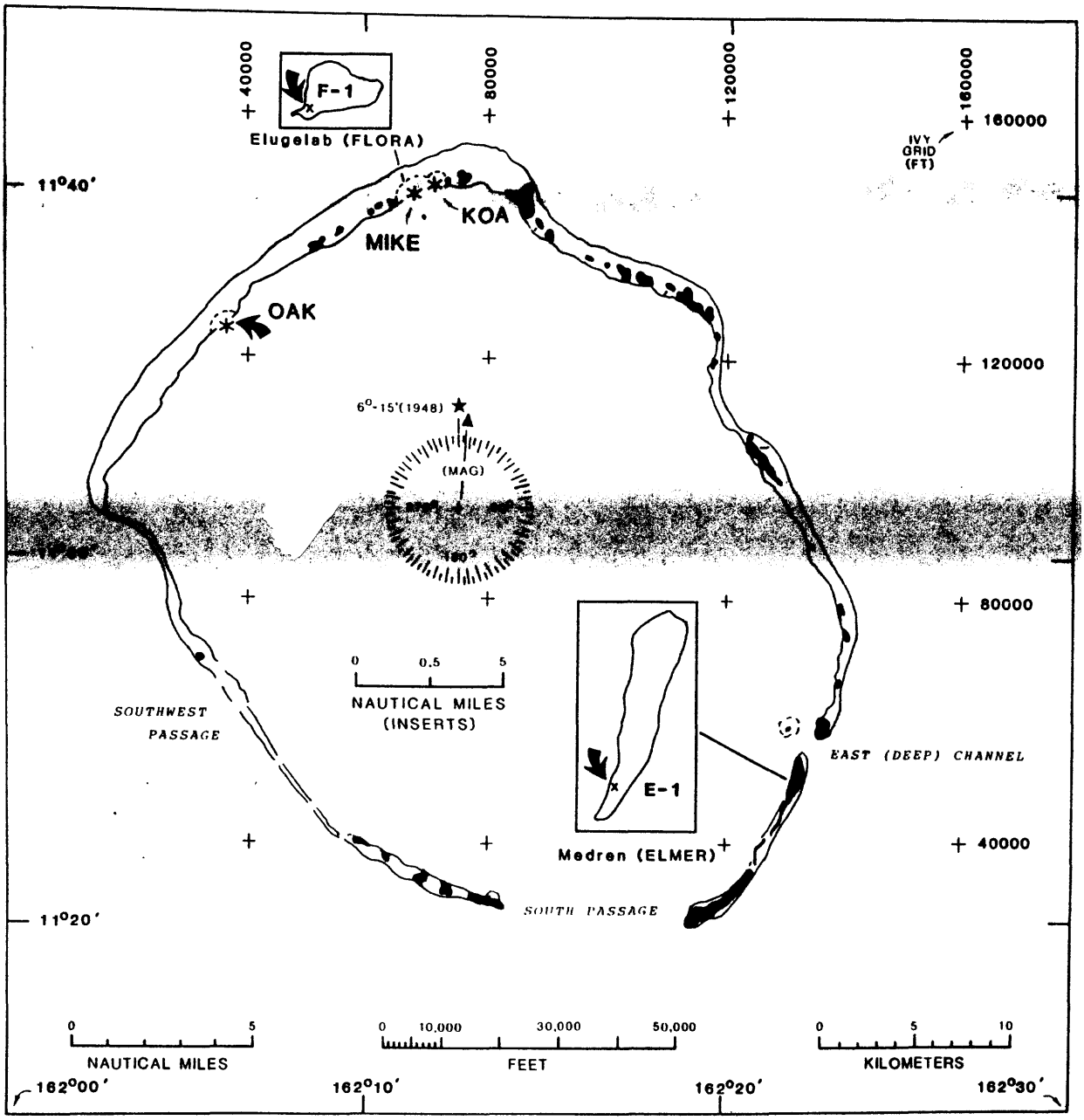

FIGURE 2-1. - Map of Enewetak Atoll showing locations of OAK, KOA, and MIKE craters and Medren (ELMER) Island. Deep boreholes E-1 and F-1 drilled in 1951 and 1952 by the USGS and AEC (Ladd and others, 1953; Ladd and Schlanger, 1960) and referred to in this paper are shown by "X"'s on the inset maps.

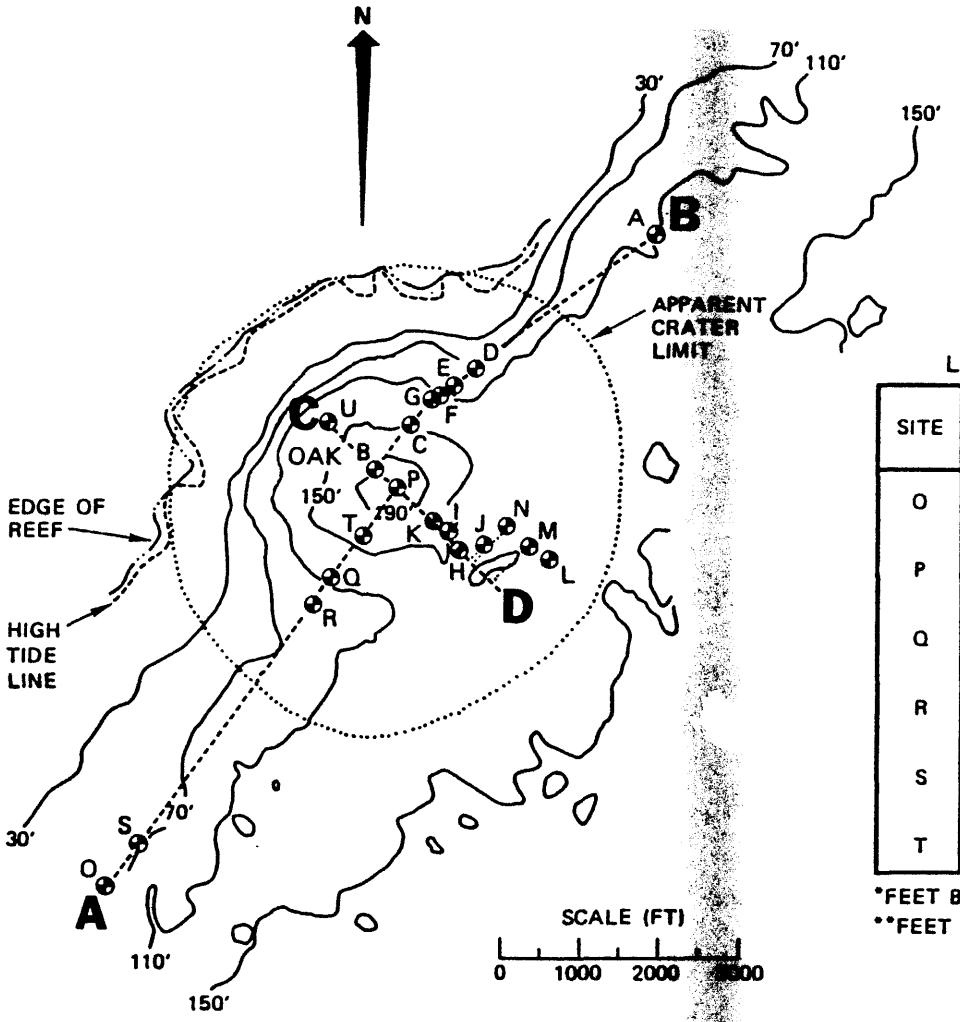

LEGEND – GRAVITY BOREHOLES

SITE	BOREHOLE	WATER* DEPTH	BOREHOLE** DEPTH
O	OOR-17	55.2	1091.1
P	OPZ-18	201.9	748.6
Q	OQT-19	117.5	701.5
R	ORT-20	101.4	491.8
S	OSR-21	84.0	354.3
T	OTG-23	164.0	587.3

*FEET BELOW SEA LEVEL (H AND N DATUM)
**FEET BELOW SEA FLOOR

FIGURE 2-2. - Map of OAK crater and vicinity showing locations of PEACE Program boreholes and cross sections AB and CD. Inset shows designation, water depth and total subsea-floor depth of boreholes in which gravity surveys were made.

The efficacy of BHG surveys to determine subtle density differences at OAK crater depends in great part on the precision of the field measurements. This is determined by making repeated Wg/Wz measurements over the same depth interval. Of 98 intervals surveyed in six boreholes, 8 percent were repeated four or more times, 81 percent were repeated three times, 10 percent were repeated two times, and 1 percent were not repeated due to operational constraints. These repeated Wg/Wz measurements indicate that the precision of the surveys is quite high and fully adequate for the purposes of the OAK study (fig. 2-3). Standard deviations of repeated measurements are given in column 3 of Tables 2-2 through 2-7 (located at the end of the current Chapter), are illustrated graphically on BHG density and porosity profiles in subsequent figures, and are explained in Appendix 8-2 of Beyer, Ristvet, and Oberste-Lehn (1986).

BOREHOLE GRAVITY ANALYSIS

The analysis of BHG measurements at OAK crater follows the only logical path available in the absence of independent data such as a detailed surface gravity anomaly map and reliable density data from gamma-gamma and/or core measurements. BHG measurements are corrected for recognizable lateral density variations so that the corrected BHG densities are reasonably accurate measures of the atoll materials within a few tens to a few hundreds of feet of each surveyed borehole. Then, comparisons of density (and porosity) can be made between different boreholes in and near OAK crater.

Corrections can be made rationally for submarine topography (Beyer, Ristvet, and Oberste-Lehn, 1986), for large-scale lateral density changes across the reef margin that are caused by natural facies changes, and for smaller-scale lateral density changes related to cratering processes. A summary of the range of corrections calculated and applied to the BHG surveys is given in Table 2-1. Individual corrections are presented in Tables 2-2 through 2-7, located at the end of the Chapter[1].

Corrections cannot be made for even smaller-scale lateral density changes on the order of tens to about a hundred feet distant from each borehole, because data needed to model these very small density changes were beyond the scope of the PEACE Program. We will note where these very small-scale effects may be present. Neglect of them does not impair the objectives of the BHG phase of the PEACE Program.

Please note that these corrections are computed as vertical gravity gradients which, when multiplied by 0.25 k, where k is the Newtonian gravitational constant, become density corrections in g/cm3. Lateral density variations that cause a downward positive vertical gravity gradient result in a positive density correction, whereas a downward negative gradient causes a negative density correction (see Appendix 8-2 of Beyer, Ristvet, and Oberste-Lehn, 1986).

---

[1]All tables are located at the end of the Chapter.

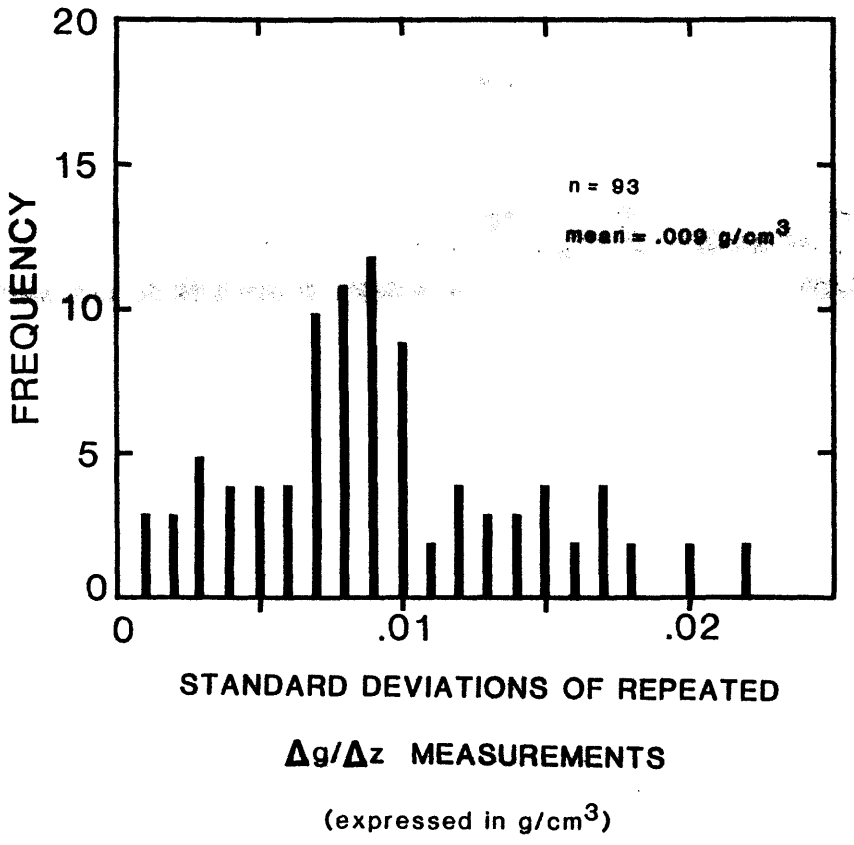

FIGURE 2-3. - Distribution of 93 sets of repeated $\Delta g/\Delta z$ measurements during borehole gravity surveys in OAK boreholes, expressed in g/cm^3. Mean is .009 g/cm^3 and is a measure of the high quality of the borehole gravity surveys (Beyer, 1968; Black and Herring, 1983).

LARGE-SCALE LATERAL DENSITY CHANGES ACROSS REEF MARGIN

A substantial body of work by many investigators at modern Pacific atolls has shown that forereef and reef core facies generally are more highly cemented (and therefore denser) than lagoon facies, and that atoll reefs generally prograde seaward (e.g., Buigues, 1985). These relationships are believed to be present along the northwest margin of Enewetak Atoll according to B. L. Ristvet, who provided the author with a sketch of the probable distribution of facies and densities across the reef margin at OAK crater. Other PEACE Program studies (Folger, 1986a) and earlier work at Enewetak, especially deep boreholes E-1 and F-1 and the XEN series of boreholes on Engebi Island (Ladd and others, 1953; Ladd and Schlanger, 1960; Couch and others, 1975), led to this assessment of atoll margin structure. Densities provided by Ristvet were modified slightly using the BHG densities from the E-1 borehole on Medren Island (see Appendix 2-1).

Deeper density contrasts (e.g., between the volcanic core and overlying carbonate rocks of the atoll) and possible incomplete isostatic compensation of the atoll also can affect the vertical gravity gradients (and BHG densities). Corrections for these possible effects are almost certainly negligibly small and, if determined, would cause only a very small, constant dc-type shift of all density data. The absence of even a rudimentary surface gravity anomaly map and more detailed deep borehole data prevent any attempt to examine these effects.

The two-dimensional density model prepared for the atoll margin at OAK crater is shown in Figure 2-4. Vertical gravity gradient corrections were calculated for the two-dimensional model with a well-established algorithm (Talwani and others, 1959) that has been modified for borehole gravity applications. These corrections are given in column 5 of Tables 2-2 to 2-7 and probably are unnecessary but their magnitudes needed to be evaluated.

CORRECTION FOR LATERAL DENSITY CHANGES DUE TO CRATERING PROCESSES

Lateral density variations due to cratering processes also can affect the BHG densities and, therefore, were evaluated. The model used to correct for these crater-related lateral density changes was developed along the southwest transect from OPZ-18 to OOR-17 by using BHG densities (corrected for submarine topography and large-scale density changes across the atoll margin) and a correlation cross section prepared by D. Oberste-Lehn and modified by B. R. Wardlaw (fig. 2-5; correlation cross section CD, fig. 2-6, also was prepared by Oberste-Lehn and Wardlaw). The density model is shown in Figure 2-7 and was assumed to have circular symmetry about OPZ-18. Trial gravity calculations taking into account the departure of OAK crater from circular symmetry about OPZ-18 (based only on correlation cross sections) showed that the assumption of circular symmetry is valid. The size of the corrections due to crater-related lateral density changes is so small that the question of true three-dimensionality versus circular symmetry about OPZ-18 is academic. The question of the actual crater density structure along cross section CD remains. A very careful sea floor gravity survey or more BHG drillholes and surveys would shed light on this question.

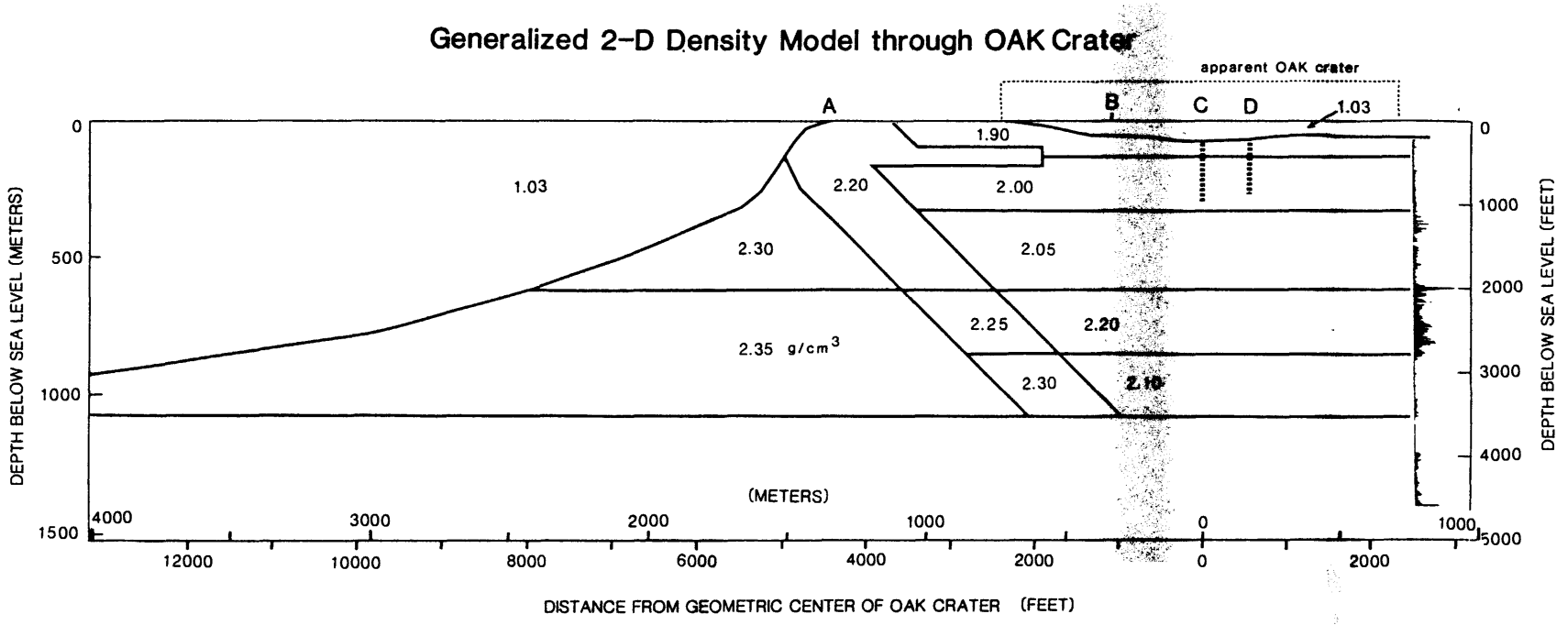

FIGURE 2-4. - Two-dimensional density model (assumed to extend as shown to great distances in directions perpendicular to page) of natural atoll facies changes in section orthogonal to reef. Labels include model element densities in g/cm^3, outer reef edge ("A"), inner reef edge prior to OAK event ("B"), position of boreholes OPZ-18, OTG-23, OQT-19, and ORT-20 ("C") and position of boreholes OSR-21 and OOR-17 ("D"). Drilling time profile (near right of depth scale) is for borehole F-1 (see fig. 2-1 for location). Remember that submarine topography correction replaced seawater (1.03 g/cm^3) with 1.90 g/cm^3 (Beyer, Ristvet, and Oberste-Lehn, 1986). No vertical exaggeration.

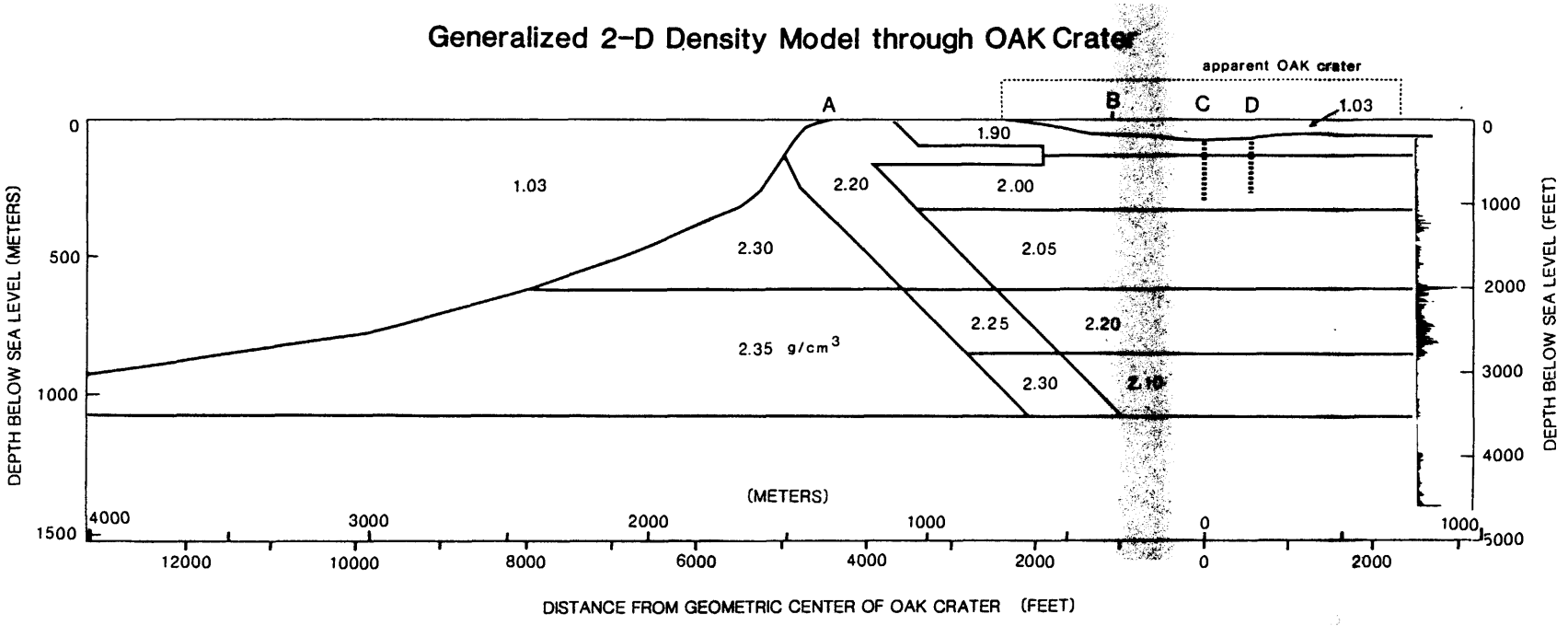

FIGURE 2-4. - Two-dimensional density model (assumed to extend as shown to great distances in directions perpendicular to page) of natural atoll facies changes in section orthogonal to reef. Labels include model element densities in g/cm^3, outer reef edge ("A"), inner reef edge prior to OAK event ("B"), position of boreholes OPZ-18, OTG-23, OQT-19, and ORT-20 ("C") and position of boreholes OSR-21 and OOR-17 ("D"). Drilling time profile (near right of depth scale) is for borehole F-1 (see fig. 2-1 for location). Remember that submarine topography correction replaced seawater (1.03 g/cm^3) with 1.90 g/cm^3 (Beyer, Ristvet, and Oberste-Lehn, 1986). No vertical exaggeration.

87-665

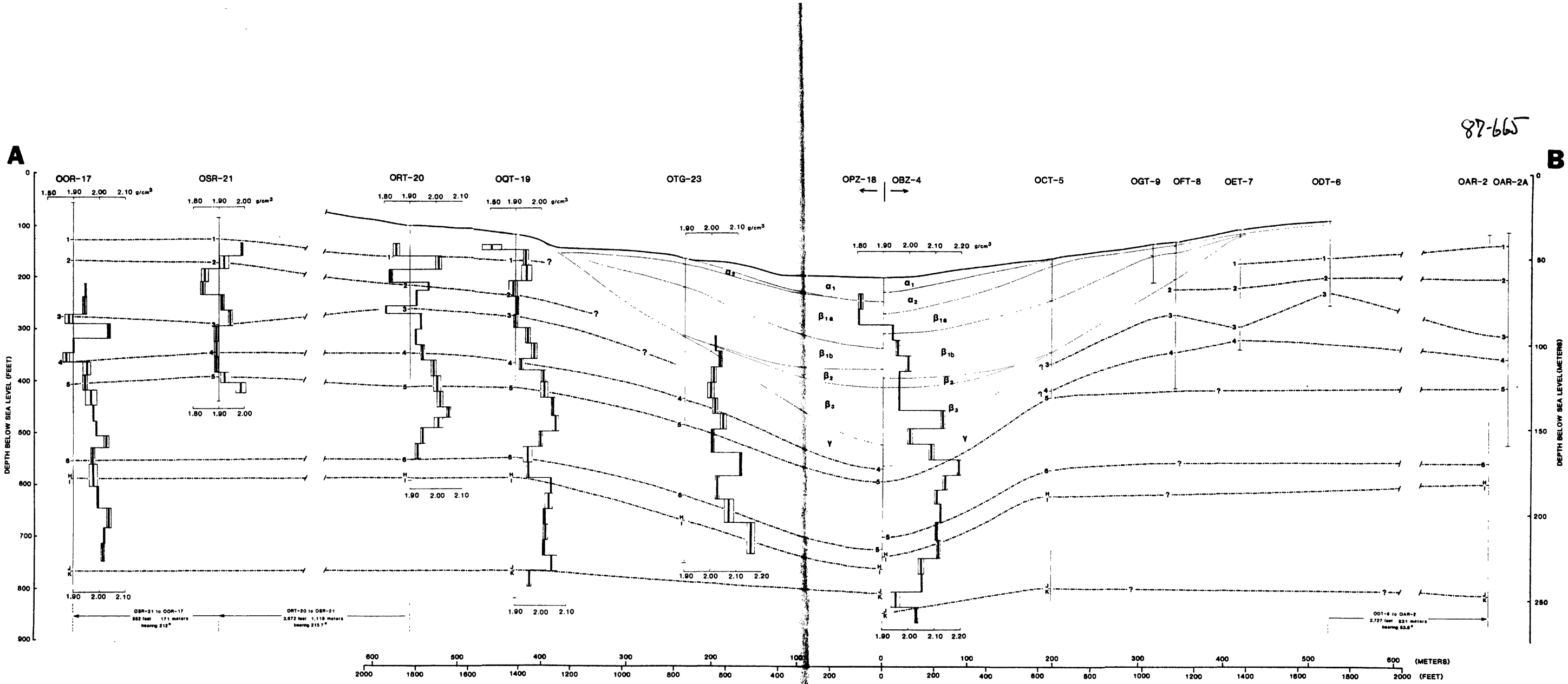

FIGURE 2-5. - Cross section AB extends from south-southwest to north-northeast through OAK crater (fig. 2-2). Section is broken at center with geologic markers in OBZ-4 extending to the right and markers in OPZ-18 extending to the left. Correlation lines tie disconformities 1 through 6, biostratgraphic zone boundaries H/I and J/K, and crater geologic zones α_1 through γ (see Wardlaw and Henry, 1986a,b). This section and that of Figure 2-6 were prepared by D. Oberste-Lehn and modified by B. R. Wardlaw. BHG density profiles are superimposed on the section for the six surveyed boreholes. The density scale labels "1.90" correspond to the positions of the surveyed boreholes in the cross section. Vertical exaggeration from ORT-20 to ODT-6 is 2X.

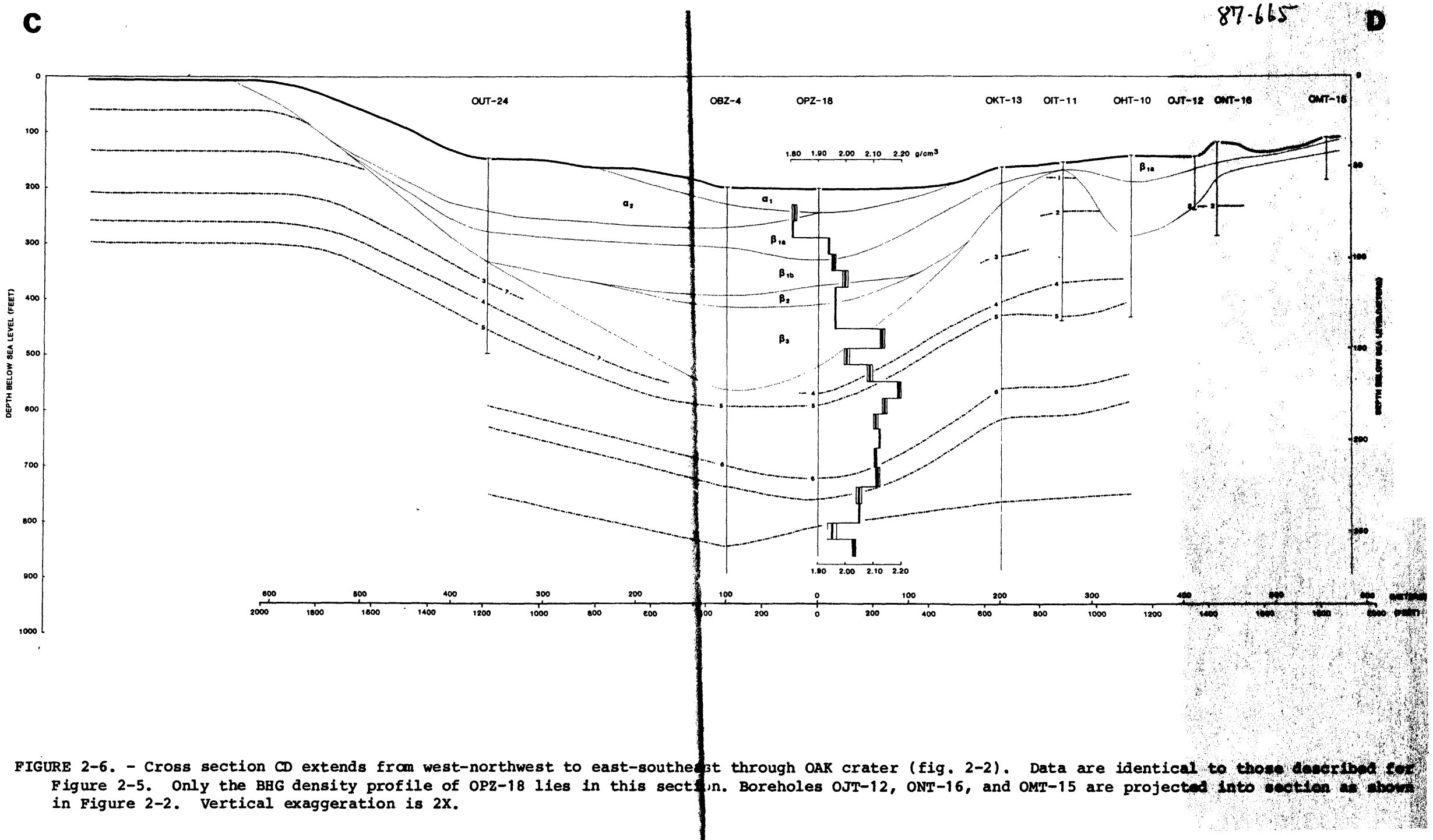

FIGURE 2-6. - Cross section CD extends from west-northwest to east-southeast through OAK crater (fig. 2-2). Data are identical to those described for Figure 2-5. Only the BHG density profile of OPZ-18 lies in this section. Boreholes OJT-12, ONT-16, and OMT-15 are projected into section as shown in Figure 2-2. Vertical exaggeration is 2X.

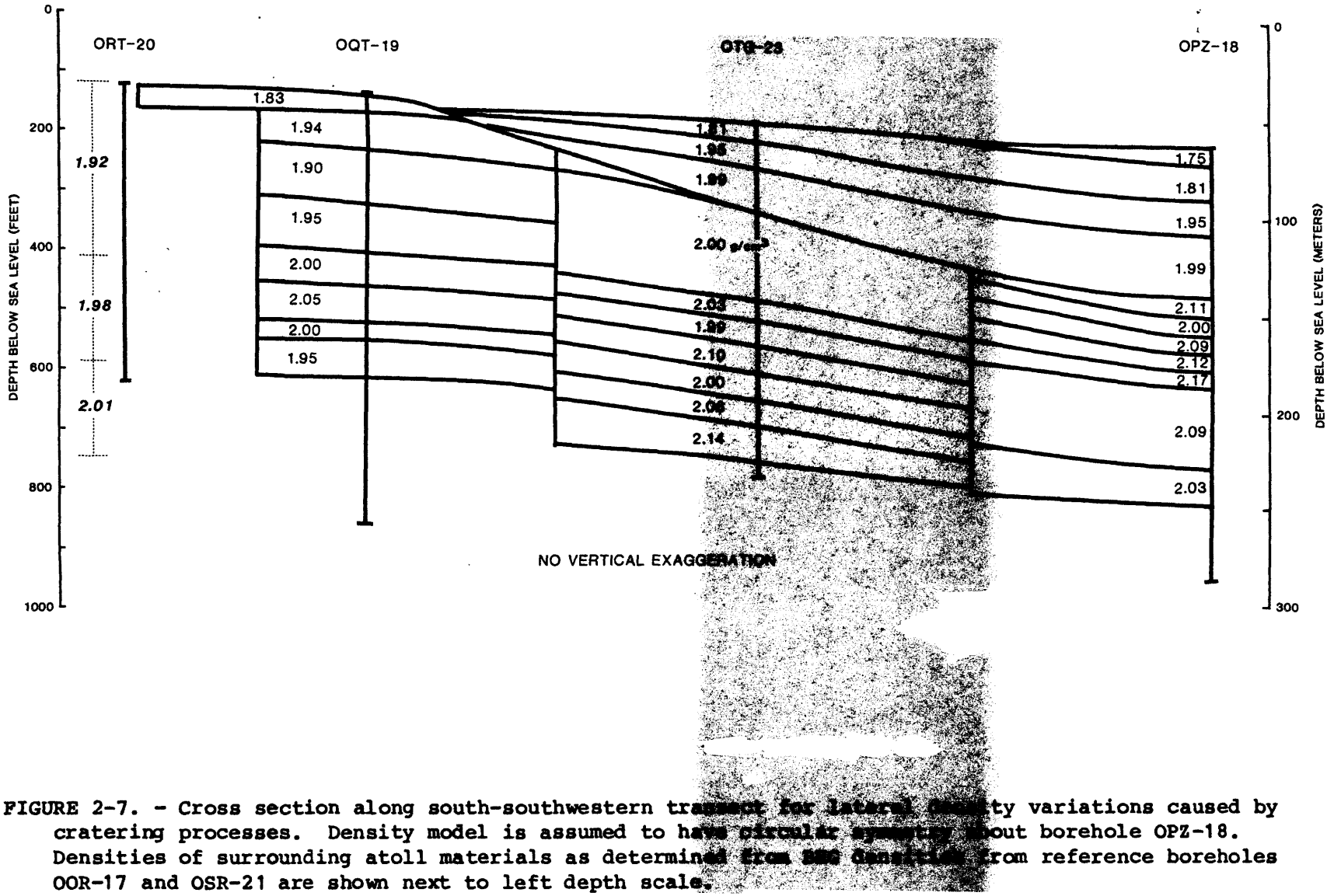

FIGURE 2-7. - Cross section along south-southwestern transect for lateral density variations caused by cratering processes. Density model is assumed to have circular symmetry about borehole OPZ-18. Densities of surrounding atoll materials as determined from [illegible] from reference boreholes OOR-17 and OSR-21 are shown next to left depth scale.

In order to perform density calculations using the model shown in Figure 2-7, the assigned densities must be recast as density contrasts relative to the surrounding medium. The density of the surrounding atoll material was determined from the BHG density profiles of reference boreholes OOR-17 and OSR-21 which were assumed to be unaltered by crater-related processes. The density model for the surrounding medium is summarized in Table 2-8, and values are shown along the left side of Figure 2-7. These reference density values were subtracted from laterally juxtaposed crater density model elements to arrive at a density contrast model.

Corrections to the BHG densities in OPZ-18, OTG-23, OQT-19, and ORT-20 were calculated from the density contrast model using a well-established algorithm for three-dimensional density elements (Plouff, 1976) modified for borehole gravity application. These corrections proved to be very small (column 6, tables 2-2 through 2-7), which could be predicted from the gentle dips of the density element boundaries as shown in Figure 2-7.

CORRECTED BOREHOLE GRAVITY DENSITY AND POROSITY AND COMPARISON WITH GAMMA-GAMMA AND NEUTRON DATA

Tabular and graphical summaries of BHG density and porosity with error estimates, grain densities with error estimates and interval-averaged density and porosity from gamma-gamma and neutron logs are presented in Tables 2-2 through 2-7 and Figures 2-8 through 2-13. Open-hole well log curves also are shown in Figures 2-8 through 2-12. Interval-averaged neutron porosity is not graphically displayed in Figures 2-8 through 2-12 because of a systematic error that has made all values too large. Interval grain density profiles are derived from individual grain density values, examination of open-hole well logs, and descriptions of cores and samples, sedimentary packages, and boreholes (Henry and Wardlaw, 1986; Wardlaw and Henry, 1986a; Holloway and Young, 1986). Errors in interval grain density are only estimates that may be increased or decreased with further information about the mineralogy of individual intervals, particularly intervals with both aragonite and calcite.

A number of questions about the reliability of the gamma-gamma density and neutron porosity logs run in OAK boreholes were raised during the analysis of the borehole data. Corrected BHG density and porosity provide a reliable standard against which gamma-gamma and neutron logs can be evaluated. In OAK boreholes, the differences between BHG density and interval-averaged gamma-gamma density decrease with increasing depth below the sea floor (fig. 2-14). This result agrees with the well-documented body of literature from the petroleum industry, which indicates that shallow-penetration radiation well logs, such as the gamma-gamma and neutron logs run in OAK boreholes, perform poorly in loosely consolidated, highly permeable sediments where formation damage caused by rotary drilling is almost always substantial.

Relatively good correspondence between BHG and gamma-gamma data is obtained for intervals deeper than 600 ft below sea level in OOR-17 and OQT-19, and deeper than 500 ft below sea level in ORT-20 where drill-induced borehole and formation damage is less because sediments are somewhat more consolidated than at shallower depths (figs. 2-8, 2-10, and 2-11). More specifically, Figure 2-14 suggests that gamma-gamma density departs

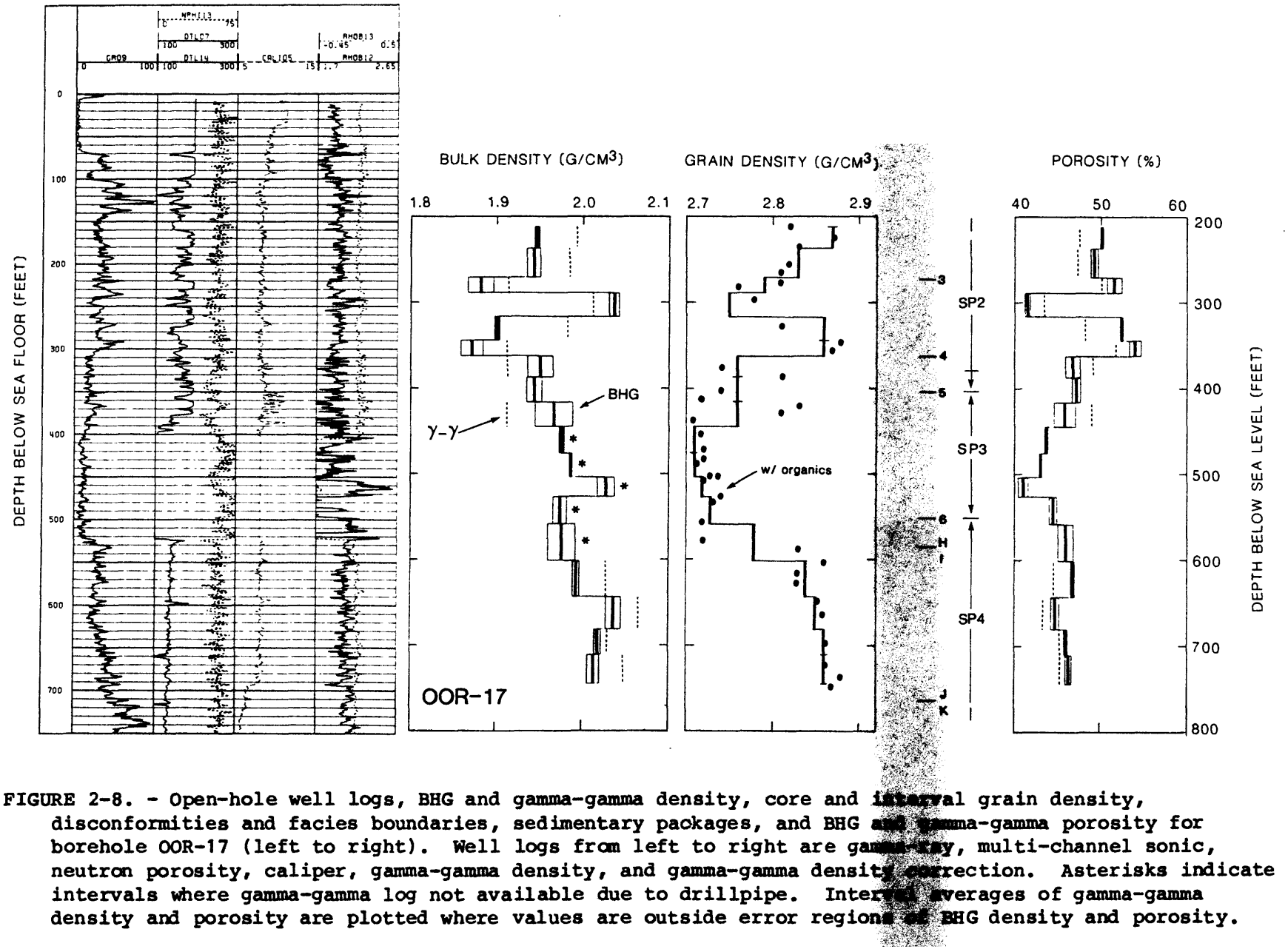

FIGURE 2-8. - Open-hole well logs, BHG and gamma-gamma density, core and interval grain density, disconformities and facies boundaries, sedimentary packages, and BHG and gamma-gamma porosity for borehole OOR-17 (left to right). Well logs from left to right are gamma-ray, multi-channel sonic, neutron porosity, caliper, gamma-gamma density, and gamma-gamma density correction. Asterisks indicate intervals where gamma-gamma log not available due to drillpipe. Interval averages of gamma-gamma density and porosity are plotted where values are outside error regions of BHG density and porosity.

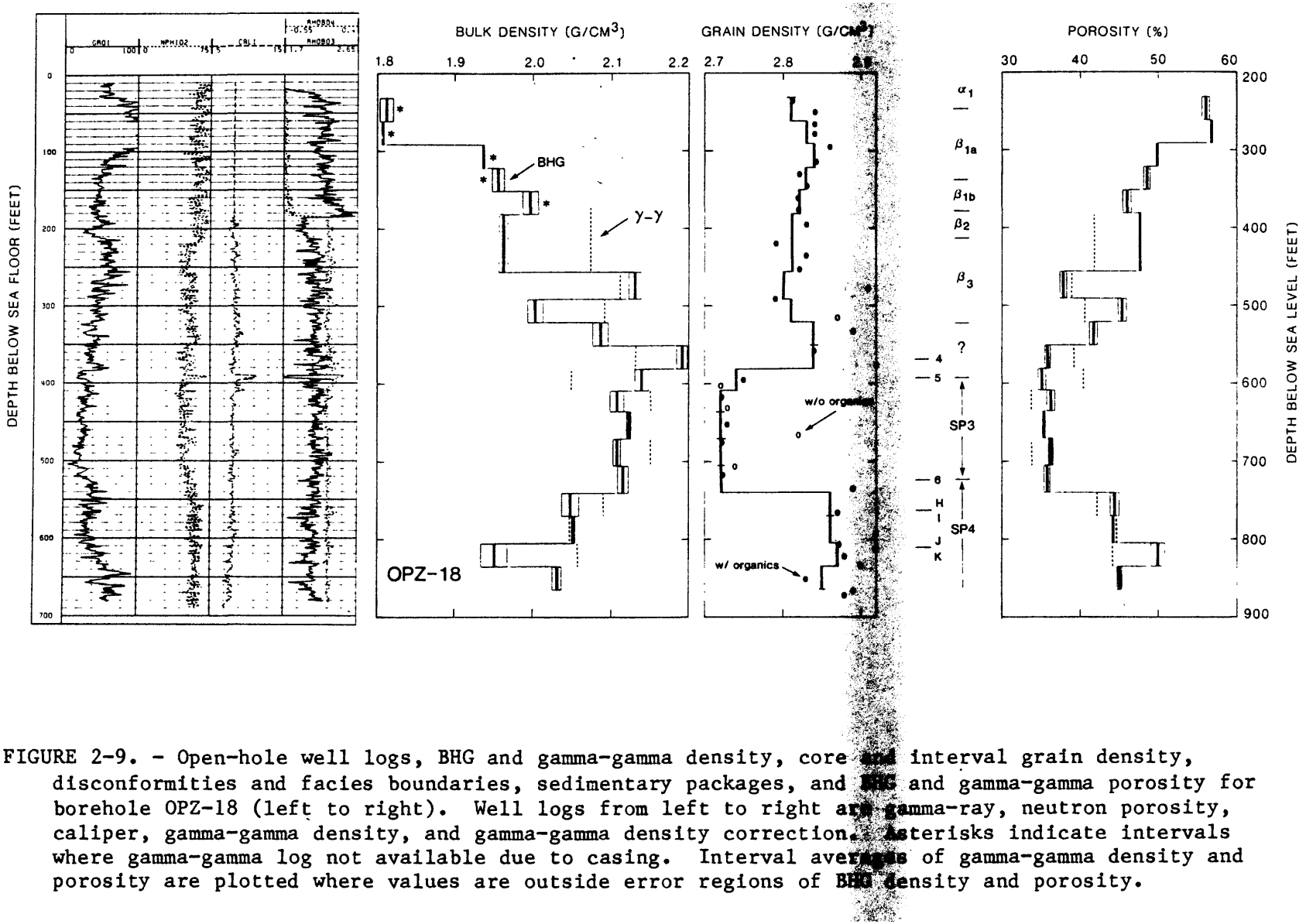

FIGURE 2-9. - Open-hole well logs, BHG and gamma-gamma density, core and interval grain density, disconformities and facies boundaries, sedimentary packages, and BHG and gamma-gamma porosity for borehole OPZ-18 (left to right). Well logs from left to right are gamma-ray, neutron porosity, caliper, gamma-gamma density, and gamma-gamma density correction. Asterisks indicate intervals where gamma-gamma log not available due to casing. Interval averages of gamma-gamma density and porosity are plotted where values are outside error regions of BHG density and porosity.

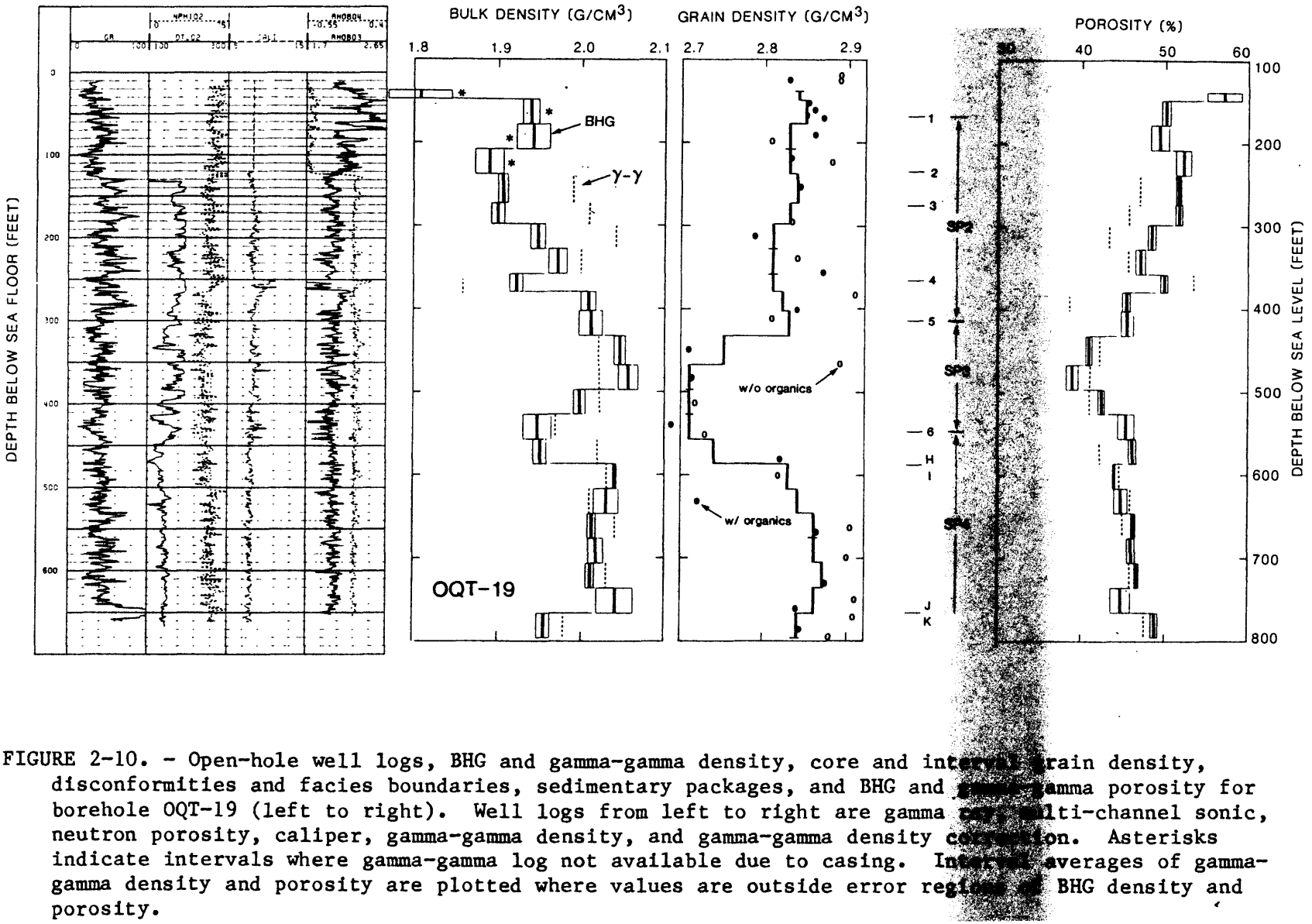

FIGURE 2-10. - Open-hole well logs, BHG and gamma-gamma density, core and interval grain density, disconformities and facies boundaries, sedimentary packages, and BHG and gamma-gamma porosity for borehole OQT-19 (left to right). Well logs from left to right are gamma ray, multi-channel sonic, neutron porosity, caliper, gamma-gamma density, and gamma-gamma density correction. Asterisks indicate intervals where gamma-gamma log not available due to casing. Interval averages of gamma-gamma density and porosity are plotted where values are outside error regions of BHG density and porosity.

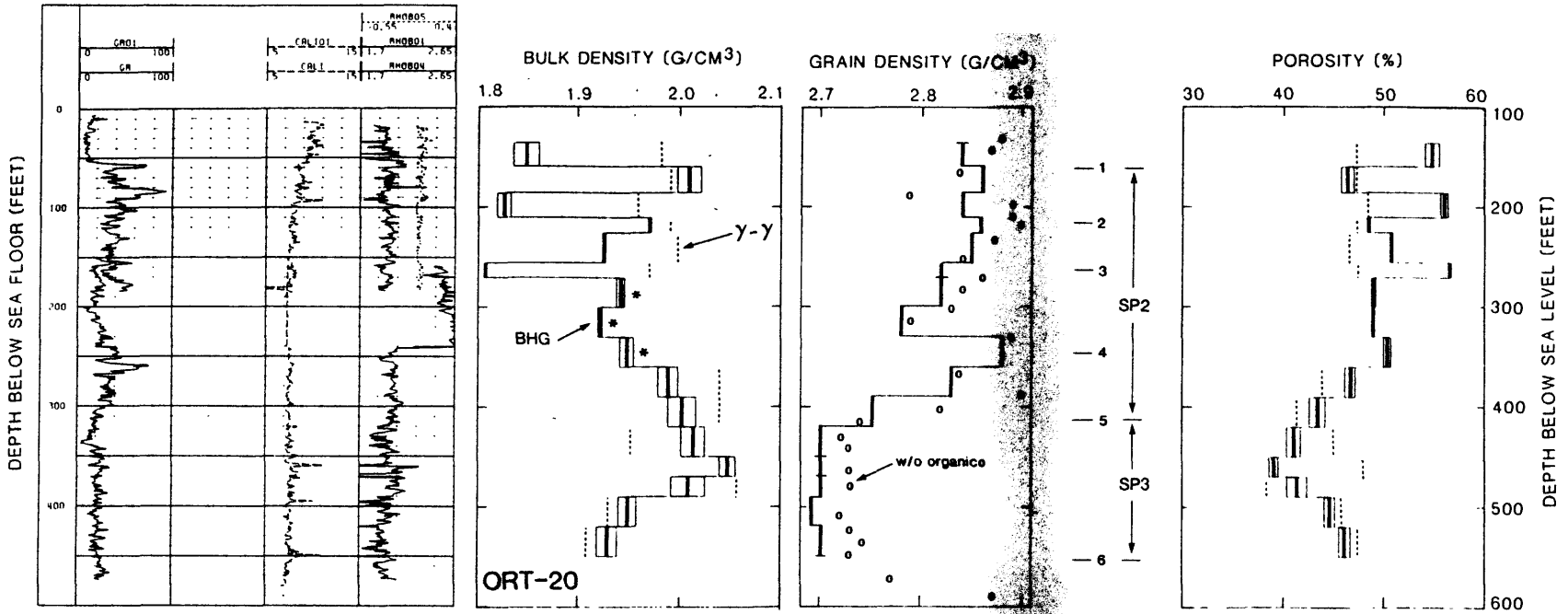

FIGURE 2-11. - Open-hole well logs, BHG and gamma-gamma density, core and interval grain density, disconformities and facies boundaries, sedimentary packages, and BHG and gamma-gamma porosity for borehole ORT-20 (left to right). Well logs from left to right are gamma ray, caliper, gamma-gamma density, and gamma-gamma density correction (partial). Asterisks indicate intervals where gamma-gamma log not available due to casing. Interval averages of gamma-gamma density and porosity are plotted where values are outside error regions of BHG density and porosity.

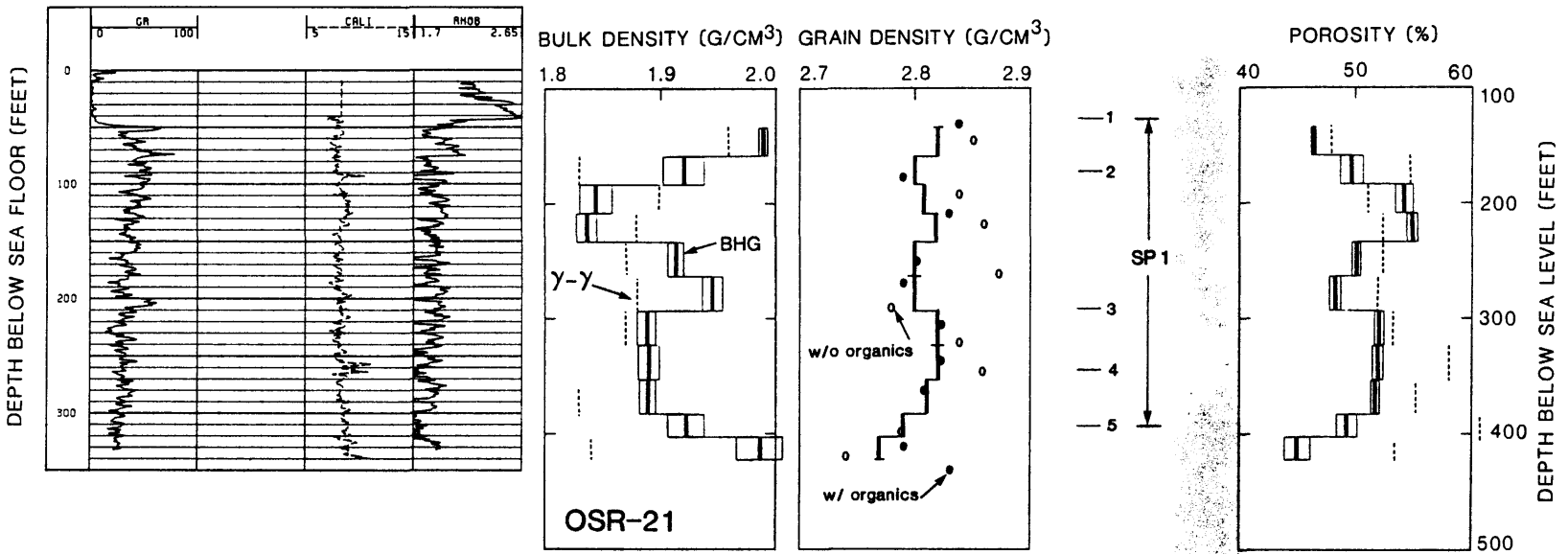

FIGURE 2-12. - Open-hole well logs, BHG and gamma-gamma density, core and interval grain density, disconformities and facies boundaries, sedimentary packages, and BHG and gamma-gamma porosity for borehole OSR-21 (left to right). Well logs from left to right are gamma ray, caliper, and gamma-gamma density. Interval averages of gamma-gamma density are plotted where values are outside error regions of BHG density and porosity.

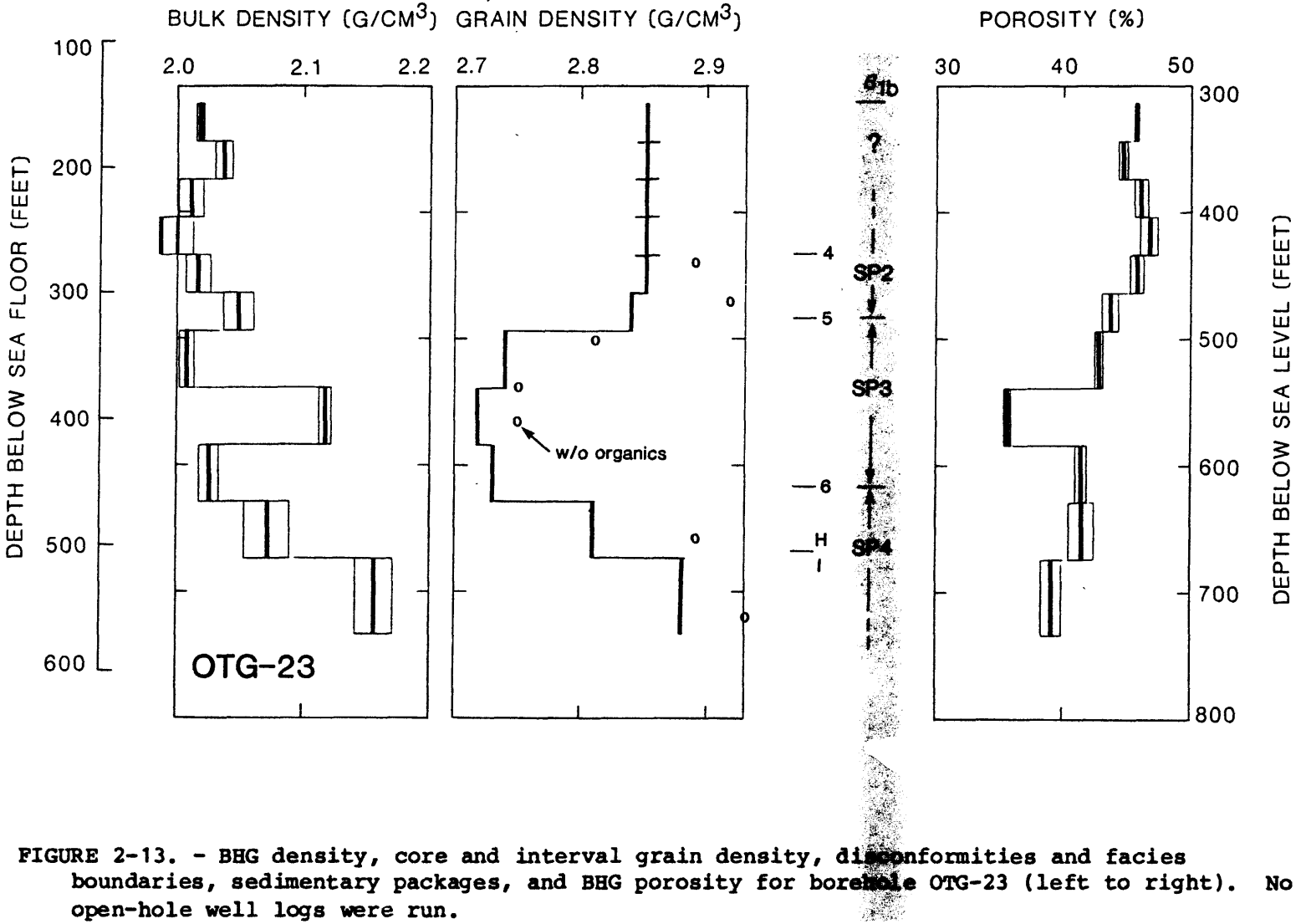

FIGURE 2-13. - BHG density, core and interval grain density, disconformities and facies boundaries, sedimentary packages, and BHG porosity for borehole OTG-23 (left to right). No open-hole well logs were run.

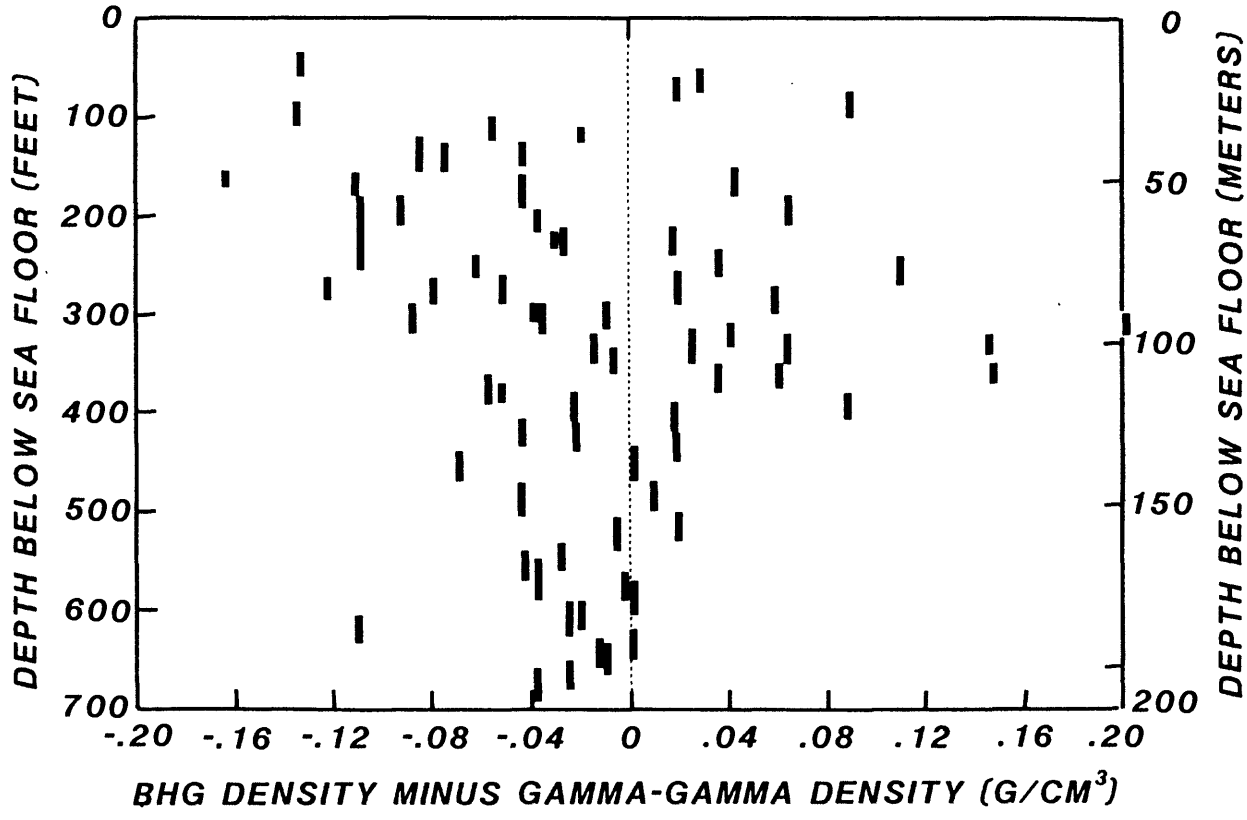

FIGURE 2-14. - Differences between BHG density and interval averages of gamma-gamma density versus depth below sea floor (bsf). Seventy differences are from boreholes OOR-17, OPZ-18, OQT-19, ORT-20 and OSR-21.

unsystematically from BHG density by as much as ±10 percent at depths shallower than about 400 ft below the sea floor. At depths greater than about 500 ft below sea level, gamma-gamma density appears to vary from BHG density by about 2 percent or less.

Cross plots between BHG porosity and neutron porosity, gamma-gamma porosity and neutron porosity, and gamma-gamma porosity versus BHG porosity confirm that the neutron data are not adequate (fig. 2-15). These cross plots, along with Figure 2-14, emphasize the need for caution in the use of the gamma-gamma logs for quantitative density or porosity evaluation. Furthermore, bulk density and total porosity data derived from core measurements should be viewed skeptically if they differ significantly and systematically from corresponding BHG density and porosity.

NATURAL DENSITY AND POROSITY VARIATIONS OF ATOLL MATERIALS

Natural variations of density and porosity of atoll materials represent the background "noise" through which density and porosity changes caused by cratering phenomena must be determined. At the volume scale of core samples of several cubic feet, a broad range of values of densities and porosities from virtual sea-water-filled voids to dense crystalline carbonate is expected. At the volume scale of BHG studies (hundreds of thousands of cubic feet--an appropriate scale for studies of large craters), one expects the range of values of natural densities and porosities to narrow considerably because of the averaging effect. This is confirmed by the BHG surveys at OAK crater where the range of densities in reference boreholes OOR-17 and OSR-21 is not great.

At shallow depths in OOR-17, OSR-21, ORT-20 and OQT-19, density fluctuations are substantial but can be averaged to give nearly identical values (fig. 2-16). Based on the similarity of averaged BHG densities for OOR-17, OSR-21, ORT-20, and parts of OQT-19, the "noise" problem connected with natural density and porosity variations is believed to be small. However, close correspondence between individual BHG intervals from borehole to borehole can not be expected because of natural variations of density in porosity.

A general systematic relationship exists between BHG porosity and interval grain density based on data from reference boreholes OOR-17 and OSR-21 (fig. 2-17). Back reef sediments dominated by aragonite have higher porosities than sediments dominated by calcite. Effects on porosity caused by mechanical compaction and grain-size distribution and uncertainty about values of interval grain density may account for some or all of the scatter of points in Figure 2-17. Nevertheless, the rate of change of porosity with respect to aragonite content, as estimated by the dashed line, is almost identical to that found by Schmoker and Hester (1986) in a study of the late Pleistocene Miami Limestone. However, porosity values of the Miami Limestone are lower than Enewetak back-reef sediments by about 15 percent for equivalent aragonite content, emphasizing the different geologic settings of these two locations.

If bulk density is held constant, the mineral volume increase accompanying simple transformation of aragonite to calcite causes porosity to decrease by about 5 percent (line A in fig. 2-17). It is clear from Figure

Page 2-25 follows

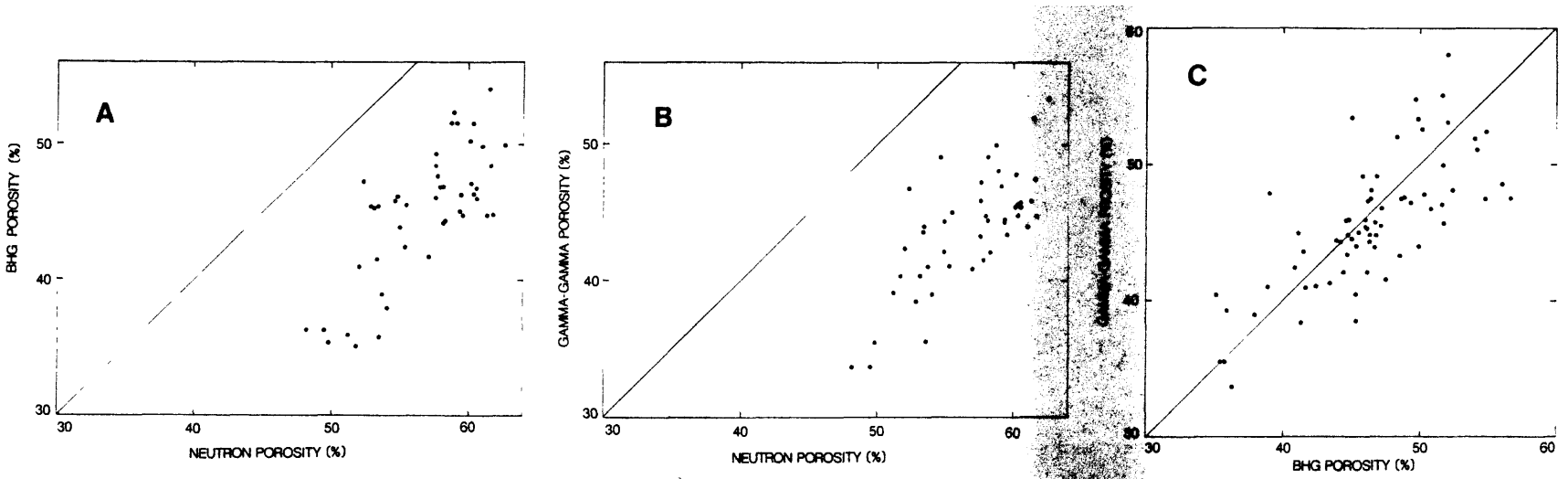

FIGURE 2-15. - Cross plot of BHG porosity and neutron porosity averaged over equivalent depth intervals (A). Cross plot of gamma-gamma porosity and neutron porosity, each averaged over BHG depth intervals (B). Cross plot of BHG porosity and gamma-gamma porosity averaged over equivalent depth intervals (C). Data are from columns 10, 13 and 14, Tables 2-2 through 2-7.

87-665

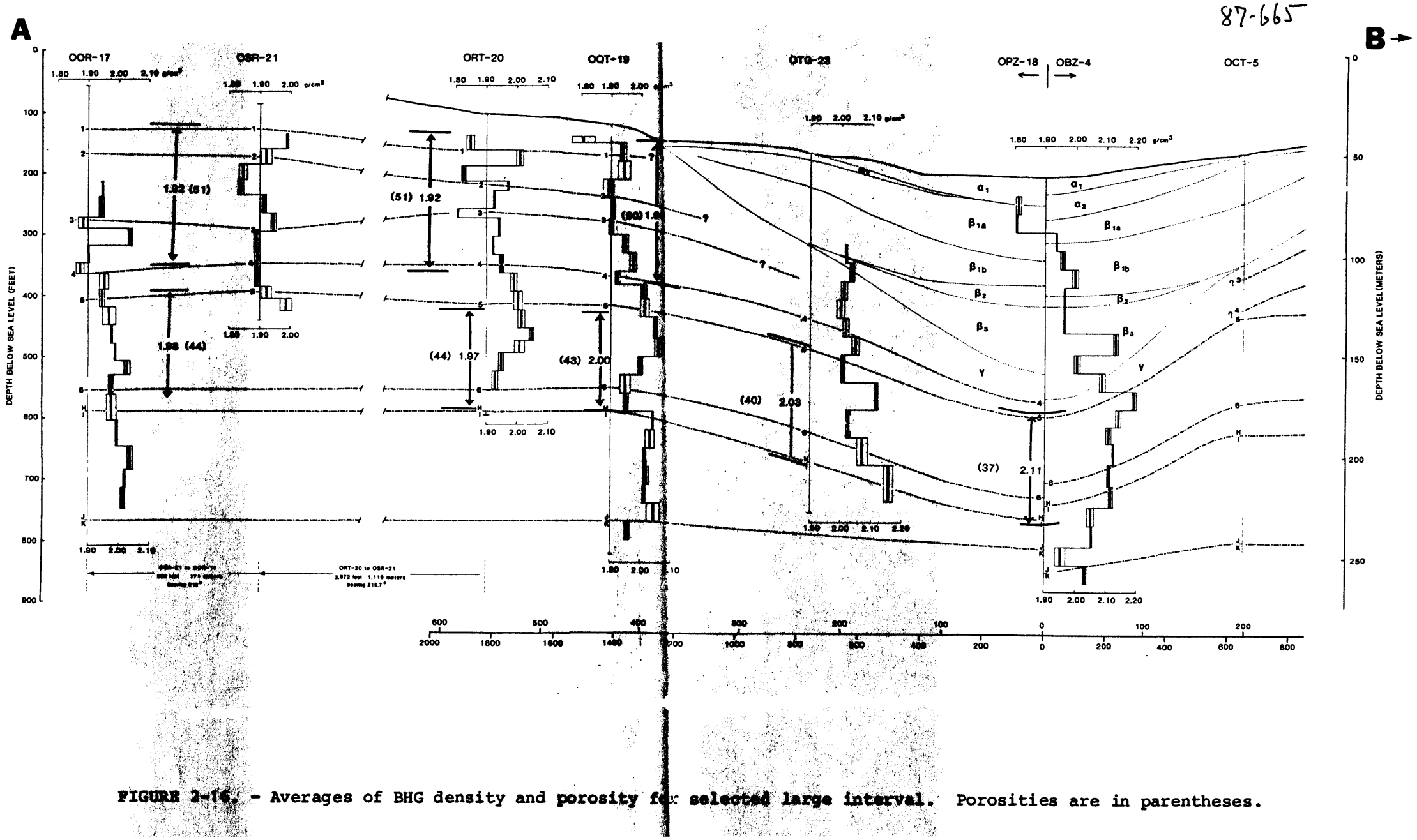

FIGURE 2-16. - Averages of BHG density and porosity for selected large interval. Porosities are in parentheses.

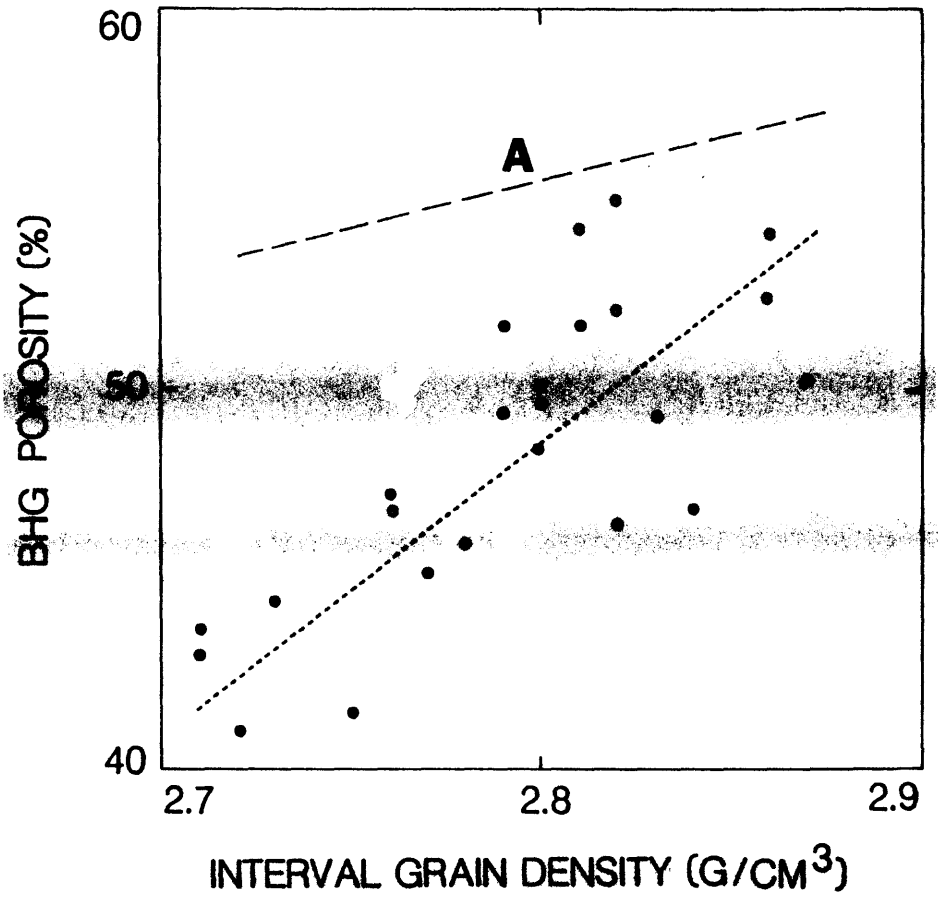

FIGURE 2-17. - Interval grain density versus BHG porosity. Data from reference boreholes OOR-17 and OSR-21. Line A shows decrease in porosity (due only to mineral volume increase) during transformation of an aragonite-bearing sediment to calcite-bearing sediment, assuming 100% aragonite sediment has porosity of 58.5%, and bulk-density is held constant.

2-17 that calcite solution and recrystallization, deposition of externally derived carbonate cement, some compaction, and other processes during well-documented cycles of atoll emergence and submergence (Ristvet and others, 1974; Tracey and Ladd, 1974) also have contributed to porosity loss in the back-reef sediments around OAK crater.

DENSITY, POROSITY, AND MASS CHANGES RELATED TO CRATERING PHENOMENA

A corrected BHG density and porosity model of the south-southwest transect of OAK crater is shown in Figure 2-18. This generalized model closely, but not exactly, follows the disconformity, facies changes, and geologic crater zone correlations defined by Wardlaw and Henry (1986a,b). The density elements of this model are based on the interval divisions of the BHG surveys that were selected during field work prior to knowledge of the exact downhole locations of the geologic boundaries. Intervals of BHG density and porosity have not been divided to correspond to the geologic boundaries because such divisions would be arbitrary in the absence of gravity station readings at the downhole locations of the geologic boundaries. Furthermore, BHG density and porosity are based on mass/volume characteristics that may or may not coincide with divisions based on the geologic characteristics of the sediments. This is clearly seen in Figure 2-5 where a significant number of major BHG density changes occur between, rather than at, the geologic boundaries defined by Wardlaw and Henry (1986a,b). Lack of exact depth correspondence of geologic and density/porosity models does not interfere with comparisons of geologically equivalent intervals between boreholes (figs. 2-16 and 2-19). (Application of the borehole gravity data to the geologic interpretation of OAK crater is expanded in Chapter 7 of the current Open-File report.)

A primary goal of the BHG phase of the PEACE Program was to determine if densification in crater-flank regions could account for observed sea-floor subsidence. BHG surveys were made in transition-zone boreholes OQT-19 and ORT-20 to investigate possible densification. There is considerable variation of BHG density and porosity in the upper parts of these boreholes but averages over larger intervals show that the sediments are not now appreciably denser than in the reference boreholes OOR-17 and OSR-21 (fig. 2-16).

Because documented subsidence of the sea floor at OQT-19 and ORT-20 cannot be explained by densification of the upper few hundred feet of underlying sediments alone, mass displacement from this region and densification of deeper materials probably occurred. Selective removal of finer fractions in this way could be investigated by comparing grain-size distributions of core samples from OQT-19 and the reference boreholes. Slight but definite densification and porosity decreases are present at greater depths in OQT-19 (figs. 2-16 and 2-19).

Unmistakable densification and porosity diminution are inferred in boreholes OTG-23 and beneath 292 ft below sea level in OPZ-18 (figs. 2-16 and 2-19). Independently documented mass transport (Wardlaw and Henry, 1986b) also can be quantified with the BHG density and porosity data. For example, the mass columns at OQT-19 and OPZ-18 are mass deficient by 3 to 5 percent and 6 to 8 percent, respectively, when compared to the mass column at reference

page 2-33 follows

87-665

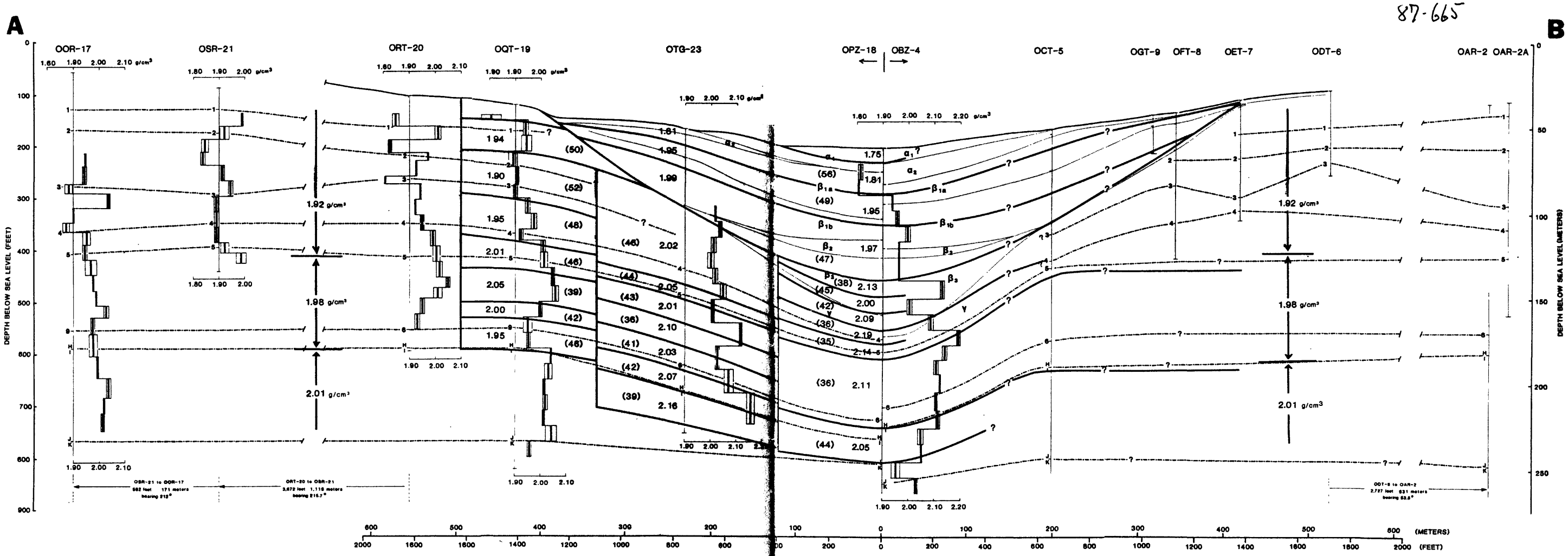

FIGURE 2-18 - BHG density and porosity model for south-southwest transect at OAK crater. Porosities are in parentheses.

87-665

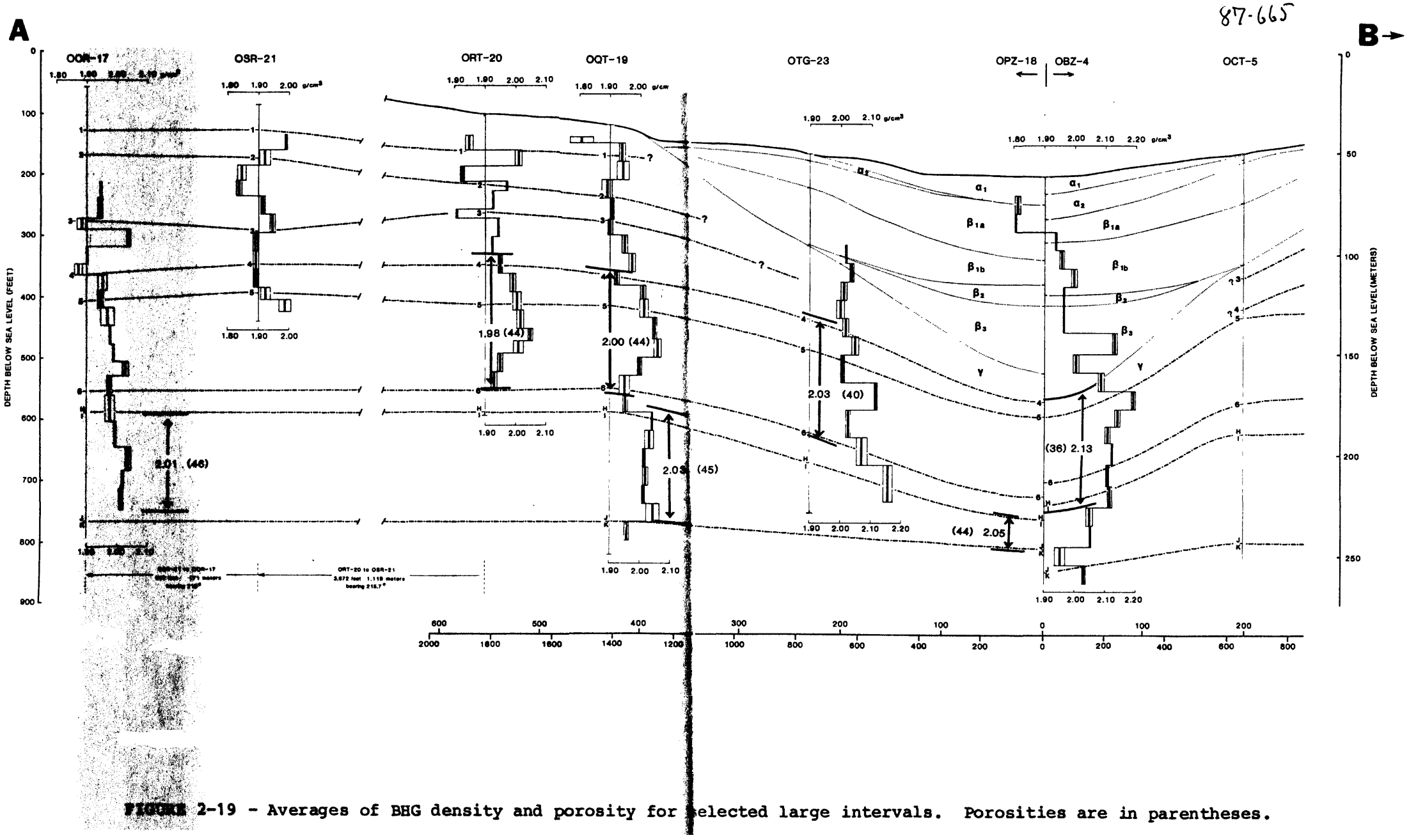

FIGURE 2-19 - Averages of BHG density and porosity for selected large intervals. Porosities are in parentheses.

(Beyer, Ristvet, and Oberste-Lehn, 1986); (2) generalized two-dimensional density variations associated with large-scale facies changes and diagenesis across the reef margin (fig. 2-4); and (3) generalized three-dimensional density changes due to cratering processes (fig. 2-7). Corrections range from .067 to .156 g/cm3 for submarine topography, .018 to .025 g/cm3 for two-dimensional density variations across the atoll margin, and +.025 to -.021 g/cm3 for generalized three-dimensional density changes due to cratering (tables 2-1 through 2-7).

The following conclusions can be drawn from the corrected BHG densities (fig. 2-5), the derived crater density model (fig. 2-18), and comparisons of corrected BHG density and porosity of geologically equivalent intervals along the south-southwest transect from OOR-17 to OPZ-18 (figs. 2-16 and 2-19):

1. Large natural variations of density and porosity of atoll materials are well-known from numerous geological observations at scales of cubic inches to hundreds of cubic feet. Serious concern was expressed prior to this study that these natural variations of density and porosity would obscure those due to cratering phenomena. The shallow portions of the BHG density profiles from OOR-17, OSR-21, ORT-20, and OQT-19 suggest that this concern may be well-founded when attempting to compare shallow vertical intervals in different boreholes that are on the order of tens of feet thick (fig. 2-5). However, averages of BHG densities over larger vertical intervals show that natural variations of density and porosity tend to average out so that valid lateral comparisons of geologically equivalent intervals can be made (figs. 2-16 and 2-19). Also, over the depths surveyed in OAK boreholes, the range of natural variation of density and porosity appears to decrease slightly with depth, allowing valid comparisons of smaller vertical intervals with increasing depth (fig. 2-5). These results are based solely on BHG surveys made on a trend nearly parallel to the reef along which facies and density changes are believed to be minimal.

2. The shallow section beneath the crater-flank region penetrated by OQT-19 and ORT-20 is not appreciably denser than the equivalent section penetrated by the more distant reference boreholes OOR-17 and OSR-21 (fig. 2-16). Crater-flank subsidence in this area cannot be explained by densification of this shallow section, but probably involved mass removal and densification of a larger vertical interval. Slight densification is evident at greater depth in OQT-19 but cannot be confirmed at greater depth in ORT-20 (figs. 2-16 and 2-19).

3. Atoll material penetrated by OTG-23 within the excavational crater is significantly denser over the surveyed intervals than the geologically equivalent sections penetrated by reference boreholes OPR-17 and OSR-21 and crater flank boreholes ORT-20 and OQT-19 (figs. 2-16, 2-18, and 2-19). Porosity reduction also has occurred as a result of cratering processes.

4. At the bathymetric center of OAK crater, the section penetrated by OPZ-18 is dominated by cratering effects. Major discontinuities of BHG density and porosity occur midway through crater zones b_{1a} and β_3. Beneath the second discontinuity midway through zone β_3, and extending at least to the J/K biostratigraphic boundary, a large amount of densification and porosity reduction has resulted from cratering processes (figs. 2-16 and

2-19). In the lower part of this densified interval, the low BHG densities compared to the indicated thinning of geologic units means that major amounts of mass have been removed (fig. 2-19). Densification and/or mass removal appears to extend beneath the depth of the BHG survey in OPZ-18, and may be evaluated by careful study of the lower portions of the gamma-gamma density logs from OAM-1/OAR-2, OBZ-4, OCT-5, and OOR-17.

5. Mass deficiencies of about 3 to 5 percent at OQT-19, and 6 to 8 percent at OPZ-18 are indicated from mass column calculations that utilize BHG densities at OOR-17, OQT-19, and OPZ-18.

Other conclusions of this study are as follows:

1. In reference boreholes OOR-17 and OSR-21, back-reef sediments dominated by aragonite have higher porosities than materials dominated by calcite (fig. 2-17). The mineral volume increase that accompanies the transformation of aragonite to calcite is not sufficient to explain the observed decrease in porosity. Not surprisingly, other diagenetic processes, such as calcite solution and recrystallization and deposition of externally derived carbonate cement, must have contributed to (or dominated) the observed natural decrease of porosity that accompanies the transformation of aragonite to calcite in these back-reef materials.

2. The BHG survey in the E-1 borehole on Medrin (ELMER) Island provided BHG densities of the shallow section that differed only slightly from those measured across Enewetak Atoll at OAK crater (figs. 2-1 and 2-20). BHG densities of the deeper section in the E-1 borehole were important to the construction of the two-dimensional density model of the reef argin (fig. 2-4). The BHG survey in the E-1 borehole also revealed a cyclical pattern of density and porosity that may be due to diagenesis caused by repeated periods of atoll emergence and submergence since middle Miocene (fig. 2-20).

3. BHG measurements permit examination of volumes of materials measured in hundreds of thousands of cubic feet. Unlike conventional, shallow penetration gamma-gamma and neutron logging methods, the large volume of material examined by the BHG method makes it immune to formation damage or borehole rugosity that commonly occurs when drilling through loosely consolidated, highly permeable strata or alternating soft and hard beds. Not unexpectedly, BHG density and porosity in the OAK study are about an order of magnitude more reliable than the next most reliable density or porosity logging method, the gamma-gamma density log, at depths less than about 400 ft below the sea floor in the five OAK boreholes where comparisons were possible (figs. 2-8 through 2-12, 2-14, and 2-15).

This first BHG study of the carbonate deposits of an atoll island and of the materials beneath a large nuclear crater affirms the unique ability of borehole gravimetry to evaluate the density and porosity of heterogeneous and/or loosely consolidated geologic formations.

Folger, D. W., ed., 1986a, Sea-floor observations and subbottom seismic characteristics of OAK and KOA craters, Enewetak Atoll, Marshall Islands: U.S. Geological Survey Bulletin 1678, 301 p., 112 figs., glossary, 2 appendices.

Henry, T. W., Wardlaw, B. R., Skipp, Betty, Major, R. P., and Tracey, J. I., Jr., 1986, Pacific Enewetak Atoll Crater Exploration (PEACE) Program; Part 1: Drilling operations and descriptions of boreholes in vicinity of KOA and OAK craters: U.S. Geological Survey Open-File Report 86-419, 497 p., 32 figs., 29 pls., 13 tbls., 3 appendices.

Holloway, G. L., and Young, A. G., 1986, Appendix II: Geotechnical Investigations, Phase II of PEACE Program: 29 p., 16 figs., 36 pls.; in Henry, T. W., Wardlaw, B. R., Skipp, Betty, Major, R. P., and Tracey, J. I., Jr., 1986, Pacific Enewetak Atoll Crater Exploration (PEACE) Program; Part 1: Drilling operations and descriptions of boreholes in vicinity of KOA and OAK craters: U.S. Geological Survey Open-File Report 86-419.

Ladd, H. S., Ingerson, E., Townsend, R. D., Russell M., and Stephenson, H. K., 1953, Drilling on Eniwetok Atoll, Marshall Islands: Bulletin of the American Association of Petroleum Geologists, v. 37, no. 10, p. 2257-2280.

Ladd, H. S., and Schlanger, S. O., 1960, Drilling operations on Eniwetok Atoll: U.S. Geological Survey Professional Paper 260-Y, p. 863-903, pls. 255-256, figs. 260-287, 3 tbls.

Plouff, D., 1976, Gravity and magnetic fields for polygonal prisms and application to magnetic terrain corrections: Geophysics, v. 41, no. 4, p. 727-741.

Ristvet, B. L., Couch, R. F., Jr., Fetzer, J. D., Goter, E. R., Tremba, E. L., Walter, D. R., and Wendland, V. P., 1974, A Quaternary diagenetic history of Eniwetok Atoll: Geological Society of America Abstracts with Programs, v. 6, p. 928-929.

Ristvet, B. L. and Tremba, E. L., 1986, Chapter 5: Total organic content of lagoon benthic sediments and of submarine samples from the PEACE drilling program: 9 p., 2 figs., 2 tbls.; in Henry, T. W., and Wardlaw, B. R., eds., Pacific Enewetak Atoll Crater Exploration (PEACE) Program, Enewetak Atoll, Republic of the Marshall Islands; Part 3: Stratigraphic analysis and other geologic and geophysical studies in vicinity of OAK and KOA craters: U.S. Geological Survey Open-File Report 86-555.

Schmoker, J. W., and Hester, T. C., 1986, Porosity of the Miami Limestone (Late Pleistocene), Lower Florida Keys: Journal of Sedimentary Petrology, v. 56, no. 5, p. 629-634.

Talwani, M., Worzel, J. L., and Landisman, M., 1959, Rapid gravity computations for two-dimensional bodies with application to the Mendocino submarine fracture zone: Journal of Geophysical Research, v. 64, no. 1, p. 49-59.

Tracey, J. I., Jr., and Ladd, H. S., 1974, Quaternary History of Eniwetok and Bikini Atolls, Marshall Islands: Proceedings of the Second International Symposium on Coral Reefs, Great Barrier Reef Committee, Brisbane, Australia, p. 537-550, 15 figs., 3 tbls.

Tremba, E. L. and Ristvet, B. L., 1986, Chapter 4: X-ray diffraction mineralogy: 49 p., 11 figs., 35 tbls.; in Henry, T. W., and Wardlaw, B. R., eds., Pacific Enewetak Atoll Crater Exploration (PEACE) Program, Enewetak Atoll, Republic of the Marshall Islands; Part 3: Stratigraphic analysis and other geologic and geophysical studies in vicinity of OAK and KOA craters: U.S. Geological Survey Open-File Report 86-555.

Wardlaw, B. R. and Henry, T. W., 1986a, Chapter 2: Physical stratigraphic framework: 36 p., 10 figs., 2 tbls.; in Henry, T. W. and Wardlaw, B. R., eds., Pacific Enewetak Atoll Crater Exploration (PEACE) Program, Enewetak Atoll, Republic of the Marshall Islands; Part 3: Stratigraphic analysis and other geologic and geophysical studies in vicinity of OAK and KOA craters: U.S. Geological Survey Open-File Report 86-555.

Wardlaw, B. R. and Henry, T. W., 1986b, Chapter 14: Geologic interpretation of OAK and KOA craters: 39 p., 21 figs., 2 tbls.; in Henry, T. W. and Wardlaw, B. R., eds., Pacific Enewetak Atoll Crater Exploration (PEACE) Program, Enewetak Atoll, Republic of the Marshall Islands; Part 3: Stratigraphic analysis and other geologic and geophysical studies in vicinity of OAK and KOA craters: U.S. Geological Survey Open-File Report 86-555.

TABLE 2-1. -- Range of corrections for lateral density changes calculated from submarine topography and density models for six BHG surveys at OAK Crater.

Borehole	Range of Corrections Expressed in g/cm^3 Due to		
	Submarine Topography	Large-Scale Lateral Density Changes Across Reef Margin	Smaller-Scale Lateral Density Changes Related to Cratering Processes
OOR-17	.156 to .144	.021 to .019	negligible
OPZ-18	.118 to .067	.025 to .021	.025 to -.021
OQT-19	.145 to .135	.024 to .020	.008 to -.004
ORT-20	.140 to .130	.023 to .020	.005 to -.005
OSR-21	.137 to .126	.020 to .018	negligible
OTG-23	.122 to .108	.022 to .024	.019 to .014

TABLE 2-2.--(on adjacent page) Bulk density, porosity, and grain density obtained from borehole gravity, gamma-gamma, and neutron measurements in borehole OOR-17 and from analysis of cores taken from OOR-17. Gamma-gamma and neutron data averages over depth intervals of BHG survey. Grain densities were calculated by the procedure described in Appendix 2-1 using data from Tremba and Ristvet (1986) and Ristvet and Tremba (1986).

→

1	2	3	4	5	6	7	8	9	10	11	12	13	14
212.-237.	1.772	.003	.156	.019	0.	1.947	2.87	.02	50.2	0.2	1.99	47.8	60.2
237.-271.	1.769	.008	.155	.019	0.	1.943	2.83	.02	49.3	0.4	1.98	47.2	57.6
271.-289.	1.709	.015	.154	.019	0.	1.882	2.79	.02	51.6	0.9	1.91	50.0	58.8
289.-317.	1.864	.006	.153	.019	0.	2.036	2.75	.02	41.5	0.3	2.00	43.6	53.3
317.-345.	1.730	.003	.152	.019	0.	1.901	2.86	.02	52.4	0.2	1.98	48.1	58.9
345.-363.	1.700	.013	.152	.020	0.	1.872	2.86	.02	54.0	0.7	1.91	51.9	61.5
363.-388.	1.780	.015	.151	.020	0.	1.951	2.76	.04	46.8	0.9	1.91	49.1	58.1
388.-417.	1.774	.009	.150	.020	0.	1.944	2.76	.04	47.2	0.5	1.95	46.8	52.3
417.-446.	1.798	.022	.149	.020	0.	1.967	2.76	.04	45.8	1.3	1.91	49.1	54.6
446.-477.	1.807	.003	.149	.020	0.	1.976	2.71	.02	43.7	0.2	0.	0.	0.
477.-505.	1.819	.001	.148	.020	0.	1.987	2.71	.02	43.0	0.1	0.	0.	0.
505.-528.	1.860	.010	.147	.020	0.	2.027	2.72	.02	41.0	0.6	0.	0.	0.
528.-560.	1.807	.008	.147	.020	0.	1.974	2.73	.02	44.5	0.5	0.	0.	0.
560.-603.	1.809	.016	.146	.021	0.	1.976	2.78	.02	45.9	0.9	0.	0.	0.
603.-645.	1.826	.004	.146	.021	0.	1.993	2.84	.02	46.8	0.2	2.03	44.8	58.0
645.-683.	1.870	.009	.145	.021	0.	2.036	2.85	.02	44.7	0.5	2.06	43.4	59.6
683.-713.	1.852	.004	.145	.021	0.	2.018	2.86	.02	46.0	0.2	2.03	45.4	60.6
713.-747.	1.848	.007	.144	.021	0.	2.013	2.86	.02	46.3	0.4	2.05	44.3	59.4

Column 1 Depth interval in feet below sea level

Column 2 Apparent BHG density in g/cm^3 (corrected for instrument calibration and drift and earth tides).

Column 3 Standard deviation of repeated $\Delta g/\Delta z$ measurements expressed in g/cm^3.

Column 4 Vertical gravity gradient correction (expressed in g/cm^3) for submarine topography out to a radial distance of 103.5 statute miles (166.7 kilometers). Correction calculated by replacing sea water with density of 1.90 g/cm^3 (see Beyer and Corbato, 1972).

Column 5 Vertical gravity gradient correction expressed in g/cm^3 for lateral density changes (assumed to be two-dimensional) caused by geologic facies changes across the reef (see Figure 2.4).

Column 6 Vertical gravity gradient correction (expressed in g/cm^3) for lateral density changes caused by crater-related processes and assumed to be symmetrical about OPZ-18 (see Figure 2.7).

Column 7 BHG density in g/cm^3 after correction for submarine topography and lateral density variations due to geologic facies changes and cratering processes.

Column 8 Mean grain density for depth interval in g/cm^3 (calculated from mineral and organic content percentages estimated from x-ray diffraction and loss-on-ignition analyses (see Appendix 2.2).

Column 9 Estimated uncertainty in mean grain density in g/cm^3.

Column 10 BHG porosity in percent calculated from BHG density (column 7), grain density (column 8) and sea-water density of 1.03 g/cm^3.

Column 11 Uncertainty in BHG porosity in porosity percent (calculated from standard deviation of BHG density (column 4) and uncertainty in mean grain density (column 8).

Column 12 Average gamma-gamma density for depth interval in g/cm^3.

Column 13 Gamma-gamma porosity in percent calculated from gamma-gamma density (column 12), grain density (column 8) and sea-water density of 1.03 g/cm^3.

Column 14 Average neutron porosity for depth interval in percent.

TABLE 2-3.--(on adjacent page) Bulk density, porosity, and grain density obtained from borehole gravity, gamma-gamma, and neutron measurements in borehole OPZ-18 and from analysis of cores taken from OPZ-18. Gamma-gamma and neutron data averages over depth intervals of BHG survey. Grain densities were calculated by the procedure described in Appendix 2-1 using data from Tremba and Ristvet (1986) and Ristvet and Tremba (1986).

→

1	2	3	4	5	6	7	8	9	10	11	12	13	14
232.-262.	1.729	.009	.067	.021	-.005	1.812	2.81	.02	56.1	0.5	0.	0.	0.
262.-292.	1.719	.001	.073	.021	-.006	1.807	2.83	.02	56.8	0.1	0.	0.	0.
292.-322.	1.844	.001	.077	.021	-.005	1.937	2.84	.02	49.9	0.1	0.	0.	0.
322.-352.	1.861	.008	.080	.021	-.006	1.956	2.83	.02	48.6	0.4	0.	0.	0.
352.-382.	1.892	.010	.084	.022	-.001	1.997	2.82	.02	46.0	0.6	0.	0.	0.
382.-457.	1.871	.	.090	.022	-.021	1.962	2.81	.02	47.6	0.	2.07	41.6	57.8
457.-492.	1.997	.008	.095	.022	0.016	2.130	2.80	.02	37.9	0.5	2.11	39.0	54.0
492.-522.	1.881	.010	.098	.022	0.002	2.003	2.81	.02	45.3	0.6	2.09	40.4	53.1
522.-552.	1.958	.010	.100	.023	0.005	2.086	2.84	.02	41.7	0.6	2.10	40.9	57.0
552.-582.	2.046	.007	.103	.023	0.019	2.191	2.84	.02	35.9	0.4	2.13	39.2	51.2
582.-610.	1.991	.009	.105	.023	0.020	2.139	2.74	.02	35.1	0.5	2.05	40.4	51.7
610.-637.	1.957	.009	.107	.023	0.020	2.107	2.72	.02	36.3	0.5	2.15	33.7	48.1
637.-672.	1.968	.003	.109	.024	0.021	2.122	2.72	.02	35.4	0.2	2.12	35.5	49.8
672.-707.	1.950	.005	.111	.024	0.022	2.107	2.72	.02	36.3	0.3	2.15	33.7	49.5
707.-742.	1.953	.007	.113	.024	0.025	2.115	2.72	.02	35.8	0.4	2.12	35.5	53.5
742.-772.	1.889	.011	.114	.024	0.021	2.048	2.86	.02	44.4	0.6	2.09	42.1	58.3
772.-807.	1.891	.002	.116	.024	0.021	2.052	2.86	.02	44.2	0.1	2.05	44.3	58.1
807.-837.	1.789	.017	.117	.024	0.021	1.951	2.87	.02	49.9	0.9	2.06	44.0	61.1
837.-867.	1.868	.006	.118	.025	0.020	2.031	2.85	.02	45.0	0.3	2.04	44.5	59.4

TABLE 2-3.

Column 1 Depth interval in feet below sea level

Column 2 Apparent BHG density in g/cm^3 (corrected for instrument calibration and drift and earth tides).

Column 3 Standard deviation of repeated $\Delta g/\Delta z$ measurements expressed in g/cm^3.

Column 4 Vertical gravity gradient correction (expressed in g/cm^3) for submarine topography out to a radial distance of 103.5 statute miles (166.7 kilometers). Correction calculated by replacing sea water with density of 1.90 g/cm^3 (see Meyer and Corbato, 1972).

Column 5 Vertical gravity gradient correction expressed in g/cm^3 for lateral density changes (assumed to be two-dimensional) caused by geologic facies changes across the reef (see Figure 2.4).

Column 6 Vertical gravity gradient correction (expressed in g/cm^3) for lateral density changes caused by crater-related processes and assumed to be symmetrical about OPZ-18 (see Figure 2.7).

Column 7 BHG density in g/cm^3 after correction for submarine topography and lateral density variations due to geologic facies changes and cratering processes.

Column 8 Mean grain density for depth interval in g/cm^3 (calculated from mineral and organic content percentages estimated from x-ray diffraction and loss-on-ignition analyses (see Appendix 2.2).

Column 9 Estimated uncertainty in mean grain density in g/cm^3.

Column 10 BHG porosity in percent calculated from BHG density (column 7), grain density (column 8) and sea-water density of 1.03 g/cm^3.

Column 11 Uncertainty in BHG porosity in porosity percent (calculated from standard deviation of BHG density (column 4) and uncertainty in mean grain density (column 8).

Column 12 Average gamma-gamma density for depth interval in g/cm^3.

Column 13 Gamma-gamma porosity in percent calculated from gamma-gamma density (column 12), grain density (column 8) and sea-water density of 1.03 g/cm^3.

Column 14 Average neutron porosity for depth interval in percent.

TABLE 2-4.--(on adjacent page) Bulk density, porosity, and grain density obtained from borehole gravity, gamma-gamma, and neutron measurements in borehole OQT-19 and from analysis of cores taken from OQT-19. Gamma-gamma and neutron data averages over depth intervals of BHG survey. Grain densities were calculated by the procedure described in Appendix 2-1 using data from Tremba and Ristvet (1986) and Ristvet and Tremba (1986).

→

1	2	3	4	5	6	7	8	9	10	11	12	13	14
138.-148.	1.646	.038	.145	.020	-.004	1.807	2.84	.02	57.1	2.1	0.	0.	0.
148.-178.	1.777	.010	.140	.020	0.002	1.939	2.85	.02	50.1	0.5	0.	0.	0.
178.-208.	1.787	.020	.134	.021	0.	1.942	2.83	.02	49.3	1.1	0.	0.	0.
208.-238.	1.737	.017	.132	.021	0.	1.890	2.83	.02	52.2	0.9	0.	0.	0.
238.-273.	1.753	.006	.131	.021	0.001	1.906	2.84	.02	51.6	0.3	1.99	47.0	59.1
273.-298.	1.747	.008	.131	.021	0.001	1.900	2.83	.02	51.7	0.4	2.01	45.6	60.4
298.-328.	1.791	.009	.131	.021	0.005	1.948	2.81	.02	48.4	0.5	2.04	43.3	57.6
328.-358.	1.814	.011	.131	.022	0.005	1.972	2.81	.02	47.1	0.6	2.00	45.5	60.2
358.-380.	1.764	.008	.132	.022	0.004	1.922	2.81	.02	49.9	0.4	1.86	53.4	62.6
380.-403.	1.846	.009	.132	.022	0.008	2.008	2.82	.02	45.4	0.5	2.13	38.5	52.8
403.-433.	1.849	.014	.132	.022	0.008	2.011	2.83	.02	45.5	0.8	2.02	45.0	55.4
433.-468.	1.885	.007	.132	.022	0.007	2.046	2.75	.02	40.9	0.4	2.02	42.4	52.0
468.-498.	1.897	.012	.133	.022	0.004	2.056	2.71	.02	38.9	0.7	2.02	41.1	53.7
498.-528.	1.842	.007	.133	.022	0.001	1.998	2.71	.02	42.4	0.4	2.02	41.1	55.3
528.-558.	1.792	.017	.133	.023	0.	1.948	2.71	.02	45.4	1.0	1.97	44.0	53.5
558.-588.	1.793	.008	.134	.023	0.001	1.951	2.74	.02	46.1	0.5	2.02	42.1	54.8
588.-618.	1.882	.002	.134	.023	0.001	2.040	2.83	.02	43.9	0.1	2.03	44.4	54.9
618.-648.	1.874	.015	.134	.023	-.001	2.030	2.84	.02	44.8	0.8	2.01	45.9	61.4
648.-678.	1.858	.005	.134	.023	-.002	2.013	2.86	.02	46.3	0.3	2.04	44.8	60.4
678.-708.	1.861	.009	.135	.024	-.002	2.018	2.86	.02	46.0	0.5	2.02	45.9	57.6
708.-738.	1.854	.005	.135	.024	-.002	2.011	2.87	.02	46.7	0.3	2.03	45.7	60.5
738.-768.	1.884	.022	.135	.024	-.002	2.041	2.86	.02	44.8	1.2	2.04	44.8	61.8
768.-798.	1.799	.008	.135	.024	-.002	1.956	2.84	.02	48.8	0.4	1.98	47.5	61.7

TABLE 2-4

Column 1 Depth interval in feet below sea level

Column 2 Apparent BHG density in g/cm^3 (corrected for instrument calibration and drift and earth tides).

Column 3 Standard deviation of repeated $\Delta g/\Delta z$ measurements expressed in g/cm^3.

Column 4 Vertical gravity gradient correction (expressed in g/cm^3) for submarine topography out to a radial distance of 103.5 statute miles (166.7 kilometers). Correction calculated by replacing sea water with density of 1.90 g/cm^3 (see Beyer and Corbato, 1972).

Column 5 Vertical gravity gradient correction expressed in g/cm^3 for lateral density changes (assumed to be two-dimensional) caused by geologic facies changes across the reef (see Figure 2.4).

Column 6 Vertical gravity gradient correction (expressed in g/cm^3) for lateral density changes caueed by crater-related processes and assumed to be symmetrical about OPZ-18 (see Figure 2.7).

Column 7 BHG density in g/cm^3 after correction for submarine topography and lateral density variations due to geologic facies changes and cratering processes.

Column 8 Mean grain density for depth interval in g/cm^3 (calculated from mineral and organic content percentages estimated from x-ray diffraction and loss-on-ignition analyses (see Appendix 2.2).

Column 9 Estimated uncertainty in mean grain density in g/cm^3.

Column 10 BHG porosity in percent calculated from BHG density (column 7), grain density (column 8) and sea-water density of 1.03 g/cm^3.

Column 11 Uncertainty in BHG porosity in porosity percent (calculated from standard deviation of BHG density (column 4) and uncertainty in mean grain density (column 8).

Column 12 Average gamma-gamma density for depth interval in g/cm^3.

Column 13 Gamma-gamma porosity in percent calculated from gamma-gamma density (column 12), grain density (column 8) and sea-water density of 1.03 g/cm^3.

Column 14 Average neutron porosity for depth interval in percent.

TABLE 2-5 (On opposite page). -- Bulk density, porosity, and grain density obtained from borehole gravity, gamma-gamma, and neutron measurements in borehole ORT-20 and from analysis of cores taken from ORT-20. Gamma-gamma and neutron data averages over depth intervals of BHG survey. Grain densities were calculated by the procedure described in Appendix 2-1 using data from Tremba and Ristvet (1986) and Ristvet and Tremba (1986).

→

1	2	3	4	5	6	7	8	9	10	11	12	13	14
136.-160.	1.693	.013	.130	.020	0.005	1.848	2.84	.02	54.8	0.7	1.98	47.5	0.
160.-186.	1.857	.012	.133	.020	0.	2.010	2.86	.02	46.4	0.7	1.99	47.5	0.
186.-211.	1.673	.007	.134	.021	-.002	1.826	2.84	.02	56.0	0.4	1.96	48.6	0.
211.-226.	1.818	.	.135	.021	-.003	1.971	2.86	.02	48.6	0.	1.99	47.5	0.
226.-256.	1.772	.	.136	.021	-.003	1.926	2.85	.02	50.8	0.	2.00	46.7	0.
256.-271.	1.653	.	.137	.021	-.004	1.807	2.82	.02	56.6	0.	1.97	47.5	0.
271.-301.	1.787	.004	.138	.021	-.004	1.942	2.82	.02	49.1	0.2	0.	0.	0.
301.-331.	1.766	.002	.139	.021	-.004	1.922	2.78	.02	49.0	0.1	0.	0.	0.
331.-361.	1.792	.007	.139	.022	-.005	1.948	2.88	.02	50.4	0.4	0.	0.	0.
361.-391.	1.833	.010	.139	.022	-.005	1.989	2.83	.02	46.7	0.6	2.04	43.9	0.
391.-421.	1.846	.014	.140	.022	-.005	2.003	2.75	.02	43.4	0.8	2.04	41.3	0.
421.-451.	1.857	.012	.140	.022	-.005	2.014	2.70	.02	41.1	0.7	1.95	44.9	0.
451.-471.	1.891	.008	.140	.022	-.005	2.048	2.70	.02	39.0	0.5	1.90	47.9	0.
471.-491.	1.852	.017	.140	.022	-.005	2.009	2.70	.02	41.4	1.0	2.06	38.3	0.
491.-521.	1.792	.009	.140	.022	-.005	1.949	2.69	.02	44.6	0.5	1.93	45.8	0.
521.-551.	1.770	.010	.140	.023	-.004	1.929	2.70	.02	46.2	0.6	1.91	47.3	0.

TABLE 2-5.

Column 1 Depth interval in feet below sea level
Column 2 Apparent BHG density in g/cm^3 (corrected for instrument calibration and drift and earth tides).
Column 3 Standard deviation of repeated $\Delta g/\Delta z$ measurements expressed in g/cm^3.
Column 4 Vertical gravity gradient correction (expressed in g/cm^3) for submarine topography out to a radial distance of 103.5 statute miles (166.7 kilometers). Correction calculated by replacing sea water with density of 1.90 g/cm^3 (see Meyer and Corbato, 1972).
Column 5 Vertical gravity gradient correction expressed in g/cm^3 for lateral density changes (assumed to be two-dimensional) caused by geologic facies changes across the reef (see Figure 2.4).
Column 6 Vertical gravity gradient correction (expressed in g/cm^3) for lateral density changes caused by crater-related processes and assumed to be symmetrical about OPZ-18 (see Figure 2.7).
Column 7 BHG density in g/cm^3 after correction for submarine topography and lateral density variations due to geologic facies changes and cratering processes.
Column 8 Mean grain density for depth interval in g/cm^3 (calculated from mineral and organic content percentages estimated from x-ray diffraction and loss-on-ignition analyses (see Appendix 2.2).
Column 9 Estimated uncertainty in mean grain density in g/cm^3.
Column 10 BHG porosity in percent calculated from BHG density (column 7), grain density (column 8) and sea-water density of 1.03 g/cm^3.
Column 11 Uncertainty in BHG porosity in porosity percent (calculated from standard deviation of BHG density (column 4) and uncertainty in mean grain density (column 8).
Column 12 Average gamma-gamma density for depth interval in g/cm^3.
Column 13 Gamma-gamma porosity in percent calculated from gamma-gamma density (column 12), grain density (column 8) and sea-water density of 1.03 g/cm^3.
Column 14 Average neutron porosity for depth interval in percent.

TABLE 2-6 (On opposite page). -- Bulk density, porosity, and grain density obtained from borehole gravity, gamma-gamma, and neutron measurements in borehole OSR-21 and from analysis of cores taken from OSR-21. Gamma-gamma and neutron data averages over depth intervals of BHG survey. Grain densities were calculated by the procedure described in Appendix 2-1 using data from Tremba and Ristvet (1986) and Ristvet and Tremba (1986).

→

1	2	3	4	5	6	7	8	9	10	11	12	13	14
134.-159.	1.845	.004	.126	.018	0.	1.989	2.82	.02	46.4	0.2	1.96	48.0	0.
159.-184.	1.776	.018	.126	.018	0.	1.920	2.80	.02	49.7	1.0	1.83	54.8	0.
184.-209.	1.698	.014	.128	.019	0.	1.845	2.81	.02	54.2	0.8	1.90	51.1	0.
209.-234.	1.689	.009	.129	.019	0.	1.837	2.82	.02	54.9	0.5	1.88	52.5	0.
234.-264.	1.763	.007	.131	.019	0.	1.913	2.80	.02	50.1	0.4	1.87	52.5	0.
264.-294.	1.794	.009	.132	.019	0.	1.945	2.80	.02	48.3	0.5	1.88	52.0	0.
294.-324.	1.735	.008	.134	.019	0.	1.888	2.82	.02	52.1	0.4	1.87	53.1	0.
324.-354.	1.736	.009	.135	.019	0.	1.890	2.82	.02	52.0	0.5	1.78	58.1	0.
354.-384.	1.734	.007	.136	.019	0.	1.889	2.81	.02	51.7	0.4	1.83	55.1	0.
384.-404.	1.765	.016	.137	.020	0.	1.922	2.79	.02	49.3	0.9	1.72	60.8	0.
404.-424.	1.829	.020	.137	.020	0.	1.986	2.77	.02	45.1	1.1	1.84	53.4	0.

TABLE 2-6.

Column 1 Depth interval in feet below sea level

Column 2 Apparent BHG density in g/cm^3 (corrected for instrument calibration and drift and earth tides).

Column 3 Standard deviation of repeated $\Delta g/\Delta z$ measurements expressed in g/cm^3.

Column 4 Vertical gravity gradient correction (expressed in g/cm^3) for submarine topography out to a radial distance of 103.5 statute miles (166.7 kilometers). Correction calculated by replacing sea water with density of 1.[illegible] g/cm^3 (see Beyer and Corbato, 1972).

Column 5 Vertical gravity gradient correction expressed in g/cm^3 for lateral density changes (assumed to be two-dimensional) caused by geologic facies changes across the reef (see Figure 2.4).

Column 6 Vertical gravity gradient correction (expressed in g/cm^3) for lateral density changes caused by crater-related processes and assumed to be symmetrical about OPZ-18 (see Figure 2.7).

Column 7 BHG density in g/cm^3 after correction for submarine topography and lateral density variations due to geologic facies changes and cratering processes.

Column 8 Mean grain density for depth interval in g/cm^3 (calculated from mineral and organic content percentages estimated from x-ray diffraction and loss-on-ignition analyses (see Appendix 2.2).

Column 9 Estimated uncertainty in mean grain density in g/cm^3.

Column 10 BHG porosity in percent calculated from BHG density (column 7), grain density (column 8) and sea-water density of 1.03 g/cm^3.

Column 11 Uncertainty in BHG porosity in porosity percent (calculated from standard deviation of BHG density (column 4) and uncertainty in mean grain density (column 8).

Column 12 Average gamma-gamma density for depth interval in g/cm^3.

Column 13 Gamma-gamma porosity in percent calculated from gamma-gamma density (column 12), grain density (column 8) and sea-water density of 1.03 g/cm^3.

Column 14 Average neutron porosity for depth interval in percent.

TABLE 2-7 (On opposite page). -- Bulk density, porosity, and grain density obtained from borehole gravity, gamma-gamma, and neutron measurements in borehole OTG-23 and from analysis of cores taken from OTG-23. Gamma-gamma and neutron data averages over depth intervals of BHG survey. Grain densities were calculated by the procedure described in Appendix 2-1 using data from Tremba and Ristvet (1986) and Ristvet and Tremba (1986).

→

1	2	3	4	5	6	7	8	9	10	11	12	13	14
314.-344.	1.869	.003	.108	.022	0.019	2.018	2.85	.04	45.7	0.2	0.	0.	0.
344.-374.	1.888	.007	.109	.022	0.018	2.037	2.85	.04	44.7	0.4	0.	0.	0.
374.-404.	1.860	.010	.111	.022	0.018	2.011	2.85	.04	46.1	0.5	0.	0.	0.
404.-434.	1.848	.013	.112	.022	0.018	2.000	2.85	.04	46.7	0.7	0.	0.	0.
434.-464.	1.864	.010	.113	.022	0.018	2.017	2.85	.02	45.8	0.5	0.	0.	0.
464.-494.	1.895	.012	.114	.022	0.018	2.049	2.84	.02	43.7	0.7	0.	0.	0.
494.-539.	1.855	.006	.116	.022	0.015	2.008	2.74	.02	42.8	0.4	0.	0.	0.
539.-584.	1.958	.005	.117	.023	0.019	2.117	2.72	.02	35.7	0.3	0.	0.	0.
584.-629.	1.867	.008	.119	.023	0.017	2.026	2.73	.02	41.4	0.5	0.	0.	0.
629.-674.	1.915	.018	.120	.023	0.014	2.072	2.81	.02	41.5	1.0	0.	0.	0.
674.-734.	1.991	.015	.122	.024	0.019	2.156	2.88	.02	39.1	0.8	0.	0.	0.

TABLE 2-7.

Column 1 Depth interval in feet below sea level

Column 2 Apparent BHG density in g/cm^3 (corrected for instrument calibration and drift and earth tides).

Column 3 Standard deviation of repeated $\Delta g/\Delta z$ measurements expressed in g/cm^3.

Column 4 Vertical gravity gradient correction (expressed in g/cm^3) for submarine topography out to a radial distance of 103.5 statute miles (166.7 kilometers). Correction calculated by replacing sea water with density of 1.90 g/cm^3 (see Beyer and Corbato, 1972).

Column 5 Vertical gravity gradient correction expressed in g/cm^3 for lateral density changes (assumed to be two-dimensional) caused by geologic facies changes across the reef (see Figure 2.4).

Column 6 Vertical gravity gradient correction (expressed in g/cm^3) for lateral density changes caused by crater-related processes and assumed to be symmetrical about OPZ-18 (see Figure 2.7).

Column 7 BHG density in g/cm^3 after correction for submarine topography and lateral density variations due to geologic facies changes and cratering processes.

Column 8 Mean grain density for depth interval in g/cm^3 (calculated from mineral and organic content percentages estimated from x-ray diffraction and loss-on-ignition analyses (see Appendix 2.2).

Column 9 Estimated uncertainty in mean grain density in g/cm^3.

Column 10 BHG porosity in percent calculated from BHG density (column 7), grain density (column 8) and sea-water density of 1.03 g/cm^3.

Column 11 Uncertainty in BHG porosity in porosity percent (calculated from standard deviation of BHG density (column 4) and uncertainty in mean grain density (column 8).

Column 12 Average gamma-gamma density for depth interval in g/cm^3.

Column 13 Gamma-gamma porosity in percent calculated from gamma-gamma density (column 12), grain density (column 8) and sea-water density of 1.03 g/cm^3.

Column 14 Average neutron porosity for depth interval in percent.

Table 2-8. -- Density model for atoll material surrounding OAK crater. Density layers are averages of BHG densities from OOR-17 and OSR-21 and are contrasted with the crater density model of Figure 2-7. Averaged grain densities and BHG porosities are also shown.

Approximate Depth Interval (feet below sea level)	Averaged BHG Density (g/cm^3)	Averaged Grain Density (g/cm^3)	Averaged BHG Porosity (%)
134 - 410	1.92	2.81	50
410 - 587	1.98	2.73	44
587 - 747	2.01	2.84	46
750 - 962	$2.09 \pm .03$ (estimate from gamma-gamma log run in OOR-17)		

Table 2-9. -- BHG density and porosity values and their contrasts with respect to reference borehole values (Table 2-8) for the averaged large intervals shown in Figures 2-16 and 2-19.

	OOR-17/OSR-21	OTG-20	OQT-19	OTG-23	OPZ-18
Interval approximately from discontinuity 1 to 4					
Density(contrast) in g/cm^3	1.92	1.92(0)	1.93(+.01)	--	--
Porosity(contrast) in %	50	51(+1)	50(0)	--	--
Interval approximately from discontinuity 4 to 6					
Density(contrast) in g/cm^3	1.97	1.98(+.01)	2.00(+.03)	2.05(+.08)	2.13(+.16)
Porosity(contrast) in %	45	44(-1)	44(-1)	41(-4)	36(-9)
Interval approximately from disconformity 5 to facies change H/I					
Density(contrast) in g/cm^3	1.98	1.97(-.01)	2.00(+.02)	2.03(+.05)	2.11(+.13)
Porosity(contrast) in %	44	44(0)	43(-1)	40(-4)	37(-7)
Interval approximately from facies change H/I to J/K					
Density(contrast) in g/cm^3	2.01	--	2.03(+.02)	--	2.05(+.04)
Porosity(contrast) in %	46	--	45(-1)	--	44(-2)
Mass columns (%)					
	100		95-97		92-94

APPENDIX 2-1

BOREHOLE GRAVITY SURVEY, BOREHOLE E-1, MEDREN ISLAND

The BHG survey in borehole E-1 on Medren (ELMER) Island (see fig. 2-20) was conducted in April, 1984, by the U.S. Geological Survey to determine if reliable BHG data could be gathered in the microseismic environment of an atoll and to evaluate the range of natural density variations of reef-forming materials. Near-surface vibrations caused by wave action were minimal and the repeatability of BHG measurements generally was excellent. The tabulated data for this survey are given in Beyer, Ristvet, and Oberste-Lehn (1986).

The borehole gravity survey in the E-1 borehole shows that the bulk density of atoll materials to a depth of 1,800 ft ranges from about 1.9 to about 2.3 g/cm^3 and averages slightly more than 2.0 g/cm^3 at the scale examined by the BHG survey. Several density patterns are evident.

1. Higher densities between 1,140 and about 1,290 ft correspond to harder rocks as indicated by slower drill rates (fig. 2-20).

2. The gravity station at 1,410 ft (point labeled "A" in fig. 2-20) probably is in close proximity to a sizable cavern that has caused measured gravity to be unexpectedly low. This one anomalous gravity reading incorporated into the overlying and underlying density calculations explains the generally high and low densities of the two adjacent intervals.

3. A repeated pattern of density variations (labeled "1" through "5" in fig. 2-20) may be due to facies changes and/or diagenesis associated with relative sea-level changes. These repeated patterns of downward decrease in density (increase in porosity) followed by more abrupt increase in density (decrease in porosity) should be examined for possible correlation with available geologic data.

Densities in the upper 600 ft are slightly higher than the densities over the same depth interval in PEACE Program reference boreholes OOR-17 and OSR-21 at OAK crater. Part of this may be due to the E-1 borehole being much closer to the ocean edge of the reef than are OOR-17 and OSR-21. Boreholes OOR-17 and OSR-21 are more likely to be in a less dense, more lagoonward facies. Corrections for submarine topography are more critical at the E-1 borehole because of its closer proximity to the outer reef slope than the PEACE Program boreholes. Unfortunately, bathymetry is less well known adjacent to the E-1 borehole, and some of the density differences between E-1 and OOR-17 and OSR-21 may be due to errors in corrections for submarine topography at E-1.

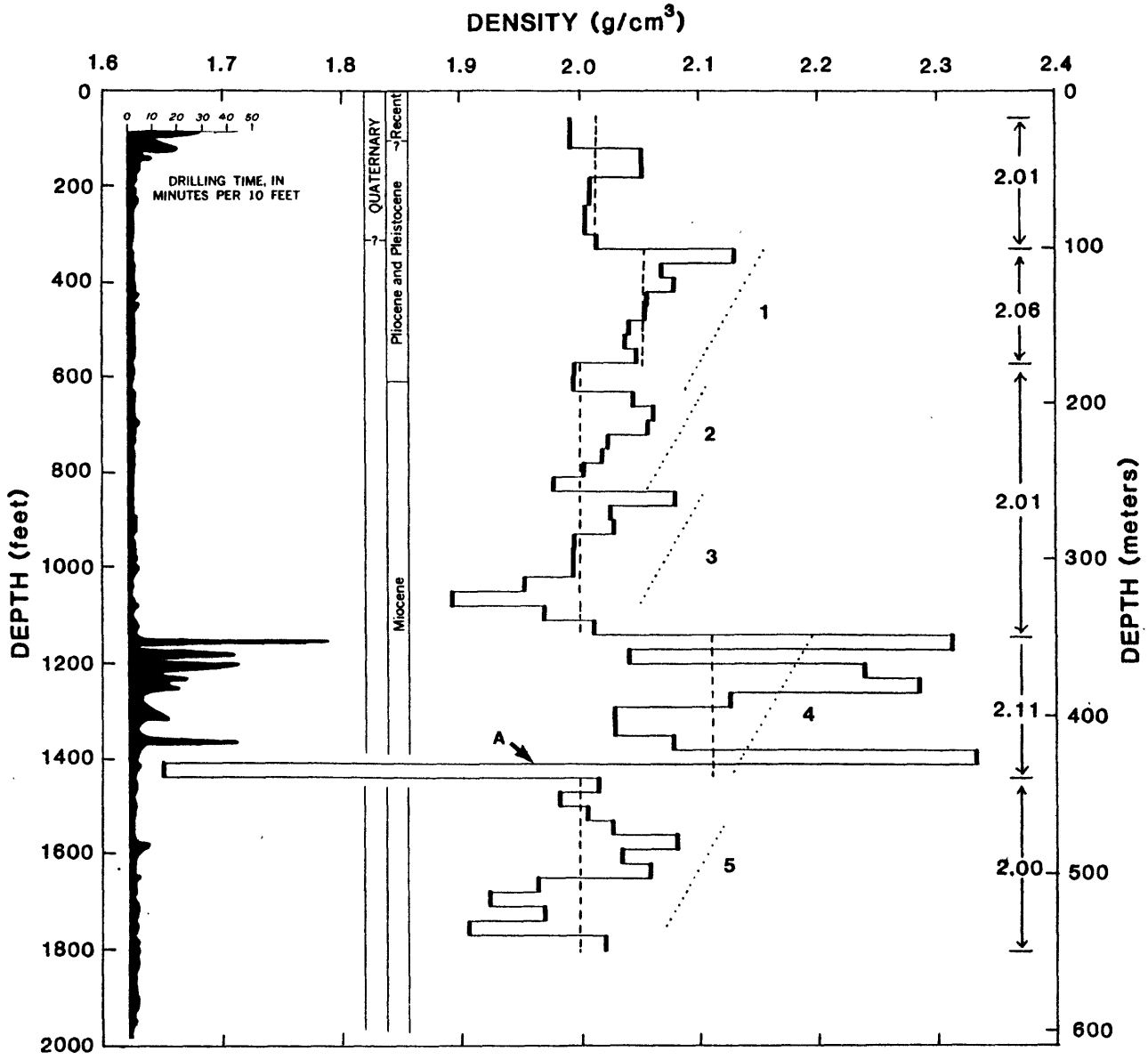

FIGURE 2-20 - BHG density profile for borehole E-1, Medren (ELMER) Island. Drilling time profile and geologic ages are from Ladd and Schlanger (1960). Large interval averages of density along righthand depth scale correspond to vertical dashed lines. Diagonal dotted lines labeled "1" through "5" designate suggested repeated density (porosity?) cycles.

APPENDIX 2-2

DETERMINATION OF INTERVAL GRAIN DENSITY

An estimate of interval grain density is needed before BHG porosity can be calculated from BHG density. Grain densities of individual core samples were estimated from x-ray mineralogy and organic analyses by Tremba and Ristvet (1986) and Ristvet and Tremba (1986) and are shown in Figures 2-8 through 2-13.

An example of how grain density was calculated from x-ray mineralogy and organic analyses follows. Calcite (and magnesium calcite), aragonite, and organic matter were assigned grain densities of 2.72, 2.93, and 1.00 g/cm^3 respectively. If organic matter was present and measured in weight percent of dry solids (generally 3 percent or less), the remainder of the dry sample was assumed to consist of inorganic material (generally 97 percent or more). Thus, for a sample with the analysis

Calcite (wt %)	Aragonite (wt %)	Organic Matter (wt %)
29	71	2.5

The grain density is

$$[(.29)(2.72) + (.71)(2.93)](1-.025) + .025 = 2.82\ g/cm^3$$

If the sample had no measurable organic matter, the grain density is

$$(.29)(2.72) + (.71)(2.93) = 2.87\ g/cm^3$$

The plots of grain densities of core samples were generalized to average grain densities for BHG intervals as shown in Figures 2-8 through 2-13. Grain densities averaged by sedimentary packages by Tremba and Ristvet (1986) were too generalized for the BHG data. Uncertainties of $\pm.02$ or $\pm.04\ g/cm^3$ were assigned in order to estimate errors in porosity calculations (columns 8, 9, 11 of Tables 2-2 through 2-7; also see Appendix 8-2, Beyer, Ristvet, and Oberste-Lehn, 1986).

CHAPTER 3:

PALEONTOLOGIC EVIDENCE FOR SEDIMENTARY MIXING IN OAK CRATER

by

Thomas M. Cronin and Thomas G. Gibson[1]

INTRODUCTION

In 1985, during the course of paleontologic studies of OAK and KOA craters, Enewetak Atoll, it was discovered that the analysis of the distribution of microfossils aided the understanding of the dynamic processes involved in the formation and evolution of the nuclear craters (Cronin, Brouwers, and others, 1986; Brouwers, Cronin, and Gibson, 1986; Henry, Wardlaw, and others, 1986; Henry and Wardlaw, 1986; and Wardlaw and Henry, 1986). These paleontologic studies were particularly useful in determining the depth of origin (or provenance) and sedimentologic history of the disturbed and mobilized materials that partially infilled KOA crater after the initial excavation by the detonation of the nuclear device.

The primary purpose of the present study is to determine the composition and provenance of crater-fill materials and the nature of sediment mixing in OAK crater using micropaleontologic data. This study is an extension of the paleontologic component by the U.S. Geological Survey for the PEACE Program (Cronin, Brouwers, and others, 1986; Brouwers, Cronin, and Gibson, 1986). In this study of OAK, we intend to establish the depth limits of mixing of: (1) surficial material, (2) sediment from the uppermost 50 ft of the stratigraphic section, and (3) material from intermediate depths (50 to 300 ft). Furthermore, we intend to determine the pattern of "piping" of deep material emplaced in the crater-fill from horizons 500 to 900 ft below the lagoon bottom or sea floor. Our results are integrated with geologic and geophysical data to form a general model of crater formation in Chapter 7 of this Open-File Report.

MATERIAL AND METHODS

To accomplish our objectives, detailed restudy of samples from reference boreholes OAR-2A and OOR-17 was necessary to refine our zonation of the microfaunal sequence in the upper 400 ft of the stratigraphic section (for discussion of the succession of microfaunal zones used on Enewetak, see Cronin, Brouwers, and others, 1986, and Brouwers, Cronin, and Gibson, 1986). The laboratory and biostratigraphic procedures used herein are the same as those described in the reports cited above. Microfossils were extracted from sediment between 63 and 850 μm in grain size. Samples from two central-crater (ground-zero) boreholes (OBZ-4 and OPZ-18) and three transition boreholes

---

[1] Branch of Paleontology and Stratigraphy, U.S. Geological Survey, Reston, VA 22092.

(OCT-5, OFT-8, and OKT-13) were examined in detail for the mixing study of OAK crater. Table 3-1 lists the depths of all 159 samples studied.

Throughout this report, depths of zonal boundaries are occasionally rounded off to whole numbers for convenience. Of course, the accuracy of any particular faunal zone is limited by the resolution of the sampling interval.

STANDARD MICROFAUNAL SEQUENCE

Quantitative data on the occurrence of diagnostic ostracode species (Appendices 3-1 and 3-2) and semiquantitative data on benthic foraminifers (Gibson and Hill, in preparation) from boreholes OAR-2/2A and OOR-17 were used to improve the standard zonation of Cronin, Brouwers, and others (1986) and Brouwers, Cronin, and Gibson (1986), in which 12 faunal zones, designated AA through MM, in descending order, were defined. In addition, the percent of specimens of the ostracode Neonesidea schulzi with preserved setae[1] was used as a new measure to quantify the amount of material mixed downward from the surface. Only living or recently dead specimens of this species found in surficial lagoon sediments have setae preserved (generally 70 to 80%). Ostracode setae normally are degraded and destroyed by natural processes soon after death of the organism and burial of the shell. Therefore, the occurrence of setae in specimens below the sediment surface in the crater-fill materials is taken to indicate mixing of specimens from the surface sediments.

The following zones were used in the quantitative analyses of ostracodes:

Surface: The percent of Neonesidea schulzi with setae preserved.

Zone AA: The combined percentages of Hermanites mooneyi and Loxoconchella sp. A.

Zone BB-CC: The combined percentages of Cletocythereis sp. A and Loxoconcha heronislandensis.

Zone EE-FF: The combined percentages of Caudites sp. A, Caudites sp. B, Cletocythereis rastromarginata, Loxonconcha labrynthica, and Loxoconchella sp. C.

Zone FF-GG: The combined percentages of Australimoosella sp. A, Bythoceratina sp. A, Cletocythereis canaliculata, Procythereis sp. A, and Semicytherura sp. A.

Zone II-MM: The combined percentages of all species restricted to zones II, JJ, KK, LL, and MM as determined by Cronin, Brouwers, and Gibson (1986). In Appendices 3-1 and 3-2 at the end of this Chapter, the totals for these species are given in row 41. Procythereis sp. B generally occurs in zones

---

[1] Setae are small hairs that occur on the exterior of the valves of some taxa of ostracodes.

TABLE 3-1. — Depth (ft bsf) in boreholes of samples examined during the study of the mixing of crater-fill materials from OAK.

OAR-2A	OBZ-4	OCT-5	OFT-8	OKT-13	OOR-17	OPZ-18
0.25	2.8	0.2	8.75	10.4	0.25	7.0
2.3	11.8	8.8	18.6	18.5	14.15	35.0
6.0	21.1	17.5	27.9	25.4	25.75	44.6
9.3	33.0	39.5	35.1	28.75	38.4	57.85
11.85	40.5	57.55	43.1	36.0	49.7	74.3
14.5	58.5	66.8	48.85	55.65	60.2	89.45
17.1	66.35	76.65	64.0	59.9	66.75	102.0
20.8	75.15	86.15	74.0	68.2	72.8	115.05
22.75	84.15	95.35	-	80.0	83.7	131.0
23.75	93.1	104.25	-	-	89.8	139.7
26.05	104.55	113.15	-	-	100.45	154.2
31.9	112.9	124.0	-	-	101.4	169.35
34.75	121.8	132.8	-	-	110.5	174.95
40.2	130.0	140.9	-	-	119.1	182.3
43.55	144.5	149.65	-	-	125.25	198.0
62.5	151.55	157.6	-	-	131.95	207.3
74.8	166.85	166.4	-	-	137.15	210.4
90.4	178.6	176.25	-	-	146.1	229.95
95.8	186.8	186.0	-	-	154.25	232.1
115.1	193.6	-	-	-	165.6	239.15
127.8	196.5	-	-	-	173.05	-
134.0	205.1	-	-	-	184.25	-
157.45	213.9	-	-	-	193.6	-
171.2	225.65	-	-	-	200.8	-
188.25	-	-	-	-	209.3	-
195.3	-	-	-	-	215.5	-
204.9	-	-	-	-	226.05	-
212.45	-	-	-	-	233.35	-
223.9	-	-	-	-	239.0	-
234.6	-	-	-	-	250.3	-
244.55	-	-	-	-	261.5	-
246.8	-	-	-	-	270.1	-
268.45	-	-	-	-	285.65	-
282.55	-	-	-	-	292.1	-
289.7	-	-	-	-	299.15	-
337.05	-	-	-	-	310.7	-
379.5	-	-	-	-	320.2	-
-	-	-	-	-	331.2	-
-	-	-	-	-	339.0	-
-	-	-	-	-	367.9	-

II-MM; however, it does occur higher in the section in single samples from OOR-17 (331.2 ft bsf) and in OAR-2A (223.9 ft). Specimens of Procythereis sp. B in crater boreholes are considered piped, so that the percent of II-MM species includes species groups 36 and 41 from the appendices.

For the companion analysis of the foraminifers, the zones used are characterized as follows:

Surface: The presence of chitinous inner linings and original (natural) coloration in several species.

Zone AA: The presence of Calcarina spengleri and C. hispida. Upper AA is characterized by coloration in specimens of C. spengleri that is not present in specimens in the lower part of this zone, as determined from the reference boreholes.

Zone BB: The presence of Epistominella tubulosa and Anomolina sp. A.

Zone CC: The presence of advanced forms of Calcarina rustica.

Zone EE: The presence of Calcarina delicata and primitive forms of Calcarina rustica.

Zone FF-GG: The presence of Calcarina calcar and Cibicides sp. A.

The percentages of ostracodes for each category (excluding the Surface[1] and II-MM categories) are plotted for boreholes OAR-2A and OOR-17 in Figures 3-1 and 3-2. These were used for comparison with the mixed faunal sequences in the central crater and transition boreholes. It is noteworthy that the two faunal sequences in OOR-17 and OAR-2A are very similar to each other, enhancing the accuracy of estimates of the original depths of mixed specimens.

A large proportion (generally about 40 to 60% of each sample) consists of long-ranging species not restricted to a particular zone. Some of these non-diagnostic species probably also were mixed during crater filling. Consequently, the percentage values for samples from crater boreholes are, in some cases, minimum values (i.e., if mixed specimens of non-diagnostic species could be identified, the true percentage of an assemblage from any particular zone would be slightly higher).

In many ways, the use in the mixing study of selected species that have acme zones (intervals of greatest abundance) is an exercise in probability. Those species chosen as diagnostic of zones AA, BB-CC, EE-FF, and FF-GG in the upper 400 ft of normal stratigraphic section have a high probability (generally about 80 to 90%) that they originated from within that interval.

---

[1] Sediments from the lagoon floor or the upper several inches of sediment below the lagoon floor itself are referred hereafter as Surface materials.

OAR-2/2A

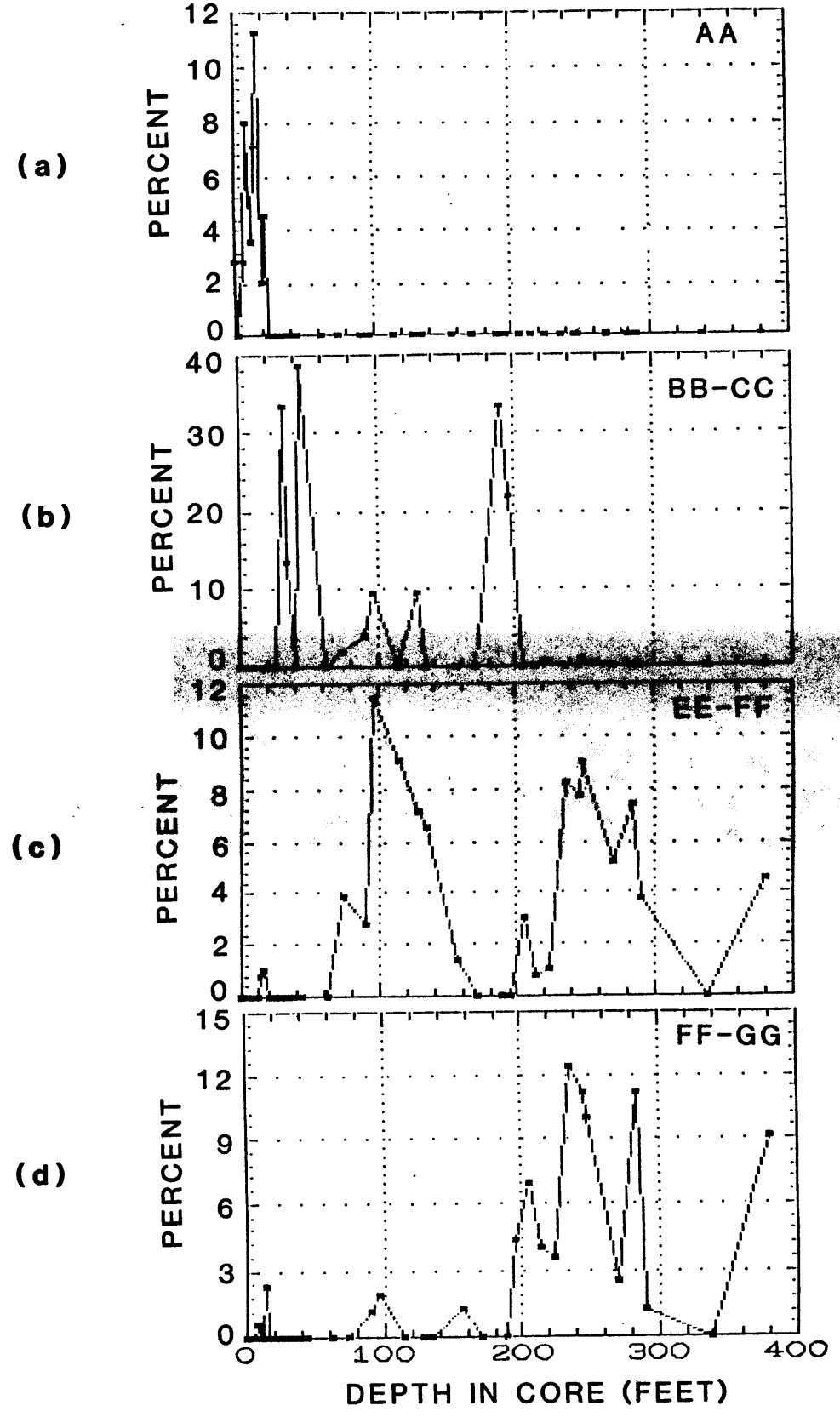

Figure 3-1. -- Borehole OAR-2/2A. Plot of percentages of diagnostic ostracode species. (1a) zone AA; (1b) zones BB-CC; (1c) zones EE-FF; (1d) zones FF-GG.

OOR-17

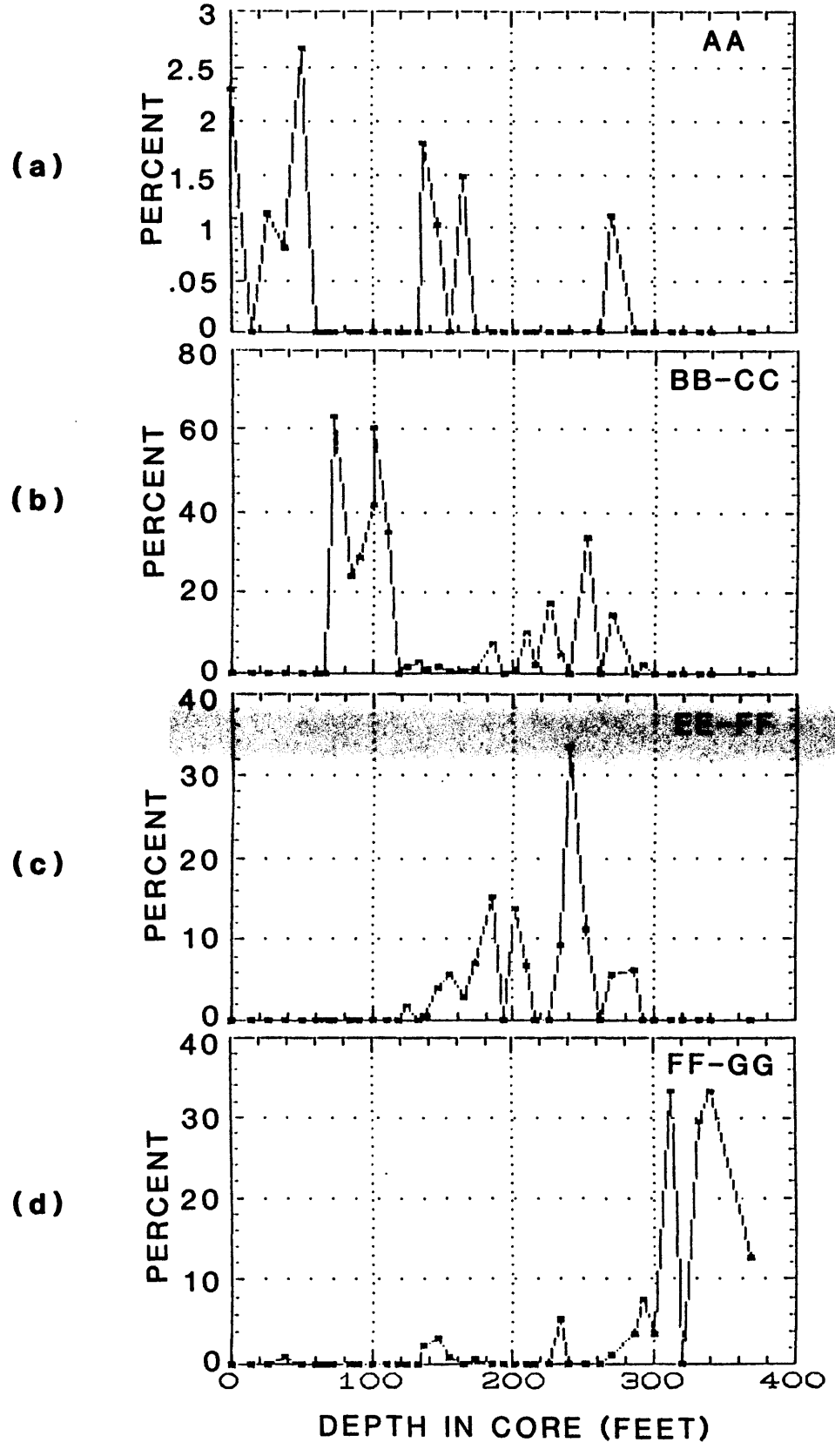

Figure 3-2. -- Borehole OOR-17: Plot of percentages of diagnostic ostracode species. (2a) zone AA; (2b) zones BB-CC; (2c) zones EE-FF; (2d) zones FF-GG.

Confirmation of a zone assignment from both fossil groups increases significantly the probability that the zone assignment is correct.

The use of percentages of specimens from zones II-MM probably underestimates the real percentages by no more than 5 to 10%, because far fewer species from the upper 300 ft of section range downward into these zones. This index of piped specimens is considered an accurate indicator of the proportion of piped material represented in a sample. The percentage piped from a depth interval may be considered representative of the entire sedimentary assemblage at that level if two assumptions are correct. First, we must assume all particles of all sizes behave the same as those between 63 and 850 μm (the size range from which ostracodes were extracted). Second, we must assume sediment particles of different shapes and densities behave the same as the ostracode valves and carapaces. With these assumptions in mind, and given the error margins associated with the limits to microfossils zonations discussed above, these data are useful in making volumetric estimates of the proportion of crater-fill sediments piped from depth.

The percentage of Neonesidea schulzi having setae is a distinct type of index that gives an approximate estimate of the actual percentage of surface material, at least to the extent that it can be determined from using this one common species of ostracodes.

A large proportion of the foraminifer assemblage in most samples is composed of Amphistigina madagascarensis. This species is abundant in the modern reef environments on Enewetak and continues downward into the Miocene strata in the Enewetak boreholes. Therefore, its occurrence alone cannot be used for biostratigraphic determination; however, its preservation state is indicative of its zone of origin or provenance. Translucent specimens of this species occur only in zone AA. Below this zone (i.e., in the Pleistocene section and in older strata), they are opaque. Thus, the occurrence of translucent specimens of A. madagascarensis indicates that their provenance is the Holocene section (zone AA). Many other foraminifer species also have long ranges and cannot be placed definitely. However, the evolutionary changes in the Calcarina lineage are most helpful for determination of the horizons, particularly because they are among the most numerous species in the assemblage.

In some other cases, the preservation of ostracodes and foraminifers also is important in identifying provenance. For example, conspicuous brown specimens of long-ranging species clearly could be identified as originating from deeper zones II-MM. Also, in the injection dikes between 189 and 208 ft bsf and at 233 ft bsf in OPZ-18, the preservation state is almost identical to that of specimens in the upper part of zone AA; therefore, the origin of even non-diagnostic species with the appropriate shell preservation can be shown confidently to be from zone AA.

RESULTS

The following results can be shown from our current studies of samples from OAK crater.

Central Crater (Ground Zero) Boreholes

Boreholes OBZ-4 and OPZ-18 were cored near ground zero in OAK crater; we examined 39 and 21 samples, respectively, from each. The following is an informal zonation of the crater-fill materials based on the characteristics of the mixing of microfossils. The zones of material in the crater-fill from top to bottom are: (1) the **Homogenized Zone,** (2) the **Upwardly Mixed Zone,** (3) the **Maximum Piping Zone,** and (4) the **Basal Mixed Zone.** The boundaries between these zones are gradational and their depths approximate. In addition, we examined material from several injection dikes. The results are based on the ostracode-occurrence data given in Appendices 3-3 and 3-4, many of which are presented graphically in Figures 3-3 and 3-4, and the benthic foraminifer data is summarized in Tables 3-2 through 3-6, located at the end of this Chapter immediately preceeding the Appendices. To appreciate the nature of the mixing described in the next few pages and to see the actual percentage values, it is useful to compare directly the "normal" pattern of ostracodes (figs. 3-1 and 3-2) with that of the mixed sequence (figs. 3-3 and 3-4).

Homogenized Zone (0 to 40 ft). -- In this interval, high percentages (50 to 60%) of Neonesidea schulzi with preserved setae and specimens of Discorbis and Cymbaloporetta with chitinous inner linings originated from the Surface. High percentages of AA species, low to moderate numbers of specimens from CC, low to moderate occurrences of EE-GG species, low percentages of presumably piped specimens of II-MM species, and 3 to 6% BB-CC mixed material also characterize the Homogenized Zone. In general, this interval is easily identified by its anomolously high species diversity, resulting from the homogenization of material from virtually all zones with apparently equal contributions from most sub-AA zones. Specimens from the Homogenized Zone are characterized by widely varying preservation states.

Upwardly Mixed Zone (40 to 100 ft). -- This interval contains consistently low percentages of EE-GG ostracodes and greater percentages of piped material from zones II-MM than occur in the upper 40 ft of OAK crater-fill. The absence of surface material is conspicuous (with the exception of a single sample from 84 ft bsf from OBZ-4). Some samples from the Upwardly Mixed Zone contain less AA material than the overlying Homogenized Zone; in others, zone AA foraminifers still predominate. This interval characteristically contains moderate amounts of BB-CC material. The boundary between the Homogenized Zone and the underlying Maximum Piping Zone is not sharp, although this may be due to sample spacing. However, the relative contributions to the Upwardly Mixed Zone of foraminifers and ostracodes from various zones are quite distinct from the rest of the crater- fill. The piped specimens from this zone are from KK-LL and possibly from MM.

Maximum Piping Zone (100 to 160 ft). -- The highest percentages of piped specimens (9 to 12% in both OBZ-4 and OPZ-18) occur in this zone. LL-MM zone foraminifers and ostracodes are common at 121.8 ft bsf in OBZ-4, where at least eight separate ostracode species were emplaced from depth. Low percentages of AA foraminifers are characteristic of the upper part of the Maximum Piping Zone; however, no definite AA ostracodes or foraminifers are recorded from below about 125 ft in OBZ-4. This interval contains low to moderate numbers of specimens from zones CC and EE-GG. Here, piped foraminifers are not as obvious in OPZ-18 as in OBZ-4. Anomolously large numbers of single ostracode valves and still-articulated carapaces are broken

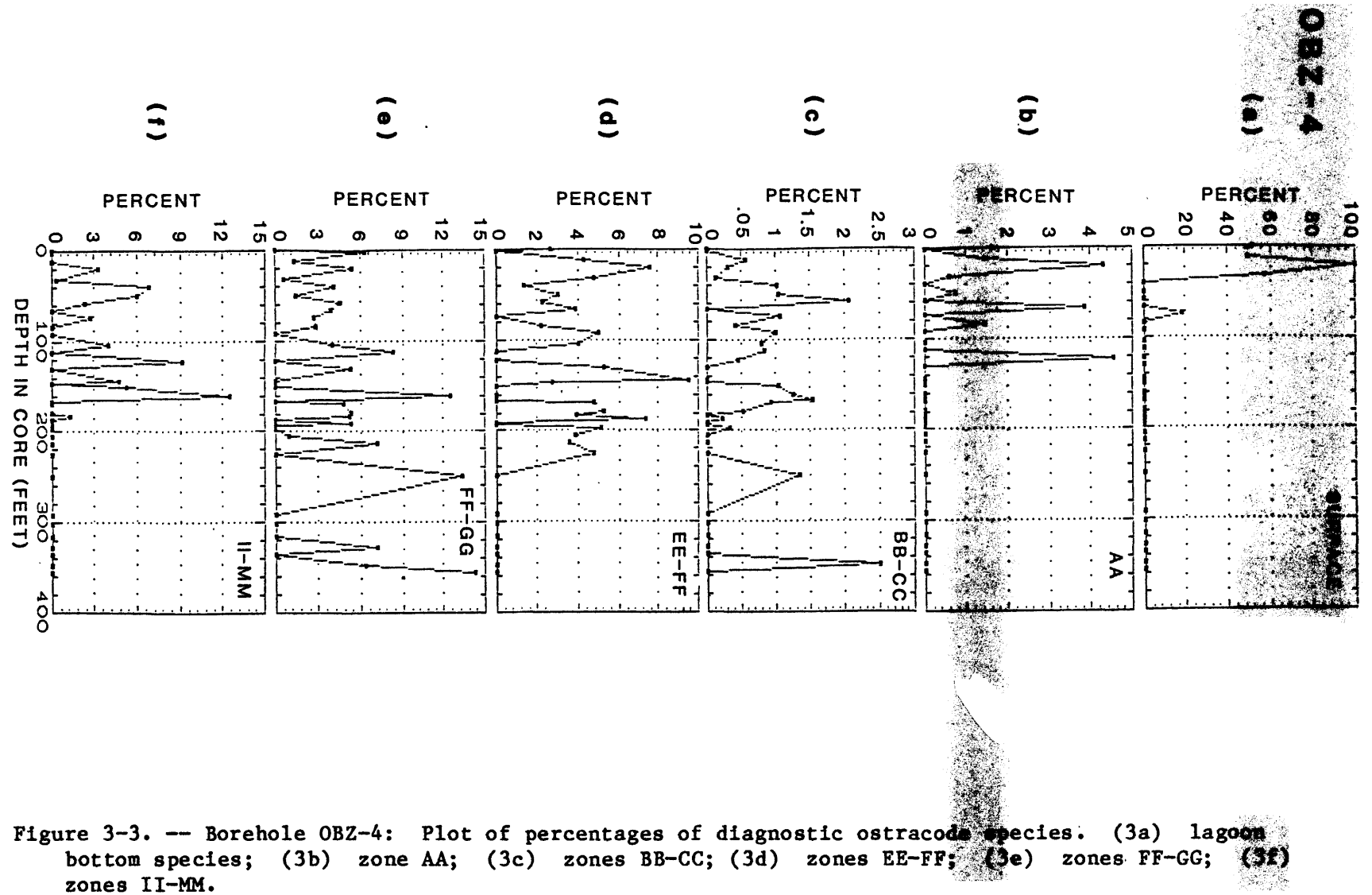

Figure 3-3. -- Borehole OBZ-4: Plot of percentages of diagnostic ostracoda species. (3a) lagoon bottom species; (3b) zone AA; (3c) zones BB-CC; (3d) zones EE-FF; (3e) zones FF-GG; (3f) zones II-MM.

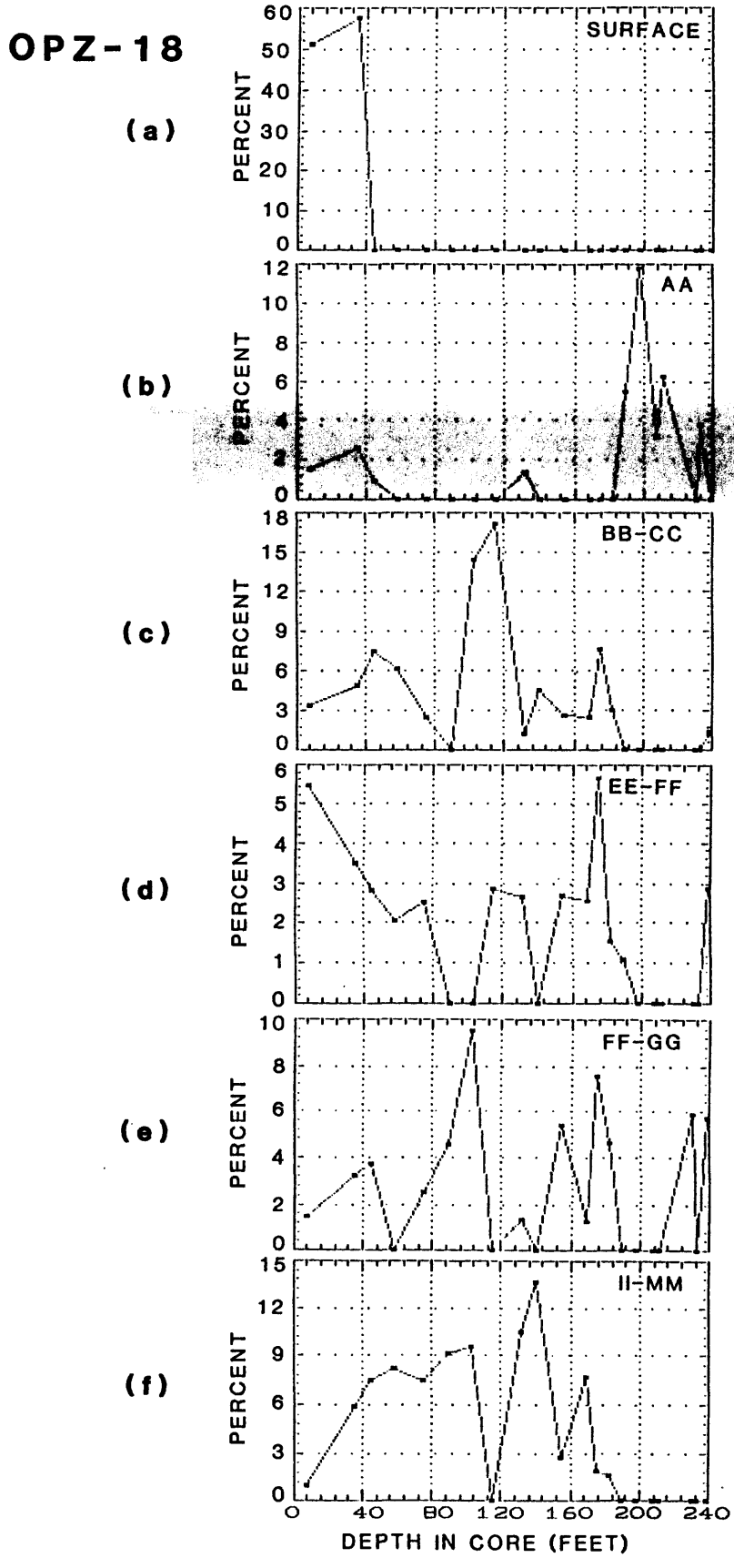

Figure 3-4. -- Borehole OPZ-18: Plot of percentages of diagnostic ostracode species. (4a) species from lagoon floor; (4b) zone AA; (4c) zones BB-CC; (4d) zones [illegible]; (4e) zones FF-GG; (4f) zones II-MM.

in samples from the Maximum Piping Zone, suggesting a kind of shock fracturing. The base of the Maximum Piping Zone is marked by an abrupt drop in the percentage of piped specimens in the samples.

Basal Mixed Zone (160 to 190 ft). -- The Basal Mixed Zone contains low percentages of piped material, low percentages of zone AA foraminifers, and high percentages of zone EE-FF material. Most of the sediment in the Basal Mixed Zone probably originated from zones EE and FF.

Statistical Analysis of Crater-Fill Materials. -- A simple linear-regression analysis of depth versus percentage of piped specimens was performed for samples from the upper 160 ft of OBZ-4 and the upper 145 ft of OPZ-18 (i.e., for all of the samples taken from above the Basal Mixed Zone in both boreholes). This statistical analysis was conducted to further analyze piping in the crater-fill from boreholes OBZ-4 and OPZ-18. Figures 3-5a and 3-5b show this relationship for 20 upper samples from OBZ-4 and 14 samples from OPZ-18. A positive correlation exists with correlation coefficients of $r = 0.46$ and $r = 0.52$, respectively. If samples from these depth intervals containing no piped specimens are excluded (9 samples in OBZ-4, 1 in OPZ-18; see Appendices 3-3 and 3-4), the correlation coeffecients are much higher, $r = 0.64$ and $r = 0.93$, respectively (figs. 3-5c and 3-5d). The absence of piped specimens in some samples may be a result of the small number of specimens that could be extracted. Nonetheless, in both boreholes there is a positive correlation, suggesting a diminishing contribution of piped material toward the upper intervals of crater-fill.

Injection Dikes. -- Injection dikes were sampled only in borehole OPZ-18 from 189 to 208 ft and 233 ft bsf. Well-preserved AA foraminifers and ostracodes and many articulated, translucent ostracode carapaces occur in these samples. Bright-red Homotrema is also common. The samples from 189.25, 198.0, and 207.3 ft bsf are composed of almost identical assemblages of species, and the preservation is almost identical also. In these dikes, material from BB-CC is conspicuously missing. All evidence suggests an origin for almost all material between 189 and 208 ft from the upper part of zone AA; however, the lack of Neonesidea schulzi with setae argues against any material originating from the Surface. The sample at 210.4 ft contains recrystallized microfossils, and the samples at 229.95 and 232.1 ft bsf contain zone AA species. These are mixed with zone EE-GG species. No piped II-MM zone material occurs in this dike.

Transition Boreholes

Transition boreholes OCT-5, OFT-8, and OKT-13 were sampled for microfossils for the current mixing study.

OCT-5. -- Samples from borehole OCT-5 were analyzed semiquantitatively for ostracodes (Appendix 3-5) and foraminifers. Both microfossil groups, particularly ostracodes, are much less abundant than in samples from OBZ-4 and OPZ-18, and the following zonation is based more heavily on the foraminifers.

0-9 ft. -- Samples from this interval in OCT-5 have anomolously high diversity, with approximately equal contributions from all mid-upper zones (AA-GG), as was the case in the Homogenized Zone of OBZ-4 and OPZ-18. A few piped foraminifers are found at 8.8 ft bsf.

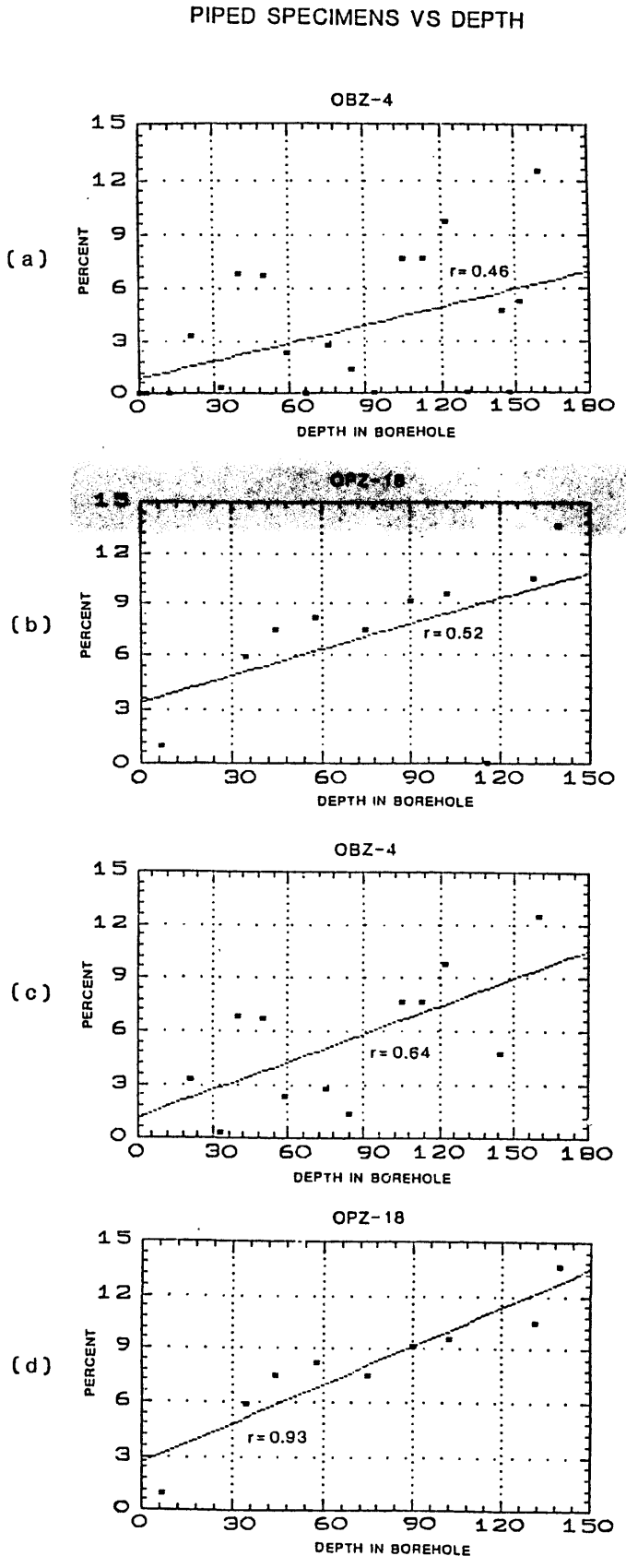

Figure 3-5. -- Plot of percentages of piped specimens versus depth. (5a) borehole OBZ-4, upper 160 ft; (5b) borehole OPZ-18, upper 145 ft; (5c) borehole OBZ-4, upper 160 ft, samples having no piped specimens omitted; (5d) borehole OPZ-18, upper 145 ft, samples having no piped specimens omitted.

39-77 ft. -- Abundant zone AA foraminifers, sparse BB-CC ostracodes, and low percentages of EE-GG material are found in samples from these depths.

86-105 ft. -- Samples from here differ from the overlying ones in lacking zone AA species; this interval has mostly CC-GG foraminifers; however both ostracodes and foraminifers are extremely sparse.

113-140 ft. -- Zone AA species predominate in these samples; preservation of the specimens is similar to specimens from zone AA and bright-red Homotrema (indicative of zone AA) also occurs; samples from here contain low percentages of CC-GG foraminifers.

149-187 ft. -- In this borehole, samples from this interval are almost barren and contain no diagnostic species of either ostracodes or foraminifers. Part of the explanation for the paucity of ostracodes may be that zone EE (normally at roughly comparable depths in the reference boreholes) typically contains few ostracodes in the normal stratigraphic section. However, samples from 149 to 187 ft in OCT-5 also lack even benthic foraminifers, which do occur in zone EE.

OFT-8. -- This borehole has diagnostic microfaunas in all samples examined, allowing a threefold subdivision of the upper 75 ft (Appendix 3-6).

0-19 ft.-- This is a mixed interval containing material from zones AA to probably no deeper than FF. Samples from this interval resemble the Homogenized Zone of the upper parts of other central crater and transitional boreholes. In the uppermost sample at 0.0 to 0.25 ft bsf, a single foraminifer and a single ostracode specimen occur, suggesting piping from zones JJ-MM.

27-50 ft. -- This interval consists almost entirely of material from zone AA, as indicated by the foraminifers. The ostracode species also occur typically in AA and are preserved like those from that zone. There is a noticable absence of zone BB-CC material, also indicating a lack of mixing.

64-75 ft. -- At 64 ft bsf, a mixture of AA and sparse FF-GG foraminifers occurs with typical BB-CC ostracodes. The 74.0-ft sample appears to be from sediment that is essentially in place and consists exclusively of BB-CC material. A detailed sampling across the interval from 50 to 75 ft would be necessary to better document the transition into undisturbed sediments at this borehole site.

OKT-18. -- This borehole contained highly diagnostic ostracodes and foraminifers that allowed a fourfold subdivision of the upper 80 ft (Appendix 3-11). The results from the two fossil groups match each other more consistently, and, thus, these zones are more definitive than in any borehole yet analyzed.

0-19 ft. -- Samples from this interval are noted for their anomolously high species diversity and homogenization of zone AA-GG material. These samples resemble those from the uppermost parts of boreholes OBZ-4, OPZ-18, and OCT-5. No piped specimens are found.

25-37 ft. -- These samples contained almost exclusively material from zone AA; small percentages from EE-GG are noted from the sample at 25.4 ft

bsf. The microfaunas from this interval resemble those from the injection dike in OPZ-18 in both species composition and preservation.

55-66 ft. -- The samples studied contain only material from zones CC-DD. Especially noteworthy is the occurrence of Paracytheridea remanei (which has its acme in DD in all reference boreholes) in OKT-13 at 55.65 (abundant), 59.9, and 68.3 ft. Also, the abundance of Orionina sp. at 59.9 ft is noteworthy. This latter very distinctive species is abundant in OAR-2A at 62 to 75 ft, and a biostratigraphic correlation is probable for strata between 59.9 ft in OKT-13 and 62-75 ft in borehole OAR-2A.

68-81 ft. -- A typical EE-FF assemblage occurs in this interval; there is no obvious mixing from AA or BB.

SUMMARY AND CONCLUSIONS

Our primary conclusions from the mixing study for the OAK crater area follow:

1. Piped material: an inverse relationship exists between sample depth and the percentage of piped material (from zones II-MM) in OBZ-4 between the surface and 160 ft bsf and in OPZ-18 between the surface and 145 ft bsf. Sparse piped specimens occur in the upper 10 ft of OCT-5 and the upper 1 ft of OFT-8; no piped specimens were found in OKT-13.

2. Mixing of abundant Surface material occurs in OBZ-4 and OPZ-18 downward to a depth of 35 ft, although sparse specimens from the Surface occur as deep as 84 ft in OBZ-4.

3. Mixing of abundant material from zone AA is evident in OBZ-4 and OPZ-18 to about 50 to 60 ft bsf; AA material is less common to a depth of about 120 ft bsf in both boreholes.

4. Mixing of moderate amounts of material from zones EE-GG (occurring from 100 to 300 ft bsf in the normal stratigraphic sequence) is encountered in the upper 100 ft of the two central-crater boreholes (OBZ-4 and OPZ-18) and in the upper 20 ft of the transition boreholes. Mixing of BB-CC material is less significant than that of EE-GG material in all boreholes.

5. An apparent injection dike between 189 and 208 ft bsf in OPZ-18 contains almost exclusively AA microfossils. In addition, sediment from these dikes is greenish-gray, like that from the normal AA section. Distinctive microfaunas at 25 to 37 ft in OKT-13 and 27 to 50 ft in OFT-8 are extremely similar to those in this injected OPZ-18 material, although it is not clear if they are genetically related.

6. A Homogenized Mixed Zone containing approximately equal proportions of AA-GG material is a general characteristic of all central-crater (ground-zero) boreholes (down to 40 ft) and in transition boreholes (down to 20 ft).

7. The overall consistency between the ostracodes and foraminifers and our ability to quantitatively revise the standard and mixing zonations to a high degree of resolution gives us confidence that the only limits to our ability to further refine zonations of mixed material, to more accurately identify provenance, and to improve volumetric computations of mixed materials are manpower constraints and sample/core recovery.

REFERENCES

Brouwers, E.M., Cronin, T.M., and Gibson, T.G., 1986, Chapter 11: Additional paleontologic studies, OAK and KOA Craters: 18 p., 5 figs., 5 tbls., 1 pl.; in Henry, T.W., and Wardlaw, B.R., editors, Pacific Enewetak Atoll Crater Exploration (PEACE) Program, Enewetak Atoll, Republic of the Marshall Islands; Part 3: Stratigraphic analysis and other geologic and geophysical studies in vicinity of OAK and KOA craters: U.S. Geological Survey Open-file Report 86-555.

Cronin, T.M., Brouwers, E.M., Bybell, L.M., Edwards, L.E., Gibson, T.G., Margerum, R., and Poore, R.Z., 1986, Pacific Enewetak Atoll Crater Exploration (PEACE) Program, Enewetak Atoll, Republic of the Marshall Islands: Part 2; Paleontology and biostratigraphy, application to OAK and KOA craters. U.S. Geological Survey Open-file Report 86-159, 39 p., 20 figs., 12 tbls., 3 appendices.

Gibson, T.G. and Hill, E.E., in preparation, Late Pliocene to Holocene benthonic Foraminifera from Enewetak Atoll.

Henry, T.W., and Wardlaw, B.R., 1986, Chapter 1: Introduction: 13 p., 3 figs., 1 tbl.; in Henry, T.W., and Wardlaw, B.R., editors, Pacific Enewetak Crater Exploration (PEACE) Program, Enewetak Atoll, Republic of the Marshall Islands; Part 3: Stratigraphic analysis and other geologic and geophysical studies in vicinity of KOA and OAK craters: U.S. Geological Survey Open-File Report 86-555.

Henry, T.W., Wardlaw, B.R., Skipp, B., Major, R.P., and Tracy, J.I., Jr., 1986, Pacific Enewetak Atoll Crater Exploration (PEACE) Program, Enewetak Atoll, Republic of the Marshall Islands: Part 1; Drilling operations and descriptions of the boreholes in the vicinity of KOA and OAK craters: U.S. Geological Survey Open-File Report 86-419, 497 p., 32 figs., 29 pls., 13 tbls., 3 appendices.

Wardlaw, B.R., and Henry, T.W., 1986, Chapter 14: Geologic interpretation of OAK and KOA craters; 39 p., 21 figs., 2 tbls.; in Henry, T.W., and Wardlaw., B.R., editors, Pacific Enewetak Atoll Crater Exploration (PEACE) Program, Enewetak Atoll, Republic of the Marshall Islands; Part 3: Stratigraphic analysis and other geologic and geophysical studies in vicinity of KOA and OAK craters: U.S. Geological Survey Open-File Report 86-555.

Table 3-2.--Summary of foraminifer occurrences in OAK crater borehole OBZ-4.

DEPTH (ft bsf)	FORAMINIFER DATA
2.8-3.05	Mostly AA, some mixing from CC-GG (most likely CC), piping from KK-MM.
11.8-12.05	Mostly AA, moderate amount of CC-GG (most likely CC), piping from JJ-KK.
21.1-21.35	Moderate amount of AA, some CC and EE-GG, piping from II-KK.
33.0-33.25	Mostly AA, mixed with minor CC.
40.05-40.3	Moderate amounts of AA, CC, and EE-GG, moderate amount of piping from II-LL.
58.50-58.75	Mixed AA, CC, and EE-GG, moderate amount of piping from KK-LL.
66.35-66.60	Mixed AA, CC, and EE-GG, more of ?CC or EE-GG than in above sample, some brown specimens presumably from KK-LL.
75.15-75.4	Mixed AA, CC, and EE-GG, more of EE-GG, some brown specimens presumably from KK-LL.
84.15-84.4	Mixed AA, CC, and EE-GG, some piping from KK-LL, possibly MM.
93.1-93.35	Mostly CC and EE-GG, sparse AA, some brown specimens presumably from KK-LL.
104.55-104.8	Mostly CC and EE-GG, sparse AA, piping from KK-LL.
112.9-113.15	No definite AA; some from ?CC, definite EE-GG, piping from KK-LL and possibly from MM.
121.8-122.05	Definite AA and CC and ?EE-GG, some piping from KK-LL.
130.0-130.25	Mostly CC with some EE-GG, sparse brown specimens possibly from deeper zones.
144.5-144.75	?CC and EE-GG.
151.55-151.8	?CC and EE-GG, some brown specimens presumably from deeper zones.
166.85-167.1	?CC and EE-GG.
178.6-178.85	?CC and EE-GG, some brown specimens presumably from deeper zones.
186.8-187.05	?CC and EE-GG.
193.6-193.85	?CC and EE-GG.
196.5-196.75	EE-GG (probably FF) with ?CC.
205.1-205.35	EE-GG (probably FF) with ?CC.
213.9-214.15	EE-GG.
225.65-225.9	EE-GG.

Table 3-3.--Summary of foraminifer occurrences in OAK crater borehole OCT-5.

DEPTH (ft bsf)	FORAMINIFER DATA
0.2-0.45	Specimens from EE-GG, abundant AA, CC; some specimens from II-MM.
8.80-9.05	Mostly specimens from EE-GG, some from AA, some from KK-MM.
17.5-17.75	Some EE-GG, probably BB-CC, no AA.
39.50-39.75	AA and EE-GG with possibly CC and possibly deep zones.
57.55-57.8	Abundant AA and EE-GG.
66.8-67.05	Abundant AA, probable CC and definite EE-GG.
76.65-76.9	Mostly AA, some EE-GG.
86.15-86.4	All from CC-GG, no AA.
95.35-95.6	Same as above sample.
104.25-104.5	Very few specimens, but similar to above sample.
113.15-113.4	Few specimens, definite AA dominant, some from CC.
124.0-124.25	Abundant AA, sparse specimens probably from CC, possibly CC-GG.
132.8-133.05	Almost entirely AA, few specimens from CC or CC-GG.
140.9-141.15	Same as above sample.
149.65-149.9	Barren.
159.6-157.85	Only 1 specimen probably from CC, possibly from BB-GG.
166.4-166.65	Only 1 specimen, provinence uncertain.
176.25-176.5	Only 1 specimen, provinence uncertain, probably CC-GG.
186.0-186.25	Few specimens of CC-GG, probably CC.

Table 3-4.--Summary of foraminifer occurrences in OAK crater borehole OFT-8.

DEPTH (ft bsf)	FORAMINIFER DATA
0.0-0.25	Few specimens, definitely AA (but not uppermost AA), few specimens from EE-GG, scattered light-brown material with 1 immature specimen possibly from JJ-MM, not certain there is deep material.
8.75-9.00	More abundant AA (with more from uppermost AA), sparse specimens from CC, moderate amount from EE-GG, no brown material.
18.60-18.85	Abundant specimens from upper AA, few specimens probably from EE-GG.
27.90-28.15	All specimens from upper part of AA.
35.1-35.35	All specimens from upper part of AA.
43.1-43.35	All specimens from AA, probably slightly lower AA than two samples above.
48.85-49.1	All specimens from AA.
64.0-64.25	Mixture of older part of AA with few from EE-GG.
74.0-74.25	Appears to be unmixed BB-CC.

Table 3-5.--Summary of foraminifer occurrences in OAK crater borehole OKT-13.

DEPTH (ft bsf)	FORAMINIFER DATA
10.4-10.65	Mostly EE-GG, some from lower AA.
18.5-18.75	Mostly CC, some from EE-GG mixed with specimens from AA.
25.4-25.65	Specimens from ?CC mixed with few from EE-GG, more abundant AA than in above two samples
28.75-29.00	All from AA.
36.00-36.25	All from AA.
55.65-55.90	All apparently from CC-DD.
59.5-59.75	All probably from CC-DD.
68.2-68.45	All probably from EE-FF, possibly some CC-DD.
80.00-80.25	All from CC-GG.

Table 3-6.--Summary of foraminifer occurrences in OAK crater borehole OPZ-18.

DEPTH (ft bsf)	FORAMINIFER DATA
7.0-7.25	Mostly AA, with some CC and EE-GG mixed, has light-brown material but no diagnostic specimens.
35.0-35.25	Mostly AA, with some CC and EE-GG mixed, has more light-brown material than above sample but only one probable specimen from KK-MM.
44.6-44.85	AA, with some CC and more EE-GG than above, moderate amount of light-brown material but no diagnostic specimens.
57.85-58.1	More AA than above sample, with EE-GG common, moderate amount of light-brown material but no diagnostic specimens.
74.3-74.55	Mostly AA with some specimens from EE-GG, moderate amount of light-brown but no diagnostic specimens.
89.45-89.7	Mostly AA with some EE-GG, moderate amount of light-brown material with 1 specimen possibly from KK-LL.
102.0-102.25	Few specimens, some AA, some EE-GG, and moderate amount of light-brown material with one specimen questionably from LL-MM.
115.05-115.3	Few specimens, some AA, some EE-GG, moderate amount of light-brown material.
131.0-131.25	Few specimens, some AA, some EE-GG, 1 specimen possibly from KK-MM.
139.7-139.95	Some AA, some EE-GG, some light-brown material.
154.2-154.45	Some AA, some EE-GG, some light-brown material.
169.35-169.6	Some AA and some EE-GG, sparse light-brown material.
174.95-175.1	Some EE-GG, some probably AA, mostly uncertain.
182.3-182.55	Some AA, some EE-GG, very little light brown material.
189.25-189.5	All AA, apparently upper AA.
198.0-198.25	All AA, apparently upper AA.
207.3-207.55	All AA, apparently upper AA.
210.4-210.65	All recrystallized, but no markers??
229.95-230.2	No diagnostic species, most look like ?CC-GG, possibly few AA.
232.1-232.35	Mostly AA, probably upper A, except for 1 specimen from EE-GG.
239.15-239.4	Appearently all EE-GG, probably FF-GG.

BOREHOLE OAR-2/2A

	DIAGNOSTIC SPECIES	SAMPLE DEPTH (ft bsf) 0.25	2.3	6.0	9.3	11.85	14.5	17.1	20.8	22.75	23.75	26.05	31.9	34.75	40.2	43.55	62.5	74.8	90.4	95.8
1.	*Australimoosella* sp.	-	-	-	-	-	-	-	-	-	-	-	-	-	-	-	-	-	1	2
2.	*Bythoceratina* sp.	-	-	-	-	-	-	-	-	-	-	-	-	-	-	-	-	-	-	-
3.	*Callistocythere* sp. A	-	-	-	-	-	-	-	6	2	2	-	-	-	1	-	4	1	-	-
4.	*C.* sp. B	-	-	1	3	-	1	2	1	-	-	-	1	-	-	-	-	-	1	2
5.	*Cardobairdia* sp.	-	-	-	-	-	3	-	1	-	1	-	-	-	-	-	-	-	-	-
6.	*Caudites* sp. A	-	-	-	-	-	-	-	-	-	-	-	-	-	-	-	-	-	2	-
7.	*C.* sp. B	-	-	-	-	-	-	-	-	-	-	-	-	-	-	-	-	-	2	2
8.	*Cletocythereis* sp. A	-	-	-	-	-	-	-	-	-	-	-	1	1	-	-	-	1	7	2
9.	*C. canaliculata*	-	-	-	-	-	-	-	-	-	-	-	-	-	-	-	-	-	-	-
10.	*C. rastromarginata*	-	-	-	-	-	-	-	-	-	-	-	-	-	-	-	-	-	-	-
11.	*Cytherelloidea* sp.	-	-	-	-	-	4	-	-	-	-	-	-	-	-	-	-	-	-	-
12.	*Hemicytherura* sp.	-	-	-	-	-	-	-	-	-	-	-	-	-	-	-	1	-	4	-
13.	*Hemicythere* sp.	-	-	1	-	-	1	1	1	-	-	-	-	-	-	-	-	-	-	-
14.	*Hermanites mooneyi*	1	-	-	10	4	9	11	2	2	-	-	-	-	-	-	-	-	-	-
15.	*H. parviloba*	1	1	9	6	-	-	-	21	-	-	-	-	-	-	2	1	-	7	4
16.	*H. transoceanica*	4	1	4	8	12	10	3	6	-	3	-	-	1	-	-	-	2	9	5
17.	*Jugosocythereis* sp.	5	-	4	16	4	5	2	33	20	-	-	-	1	-	-	-	17	9	5
18.	*Keijia demissa*	-	-	-	-	-	-	-	-	-	-	-	-	-	-	-	-	-	2	3
19.	*Loxoconcha heronislandensis*	-	-	-	-	-	-	-	-	-	-	-	16	3	-	5	-	-	-	8
20.	*L. huahinensis*	8	2	9	32	45	31	30	17	4	1	8	4	-	-	-	10	6	61	20
21.	*L. insulardasnsis*	-	-	-	-	-	-	-	-	-	-	-	-	-	-	2	-	3	11	1
22.	*L. labrynthica*	-	-	-	-	-	-	-	-	-	-	-	-	-	-	-	-	2	1	7
23.	*L.* n. sp. A	-	-	-	-	-	-	-	-	-	-	-	-	-	-	-	-	-	-	-
24.	*Loxoconchella* sp. A	-	-	2	2	-	-	-	2	2	-	-	-	-	-	-	-	-	-	-
25.	*L.* sp. B	-	-	-	-	-	-	-	-	-	-	-	-	-	-	-	-	-	1	-
26.	*L.* sp. C	-	-	-	-	-	1	1	-	-	-	-	-	-	-	-	-	-	-	3
27.	*Miocypridеis* sp.	-	-	-	-	-	-	-	-	-	-	-	-	-	-	-	-	-	-	-
28.	*Morkhovenia inconspicua*	-	-	-	-	2	-	-	-	-	1	-	1	-	-	-	2	-	-	-
29.	*Neonesidea schulzi*	3	-	11	23	1	13	9	28	23	54	-	21	-	-	-	1	5	9	9
30.	*Occultocythereis* sp.	-	-	-	-	-	1	1	-	-	-	-	-	-	-	-	-	-	-	-
31.	*Orionina* sp.	-	-	-	-	-	-	-	-	-	-	-	-	-	-	-	14	5	-	-
32.	*Ornatoleberis* sp.	2	-	4	6	5	5	9	3	-	-	-	-	-	-	-	-	1	-	-
33.	*Paracytheridea remani*	1	-	-	1	-	3	3	1	-	-	-	-	-	-	-	-	-	10	3
34.	*Ponticocythereis* sp.	-	-	-	-	-	-	-	-	-	-	-	-	-	-	-	1	-	-	-
35.	*Procythereis* sp. A	-	-	-	-	-	-	-	-	-	-	-	-	-	-	-	-	-	-	-
36.	*P.* sp. B	-	-	-	-	-	-	-	-	-	-	-	-	-	-	-	-	-	-	-
37.	*Pterobairdia maddocksae*	-	-	-	-	-	-	-	-	-	-	-	-	-	-	-	-	-	-	-
38.	*Semicytherura* sp.	-	-	-	1	-	3	-	-	-	-	-	-	-	-	-	-	-	1	-
39.	*Triebelina sertata*	-	-	-	-	-	-	1	-	-	-	-	-	-	-	-	-	-	-	-
40.	Other	10	1	24	43	37	37	25	67	35	39	7	7	24	17	4	9	9	42	29
	TOTAL	35	5	69	151	110	127	98	189	88	101	15	51	30	23	13	43	52	180	105

(continued on next page)

BOREHOLE OAR-2/2A (continued)

	DIAGNOSTIC SPECIES	SAMPLE DEPTH (ft bsf)																		
		115.1	127.8	134.0	157.45	171.2	188.25	195.3	204.9	212.45	223.9	234.6	244.55	246.8	268.45	282.55	289.7	337.05	379.5	TOTAL
1.	*Australimoosella* sp.	-	-	-	-	-	-	1	1	1	1	1	2	9	2	3	1	-	-	25
2.	*Bythoceratina* sp.	-	-	-	-	-	-	-	1	-	-	-	-	-	-	-	-	-	-	1
3.	*Callistocythere* sp. A	-	-	-	-	-	-	-	-	-	-	-	-	-	-	-	-	-	-	16
4.	*C.* sp. B	2	-	-	1	-	-	-	2	5	13	-	1	-	2	-	-	-	-	38
5.	*Cardobairdia* sp.	-	-	-	-	-	-	-	-	-	-	-	-	-	-	-	-	-	-	5
6.	*Caudites* sp. A	-	-	-	-	-	-	-	1	-	2	-	-	2	-	1	-	-	-	8
7.	*C.* sp. B	-	-	-	-	-	-	-	-	-	-	-	4	1	-	-	1	-	-	10
8.	*Cletocythereis* sp. A	-	-	-	-	-	2	5	-	-	1	-	-	1	-	-	-	-	-	21
9.	*C. canaliculata*	-	-	-	1	-	-	-	-	-	-	6	3	-	-	1	-	-	1	12
10.	*C. rastromarginata*	1	1	-	-	-	-	-	6	1	-	-	-	-	-	-	-	-	-	9
11.	*Cytherelloidea* sp.	-	-	-	-	-	-	-	-	-	-	-	-	-	-	-	-	-	-	4
12.	*Hemicytherura* sp.	-	-	-	-	-	-	-	-	-	3	-	1	-	-	-	-	-	-	9
13.	*Hemicythere* sp.	-	-	1	-	-	-	-	4	-	-	-	-	-	-	-	-	-	-	9
14.	*Hermanites mooneyi*	-	-	-	-	-	-	-	-	-	-	-	-	-	5	-	-	-	-	44
15.	*H. parviloba*	-	-	9	-	-	-	-	16	2	23	1	-	5	-	-	3	-	-	111
16.	*H. transoceanica*	5	-	8	-	-	-	-	4	1	14	3	10	13	7	-	8	-	1	142
17.	*Jugosocythereis* sp.	2	2	4	1	-	-	1	9	7	13	7	9	20	7	-	10	-	5	218
18.	*Keijia demissa*	-	-	-	-	-	-	-	-	-	-	-	-	-	-	-	-	-	-	5
19.	*Loxoconcha heronislandensis*	-	4	-	-	-	-	-	-	-	-	-	-	-	-	-	-	-	-	36
20.	*L. huahinensis*	1	18	30	37	-	2	7	82	34	51	8	31	12	15	10	24	-	27	679
21.	*L. insulardaensis*	-	-	-	-	-	-	-	13	8	3	7	9	4	3	2	4	-	4	77
22.	*L. labrynthica*	2	-	5	-	-	-	-	-	-	-	6	5	6	6	3	2	-	1	46
23.	*L.* n. sp. A	-	-	-	-	-	-	-	-	-	-	-	-	-	10	7	6	-	2	25
24.	*Loxoconchella* sp. A	-	-	-	-	-	-	-	-	-	-	-	-	-	-	-	-	-	-	8
25.	*L.* sp. B	-	-	-	1	-	-	-	-	-	-	-	-	-	-	-	-	-	-	2
26.	*L.* sp. C	-	2	-	1	-	-	-	-	-	-	-	-	1	-	-	-	-	3	12
27.	*Miocyprideis* sp.	-	-	-	-	-	-	-	15	14	9	-	-	-	2	4	-	-	1	45
28.	*Morkhovenia inconspicua*	-	-	2	-	-	-	-	4	-	-	-	3	4	1	-	1	-	-	21
29.	*Neonesidea schulzi*	8	-	3	15	1	1	-	10	4	1	2	3	-	-	-	1	-	1	260
30.	*Occultocythereis* sp.	-	-	-	-	-	-	-	-	-	-	-	-	-	-	-	-	-	-	2
31.	*Orionina* sp.	-	-	-	-	-	-	-	-	-	-	-	-	-	-	-	-	-	-	19
32.	*Ornatoleberis* sp.	-	1	5	-	-	-	-	9	-	3	-	-	-	-	-	-	-	-	53
33.	*Paracytheridea remani*	-	-	-	1	-	-	-	-	-	1	-	-	-	-	-	-	-	1	25
34.	*Ponticocythereis* sp.	-	-	-	-	-	-	-	-	-	-	-	-	-	-	-	-	-	-	1
35.	*Procythereis* sp. A	-	-	-	-	-	-	-	13	4	5	-	2	-	-	1	-	-	7	32
36.	*P.* sp. B	-	-	-	-	-	-	-	-	-	11	-	-	-	-	-	-	-	-	11
37.	*Pterobairdia maddocksae*	-	-	-	-	-	-	1	-	-	-	1	-	-	-	-	-	-	-	2
38.	*Semicytherura* sp.	-	-	-	-	-	-	-	1	-	1	2	6	2	1	1	-	-	-	19
39.	*Triebelina sertata*	-	-	-	-	-	-	1	1	-	-	-	-	-	-	-	-	-	-	3
40.	Other	12	14	9	18	-	1	7	38	44	41	29	28	31	55	21	19	1	34	868
	TOTAL	33	42	76	76	1	6	23	230	125	196	73	117	111	116	54	80	1	88	2933

BOREHOLE OOR-17

	DIAGNOSTIC SPECIES	SAMPLE DEPTH (ft bsf)																					
		0.25	14.15	25.75	38.4	49.7	60.2	66.75	72.8	83.7	89.8	100.45	101.4	110.5	119.1	125.25	131.95	137.15	146.1	154.25	165.6	173.05
1.	*Australimoosella* sp.	-	-	-	-	-	-	-	-	-	-	-	-	-	-	-	-	2	2	-	-	-
2.	*Bythoceratina* sp.	-	-	-	-	-	-	-	-	-	-	-	-	-	-	-	-	-	-	-	-	-
3.	*Callistocythere* sp. A	-	-	-	18	-	2	2	1	1	2	6	1	-	-	3	3	1	1	-	1	-
4.	*C.* sp. B	-	-	-	-	-	-	-	-	-	-	-	-	-	-	9	-	-	-	-	1	10
5.	*Cardobairdia* sp.	-	-	2	-	1	-	1	-	-	-	1	-	-	-	-	-	-	-	-	-	-
6.	*Cauditee* sp. A	-	-	-	-	-	-	-	-	-	-	-	-	-	-	-	-	-	1	1	1	-
7.	*C.* sp. B	-	-	-	-	-	-	-	-	-	-	-	-	-	-	1	-	-	-	-	-	-
8.	*Cletocythereis* sp. A	-	-	-	-	-	-	-	42	16	8	-	1	3	-	1	1	2	2	1	1	2
9.	*C. canaliculata*	-	-	-	-	-	-	-	-	-	-	-	-	-	-	-	-	-	-	-	-	-
10.	*C. rastromarginata*	-	-	-	-	-	-	-	-	-	-	-	-	-	-	-	-	1	-	-	-	-
11.	*Cytherelloidea* sp.	-	-	1	-	-	-	-	-	-	-	-	-	-	-	-	-	-	-	-	-	-
12.	*Hemicytherura* sp.	-	-	-	-	-	-	-	-	-	-	-	-	-	-	1	-	-	-	-	1	1
13.	*Hemicythere* sp.	-	1	-	-	-	-	-	-	-	-	-	-	1	-	-	-	-	-	-	-	-
14.	*Hermanites mooneyi*	-	-	2	-	1	-	-	-	-	-	-	-	-	-	-	-	3	1	-	2	-
15.	*H. parviloba*	1	2	2	3	2	17	19	-	-	-	-	-	-	-	2	1	6	-	2	-	-
16.	*H. transoceanica*	12	11	12	9	2	7	3	-	10	4	2	-	8	-	2	-	3	8	6	12	22
17.	*Jugosocythereis* sp.	8	2	1	-	2	7	18	-	-	-	-	-	1	-	3	-	8	-	6	10	11
18.	*Keijia demissa*	-	-	-	-	-	-	-	-	-	-	-	-	-	-	-	-	-	1	1	1	1
19.	*Loxoconcha heronislandensis*	-	-	-	-	-	-	-	7	8	6	10	2	23	-	-	-	-	-	-	-	-
20.	*L. huahineneis*	30	10	34	9	24	6	9	-	-	-	1	-	2	-	7	5	35	11	24	15	12
21.	*L. insulardaensis*	-	-	-	-	-	-	-	-	2	1	-	-	-	-	8	-	24	12	6	1	-
22.	*L. labrynthica*	-	-	-	-	-	-	-	-	-	-	-	-	-	-	-	-	-	2	6	3	10
23.	*L.* n. sp. A	-	-	-	-	-	-	-	-	-	-	-	-	-	-	-	2	-	-	-	-	-
24.	*Loxoconchella* sp. A	4	-	-	1	1	-	-	-	-	-	-	-	-	-	-	-	-	-	-	-	-
25.	*L.* sp. B	-	-	-	-	-	-	-	-	-	-	-	-	-	-	-	-	-	-	-	-	1
26.	*L.* sp. C	-	-	-	-	-	-	-	-	-	-	-	-	-	-	-	-	-	1	-	-	-
27.	*Miocyprideis* sp.	-	-	-	-	-	-	-	-	-	-	-	-	-	-	-	-	-	-	-	-	-
28.	*Morkhovenia inconspicua*	-	-	-	-	-	1	-	-	-	-	-	-	-	-	4	-	-	-	-	-	-
29.	*Neonesidea schulzi*	45	32	41	32	12	32	39	3	2	-	-	-	2	-	-	1	7	2	12	29	17
30.	*Occultocythereis* sp.	-	-	-	-	-	-	-	-	-	-	-	-	-	-	-	-	-	-	-	-	-
31.	*Orionina* sp.	-	-	-	-	-	-	-	-	-	-	-	-	-	-	-	13	-	-	-	-	-
32.	*Ornatoleberis* sp.	1	3	4	1	1	-	-	6	5	-	-	-	-	-	1	-	-	-	1	2	2
33.	*Paracytheridea remani*	2	1	1	-	-	-	-	1	-	-	-	-	31	-	2	-	6	2	7	5	6
34.	*Ponticocythereis* sp.	-	-	-	-	-	-	-	-	-	-	-	-	-	-	-	1	-	-	-	-	-
35.	*Procythereis* sp. A	-	-	-	-	-	-	-	-	-	-	-	-	-	-	-	-	-	-	-	-	-
36.	*P.* sp. B	-	-	-	-	-	-	-	-	-	-	-	-	-	-	-	-	-	-	-	-	-
37.	*Pterobairdia maddocksae*	-	-	1	-	-	-	-	-	-	-	-	-	-	-	-	-	-	-	-	-	-
38.	*Semicytherura* sp.	-	-	-	1	-	-	-	-	-	-	-	-	-	-	-	-	2	1	1	-	1
39.	*Triebelina sertata*	-	1	-	-	1	-	-	-	-	-	-	-	-	-	-	-	-	-	-	-	-
40.	Other	72	31	75	48	28	53	36	18	55	28	4	1	4	-	13	6	68	51	51	52	45
	TOTAL	175	94	176	122	75	125	127	78	99	49	24	5	75	-	57	33	168	98	125	137	141

(continued on next page)

BOREHOLE OOR-17 (continued)

	DIAGNOSTIC SPECIES	SAMPLE DEPTH (ft bsf)																			TOTAL
		184.25	193.6	200.8	209.3	215.5	226.05	233.35	239.0	250.3	261.5	270.1	285.65	292.1	299.15	310.7	320.2	331.2	339.0	367.9	
1.	*Australimoosella* sp.	-	-	-	-	-	-	1	-	-	-	-	4	-	-	-	-	3	2	0	14
2.	*Bythoceratina* sp.	-	-	-	-	-	-	-	-	-	-	1	-	-	-	-	-	-	-	-	1
3.	*Callistocythere* sp. A	5	-	-	-	-	-	-	-	-	-	-	-	-	-	-		-	-	-	47
4.	*C.* sp. B	-	-	-	-	-	1	2	-	1	-	-	-	-	1	-	-	-	-	-	25
5.	*Cardobairdia* sp.	-	-	-	-	-	-	-	-	-	-	-	-	-	-	-	-	-	-	-	5
6.	*Caudites* sp. A	1	-	-	-	-	-	4	1	-	-	1	1	-	-	-	-	-	-	-	11
7.	*C.* sp. B	-	-	-	-	-	-	-	-	-	-	4	-	-	-	-	-	-	-	-	5
8.	*Cletocythereis* sp. A	-	-	1	6	1	3	6	-	3	-	13	-	-	-	-	-	-	-	-	113
9.	*C. canaliculata*	-	-	-	-	-	-	3	-	-	-	-	-	-	1	-	-	1	2	-	7
10.	*C. rastromarginata*	2	-	1	1	-	-	1	-	-	-	-	1	-	-	-	-	-	-	-	7
11.	*Cytherelloidea* sp.	-	-	-	-	-	-	-	-	-	-	1	-	-	-	-	-	-	-	-	2
12.	*Hemicytherura* sp.	-	-	-	-	1	-	-	-	-	-	-	-	-	-	-	-	1	-	-	5
13.	*Hemicythere* sp.	-	1	1	-	-	-	-	-	-	-	-	-	-	-	-	-	-	-	-	4
14.	*Hermanites mooneyi*	-	-	-	-	-	-	-	-	-	-	-	-	-	-	-	-	-	-	-	9
15.	*H. parviloba*	1	-	11	5	-	-	-	-	-	-	-	9	-	4	-	-	-	-	-	87
16.	*H. transoceanica*	8	1	9	2	4	-	2	-	1	-	7	4	1	4	-	-	-	-	1	177
17.	*Jugosocythereis* sp.	11	-	6	4	2	-	-	-	-	-	1	1	2	2	1	1	7	2	-	117
18.	*Keijia demissa*	-	-	-	-	-	-	-	-	-	-	-	-	-	-	-	-	-	-	-	4
19.	*Loxoconcha heronislandensis*	3	-	-	-	-	-	-	-	-	-	-	-	1	-	-	-	-	-	-	60
20.	*L. huahinensis*	-	3	35	25	14	7	62	-	1	1	16	31	12	26	1	-	3	3	1	475
21.	*L. insulardaensis*	-	-	-	-	3	3	5	-	-	-	5	3	2	2	-	-	-	2	-	79
22.	*L. labrynthica*	3	-	11	3	-	-	7	-	1	-	-	-	-	-	-	-	-	-	-	46
23.	*L.* n. sp. A	-	-	-	-	-	-	-	-	-	-	-	-	-	-	-	-	-	-	2	4
24.	*Loxoconchella* sp. A	-	-	-	-	-	-	-	-	-	-	1	-	-	-	-	-	-	-	-	7
25.	*L.* sp. B	-	-	-	-	-	-	4	-	-	-	3	-	-	-	-	-	-	-	-	8
26.	*L.* sp. C	-	-	-	-	-	-	-	-	-	-	-	5	-	-	-	-	-	-	-	6
27.	*Miocyprideis* sp.	-	-	-	-	-	-	-	-	-	-	-	-	-	-	-	-	-	-	-	-
28.	*Morkhovenia inconspicua*	-	1	-	-	2	-	2	-	-	-	-	-	3	-	-	-	-	-	-	13
29.	*Neonesidea schulzi*	1	-	5	2	2	2	9	1	-	-	3	-	3	-	-	-	-	-	-	336
30.	*Occultocythereis* sp.	-	-	-	-	-	-	-	-	-	-	-	-	-	-	-	-	-	-	-	-
31.	Orionina sp.	-	-	-	-	-	-	-	-	-	-	-	-	-	-	-	-	-	-	-	13
32.	*Ornatoleberis* sp.	-	-	6	-	-	-	1	-	-	-	1	4	-	-	-	-	-	-	-	39
33.	*Paracytheridea remani*	-	-	-	-	-	1	2	-	-	-	8	2	-	-	-	-	-	-	2	79
34.	*Ponticocythereis* sp.	-	-	-	-	-	-	-	-	-	-	-	-	-	-	-	-	-	-	-	1
35.	*Procythereis* sp. A	-	-	-	-	-	-	-	-	-	-	-	-	3	2	1	-	1	-	-	7
36.	*P.* sp. B	-	-	-	-	-	-	-	-	-	-	-	-	-	-	-	-	1	-	-	1
37.	*Pterobairdia maddockeae*	-	-	-	-	-	-	-	-	-	-	-	-	-	-	-	-	-	-	-	1
38.	*Semicytherura* sp.	-	-	-	-	-	-	3	-	-	-	-	-	-	-	-	-	-	-	1	10
39.	*Triebelina sertata*	-	-	-	-	-	-	-	-	-	-	-	-	-	3	-	-	-	-	-	5
40.	Other	5	-	2	12	12	-	17	1	2	-	24	47	12	38	-	-	-	1	1	913
	TOTAL	40	6	88	60	41	17	131	3	9	1	89	112	39	83	3	1	17	12	8	2743

BOREHOLE OBZ-4

	DIAGNOSTIC SPECIES	SAMPLE DEPTH (ft bsf)																				
		0.0	2.8	11.8	21.1	33.0	40.05	49.7	58.5	66.35	75.15	84.15	93.1	104.55	112.9	121.8	130.0	144.5	147.75	151.55	160.05
1.	*Australimoosella* sp.	-	-	-	2	-	1	1	2	1	-	2	-	-	-	1	-	-	-	-	-
2.	*Bythoceratina* sp.	-	-	-	1	-	-	-	-	-	-	1	-	-	-	-	-	-	-	-	-
3.	*Callistocythere* sp. A	7	-	-	1	-	1	-	-	-	-	1	-	-	-	-	-	-	-	-	-
4.	*C.* sp. B	1	-	-	-	4	-	1	-	1	-	2	1	-	-	1	-	-	-	1	-
5.	*Cardobairdia* sp.	-	-	-	-	-	-	-	-	-	-	-	-	-	-	-	-	-	-	-	-
6.	*Caudites* sp. A	-	-	1	-	1	-	1	-	-	-	-	-	1	-	-	-	1	-	-	-
7.	*C.* sp. B	-	-	-	-	-	-	-	-	-	-	-	-	-	-	2	1	-	-	-	-
8.	*Cletocythereis* sp. A	-	-	3	1	-	7	3	3	-	1	2	1	-	-	1	-	-	-	1	1
9.	*C. canaliculata*	-	-	-	-	-	2	-	-	-	-	-	-	-	-	1	-	-	-	-	-
10.	*C. rastromarginata*	-	-	-	-	-	-	-	-	-	-	-	-	-	-	-	-	-	-	-	-
11.	*Cytherelloidea* sp.	1	-	1	-	-	1	1	-	-	-	-	-	-	-	-	1	-	-	-	-
12.	*Hemicytherura* sp.	-	-	-	-	-	-	-	-	-	-	-	-	-	-	-	-	-	-	-	-
13.	*Hemicythere* sp.	-	-	1	-	2	2	3	-	-	1	1	-	-	-	-	-	-	-	-	-
14.	*Hermanites mooneyi*	3	-	1	3	2	-	1	-	1	-	2	-	-	-	2	-	-	-	-	-
15.	*H. parviloba*	5	-	10	2	2	-	-	-	1	1	7	-	4	-	10	3	-	2	3	-
16.	*H. transoceanica*	8	2	-	-	25	5	8	-	-	2	3	2	-	1	11	1	-	1	2	-
17.	*Jugosocythereis* sp.	7	3	1	7	6	11	12	4	-	3	10	1	2	1	9	-	4	2	1	1
18.	*Keijia demissa*	-	-	-	-	1	-	-	-	-	-	1	-	1	-	1	-	-	-	-	-
19.	*Loxoconcha heronislandensis*	-	-	1	2	4	8	11	6	-	3	4	3	2	1	-	-	-	-	1	-
20.	*L. huahinensis*	18	9	11	27	25	24	26	5	3	9	31	8	3	4	22	2	6	13	6	2
21.	*L. insulardaensis*	5	1	5	2	7	7	5	1	1	1	4	1	-	-	6	-	1	1	1	-
22.	*L. labrynthica*	-	-	-	6	1	2	3	1	1	-	3	2	-	-	2	-	1	1	-	-
23.	*L.* n. sp. A	-	-	-	-	-	-	-	-	-	-	-	-	-	-	-	-	-	-	-	-
24.	*Loxoconchella* sp. A	-	-	-	1	-	-	-	-	-	-	-	-	-	-	-	-	-	-	-	-
25.	*L.* sp. B	-	-	-	-	-	-	-	-	-	-	-	-	-	-	-	-	-	-	-	-
26.	*L.* sp. C	5	-	2	1	14	-	-	-	-	-	-	-	-	-	-	-	-	-	-	-
27.	*Miocyprideis* sp.	-	1	-	-	-	3	4	-	-	-	-	-	-	-	-	-	-	-	-	-
28.	*Morkhovenia inconspicua*	1	1	-	-	3	3	1	-	-	-	3	-	2	-	-	-	-	-	-	-
29.	*Neonesidea schulzi*	33	2	8	2	61	-	13	7	4	5	11	1	-	-	-	-	-	3	1	-
30.	*Occultocythereis* sp.	-	-	-	-	1	-	-	-	-	-	-	-	-	-	-	-	-	-	-	-
31.	*Orionina* sp.	-	1	-	-	-	3	1	-	-	-	1	1	-	-	2	-	-	1	-	-
32.	*Ornatoleberis* sp.	4	-	1	-	-	1	3	-	-	-	2	2	-	-	-	-	-	1	1	-
33.	*Paracytheridea remani*	2	-	-	3	3	6	3	-	-	2	2	-	-	-	8	2	1	-	-	-
34.	*Ponticocythereis* sp.	-	-	-	-	-	-	-	-	-	-	-	-	-	-	-	-	-	-	-	-
35.	*Procythereis* sp. A	-	1	-	1	-	2	1	-	-	-	-	-	1	1	-	1	-	-	-	1
36.	*P.* sp. B	-	-	-	-	-	1	2	-	-	1	-	-	1	-	-	-	1	-	-	-
37.	*Pterobairdia maddocksae*	-	-	-	-	-	-	-	-	-	-	-	-	-	-	-	-	-	-	-	-
38.	*Semicytherura* sp.	-	1	1	1	2	1	-	-	-	1	1	-	-	-	4	-	-	-	-	-
39.	*Triebelina sertata*	-	-	-	-	-	-	-	-	-	-	-	-	-	-	-	-	-	-	-	-
40.	Other	88	10	23	27	171	47	23	14	13	7	44	17	8	4	37	8	6	12	-	2
41.	"Piped" specimens	-	-	-	3	1	9	7	1	-	-	2	-	1	1	13	-	-	-	1	1
	TOTAL	188	32	70	93	336	147	134	44	26	37	140	40	26	13	133	19	21	37	19	8

(continued on next page)

BOREHOLE OBZ-4 (continued)

	DIAGNOSTIC SPECIES	SAMPLE DEPTH (ft bsf)																			
		166.85	169.85	178.6	182.35	186.8	190.3	193.6	196.5	205.1	213.9	225.65	250.05	291.45	300.5	314.75	327.1	336.25	347.15	356.45	TOTAL
1.	*Australimoosella* sp.	-	1	1	4	-	1	-	-	-	-	-	1	-	-	-	-	-	2	1	21
2.	*Bythoceratina* sp.	-	-	-	-	-	-	-	-	1	1	-	-	-	-	-	-	-	-	-	4
3.	*Callistocythere* sp. A	-	-	-	-	2	-	-	9	6	-	-	-	-	-	-	-	-	-	-	27
4.	*C.* sp. B	-	-	1	-	1	-	-	-	-	1	-	-	-	-	-	1	-	1	-	17
5.	*Cardobairdia* sp.	-	-	-	-	-	-	-	-	-	-	-	-	-	-	-	-	-	1	-	1
6.	*Caudites* sp. A	-	-	-	-	-	-	-	2	-	1	-	-	-	-	-	-	-	-	-	8
7.	*C.* sp. B	-	-	-	-	-	-	-	-	-	-	-	-	-	-	-	-	-	-	-	3
8.	*Cletocythereis* sp. A	1	-	1	-	-	-	-	6	-	-	-	2	-	-	-	-	-	1	-	35
9.	*C. canaliculata*	-	-	-	-	-	-	-	-	-	-	-	-	-	-	-	-	-	-	-	3
10.	*C. rastromarginata*	-	-	-	-	2	-	-	-	-	-	-	-	-	-	-	-	-	-	-	2
11.	*Cytherelloidea* sp.	-	-	-	-	-	-	-	1	-	-	-	-	-	-	-	-	-	-	-	6
12.	*Hemicytherura* sp.	-	-	-	-	-	-	-	-	-	-	-	-	-	-	-	-	-	-	-	-
13.	*Hemicythere* sp.	-	-	-	-	-	-	-	-	-	-	-	-	-	-	-	-	-	-	-	10
14.	*Hermanites mooneyi*	-	-	-	-	-	-	-	-	-	-	-	-	-	-	-	-	-	-	-	15
15.	*H. parviloba*	1	-	1	7	5	-	1	6	3	-	1	-	-	-	-	-	-	2	1	78
16.	*H. transoceanica*	-	-	-	2	-	3	-	4	1	-	-	-	-	1	-	-	-	-	-	82
17.	*Jugosocythereis* sp.	-	1	3	6	4	-	2	17	22	2	8	2	3	-	1	2	-	-	-	158
18.	*Keijia demissa*	-	-	-	-	-	-	1	-	-	-	-	-	-	-	-	-	-	-	-	5
19.	*Loxoconcha heronislandensis*	1	2	-	-	1	-	-	-	-	-	-	-	-	-	-	-	-	7	-	57
20.	*L. huahinensis*	2	7	4	17	6	5	4	27	12	14	4	2	-	1	-	3	-	1	-	363
21.	*L. insulardaensis*	-	-	1	4	1	1	2	11	13	1	1	1	1	-	-	-	-	1	1	88
22.	*L. labrynthica*	-	1	1	2	1	-	-	7	4	-	1	-	-	-	-	-	-	-	-	40
23.	*L.* n. sp. A	-	-	-	-	-	-	-	-	-	-	-	-	-	-	-	-	-	-	-	-
24.	*Loxoconchella* sp. A	-	-	-	-	-	-	-	-	-	-	-	-	-	-	-	-	-	-	-	1
25.	*L.* sp. B	-	-	-	-	-	-	-	-	-	-	-	-	-	-	-	-	-	-	-	-
26.	*L.* sp. C	-	-	-	1	-	-	-	-	-	-	-	-	-	-	-	-	-	-	-	23
27.	*Miocyprideis* sp.	-	-	-	-	-	-	-	-	-	-	-	-	-	-	-	-	-	-	-	8
28.	*Morkhovenia inconspicua*	-	-	-	2	-	-	-	-	-	-	-	1	-	-	-	-	-	-	-	17
29.	*Neonesidea schulzi*	-	3	1	5	3	-	-	7	4	2	1	-	-	1	-	-	-	2	-	180
30.	*Occultocythereis* sp.	-	-	-	-	-	-	-	-	-	-	-	-	-	-	-	-	-	-	-	-
31.	*Orionina* sp.	-	-	-	-	-	-	-	22	14	-	-	-	-	-	-	-	-	-	-	46
32.	*Ornatoleberis* sp.	-	-	-	-	-	-	-	4	-	-	-	-	-	-	-	1	-	3	-	23
33.	*Paracytheridea remani*	-	1	-	1	2	-	1	-	-	-	-	-	-	-	-	1	-	-	1	39
34.	*Ponticocythereis* sp.	-	-	-	-	-	-	-	-	-	-	-	-	-	-	-	-	-	-	-	-
35.	*Procythereis* sp. A	-	-	-	-	-	-	-	-	-	-	-	-	-	-	-	-	-	-	-	9
36.	*P.* sp. B	-	-	-	-	-	-	-	-	-	-	-	-	-	-	-	-	-	-	-	6
37.	*Pterobairdia maddocksae*	-	-	-	-	-	-	-	1	-	-	-	-	-	-	-	-	-	-	-	1
38.	*Semicytherura* sp.	-	-	-	-	-	-	-	-	-	1	-	1	-	-	-	1	-	-	-	15
39.	*Triebelina sertata*	-	-	-	-	-	-	-	-	-	-	-	-	-	-	-	-	-	-	-	-
40.	Other	8	5	5	25	13	9	7	51	23	5	5	5	2	-	2	5	2	11	3	747
41.	"Piped" specimens	-	-	-	1	-	-	-	-	-	-	-	-	-	-	-	-	-	-	-	41
	TOTAL	13	21	19	77	41	19	18	175	103	28	21	15	6	3	3	14	2	32	7	2180

BOREHOLE OPZ-18

	DIAGNOSTIC SPECIES	SAMPLE DEPTH (ft bsf)																					TOTAL
		7.0	35.0	44.6	57.85	74.3	89.45	102.0	115.05	131.0	139.7	154.2	169.35	174.95	182.3	189.25	198.0	207.3	210.4	229.95	232.1	239.15	
1.	*Australimoosella* sp.	1	4	1	-	-	-	1	-	1	-	-	-	1	1	-	-	-	-	1	-	1	12
2.	*Bythoceratina* sp.	1	1	1	-	-	-	-	-	-	-	-	1	-	-	-	-	-	-	-	-	-	4
3.	*Callistocythere* sp. A	-	1	-	1	1	-	-	-	-	-	2	-	-	-	-	-	-	-	-	-	-	5
4.	*C.* sp. B	1	2	1	-	-	2	-	1	-	-	-	2	2	2	1	4	4	-	1	1	2	26
5.	*Cardobairdia* sp.	-	-	-	-	-	-	-	-	-	-	-	-	-	-	-	-	-	-	-	-	-	-
6.	*Caudites* sp. A	-	6	1	-	-	-	-	-	-	-	-	1	2	-	-	-	-	-	-	-	1	11
7.	*C.* sp. B	-	-	-	-	-	-	-	-	-	-	-	-	-	-	-	-	-	-	-	-	-	-
8.	*Cletocythereis* sp. A	3	14	-	2	-	-	2	-	1	-	-	-	-	-	-	-	-	-	-	-	1	23
9.	*C. canaliculata*	1	2	-	-	-	-	-	-	-	-	-	-	2	-	-	-	-	-	-	-	-	5
10.	*C. rastromarginata*	-	1	-	-	-	-	-	-	-	-	-	-	-	-	-	-	-	-	-	-	1	2
11.	*Cytherelloidea* sp.	1	1	-	1	-	-	-	-	-	-	-	-	-	-	-	-	-	-	-	1	-	4
12.	*Hemicytherura* sp.	-	-	-	-	-	-	-	-	-	-	-	-	-	-	-	-	-	-	-	-	-	-
13.	*Hemicythere* sp.	2	2	-	-	-	-	-	-	-	-	1	-	-	1	-	-	-	-	1	-	1	8
14.	*Hermanites mooneyi*	1	6	1	-	-	-	-	-	1	-	-	-	-	-	5	22	3	1	-	3	-	43
15.	*H. parviloba*	8	18	10	5	-	-	1	-	3	2	5	-	3	4	-	4	2	2	2	3	3	75
16.	*H. transoceanica*	16	11	8	-	1	-	-	-	2	-	3	3	3	-	14	28	8	-	2	5	6	110
17.	*Jugosocythereis* sp.	8	17	11	5	4	-	-	3	11	-	-	7	-	11	6	2	11	1	-	9	5	111
18.	*Keijia demissa*	-	1	-	-	-	-	-	1	1	1	1	-	1	-	-	-	-	-	-	-	-	6
19.	*Loxoconcha heronislandensis*	4	3	8	1	1	-	1	6	-	1	2	2	4	2	-	-	-	-	-	-	-	35
20.	*L. huahinensis*	29	82	17	13	7	4	7	-	11	5	19	23	13	17	33	72	40	3	5	34	13	447
21.	*L. insulardaensis*	6	16	3	1	2	-	-	3	4	-	4	2	2	4	-	1	-	1	1	-	2	52
22.	*L. labrynthica*	4	4	2	1	1	-	-	1	2	-	2	1	1	1	-	-	-	-	-	-	-	20
23.	*L.* n. sp. A	-	-	-	-	-	-	-	-	-	-	-	-	-	-	-	-	-	-	-	-	-	-
24.	*Loxoconchella* sp. A	2	3	-	-	-	-	-	-	-	-	-	-	-	-	-	2	-	-	-	1	-	8
25.	*L.* sp. B	-	-	-	-	-	-	-	-	-	-	-	-	1	-	-	-	-	-	-	-	-	1
26.	*L.* sp. C	7	1	-	-	-	-	-	-	-	-	-	-	-	-	1	-	-	-	-	-	-	9
27.	*Miocyprideis* sp.	-	-	-	-	-	-	-	-	-	-	-	-	-	-	-	-	-	-	-	-	-	-
28.	*Morkhovenia inconspicua*	1	2	1	-	1	-	-	-	-	-	2	2	-	1	-	2	1	-	1	-	1	15
29.	*Neonesidea schulzi*	41	19	-	1	6	-	-	3	-	-	-	-	-	-	-	6	4	-	-	5	-	85
30.	*Occultocythereis* sp.	1	-	-	-	-	-	-	-	-	-	-	-	-	-	-	-	-	-	-	-	-	1
31.	*Orionina* sp.	-	-	-	-	-	-	-	-	1	-	-	-	1	1	-	-	-	-	-	-	-	3
32.	*Ornatoleberis* sp.	3	7	1	1	-	1	-	-	-	-	-	-	-	1	6	9	2	-	-	1	-	32
33.	*Paracytheridea remani*	1	22	5	2	2	-	1	-	1	2	10	9	1	3	6	27	5	-	-	2	8	107
34.	*Ponticocythereis* sp.	-	-	-	-	-	-	-	-	-	-	-	-	-	-	-	-	-	-	-	-	-	-
35.	*Procythereis* sp. A	-	-	-	-	-	-	-	-	-	-	-	-	-	-	-	-	-	-	-	-	-	-
36.	*P.* sp. B	-	1	-	-	-	-	-	-	-	-	-	-	-	1	-	-	-	-	-	-	-	2
37.	*Pterobairdia maddocksae*	1	-	-	-	-	-	-	-	-	-	-	-	-	-	-	-	-	-	-	-	-	1
38.	*Semicytherura* sp.	-	4	2	-	1	1	1	-	-	-	4	-	1	2	-	-	-	-	-	-	3	19
39.	*Triebelina sertata*	-	-	-	-	-	-	-	-	-	-	-	-	-	-	-	-	-	-	-	-	-	-
40.	Other	58	73	26	11	10	12	5	17	29	8	17	19	14	13	20	26	15	8	3	41	22	447
41.	"Piped" specimens	2	19	8	4	3	2	2	-	8	3	2	6	1	-	-	-	-	-	-	-	-	60
	TOTAL	202	343	107	49	40	22	21	35	76	22	74	78	53	65	92	205	95	16	17	106	70	1788

BOREHOLE OCT-5

	DIAGNOSTIC SPECIES	SAMPLE DEPTH (ft bsf) 0.2	8.8	17.5	39.5	48.05	57.55	66.8	76.65	86.15	95.35	104.25	113.15	[illegible]	[illegible]	140.9	149.65	157.6	166.4	176.25	186.0	TOTAL
1.	*Australimoosella* sp.	-	-	-	-	-	-	-	-	-	-	-	-	-	-	-	-	-	-	-	-	-
2.	*Bythoceratina* sp.	-	-	-	-	-	-	-	-	-	-	-	-	-	-	-	-	-	-	-	-	-
3.	*Callistocythere* sp. A	4	-	-	-	-	-	-	-	-	-	-	-	-	-	-	-	-	-	-	-	4
4.	*C.* sp. B	1	-	1	-	-	-	-	-	-	-	-	-	-	-	-	-	-	-	-	-	2
5.	*Cardobairdia* sp.	-	-	1	-	-	-	-	-	-	-	-	-	-	-	-	-	-	-	-	-	1
6.	*Caudites* sp. A	1	-	-	-	-	-	-	-	-	-	-	-	-	-	-	-	-	-	-	-	1
7.	*C.* sp. B	3	-	-	-	-	-	-	-	-	-	-	-	-	-	-	-	-	-	-	-	3
8.	*Cletocythereis* sp. A	3	-	1	1	-	-	1	-	-	-	-	-	-	-	-	-	-	-	-	-	6
9.	*C. canaliculata*	-	-	-	-	-	1	-	-	-	-	-	-	-	-	-	-	-	-	-	-	1
10.	*C. rastromarginata*	1	-	-	-	-	-	-	-	-	-	-	-	-	-	-	-	-	-	-	-	1
11.	*Cytherelloidea* sp.	-	-	-	-	-	-	-	-	-	-	-	-	-	-	-	-	-	-	-	-	-
12.	*Hemicytherura* sp.	-	-	-	-	-	-	-	-	-	-	-	-	-	-	-	-	-	-	-	-	-
13.	*Hemicythere* sp.	1	-	-	-	-	3	-	1	-	-	-	-	-	-	-	-	-	-	-	-	5
14.	*Hermanites mooneyi*	2	-	-	-	-	-	-	-	-	-	-	-	-	-	-	-	-	-	-	-	2
15.	*H. parviloba*	4	-	-	-	-	2	-	-	-	-	-	-	-	-	-	-	-	-	-	-	6
16.	*H. transoceanica*	13	-	1	-	-	1	-	-	-	-	-	-	2	-	-	-	-	-	-	-	17
17.	*Jugosocythereis* sp.	13	1	-	-	-	8	-	1	-	-	-	-	1	-	4	-	-	-	-	-	28
18.	*Keijia demissa*	2	-	-	-	-	-	-	-	-	-	-	-	-	-	-	-	-	-	-	-	2
19.	*Loxoconcha heronislandensis*	5	-	-	1	-	-	-	-	-	-	-	-	-	-	-	-	-	-	-	-	6
20.	*L. huahinensis*	35	1	1	2	-	13	-	2	-	-	-	3	-	-	1	1	-	1	1	-	61
21.	*L. insulardaensis*	6	-	-	-	-	4	-	1	-	-	-	-	-	-	-	-	-	-	-	-	11
22.	*L. labrynthica*	2	-	-	-	-	2	-	-	-	-	-	-	-	-	-	-	-	-	-	-	4
23.	*L.* n. sp. A	-	-	-	-	-	-	-	-	-	-	-	-	-	-	-	-	-	-	-	-	-
24.	*Loxoconchella* sp. A	-	-	-	-	-	-	-	-	-	-	-	-	-	-	-	-	-	-	-	-	-
25.	*L.* sp. B	1	-	-	-	-	-	-	-	-	-	-	-	-	-	-	-	-	-	-	-	1
26.	*L.* sp. C	-	-	-	-	-	-	-	-	-	-	-	-	-	-	-	-	-	-	-	-	1
27.	*Miocypridеis* sp.	-	-	-	-	-	-	-	-	-	-	-	-	-	-	-	-	-	-	-	-	-
28.	*Morkhovenia inconspicua*	5	-	-	-	-	-	-	-	-	-	-	-	-	-	-	-	-	-	-	-	5
29.	*Neonesidea schulzi*	4	-	-	-	-	-	-	-	-	-	-	-	-	-	-	-	1	2	3	-	11
30.	*Occultocythereis* sp.	-	-	-	-	-	-	-	-	-	-	-	-	-	-	-	-	-	-	-	-	-
31.	*Orionina* sp.	-	-	-	-	-	1	-	-	-	-	-	-	-	-	-	-	-	-	-	-	1
32.	*Ornatoleberis* sp.	1	-	-	-	-	-	-	-	-	-	-	-	-	-	-	-	-	-	-	-	1
33.	*Paracytheridea remani*	13	-	-	-	-	5	-	-	-	-	-	-	-	-	-	-	-	-	-	-	18
34.	*Ponticocythereis* sp.	-	-	-	-	-	-	-	-	-	-	-	-	-	-	-	-	-	-	-	-	-
35.	*Procythereis* sp. A	-	-	-	-	-	-	-	-	-	-	-	-	-	-	-	-	-	-	-	-	-
36.	*P.* sp. B	2	-	-	-	-	-	-	-	-	-	-	-	-	-	-	-	-	-	-	-	2
37.	*Pterobairdia maddocksae*	-	-	-	-	-	-	-	-	-	-	-	-	-	-	-	-	-	-	-	-	-
38.	*Semicytherura* sp.	3	-	-	-	-	-	-	-	-	-	-	-	-	-	-	-	-	-	-	-	3
39.	*Triebelina sertata*	-	-	-	-	-	-	-	-	-	-	-	-	-	-	-	-	-	-	-	-	-
40.	Other	45	-	3	-	1	15	-	5	1	3	-	4	-	-	3	4	-	-	2	-	88
41.	"Piped" specimens	-	-	-	-	-	-	-	-	-	-	-	-	-	-	-	-	-	-	-	-	-
	TOTAL	170	2	8	4	1	55	1	10	1	3	-	7	[illegible]	[illegible]	8	5	1	3	6	-	292

APPENDIX 3-6
BOREHOLE OPT-8

	DIAGNOSTIC SPECIES	SAMPLE DEPTH (ft bsf)									
		0.0	8.75	18.6	27.9	35.1	43.1	48.85	64.0	74.0	TOTAL
1.	*Australimoosella* sp.	-	-	-	-	-	-	-	-	-	-
2.	*Bythoceratina* sp.	-	-	-	-	-	-	-	-	-	-
3.	*Callistocythere* sp. A	-	-	-	-	-	1	-	1	-	2
4.	*C.* sp. B	-	-	-	-	-	-	-	-	-	-
5.	*Cardobairdia* sp.	-	-	-	1	-	-	-	-	-	1
6.	*Caudites* sp. A	-	1	-	-	-	-	-	-	-	1
7.	*C.* sp. B	-	-	-	-	-	-	-	-	-	-
8.	*Cletocythereis* sp. A	-	-	1	-	-	-	-	1	-	2
9.	*C. canaliculata*	-	-	-	-	-	-	-	-	-	-
10.	*C. rastromarginata*	-	-	-	-	-	-	-	-	-	-
11.	*Cytherelloidea* sp.	-	-	-	-	-	-	-	-	-	-
12.	*Hemicytherura* sp.	-	-	-	-	-	-	-	-	-	-
13.	*Hemicythere* sp.	-	1	-	-	-	-	-	-	-	1
14.	*Hermanites mooneyi*	-	-	-	1	1	-	-	-	-	2
15.	*H. parviloba*	1	-	-	-	-	-	-	-	-	1
16.	*H. transoceanica*	-	-	-	3	4	-	-	-	-	7
17.	*Jugosocythereis* sp.	-	1	-	-	-	8	-	4	-	13
18.	*Keijia demissa*	-	-	-	-	-	-	-	-	-	-
19.	*Loxoconcha heronislandensis*	-	2	-	-	-	-	-	2	-	4
20.	*L. huahinensis*	1	4	1	5	3	3	1	9	1	28
21.	*L. insulardaensis*	-	1	-	-	-	-	-	1	-	2
22.	*L. labrynthica*	-	-	-	-	-	-	-	-	-	-
23.	*L.* n. sp. A	-	-	-	-	-	-	-	-	-	-
24.	*Loxoconchella* sp. A	-	-	-	-	-	-	-	-	-	-
25.	*L.* sp. B	-	-	-	-	-	-	-	-	-	-
26.	*L.* sp. C	-	-	-	-	-	-	-	-	-	-
27.	*Miocyprideis* sp.	-	-	-	-	-	-	-	-	-	-
28.	*Morkhovenia inconspicua*	-	-	-	-	-	-	-	-	-	-
29.	*Neonesidea schulzi*	-	2	-	-	-	1	-	1	-	4
30.	*Occultocythereis* sp.	-	-	-	-	-	-	-	-	-	-
31.	*Orionina* sp.	-	-	-	-	-	-	-	-	-	-
32.	*Ornatoleberis* sp.	-	1	-	3	-	-	-	-	-	4
33.	*Paracytheridea remani*	-	1	-	2	1	1	-	-	-	5
34.	*Ponticocythereis* sp.	-	-	-	-	-	-	-	-	-	-
35.	*Procythereis* sp. A	-	-	-	-	-	-	-	-	-	-
36.	*P.* sp. B	-	-	-	-	-	-	-	-	-	-
37.	*Pterobairdia maddocksae*	-	-	-	-	-	-	-	-	-	-
38.	*Semicytherura* sp.	-	-	-	-	-	-	-	-	-	-
39.	*Triebelina sertata*	-	-	-	-	-	-	-	-	-	-
40.	Other	7	7	2	6	4	4	-	10	-	40
41.	"Piped" specimens	1	-	-	-	-	-	-	-	-	1
	TOTAL	10	21	4	21	13	18	1	29	1	118

APPENDIX 3-7

BOREHOLE OKT-13

	DIAGNOSTIC SPECIES	SAMPLE DEPTH (ft bsf)									
		10.4	18.5	25.4	28.75	36.0	55.65	59.9	68.2	80.0	TOTAL
1.	*Australimoosella* sp.	-	1	-	-	-	-	-	-	-	1
2.	*Bythoceratina* sp.	-	1	-	-	-	-	-	-	-	1
3.	*Callistocythere* sp. A	-	-	-	-	-	-	13	-	3	16
4.	*C.* sp. B	3	2	-	-	-	-	-	-	-	5
5.	*Cardobairdia* sp.	-	-	-	-	-	-	-	-	-	-
6.	*Caudites* sp. A	1	-	-	-	-	-	-	-	-	1
7.	*C.* sp. B	-	-	-	-	-	2	-	-	-	2
8.	*Cletocythereis* sp. A	2	2	2	-	-	2	-	3	3	14
9.	*C. canaliculata*	-	-	-	-	-	-	-	-	-	-
10.	*C. rastromarginata*	-	-	-	-	-	-	-	-	-	-
11.	*Cytherelloidea* sp.	-	1	-	-	-	-	-	-	-	1
12.	*Hemicytherura* sp.	-	-	-	-	-	-	-	-	-	-
13.	*Hemicythere* sp.	-	-	-	-	-	-	-	1	-	1
14.	*Hermanites mooneyi*	-	-	4	5	2	-	-	-	-	11
15.	*H. parviloba*	2	1	3	8	3	1	-	1	-	19
16.	*H. transoceanica*	3	3	5	6	3	1	5	3	4	33
17.	*Jugosocythereis* sp.	5	7	1	-	3	-	12	3	11	42
18.	*Keijia demissa*	-	1	-	-	-	1	-	-	-	2
19.	*Loxoconcha heronislandensis*	2	2	-	-	-	-	-	-	-	4
20.	*L. huahinensis*	11	19	17	19	11	12	3	8	12	112
21.	*L. insulardaensis*	-	1	-	-	-	-	2	2	4	9
22.	*L. labrynthica*	-	-	4	-	-	-	2	2	3	11
23.	*L.* n. sp. A	-	-	-	-	-	-	-	-	-	-
24.	*Loxoconchella* sp. A	-	-	1	3	-	-	-	-	-	4
25.	*L.* sp. B	-	-	-	-	-	-	-	-	-	-
26.	*L.* sp. C	1	-	-	-	-	-	-	-	-	1
27.	*Miocyprideis* sp.	-	-	-	-	-	-	-	-	-	-
28.	*Morkhovenia inconspicua*	-	-	-	-	-	-	-	1	-	1
29.	*Neonesidea schulzi*	1	3	11	15	8	1	1	2	-	42
30.	*Occultocythereis* sp.	-	-	-	-	-	-	-	-	-	-
31.	*Orionina* sp.	-	-	1	-	-	-	12	-	1	14
32.	*Ornatoleberis* sp.	-	1	1	1	5	-	-	-	-	8
33.	*Paracytheridea remani*	4	6	5	-	2	8	1	3	-	29
34.	*Ponticocythereis* sp.	-	-	-	-	-	-	-	-	-	-
35.	*Procythereis* sp. A	-	-	-	-	-	-	-	-	-	-
36.	*P.* sp. B	-	-	-	-	-	-	-	-	-	-
37.	*Pterobairdia maddocksae*	-	-	1	-	-	-	-	-	-	1
38.	*Semicytherura* sp.	1	4	-	2	-	2	-	7	-	16
39.	*Triebelina sertata*	-	-	-	-	-	-	-	-	-	-
40.	Other	11	21	29	22	13	7	11	7	26	147
41.	"Piped" specimens	-	-	-	-	-	-	-	-	-	-
	TOTAL	47	76	84	81	50	37	62	43	67	547

CHAPTER 4:

ELECTRON PARAMAGNETIC RESONANCE STUDIES OF SELECTED BOREHOLE SAMPLES AND DEBRIS MATERIAL FROM OAK CRATER

by

Carol A. Polanskey[1] and Thomas J. Ahrens[1]

INTRODUCTION

Electron paramagnetic resonance (EPR) spectrometry was used to measure the peak shock stress experienced by a variety of carbonate samples as a result of the detonation of the OAK nuclear device. The following results are based on EPR spectra from 136 samples taken from six boreholes and 17 debris samples recovered from the crater floor. Shock pressures were determined by comparing the sample spectra with spectra of Enewetak carbonate samples and Solenhofen Limestone that had been shocked to known pressures in the laboratory. Preliminary work on this procedure was developed by Vizgirda and Ahrens (1980) using Enewetak material from CACTUS crater obtained during Project EXPOE. Their work demonstrated a linear relationship between shock pressure and the hyperfine splitting of Mn^{2+} in the calcite component of CACTUS carbonate samples. The current report contains the analysis of the OAK samples and expands upon the previous calibration technique.

EPR ANALYSIS

The EPR spectrum of calcium carbonate, $CaCO_3$, is a result of Mn^{2+} substituting for Ca^{2+} in a single site in the crystal lattice. The theory of Mn^{2+} resonance absorption in single crystal of calcite is described by Hurd and others (1954). The calcite spectrum is dominated by six hyperfine peaks due to the central transitions $M = +1/2$, where M is the electronic magnetic quantum number. The hyperfine splitting results from the coupling between electronic and nuclear magnetic moments (Hurd and others, 1954). The spectrum of a powdered sample of single crystal calcite, Iceland spar, is shown in Figure 4-1. The central transitions are labeled along with the forbidden transitions. Of particular interest to this study are the two outer most peak doublets at the lowest and highest field positions.

Sample Preparation and Spectrometer Settings

The carbonate samples were ground into a coarse powder and placed into Wilmad© 707SQ fused EPR tubes. The spectra were taken at room temperature with a Varian© E-Line Century Series spectrometer. The calcite spectrum is centered near 3,400 Gauss (G), and ranges from approximately 3,150 to 3,650 G.

---

[1]California Institute of Technology, Division of Geological and Planetary Sciences; Pasadena, California 91125.

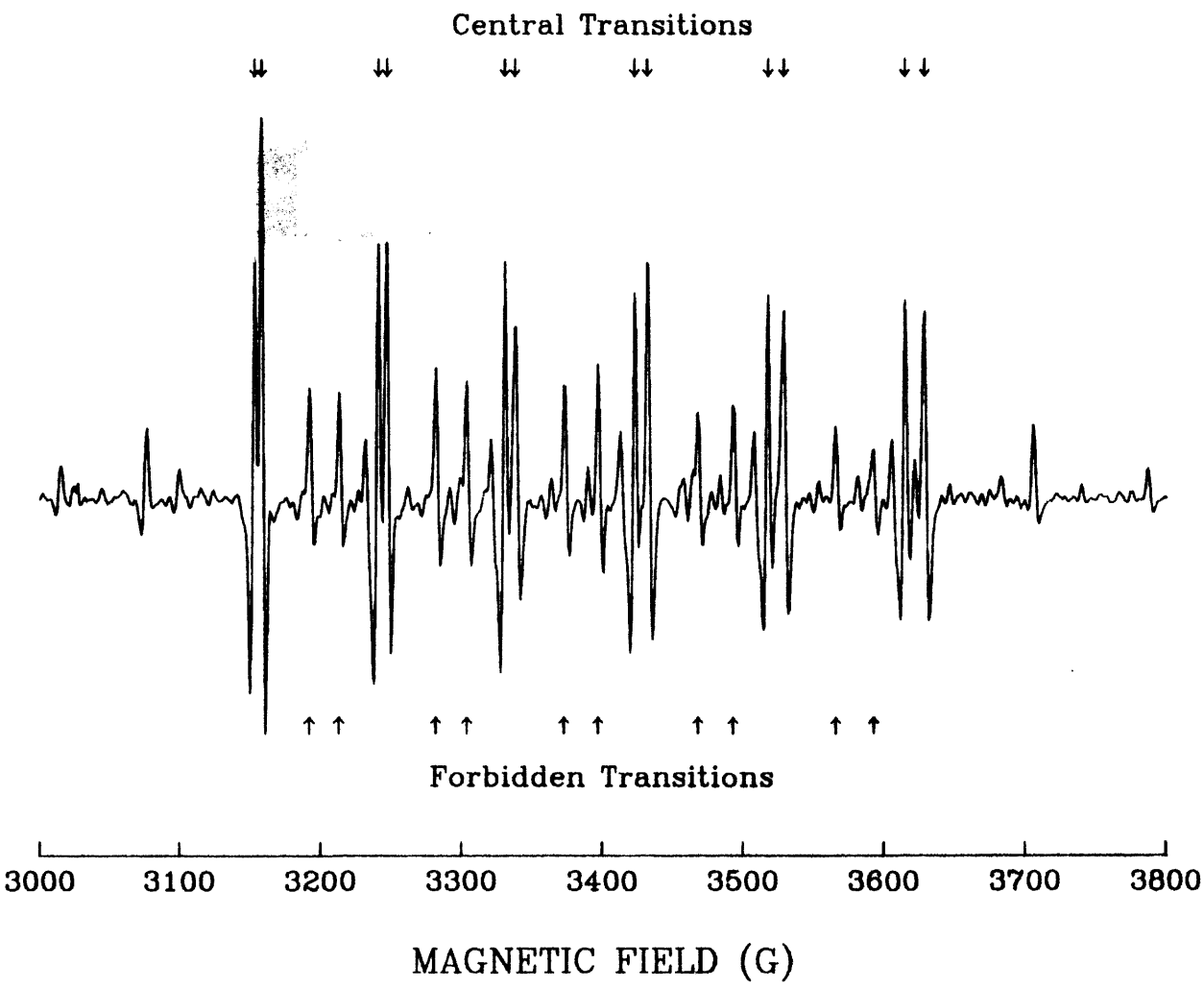

FIGURE 4-1. -- EPR spectrum of powdered single crystal calcite. The central transitions are due to $M = +1/2$, $\Delta m = 0$, where M and m are the electronic and nuclear magnetic quantum numbers, respectively. The forbidden transitions occur when $\Delta m = 1$. G = Gauss.

The spectrometer was set at a microwave frequency of 9.56 GigaHertz (GHz), modulation amplitude of 3.2 G, time constant of 0.25 seconds (sec), and microwave power of 20 milliwatts (mWatt). A scan time of 8 minutes (min) was used to obtain the full spectrum over a 1000-G scan range; however, high-resolution spectra were also recorded for both the extreme lower and higher field components of the spectrum. For these spectra, the magnetic field was swept over 100 G in 4 min. The high resolution spectra provided greater details of the modification of the hyperfine doublets from the shocked samples. As a result, the high-resolution spectra were used in all of the subsequent analyses.

In addition, all spectra were recorded digitally by the spectrometer. Therefore, it was possible to average several scans to improve the signal-to-noise ratio in samples with low signal strength. Signal averaging proved to be extremely useful for the highly shocked samples because there is a definite correlation between decreasing signal strength and increasing shock pressure. Finally, to remove the slope from the spectrum and reduce the line width of the signal, the spectrometer was operated in the second derivative mode. This was accomplished by setting the modulation frequency of the cavity 90 degrees out of phase with the receiver frequency.

SHOCK PRESSURE CALIBRATION OF EPR SPECTRA

Shock-Wave Calibration Experiments

The calibration experiments were a combination of two different data sets. The first set consisted of Enewetak carbonate samples shocked in the laboratory over 10 years ago. The samples were taken from two different depths, 10 ft and 146 ft, from the borehole XRU-3 located outside of CACTUS crater on the eastern side of Enewetak Atoll. These samples and experiments are described in detail by Vizgirda and Ahrens (1980). One reason for reprocessing these samples was to determine if the shock effects observed by Vizgirda and Ahrens (1980) had changed with time. New spectra were taken of each sample and the results confirmed that the effect of shock on the hyperfine splitting had not altered over the time scale of a decade. Secondly, high-resolution spectra were taken from these samples in order to test the pressure-calibration technique; however, these samples were not used for the pressure calibration which is described subsequently in this Chapter.

A series of Solenhofen Limestone samples also were shocked in the laboratory, and these samples became the basis for the pressure calibration. This material was chosen because its EPR spectrum, also due to Mn^{2+} substitution, is orders of agnitude more intense than the Enewetak samples. The Solenhofen is also more chemically homogeneous, although it is still a polycrystalline material. Limestone cores (diameter 0.25 in.) were cut into 0.4-in.-long cylinders and pressed into stainless-steel sample chambers. The sample chambers were sealed in the rear by a stainless-steel plug which was notched to vent any impact generated gases. The sample chamber was then inserted into a large stainless-steel momentum trap and mounted in a 40-mm propellant gun. Projectiles were made of polycarbonate-resin plastic (Lexan) that contained flyer plates of aluminium or Lexan. These impacted the target assembly at velocities between 0.8 and 1.6 km/sec to yield initial shock

pressures of 1.3 to 9.8 Giga Pascals (GPa). Initial shock pressure (rather than final reverberated shock pressure) is reported, because most of the entropy generated by the shock (and hence the shock damage) is associated with the initial shock wave.

Shock pressures were calculated using the projectile velocities and the impedance match technique (Stoffler, 1972). The average bulk density of the limestone samples was 2.61 g/cm^3, and the Hugoniot for Solenhofen Limestone samples was taken from Tyburczy and Ahrens (1986). The remaining Hugoniots for Lexan© aluminium 2024, and stainless steel 304 are found in Marsh (1980).

Description of Shocked Spectra

Figure 4-2 shows a series of shocked-limestone spectra. The spectra have all been normalized such that the highest peaks (low-resolution spectra) or the highest subpeaks (high-resolution spectra) are of equal height. The shocked-limestone spectra not only reflect in much greater detail the decrease in the hyperfine splitting as a function of increasing pressure, observed previously in the carbonate, but also reveal that the relative signal strength and width of the two subpeaks also varies in a consistent manner with increasing pressure. It is clear from the last two columns in Figure 4-2 that the extreme low-field subpeak in the low-field doublet and the extreme high-field subpeak in the high-field doublet both decrease in relative amplitude and broaden with increasing shock pressure. Because the spectrum of each doublet is the sum of two individual subpeaks, a change in the magnitude or shape of one subpeak can be enough to create the observed decrease in peak separation of the doublet as a whole. In this case, a shift in the actual line position of either subpeak is not required.

The same general trend in peak variation also can be seen in the shocked-carbonate spectra shown in Figure 4-3. Because of the low signal in several samples, these spectra were not uniformly normalized. The specific behavior of the subpeaks in the high-field doublet is less obvious in this series, and the subpeaks are difficult to distinguish at higher shock pressures. The high-field doublet is ultimately lost in the noise (as seen in the sample shocked to 10 GPa). Another factor which complicates the carbonate analysis is that there is also variation between spectra of some of the "unshocked" carbonate samples. Material from two different depths in borehole XRU-3 was used in the calibration experiments of Vizgirda and Ahrens (1980). It appears that the material taken from a depth of 10 ft is not typical of the bulk of the unshocked samples analyzed from Enewetak Atoll. As a result, a systematic difference exists between the spectra taken from these calibration shots and that of the shocked material from 146 ft depth. Both sets of spectra show consistent variation in hyperfine splitting with increasing shock pressure; however, they do differ in the degree to which they are affected by shock deformation.

A second observation, mentioned earlier, is that the amplitude of the entire spectrum tends to decrease with increasing shock pressure. This effect is much more obvious in the Enewetak samples than in the Solenhofen Limestone samples. A loss of signal could be due to a reduction of the Mn^{2+} concentration in the Ca^{2+} lattice sites. The specific mechanism responsible for this reduction has not yet been identified.

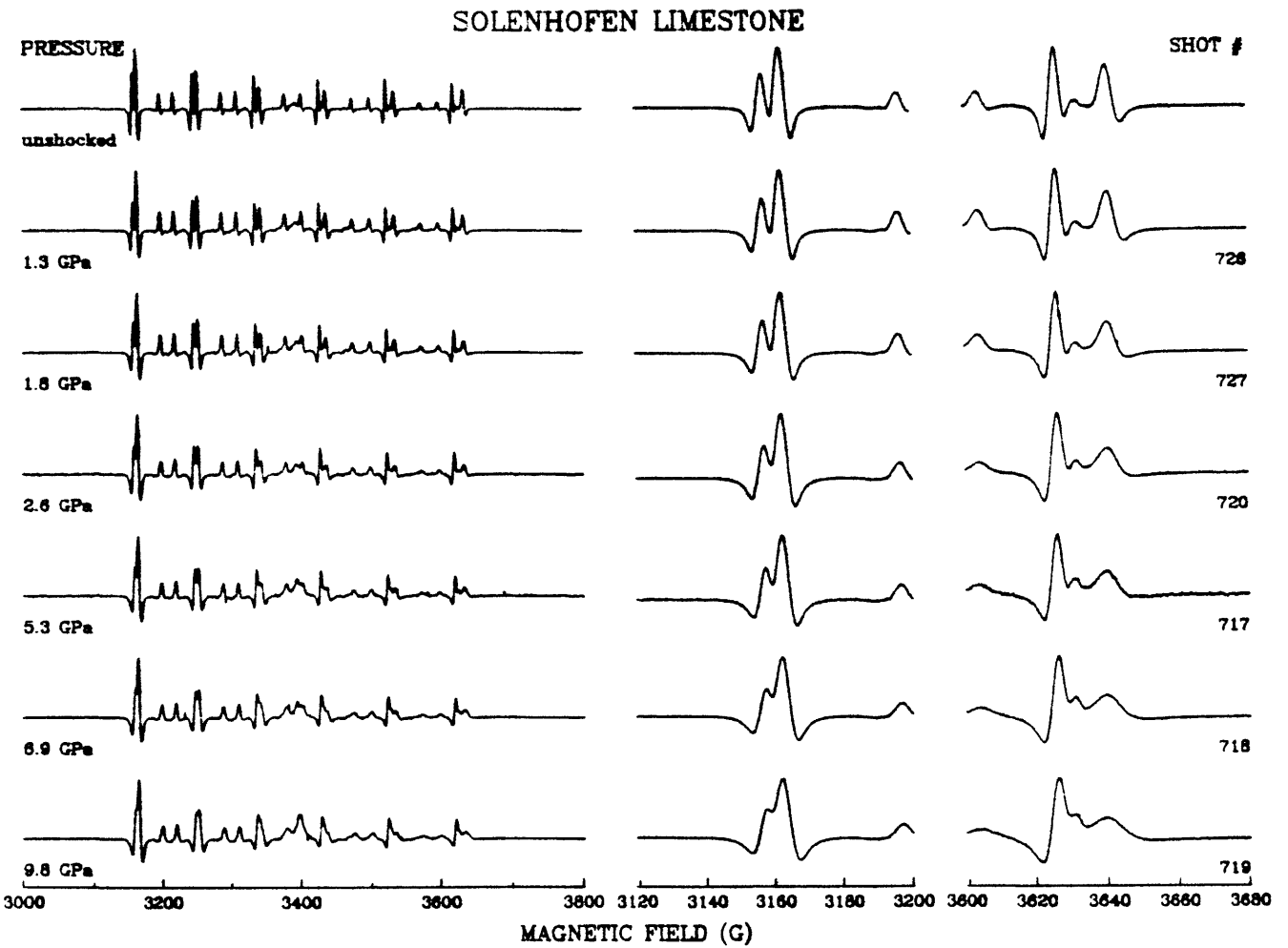

FIGURE 4-2. -- Comparison of limestone spectra shocked in the laboratory. The full spectrum is shown in the first column and centered at 3,400 Gauss (G). High-resolution spectra of the lowest and highest field components are shown in the latter two columns and centered at 3,160 G and 3,630 G, respectively.

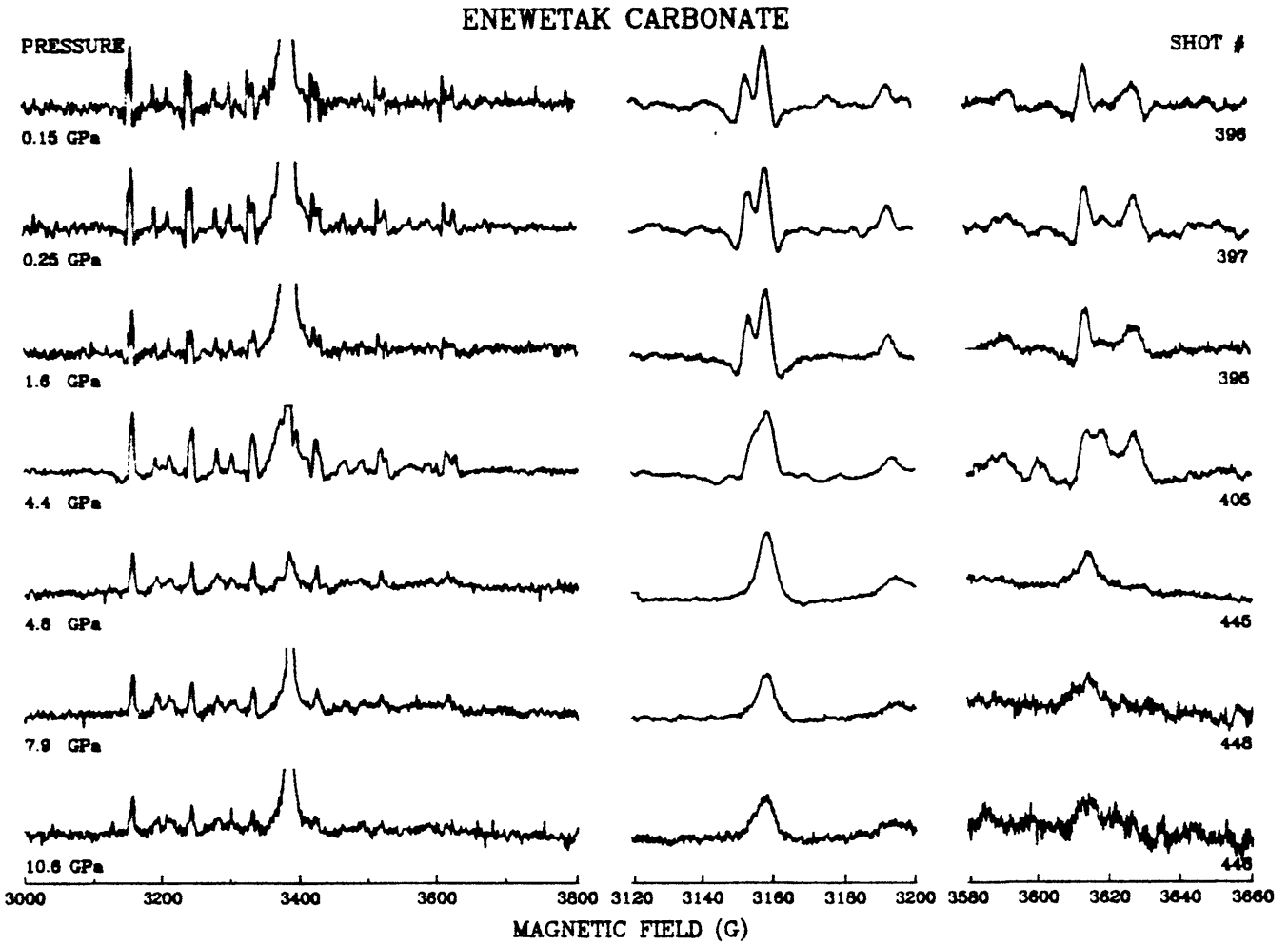

FIGURE 4-3. -- Comparison of coral spectra shocked in the laboratory. The full spectrum is shown in the first column and centered at 3,400 Gauss (G). High-resolution spectra of the lowest and highest field components are shown in the latter two columns and centered at 3,160 G and 3,630 G, respectively.

Pressure Calibration by Differencing Spectra

The previous calibration technique of Vizgirda and Ahrens (1980) relied on measuring the separation, in Gauss (G), of the two subpeaks of the highest field component of each spectrum. The hyperfine peak splitting, HPS, was related to shock pressure, P, by the relationship:

$$HPS(G) = -0.60P(GPa) + 13.85 \qquad \text{(high field)}$$

Although the decrease in hyperfine splitting is most evident in the high field component, the signal strength of this peak is also the lowest. Therefore, as the signal intensity decreases, the error in measuring hyperfine peak splitting increases. The following technique was developed to incorporate the variations in hyperfine splitting as well as relative peak amplitudes and widths. In addition, the analysis will work equally well for the lowest field component of the spectrum which always has a higher amplitude.

Digital spectra were used to compare each carbonate sample to a pure, single-crystal calcite standard. Both high-resolution spectra from each end of the spectrum were used in the comparison. The digital spectra consisted of 1000 amplitude values evenly spaced over a 100-G field range. Both sample and standard spectra were first normalized by the amplitude of their respective highest subpeaks. The sample spectrum was then translated along the magnetic-field axis until the position of its highest subpeak coincided with that of the standard spectrum. Next the absolute value of the difference in amplitude between the two spectra was calculated for each point over the extent of the doublet. Finally, these individual differences were summed to determine a measure of the "likeness" or "unlikeness" of the sample spectrum to the standard. This number shall be referred to as the integrated difference, or ID, of the sample, which is given analytically by the equation:

$$ID = \int_{n=n_o}^{n=400} \left| Y[\text{standard}] - Y[\text{sample}] \right| / 40G$$

where n_0 is the index of the amplitude array corresponding to a magnetic field value 20 G below that of the highest peak of the standard spectrum; Y[standard](i) and Y[standard](i) are the normalized amplitudes of the standard and sample spectra, respectively, and N is the number of data points that are integrated. In this case, N is 400. The error in ID is determined by performing a similar calculation, where Y[sample](i) are points in the flat baseline signal on either side of the Mn^{2+} peak.

Figure 4-4 illustrates this procedure with examples of two spectra from the limestone calibration experiments. The first frame shows an unshocked Solenhofen Limestone spectrum normalized, translated, and plotted over the standard calcite spectrum. The second frame is a plot of the absolute value of the difference between the amplitudes at each point over a 40-G range in magnetic field. The final two frames demonstrate the same technique using a sample which has been shocked to 9.8 GPa. The error is determined by using the same scheme to calculate the integrated difference along a flat portion of the spectrum. This value gives an estimate of the contribution of noise to the ID over the region containing the signal.

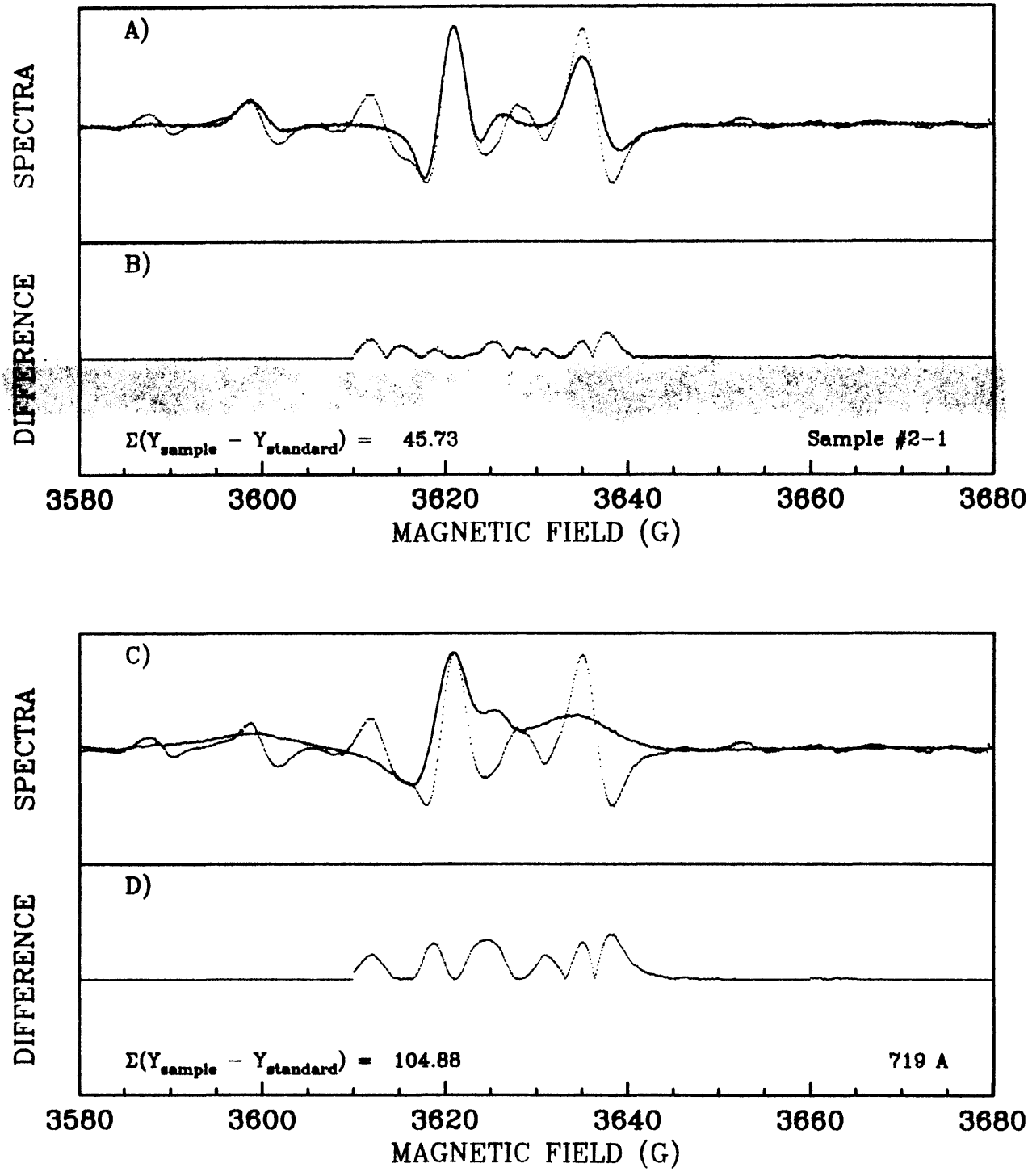

FIGURE 4-4. -- Illustration of the differencing technique showing (A) an overlay of the standard spectra and an unshocked Solenhofen Limestone sample; and (B) a plot of the individual absolute differences at each point along the field. Frames (C) and (D) correspond to (A) and (B) for a limestone sample shocked to 9.8 GigaPascals (GPa).

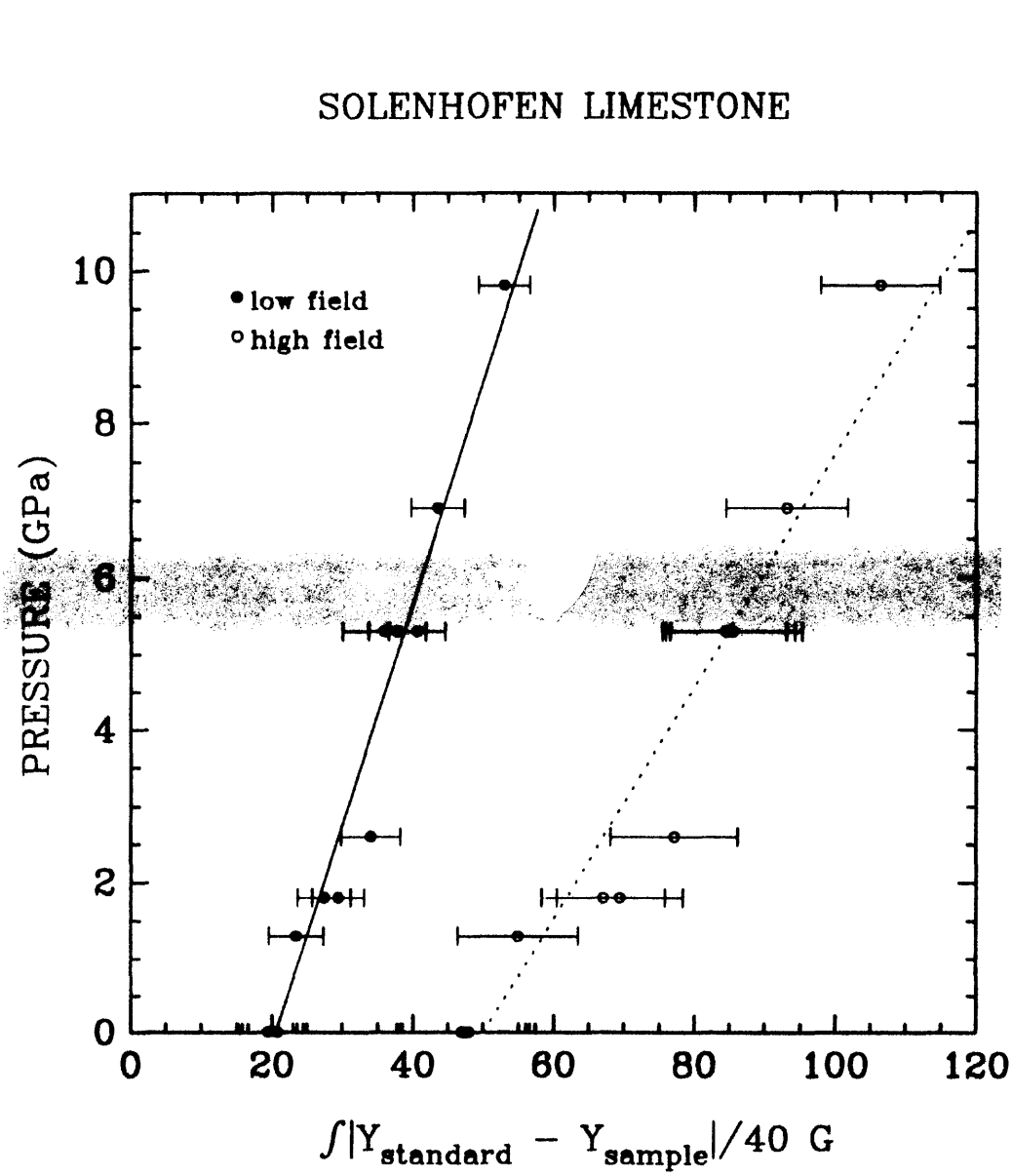

FIGURE 4-5. -- Plot of the summed differences for the low and high field components of the Solenhofen Limestone samples as a function of shock pressure. The ID value is normalized by 40 Gauss (G), the magnetic field range over which the differences were integrated.

TABLE 4-1. Pressure (Giga Pascal) and Integrated Difference (ID) Data for High Resolution Spectra from Samples Shocked in Laboratory Recovery Experiments.

SOLENHOFEN LIMESTONE

SHOT NUMBER	P (GPa)	ID Low Field	ID High Field
—	0.0	20.79	47.61
717	5.3	38.12	85.13
718	6.9	43.53	93.17
719	9.8	52.99	106.43
720	2.6	34.03	77.16
726	1.3	23.44	55.14
727	1.8	28.42	68.23

ENEWETAK CARBONATES

SHOT NUMBER	P (GPa)	ID Low Field	ID High Field
394	1.4	37.43	74.68
395	1.6	37.83	84.80
396	0.2	33.67	66.51
397	0.3	33.00	74.79
405	4.4	73.85	146.09
442	1.9	78.25	146.22
443	1.5	68.33	166.97
445	4.8	73.61	165.60
446	10.6	75.70	181.03
448	7.9	70.71	161.79

ACKNOWLEDGEMENTS

I am especially indebted to several key people. D. Oberste-Lehn, of R & D Associates, one of several people who initially recognized the potential value of borehole gravity surveys to the PEACE Program, solicited my involvement and worked closely with me during the past several years. Her persistent questions, stimulating ideas, and material support have been invaluable. Crucial leadership and considerable effort during the difficult field surveys were very ably provided by B. L. Ristvet of S-Cubed, Inc. Early recognition of the value of BHG surveys and strong backing from within the cratering community came from J. G. Trulio of Applied Theory, Inc. I also benefited greatly from information provided at various stages by J. J. Daniels, J. A. Grow, R. B. Halley, J. C. Hampson, T. W. Henry, L. S. Melzer, B. L. Ristvet, E. L. Tremba, J. G. Trulio, and B. R. Wardlaw.

REFERENCES

Beyer, L. A., 1968, Recent tests of the United States Geological Survey -- La Coste and Romberg borehole gravimeter system (abs.): Geophysics, v. 33, no. 6, p. 1030.

Beyer, L. A., and Corbato, C. E., 1972, A FORTRAN IV computer program for calculating borehole gravity terrain corrections: U.S. Geological Survey Open-File Report, 30 p.; available as report PB-208-679 from National Techinical Information Service, Springfield, Virginia.

Beyer, L. A., Ristvet, B. L., and Oberste-Lehn, D., 1986, Chapter 8: Preliminary density and porosity data and field techniques of borehole gravity surveys, OAK crater: 28 p., 4 figs., 10 tbls.; in Henry, T. W., and Wardlaw, B. R., eds., Pacific Enewetak Atoll Crater Exploration (PEACE) Program, Enewetak Atoll, Republic of the Marshall Islands; Part 3: Stratigraphic analysis and other geologic and geophysical studies in vicinity of OAK and KOA craters: U.S. Geological Survey Open-File Report 86-555.

Black, A. J., and Herring, A. T., 1983, Borehole gravity: Expanded operating limits and performance: Expanded Abstracts with Bibliographies, 1983 Technical Program, 53rd Annual International Society of Economic Geologists Meeting, September 11-15, 1983, Las Vegas, Nevada, p. 21-33.

Buigues, D., 1985, Principal facies and their distribution at Mururoa Atoll: Proceedings of the Fifth International Coral Reef Congress, v. 3, p. 249-255.

Couch, R. F., Jr., Fetzer, J. A., Goter, E. R., Ristvet, B. L., Tremba, E. L., Walter, D. R., and Wendland, V. P., 1975, Drilling operations on Eniwetok Atoll during Project EXPOE: Air Force Weapons Laboratory Technical Report AFWL-TR-75-216, Kirtland Air Force Base, New Mexico, 270 p., 17 figs., 4 tbls. [Unclassified].

The results of these calculations for the limestone calibration experiments are plotted in Figure 4-5. The ID values are plotted against pressure for both the low- and high-field components of the spectrum. To determine the pressure to integrated difference calibration, a line was fit to each data set using linear least squares. The resulting equations are listed below:

$$P\ (GPa) = 0.290(ID) - 5.97 \qquad \text{(low field)}$$
$$P\ (GPa) = 0.152(ID) - 7.59 \qquad \text{(high field)}$$

The correlation coefficients for the fit were 0.966 and 0.943, respectively. Table 4-1 contains a list of the ID results for both limestone and Enewetak sample experiments. The average ID values are given for shots where several samples were analyzed.

Using the calibration curves above, shock pressures were then assigned to the OAK carbonate samples. In general, the Enewetak carbonate samples have a much weaker EPR signal than those from the Solenhofen Limestone. Therefore, it was necessary to adjust the intercept of the calibration curves to compensate for the average ID value of the unshocked Enewetak samples. It follows that this method will then assign negative pressures to some samples, because the previous adjustment was made to accomodate the "average" background noise. To avoid this obviously unphysical result, and because this technique is not extremely sensitive for low-shock damage, all samples with shock pressures calculated to be below 2.0 GPa were classified as unshocked. Similarly, the high-pressure cut-off was chosen to be 15 GPa. This is necessary because: (1) no data exist for very high shock pressures, and (2) the intensity of the Enewetak sample spectrum is low even at 10 GPa. Samples with shock pressures calculated to be above 10 GPa were classified as highly shocked.

In most cases, shock pressures were calculated for each sample using both the low- and high-field components of the spectrum. These values were then averaged to determine the final calculated pressure.

OAK DATA

Borehole Sample Selection

The borehole samples consisted of uncemented sediments and carbonate rock clasts from boreholes OAR-2A, OBZ-4, OCT-5, OET-7, OFT-8, and OPZ-18, the locations of which are shown on Figure 4-6. Samples are referred by the appropriate borehole name succeeded by depth in feet below sea level (bsl).

The carbonate material from Enewetak is extremely inhomogeneous and consists of a mixture of both calcite and aragonite. Because aragonite does not have a detectable EPR spectrum (Low and Zeira, 1972), samples were selected, where possible, for their high-calcite content. For example, those samples containing carbonate grains replaced by solution-deposited calcite crystals were preferred because they would yield stronger EPR signals. Choosing good sample material is important because it provides a consistent base for analysis, and because it guards against mistaking a sample with an inherently poor EPR spectrum as being highly shocked. The difference between the two cases generally can be recognized by visual inspection, although it is

more difficult to assess with numerical techniques. As a result, the samples chosen were much less porous than the CACTUS samples used in the earlier shock-wave experiments; consequently, the OAK spectra tended to resemble the Solenhofen Limestone spectra more closely. For each borehole, the majority of samples were taken from depths above the gamma (γ) geologic crater zone, defined by Wardlaw and Henry (1986, p. 3) as that interval of rock and sediment that is fractured and displaced beneath the crater. A more specific description of each sample analyzed is given in Tables 4-2 through 4-7 (located at the end of this Chapter). Detailed descriptions of each borehole are given in Henry, Wardlaw, and others (1986).

Results of Borehole Sample Analysis

The two boreholes drilled almost directly below the position of the explosive device (ground-zero, GZ, and bathymetric-center boreholes OBZ-4 and OPZ-18, respectively) were the most heavily sampled for the EPR study. A very highly shocked layer of uncemented material was found in samples from borehole OPZ-18 between 399.9 ft and 415.9 ft bsl. This layer was distinguished visually by the characteristic greenish color of the muddy carbonate sand. The shocked zone was interrupted at 412.4 ft bsl by a thin zone of lighter-colored material. The location and nature of this shocked material coincides with a zone of Holocene sediments described by Wardlaw and Henry (1986) as a possible example of material that has been injected. The present results are consistent with such an hypothesis since this material most likely originated near the pre-shot sea-floor surface. Three other sand samples above this layer, 386.9 ft, 368.5 ft, and 357.2 ft bsl, were moderately shocked to at most 3.2 GPa. The highly shocked samples were located primarily in the geologic crater zone beta-2 (β_2) --the transition sands-- whereas the moderately shocked material came from zone beta-1b (β_{1b}) (Wardlaw and Henry, 1986; and Chapter 6 of current Report). The remaining 24 of the 31 samples from OPZ-18 appear to be unshocked.

Remarkably, not one of the 26 samples from OBZ-4 showed significant shock damage. Three samples from the β_{1b} zone registered only marginally detectable degrees of shock damage. Sufficient samples were analyzed from the transition sands and vicinity to characterize the core; therefore, it appears that OBZ-4 did not share the same history as OPZ-18.

Thick zones of highly shocked material were found in each of the three northeastern-radial transition boreholes OCT-5, OET-7, and OFT-8. The transition sands have not been identified in any of these boreholes; however, the spectra of the shocked material are similar to those from the shocked material in OPZ-18.

Spectra were taken of 25 samples from borehole OCT-5, drilled 658 ft from GZ. The results of six of these samples define a heavily shocked zone at least 25 ft thick, extending from 285.3 ft to 309.9 ft bsl. This region occurs within zone β_{1b} (early stage collapse rubble), and these samples are also primarily uncemented sands. Aside from the highly shocked material in this region, four widely dispersed samples appear to be moderately shocked. However, two of these samples (368.4 and 464.0 ft bsl in OCT-5) are examples of the aforementioned situation where poor signal quality biases a pressure determination. Simple visual analysis of these spectra suggest that both samples are actually unshocked. The elevated pressures calculated for

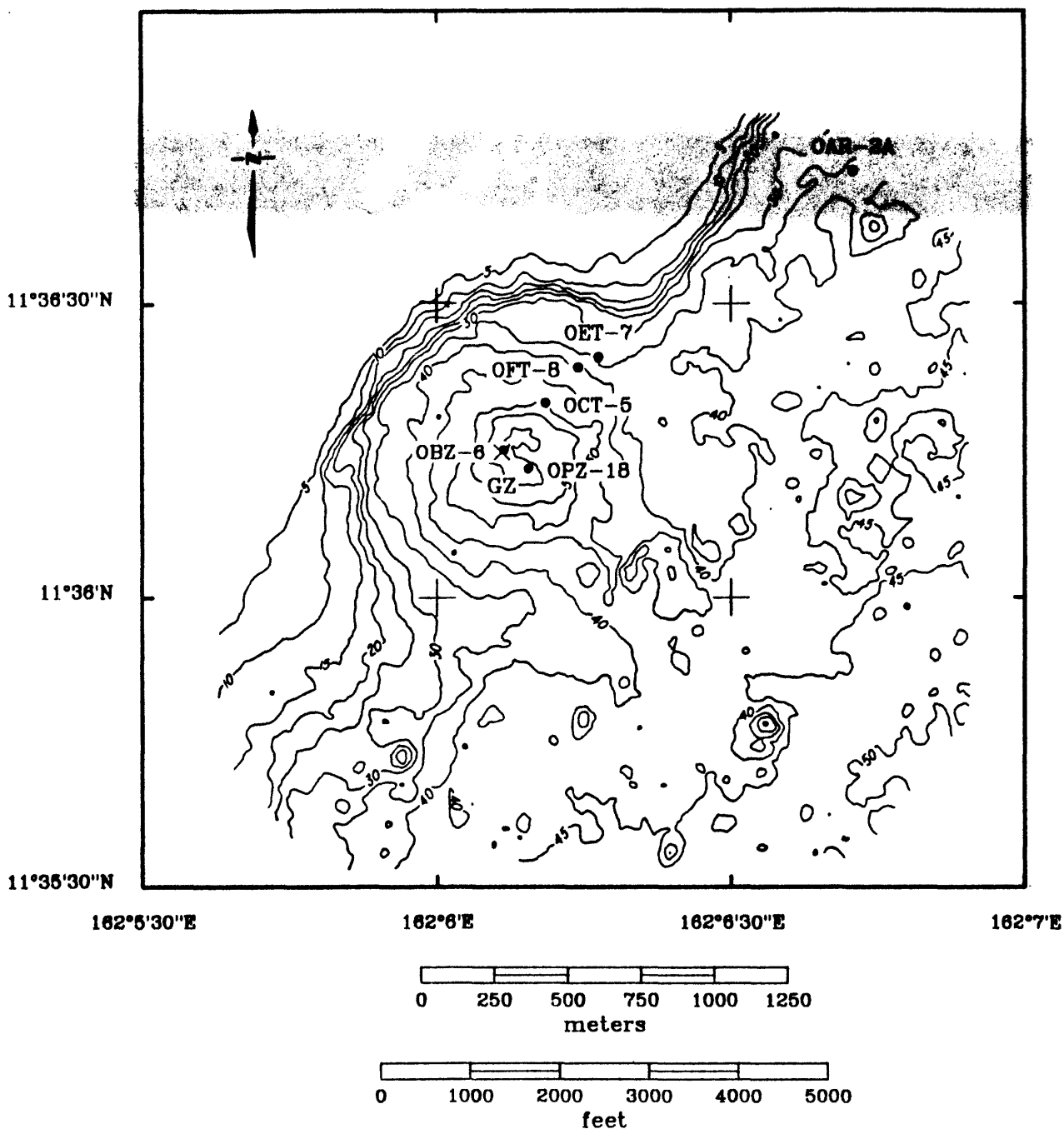

FIGURE 4-6. -- Map of OAK crater showing the location of the boreholes sampled for this study. Bathymetric contours given in 5-meter intervals.

these depths are an artifact of the noisiness of the spectra due to the small fraction of calcite in these samples.

Borehole OFT-8 is located 1,129 ft from GZ, just within the excavational crater (Henry, Wardlaw, and others, 1986). This borehole was sampled at 24 depths. In OFT-8, the region of heavily shocked material begins near the top of the β_{1b} zone and extends downward for approximately 27 ft. Included within this zone were seven heavily shocked samples located between 153.6 ft and 180.9 ft bsl. Bordering this region above and below are zones containing moderately shocked material. Two moderately shocked samples, 149.2 ft and 151.3 ft bsl, were taken at the base of the β_{1a} (late-stage collapse rubble) geologic zone, and three samples deeper in the β_{1b} extending to a depth of 195.3 ft bsl.

The next farthest borehole (OET-7) is 1,374 ft from GZ. Based on seismic-reflection, paleontologic, and lithostatigraphic data, this borehole is thought to be located outside of the excavational crater (Henry, Wardlaw, and others, 1986). The majority of the nine samples were from the GAMMA zone; however, all but the uppermost sample were heavily to moderately shocked. Of the highly shocked samples, six out of seven were uncemented sediment samples. The highly shocked zone extended from 118.9 to 147.5 ft bsl, and a moderately shocked, cemented sample was detected at 173.6 ft bsl.

Borehole OAR-2A, located 4,458 ft from OAK GZ, initially was sampled only as a reference core; however, six of 21 samples from this borehole have been heavily shocked. Two other samples were moderately shocked to pressures of 3.5 and 4.4 GPa. All of the shocked samples were located within the top 39 ft of the core and the most heavily shocked material within the first 24 ft. The proximity of this borehole to the reef may suggest that some highly shocked, fine-grain ejecta was transported from the slope and deposited at the site of OAR-2A.

The combined results from the OAK borehole sample analysis are presented in Figure 4-7. The solid horizontal line in each panel indicates the present sea-floor depth. The depth and thickness of each zone containing highly shocked material ($P > 10$ GPa) as a function of the distance of the borehole from GZ is shown in a simplified manner in Figure 4-8.

Results from Debris Samples

The debris analyzed consists of 14 samples collected throughout the crater by submersible and three samples collected by scuba divers from roughly a single site. The former samples are a subset of a series of debris samples analyzed by Halley, Ludwig, and others (1986). Figure 4-9 shows the locations where each debris sample was recovered. The range values that will be discussed in a subsequent section were measured from this map. Unfortunately, the debris samples included in this study were all taken from roughly the same distance from GZ. Only one sample (OAK 201) was recovered at a significantly different range.

The results of the debris analysis are plotted in Figure 4-10A and listed in Table 4-8 (located at end of Chapter). The majority of the debris samples were relatively unshocked; however, all of the highly shocked debris was found

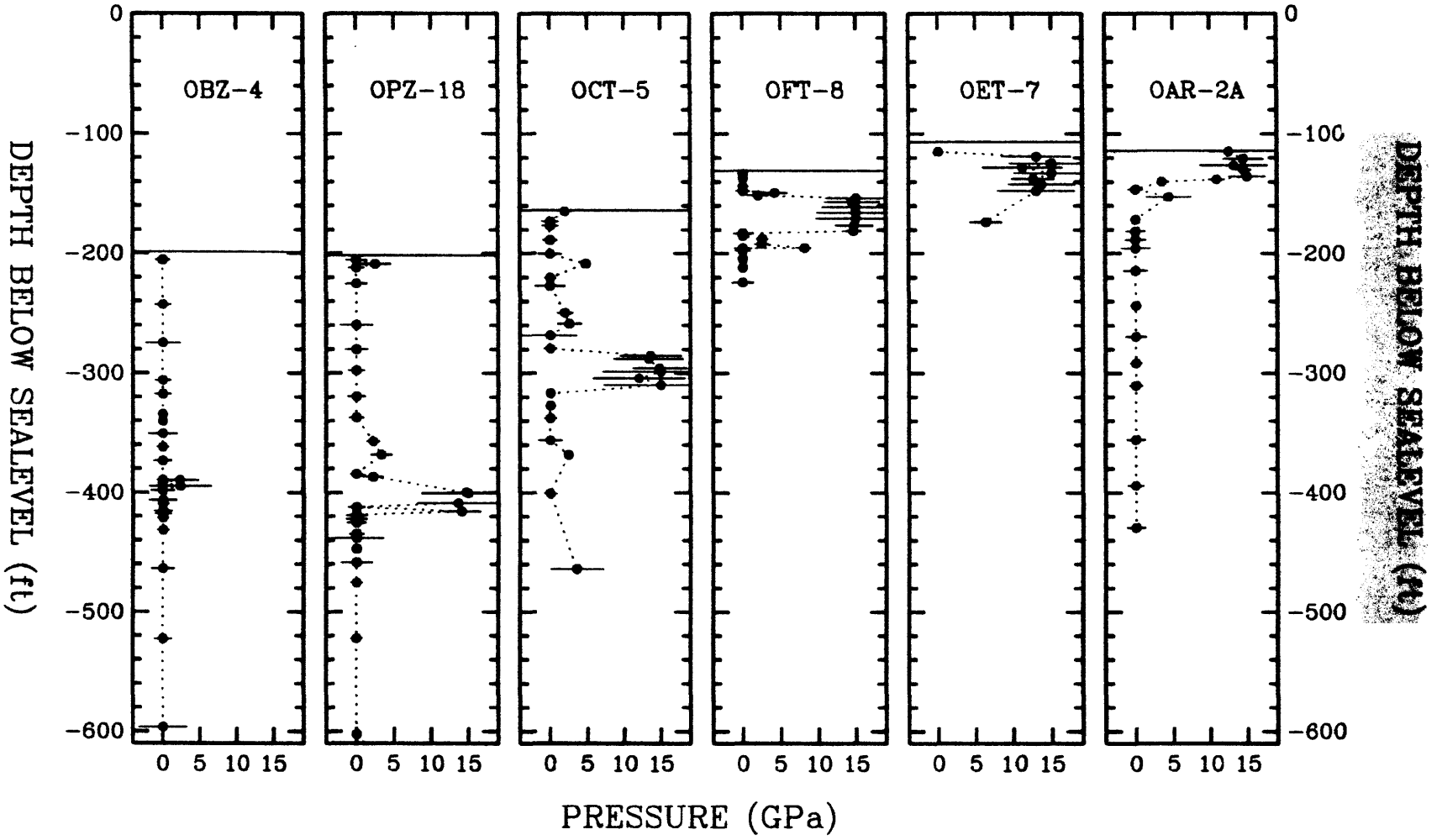

FIGURE 4-7. -- Combined results of the borehole-sample analysis showing the calculated shock pressure in relation to the sample depth in ft below sea level. The boreholes are presented in order of increasing distance from ground zero.

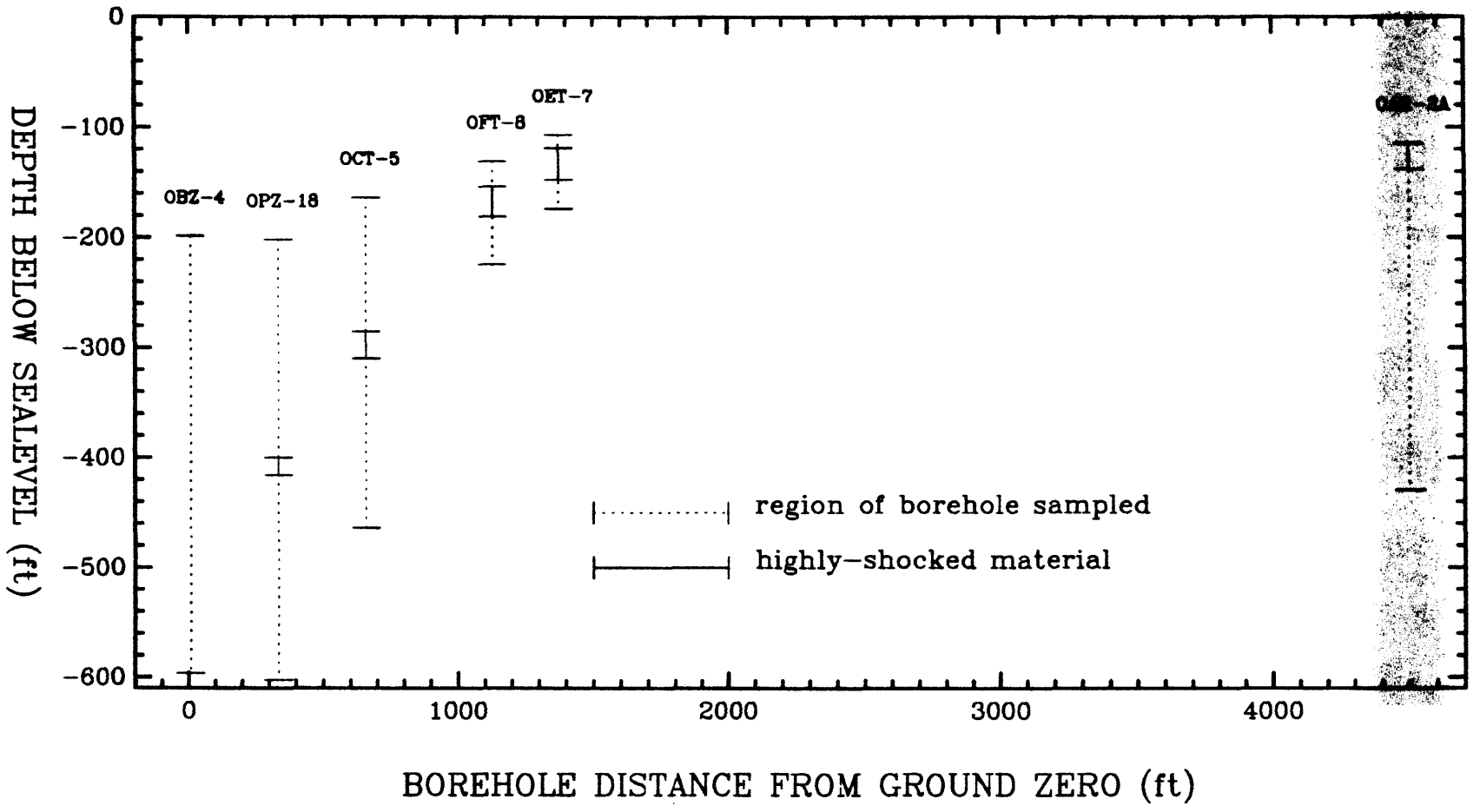

FIGURE 4-8. -- Illustration of the depth and thickness of regions of highly shocked carbonates recovered from each borehole. The dotted line indicates the extent of the borehole sampled, and the solid line defines the highly shocked zone.

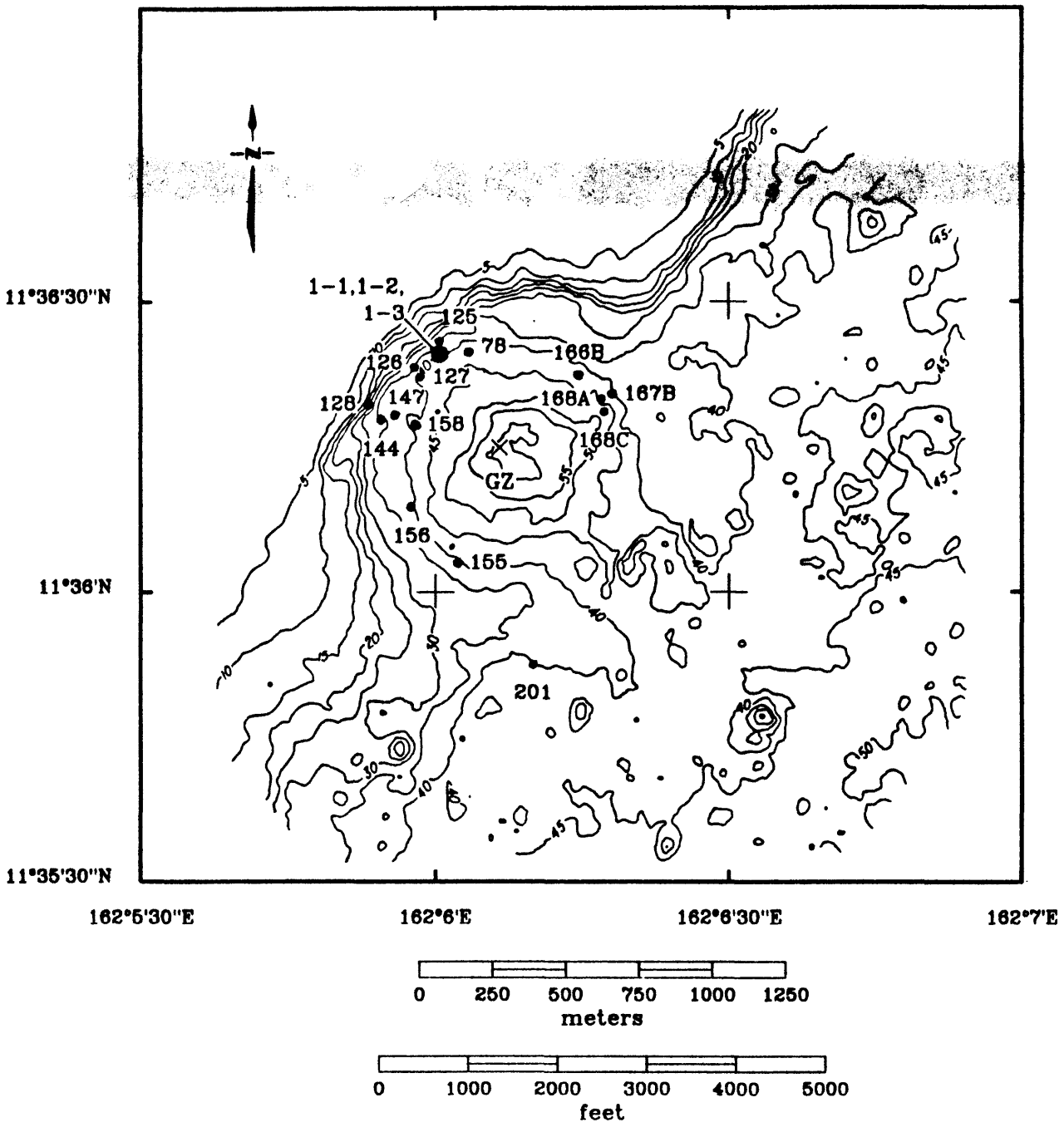

FIGURE 4-9. -- Map of OAK crater showing the debris-sample recovery sites. Bathymetric contours given in 5-meter intervals.

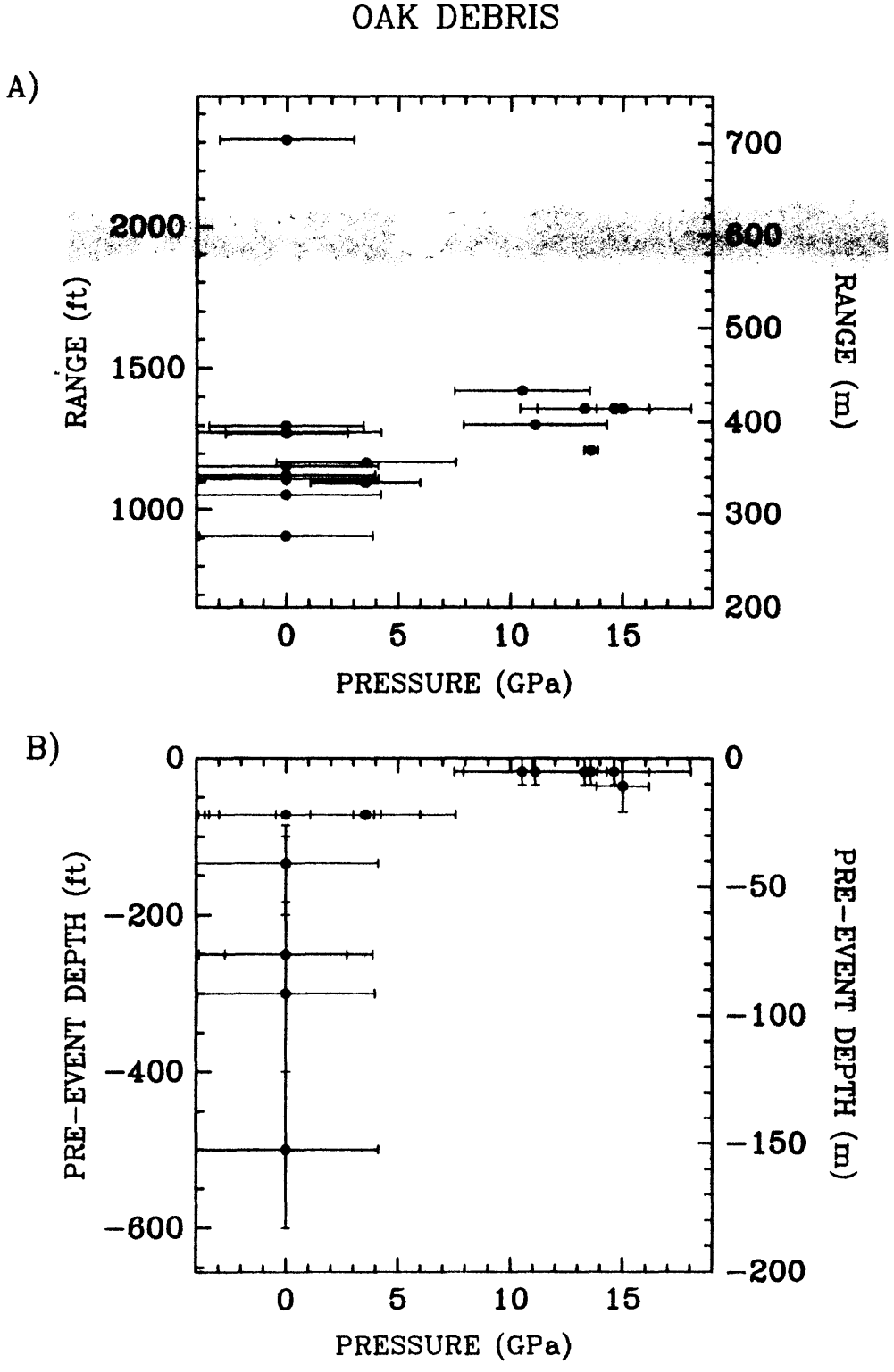

FIGURE 4-10. -- Results of the debris-sample analysis showing (A) shock pressure as a function of range from ground zero, and (B) shock pressure versus estimated pre-event depth below sea level.

at the base of the reef slope. The reef may have blocked some of the highly shocked material from leaving the crater as ejecta, or this material (ejected from the crater) could have been transported craterward back down the reef slope some time after the crater was formed.

In addition to the range measurements, the estimated pre-event initial depth of a limited number of the debris samples was available from strontium-isotope analysis (Halley, Major, and others, 1986; and Ludwig, Halley, and others, 1986) and gross paleontologic and petrographic analysis by B.L. Ristvet in 1981 (see Ristvet, 1986) and corroborated by subsequent analysis by USGS personnel. The pre-event depth below sea level is plotted against shock pressure for these samples in Figure 4-10. Although the pre-event depth estimates are crude in some cases, a strong correlation is evident between shock pressure and depth for this limited data set. This correlation is consistent with the assertion that the pre-event surface material near GZ was the most severely shocked.

DISCUSSION

With a few exceptions, the bulk of the samples analyzed can be split into two catagories, unshocked and very highly shocked. There were relatively few samples which can be assigned to intermediate pressure categories. This suggests that the majority of the shocked material shares a common origin. Presumably, the material right at or near the surface near GZ received the highest shock pressure from the blast. During the cratering event, some of this material was incorporated in the lining of the transient crater cavity and was then buried almost immediately by the collapse of the crater walls. Subsequent backwash of ejecta and slumping and deformation of the crater would tend to mix this highly shocked material with other rubble and breccia and consequently obscure any stratigraphically discernable zone of highly shocked material.

This hypothesis can be applied to explain the presence of the shocked regions in OPZ-18 and in the transition boreholes. Because slumping and collapse become increasingly more important toward the rim of the crater, it is not unreasonable that OPZ-18 is the only borehole to have the shocked material preserved in a stratigraphically discernable unit such as the transition sands. The thickness of the region of highly shocked material does remain fairly constant throughout the three transition boreholes (Figure 4-8), although the region is located at consistently shallower depths as the distance between the borehole and GZ increases. This is a further indication that these regions were at one time related.

Late-stage debris slumping and the influence of sedimentation also have contributed to borehole stratigraphy. Post-event slumps from the reef have deposited at least 8 ft of unshocked debris at OET-7, and possibly as much as 17 ft at OFT-8. The location of the shocked debris samples collected from the floor of the crater suggest that highly shocked ejecta may also be deposited from the reef slope, and the shocked upper layer of OAR-2A could be the result of accumulated deposition over many years.

ACKNOWLEDGEMENTS

The authors would like to thank the following people: Lt. Col. Robert F. Couch, Jr., for his support of this project; Thomas W. Henry for assistance with sample acquisitions from the boreholes; Robert B. Halley for providing debris samples; Papo Gelle, Mike Long, and Leon Young for preparing the recovery samples for the shock-wave experiments; and Sunney Chan for use of the EPR facilities.

Contribution # 4473, Division of Geological and Planetary Sciences, California Institute of Technology, Pasadena, CA 91125.

REFERENCES CITED

Blanchard, S.C., and Chasteen, N.D., 1976, Electron paramagnetic resonance spectrum of a sea shell, Mytilus edulis: Journal of Physical Chemistry, v. 80, p. 1362-1367.

Halley, R.B., Major, R.P., Ludwig, K.R., Peterman, Z.L., and Matthews, R.K., 1986, Preliminary analyses of OAK debris samples; 11 p., 7 figs., 4 tbls.; in Folger, D.W., ed., Sea-floor observations and subbottom seismic characteristics of OAK and KOA craters, Enewetak Atoll, Marshall Islands: U.S. Geological Survey Bulletin 1678.

Henry, T. W., Wardlaw, B. R., Skipp, B., Major, R.P., and Tracey, J. I.,Jr., 1986, Pacific Enewetak Atoll Crater Exploration (PEACE) Program Enewetak Atoll, Republic of the Marshall Islands; Part 1: Drilling operations and descriptions of boreholes in vicinity of KOA and OAK craters: U.S. Geological Survey Open-File Report 86-419, 502 p., 29 figs., 13 tbls., 3 appendicies.

Hurd, F. K., Sachs, M., and Hershberger, W. D., 1954, Paramagnetic resonance absorption of Mn^{++} in single crystals of $CaCO_3$: Physics Review, vol. 93, p. 373-380.

Low, W. and Zeira, S., 1972, ESR spectra of Mn^{++} in heat-treated aragonite: American Mineralogist, v. 57, p. 1115-1124.

Ludwig, K.R., Halley, R.B., Simmons, K.R., and Peterman, Z.E., 1986, Sr-isotope stratigraphy of disturbed and undisturbed carbonates; 23 p., 8 figs., 6 tbls.; in Henry, T.W., and Wardlaw, B.R., eds., Pacific Enewetak Atoll Crater Exploration (PEACE) Program Enewetak Atoll, Republic of the Marshall Islands; Part 3: Stratigraphic analysis and other geologic and geophysical studies in vicinity of OAK and KOA craters: U.S. Geological Survey Open-File Report 86-555.

Marsh, S.P. (Ed.), 1980, LASL Shock Hugoniot Data; University of California Press, Berkeley.

Ristvet, B.L, 1986, Personal oral communication.

Stoffler, D., 1972, Deformation and transformation of rock-forming minerals by natural and experimental shock processes: Fortschrift Mineralogie, v. 49, p. 50-113.

Tyburczy, J.A., and Ahrens, T.J., 1986, Dynamic compression and volatile release of carbonates: Journal of Geophysical Review, v. 91, p. 4730-4744.

Vizgirda, J. and Ahrens, T. J., 1980, Shock-induced effects in calcite from Cactus Crater: Geochimica Cosmochimica Acta, v. 44, p. 1059-1069.

Wardlaw, B. R., and Henry, T. W., 1986, Geologic interpretation of OAK and KOA craters; 39 p., 21 figs., 3 tbls., 1 appendix; in Pacific Enewetak Atoll Crater Exploration (PEACE) Program Enewetak Atoll, Republic of the Marshall Islands; Part 3: Stratigraphic analysis and other geologic and geophysical studies in vicinity of OAK and KOA craters: U.S. Geological Survey Open-File Report 86-555.

****

TABLE 4-2. Results for Borehole OAR-2A Samples. The pressures and accompanying errors are given in Giga Pascal (GPa). Depths are provided in both feet below seafloor (ft bsf) and feet below sealevel (ft bsl). For explanation of carbonate petrographic names used under DESCRIPTION column in this and succeeding tables, see Henry, Wardlaw, and others (1986, p. 83-97).

DEPTH (ft bsf)	DEPTH (ft bsl)	P (GPa)	ERROR (GPa)	DESCRIPTION
0.6	111.1	12.5	2.6	uncemented sand
6.6	117.1	14.5	2.7	uncemented wackestone
12.2	122.7	13.2	4.5	uncemented wackestone
15.8	126.3	14.5	1.0	uncemented wackestone
21.4	131.9	15.0	2.4	uncemented packstone
23.8	134.3	10.9	1.0	uncemented wackestone/packstone
25.8	136.3	3.5	0.6	uncemented packstone below AA/BB bndry
32.2	142.7	0.0	1.0	cemented packstone
38.4	148.9	4.4	3.0	poorly-cemented packstone
57.3	167.8	0.0	0.7	cemented packstone
67.1	177.6	0.0	1.2	poorly-cemented wackestone
74.2	184.7	0.0	1.3	uncemented wackestone
81.6	192.1	0.0	1.9	uncemented wackestone
100.3	210.8	0.0	1.6	coral fragment, *Astreopora*
129.3	239.8	0.0	0.6	cemented wackestone
155.3	265.8	0.0	1.4	spar-replaced coral
177.4	287.9	0.0	0.7	well-cemented mudstone
196.3	306.8	0.0	0.8	cemented wackestone
241.6	352.1	0.0	1.2	uncemented grainstone
280.0	390.5	0.0	0.9	cemented wackestone burrow
315.6	426.1	0.0	1.1	cemented wackestone

TABLE 4-3. Results for Borehole OBZ-4 samples. The pressures and accompanying errors are given in Giga Pascal (GPa). Depths are provided in both feet below seafloor (ft bsf) and feet below sealevel (ft bsl).

CRATER ZONE	DEPTH (ft bsf)	(ft bsl)	P (GPa)	ERROR (GPa)	DESCRIPTION
α_1	6.7	205.4	0.0	0.9	mud
α_2	44.0	242.7	0.0	1.0	wackestone
	75.9	274.6	0.0	2.3	coarse-grain packstone
β_{1a}	107.5	306.2	0.0	1.0	cemented
	119.1	317.8	2.3	1.0	cemented packstone
	136.0	334.7	0.0	0.6	cemented packstone
	141.8	340.5	0.0	0.5	cemented
	152.1	350.8	0.0	2.0	cemented
	163.3	362.0	0.0	0.8	cemented
β_{1b}	174.8	373.5	0.0	1.2	spar
	190.8	389.5	0.0	0.7	cemented wackestone burrow
	191.0	389.7	2.3	2.6	lithoclast and spar
	193.2	391.9	0.0	0.6	cemented packstone
	196.1	394.8	2.4	4.2	spar-replaced *Favia*
	199.6	398.3	0.0	1.6	fine grain muddy sand
	199.9	398.6	0.0	0.7	uncemented wackestone
β_2	207.7	406.4	0.0	1.8	cemented wackestone burrow
	210.9	409.6	0.0	0.7	cemented packstone burrow
	216.6	415.3	0.0	0.7	recrystallized *Tridacna*
	217.1	415.8	0.0	1.2	well-cemented tea-brown micrite
	219.4	418.1	0.0	1.1	spar-replaced coral
β_3	222.7	421.4	0.0	0.7	cemented packstone
	233.0	431.7	0.0	0.7	uncemented
	265.1	463.8	0.0	1.5	poorly-cemented
	324.0	522.7	0.0	1.1	cemented burrow
γ	397.7	596.4	0.0	3.2	spar-replaced coral

TABLE 4-4. Results for Borehole OCT-5 Samples. The pressures and accompanying errors are given in Giga Pascal (GPa). Depths are provided in both feet below seafloor (ft bsf) and feet below sealevel (ft bsl).

CRATER ZONE	DEPTH (ft bsf)	(ft bsl)	P (GPa)	ERROR (GPa)	DESCRIPTION
α_1	0.9	164.6	0.0	1.0	uncemented grainstone
α_2	9.4	173.1	0.0	1.1	coarse-grain packstone
	13.0	176.7	0.0	1.0	uncemented packstone
	25.0	188.7	0.0	0.9	fall-in (?)
	36.7	200.4	0.0	1.5	cemented wackestone burrow
β_{1a}	45.0	208.7	4.8	0.6	echinoid spine
	56.7	220.4	0.0	0.8	cemented packstone lithoclast
	63.4	227.1	0.0	2.0	rounded cemented burrow
	85.8	249.5	0.0	1.0	cemented packstone
	95.1	258.8	2.6	1.6	*Cardium* with internal filling
	104.7	268.4	0.0	3.5	spar-replaced *Cardium*
	115.7	279.4	0.0	0.8	cemented wackestone
	121.6	285.3	13.6	4.2	uncemented med-grained grainstone
	124.3	288.0	13.3	4.7	uncemented coarse-grained grainstone
β_{1b}	131.9	295.6	14.8	3.6	uncemented grainstone
	135.1	298.8	15.0	8.0	cemented grainstone
	140.6	304.3	12.0	6.3	uncemented *Halimeda* packstone
	146.2	309.9	15.0	7.8	uncemented *Halimeda* packstone
	153.4	317.1	0.0	0.6	cemented burrow
	163.6	327.3	0.0	0.6	cemented packstone
	174.1	337.8	0.0	0.8	cemented packstone
	192.6	356.3	0.0	1.6	cemented packstone
	204.7	368.4	2.5	0.4	tea-brown cemented rhizolith
γ	237.0	400.7	0.0	0.8	tea-brown cemented packstone
	300.3	464.0	3.6	3.5	spar-replaced coral

TABLE 4-5. Results for Borehole OET-7 Samples. The pressures and accompanying errors are given in Giga Pascal (GPa). Depths are provided in both feet below seafloor (ft bsf) and feet below sealevel (ft bsl).

CRATER ZONE	DEPTH (ft bsf)	(ft bsl)	P (GPa)	ERROR (GPa)	DESCRIPTION
	8.3	115.2	0.0	0.7	pebble-sized lithoclast
α_2	12.0	118.9	13.0	4.5	uncemented grainstone
	17.8	124.7	15.0	5.5	coral pebble
	21.2	128.1	11.2	5.2	uncemented *Halimeda* grainstone
	25.9	132.8	15.0	4.8	uncemented packstone-grainstone
γ	30.7	137.6	12.6	2.7	uncemented packstone-grainstone
	35.3	142.2	13.7	4.3	uncemented packstone-grainstone
	40.6	147.5	13.0	5.0	uncemented fine-grain packstone
	66.7	173.6	6.4	2.1	cemented pebble-sized

TABLE 4-6. Results for Borehole OFT-8 Samples. The pressures and accompanying errors are given in Giga Pascal (GPa). Depths are provided in both feet below seafloor (ft bsf) and feet below sealevel (ft bsl).

CRATER ZONE	DEPTH (ft bsf)	(ft bsl)	P (GPa)	ERROR (GPa)	DESCRIPTION
	2.7	133.5	0.0	0.6	tea-brown cemented rhizolith
α_2	6.4	137.2	0.0	0.6	tea-brown cemented lithoclast
	13.1	143.9	0.0	0.6	tea-brown cemented packstone
	17.0	147.8	0.0	0.9	cemented packstone
β_{1a}	18.4	149.2	4.2	1.6	cemented matrix within pelecypod
	20.5	151.3	2.0	1.4	partly spar-replaced coral
	22.8	153.6	15.0	4.0	uncemented packstone
	26.0	156.8	14.5	3.7	uncemented grainstone
	30.4	161.2	15.0	4.5	uncemented *Halimeda*
	35.0	165.8	15.0	5.2	uncemented packstone
	39.8	170.6	15.0	5.3	uncemented packstone
	45.5	176.3	14.8	2.5	partly spar-replaced coral
	50.1	180.9	14.7	1.0	uncemented packstone
β_{1b}	52.3	183.1	0.0	1.2	*Cardium* with cemented matrix
	52.6	183.4	0.0	0.9	partly spar-replaced coral
	54.4	185.2	0.0	0.6	moderately cemented packstone
	57.0	187.8	2.6	0.7	moderately cemented *Halimeda*
	61.1	191.9	2.5	0.9	poorly-cemented packstone
	64.5	195.3	8.1	0.8	cemented shell rubble
	64.9	195.7	0.0	1.1	spar-replaced *Astreopora*
	67.0	197.8	0.0	1.0	mudstone filled cemented burrow
	73.8	204.6	0.0	0.4	moderately cemented packstone
γ	81.2	212.0	0.0	0.5	cemented packstone
	93.5	224.3	0.0	1.4	spar-replaced *Porites*

TABLE 4-7. Results for Borehole OPZ-18 Samples. The pressures and accompanying errors are given in Giga Pascal (GPa). Depths are provided in both feet below seafloor (ft bsf) and feet below sealevel (ft bsl).

CRATER ZONE	DEPTH (ft bsf)	(ft bsl)	P (GPa)	ERROR (GPa)	DESCRIPTION
	3.6	205.5	0.0	1.4	uncemented mudstone
	7.0	208.9	2.5	2.1	uncemented mudstone
α_1	10.0	210.9	0.0	1.0	uncemented mudstone
	23.3	225.2	0.0	1.4	uncemented mudstone
	57.8	259.7	0.0	2.1	uncemented wackestone
	78.2	280.1	0.0	1.4	uncemented grainstone
β_{1a}	95.9	297.8	0.0	1.0	uncemented grainstone
	117.8	319.7	0.0	1.1	uncemented grainstone
	135.3	337.2	0.0	0.9	uncemented grainstone
	155.3	357.2	2.2	0.9	uncemented packstone
β_{1b}	166.6	368.5	3.3	1.4	uncemented packstone
	182.6	384.5	0.0	0.8	spar-cemented grainstone
	185.0	386.9	2.2	1.3	uncemented
β_2	198.0	399.9	14.7	2.5	uncemented
	198.6	400.5	15.0	6.3	green Holocene wackestone mud
	207.0	408.9	13.6	5.4	uncemented
	210.5	412.4	0.0	1.1	cemented packstone burrow
	214.0	415.9	14.1	2.5	uncemented
	217.0	418.9	0.0	0.9	tea-brown cemented packstone
	217.1	419.0	0.0	0.7	cemented wackestone
	217.5	419.4	0.0	1.4	cemented wackestone burrow
	220.4	422.3	0.0	1.3	coarse-grain spar
	220.5	422.4	0.0	0.8	cemented packstone
β_3	223.5	425.4	0.0	1.2	cemented packstone burrow
	232.9	434.8	0.0	0.9	poorly-cemented packstone
	236.3	438.2	0.0	3.5	partially spar-replaced coral
	245.4	447.3	0.0	0.6	cemented wackestone
	256.9	458.8	0.0	2.0	spar-replaced coral
	273.8	475.7	0.0	0.7	spar-cemented packstone burrow
	320.5	522.4	0.0	0.7	spar-filled grstropod
γ	400.5	602.4	0.0	0.6	cemented wackestone

TABLE 4-8. Results for OAK Debris Samples. The pressures and accompanying errors are given in Giga Pascal (GPa). Source-depths are converted to feet below sea level from Ludwig and others (1987) and Ristvet (1981).

SAMPLE	RADIUS (ft)	ERROR (ft)	P (GPa)	ERROR (GPa)	SOURCE-DEPTH (ft bsl)
78	1053	13	0.0	0.9	–
125a	1273	13	0.0	1.8	200-500
126	1211	13	13.6	4.2	105–140
127	1095	13	3.0	2.0	–
128	1421	13	10.5	8.0	105–140
144	1302	13	12.5	2.3	105–140
147	1170	30	2.7	0.9	–
155	1299	13	0.0	1.4	–
156	1109	13	0.0	1.1	–
156b	1109	13	0.0	0.9	–
158	906	13	0.0	1.0	200-500
166B	1109	13	0.0	1.0	500-700
167B	1276	13	0.0	0.6	–
168A	1155	13	0.0	0.8	–
168C	1122	13	0.0	1.4	300-500
201	2310	16	0.0	1.4	420
1–1	1358	157	13.1	1.6	105–140
1–2	1358	157	15.0	3.4	>140
1–3	1358	157	14.6	1.6	105–140

CHAPTER 5:

BATHYMETRIC STUDIES OF OAK CRATER

By

John L. Peterson[1] and Robert W. Henny[2]

INTRODUCTION

This chapter summarizes recent work done by the Air Force Weapons Laboratory (AFWL) and the New Mexico Engineering Research Institute (NMERI) in a first-order assessment of OAK crater bathymetry (Peterson and Henny, 1987). The starting points for this study were the 1958 pre- and postshot bathymetric maps and a new 1984 bathymetric map of the OAK crater (ALICE reef) area of Enewetak Atoll (fig. 5-1).

Objectives and General Procedures

The primary objectives were to characterize and to quantify changes in bathymetry resulting both from the detonation of the OAK device and from subsequent geologic processes. A secondary objective was to provide a set of working maps at a common scale of 1:2400 for use both by the PEACE Program and future investigations.

The approach was to prepare contour maps by digitizing and reprocessing each of the three bathymetric basemaps and to construct three isopach maps from the contour-map pairs with the aid of a computer. Areas and volumes were computed by contour interval for each of the isopach maps, and planar and cross-sectional features were examined critically on all six maps.

Terminology

The following terms are used in this Chapter. No attempt is made here to correlate the cratering terms with those used in other portions of this Open-File Report; this can only be accomplished after synthesis of the various data sets (see statement 8 of the Conclusions).

Circular crater -- crater region consisting of an inner circular component, as defined by the minus 145-ft closed contour in the postshot contour maps, which is enclosed by an outer-circular component as defined by approximately the minus 50-ft partially closed contour on the same maps.

---

[1] New Mexico Engineering Research Institute, Albuquerque, NM.

[2] Air Force Weapons Laboratory, Kirtland Air Force Base, NM.

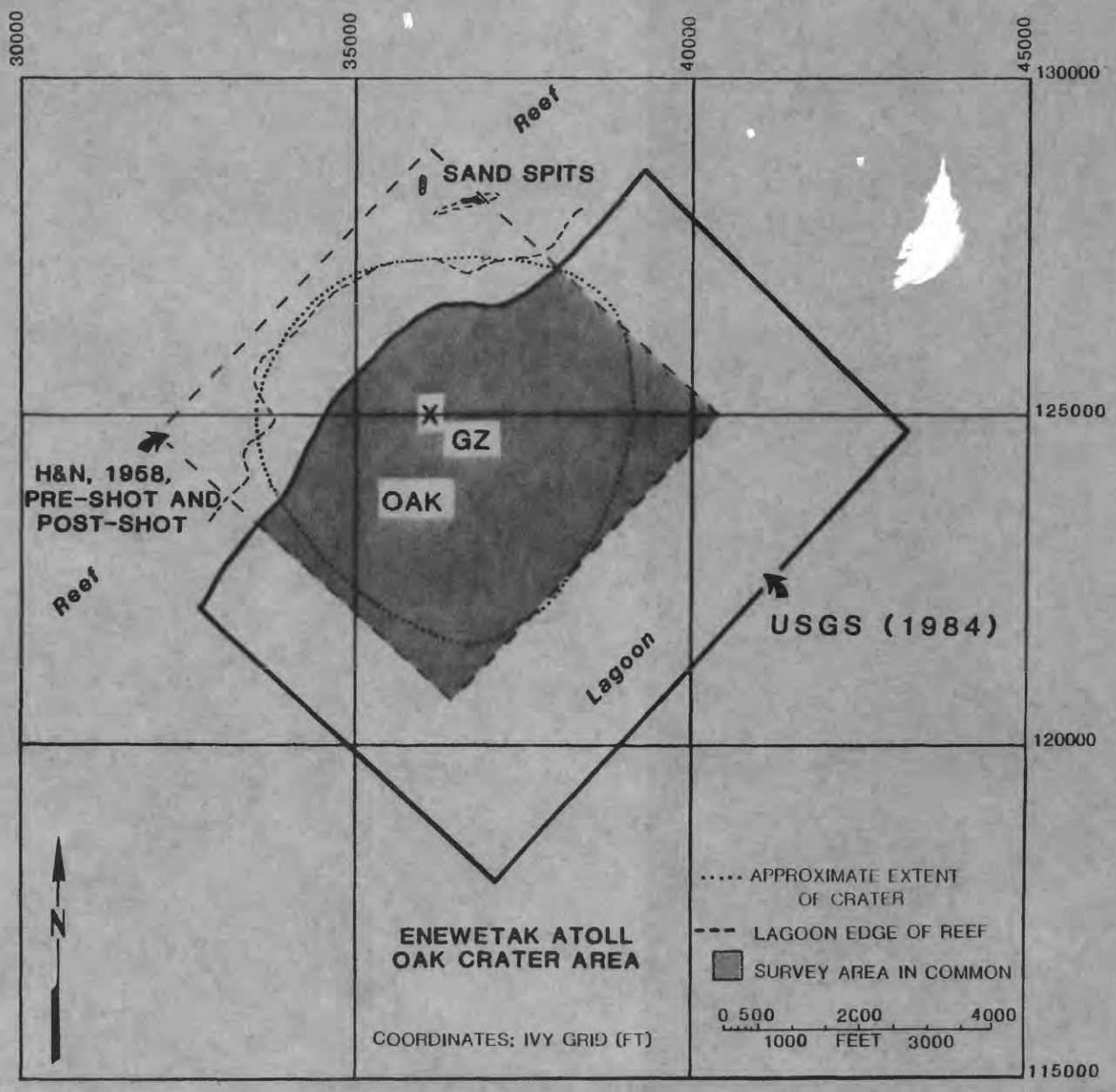

FIGURE 5-1. -- Map showing OAK crater region and areas included in Holmes and Narver pre- and postshot surveys (H&N, 1958a and 1958b) and the U.S. Geological Survey map (USGS, 1984). Area in common to all three basemaps shown in stippled pattern. OAK surface ground zero (SGZ) depicted by "X", and apparent crater shown by dotted line.

Crater wings -- areas primarily within the reef slope and just beyond the boundary of the circular crater.

Elliptical crater -- crater region consisting of the circular crater and portions of the crater wings as defined by the closed minus 20-ft contour of the isopach maps.

Apparent crater -- the final observed crater, composed of the elliptical crater and the encompassing areas of subsidence. Note that the apparent crater boundary extends beyond the mapped areas of this study.

Differential relief (subsequently abbreviated Δ-relief) -- term used in describing the net positive and negative changes in relief of an area with time. This is depicted by isopach maps showing the areas of change of relief derived from comparison of the digitized bathymetric base maps.

Subsidence -- term used to denote an increase in negative Δ-relief without subscribing to any particular mechanism.

Units used in this Chapter are those of the original works; metric for the 1984 bathymetry, engineering for the remainder.

DATA BASE

H&N Preshot Bathymetric Map

Prior to the OAK nuclear event (29 June 1958), a bathymetric survey of the site (ALICE-reef area) was conducted between 3 and 26 June by Holmes and Narver Engineering Company (H&N) for the U.S. Atomic Energy Commission (AEC) using standard rod, fathometer, and lead-line surveying techniques (fig. 5-1). Datum was 0.5 ft below Approximate Mean Low Water Spring (AMLWS). The survey, tied into the Eniwetok Ivy Grid Coordinate System (H&N, 1952; U.S. Army, 1970), originally was planned to cover a 6,000- x 6,000-ft square centered on the OAK surface ground zero (SGZ) and aligned with the oceanward edge of ALICE reef. A baseline approximately 6,000-ft long was established along the highest topographic area of the reef flat (specifically, along a line of sand bars midway on the reef flat) with benchmarks (BMs) placed on 300-ft centers.

A standard rod survey was conducted perpendicular to the baseline at each BM oceanward to near the reef edge and lagoonward to approxi ately the minus 5-ft elevation. Each survey line was continued lagoonward to 3,000 ft beyond SGZ using an LCM vessel equipped with a Raytheon Recording Fathometer. Vessel course was controlled by theodolite from each BM and at 300-ft intervals by triangulation from the two terminal baseline BMs. Vertical control was provided at these 300-ft intervals by a lead-line sounding. No cross-tie survey lines were run, and a data gap of a few hundred feet at the lagoonward reef edge resulted because of the inability of the LCM-vessel to obtain fathometer readings in water shallower than 10 to 15 ft (H&N, 1958a).

The resultant bathymetric map was hand-contoured with 5-ft intervals (1-ft intervals above the minus 5-ft contour) (pl. 5-1)[1]. The map did not include the surveyed ocean side of the reef for reasons discussed below.

H&N Postshot Bathymetric Map

A postshot survey of the OAK crater area, using the same techniques described above, was run between 16 August and 4 September 1958 (D + 47 to 67 days). Numerous major problems were encountered in relocating the baseline along the reef flat opposite the crater because it was significantly disturbed (lowered and covered with debris) by the event. Eventually, the terminal BMs were located and the baseline reconstructed. As in the preshot survey, there was a data gap between rod and fathometer surveys that probably was increased by the difficult postshot conditions. These conditions also resulted in little of the reef oceanward of the baseline being resurveyed. Finally, toward the end of the survey, operationally imposed time constraints may have resulted in only every other line being surveyed in the far eastern quadrant of the grid. The resultant map (H&N, 1958b), contoured at a 5-ft interval, covered the same area as the preshot survey except oceanward of the reef baseline (fig. 5-1), thus giving a common pre-/postshot map area of approximately 6,000 x 5,000 ft or 30 million sqft (pl. 5-2).

Detailed documentation of the H&N surveys does not exist. Most of the information presented here is from B.L. Ristvet (oral communication, 1986) who has reviewed the original field survey books and maps referenced and has conducted extended discussions with several of the original workers.

USGS 1984 Bathymetric Map

The third basemap used in this study was the bathymetric map of the OAK crater and surrounding area prepared from a detailed echo-sounder survey conducted in 1984 (D + 26 years) by the U.S. Geologic Survey (USGS) during the Marine Phase of the PEACE Program (USGS, 1984; see Folger, Hampson, and others, 1986, for details of the survey). This survey also was tied into the Eniwetok Ivy Grid; however, datum was Mean Lower Low Water (MLLW), which is 0.18 m (0.6 ft) below the MLWS established for the earlier H&N surveys. Most of the echo-sounder data were collected along 25-m- (82-ft-) spaced lines oriented parallel to the reef. Perpendicular tie lines were run on the average at 180-m (590-ft) intervals (fig. 5-2). Thus, the USGS survey had a sampling density greater than four times that of the H&N surveys. Although smaller boats provided some data at shallower water depths, nearly all data contoured were obtained from the 41-m R/V Egabrag II, which, because of her draft, effectively excluded data above minus 4 m (minus 13 ft). Therefore, although the greatly increased sample density allowed a 1-m contour interval and the survey extended a 1,000 ft both farther out into the lagoon and along the reef slope (figs. 5-1 and 5-2), no bathymetric data were obtained from

---

[1] Plates 5-1, 5-2, and 5-3 are digitized, reprocessed versions of the referenced original bathymetric maps; these are located at the end of the Open-File Report in the map pocket.

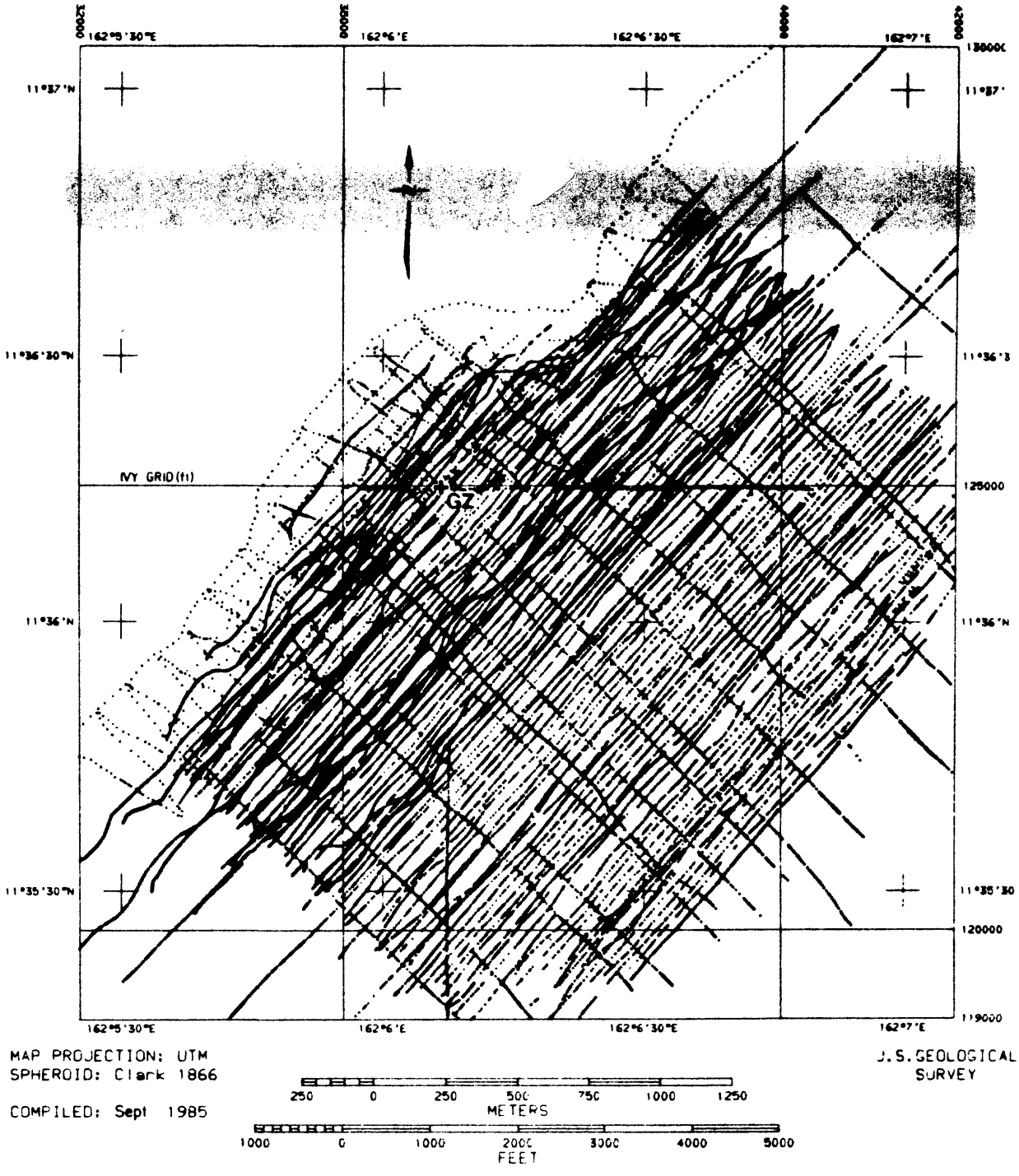

FIGURE 5-2. -- Fathometer lines used in the 1984 USGS study (from Folger, Hampson, and others, 1986, fig 2, p. A-3).

near the reef or on the reef flat itself. This reduced the contoured area common to all three maps to approximately 25.5 million sqft or 85 percent of the digitized H&N maps (see fig. 5-1).

DATA PROCESSING

Digitized Base Contour Maps

All data input and processing were performed using an Arc/Info Geographic Information System software package (ESRI, 1986). Processing was done on a VAX 11/750 computer at the Technology Application Center (TAC), University of New Mexico.

The data-input process for the two H&N maps (pls. 5-1 and 5-2, located in the map pocket at the end of the Report) was complicated because the maps were not on base-stable media. Both were digitized manually from 1:2400-scale bluelines using a 36- x 48-in. Summagraphics Digitizer Tablet operating in the continuous-string sampling mode. All data entered into the system were initialized and recorded in the Eniwetok Ivy Grid Coordinate System.

Digitization of the 1984 USGS basemap (pl. 5-3) required that a photographic enlargement be made from the original mylar map (1:6000). The enlargement was redrafted to separate contour lines along steep slopes within the study area. This redrafted map was photographically enlarged again to increase digitizing accuracy of the contours.

Three minor corrections were required to standardize and update the USGS map. The first was a simple conversion of metric contours to feet. However, since no interpolation was applied to the converted metric units, non-integer engineering-unit contours were generated. The second was a depth correction. This resulted from the comparison of the water-depth values interpolated from the USGS bathymetric map to those measured at each borehole site during the Drilling Phase of the PEACE Program. Linear fits to these data pairs showed that fathometer depths exceeded borehole-site depths by 1 percent down to minus 120 ft, and that borehole-site depths exceeded fathometer depths by 2 percent below minus 120 ft (E.L. Tremba, oral communication, 1986). Third, only those portions of the USGS map that overlayed the H&N map boundaries were digitized.

All digitized basemaps were quality-control checked by interactive zoom editing with a 13-in. Techtronix 4107A Color Graphics Terminal. The maps were scale-corrected by the computer to be compatible for overlaying data sets.

Derived Isopach Maps

Three pairs of isopach maps were computer-generated by digitally subtracting combinations of the three contour maps. The contour-map combinations and descriptions of the resulting three pairs of isopach maps are listed below. The first isopach map of each pair presents negative Δ-relief; the second map shows the positive Δ-relief. All (as plates) are located in the pocket in the back of this Report.

H&N Postshot - H&N Preshot Map Pair: Plates 5-4 and 5-5 display distribution of short-term elevation changes (event to D + 67 days) primarily due to cratering effects.

USGS 1984 - H&N Preshot Map Pair: Plates 5-6 and 5-7 display distribution of long-term elevation changes (event to D + 26 years) primarily due to cratering effects and redistribution of crater-produced and natural debris.

USGS 1984 - H&N Postshot Map Pair: Plates 5-8 and 5-9 display distribution of post-crater long-term elevation changes (from D + 67 days to D + 26 years) primarily due to continued subsidence and redistribution of crater-produced and natural debris.

Figure 5-3 illustrates how vertical differences in elevation were calculated within the Arc/Info computer framework. As indicated, a polygon is formed where the two sets of elevation contours, one from each map, intersect. To account for as much of the elevation variance inside the polygon as possible, the mean between the two contours was always used. The vertical difference for each polygon, therefore, is the difference between the means of the two contour sets. In the production of the isopach maps, vertical differences were computed for all polygons formed by the intersection of one map overlaid on another. Typically, five thousand polygons were formed per isopach map. Areas for each polygon were computed in square feet and stored as associated attributes. The vertical-difference files and individual polygons were then sorted into 5-ft increments by a decision rule that grouped polygons with similar vertical differences (i.e.; 0 to 5 ft, 5 to 10 ft, etc.) into the same file.

To reduce required computer memory for the graphic displays, a dissolve module was run on the computer map files that combined adjacent polygons having the same 5-ft increment. Tabular data used to compute areas and volumes for each polygon were saved separately. The final groupings of polygons, representing an increment of 5 ft of positive or negative elevation difference (Δ-relief) between two maps, was then assigned a color and/or symbol for the slides or a shade and/or symbol for the hardcopy maps presented in this Report (pls. 5-4 through 5-9). The jagged appearance of many boundaries on the isopach maps results from the oblique angles formed by intersecting contour sets.

Map Products

Table 5-1 summarizes all maps produced during this study. Each map was produced as a color 35-mm slide, and selected maps were output as hardcopy at a scale of 1:2400 using a 36-in. Versatec Electrostatic Plotter. Because of the large number of contour increments required to fully delineate the crater and disturbed region, the color slides provided the best means to make first-order assessments of the maps. Hardcopy maps were necessary for more detailed analysis and publication. The three digitized contour maps are presented as Plates 5-1 through 5-3, and a positive and a negative display for each of the three derived isopach-map pairs are presented as Plates 5-4 thru 5-9, located in the map pocket of this Report.

EXAMPLE OF VERTICAL DIFFERENCE CALCULATION

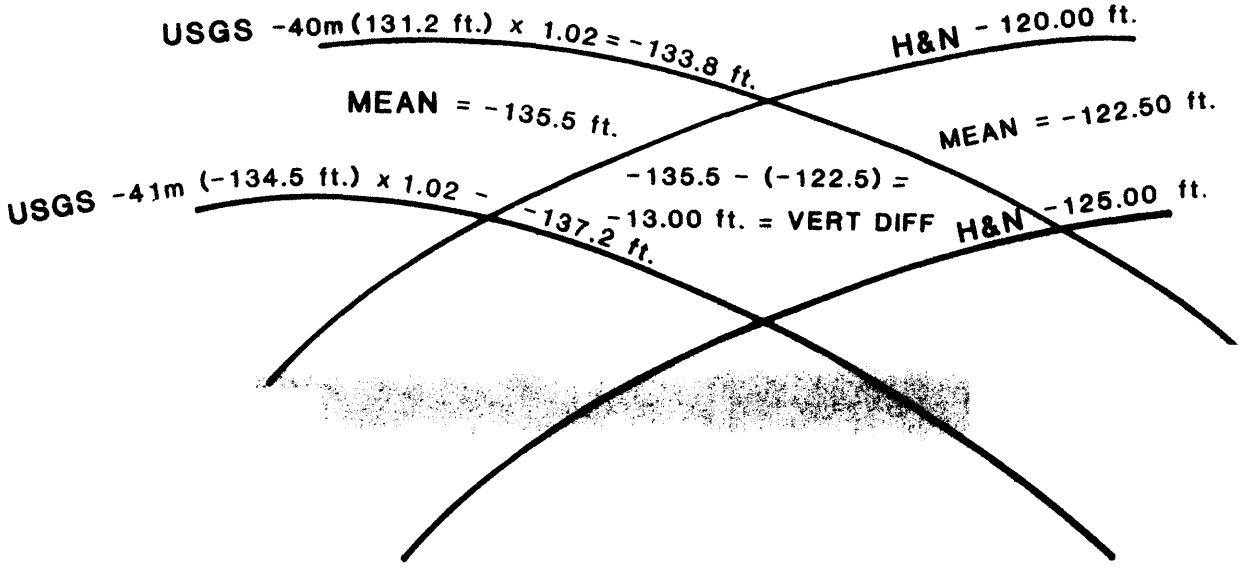

VOLUME OF POLYGON = AREA OF POLYGON X VERT DIFF

FIGURE 5-3. -- Diagram showing isopach computational grid.

TABLE 5-1. -- Summary of digitized bathymetric map products for OAK crater for PEACE Program. Note that the 10-ft contour increment is depicted on the negative Δ-relief isopach maps (i.e., pls. 5-4, 5-6, and 5-8) for depth increments greater than minus 20 ft.

MAP PRODUCTS

MAP TYPE	PLATE	MAP TITLE		CONTOUR INTERVAL (ft)				SLIDE SETS	PAPER MAPS	AREA & VOLUME SUMMARY
				3.3	5	10	25			
Contour	5-1	H&N Preshot		-	+	-	-	+	+	-
	5-2	H&N Postshot		-	+	-	-	+	+	-
	5-3	USGS Postshot		+	-	-	-	+	+	-
Overlaid Contour	-	H&N Post- on H&N Pre- Overlay (contours only)		-	+	-	-	+	-	-
	-	USGS on H&N Pre- Overlay (contours only)		-	+	-	-	+	-	-
	-	USGS on H&N Post- Overlay (contours only)		+	+	-	-	+	-	-
Isopach	5-4	H&N Isopach (Pre- & Post-)	Negative Δ-relief	-	+	-	-	+	+	+
	5-5	H&N Isopach (Pre- & Post-)	Positive Δ-relief	-	+	-	-	+	+	+
	-	H&N Isopach (Pre- & Post-)	Combined Pos. & Neg. Δ-relief	-	-	-	+	+	+	+
	5-6	USGS/Pre- H&N Isopach	Negative Δ-relief	-	+	+	-	+	+	+
	5-7	USGS/Pre- H&N Isopach	Positive Δ-relief	-	+	-	-	+	+	+
	5-8	USGS/Post- H&N Isopach	Negative Δ-relief	-	+	+	-	+	+	+
	5-9	USGS/Post- H&N Isopach	Positive Δ-relief	-	+	-	-	+	+	+

Plus (+) symbol indicates presence of product, minus (-) absence.

ANALYSIS

On comparing the three bathymetric basemaps discussed above (see fig. 5-1) and knowledge of the extent of the apparent crater of OAK, it is obvious that neither the 1958 H&N maps nor the 1984 USGS map continue outward far enough in any direction to fully cover the total area affected by the OAK event. This forms a significant limitation to any bathymetric analysis.

Map Derived Quantities

Several problems are associated with obtaining numerical values from the contour and isopach maps. These are complexly related to the previously discussed survey-sampling differences and deficiencies. They include the following: (1) the differences in areas mapped between surveys; (2) problems with positioning of the survey and drilling ships; and (3) the continuing redistribution of debris with time. The interpretation of the results are further hampered by the fact that both the pileup of debris from the crater (positive Δ-relief) and subsidence after the event (negative Δ-relief) occur over nearly the entire map area yet are inseparable solely from bathymetric data alone. However, even cursory examination of the maps shows clearly recognizable Δ-relief patterns that are easily followed from map to map (i.e., with time). Therefore, in general, the larger the area over which measurements are averaged, the higher the confidence of those values. Below are presented selected point (depths), line (cross sections), and area (areas and volumes) estimates.

Water Depths. -- Table 5-2 compares water depths at each borehole drilled during the PEACE Program that are located within the map areas. Borehole-site depths are those measured in the field at time of drilling and reported by the USGS (Henry, Wardlaw, and others, 1986a), whereas bathymetric water depths are the arithmetic mean of the bounding contours (3.3-ft contour interval). Thus, although the precision of the former are probably to within 0.1 ft, the latter could be in error by up to 1.7 ft. Additional errors probably occur due to borehole location uncertainties (± 10 ft), which could easily translate into several vertical feet in areas of rough postshot terrain.

Because the USGS bathymetry and drilling programs were completed within a year of each other, the differences in water depths provide a measure of the inaccuracies inherent on the USGS contour map. Fourteen of the boreholes exhibit differences ranging from plus 2.9 to minus 1.7 ft, with a mean of only 0.4 ft and an absolute average of 1.6 ft. The other four boreholes (OCT-5, ODT-6, OLT-14, and OUT-24) exhibit differences exceeding 4 ft (range from plus 4.8 to minus 5.8 ft), have a mean difference of 1.9 ft and an absolute average of 4.9 ft. For OLT-14, there was a problem in locating the position of the borehole (see Henry, Wardlaw, and others, 1986b, p. 390-391). For the other three, no trends are obvious nor is the reason for the larger differences known. These differences do illustrate the problem in relying solely on the bathymetric data to obtain point estimates.

Another important observation is that postshot water depths for boreholes located at roughly equal distances, but on opposite sides of SGZ, are similar

TABLE 5-2. -- Summary of water depths and vertical differences at PEACE Program borehole locations. Water depths are compared between measured values at borehole sites in 1985 (Henry, Wardlaw, and others, 1986, p. 60, tbl. 10) and interpolated values from Holmes and Narver preshot and postshot maps (H&N, 1958a, 1958b) and U.S. Geological Survey postshot map (USGS, 1984), compiled from echo-sounding data from Marine Phase of PEACE Program. All depths given in ft below sea level (bsl); vertical differences are given in ft. Note that the location of borehole OLT-14 is questionable (see Henry, Wardlaw, and others, 1986, p. 390-391).

WATER DEPTHS AND VERTICAL DIFFERENCES

	BOREHOLE NUMBER	H&N PRESHOT DEPTH*	USGS DRILL LOG DEPTH** (1985)	USGS MAP DEPTH* (1984)	USGS 1984-85 DIFF.	H&N POSTSHOT DEPTH*	H&N POSTSHOT VS USGS 1984 DIFF.
				PARALLEL TO REEF			
1	ORT-20	67.5	101.4	102	-0.9	87.5	-14.8
2	OQT-19	47.5	117.5	115	2.2	107.5	- 7.8
3	OTG-23	47.5	164.0	166	-1.6	152.5	-13.1
4	OPZ-18	47.5	201.9	199	2.8	197.5	- 1.6
5	OBZ-4	12.5	198.7	199	-0.4	197.5	- 1.6
6	OCT-5	17.5	163.7	159	4.8	142.5	-16.4
7	OGT-9	17.5	134.8	136	-0.7	122.5	-13.0
8	OFT-8	17.5	130.8	129	2.0	117.5	-11.3
9	OET-7	17.5	106.9	106	1.4	92.5	-13.0
10	ODT-6	17.5	90.1	86	4.0	72.5	-13.6
				PERPENDICULAR TO REEF			
1	OUT-24	1.5	147.0	142	4.8	127.5	-14.7
2	OBZ-4	12.5	198.7	199	-0.4	197.5	- 1.6
3	OPZ-18	47.5	201.9	199	2.8	197.5	- 1.6
4	OKT-13	102.5	164.7	166	-0.9	152.5	-13.1
5	OIT-11	122.5	155.0	152	-2.8	147.5	- 4.7
6	OHT-10	122.5	137.3	139	-1.5	122.5	-16.3
7	OJT-12	112.5	143.8	146	-1.7	132.5	-13.0
8	ONT-16	132.5	135.1	132	2.9	122.5	- 9.7
9	OMT-15	142.5	110.9	112	-1.1	127.5	15.5
10	OLT-14	127.5	139.7	146	-5.8	132.5	-13.0

* From Arc/Info File.
** From Henry, Wardlaw, and others (1986, p. 60, tbl. 10).

regardless of differences in the preshot water depths. For example, at roughly 900 ft from SGZ, preshot differences in water depths between OUT-24 on the reefward side and OKT-13 on the lagoonward side are 101 ft; postshot differences are only 18 ft. At 1,800 ft from SGZ, ODT-6 and ORT-20 differ by 50 ft preshot compared to only 11 ft postshot. Another pair (OQT-19 and OET-7 at 1,400 ft) exhibit preshot and postshot differences of 30 and 10 ft, respectively. These data suggest that the net cratering effects in both the "coral" media and water were about the same.

Except for OMT-15, which lies along the lagoon radial (southwest transect) of a large debris tongue, all 1984 USGS water depths at borehole locations exceed the 1958 H&N postshot depths by 2 to 16 ft (see tbl. 5-2). Although no other trends are obvious, these values represent the minimum net downward displacement (i.e., downward movement of the surface plus any addition of debris that may have occurred between surveys). At OMT-15, there is a 15-ft decrease in water depth which, if valid, can only be explained by a late-time addition of debris possibly from a neighboring high.

Cross Sections. -- Figure 5-4 presents two composite cross sections through the OAK SGZ parallel to (southwest to northeast) and perpendicular to (northwest to southeast) the trend of the reef. Each profile of the composite was prepared by manually digitizing the respective contour maps. Note that a vertical exaggeration of 10:1 results in slopes accordingly out of proportion. The H&N preshot profiles illustrate that the OAK device was placed above a sharp break in slope of the lagoonward edge of the reef. Comparisons of the H&N pre- and postshot profiles show that a large part of the lagoon side of the crater was originally water, and, therefore, most of the ejecta from that side of the crater was water. Within the circular crater, the flat floor is offset lagoonward from SGZ by 300 ft, and sets of terraces on the reefward side of the crater are evident.

The H&N postshot profile, perpendicular to the reef, crosses the most complex portion of the map near the apex of a large debris mass rising over 50 ft above the preshot level near the 1,900-ft mark. A slightly smaller debris mass, 500 ft further out, is some 30 ft above the preshot level and appears to have built up against and engulfed a preshot coral knoll. The cross section parallel to the reef shows the break at the boundary of the circular crater and the crater wings. Several distinct terraces within the crater are visible.

Comparisons of the 1984 USGS and 1958 H&N profiles show that the entire region subsided. Maximum downward displacement is concentrated in the mid- to lower depths of the circular crater and out into the lagoon. Significantly less downward displacement has occurred on the wings of the crater, whereas, on the reefward side, material has moved up and in toward SGZ. In assessing these profiles it is important to consider that redistribution of sediments probably resulted in material moving out of and into the plane of the cross sections.

Areas and Volumes. -- Tabulated areas and volumes for each of the three computed isopach maps are given in Tables 5-3 thru 5-5, located at the end of

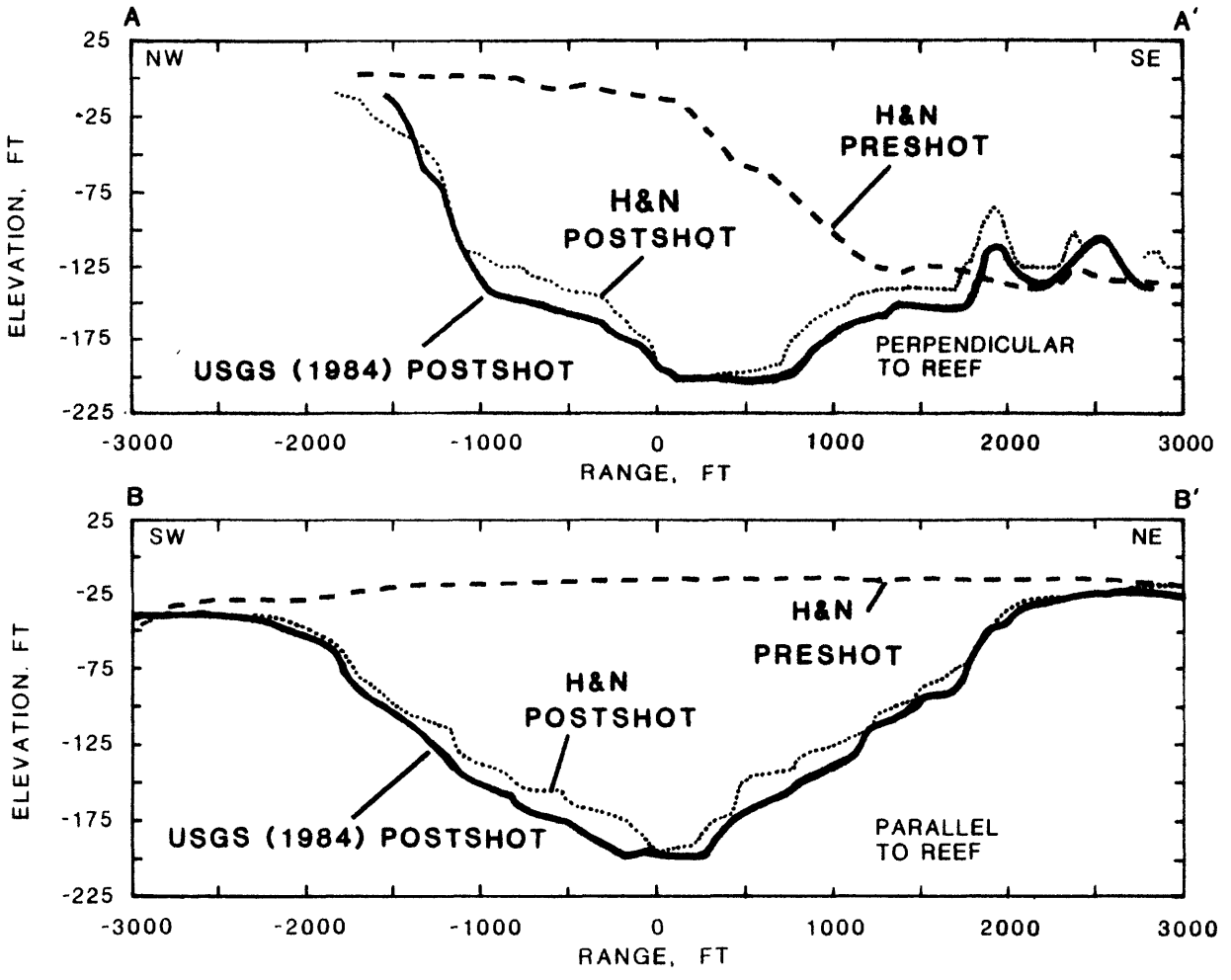

FIGURE 5-4. -- Cross sections through surface ground zero (SGZ) of OAK crater.

the Chapter[1], and summarized in Table 5-6. Volumes were computed in 5-ft increments by multiplying the vertical differences for each polygon by their respective areas and then totaling all of the volumes. Dimensions given are for each map area which, as discussed previously, differ somewhat between maps. The data demonstrate clearly that the entire area subsided an average of 23 ft by D + 67 days and another 12 ft during the next 26 years. As the surface of the crater and surrounding areas dropped, so did the coverage of positive relief, from 27 percent of the area at D + 67 days to only 14 percent of the area after 26 years.

MAP CHARACTERISTICS

The following is a first-order assessment of each contour and isopach map in terms of topographic patterns and characteristics. Because it is difficult to accurately quantify many of the features discussed, dimensions stated are only approximate.

H&N Preshot Contour Map

The northwest one-third (reefward side) of the 1958 H&N preshot map (pl. 5-1) shows the lagoonward side of the reef flat with sand bars along the upper margin. At the wave-break line, there is a well-defined, nearly linear scarp that is distinctly sharper north of SGZ. Approximately 400 ft reefward from SGZ, the scarp is cut by a 400 x 400-ft embayment. Beyond the scarp, a gently sloping shelf, dipping 1.5 degrees into the lagoon, ranges in width from 1,000 ft south of SGZ to less than 500 ft north of SGZ.

The southeast two-thirds of the H&N map (lagoonward side) comprises the reef slope and the lagoon floor, which contains numerous patch reefs. The reef slope, steepest (up to 15 degrees) north and shallowest (up to 5 degrees) south of SGZ, extends 1,000 ft beyond SGZ. Lagoonward from the foot of the reef slope, the lagoon floor slopes very gently (1 degree) toward the lagoon interior. Just south of SGZ is a 75-ft deep, 200-ft wide ravine with a steep, 25-degree headwall. This ravine flattens and widens lagoonward over a distance of about 1,500 ft but retains its identity to at least 2,500 ft as a clear path extending through the patch reefs. On the lagoon floor, numerous patch reefs, roughly aligned in two lineaments parallel to the reef at 1,700 and 2,600 ft lagoonward of SGZ, rise as high as 40 ft above the bottom and range up to several hundred feet in diameter. Their elliptical to triangular shapes on the map are due to the 300-ft H&N-survey spacing. Actually, they are in fact smaller and nearly circular as shown in the 1984 USGS map with its nearly fourfold increase in sampling density.

---

[1] Tables 5-3 through 5-5, summarizing the data calculated from the computer analysis of the pairs of derivative maps, and Table 5-6, presenting the grand summary of Tables 5-3 through 5-5, are all located at the end of the current Chapter.

Inspection of the H&N Preshot Contour Map (pl. 5-1) shows that the device was placed at a position along the Alice Reef marked by a large embayment. In addition, SGZ was located near the beginning of the lagoonward edge of the reef slope and close to the head of the large ravine that cuts into that slope. Although water depth, interpolated from the preshot map for the OAK SGZ, was almost 13 ft at shot time, according to B.L. Ristvet (oral communication, 1986), it was closer to 14 ft due to a 1.4-ft tide.

H&N Postshot Contour Map

The most striking feature of the OAK crater is its symmetry with respect to the geometric center (GC), which is offset nearly 300 ft lagoonward of SGZ. This is shown clearly in the 1958 H&N postshot map (pl. 5-2). All contours from the bottom of the crater up to the minus 145-ft contour, averaging 850 ft from the GC, are closed. The minus 125-ft contour, averaging 1,200 ft from the GC, closes except for a 45-degree sector on the lagoonward side. Furthermore, on the same side at roughly 1,500 ft from GC, the minus 100-ft contour closes to within 120 degrees. Slopes within the crater are much steeper on the reef side with distinct terraces and slump features evident throughout. Contours in the preshot embayment area are noticeably more distorted than at other locations along the reef.

A second major feature shown by the H&N postshot map is the extension of the debris blanket into the lagoon. This blanket is dominated by a 3,000-ft-long tongue of material, 1,500 ft wide at the crater edge and 55 ft thick at the highest point. Actually, the maximum thickness must be at least 75 ft due to an estimated subsidence in that region of at least 20 ft. The debris tongue is cut radially near the middle by a 400-ft wide channel closely aligned with the preshot ravine. This channel, breaching the crater rim at 1,200 ft from SGZ, passes between two topographic highs at 1,500 ft and bifurcates against another topographic high at 2,700 ft from SGZ.

A third major characteristic is the difference in the preshot to postshot topography in the area of the crater wings along the reef slope. North of SGZ the postshot contours virtually overlay the preshot contours, whereas south of SGZ, the contours have changed considerably and most of the reef slope clearly has been modified by the event.

Many of the patch reefs surveyed preshot do not appear on the H&N postshot map. Some were obviously destroyed, others buried by debris; however, many were probably not mapped in the H&N surveys. Resolution of this issue will require a better understanding of the exact survey lines used by H&N. The 1984 USGS Map (pl. 5-3), with its greater sampling density, adds important information regarding these features and probably could be used as a base to rectify the H&N maps.

USGS 1984 Contour Map

The 1984 USGS map (pl. 5-3) depicts many of the same features shown in the 1958 H&N postshot map (pl. 5-2), except that, with its fourfold increase in sampling density, features such as the coral patch reefs, crater terraces, and slump regions are much more sharply defined. After 26 years, the crater

is larger but retains its basic circular appearance; the crater wings have broadened, especially to the southwest. The inner component of the circular crater, still defined by the minus 145-ft contour, has expanded in radius about the GC from 850 to 1,050 ft. Contours are noticeably smoother, and slopes within the crater are steeper, particularly along the reef where at least two distinct scarps are now present. The debris tongue continues to dominate the lagoonward side, and the preshot ravine is still clearly visible as a remnant feature. Folger, Hampson, and others (1986) discuss the features of the 1984 USGS bathymetric map in terms of "physiographic provinces" and compare them to observations from the submersible, scuba-diving, and sidescan-sonar operations.

H&N Postshot - H&N Preshot Isopach Map

This pair of isopach maps (pls. 5-4 and 5-5) documents the areal distribution of Δ-relief (the net changes in negative and positive elevations), referenced to the preshot datum, resulting from OAK and extending to 67 days after the event.

The most striking feature of the map pair is the nature and distribution of the Δ-relief. Areas of positive Δ-relief, ranging up to 55 ft, cover only 27 percent of the total map of which Δ-relief greater than 5 ft (16 percent of the total map) is restricted to areas lagoonward of the crater. Negative Δ-relief dominates all other areas and covers 63 percent of the map, approximately one-half of that is outside the elliptical crater. The remaining 10 percent of the area shows no change in Δ-relief.

Although it is likely that at least some debris from the crater extends over nearly all of the area covered by the H&N postshot map, most of the reef and large regions on the crater wings and beyond are at a lower elevation than preshot. Therefore, this isopach map grossly understates the amount of debris present because of the unknown amount of event-related subsidence which is very difficult to isolate and measure. In fact, the total amount of debris is further understated because a substantial amount of the debris mass, particularly on the lagoon side, was water. Also, a small amount of ejecta impacted beyond the map area. And finally, an unknown amount of the debris mass may have been transported beyond the confines of the map.

A first-cut estimate of the downward displacement can be obtained by viewing the upper corners of the map (north and west of SGZ) that contain the reef flat. Most distant from SGZ, at 3,000 ft from SGZ, there are areas with a maximum of 5 ft of positive Δ-relief. In contrast at 2,000 ft along the same radials, but still beyond the elliptical crater, there are regions of 5 to 10 ft of negative Δ-relief. Because the positive Δ-relief is probably due to debris, and because debris thickness should increase toward the crater, it is concluded that at least 10 to 15 ft of negative Δ-relief is present at the 2,000 ft range. High-explosive craters in wet media typically display such downwardly displaced profiles, although large azimuthal variations often exist.

A second striking feature of this isopach pair is the elliptically shaped crater, defined by the minus 20-ft contour, which is in sharp contrast to the circular crater of the postshot contour maps (see pls. 5-2 and 5-3). This

elliptical crater, composed of the inner and outer components of the circular crater and the crater wings, has a long axis (4,000 ft) parallel to the reef and a short axis (2,800 ft) perpendicular to the reef.

Difference contours from the deepest point on the crater floor up to the minus 140-ft contour (400-ft radius) are roughly circular and symmetric about the GC of the crater. Above and up to the minus 110-ft contour (1,000-ft radius), the contour lines are roughly circular, but about the SGZ. Above, the largest rates of increasing difference (narrowest contour bands) occur between the minus 60- and minus 20-ft contours and probably represent a series of scarps surrounding the elliptical crater.

The elliptical shape of the crater is primarily due to the crater wings and to the sloping lagoon floor. This suggests that the crater wings, although controlled by the reef structure, are related to the circular crater. The elliptical crater is notably broken along the southeast by a remnant feature of the ravine and its headwall, previously described for the 1958 H&N preshot map. Finally, beyond the crater wings and predominately to the southwest, the en echelon pattern of difference contours suggests successive slumping parallel to the reef and well out into the lagoon.

USGS 1984 - H&N Preshot Isopach Map

This isopach map set (pls. 5-6 and 5-7) documents the distribution of net positive and negative Δ-relief from the preshot datum to 26 years after the detonation of the OAK device. Generally, the same basic difference patterns and features are displayed as at 67 days (previously discussed isopach map), but with some notable changes.

First, the entire area has subsided further so that now 86 percent of the map area exhibits a negative Δ-relief and only 14 percent exhibits a positive Δ-relief. The reef flat in the upper right corner of the map (north of SGZ) indicates an additional 5 to 10 ft of subsidence since the detonation of OAK. At the bottom of the map, 3,300 ft southeast of SGZ, an additional drop of 5 to 10 ft has occurred since the event. The previous maximum high of 55 ft on the ejecta tongue is now only 40 ft, indicating subsidence and possibly some redistribution of debris. Note that the new small circular highs in the bottom right of the map (east of SGZ) are probably artifacts of the higher density sampling by the USGS and were not detected by the earlier H&N surveys.

Second, the elliptical crater, as defined by the minus 20-ft contour, has expanded parallel to the reef in the crater wings and into the lagoon, but has contracted reefward. The net result is an increase of 500 ft in the long axis to 4,500 ft, but only an increase in the short axis of 100 ft to 2,900 ft.

Third, the difference contours near the crater floor have changed from circular to elliptical. However, the contours above that level (i.e., the minus 160- to minus 100-ft contours) have remained circular, expanded considerably, and shifted toward the reef.

USGS 1984 - H&N Postshot Isopach Map

This pair of isopach maps (pls. 5-8 and 5-9) shows the negative and positive changes in Δ-relief relative to the H&N postshot datum (47 to 67 days after the event) caused by redistribution of debris and long-term subsidence. In general, the entire map area is displaced downward increasing from 5 ft at the map boundaries (3,500 ft from SGZ) to 20 ft over much of the lagoon to 30 ft within the crater. Areas of negative Δ-relief now constitute 89 percent of the map area.

Areas of maximum negative Δ-relief are associated with deeper portions of the crater, the debris tongue, and isolated topographic highs in the lagoon. The concentric patterns of increasing negative Δ-relief vary from 5 to 10 ft at the edge of the circular crater (1,700 ft from SGZ) up to 25 to 30 ft just above the crater floor. This indicates that the circular crater has continued to subside with time. The multiple, repeating circumferential patterns in the elliptical-crater walls and along portions of the reef probably represent en echelon slumping of debris.

Beyond the elliptical crater, the debris tongue exhibits 5 to 15 ft greater negative Δ-relief compared with surrounding areas, even at its maximum extent of 3,300 ft, where a negative change of 20 to 25 ft is measured. Localized areas of 30 to 45 ft of negative Δ-relief occur in the lagoon associated with topographic highs. These areas are complex with converging zones of negative and positive Δ-relief probably representing slumping and redistribution of debris.

Areas of positive Δ-relief are associated with the flanks of several topographic highs, suggesting (as mentioned above) movement of debris downslope. The small positive Δ-relief on the floor of the crater is due to infillin and probably masks a 20-ft plus Δ-relief. The positive lineaments along the reef scarp probably reflect movement of reef blocks and washback of debris into the crater. The narrow positive lineaments bordering the extended crater probably represent movement of debris downslope along the crater rim scarps. The positive circular highs on the middle and lower right side of the map are probably artifacts of the previously mentioned bathymetry sampling density. The positive highs in the lower left portion of the map (south of SGZ) are unexplained.

CONCLUSIONS

Based primarily on analysis of the OAK bathymetric data presented herein, the following conclusions are reached:

1. The OAK event produced a circular explosion-type crater with debris distributed outward in all directions, probably continuously, to at least 3,000 ft from SGZ.

2. The circular crater, consisting of an inner circular component on the order of 850 ft in radius, probably formed initially by ejection and outward flow of material. This expanded outward by crater-wall collapse, slumping, and inflow of material to form an outer circular component. By D + 67 days, and probably much sooner, the circular crater had grown to a radius of 1,700 ft and a depth of 200 ft.

3. A very large tongue of debris, 1,500 ft wide at the crater edge and tapering to 500 ft at 3,000 ft from SGZ, was deposited outward onto the lagoon floor. This is cut by a 400-ft-wide channel that closely tracks the preshot ravine.

4. Also by D + 67 days, the entire area out to at least 3,000 ft from SGZ had subsided 5 to 10 ft with crater wings forming and expanding along the reef slope on either side of the circular crater. This resulted in an elliptical crater 4,000 ft parallel to and 2,800 ft perpendicular to the reef.

5. Over the next 26 years, the entire area continued to subside. This subsidence ranged from a minimum of 5 to 10 ft at 3,000 ft from SGZ up to 10 to 20 ft just outside the elliptical crater. Even greater subsidence occurred within the circular crater, particularly the lower portions, and out on the debris tongue. The length of the elliptical crater increased 500 ft (from 4,000 to 4,500 ft), but the width increased only 100 ft (from 2,800 to 2,900 ft).

6. Also, over this 26-year period, debris within the crater, on the debris tongue, and along the crater walls continued to slump. Elsewhere debris was selectively redistributed.

7. In retrospect, preshot topographic features (reef, embayment, ravine, and reef/lagoon slope) had a significant influence on the final size and shape of the crater and on the initial distribution and subsequent reworking of debris.

8. Finally, it is believed that a synthesis of the bathymetric data with the drilling, seismic, side-scan sonar, and gravity data will lead to a significant improvement in the quantification of the postshot topography which, in turn, should provide substantial improvement in the understanding of the cratering mechanics of the OAK event.

ACKNOWLEDGEMENTS

We are indebted to Gar Clark and his staff at the Technology Application Center (TAC), University of New Mexico, for their excellent and painstaking work in digitizing the basemaps and producing the contour and isopach maps. We also greatly appreciate the extended discussions with B.L. Ristvet of S-Cubed on the many details of the 1958 H&N surveying and for providing us the last "originals" of those maps.

This effort was jointly funded by the Defense Nuclear Agency (DNA). Project Officer for DNA was Lt. Col. Robert Couch; the Air Force Systems Command Project Officer was Maj. William Clark.

REFERENCES CITED

Environmental Systems Research Institute (ESRI), 1986, ARC/INFO Users Manual; v. 3.2, April 1986.

Folger, D.W., Hampson, J.C., Robb, J.M., Woellner, R.A., Foster, D.S., and Tavares, L.A., 1986, Bathymetry of OAK and KOA craters; 32 p., 12 figs., 2 appendices; in Folger, D.W., editor, Sea-floor observations and subbottom seismic characteristics of OAK and KOA craters, Enewetak Atoll, Marshall Islands: U.S. Geological Survey Bulletin 1678.

Henry, T.W., and Wardlaw, B.R., editors, 1986, Pacific Enewetak Atoll Crater Exploration (PEACE) Program, Enewetak Atoll, Republic of the Marshall Islands; Part 3: Stratigraphic analysis and other geologic and geophysical studies in vicinity of KOA and OAK craters: U.S. Geological Survey Open-File Report 86-555, 486 p., 92 figs., 90 tbls., 34 pls.

Henry, T.W., Wardlaw, B.R., Skipp, B.A., Major, R.P., and Tracey, J.I., Jr., 1986, Pacific Enewetak Atoll Crater Exploration (PEACE) Program, Enewetak Atoll, Republic of the Marshall islands; Part 1: Drilling operations and descriptions of boreholes in vicinity of KOA and OAK craters: U.S. Geological Survey Open-File Report 86-419, 497 p., 32 figs., 29 pls., 13 tbls., 3 appendices.

Holmes and Narver Engineering Co. (H&N), 1952, Completion Report, Enewetak Proving Ground Facilities, Operation IVY; v. 1, book 1, p. 2-11 through 2-25, Los Angeles, CA, 31 December 1952 [Unclassified]. Survey conducted for U.S. Atomic Energy Commission (AEC).

Holmes and Narver Engineering Co. (H&N), 1958a, OAK preshot topography and hydrography map; Alice Reef Station #25: Field Book # 337, p. 2-28 [dated June 9 through 26, 1958)], Map Sheets J/S 03-001-C11 [compiled September 13, 1958]. Survey conducted for U.S. Atomic Energy Commission (AEC).

Holmes and Narver Engineering Co. (H&N), 1958b, OAK postshot topography and hydrography map; Alice Reef Station #25: Field Book # 242, p. 7-21 [dated August 14 thru September 4, 1958], Map Sheets J/S 03-001-C11 [compiled October 1, 1958]. Survey conducted for U.S. Atomic Energy Commission (AEC).

Peterson, J.L., and Henny, R.W., 1987, Bathymetric studies of the 1958 OAK nuclear cratering event, Pacific Proving Grounds: New Mexico Engineering Research Institute Task Report WA6-16, September 1987, Albuquerque, NM.

U.S. Army, 1970, Eniwetok Trig List: U.S. Army Topographic Command, Ft. Belvoir, VA.

U.S. Geological Survey (USGS), 1984 [1985], Bathymetric Map of the OAK Crater Area, Enewetak Atoll [surveyed June 17 thru September 20, 1984, compiled September 1985]. [This is a working-scale map at 1:6000 of the map published as fig. 7, p. A8, of Folger, Hampson, and others, 1986.] Survey conducted for Defense Nuclear Agency (DNA).

TABLE 5-3. -- Summary of areas and volumes calculated from derivative map pair formed by combination of Holmes and Narver (H&N) preshot bathymetric/topographic map (pl. 5-1) and H&N postshot isopach map (pl. 5-2). Corresponding maps are Plates 5-4 for the negative Δ-relief and Plate 5-5 for the positive Δ-relief, respectively.

H&N PRESHOT VS H&N POSTSHOT -- VOLUMES AND AREAS

Δ-RELIEF CATEGORY	CONTOUR INTERVAL (ft)	AREA (sq ft)	TOTAL MAP AREA (%)	VOLUME (cu ft)
	50-55	1,348	0.004	74,160
	45-50	4,176	0.01	208,796
	40-45	6,201	0.02	279,045
Positive	35-40	21,735	0.07	869,394
	30-35	122,071	0.4	4,272,490
Δ-relief	25-30	299,352	1.0	8,980,567
	20-25	317,622	1.1	7,940,551
	15-20	727,271	2.4	14,545,419
	10-15	1,265,755	4.2	18,986,338
	5-10	2,118,996	7.0	21,187,252
	>0-5	3,134,338	10.4	13,788,992
Total Positive Δ-relief		8,018,865	26.6	91,132,994
Total Zero (0) Δ-relief		3,223,946	10.6	0
	>0-5	4,597,830	15.2	19,366,933
	5-10	3,090,431	10.2	29,015,023
	10-15	1,856,139	6.1	27,033,099
	15-20	1,133,271	3.8	22,237,414
	20-25	700,073	2.3	17,178,469
	25-30	454,545	1.5	13,423,574
	30-35	375,716	1.2	12,903,993
	35-40	330,047	1.1	13,017,456
	40-45	276,989	0.9	12,300,535
	45-50	307,840	1.0	15,220,082
	50-55	256,148	0.8	13,975,590
	55-60	294,104	1.0	17,531,655
	60-65	254,941	0.8	16,485,412
	65-70	258,831	0.9	18,033,970
	70-75	264,372	0.9	19,743,284
	75-80	244,716	0.8	19,493,811
	80-85	274,512	0.9	23,247,576
	85-90	269,727	0.9	24,166,199
	90-95	294,963	1.0	27,771,543
	95-100	338,887	1.1	33,472,777
Negative	100-105	291,624	1.0	30,298,728
	105-110	346,830	1.1	37,791,053
Δ-relief	110-115	355,535	1.2	40,539,123
	115-120	320,563	1.1	38,067,852
	120-125	391,098	1.3	48,674,321
	125-130	401,628	1.3	51,943,142
	130-135	324,904	1.1	43,586,633
	135-140	230,240	0.8	31,933,508
	140-145	76,917	0.3	11,138,920
	145-150	63,249	0.2	9,487,333
	150-155	63,632	0.2	9,862,944
	155-160	55,269	0.2	8,843,002
	160-165	41,603	0.1	6,864,333
	165-170	32,152	0.1	5,465,870
	170-175	28,008	0.1	4,901,403
	175-180	22,978	0.1	4,135,995
	180-185	23,807	0.1	4,404,334
	185-190	7,449	0.03	1,415,289
Total Negative Δ-relief		18,951,568	62.8	784,972,178

TABLE 5-4. -- Summary of areas and volumes calculated from derivative map pair formed by combination of U.S. Geological Survey (USGS, 1984) postshot isopach map (pl. 5-3) and Holmes and Narver (H&N) preshot map (pl. 5-1). Corresponding figures are Plates 5-6 for the negative Δ-relief and Plate 5-7 for the positive Δ-relief, respectively

H&N PRESHOT VS USGS POSTSHOT -- AREAS AND VOLUMES

Δ-RELIEF CATEGORY	CONTOUR INTERVAL (ft)	AREA (sq ft)	TOTAL MAP AREA (%)	VOLUME (cu ft)
	35-40	3,874	0.01	142,868
	30-35	45,563	0.20	1,431,651
Positive	25-30	83,634	0.30	2,269,071
	20-25	222,615	0.9	5,202,429
Δ-relief	15-20	203,841	0.8	3,683,457
	10-15	399,046	1.6	4,865,145
	5-10	897,017	3.5	6,635,921
	0- 5	1,678,303	6.5	3,792,121
Total Positive Δ-relief		3,533,893	13.7	28,022,645
	0- 5	2,933,886	11.4	9,388,814
	5-10	3,826,724	15.0	30,180,137
	10-15	3,220,256	12.5	40,631,938
	15-20	2,359,641	9.2	40,622,228
	20-25	1,191,911	4.6	26,888,750
	25-30	676,404	2.6	18,651,376
	30-35	450,900	1.8	14,086,245
	35-40	371,889	1.5	14,686,246
	40-45	324,188	1.3	13,924,608
	45-50	312,580	1.2	14,938,353
	50-55	302,003	1.2	15,895,082
	55-60	289,656	1.1	16,678,999
	60-65	275,562	1.1	17,264,649
	65-70	253,538	1.0	17,161,790
	70-75	245,220	1.0	17,773,609
	75-80	223,971	0.9	17,360,741
	80-85	252,353	1.0	20,796,354
	85-90	288,305	1.1	25,364,923
	90-95	286,225	1.1	26,602,615
Negative	95-100	270,795	1.1	26,505,055
	100-105	317,440	1.2	32,581,804
Δ-relief	105-110	338,915	1.3	36,342,656
	110-115	292,983	1.1	33,043,380
	115-120	256,188	1.0	30,203,709
	120-125	339,398	1.3	41,854,235
	125-130	306,752	1.2	39,182,244
	130-135	329,502	1.3	43,734,343
	135-140	274,305	1.9	37,830,734
	140-145	285,822	1.1	40,886,445
	145-150	387,055	1.5	57,054,055
	150-155	244,093	1.0	37,287.965
	155-160	127,398	0.5	20,112,373
	160-165	70,272	0.3	11,453,367
	165-170	67,390	0.3	11,340,488
	170-175	54,923	0.2	9,519,263
	175-180	48,496	0.2	8,659,313
	180-185	58,401	0.2	10,717,498
	185-190	41,979	0.2	7,869,618
Total Negative Δ-relief		22,197,319	86.3	935,058,002

TABLE 5-5. -- Summary of areas and volumes calculated from derivative map pair formed by combination of U.S. Geological Survey postshot map (USGS, 1984) and Holmes and Narver (H&N) postshot isopach map. Corresponding figures are Plates 5-8 for the negative Δ-relief and Plate 5-9 for the positive Δ-relief, respectively.

H&N PRESHOT VS USGS POSTSHOT -- AREAS AND VOLUMES

Δ-RELIEF CATEGORY	CONTOUR INTERVAL (ft)	AREA (sq ft)	TOTAL MAP AREA (%)	VOLUME (cu ft)
	35-40	478	0.002	16,843
	30-35	844	0.003	26,802
Positive	25-30	3,856	0.02	102,241
Δ-relief	20-25	17,189	0.1	378,356
	15-20	112,704	0.4	1,976,874
	10-15	272,512	1.1	3,386,556
	5-10	721,865	2.8	5,217,536
	0- 5	1,820,125	7.1	3,739,364
Total Positive Δ-relief		2,949,573	11.5	14,844,523
	0- 5	4,053,640	15.8	11,485,025
	5-10	6,555,275	25.5	51,868,217
	10-15	7,707,037	30.0	97,957,905
	15-20	3,372,562	13.1	59,101,780
Negative	20-25	857,090	3.3	19,181,484
Δ-relief	25-30	178,053	0.7	4,838,022
	30-35	28,472	0.1	921,606
	35-40	6,822	0.03	257,019
	40-45	3,177	0.01	136,916
	45-50	2,052	0.01	99,545
	50-55	579	0.002	30,640
Total Negative Δ-relief		22,764,759	88.5	245,878,159

TABLE 5-6. -- Grand summary of areas and volumes of negative, zero, and positive Δ-relief for OAK crater area. Summary derived from Tables 5-2 through 5-5. Area given in sq ft, volume in cu ft, net Δ-relief in ft.

TYPE Δ-RELIEF	H&N PRESHOT VS. H&N POSTSHOT Value	Percent	USGS POSTSHOT VS. H&N PRESHOT Value	Percent	USGS POSTSHOT VS. H&N POSTSHOT Value	Percent
AREA: (sq ft)						
Positive Δ-relief	8,018,865	26.56	3,533,893	13.73	2,949,573	11.47
Negative Δ-relief	18,951,568	62.77	22,197,319	86.27	22,764,759	88.53
Zero (0) Δ-relief	3,223,337	10.68	------	---	------	---
TOTAL	30,193,770 sq ft		25,731,212 sq ft		25,714,302 sq ft	
VOLUME: (cu ft)						
Positive Δ-relief	91,132,994	10.39	28,022,645	2.91	14,844,523	5.69
Negative Δ-relief	789,972,178	89.61	935,058,002	97.09	245,878,159	94.31
NET	(693,809,189) cu ft		(907,035,357) cu ft		(231,033,636) cu ft	
AVERAGE NET Δ-RELIEF:	minus 22.99 ft		minus 35.25 ft		minus 8.98 ft	

CHAPTER 6:

CONSTRAINTS ON DENSIFICATION AND PIPING FOR THE OAK EVENT

By

John G. Trulio[1]

BACKGROUND AND SUMMARY

PPG (Pacific Proving Grounds) sites differ widely from typical CONUS (Continental U.S.) sites in structure and composition. Hence, plausibly, high-yield near-surface nuclear explosions might dig much different craters in one setting than the other. But do they? The question cannot be answered by direct comparison of craters from such bursts. It therefore raises the kindred one of mechanism: The crater from a given burst could vary greatly from a CONUS site to the PPG, because dominant cratering mechanisms might -- but do they?

A "subsidence hypothesis" proposed in the early 1980's got to the physical nub of this issue:[2]

> Explosive loading causes widespread fracturing of PPG coral, whose parts then settle slowly under gravity to form the outer one-half to three-fourths (in radius) of the apparent crater -- its "wing." By contrast, the inner one-half to one-fourth grows in several ways, including ejection of solid; indeed, virtually all ejecta come from that inner region -- or (hence) "excavation crater."

In sum, the subsidence hypothesis posits cave-in of a "coral" skeleton[3] to fill the space left by water flowing out of it. Here, we call that process "simple subsidence." Its hallmark is an increase in coral density, since coral solids are denser than the water they replace [but for that, gravity (its cause) could not drive it]. Hence, alternatively, we speak of simple subsidence as "densification."

---

[1] Applied Theory, Inc., Los Angeles, CA 90036.

[2] The basic idea appears to have been suggested independently by S. Blouin, H.L. Brode, and B.L. Ristvet, years before the PEACE Program began. In the form stated here, the simple subsidence hypothesis is credited mainly to K.D. Pyatt and K. Kreyenhagen.

[3] The OAK medium is referred to herein simply as coral. Said medium is a mixture of carbonate sediment, carbonate rock, and sea water with small amounts of other substances (see Chapter 7 of this Report for details of composition of the OAK medium). Used as an adjective herein, the meaning of coral is controlled by the noun it modifies; for example, "coral solid" denotes the solid components of the medium just described.

PEACE Program data do tell of excavation craters about one-fourth to one-third as large in radius as present apparent craters, widened by later slumping of their walls to about 0.4 of the latter radii (B.R. Wardlaw, oral communication, November 9, 1987). Thus, if the wings of apparent PPG craters did form by simple subsidence, then, for a given burst, most CONUS craters would have half the radii (or less) seen at the PPG. By the same token, coral under the wings would be denser now than pre-shot. PEACE Program measurements [borehole gravimetry and gamma-gamma (γ-γ) logging], however, disclose only minor changes in density there: Layers of coral (roughly horizontal) from the sea floor to clearly identified interfaces below have thinned much more than the measured densities alone imply. Hence, on the available data, most of the sea-floor lowering had other causes than simple subsidence. Succeeding sections summarize the evidence for and against this last statement; though not airtight, the case for it is strong.

When the mean density of solids in a column grows by a smaller factor than the column's vertical compression, lateral transport must take place. Such transport can occur during plastic flow, as in a tube of toothpaste. Another kind, termed "piping", calls for the flow of slurry (here, water plus coral particles) to the sea floor, where currents may sweep it out of the crater. Signs of piping abound in the OAK crater (Wardlaw and Henry, 1986b, p. 10; Halley and others, 1986, p. 4), but not in its wing, reducing the importance of PEACE measurements as constraints on piping (nonetheless discussed below). Plastic flow, perhaps with some "internal piping" (transport), seems the most likely means whereby the wings of OAK's crater formed. If so, similar wings could form at most CONUS sites -- and early, relative to such gravity-driven processes as slumping and densification. For structures, the wing would still be more benign than the excavation crater, but operating there would be no cinch.

BASIC FACTS AND PARAMETERS

Both the OAK and KOA craters were explored during the PEACE Program, but emphasis fell on OAK because many nearby shots preceded KOA; cratering-mechanism puzzles are made knottier by the effects of prior shots (example: How did MIKE affect KOA coral?). Indeed, even with the focus on OAK, and OAK's relative simplicity, the data base for assessing density changes remains slim. Priority rightly went to OAK.

In the OAK crater area, vital maps of the sea floor were drawn before the event, shortly after, and during the PEACE Program (see Chapter 5 of this Report). The bathymetric maps tell us how far the sea floor has sunk as a result of the shot. That does more than quantify what it is that we have to explain (essential enough). For, PEACE exploration has shown that, in the wing and beyond, the coral is split into layers by clearly identifiable Lagrangian surfaces (termed "horizons" by the geologists) that are critical here; several appear in Figure 6-1.

The horizons' great value lies in knowledge of their undisturbed (hence pre-shot) depths. By geologic means, those depths are reproducible down boreholes to within a few tens of feet, and most often to $\pm$10 ft, in this part of the atoll. More important still, they can be located generally to within a foot in any one borehole. Thus, the depth of each has been determined in boreholes inside the crater and out. So, therefore, has the shortening of

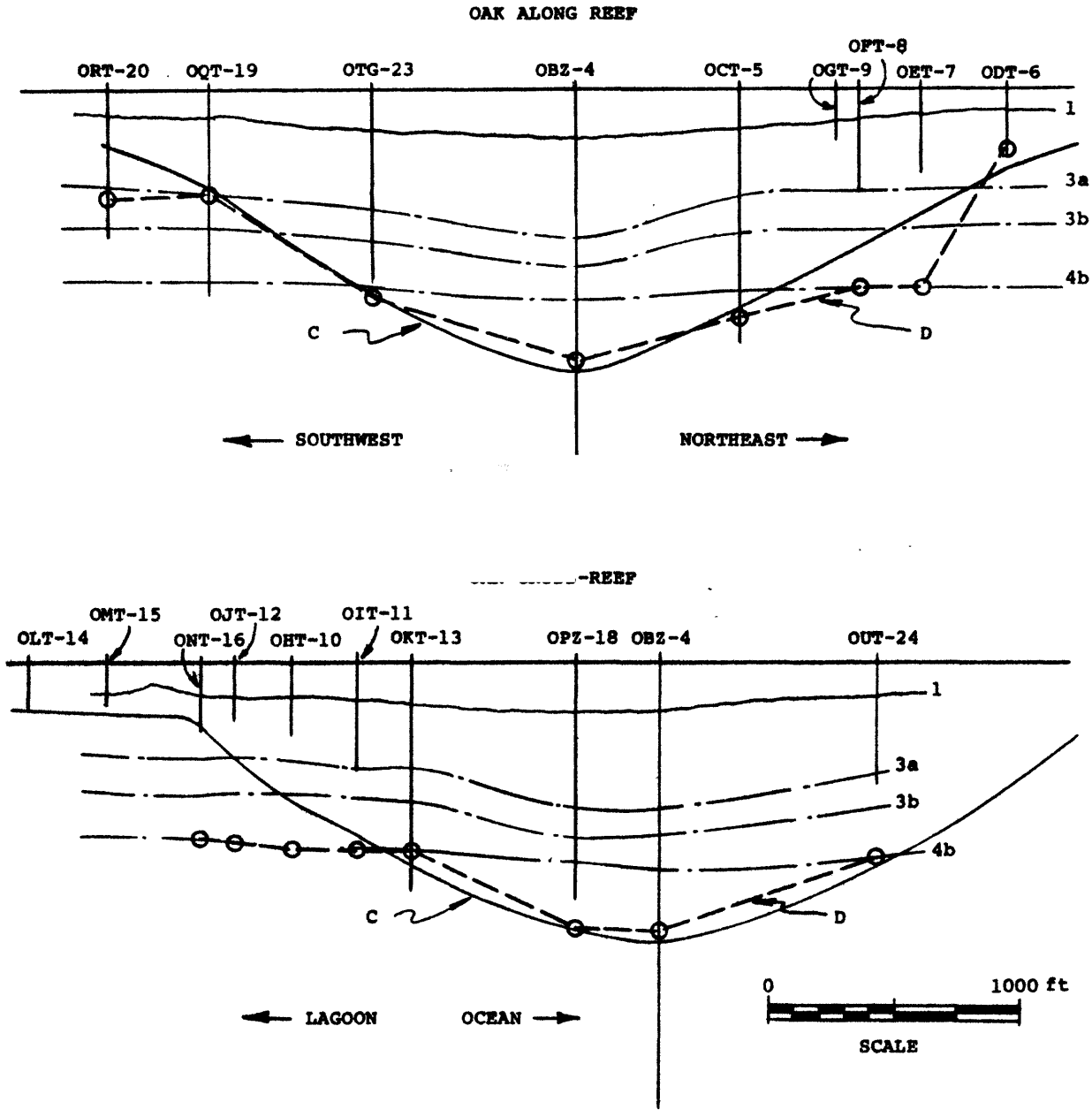

FIGURE 6-1. -- Vertical sections at the OAK site. Contours C and D, respectively, mark the bases of regions of (a) measurable decrease in sonic wavespeed and (b) measurable downward displacement. The SCALE (in ft) applies to all distances.

vertical columns between the sea floor and these horizons.[1] Mapped out too is the base of the region of sensible downward displacement of coral below the crater (contour D; fig. 6-1); its border lies close to the contour (C; fig. 6-1) that marks the limit of the region in which seismic wave-speed has decreased measurably (see Chapter 7 of this Report, particularly tbls. 7-2 and 7-4). Evidently, the shortening of any vertical coral column, flagged by lowering of the sea floor, takes place above the contour D -- and the column's mean vertical shrinkage is given by the ratio of sea-floor lowering at the top of the column, to the column's pre-shot height (current height plus sea-floor drop).

The OAK boreholes lay along two lines through the center of the crater (see Chapter 1, fig. 1-3), one parallel to the reef ("reef-wise") and the other at right angles to it ("cross-reef"). By design, most density logs (and results on densification) came from the reef-wise line (see Chapter 2, fig. 2-2). The reason: We need pre-shot density profiles to compute density changes and their effects. Now -- long after OAK -- those profiles have to come from logging in near-pristine coral outside the crater. For geologic reasons, however, systematic changes in material properties occur along cross-reef lines; on well-chosen reef-wise lines, the medium is subject mainly to smaller, random, local variations. Most actual borehole locations were chosen for OAK by PEACE geologists on that basis. The line those holes form runs close to the crater's center, so that density profiles along it can stand as rough cylindrical crater-averages at their respective reef-wise stations. What "rough" means rests with actual PPG measurements; so does the gut issue of reef-wise fluctuations in natural density profiles (below).

Table 6-1 presents basic PEACE data from the OAK crater, including the mean compressions of coral columns at borehole locations. All OAK boreholes are listed in the table; for reference, so is the estimated peak airblast pressure that acted above each. Of special weight are the table's mean vertical shrinkages $\Delta D/L$. Their average of 13 percent (16-1/2 percent for the reef-wise holes), if achieved via simple subsidence, would entail a mean density increase of ~.13 g/cc (.18 g/cc reef-wise). That is larger by almost a factor of ten than the limit of BHG (and γ-γ) resolution achieved in the PEACE Program (.01 to .02 g/cc). Hence, direct on-site evaluation of the subsidence hypothesis was indeed feasible (not known when the program began). Concern therefore lies instead with systematic error and the natural reef-wise scatter of density/depth profiles. Further, as readily confirmed,

---

[1] The pre-shot depth of the sea floor is known at borehole locations, as are the depths of some horizons (depth uncertainties and confidence questions are taken up later). For a given borehole and horizon, the difference between horizon depth and sea-floor depth is the pre-shot height of the vertical column between horizon and sea floor. Likewise, for that same borehole and horizon, the post-shot height of the column from horizon to sea floor is also known. Between those two levels (horizon and sea floor), the particles of solid in the column may or may not be the same pre-shot as post-shot. The simple subsidence hypothesis says they are the same. The hypothesis is tested herein by adopting it, and comparing the column shortening it implies (when coupled with measured densities) to the observed shortening.

Hole	Range (ft) from GZ	LINE	Preshot Depth L, (ft); Sea Floor to C	to D	Water Depth (ft) Preshot D_1	PEACE D_2	ΔD, ft $D_2 - D_1$	Shrinkage $\Delta D / L$, %; Column to D	Peak Overpressure MPa
OOR-17	6057.8		NA	NA	-	55.2	0	NA	1.0
OSM-22	5538.6		NA	NA	-	76.0	0	NA	1.3
OSR-21	5495.3	A	NA	NA	-	84.0	0	NA	1.3
ORT-20	1845.8	L	144.5	375	70.0	101.4	31.4	8	34
OQT-19	1444.3	O	360.0	380	46.0	117.5	71.5	19	72
OTG-23	804.6	N	796.4	787	45.6	164.0	118.4	15	620
OBZ-4	7.1	G	1125.6	1068	13.1	198.7	185.6	17	>690
OCT-5	658.3		841.5	891	16.2	163.7	147.5	17	>690
OGT-9	1043.5	R	-	-	16.0	134.8	118.8	-	228
OFT-8	1129.1	E	598.8	779	15.4	130.8	115.4	15	172
OET-7	1374.8	E	471.7	775	18.4	106.9	88.5	11	85
ODT-6	1714.9	F	291.6	211	20.0	87.4	67.4	32	41
OAM-3	4510.2		NA	NA	-	108.0	0	NA	2.3
OAR-2A	4500.2		NA	NA	-	110.5	0	NA	2.3
OAM-1) OAR-2)	4458.4		NA	NA	-	114.2	0	NA	2.4
OLT-14	2511.2	C	-	-	132.5	139.7	7.2	-	13
OMT-15	2203.6	R	-	-	141.8	110.9	30.9	-	19
ONT-16	1827.3	O	93.0	207	130.9	135.1	4.2	2	34
OJT-12	1695.5	S	257.3	617	115.0	143.8	28.8	5	43
OHT-10	1462.2	S	446.5	626	124.6	137.3	12.7	2	70
OIT-11	1205.5		568.5	636	121.6	155.0	33.4	5	136
OKT-13	988.7	R	730.0	664	101.7	164.7	63.0	9	269
OPZ-18	334.8	E	1032.6	1043	46.3	201.9	155.6	15	>690
OBZ-4	7.1	E	1125.6	1068	13.1	198.7	185.6	17	>690
OUT-24	858.0	F	828.4	782	1.6	147.0	145.4	19	510

TABLE 6-1. -- Column-height changes down boreholes at the OAK site. Contour C is the base of region of decrease in sonic wavespeed; contour D is the base of the region of downward displacement; GZ is ground zero.

Heading	Hole	RANGE, ft to OBZ-4	Hole Base	Surface D	PEACE Depth, in ft bsl Horizon 2b	2c	2d	3a	3b	4b	5a	5b	5c
SW	OOR-17	6060.6	1146.3	NA			363.1	405.7	552.4	765.2	961.2		
	OSR-21	5498.2	438.3	NA		290.1	344.2	391.7					
REFWISE	ORT-20	1847.8	593.2	445	216.2	262.7	346.7	411.7	552.0	(767.0)	(1013.5)		
	OQT-19	1446.1	819.0	426	233.9	274.7	365.3	413.3	548.3	766.5	(1020.1)		
	OTG-23	805.5	751.3	(834)			434.0	484.0	610.0	(787.0)	(1000.4)		
	OBZ-4	0	1803.9	1081				593.0	701.2	847.7	1013.8	1065.1	1114.6
	OCT-5	654.3	1015.2	907½		368.4	417.9	432.7	572.2	799.7	944.6		
	OGT-9	1039.6	209.8										
	OFT-8	1125.0	414.3	(794)	223.3	272.0	344.6	(419.8)	(565.0)	(794.0)	(925.0)		
	OET-7	1370.5	338.6	(793)	220.6	294.7	320.4	(410.0)	(555.0)	(793.0)	(925.0)		
	ODT-6	1710.5	251.6	231	219.0	231.3	(315.0)	(397.0)	(546.0)	(792.0)	(925.0)		
NE	OAR-2A	4495.5	521.0	NA		310.0	355.6	410.6	(556.8)	(812.2)	(918.2)		
SE	OLT-14	2517.3	188.9	(700)	(227.0)		(341.1)	(383.8)	(534.6)	(700.0)	(1010.2)		
ACROSSREEF	OMT-15	2209.7	187.5	(702)	(225.0)		(334.6)	(373.9)	(529.7)	(701.9	(1013.5)		
	ONT-16	1833.4	287.4	(715)	238.6		(337.8)	(395.2)	(537.9)	(715.0)	(993.8)		
	OJT-12	1701.6	241.1	(732)	238.0		(350.0)	(390.3)	(531.0)	(732.0)	(991.0)		
	OHT-10	1456.3	299.8	(751)	213.3		(360.8)	(403.4)	(531.4)	(751.0)	(987.3)		
	OIT-11	1199.4	441.5	(758)	274.4		375.0	434.8	(562.0)	(758.0)	(980.0)		
	OKT-13	982.7	920.0	766	232.9	326.1	411.6	431.3	564.0	765.8	(974.5)	(1036.5)	
	OPZ-18	329.1	950.5	(1089)			568.9	593.0	723.5	809.9	(1000.0)	(1063.0)	(1114.0)
	OBZ-4	0	1803.9	1081				593.0	701.2	847.7	1013.8	1065.1	1114.6
NW	OUT-24	864.2	498.1	(784)		373.0	407.0	457.1	(592.0)	784.0	(925.0)	(1025.0)	

TABLE 6-2. -- Uniformity of horizons in OAK area. Parentheses () signifies seismic data because borehole ends above depth shown; cross-hatching covers downward-displacement region; blank spaces signify missing values. Below sea level (given in ft) is abbreviated bsl.

the few tens of feet or less by which horizon depths vary (tbl. 6-2) have scant effect on the values of $\Delta D/\Delta z$ in Table 6-1.

SHORTENING OF CORAL COLUMNS BY DENSIFICATION: BOOKKEEPING

Let subscripts L and S refer, respectively, to the liquid and solid components of saturated coral. In a volume V of the mixture, let V_L and V_S be the volumes of the two components and ρ_L and ρ_S their densities. The mass, m, of the mixture is then equal to the mass of its liquid component ($=\rho_L V_L$) plus the mass of its solid component ($=\rho_S V_S$). Hence, if ρ denotes the density of the mixture, we can write:

$$\rho_L V_L + \rho_S V_S = m = \rho V$$

or

$$\rho_L \alpha_L + \rho_S \alpha_S = \rho \qquad \text{Eq. (1)}$$

where α_L amd α_S denote the volume-fractions of liquid and solid in the mixture:

$$\alpha_L \equiv V_L/V \;\; ; \;\; \alpha_S \equiv V_S/V \;\; ; \;\; \alpha_L + \alpha_S = 1 \qquad \text{Eq. (2)}$$

Using the last of Eqs. (2) to eliminate α_L from Eq. (1), and rearranging, we get:

$$\text{Volume Fraction of Solid in Mixture} = \alpha_S = (\rho-\rho_L)/(\rho_S-\rho_L) \qquad \text{Eq. (3)}$$

Hence, in volume V of the mixture, we find that:

$$\text{Mass of Solid} = \rho_S V_S = \rho_S \alpha_S V = V\rho_S(\rho-\rho_L)/(\rho_S-\rho_L) \qquad \text{Eq. (4)}$$

Now consider a vertical column of coral of unit cross-section. Let the column be divided into short vertical sections. A section of the column of height dh then subtends a volume V, and Eq. (4) -- with dh replacing V -- gives the mass of solid in that section. Summing over all sections of the column from a height z_o to a greater height z, the total solid mass m_S between those heights is given by:

$$M_S = \rho_S \frac{\rho-\rho_L}{\rho_S-\rho_L}\, dh \qquad \text{Eq. (5)}$$

In Eq. (5), ρ_L, ρ_S, and ρ can all vary with height h in the column. Here however ρ_L (the density of sea water) is constant, while ρ_S can run only from about calcite's density to aragonite's (ρ_S can be set uniformly to the mean of the calcite/aragonite densities, with negligible error in m_S; below). Thus,

the measured density of the mixture, ρ, holds the key to simple subsidence in the OAK event.

With the key, goes a key assumption: The pre-shot density profile down any crater hole is the same as that found now in holes outside the crater ("control holes"), where the medium is almost unmarred. Then, taking z_o [Eq. (5)] at a level in the column where coral has not been vertically displaced, the vertical thickness subtended by solid mass m_S [from Eq. (5)] in a control hole, is equal to the pre-shot thickness of mass m_S of solid in the crater hole. On that basis, the hypothesis of simple subsidence can be tested via its mandate to conserve the column's solid mass. For, the present thickness of that mass [also from Eq. (5)], subtracted from its pre-shot thickness, will give the actual change in height of its topmost particle -- <u>if</u> that change is due to simple subsidence.

In particular, if z [Eq. (5)] refers to the crater floor, the change in question should equal the observed sea-floor lowering. Moreover, knowledge of the pre- and post-shot depths of horizons below the crater allows us a stronger result: By letting z_o and z refer to any two horizons, Eq. (5) should give the same solid mass m_S pre-shot as now -- <u>if</u> the distance between horizons changed by means of simple subsidence. We therefore integrate upward from one and the same horizon R, both pre-shot ($z_o=z_r^p$) and now ($z_o=z_r^n$). When that is done (with a control-hole profile taken as "pre-shot"), a given solid mass m_S, reached at $z=z^p$ pre-shot, will be reached at $z=z^n$ now. For that solid (between z_r^p and z^p pre-shot), the difference $(z^n-z_r^n) - (z^p-z_r^p) \equiv \delta z$ specifies the change in thickness implied by the observed density-profile changes, if the solid moved only up or down. Thus, the meaning of measured density profiles for simple subsidence is shown by plotting δz (but with z increasing downward, not upward; i.e., with depth in place of altitude). Such plots tell how coral solid at any depth below the present OAK crater had its depth changed by the shot -- <u>if</u> simple subsidence caused the change.

DENSITY PROFILES, THEIR TREATMENT, AND DOWNWARD DISPLACEMENTS

Logs of back-scattered neutron and γ-ray intensity (see Melzer, 1986), and of gravity-field variations (Beyer, Ristvet, and Oberste-Lehn, 1986) furnished density profiles down boreholes in the OAK crater region ("neutron", "γ-γ", and "BHG" profiles, respectively). On the reef-wise line (see second section), control-holes OOR-17 and OSR-21 were logged in all three ways, whereas neutron and γ-γ logs were taken in control-hole OAR-2A. There were no cross-reef control holes. On the crater's wing, however, the only reef-wise holes logged close to contour C or D were OQT-19 and ORT-20;[1] that was done by all three methods, save for neutron logging of ORT-20.

---

[1] That can be seen by comparing (1) the depths listed for contours C and D in Table 6-2 and (2) the density profiles presented in full in Appendix 6-1.

It was known before PEACE operations began at the PPG that we would have to look mainly to BHG for density profiles. Why? Because γ-γ logs tell about the medium only within a few centimeters of our 4-inch-diameter boreholes, where the drilling disturbance is greatest; neutron logs "see" about 4 inches farther out (L.S. Melzer, conversations, summer 1987). By contrast, BHG logs give average densities out to about 10 times the vertical interval between readings (generally an interval of 25 ft for the boreholes in question); BHG densities are thus virtually free of man-made or natural local variations in the medium. It was not known, however, whether BHG logging could be done with useful precision under PPG conditions; doing so was a first, and a major PEACE Program success (see Beyer, Ristvet, and Oberste-Lehn, 1986, and Chapter 2 of this Report).

BHG aside, steel borehole casing that ran downward from the sea floor for 100 to 150 ft, interfered with γ-γ logs; the tool was not calibrated for measurement in coral through such a pipe (L.S. Melzer, conversations, summer 1987). In view of that problem, and of changes to the medium from drilling, γ-γ density profiles are probably reliable only at depths greater than a few hundred feet (where they match BHG profiles fairly well). Further, if neutron logs are to add density profiles to the BHG/γ-γ set, a way will be needed to calibrate the neutron tool for PPG coral (L.S. Melzer, conversations, early summer 1987). Thus, at present, density changes from the OAK event must be evaluated from BHG density profiles, augmented somewhat by γ-γ profiles.

Copies of all BHG density profiles from OAK's reef-wise line are shown in Figure 6-2, and the γ-γ profiles in Figure 6-3; all profiles appear at full scale in Appendix 6-1. For use in Eq. (5), each profile was fit by a piecewise linear function, an especially simple matter for the BHG step-profiles; the linear coefficients are listed in Appendix 6-1, where the fits are also plotted. At full scale, the fits overlap the measured profiles everywhere, reproducing them about as closely as their finite line width allows. Those fits embody almost all the depth-dependence of the integrand of Eq. (5); the rest stems from the solid component's density ρ_S, whose extremes lie within 4 percent of their mean (see preceding section). As measured, the variation of ρ_S over that small range is also no more than piecewise-linear with depth. Thus, at its worst, Eq. (5) calls only for integrating a ratio of two linear functions [since $\rho_S/(\rho_S-\rho_L)=1+\rho_L/(\rho_S-\rho_L)$] -- whence, down a given borehole, the solid mass m_S is easily found in closed form vs. depth. When m_S for a crater hole is equated to m_S for a borehole, however, the resulting equation for z^p in terms of z^n is transcendental. By taking ρ_S as constant over each of the many linear intervals of measured density ρ, we avoid that complication; m_S becomes (at worst) piecewise-quadratic in depth, and z^n-z^p becomes an explicit function of z^n. The results, plotted in Figures 6-4 through 6-7, are identical (when plotted) with those obtained by solving the transcendental equation; indeed, simply replacing ρ_S by its mean (2.821 g/cc), and ignoring its depth-dependence, makes no significant change in the figures. Full equations and details of calculation, including the fits to ρ_S, are presented in Appendix 6-2.

The dotted and dashed curves in our thickness-change figures (figs. 6-4 through 6-7) and in Appendix 6-1 speak to a subtler point in the treatment of density profiles: They make direct use of all horizon-depths measured for a given control-hole/crater-hole pair. Specifically, Eq. (5) was integrated from any one horizon to the next higher one in the given control hole. Starting from the same lower horizon in the crater hole, the z^n-value dictated by equal solid mass m_s in the two holes, was computed from Eq. (5) (in the usual way; above) for each z^p-value. On reaching the next horizon in the control hole, z^n fell above or below -- but not on -- that horizon in the crater hole; the reasons: natural density-profile variations along the reef-wise line, and sources of thickness-change other than simple subsidence. Integration proceeded nonetheless from that horizon in both holes, until the horizon above it was reached in the control hole -- and so on until density data gave out in one hole or the other. A full thickness-change curve was thus developed in sections, with the assurance that integration started for each section from the bottom of the same geologic (bio- or lithostratigraphic) layer -- and hence in as nearly equivalent material as possible in both holes. Dots track that curve in our plots of thickness change. The process was then repeated with the roles of crater hole and control hole reversed (i.e., going from one horizon to the next higher one in the crater hole); dashes limn that curve in our plots of thickness-change. The mean of the dotted and dashed curves -- a solid curve -- also appears in the plots. All three curves are clearly distinguishable on the right half of Figure 6-4 (for example); note the horizontal step on the dotted curve, where integrating to the upper surface of a layer in control-hole OOR-17 took us past the corresponding surface in the crater hole (OPZ-18).

As the density profiles show (figs. 6-2, 6-3, and Appendix 6-1), logging began in each hole at a significant depth below the sea floor (not at it). Calculated thickness changes (figs. 6-4 through 6-7 and Appendix 6-2) must therefore be extrapolated up to the sea floor from the smallest depths the logs cover. With OSR-21 as the control hole, the gaps spanned by extrapolation at boreholes OQT-19 and ORT-20, respectively, come to about 5 and 6 percent of the present distance between the sea floor and surface D (downward displacement limit; see preceding section). Using control-hole OOR-17, these figures grow to 23 and 21 percent -- large enough to have three people separately set reasonable upper and lower limits of extrapolation; arrows on Figures 6-6 and 6-7 mark the lines that gave the extremes of the six estimates and their mean.

The downward trend of every BHG-derived curve near its shallow end probably influenced all extrapolations (γ-γ curves go both ways; Appendix 6-2). If so, the bias can hardly be called a defect, given the trend's persistence. Indeed, it suggests forcibly that, down to 100 to 200 ft below the sea floor, the medium is somewhat less dense now than pre-shot.

CONTRIBUTION OF SIMPLE SUBSIDENCE TO THE OAK CRATER

The solid curves of Figures 6-4 through 6-7 (and Appendix 6-1) present final estimates of thickness change due to densification below OAK crater. Extrapolating those curves to the sea floor produced the mean values listed as δz in Table 6-3.

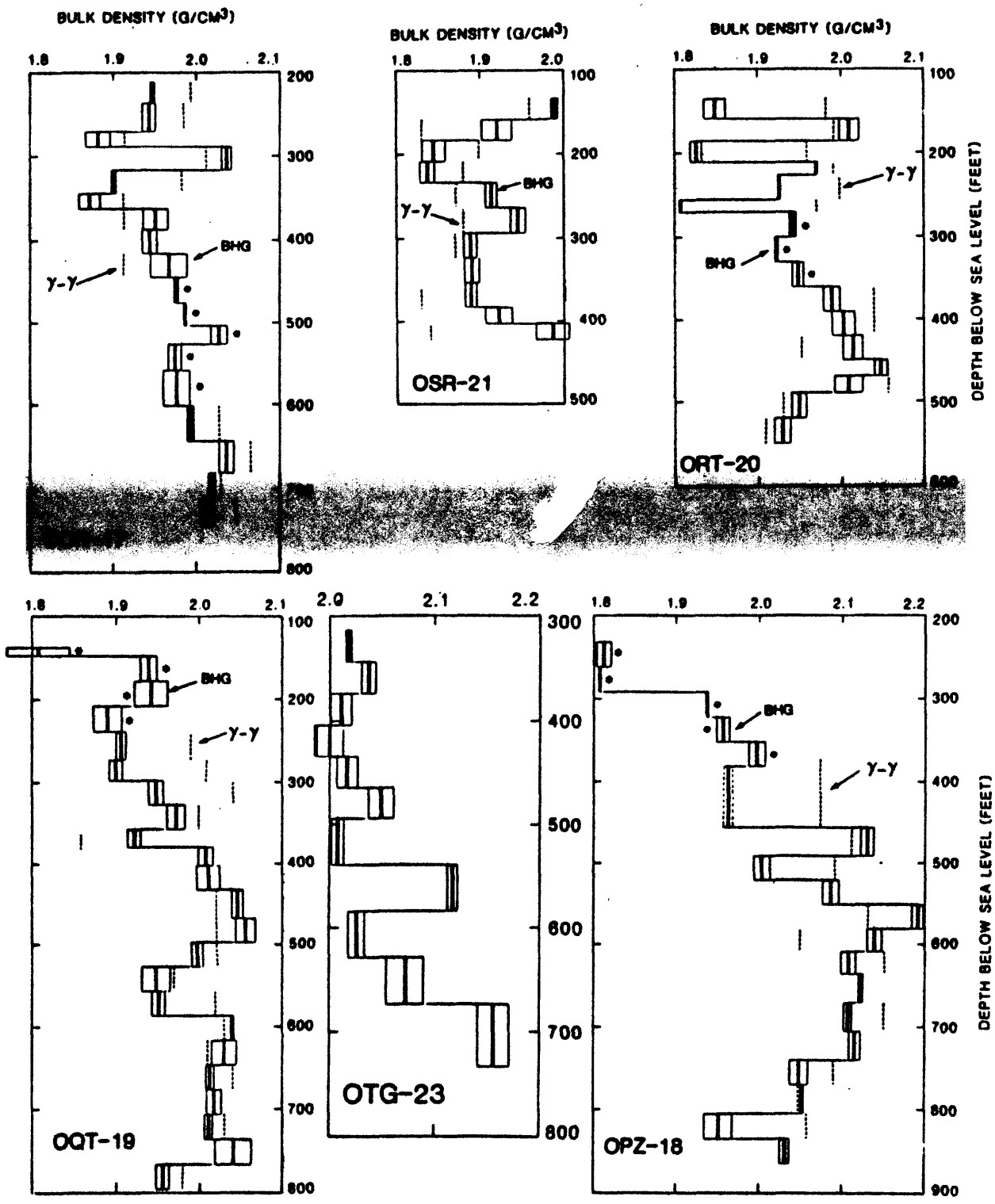

FIGURE 6-2. --Density profiles determined by borehole gravimetry (BHG) in the OAK crater area (Courtesy of L. Beyer, see Chapter 2). Depth below sea level (bsl) given in ft; bulk density in g/cm^3. Inferred densities derived from gamma-gamma (γ-γ) logs shown as dotted lines. Asterisks (*) denote intervals where γ-γ logs are not available due to drillpipe.

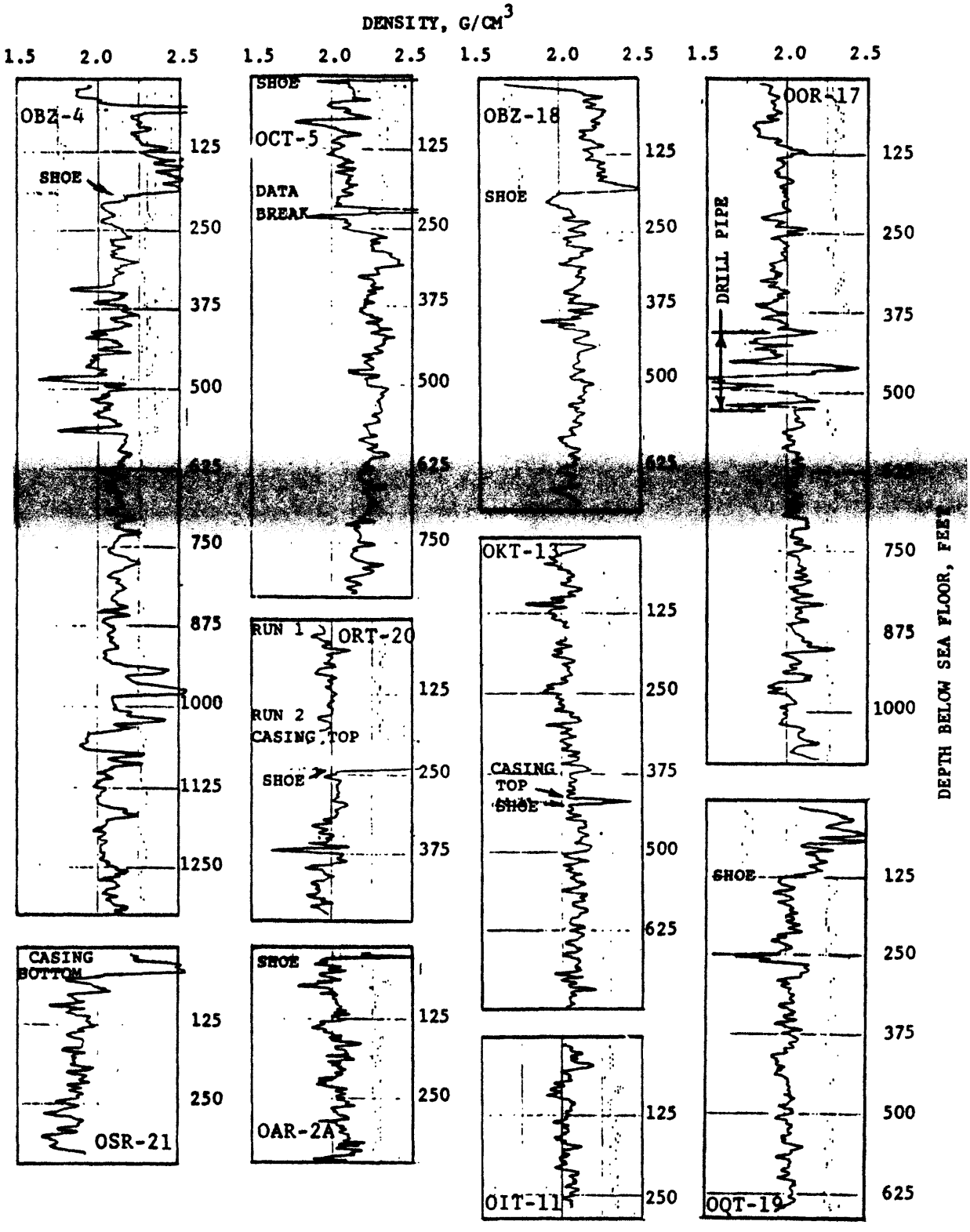

FIGURE 6-3. — Density profiles from gamma-gamma (γ-γ) logging in OAK crater area (data from Melzer, 1986). Depth below sea floor given in ft.

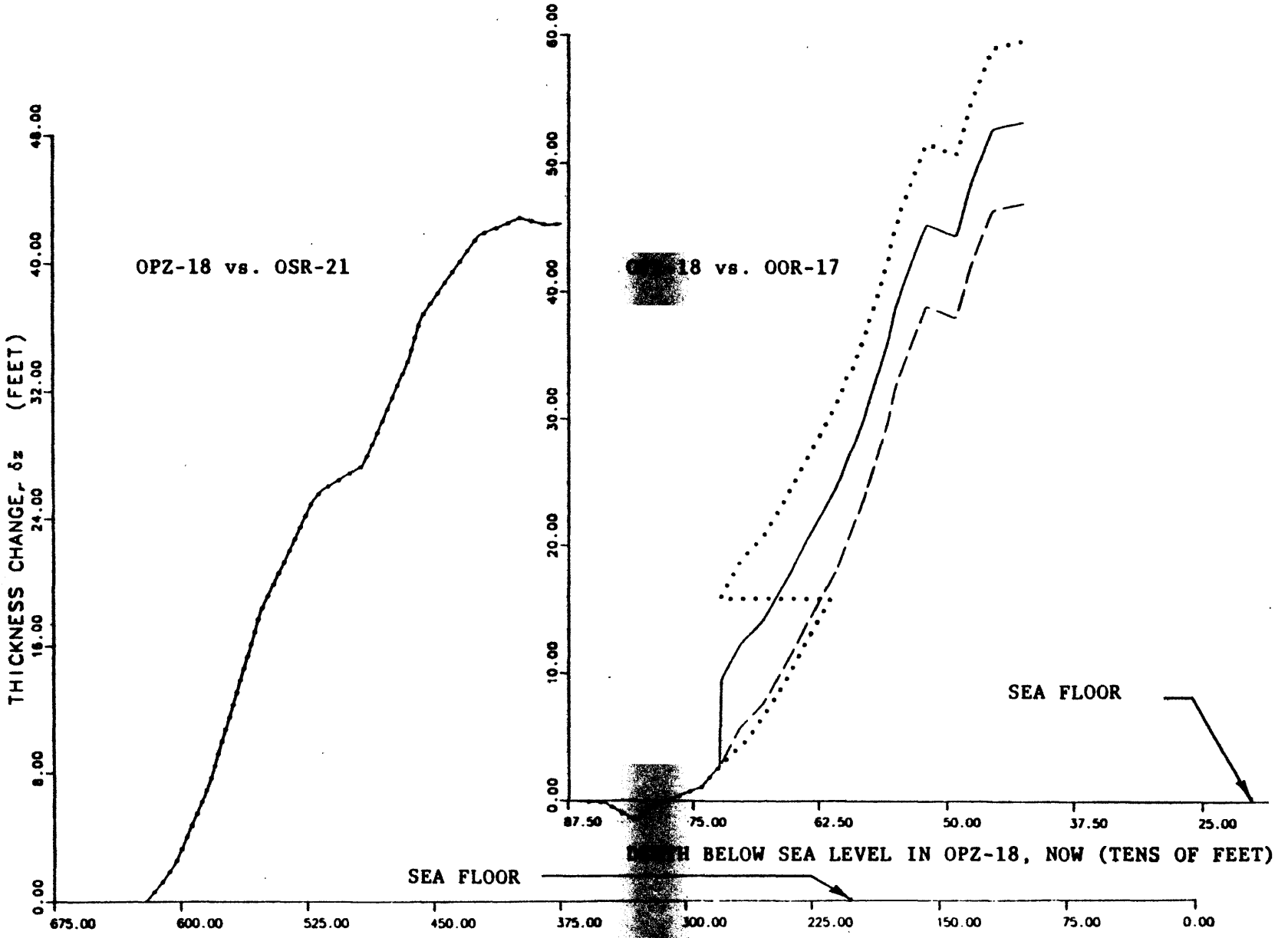

FIGURE 6-4. -- Change in rock thickness [illegible] borehole-gravity (BHG) densities, assuming simple subsidence. Boreholes OPZ-18 vs OSR-21 and OPZ-18 vs OOR-17. Strictly speaking, "NOW" refers to December 1984 throughout this Chapter.

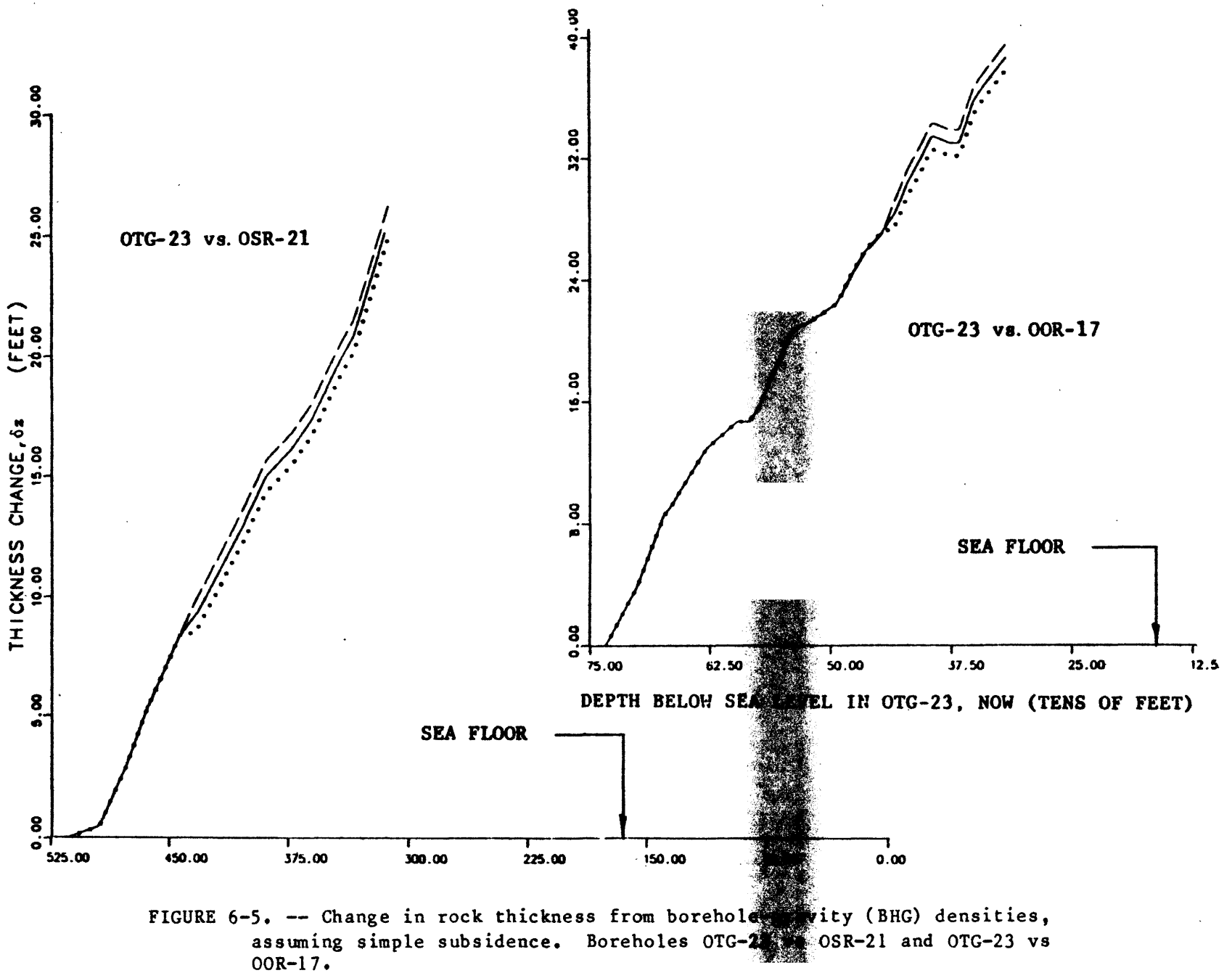

FIGURE 6-5. -- Change in rock thickness from borehole gravity (BHG) densities, assuming simple subsidence. Boreholes OTG-23 vs OSR-21 and OTG-23 vs OOR-17.

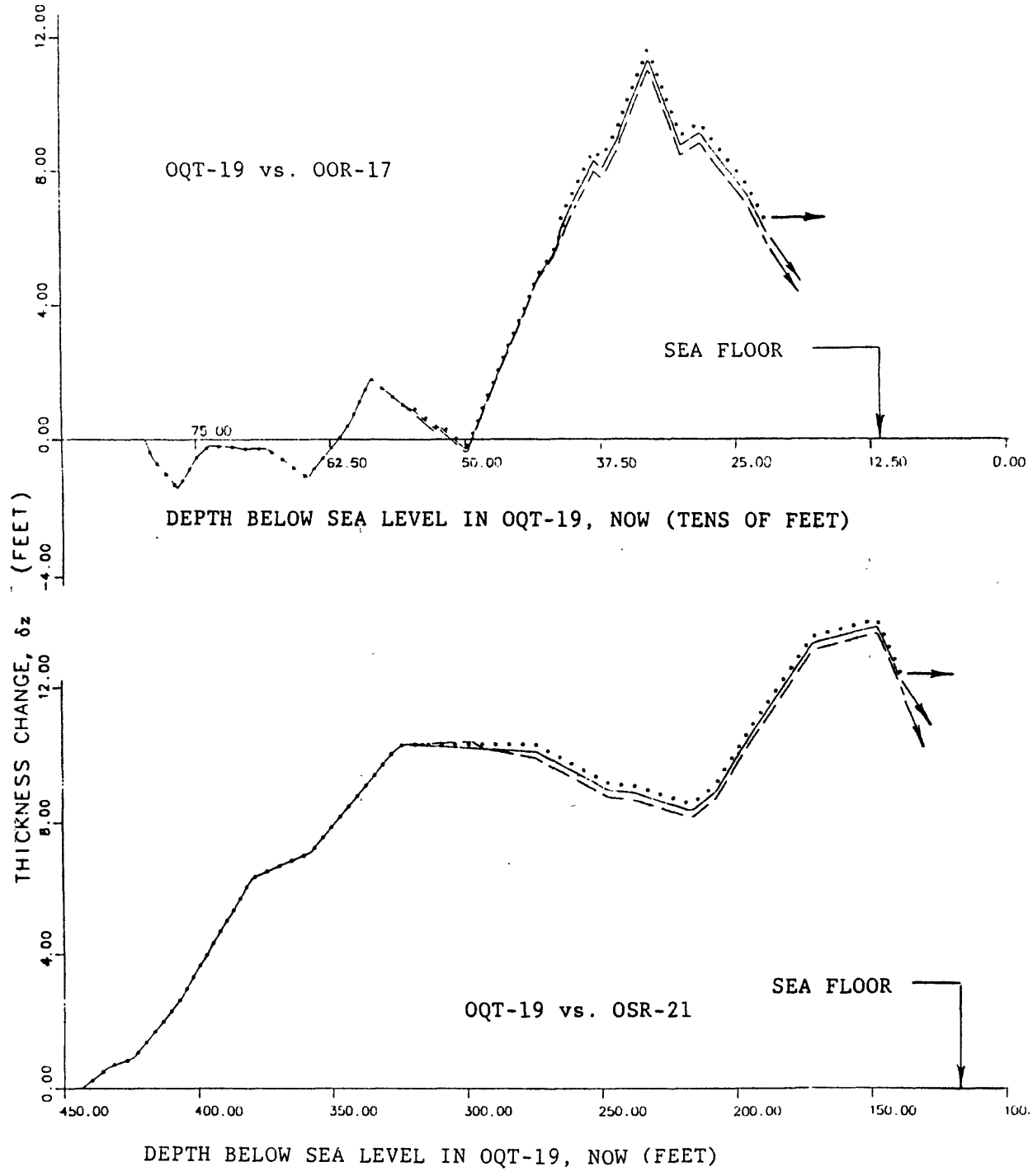

FIGURE 6-6. -- Change in rock thickness from borehole-gravity (BHG) densities, assuming simple subsidence. Boreholes OQT-19 vs OSR-21 and OQT-19 vs OOR-17.

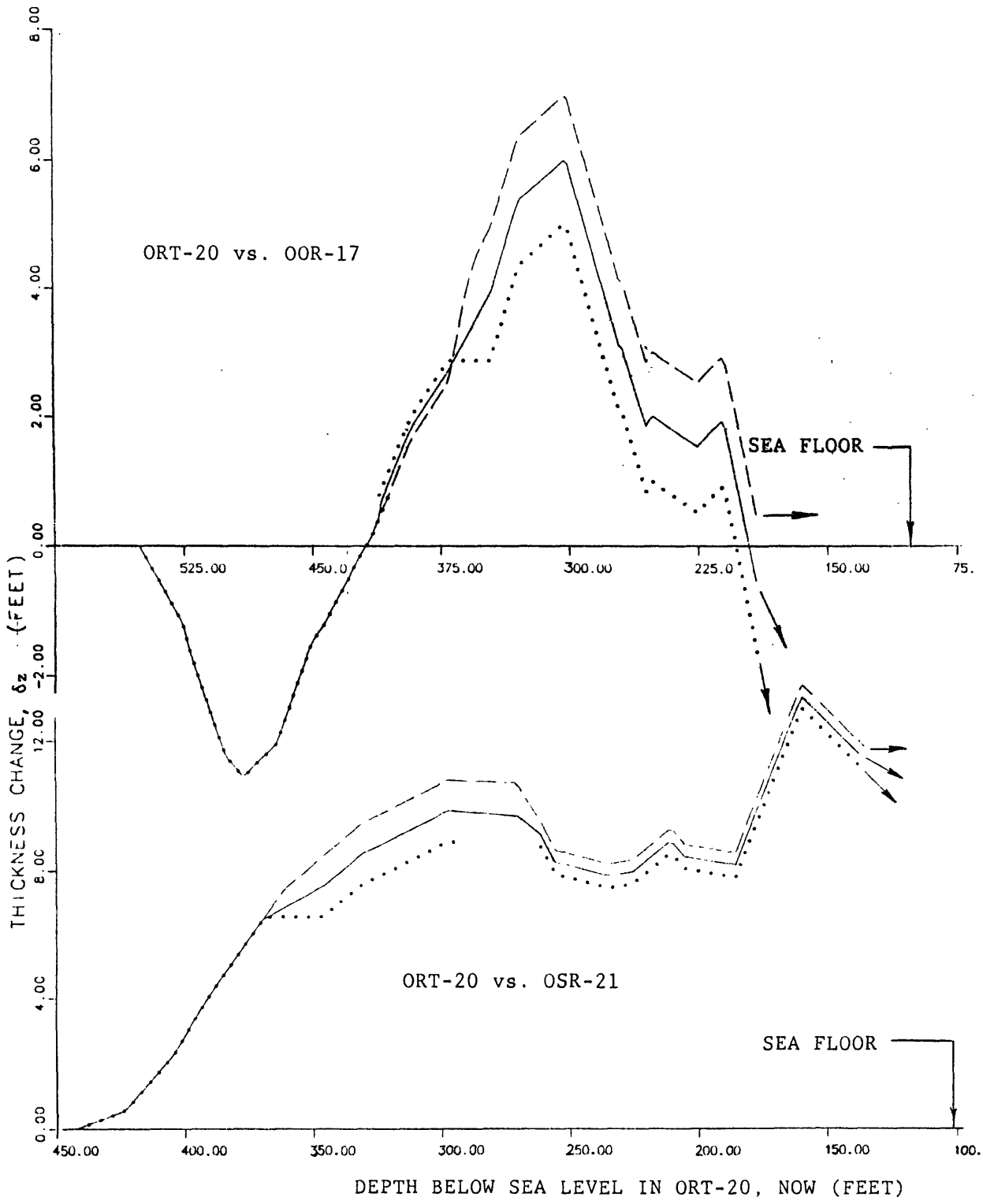

FIGURE 6-7. -- Change in rock thickness from borehole-gravity (BHG) densities, assuming simple subsidence. Boreholes ORT-20 vs. OSR-21 and ORT-20 vs OOR-17.

(Length Unit = 1 ft; $f \equiv \delta z/\Delta z$)

		AS MEASURED: D: 423 ft bsl for OQT-19, 442 ft bsl for ORT-20			BIASED TO INCREASE f: D: 498 ft bsl for OQT-19, δz = 3 ft at D for ORT-20			
Pairs	Δz	δz	f	σ_3	δz	f	σ_3	
19/17	71.5	1.6	.02	.17	7.0	.10	.17	High Estimate
19/21	71.5	11.4	.16	.20	16.8	.23	.20	
20/17	31.4	1.6	.05	.18	4.6	.15	.19	<f> = { .153, no bias; .238, bias up
20/21	31.4	11.9	.38	.07	14.9	.47	.07	
19/17	71.5	-3.6	-.05	.24	1.8	.03	.24	Best Estimate
19/21	71.5	8.6	.12	.25	14.0	.20	.25	
20/17	31.4	-4.7	-.15	.19	-1.7	-.05	.20	<f> = { .060, no bias; .146, bias up
20/21	31.4	10.1	.32	.14	13.1	.42	.13	
19/17	71.5	-4.2	-.06	.30	1.2	.02	.30	Low Estimate
19/21	71.5	6.5	.09	.29	11.9	.17	.30	
20/17	31.4	-10.3	-.32	.16	-7.3	-.23	.17	<f> = { -.009, no bias; .077, bias up
20/21	31.4	8.2	.26	.21	11.2	.36	.20	

TABLE 6-3. -- Column-height changes (in ft) due to densification. Borehole pairs shown in left-hand column; f denotes the fraction $\delta z/\Delta z$.

If a column of material between D and the sea floor changed thickness via simple subsidence, then the thickness change δz computed from density profiles measured pre-shot (under our key assumption, see p. 6-8 above) and post-shot should equal the observed sea-floor lowering at the top of the column. The latter lowering is the column's actual thickness-change Δz (tbl. 6-3), whereas δz is the virtual change which densification provides, as computed from measured density profiles. For each control-hole/crater-hole pair, the ratio $\delta z/\Delta z$ appears in Table 6-3 as the fraction "f" of the sea-floor drop due to simple subsidence. On the wing of the OAK crater, the BHG profiles at hand (crater-holes OQT-19, ORT-20; control-holes OOR-17, OSR-21) tell a clear story: Only a small part of the sea-floor drop can be laid to simple subsidence. The highlights, subsumed in the f-values of Table 6-3, follow:

(1). For the sea-floor drop, best estimates of the fraction (f) due to densification run from -.15 to .32, with a mean of .06.

(2). With each variable (some not yet discussed) pushed to a reasonable extreme so as to increase f, the minimum, maximum, and mean of f are .02, .38, and .15.

(3). With each variable pushed to a reasonable extreme to decrease f, the least, greatest, and mean f-values are -.32, .26, and .01.

(4). With further possible but unlikely increases in all δz-values (right side of tbl. 6-3), the best-estimate values of f [(1), above] increase by .10, .10, and .09, respectively; the f-values in (2) and (3), above, also increase by about those amounts.

Items (1) through (4) above cover systematic errors in determining the fractions by which densification changed column-heights. A major question remains, however, especially with so small a data-set: What confidence can be placed in these results?

CONFIDENCE ASSESSMENT

To fix levels of confidence, we look first at "thickness-changes" caused not by the OAK shot but by natural density-profile variations from one reef-wise borehole to another. To that end, the profile from OSR-21 has been used as a crater profile with the one from control-hole OOR-17 (fig. 6-8) -- and vice versa (fig. 6-9). With OSR-21 as crater hole, extrapolation to the sea floor gives "thickness-change" extremes of -16.3 and -22.5 ft; with OOR-17 as the crater hole, the extremes become 19.8 and 30.4 ft. These are thickness-changes that the two profiles would imply if simple subsidence, in a single coral column down to about 400 ft below sea level (bsl), turned one profile into the other. Thus, not only is density steadily higher in OOR-17 than OSR-21 to about 442 ft bsl, but, as forseen,[1] the "changes" in question are a good deal larger than those due to the burst (the measured $[\delta z[$'s in tbl. 6-3

---

[1] Letters of July 12, 1984, and April 21, 1985, from author to Dean Oberste-Lehn, Research and Development Associates (RDA), and to Maj. Robert F. Couch, Defense Nuclear Agency (DNA), respectively.

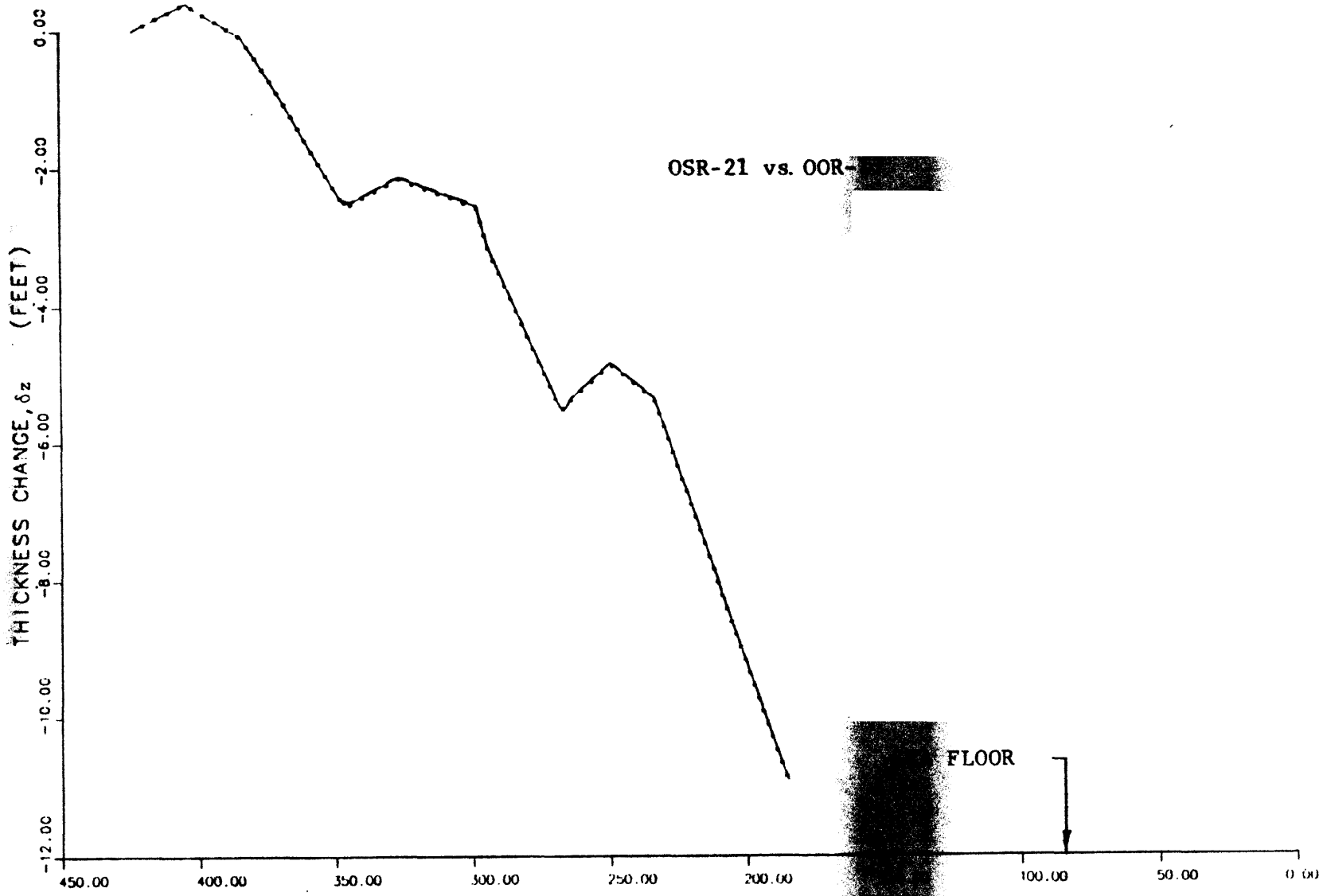

FIGURE 6-8. -- Change in rock thickness from borehole [illegible]y (BHG) densities, assuming simple subsidence. Boreholes OSR-2[illegible]OR-17.

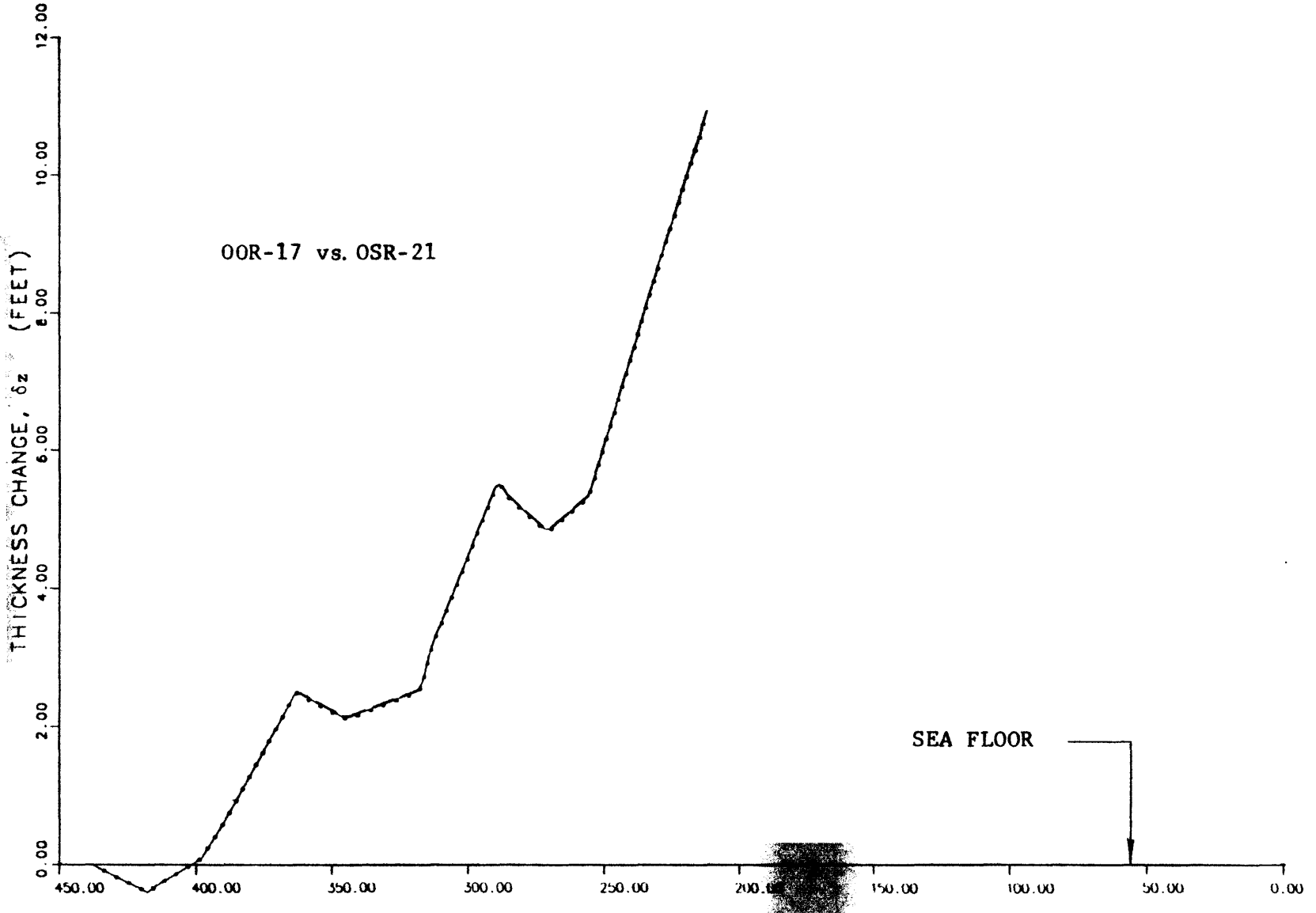

FIGURE 6-9. -- Change in rock thickness from bo[illegible]-gravity (BHG) densities, assuming simple subsidence. Boreholes [illegible]7 vs OSR-21.

are ≤12.4 ft and average 3.0, 6.1, and .1 ft, respectively, for our best, high, and low extrapolations). With nature causing so much variation (presumably at random) in our calculated thickness-change δz, natural density variations dominate the δz-values. Indeed, for equal depths (442 ft) and the same control hole, absolute differences in δz between OQT-19 and ORT-20 come to <4 ft and average only 1.8 ft. Hence, treating all four of the resulting f-values as randomly distributed about a mean appears, at the least, a fair approximation (actually, three sets of four must be dealt with, owing to uncertainty in extrapolating δz to the sea floor). On that basis, the question of confidence turns to one of confidence in the estimated mean of a distributed random variable, and can be answered for a data-set of any size by standard statistical methods.

By reason of central tendency, and lacking data that would establish a precise distribution, we assume (as usual) that f-values are normally distributed. In each case (best, highest, and lowest extrapolation), the data of Table 6-3 then supply both a sample mean of f and a sample standard deviation. In computing the latter, however, it must be recognized that only three of the four f-values are independent. For example, given z in both OQT-19 and ORT-20, vs. z in OOR-17, we know z in OQT-19 vs. z in ORT-20; z in OQT-19 vs. z in OSR-21, then yields z in ORT-20 vs z in OSR-21. Since any three of the four f-values can be taken as independent, four estimates emerge of the standard deviation σ_3; two degrees of freedom enter the calculation of each (par for the standard deviation of three independent measurements). For each mode of extrapolation (high, best, low), every one of the four σ_3-estimates is listed in Table 6-3 alongside the f-value omitted in its calculation; also listed are the drop Δz of the sea floor, and the part (δz) of the sea-floor drop due to densification.

For each estimate in Table 6-3 (high, best, and low) the mean $\langle f \rangle$ and a standard deviation imply a distribution of the true mean of the densification-fraction f. In its cumulative form, that "t-distribution" states the probability Prob(f>v) that the true mean of f (denoted f) lies above any stated value v. Since Prob(f>v) increases monotonically with σ_3 for a given sample mean $\langle f \rangle$, the largest of the four pertinent σ_3-values was chosen to get a high estimate of Prob(f>v), and the smallest σ_3-value for a low estimate; for the best estimate, the four σ_3-values were averaged. With those respective values of the standard deviation σ_3, we computed Prob(f>.5) and Prob(f>1) for each estimate of $\langle f \rangle$ [high, low, and best; a value of about 1/2 would be expected for Prob(f>1) if densification accounted for all of the sea-floor drop]. The net result -- fundamental to the whole study -- is that every case Prob(f>.5) ≤.05, with much smaller values for Prob(f>1). That is, the odds against densification having caused as much as half the observed sea-floor drop are at least 20-to-1. The left side of Table 6-4 presents a detailed, though brief, summary of all key quantities. As for the right sides of Tables 6-3 and 6-4, the following applies.

The thickness-change curve for OQT-19 vs OOR-17 rises at its greatest rate at a depth of about 426 ft, from a minimum at 498 ft (fig. 6-6). The rise between 498 and 426 ft, and the curve's wiggles below 498 ft, may well stem from the medium's random reef-wise variations, rather than any error in estimating the depth of D at OQT-19. In addition, at ORT-20 (and elsewhere), non-zero downward displacement of a few feet might have been missed at D. Both hypothetical errors would act to decrease f; errors of opposite sign -- about as likely -- would make our f-values too large. Nonetheless, to bias f

	AS MEASURED: D: 423 ft bsl for OQT-19 442 ft bsl for ORT-20						BIASED TO INCREASE f D: 498 ft bsl for OQT-19 δz = 3 ft at D for ORT-20					
			$\bar{f}$ >.5		$\bar{f}$ >1				$\bar{f}$ >.5		$\bar{f}$ >1	
Estimate	<f>	σ_3	t	Prob	t	Prob	<f>	σ_3	t	Prob	t	Prob
	.153	.07	8.31	.007	20.29	.001	.238	.07	6.52	.011	18.98	.001
High	.153	.15	3.89	.030	9.50	.005	.238	.16	2.85	.052	8.31	.007
	.153	.20	3.03	.047	7.40	.009	.238	.20	2.21	.079	6.44	.012
	.060	.14	5.58	.015	11.92	.003	.146	.13	4.80	.020	11.58	.004
Best.	.060	.20	3.77	.032	8.06	.008	.146	.20	3.02	.047	7.28	.009
	.060	.25	3.06	.046	6.55	.011	.146	.25	2.43	.068	5.86	.014
	-.009	.16	5.50	.016	10.92	.004	.077	.17	4.30	.025	9.39	.006
Low	-.009	.24	3.63	.034	7.20	.009	.077	.24	3.03	.047	6.61	.011
	-.009	.30	2.91	.050	5.76	.014	.077	.30	2.44	.068	5.32	.017

TABLE 6-4. -- Likelihood that true mean $\bar{f}$ exceeds .5 or 1, given a sample mean <f>. Symbol f denotes the fraction of column-height change due to densification. For each estimate (high, best, low), the three standard deviations shown are are the greatest, mean, and least of the four values of Table 6-3.

as far toward higher values as common sense allows, we have assumed on the right of Tables 6-3 and 6-4 that: (a) the depth of D at OQT-19 is 498 ft, causing δz to increase by 5.4 ft (vs. OOR-17); (b) δz is also greater by 5.4 ft at D for OQT-19 vs OSR-21; (c) for ORT-20, the downward displacement is 3 ft (not zero) at 442 ft bsl, where the geologist's horizons place D; and (d) the 3-ft drop at D for ORT-20 is due entirely to densification at greater depths (contrary to all evidence above D). These assumptions lead to the values of f on the right of Figures 6-2 and 6-3, under the heading "BIASED TO INCREASE f". The main result (besides raising <f>-values by ~.10): Prob(f>.5)$\leq$.08. Strengthened, therefore, is our central conclusion: Densification accounts for just a small part of the wing of OAK's crater.

LONG-TERM SETTLING

Within 67 days of the OAK shot (viz., B+67 days), the sea floor had been re-surveyed to ~3,000 ft from ground zero (GZ). Coupling that survey with PEACE bathymetry has brought to light notable changes in sea-floor depth between August 1958 and December 1984 (see Chapter 5 of this Report). Specifically, in that period, the sea floor sank by ~12 ft at ORT-20, 11 ft at OQT-19, and 4-1/2 ft outside the crater (3,000 ft southwest of GZ on the reef-wise line). That cuts the respective sea-floor drops at ORT-20 and OQT-19 to ~20 and 60 ft seven to ten weeks after the event; i.e., "early". What those results mean for densification -- still our working hypothesis -- is perhaps plainest in terms of ORT-20.

Suppose first that the 1958 to 1984 sea-floor drop was caused by vertical settling of coral from the floor down to surface D; such densification is both simple and credible (any net settling below D, for example, would entail an error in present estimates of D's depth). The early sea-floor drop of ~20 ft at ORT-20 would take less densification to produce than the drop from pre-shot time to now (31.4 ft) -- but the column between D and the sea floor would have been 12 ft taller in 1958 than now, lowering its mean density. More precisely, the sea-floor drop δz due to densification would be less by 12 ft than in 1984 (see tbl. 6-3); the high, best, and low estimates of its value would all fall by that amount, making negative every f on Table 6-3 but one (for ORT-20). The opposite, less likely scenario has contour D move downward by the same amount as the sea floor above it. Above D, density profiles (and hence δz) are then unaffected; mean densification there stays in the small positive range shown in Tables 6-3 and 6-4 [$f=\delta z/(\Delta z-\Delta z_D)$; δz unaffected; equal changes in Δz and in the drop Δz_D at D] -- even if the drop Δz_D has other causes than densification.

Both extremes (D-depth unchanged vs. equal change at D and at sea floor) lead to the same fraction f of the sea-floor drop due to densification. For, if h_D is the increase in D-depth due to slow densification below D, then δz_D (the part of Δz_D due to densification) evolved to zero in 1984 from $-h_D$ at B+67 days (48 to 67 days after the OAK burst); similarly, if h denotes the increase in sea-floor depth due to slow densification above D, then (for coral above D) δz in 1984 becomes $\delta z-h$ at B+67 days. On the densification hypothesis, we have $h+h_D$ = 11.8 ft (the total sea-floor drop at ORT-20 from B+67 to 1984) for any value of h_D; at OQT-19, $h+h_D$ = 11.2 ft. Hence δz (densification's part of the total sea-floor drop by 1984) becomes $\delta z-h-h_D$ at day B+67 -- i.e., δz-11.8 ft for ORT-20 and δz-11.2 ft for OQT-19. Likewise,

the sea-floor drop Δz (in 1984) becomes Δz-11.8 ft for ORT-20 at day B+67, and Δz-11.2 ft for OQT-19. The f's, reckoned as $\delta z/\Delta z$ for 1984, change to $(\delta z\text{-}h\text{-}h_D)/(\Delta z\text{-}h\text{-}h_D)$ for day B+67. Thus, with the 1958 to 1984 sea-floor drop $h+h_D$ fixed (no matter how it is split into parts h and h_D due to densification above and below D), the change in f during that period is also fixed. Accordingly, at B+67, the f- and σ_3-values of Table 6-3, and the probabilities of Table 6-4, becomes those of Table 6-5 below.

Table 6-5, like Tables 6-3 and 6-4, tells a clear and simple tale: As in 1984, the odds against densification having caused half or more of the sea-floor drop measured at B+67, are $\geq$ 18-to-1 in all cases; biased to favor densification, the odds remain $\geq$ 16-to-1. At B+67, however, all values of $\langle f \rangle$ are negative, with a best estimate of -.30 (vs. .06 in 1984). Hence, had f-values been as precise for B+67 as for 1984, Prob(f>.5) would have been a good deal smaller than .05; higher σ_3's at B+67 blocked that (the largest were almost twice as big at B+67). Still, simple subsidence points to negative densification at B+67 (f-values < 0), and it may actually have been negative then (dilatancy). More likely, though, the simple subsidence hypothesis is at fault; it is hard to believe that a medium with 40 to 60 percent porosity, even though fully saturated, would show sizable volume increases on loading and unloading either in uniaxial strain [peak overpressures: ~30 to 78 MegaPascals (MPa) (Table 6-1)] or thereafter.

Larger σ_3's, and the increased scatter of f-values they reflect, take some explaining. They stem primarily from the reduced value, for ORT-20, of the column-height change that forms the denominator of f (a factor of 1.6 smaller at B+67 than 1984). Physically, small column-height changes can flag a breakdown of the f-criterion for measuring the part densification played in forming the crater. That measure makes sense only if the column-height change ($\Delta z\text{-}h\text{-}h_D$ in this case) is large compared to random ups and downs (standard deviation) in the part densification contributes to the change. Otherwise values of f for columns with small changes in height (changes adding little to the sea-floor drop and crater volume) will dominate the mean value $\langle f \rangle$ used to characterize the whole set of f's (including f's for holes with much larger changes in height). The problem can perhaps be finessed (below, last setion), but the true cure lies in computing f as a fraction of crater volume due to densification -- given axial symmetry, a sum (over all crater holes) of products $R\delta z$, divided by a sum of products $R\Delta z$ (R = horizontal range at a given crater hole). That fraction, after all, is the ultimate object sought. On present knowledge, its uncertainty would come mostly from its dependence on the choice of control hole for computing each δz. Here, however, we have density profiles from just two crater holes and two control holes. They yield too small a sample (2 ratios) to make such a criterion practical; the one adopted here, despite the drawback under discussion, permits more efficient use of those data (3 independent f's). Given profiles from a half-dozen or more holes of each kind, the volume criterion appears the better choice.

As for slow settling beyond the presently defined crater, pre-shot and 1984 contour maps show ~4 to 6 ft of it. So do the maps for B+67. The drop appears widespread as to direction, occurring (for example) at both 2-to-4 o'clock relative to GZ (north = 12 o'clock), and 6-to-8 o'clock. Here, however, it matters only if it means that the shot appreciably disturbed control-hole material. That is not at all likely for the following reasons:

Pairs	Δz	AS MEASURED			BIASED TO INCREASE f			
		$\delta z-(h+h_D)$	f	σ_3	$\delta z-(h+h_D)$	f	σ_3	
19/17	60.3	1.6-11.2	-.16	.30	7.0-11.2	-.07	.29	High
19/21	60.3	11.4-11.2	.00	.27	16.8-11.2	.09	.26	Estimate
20/17	19.6	1.6-11.8	-.52	.09	4.6-11.8	-.37	.12	<f>= -.17, no bias
20/21	19.6	11.9-11.8	.01	.27	14.9-11.8	.16	.23	<f>= -.05, bias up
19/17	60.3	-3.6-11.2	-.25	.45	1.8-11.2	-.16	.43	Best
19/21	60.3	8.6-11.2	-.04	.40	14.0-11.2	.05	.39	Estimate
20/17	19.6	-4.7-11.8	-.84	.11	-1.7-11.8	-.69	.12	<f>= -.30, no bias
20/21	19.6	10.1-11.8	-.09	.42	13.1-11.8	.07	.38	<f>= -.18, bias up
19/17	60.3	-4.2-11.2	-.26	.58	1.2-11.2	-.17	.56	Low
19/21	60.3	6.5-11.2	-.08	.53	11.9-11.2	.01	.51	Estimate
20/17	19.6	-10.3-11.8	-1.13	.09	-7.3-11.8	-.97	.09	<f>= -.41, No bias
20/21	19.6	8.2-11.8	-.18	.56	11.2-11.8	-.03	.53	<f>= -.29, bias up

LIKELIHOOD THAT THE TRUE MEAN $\bar{f}$ EXCEEDS .5 or 1, GIVEN A SAMPLE MEAN <f>

Estimate	AS MEASURED:						BIASED TO INCREASE f					
			$\bar{f}$ >.5		$\bar{f}$ >1				$\bar{f}$ >.5		$\bar{f}$ >1	
	<f>	σ_3	t	Prob	t	Prob	<f>	σ_3	t	Prob	t	Prob
High	-.17	.09	12.26	.003	21.44	.001	-.05	.12	8.07	.008	15.45	.002
	-.17	.23	4.95	.019	8.66	.007	-.05	.23	4.20	.026	8.05	.008
	-.17	.30	3.81	.031	6.68	.011	-.05	.29	3.30	.040	6.33	.012
Best	-.30	.11	13.08	.003	21.22	.001	-.18	.12	9.62	.005	16.66	.002
	-.30	.34	4.07	.028	6.60	.011	-.18	.33	3.58	.035	6.20	.013
	-.30	.45	3.10	.045	5.03	.019	-.18	.43	2.75	.055	4.76	.021
Low	-.41	.09	17.68	.002	27.38	.001	-.29	.09	14.76	.002	24.10	.001
	-.41	.44	3.60	.035	5.57	.015	-.29	.42	3.25	.042	5.30	.017
	-.41	.58	2.73	.056	4.23	.026	-.29	.56	2.45	.067	4.01	.029

TABLE 6-5. -- Column-height changes due to densification in OAK crater 48 to 67 days after burst. Borehole pairs given in left-hand column.

(1). Whereas 4-to-6 ft of subsidence appears to have occurred around most of the crater, the pre-shot map runs only about 1.2 crater radii; there, peak overpressure was greater by a factor of 5-to-10 than at control-holes OSR-21 and OOR-17.

(2). As horizontal range increases, a steady decrease occurs in the sea-floor drop observed between 1958 (pre-shot) and 1984. On the reef-wise line of BHG logging, those drops run from ~120 ft one-fourth of the way to the crater's edge, to ~64 ft halfway there, to ~5 ft at the edge itself. They and their rapid decrease with range were doubtless both caused by the explosive loads the medium bore -- loads which also decreased rapidly with range. Like those loads, the sea-floor drop should be a good deal smaller at two crater radii than one -- and the drop of 5 ft at the crater's edge is already small, whether it came about by densification or not.

(3). Uncemented layers were breached in the crater's central region, opening new routes for leakage of water to the surface from great ranges; at a speed of only 1 cm/hr, water would have flowed ~7,500 ft by 1984. Driving such flow, however, would be gravity, just as it has tended over geologic ages to force water upward through the local fissures and passages present in coral. Balancing gravity over that time has been the ability of the solid skeleton to support vertical loads without transferring them to interstitial water; owing to those very loads, the strength of uncemented sand is >0. Gravity and strength act no differently now than in the past -- and the absence of detectable change in the separation of horizons in control holes argues that the balance between them remains where it was struck ages ago.

PIPING

During simple subsidence, skeletal coral replaces water that flows from it; since coral solids are denser than water, the medium then densifies, in accord with Eqs. (1)-(5). Yet, as discussed above, applying Eqs. (1)-(5) to the observed density profiles accounts for only some of the observed sea-floor drop; in material below the crater floor, density has increased by only a small fraction of the requisite amount. However, the finding that material hundreds of feet below the excavation crater had risen to the crater floor (see Wardlaw and Henry, 1986b; and Chapters 3 and 7 of this Report), suggests a way out -- namely, transport of solid particles by upwelling water. Any observed changes in density and column-height can be brought about by such "piping", given the right ratio of solid to liquid in piped slurry; for example, no density changes will be seen if the density of the slurry equals that of the pre-shot medium. In addition, of course, the right amount of material must be piped. On that point, the idea founders; evidence of

substantial piping is limited to the central crater region.[1] There is also an implicit demand that piped solid be transported not just to the sea floor, but out of the apparent crater; that puts direct measurement of the amount of piped material beyond reach now. Nevertheless, piping was noted at OAK; some of its properties follow.

Eqs. (1)-(5) remain valid, but it is no longer useful to ask what pre- and post-shot heights are subtended in a column by a given solid mass m_s. Rather, with solid leaving the column, the mass of solid between two coral particles that remain in it will be different before the shot than after; moreover, the distance between them changes as both solids and liquid are lost. To compute the effects of both losses, let V denote a pre-shot control volume of the medium in which the following definitions apply:

α = pre-shot volume-fraction of liquid in V

β = pre-shot volume fraction of solid in V = $1-\alpha$

ρ_L = density of liquid component

ρ_S = density of solid component

ρ = mean pre-shot density of mixture in V.

As on page 6-7 of this Chapter, it then follows that:

$$\alpha\rho_L + \beta\rho_S = \rho \qquad \text{Eq. (6)}$$

To describe the post-shot state of the same material, let

γ = piped-out fraction (volume or mass) of the liquid within V

$k\gamma$ = piped-out fraction (volume or mass) of the solid within V

$\bar{\rho}$ = present mean density of mixture not piped from V.

---

[1] For a cratering mechanism, a useful measure of significance lies in the fraction of the apparent crater's volume that can be laid to it. The piping observed at OAK crater occurred only within ~.4 apparent radii from GZ -- the central crater -- whereas the main PEACE problem is to account for the wing beyond the central crater. Piping will merit great attention if it can be shown, by tight quantitative arguments, to have produced something like half the wing's volume. By that standard, the fact that piping occurred can only suggest it as a possibly significant mechanism. The same holds for other observations as well, applying (for example) to any sand boils outside the apparent KOA crater; what their quantitative relation might be to the volume of KOA crater (let alone OAK's) is not at all obvious [mud boils also appeared above the Tatum salt dome after the SALMON event (Werth and Randolph, 1966, p. 3409) -- clear proof of piping, but piping played no role in forming SALMON's cavity].

Since αV and βV are the respective pre-shot volumes of liquid and solid, the volumes of liquid and solid piped out of V equal $\gamma\alpha V$ and $k\gamma\beta V$. Hence, of the volume V, the piped-out fraction ϕ is given by:

$$\phi = \frac{\text{Volume of Mixture Piped}}{\text{Pre-shot Volume, V}} = (\gamma\alpha V + k\gamma\beta V)/V = \gamma(\alpha+k\beta) \qquad \text{Eq. (7)}$$

Likewise, the mean density of the remaining mixture becomes:

$$\bar{\rho} = [(1-\gamma)\alpha V\rho_L + (1-k\gamma)\beta V\rho_S)]/[(1-\phi)V]$$

$$= [(\alpha\rho_L+\beta\rho_S)-\gamma(\alpha\rho_L+k\beta\rho_S)]/(1-\phi) = [\rho-\gamma(\alpha\rho_L+k\beta\rho_S)]/(1-\phi) \qquad \text{Eq. (8)}$$

Using Eq. (7) to eliminate γ from Eq. (8), the direct result is:

$$\bar{\rho} = [\rho-(\alpha\rho_L+k\beta\rho_S)\phi/(\alpha+k\beta)]/(1-\phi)$$

Slight rearrangement of this last equation makes it linear in $k\beta/\alpha$, whence

$$k\beta/\alpha = [(\bar{\rho}-\rho_L)\phi - (\bar{\rho}-\rho)\phi + (\bar{\rho}-\rho)]$$

$$= \frac{k\gamma\beta V}{\gamma\alpha V} = \frac{\text{Volume of Solid Piped}}{\text{Volume of Liquid Piped}} \equiv \frac{V_{SP}}{V_{LP}} \qquad \text{Eq. (9)}$$

The sludge density, $\bar{\rho}_{SL}$, follows from the ratio V_{SP}/V_{LP}:

$$\bar{\rho}_{SL} = (\rho_L V_{LP} + \rho_S V_{SP})/(V_{LP}+V_{SP}) = [\rho_L + \rho_S(V_{SP}/V_{LP})]/[1+(V_{SP}/V_{LP})] \qquad \text{Eq. (10)}$$

Values for the mean densities ρ and $\bar{\rho}$ come from density profiles measured, respectively, in control holes and crater holes. Also, for a vertical column of OAK coral, the fraction ϕ is just the change in column-height, divided by the column's pre-shot height. Hence, from PEACE observations, Eq. (9) allows us to compute the ratio of solid and liquid volumes in piped material, and Eq. (10) its density, if piping caused the changes observed. Perforce, then, those quantities constrain the piping process, whereas γ and $k\gamma$ simply fix the unmeasurable total amount piped. For example, if no density changes occur ($\bar{\rho}=\rho$), then the volume and mass ratios implied by Eq. (9) will be those of pre-shot material, and piped sludge will have the same density as the rest of the medium -- in which case, gravity cannot cause it to be piped. However, if a shot raises the medium's density a bit (as the PEACE logs indicate for OAK), the resulting small pressure head can push sludge upward. To help quantify that push, estimates of the density of piped material have been made from PEACE measurements using Eqs. (7), (9), and (10).

In Table 6-6 below are recorded: (a) the mean densities (ρ and $\bar{\rho}$) measured for OOR-17, OSR-21, OQT-19, and ORT-20 from their shallowest common horizon, down to each of three others (the deepest at base D of the downward-displacement region); (b) the depths z and z_Q, respectively, of the top and bottom of the column to which each mean density refers; (c) the measured

column shrinkage, ϕ, between z and z_o for OQT-19 and ORT-20 [1] (together with the changes in depth Δz and Δz_o at z and z_o)[2]; (d) volume ratios implied by those data and Eq. (9), for the four control-hole/crater-hole pairs; (e) a mean density of piped material (also listed) follows from each volume ratio by Eq. (10), and with it (f) a "density decrement" $\rho_{SL}-\bar{\rho}$ (the difference between the densities of piped and remaining material). Evidently, subsidence by piping would require extruded material to have a bit lower density than that not piped. Note, however, that the residue's density $\bar{\rho}$ runs from slightly greater than that of the supposed sludge, to ~.45 g/cc less. That wide spread reflects sensitivity of the volume ratio [Eq. (9)] to random differences among borehole density profiles, when column shrinkages (ϕ) are $<<1$. Thus, the most consistent sludge densities and density decrements are obtained for the longest columns (third quartet of tbl. 6-6, running down to D at ~443 ft bsl for OQT-19 and ORT-20).

From the decrements in Table 6-6, it appears that slurry would be driven upward by pressures of about a tenth of the lithostatic head (mean decrement ~.2 g/cc), though the standard deviation of decrements is also that large (.21 and .26 g/cc; second and third quartets). At an upward acceleration of .1 g (decrement ~.2 g/cc), sludge would take ~11 sec to rise 200 ft in a wide, unobstructed pipe -- but there's more to piping than that.

OTHER CONSTRAINTS; HORIZONTAL PIPING

The densities in Table 6-6 apply to vertical columns 200 to 300 ft in height. Within such a column, single layers could have been driven by a density decrement as large as 1/3 g/cc. However, the path of sludge piped from the crater's wing leads first to the central crater, where lie nearly all the vents known to have guided solids from depth to the sea floor. That first path-leg has its pitfalls. For one, all horizons grow in depth along it; the horizons crossed by contour D at boreholes OQT-19 and ORT-20 (roughly 3a in fig. 6-1) run ~70 ft deeper at OTG-23, 800 ft from GZ (tbl. 6-2), and the sea floor lies ~55 ft deeper. Adding 55 ft of sea water and 15 ft (70 minus 55 ft) of coral makes the overburden ~11 percent greater than at the intersection of D with OQT-19 (or ORT-20). Along the horizon in question (H, say), the resulting overburden gradient opposes inward flow to the vents -- and while 11

---

[1] The "Volume of Mixture Piped", needed to calculate ϕ by Eq. (7), is equal to the change in depth Δz_o of the column's bottom end, minus the change in depth Δz of its top end. The column's "Pre-shot Volume, V" is equal to the pre-shot depth $z_o-\Delta z_o$ of its bottom end minus the pre-shot depth $z-\Delta z$ of its top end, where z_o and z are the current (1984) depths of its bottom and top ends, respectively.

[2] Values of z, z_o, Δz and Δz_o were obtained for Table 6-6 from Table 7-4 of the present Report. For several horizons, the latter table lists both 1984 depths measured in crater holes, and estimates of pre-shot depth based on the full set of 1984 measurements (including horizon depths in control holes). Given a 1984 depth, the pre-shot depth of the same horizon was obtained for Table 6-6 by linear interpolation in Table 7-4 -- with the change in its depth equal to the difference between the 1984 and pre-shot values.

Pair	z_o	z	Δz_o	Δz	ϕ	$\bar{\rho}$	ρ	V_{SP}/V_{LP}	$\bar{\rho}_{SL}$	$\bar{\rho}_{SL}-\bar{\rho}$
19/17	309	220	35.0	38.9	.042	1.91	1.96	<0	>ρ	>0
19/21	309	220	35.0	38.9	.042	1.91	1.89	.36	1.50	-.40
20/17	300	192	19.7	29.7	.085	1.91	1.96	4.66	>ρ	>0
20/21	300	192	19.7	29.7	.085	1.91	1.89	.62	1.71	-.19
19/17	410	220	9.2	38.9	.135	1.94	1.94	1.04	1.94	.00
19/21	410	220	9.2	38.9	.135	1.94	1.89	.44	1.57	-.37
20/17	408	192	6.0	29.7	.099	1.94	1.94	1.14	1.98	.04
20/21	408	192	6.0	29.7	.099	1.94	1.89	.34	1.48	-.46
19/17	444	220	0	38.9	.148	1.95	1.94	.92	1.89	-.06
19/21	444	220	0	38.9	.148	1.95	1.90	.47	1.60	-.35
20/17	442	192	0	29.7	.106	1.95	1.94	.97	1.91	-.04
20/21	442	192	0	29.7	.106	1.95	1.90	.37	1.51	-.44

TABLE 6-6. -- Piping hypothesis. Symbol $\bar{\rho}_{SL}$ denotes density of piped material; densities in g/cm^3; lengths in ft.

percent of overburden may be a small pressure, it is two-thirds or more of the total head available to pipe sludge from H. That head acts at the vents; slurry near them can, of course, be piped upward. At bigger ranges, however, their influence weakens relative to that of overburden. Hence, if we are dealing with a liquefied layer (all sludge), the denser layers above probably settle soonest near the vents, replacing piped material but pinching off the flow. Note also that slurry converges cylindrically as it moves inward, slowing its passage to the vents. The "aperture" available to it (proportional to horizontal radius) decreases by a factor of 2-1/2, for example, as slurry goes from 2,000 ft of radius to 800.

An unliquefied layer presents added bars to piping. For, in a layer with strength, unpiped material bears at least part of the overburden; the pressure that drives piping is smaller than the head that the density decrement would otherwise supply. Indeed, the slurry pressure may simply equal its own head, as in any drained unit; then no piping occurs. More generally, creep of the layer's strong component, like weakening induced by the blast, provides some impetus for piping -- but reduced from that which the full density decrement could furnish, and on a wholly different time-scale. Indeed, creep can be so slow that almost no solid particles are entrained by piped water (simple subsidence), which may well have been the mechanism for settling between B+67 and 1984 (see preceding section). In addition, members with strength physically block piping; sludge has to flow between and around those solid parts. Such flow -- through a porous solid -- is described in simplest quantitative terms as diffusion, in accord with D'Arcy's Law, with flow rates set mainly by the medium's permeability. The lower the rates, however, the more solid settles out (under gravity) on its way to the crater's floor; further, at any given rate, entrained particles will not accelerate upward unless the drag on them exceeds their submerged weight.

These remarks suggest detailed calculations of upward/inward diffusion that have not been made, partly because the medium's post-shot permeability is poorly known, but more because PEACE disclosed no piping of note on the crater's wing.

Once at the surface, slurry particles would have to ride out of the crater on reef-wise currents of perhaps 1 knot (~1.5 ft/sec) (Halley and others, 1986, p. 5). During that half-hour trip, gravity would cause particles to settle; those with diameters >1/8 mm would drop an estimated 100 ft or more along the way (Stokes flow), and hence would leave the crater, if at all, only by other, slower means. The same forces of drag, weight and buoyancy also act on the particles during their rise to the crater's floor; treating them again as isolated spheres, the buoyancy and drag of water rising 200 ft in one hour (1/18 ft/sec) can move them only if their diameters are <1/8 mm, while for 10 and 100 hours of rise, respectively, the critical diameters are 3/80 and 1/80 mm. These estimates are rough, since the particles are not spheres (nor do spheres bound drag ÷ mass), they and their wakes overlap [increasing drag ÷ mass if they do not clump (Soo, 1967, Ch. 5)], and they rise in ragged, twisty channels (not straight, free streams) that may be <10 diameters wide in places.

Fissures, and cones of debris containing coral fragments raised hundreds of feet, were seen in the central region, where coral was most damaged (Halley and others, 1986; Slater, and others, 1986). Piping accounts neatly for that, and much of it could have occurred in a few seconds or less. For, with

overpressure at the .1-MPa level, burst-induced sub-crater pressures up to ~100 MPa would furnish the required vertical stress gradients. Relief of those pressures would be rapid, requiring a volume increase of <1/2 percent for decay to .1 MPa (from 100 MPa). Though slight in relation to crater volume, enough material would be extruded in such an expansion to make impressive deposits on the sea floor, and cloud the reef currents that cross the crater.

DENSIFICATION: SUMMARY AND CRITIQUE

Borehole cores have let geologists fix the depths of many layer interfaces ("horizons") below and outside the OAK crater. Further, in two holes on the crater's wing, gravimetry has furnished density profiles down to horizons not moved by the OAK burst; to the same horizons, but well outside the crater, borehole gravimetry (BHG) also has given two density profiles. All four holes lie on a curve roughly parallel to the reef. There, in pristine coral, geology argues for random density-profile variations about some mean. The present coral medium formed in about the same way at different points on any one of a set of curves roughly parallel to the reef. Moreover, PEACE cores and density profiles support the idea of such variations about a mean. Treating the far-field pair as pristine profiles then yields density changes due to the burst, from depth to 20-100 ft below the crater floor. From those changes come the downward displacements that densification implies for sub-crater coral, vs. depth, and for the crater floor itself. Comparing the latter displacements to actual sea-floor drops yields the result that densification played but a small role in forming the crater's wing.

Except for converting density profiles to downward displacements, significant uncertainty attends each step noted:

1. The general increase of coral density from lagoon to ocean is a source of systematic error in the measured profiles. Specifically, prior to OAK, departures from the mean density profile would have been random along the curve on which boreholes were supposed to lie. That curve is not known precisely. Actual boreholes therefore depart from it, but are about as likely to fall on one side of it as the other. Hence, given the oceanward density gradient, the general effect of such misplacement is to increase the differences among measured profiles. The unlikely opposite result, however, is more apt to have occurred in our four-profile set than in a large set. The scatter of profiles would then have been underestimated.

2. A horizon's drop (or rise) by a few feet could have escaped notice. That holds for the "unmoved" horizons above which we reckoned density-change effects in the two crater-wing holes.

3. From the shallowest point of BHG logging in a given borehole to the sea floor, horizon-depth changes due to densification were estimated by extrapolation from below.

4. Limits of precision render BHG-measured densities uncertain, but by $< \pm .02$ g/cc. Further, BHG densities are averages over such large regions that the effects of them of local site inhomogeneities (vugs, etc.) are believed negligible (for PEACE, a great advantage of BHG over other methods).

5. The sea-floor drop δz implied by density changes down a borehole, divided by the actual sea-floor drop at the hole (Δz), measures the contribution of densification to the crater. That ratio (f), however, gives too much weight to holes where the actual drop is small. Further, though f is a random variable, its distribution may not be near-normal (as assumed).

6. The largest values of δz (vs. depth) come from pairing the two wells outside the crater, just 560 ft apart ("control-holes," ~5,500 and 6,000 ft from GZ). Moreover, paired with the same control hole, the two holes 400 ft apart in the crater's wing (~4,000 ft from the control holes) have much the same curve of δz-vs.-depth. Nature, not the OAK burst, thus appears the chief source of variation among the four density profiles; our signals (density changes due to OAK) were buried in noise (random natural differences in density). As a result, the likelihood that the crater wing formed by simple subsidence could be assessed using three independent values of δz (the maximum from four profiles) -- despite our having just two profiles from the wing. Strictly, that can be correct only as f, divided by its standard deviation, approaches zero. The crater-wing profiles show some densification ($f>0$), however, and may differ systematically therein owing to their different ranges.

Caveats 1 through 6 forced us to assess confidence in the overall finding of low densification ($\delta z < .1\ \Delta z$). To that end, our data base and calculations were altered (within reason) to maximize f:

i) Since oceanward density gradients could have acted to reduce differences among our f-values [caveat 1 above], the standard deviation of f was assigned the largest value found from the data (of the four deviations at hand when three of four f's are independent).

ii) For each borehole, δz was set at the sea floor to the highest δz-value found by extrapolating δz-vs.-depth to the floor [point 2 above].

iii) Unseen displacement of the shallowest "unmoved horizon" D in a given borehole would probably have been downward. Each δz-value from item (ii) above was increased by 3 ft or more to offset such an error [caveat 3 above].

iv) Adding offsets (iii) directly to δz-values credits the unseen drop of D entirely to densification below D -- even though densification accounted for just a small part of the horizon-drops observed above D (in the crater's wing).

v) On the PEACE data, the tendency of f to place undue weight on holes with small sea-floor drops [point 5 above] led to high -- but accepted -- values of both f and its standard deviation (ORT-20 has smaller Δz-values than OQT-19 and higher f-values).

The overstatement of f flagged by item (v) looks correctible (next section). That correction would probably be cancelled, and then some, if no appeal were made to the limit where f, divided by its standard deviation, tends to zero (item 6 above). How to avoid that limit without giving f another strong ad hoc lift is not clear. As it is, each upward bias lent to f appears within reason. Having them all act at once to make high f-values likely does not. But even so, only minor densification results.

CONCLUSIONS

If the wing of the OAK crater resulted from densification, then the sea-floor drop at a wing-station, W, can be computed exactly from density profiles before and after the shot in a vertical column below W. No such profiles were measured pre-shot. That heightens the problem of reading density increases due to OAK through the noise of random natural variations in density. Below the crater's wing, those variations were found to dominate shot-driven changes in density. More important, however, the noise level proved low enough to admit a clear answer to the main question posed -- **on the wing of OAK's crater, most of the sea-floor drop had causes other than densification.**

As a best estimate, 6 percent of the sea-floor drop on the crater's wing can be laid to density increases caused by the burst. That figure follows from profiles down two crater holes and down two control holes outside the crater -- profiles that yield four estimates (3 independent) of the fraction, f, contributed by densification to the sea-floor drop. Each of the four has a high, best, and low value, depending on how a gap in data just below the sea floor is bridged (fig. 6-10). To be sure, the sample is small, but its size has been taken into account in assessing confidence in the mean of f. The results: The probability that densification caused half or more of the sea-floor drop is $<.1$. That result holds even if the main parameters of the calculation are all varied at once (each within reasdonable limits) so as to increase f. The PEACE density profiles could be of course atypical, but, at most, that observation only supports measuring more profiles; with the data at hand, the results are as stated.

Extant maps show that, in the crater wing, the sea floor sank appreciably between August 1958 (a few months after OAK) and December 1984 (PEACE). The crater was therefore significantly shallower in 1958 than now. By the same token, given simple subsidence, the medium was notably less dense (on average), from the base of the region of downward displacement to the crater floor. Combining that slow sea-floor drop with the PEACE density profiles leads to a best estimate of $\sim -.2$ for f at August 1958 -- and again (by chance) the probability that densification caused half or more of the sea-floor drop at that date is $<.1$.

The same data base of sea-floor maps and PEACE density profiles also yields mean values for the density of materials piped up to the sea floor, if the piping hypothesis is correct. From those values, the densities of piped and residual material differ by an average of $\sim .2$ g/cc, but with a standard deviation at least that large. A density difference of .2 g/cc can drive piping, but weakly -- and the chain of events leading to transport of piped material out of the crater has many weak links (e.g., it appears that particles $>.1$ mm in diameter will settle before they can exit).

The statistical grounds for assessing densification probably can be strengthened, using only extant data. Given the cost of the data, that should be done. Specifically, both the sea-floor drop (Δz) and the part of it due to density changes (δz) can be expressed as fractions of the pre-shot depth to D. The probability that the latter fraction exceeds half (say) of the former can then be computed, using standard deviations supplied by PEACE data. A BHG profile from the central region could also be added to the present set, but not without giving a further strong upward bias to the estimated extent of

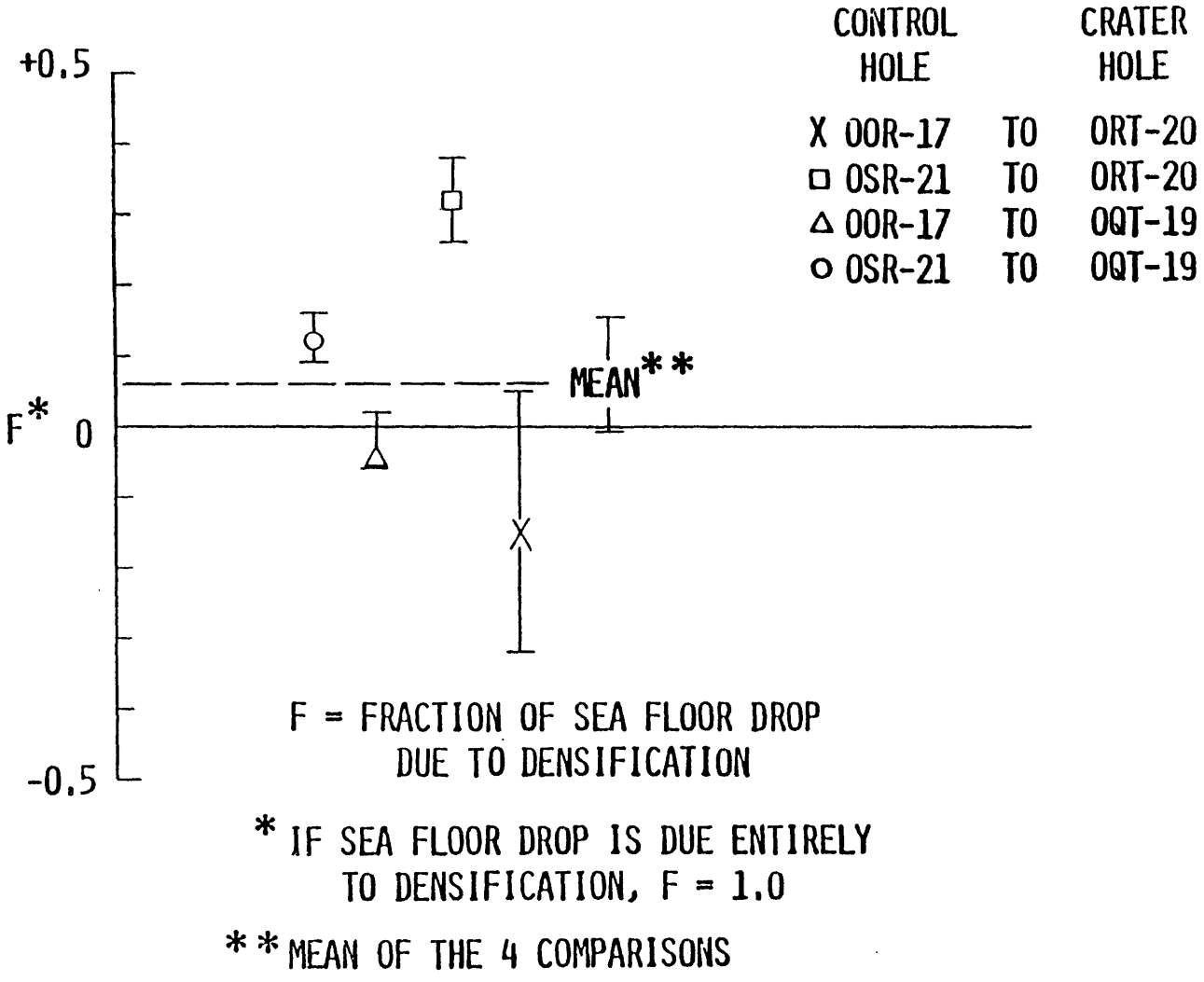

FIGURE 6-10. -- High, low, and best estimates of the fraction contributed to sea-floor drop by densification at boreholes OQT-19 and ORT-20.

densification. In addition, the plausibility of the piping hypothesis should be examined further. With densification as an unlikely mechanism for forming OAK's crater-wing, however, plastic flow appears to offer the simplest and most plausible explanation for it. Whether that explanation will withstand close scrutiny is unclear; flow is well understood in principle, but not much is known about the displacement field around a flow crater.

ACKNOWLEDGEMENTS

For the PEACE Program data herein, and much kind assistance besides, my sincere thanks go to Larry Beyer, Scott Blouin, Bob Henny, Woody Henry, Steve Melzer, Dean Oberste-Lehn, John Peterson, Byron Ristvet, Ed Tremba, and Bruce Wardlaw. Larry, John, Woody, and Byron, and (above all) Steve and Bruce are due special thanks for extended discussions of both the data and its implications; so are my co-workers Neil Perl, Jim Workman, and Ken Burrell, for reducing PEACE data to forms from which conclusions more readily follow.

REFERENCES CITED

Beyer, L.A., Ristvet, B.L., and Oberste-Lehn, D., Chapter 8, Preliminary density and porosity data and field techniques of borehole gravity surveys, OAK crater; 28 p., 4 figs. 10 tbls; in Henry, T.W., and Wardlaw, B.R., eds., Pacific Enewetak Atoll Crater Exploration (PEACE) Program, Enewetak Atoll, Republic of the Marshall Islands; Part 3: Stratigraphic analysis and other geologic and geophysical studies in vicinity of KOA and OAK craters: U.S. Geological Survey Open-File Report 86-555.

Halley, R.B., Slater, R.A., Shinn, E.A., Folger, D.W., Hudson, J.H., Kindinger, J.L., and Roddy, D.J., 1986, Observations of OAK and KOA craters from the submersible; 32 p., 13 figs., 1 appendix; in Folger, D.W., ed., Sea-floor observations and subbottom seismic characteristics of OAK and KOA craters, Enewetak Atoll, Marshall Islands: U.S. Geological Survey Bulletin 1678.

Melzer, L.S., 1986, Chapter 7, Downhole geophysical logs; 32 p., 16 figs., 7 tbls., in Henry, T.W., and Wardlaw, B.R., eds., Pacific Enewetak Atoll Crater Exploration (PEACE) Program, Enewetak Atoll, Republic of the Marshall Islands; Part 3: Stratigraphic analysis and other geologic and geophysical studies in vicinity of KOA and OAK craters: U.S. Geological Survey Open-File Report 86-555.

Pierce, B.O., 1929, A Short Table of Integrals; Third Revised Edition, Ginn and Company, Boston, New York (etc.).

Slater, R.A., Roddy, D.J., Folger, D.W., Halley, R.B., and Shinn, E.A., 1986, Chapter 13; Additional submersible studies; detailed observations of the sea floor of OAK, KOA, and MIKE craters; 153 p., 2 tbls., 4 pls.; in Henry, T.W., and Wardlaw, B.R., eds., Pacific Enewetak Atoll Crater Exploration (PEACE) Program, Enewetak Atoll, Republic of the Marshall Islands; Part 3: Stratigraphic analysis and other geologic and geophysical studies in vicinity of KOA and OAK craters: U.S. Geological Survey Open-File Report 86-555.

Soo, S.L., 1967, Chapter 5; in Fluid Dynamics of Multiphase Systems; Blaidsell Publishing Company, Division of Ginn and Company, Waltham, Massachusetts, Toronto, London.

Tremba, E.L., and Ristvet, B.L., 1986, Chapter 4; X-ray diffraction mineralogy; 49 p., 11 figs., 35 tbls., in Henry, T.W., and Wardlaw, B.R., eds., Pacific Enewetak Atoll Crater Exploration (PEACE) Program, Enewetak Atoll, Republic of the Marshall Islands; Part 3: Stratigraphic analysis and other geologic and geophysical studies in vicinity of KOA and OAK craters: U.S. Geological Survey Open-File Report 86-555.

Wardlaw, B.R., and Henry, T.W., 1986b, Chapter 14; Geologic interpretation of OAK and KOA craters; 39 p., 21 figs., 2 tbls.; in Henry, T.W., and Wardlaw, B.R., eds., Pacific Enewetak Atoll Crater Exploration (PEACE) Program, Enewetak Atoll, Republic of the Marshall Islands; Part 3: Stratigraphic analysis and other geologic and geophysical studies in vicinity of KOA and OAK craters: U.S. Geological Survey Open-File Report 86-555.

Werth, G., and Randolph, P., 1966, The Salmon seismic experiment: Journal of Geophysical Research, v. 71, no. 14, p. 3405-3413.

****

APPENDIX 6-1

This appendix contains (1) all PEACE density profiles measured in the OAK area, with (2) plots of the fits made to those profiles as part of the work reported here. Also presented are (3) tables of coefficients for the piecewise linear function used to fit all profiles. That function is defined as follows:

$$\rho = [(z-z_j)\ \rho^-_{j+1} + (z_{j+1}-z)\ \rho^+_j] \ /\ (z_{j+1} - z_j);\ j = 1,2,..,J \qquad \textbf{Eq. (11)}$$

where ρ and z denote density and depth, respectively. For the BHG profiles [received as step-functions from L.A. Beyer, written communication, May 15, 1987); see Chapter 2, this Report], ρ^+_j and ρ^-_{j+1} have the same value $\rho_{j+1/2}$. Otherwise, $\rho^-_j = \rho^+_j = \rho_j$, and (ρ_j,z_j) gives the coordinates of an endpoint of either two or one straight-line segments of the complete function. Specifically, for $j \neq 1$ or J, a segment runs from (ρ_{j-1},z_{j-1}) to (ρ_j, z_j), and another from (ρ_j,z_j) to (ρ_{j+1},z_{j+1}); the single segment for j=1 runs from (ρ_1,z_1) to (ρ_2,z_2), and the single segment for j=J connects (ρ_J,z_J) to (ρ_{J+1},z_{J+1}).

The measured BHG profiles, in graphic form, comprise the first exhibit below (figs. 6-11 to 6-16). In each case, for ready comparison, a graph of the density-function fit to a given profile [Eq. (11)] is shown next to it, with the pair on identical scales. Then, in exactly the same format, a set of figures (6-17 to 6-26) follows in which appear all the profiles derived from γ-γ logging, together with the density function fit to each. Next, on a single page (tbl. 6-7), come all the (ρ_j,z_j)-points that specify the functions fit to BHG profiles (points supplied by the tables of Chapter 2 of this report). A corresponding table for fits to all the γ-γ profiles comes last (tbl. 6-8). The latter table was compiled by measuring coordinates from the profiles themselves, having overlain them with thin graph paper; thus, at the outset, our measures of density and depth, denoted "DIV" in the tables, were a pair of coordinates read off graph paper. Conversion was made from DIV to g/cc, and from DIV to ft, by means of the following formulas:

$$\text{density (g/cc)} = Q + (\text{DIV}-Y_o)/S; \quad \text{depth (ft)} = A + B(\text{DIV}-X_o)/C \qquad \textbf{Eq. (12)}$$

Values of Q, Y_o, S, A, B, X_o, and C are given for each profile in Table 6-8.

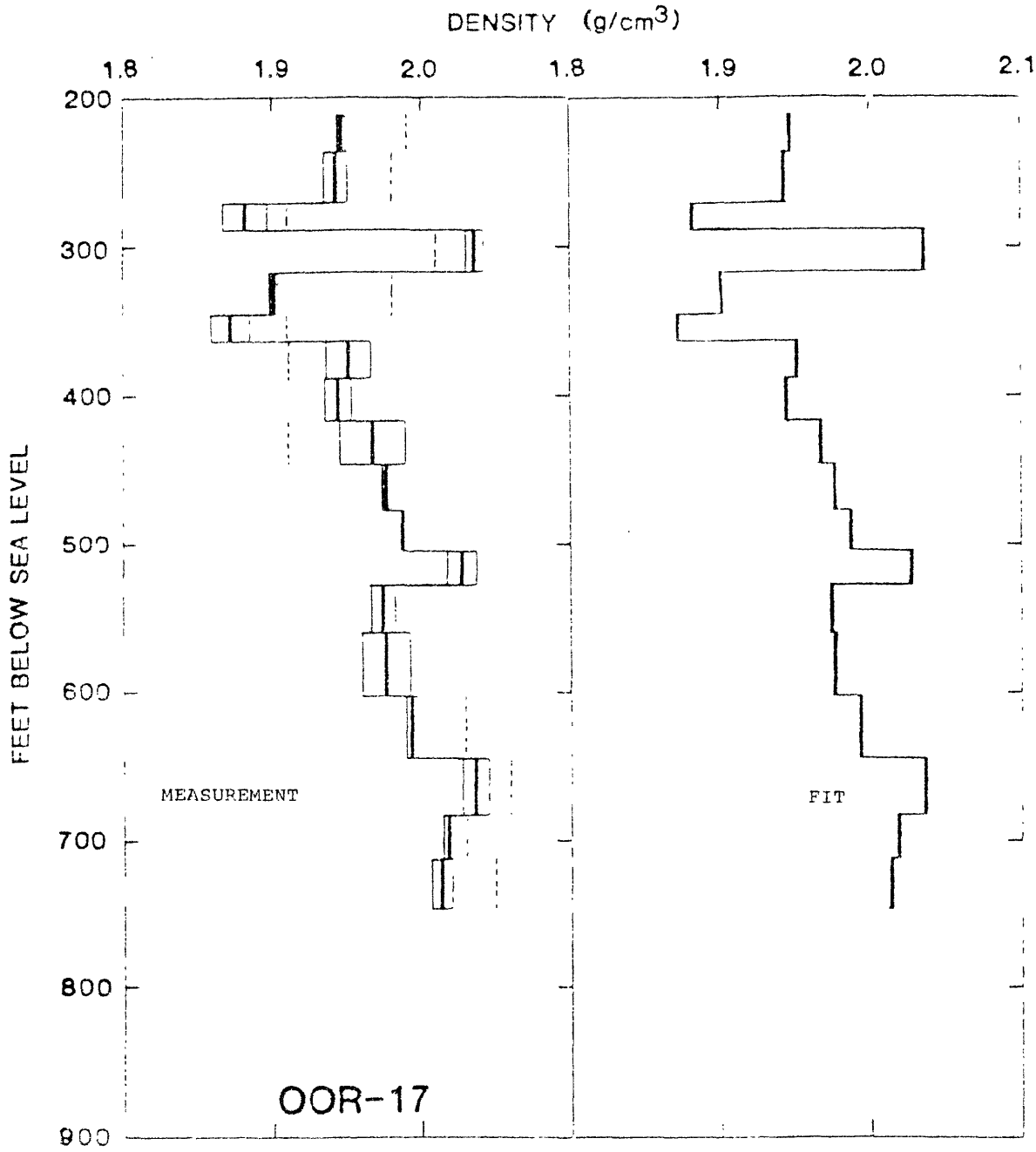

FIGURE 6-11. -- Left: profile of density vs. depth from BHG logging in control hole OOR-17, as received. Right: plot of broken-straight-line fit [Eq. (11)] to profile at left. The left- and right-hand plot scales are identical.

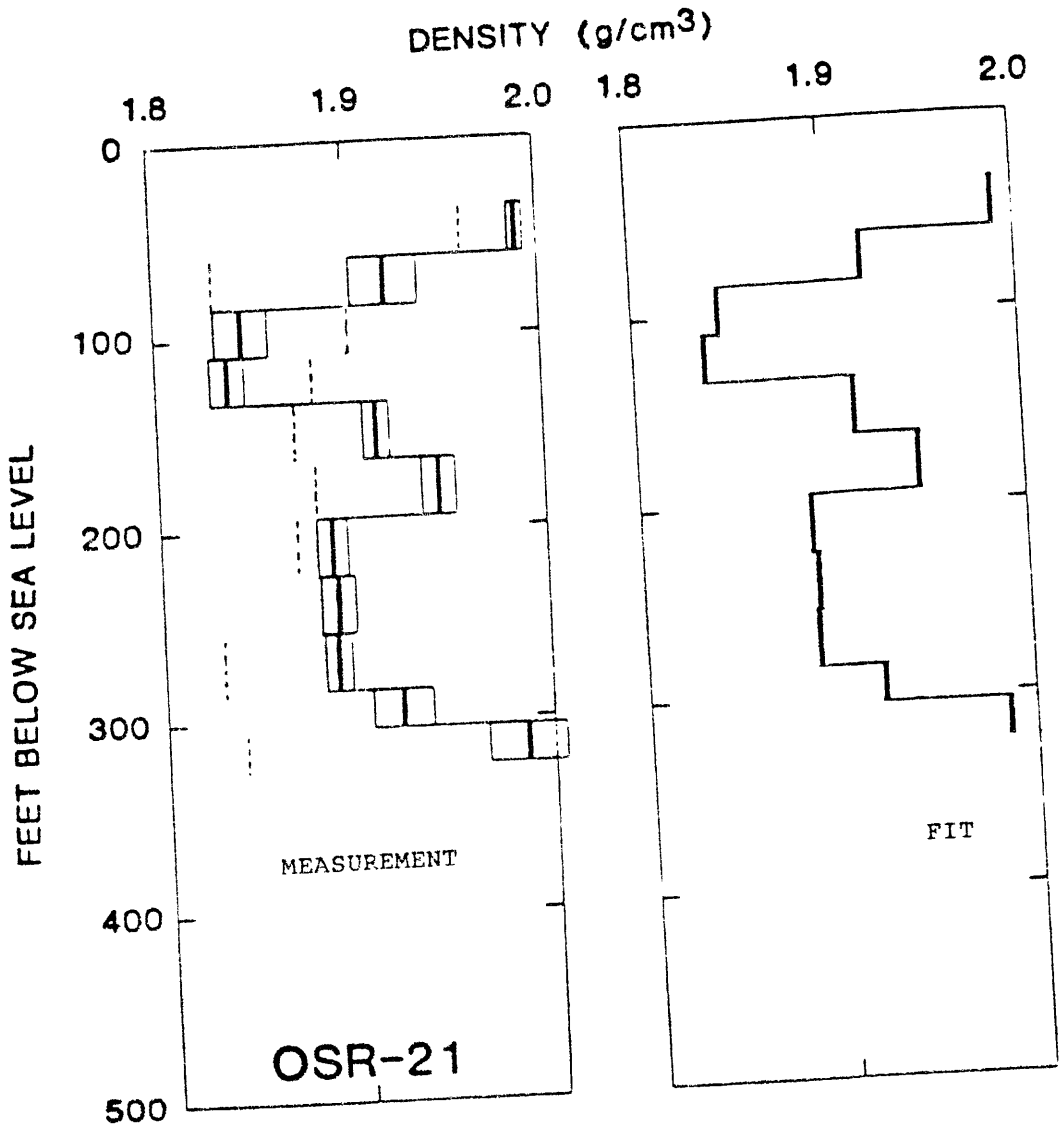

FIGURE 6-12. — Left: profile of density vs. depth from BHG logging in control hole OSR-21, as received. Right: plot of broken-straight-line fit [Eq. (11)] to profile at left. The left- and right-hand plot scales are identical.

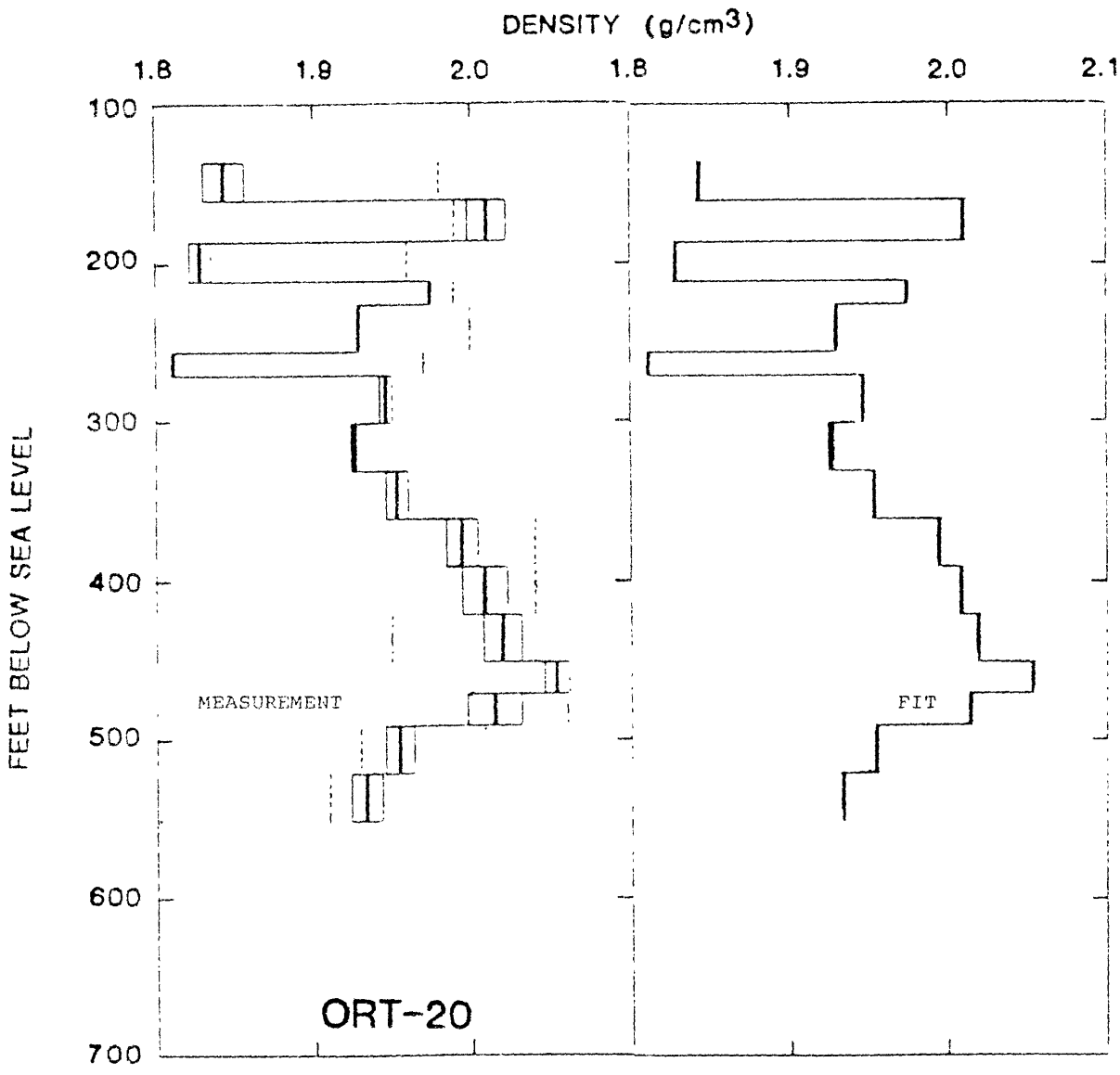

FIGURE 6-13. -- Left: profile of density vs. depth from BHG logging in crater hole ORT-20, as received. Right: plot of broken-straight-line fit [Eq. (11)] to profile at left. The left- and right-hand plot scales are identical.

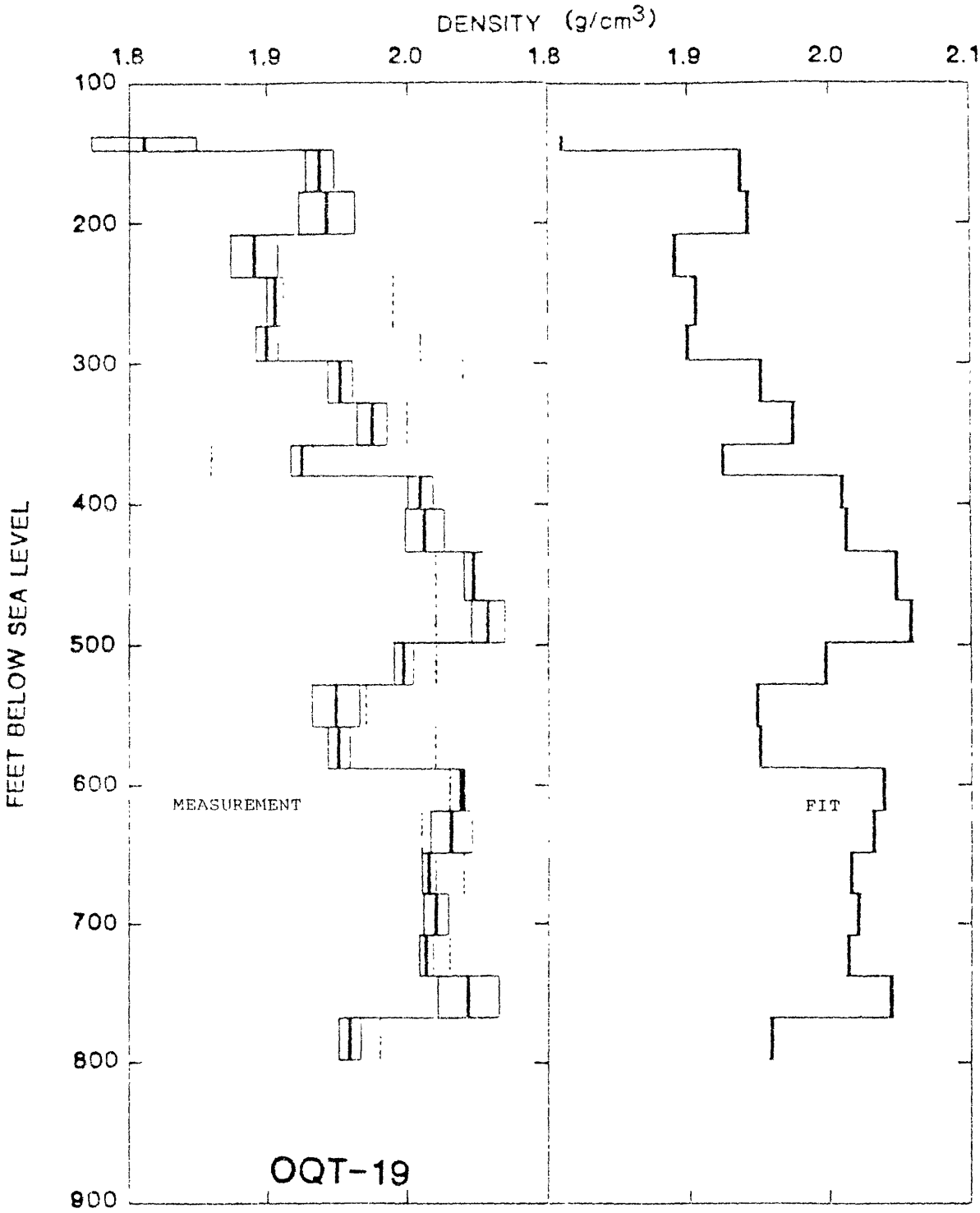

FIGURE 6-14. -- Left: profile of density vs. depth from BHG logging in crater hole OQT-19, as received. Right: plot of broken-straight-line fit [Eq. (11)] to profile at left. The left- and right-hand plot scales are identical.

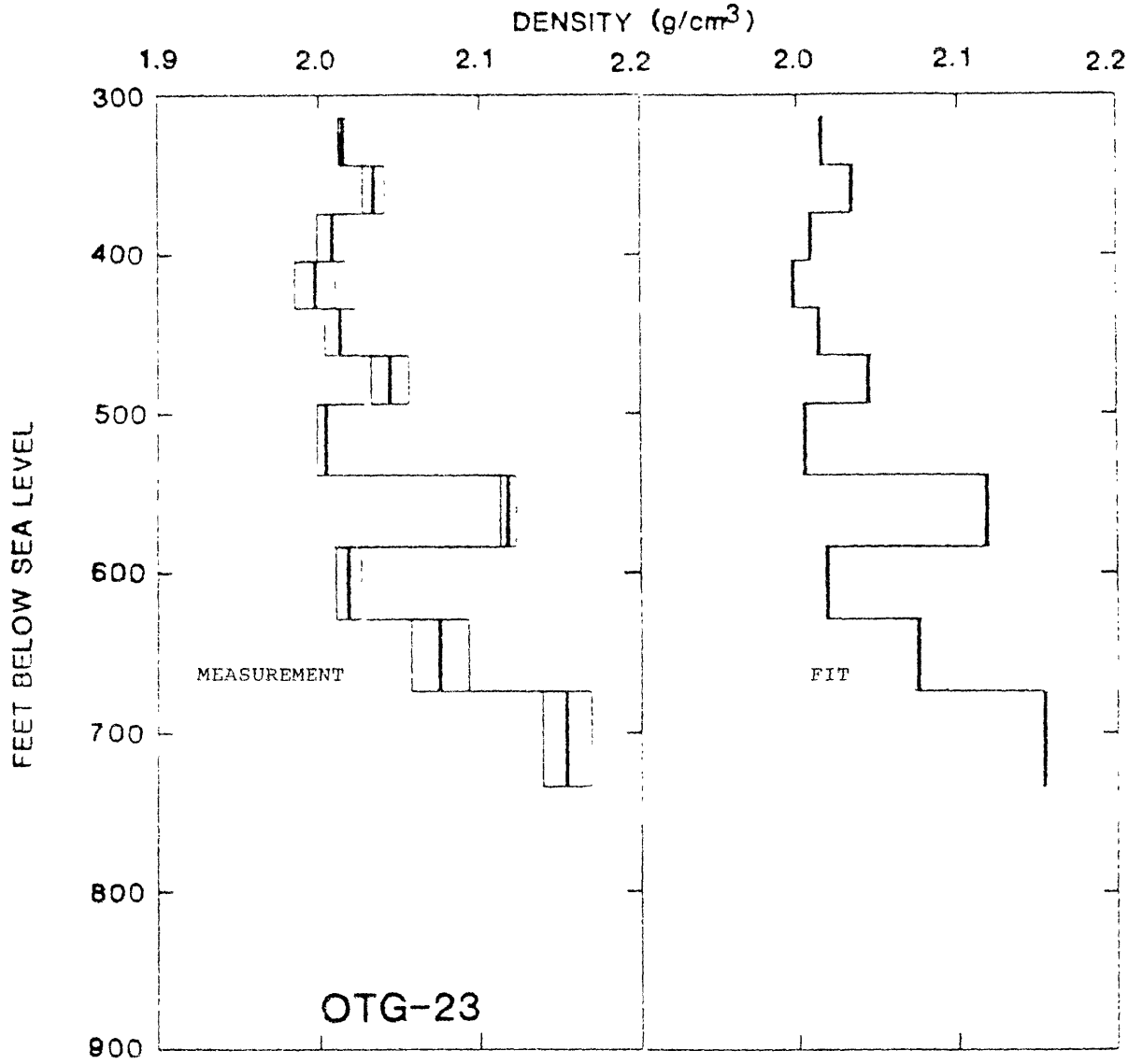

FIGURE 6-15. -- Left: profile of density vs. depth from BHG logging in crater hole OTG-23, as received. Right: plot of broken-straight-line fit [Eq. (11)] to profile at left. The left- and right-hand plot scales are identical.

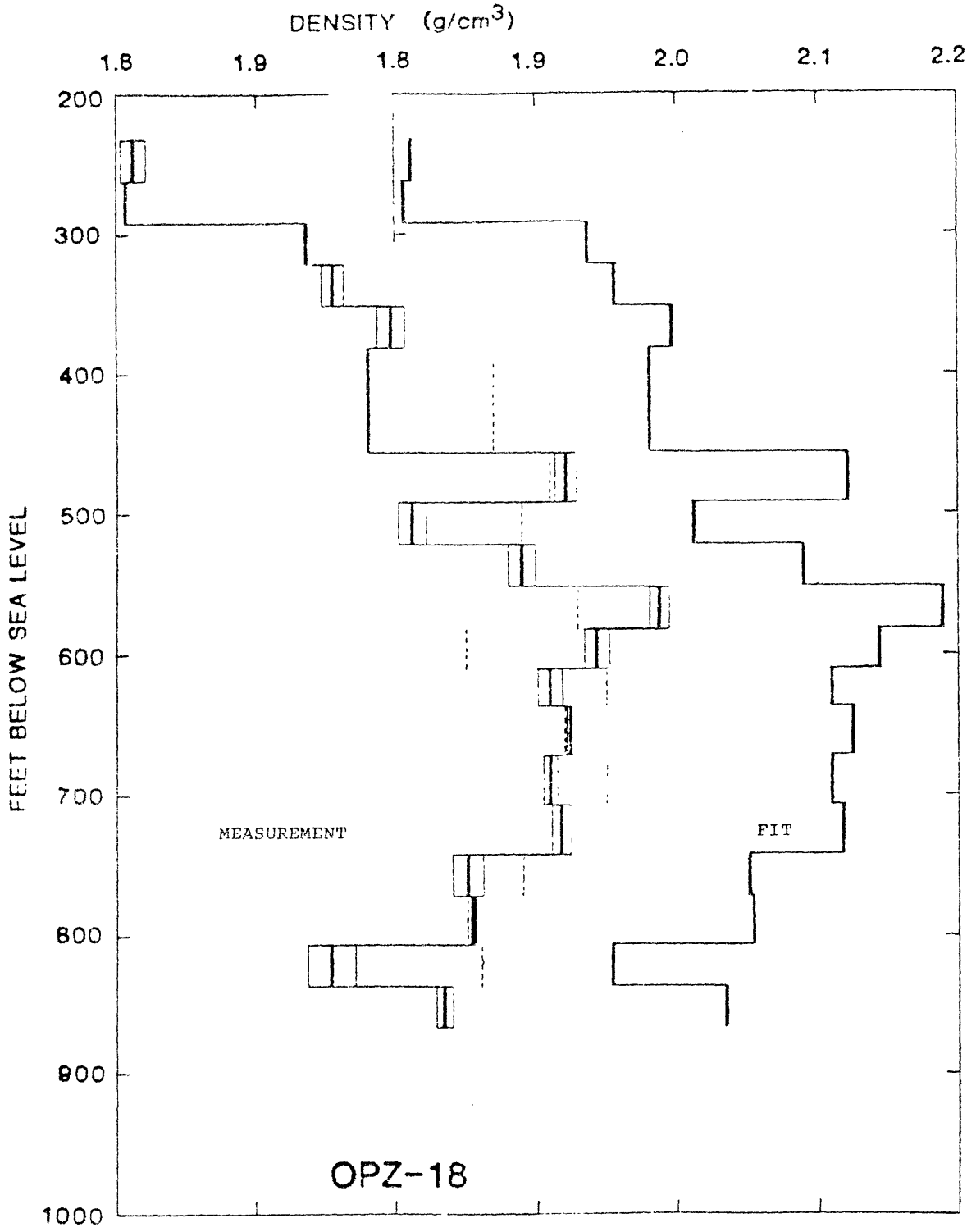

FIGURE 6-16. -- Left: profile of density vs. depth from BHG logging in crater hole OPZ-18, as received. Right: plot of broken-straight-line fit [Eq. (11)] to profile at left. The left- and right-hand plot scales are identical.

BOREHOLE OOR-17: GAMMA-GAMMA LOGGING

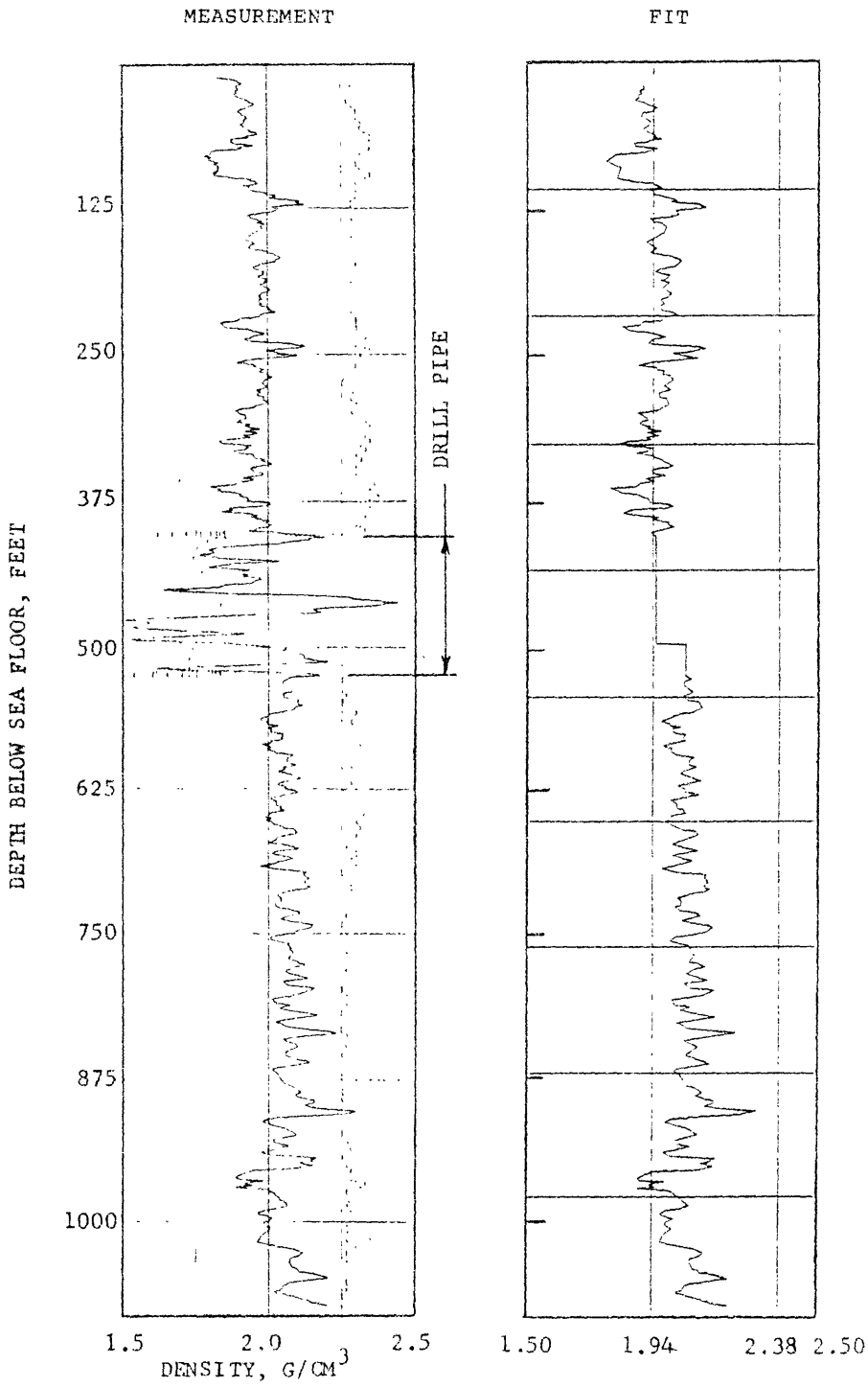

FIGURE 6-17. -- Left: profile of density vs. depth from γ-γ logging in control hole OOR-17, at .70 times the scale of the plot as received. Right: plot of broken-straight-line fit [Eq. (11)] to profile at left. The left- and right-hand plot scales are identical.

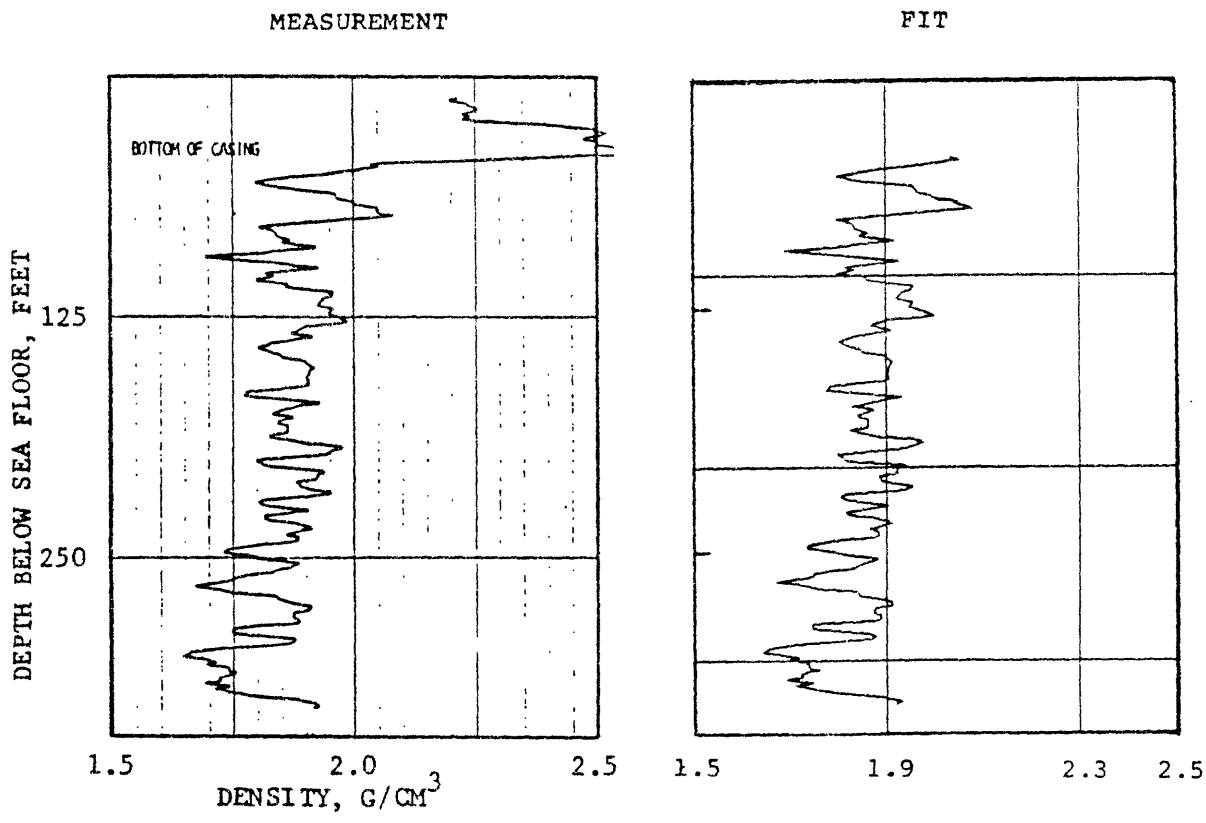

FIGURE 6-18. -- Left: profile of density vs. depth from γ-γ logging in control hole OSR-21, at 1.0 times the scale of the plot as received. Right: plot of broken-straight-line fit [Eq. (11)] to profile at left. The left- and right-hand plot scales are identical.

BOREHOLE ORT-20: GAMMA-GAMMA LOGGING

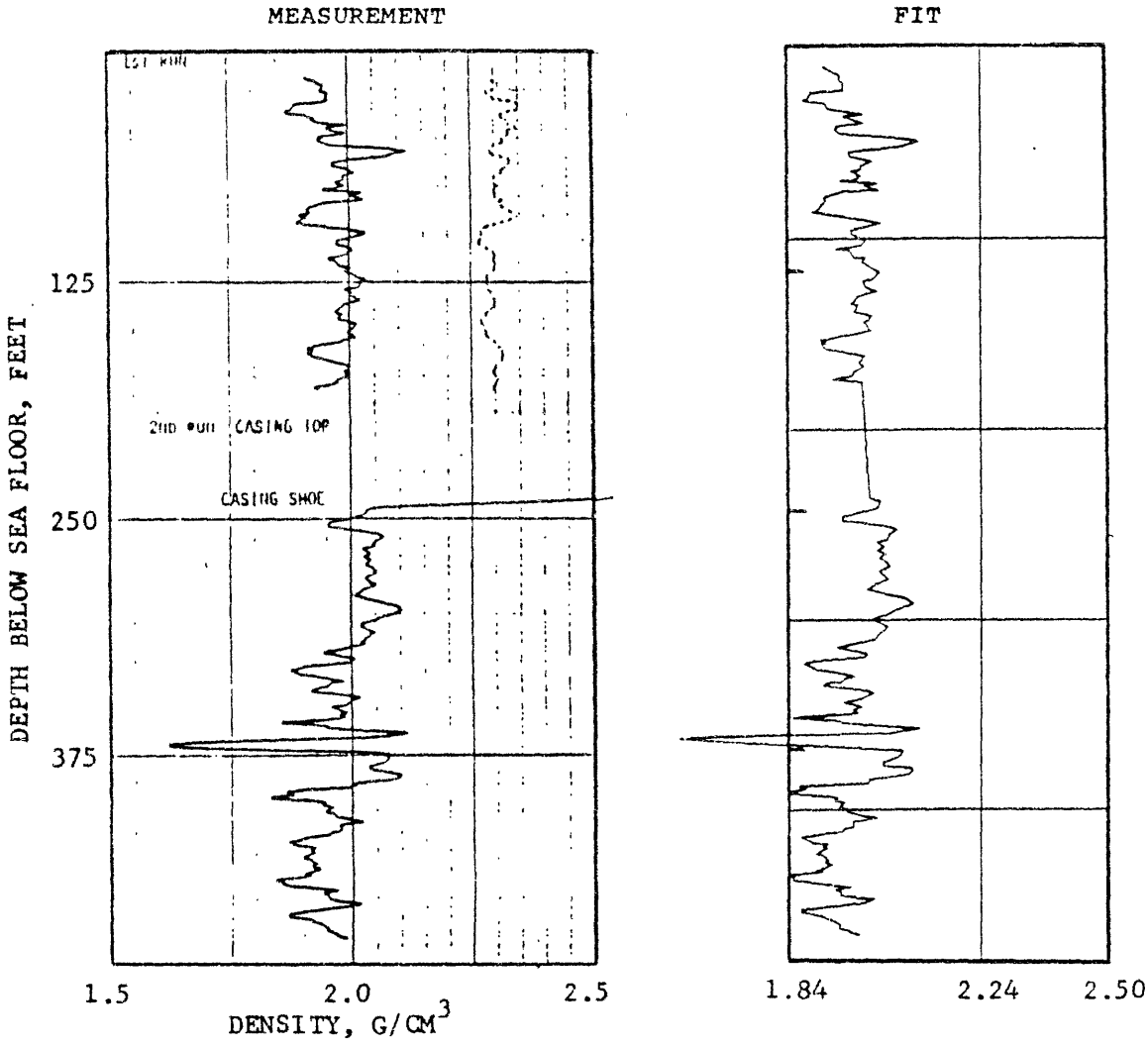

FIGURE 6-19. -- Left: profile of density vs. depth from γ-γ logging in crater hole ORT-20 at 1.0 times the scale of the plot as received. Right: plot of broken-straight-line fit [Eq. (11)] to profile at left. The left- and right-hand plot scales are identical.

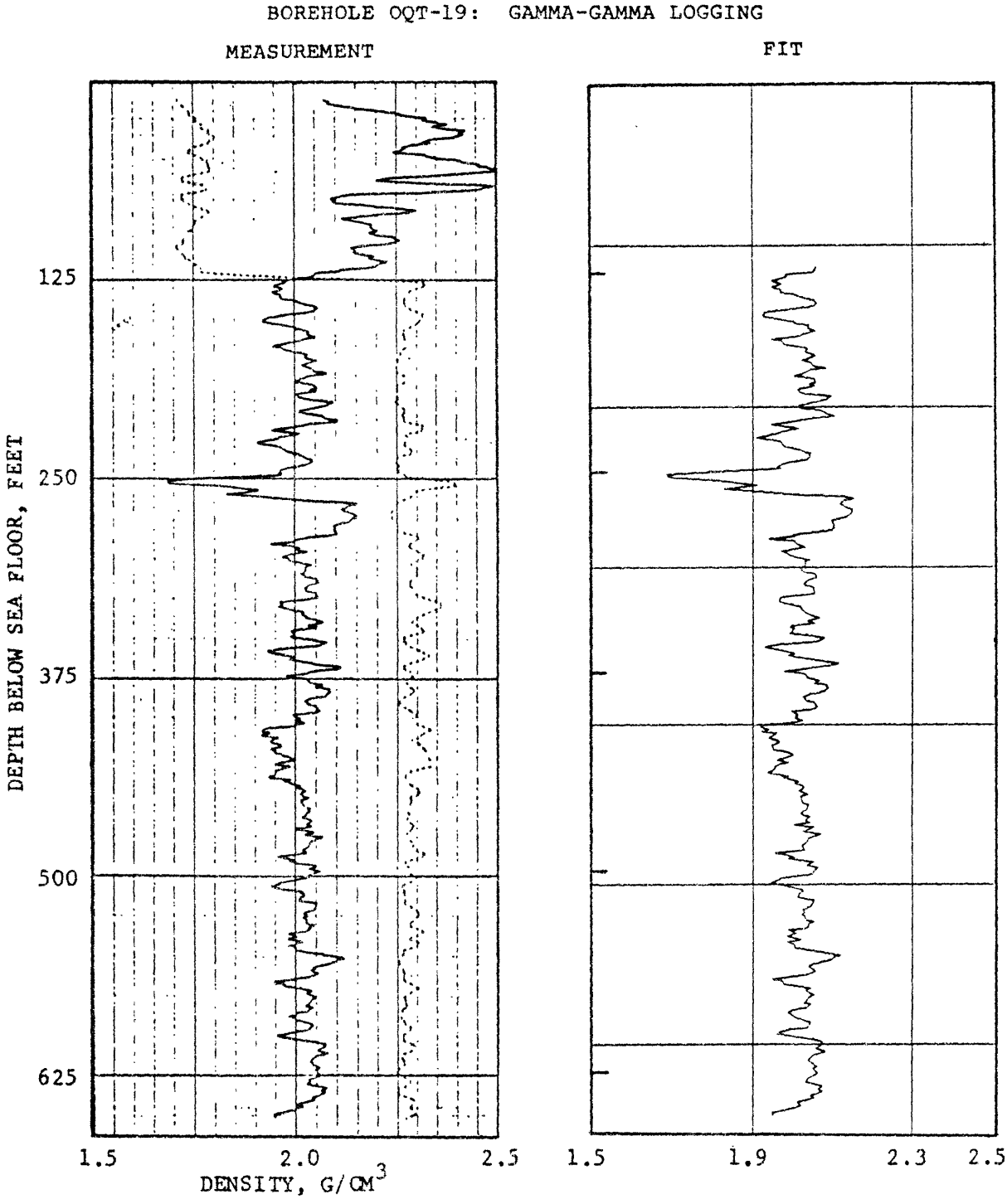

FIGURE 6-20. -- Left: profile of density vs. depth from γ-γ logging in crater hole OQT-19, at 1.0 times the scale of the plot as received. Right: plot of broken-straight-line fit [Eq. (11)] to profile at left. The left- and right-hand plot scales are identical.

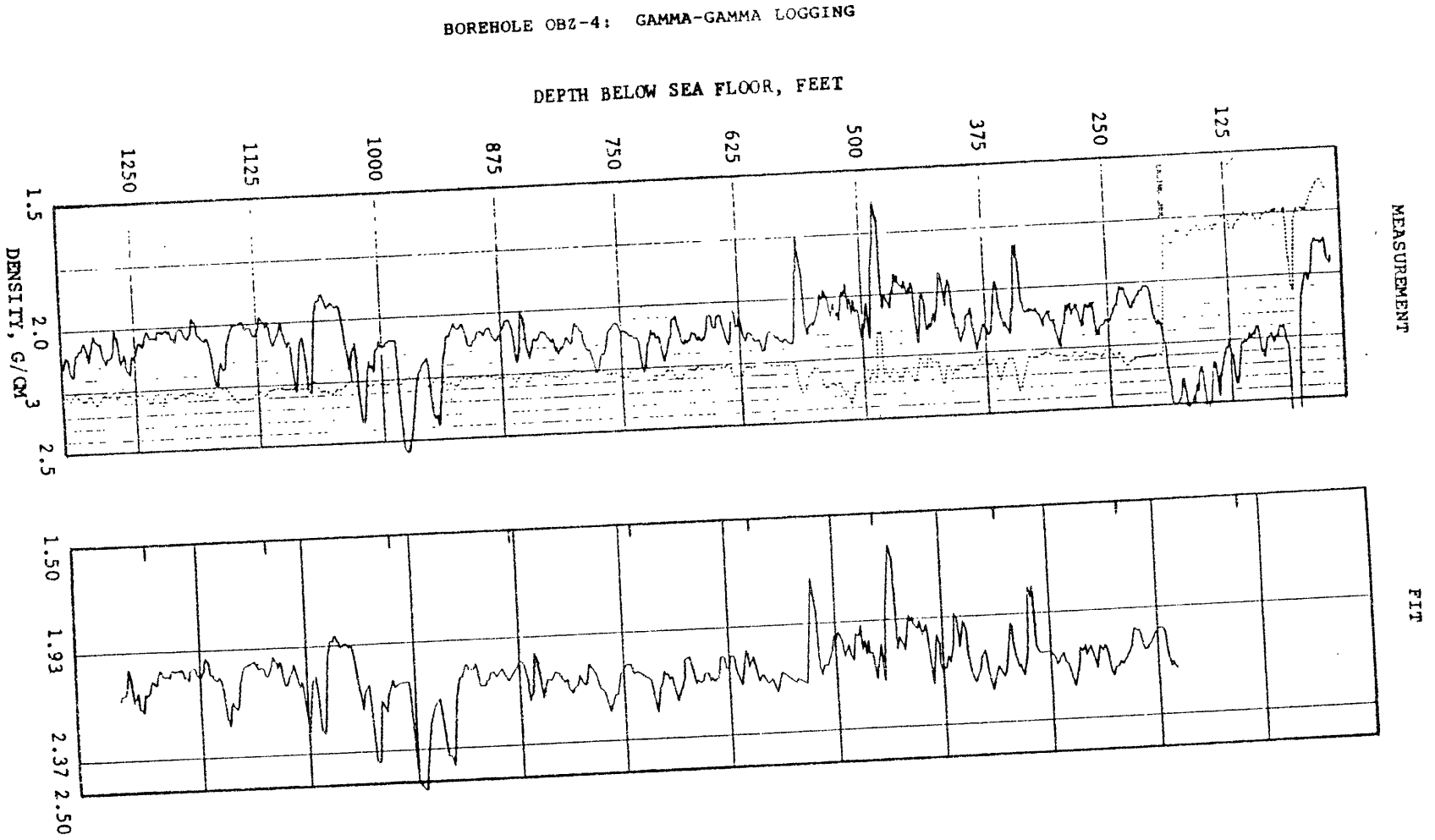

FIGURE 6-21. -- Left: profile of density vs. depth from γ-γ logging in crater hole OBZ-4, at .70 times the scale of the plot as received. Right: plot of broken-straight-line fit [Eq. (11)] to profile at left. The left- and right-hand plot scales are identical.

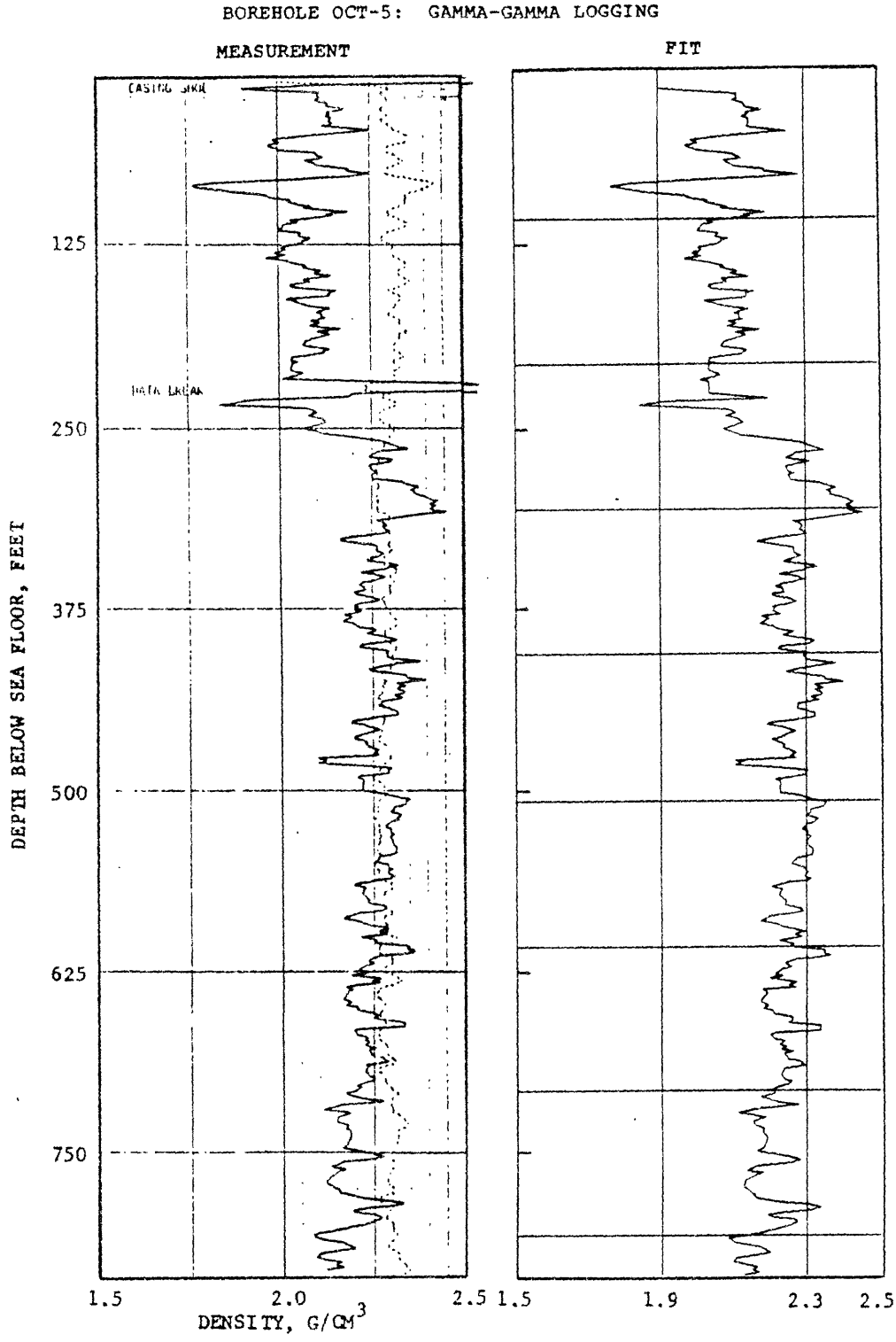

FIGURE 6-22. -- Left: profile of density vs. depth from γ-γ logging in crater hole OCT-5, at 1.0 times the scale of the plot as received. Right: plot of broken-straight-line fit [Eq. (11)] to profile at left. The left- and right-hand plot scales are identical.

BOREHOLE OAR-2A: GAMMA-GAMMA LOGGING

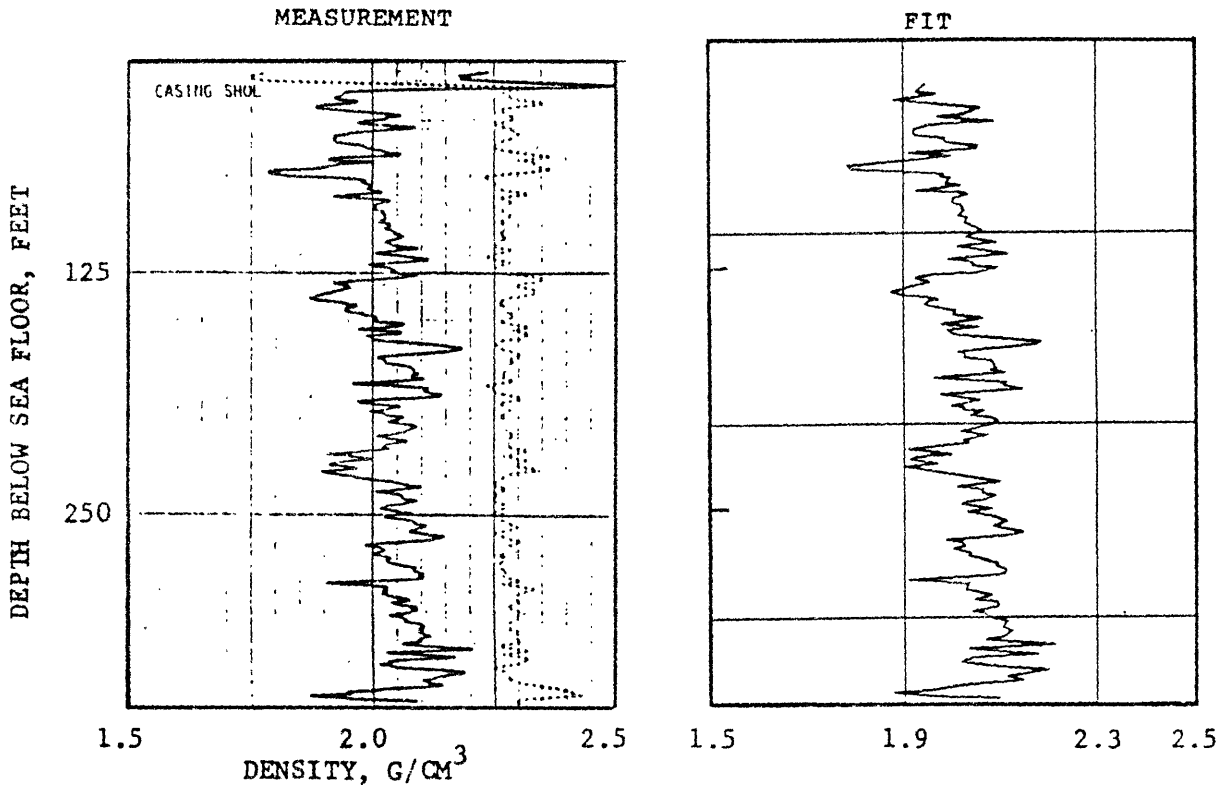

FIGURE 6-23. -- Left: profile of density vs. depth from γ-γ logging in control hole OAR-2A, at 1.0 times the scale of the plot as received. Right: plot of broken-straight-line fit [Eq. (11)] to profile at left. The left- and right-hand plot scales are identical.

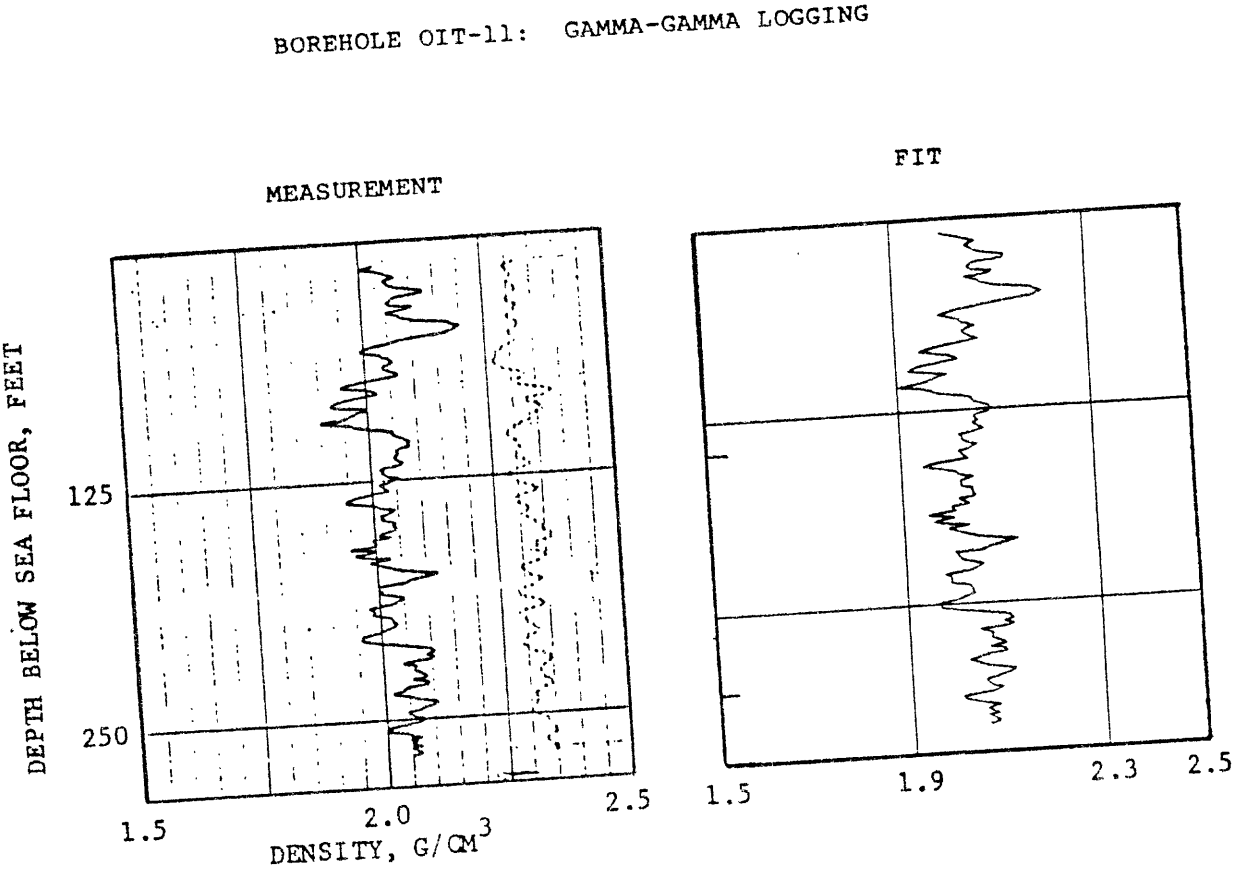

FIGURE 6-24. -- Left: profile of density vs. depth from γ-γ logging in crater hole OIT-11, at 1.0 times the scale of the plot as received. Right: plot of broken-straight-line fit [Eq. (11)] to profile at left. The left- and right-hand plot scales are identical.

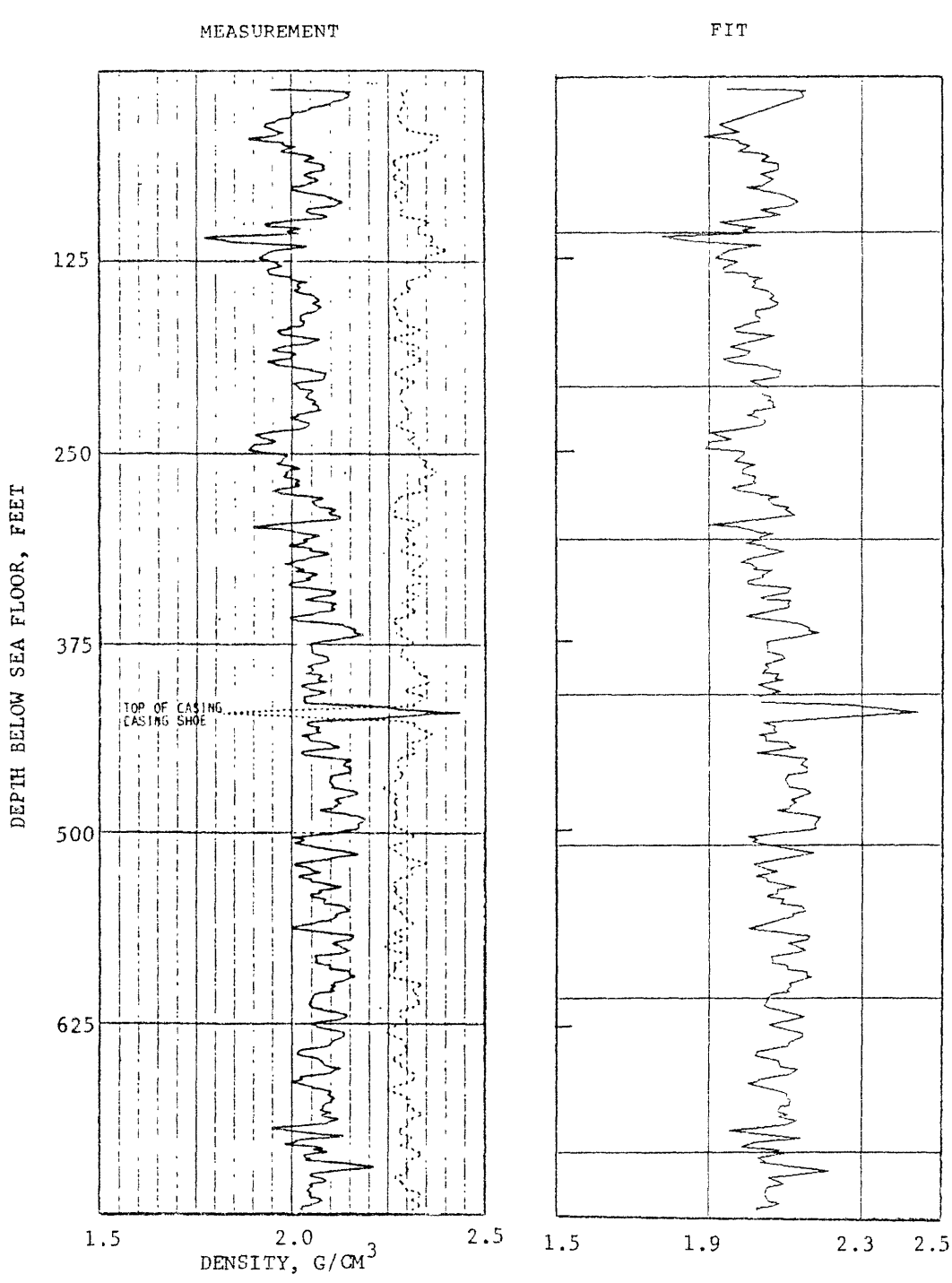

FIGURE 6-25. -- Left: profile of density vs. depth from γ-γ logging in crater hole OKT-13, at 1.0 times the scale of the plot as received. Right: plot of broken-straight-line fit [Eq. (11)] to profile at left. The left- and right-hand plot scales are identical.

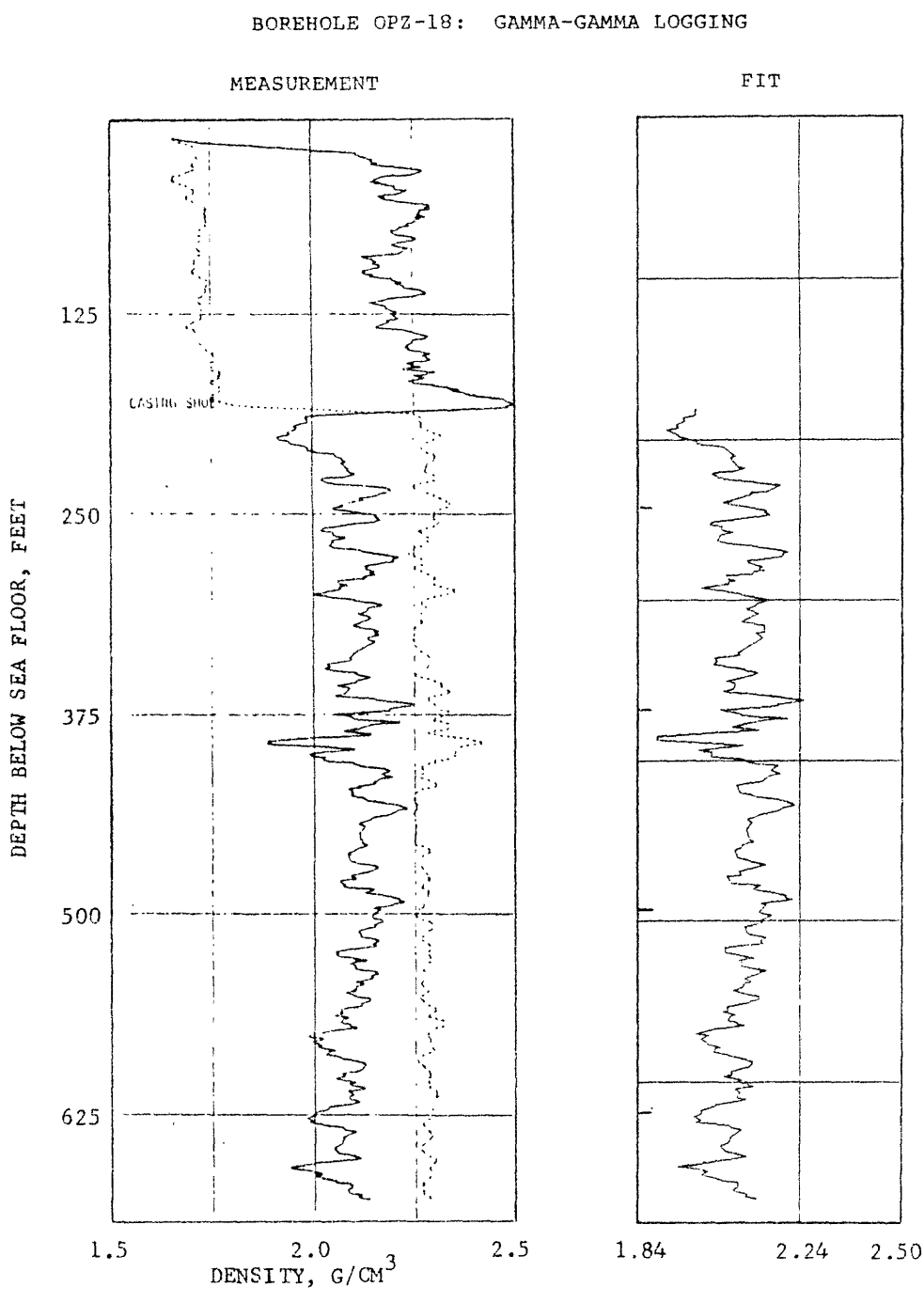

FIGURE 6-26. -- Left: profile of density vs. depth from Y-Y logging in crater hole OPZ-18, at 1.0 times the scale of the plot as received. Right: plot of broken-straight-line fit [Eq. (11)] to profile at left. The left- and right-hand plot scales are identical.

PEACE BOREHOLE UOR-17		
J	DEPTH (FT)	DENSITY (GM/CC)
1	212	1.947
2	237	1.947
2	237	1.943
3	271	1.943
3	271	1.882
4	289	1.882
4	289	2.036
5	317	2.036
5	317	1.901
6	345	1.901
6	345	1.872
7	363	1.872
7	363	1.951
8	388	1.951
8	388	1.944
9	417	1.944
9	417	1.967
10	446	1.967
10	446	1.976
11	477	1.976
11	477	1.987
12	505	1.977
12	505	2.027
13	528	2.027
13	528	1.974
14	560	1.974
14	560	1.976
15	603	1.976
15	603	1.993
16	645	1.993
16	645	2.036
17	683	2.036
17	683	2.018
18	713	2.018
18	713	2.013
19	747	2.013

PEACE BOREHOLE OPZ-18		
J	DEPTH (FT)	DENSITY (GM/CC)
1	252	1.812
2	252	1.812
2	282	1.807
3	292	1.807
3	292	1.937
4	322	1.937
4	342	1.956
5	352	1.956
5	352	1.937
6	382	1.937
6	382	1.962
7	407	1.962
7	407	2.130
8	442	2.130
8	442	2.003
9	522	2.003
9	522	2.086
10	552	2.086
10	552	2.191
11	582	2.191
11	582	2.139
12	610	2.139
12	610	2.107
13	637	2.107
13	637	2.122
14	672	2.122
14	672	2.107
15	707	2.107
15	707	2.115
16	742	2.115
16	742	2.048
17	772	2.048
17	772	2.052
18	807	2.052
18	807	1.951
19	837	1.951
19	837	2.031
20	867	2.031

PEACE BOREHOLE OUT-19		
J	DEPTH (FT)	DENSITY (GM/CC)
1	138	1.807
2	143	1.807
2	143	1.939
3	178	1.939
3	178	1.942
4	208	1.942
4	208	1.890
5	238	1.890
5	238	1.906
6	273	1.906
6	273	1.900
7	298	1.900
7	298	1.948
8	328	1.948
8	328	1.972
9	358	1.972
9	358	1.922
10	390	1.922
10	390	2.008
11	403	2.008
11	403	2.011
12	433	2.011
12	433	2.046
13	468	2.046
13	468	2.056
14	498	2.056
14	498	1.994
15	528	1.994
15	528	1.948
16	558	1.948
16	558	1.951
17	588	1.951
17	588	2.040
18	618	2.040
18	618	2.030
19	648	2.030
19	648	2.013
20	678	2.013
20	678	2.018
21	708	2.018
21	708	2.011
22	738	2.011
22	738	2.041
23	768	2.041
23	768	1.956
24	798	1.956

PEACE BOREHOLE UNT-20		
J	DEPTH (FT)	DENSITY (GM/CC)
1	136	1.845
2	160	1.848
2	160	2.010
3	186	2.010
3	186	1.826
4	211	1.826
4	211	1.971
5	226	1.971
5	226	1.926
6	256	1.926
6	256	1.907
7	271	1.907
7	271	1.942
8	301	1.942
8	301	1.922
9	331	1.922
9	331	1.948
10	361	1.948
10	361	1.989
11	391	1.989
11	391	2.003
12	421	2.003
12	421	2.014
13	451	2.014
13	451	2.048
14	471	2.048
14	471	2.009
15	491	2.009
15	491	1.949
16	521	1.949
16	521	1.929
17	551	1.929

PEACE BOREHOLE OSH-21		
J	DEPTH (FT)	DENSITY (GM/CC)
1	134	1.989
2	159	1.989
2	159	1.920
3	184	1.920
3	184	1.845
4	209	1.845
4	209	1.937
5	234	1.937
5	234	1.913
6	264	1.913
6	264	1.945
7	294	1.945
7	294	1.888
8	324	1.888
8	324	1.890
9	354	1.890
9	354	1.889
10	384	1.889
10	384	1.922
11	404	1.922
11	404	1.986
12	424	1.986

PEACE BOREHOLE OTG-23		
J	DEPTH (FT)	DENSITY (GM/CC)
1	314	2.018
2	344	2.018
2	344	2.037
3	374	2.037
3	374	2.011
4	404	2.011
4	404	2.000
5	434	2.000
5	434	2.017
6	464	2.017
6	464	2.049
7	494	2.049
7	494	2.003
8	524	2.003
8	524	2.117
9	554	2.117
9	554	2.026
10	629	2.026
10	629	2.072
11	674	2.072
11	674	2.156
12	734	2.156

TABLE 6-7. -- Endpoints of segments of piecewise linear fits [Eq. (11)] to density profiles from borehole gravity surveys.

PEACE BOREHOLE OOR-17

J	DIGITIZED DEPTH, X (DIV)	DIGITIZED DENSITY, Y (DIV)	COMPUTED DEPTH (FT)	COMPUTED DENSITY (GM/CC)
1	5.00	23.30	72.79	1.903
2	5.40	23.50	74.44	1.907
3	5.70	22.50	75.73	1.889
4	6.30	23.00	78.31	1.898
5	6.70	22.40	80.03	1.888
6	7.30	22.50	82.61	1.889
7	7.60	21.60	83.90	1.874
8	9.20	26.00	90.78	1.950
9	10.00	24.80	94.22	1.929
10	10.20	23.20	95.08	1.901
11	10.60	22.80	97.65	1.894
12	12.00	24.90	102.81	1.931
13	12.60	24.20	106.25	1.919
14	13.40	23.40	108.83	1.905
15	14.00	24.20	111.41	1.919
16	14.70	25.60	114.42	1.946
17	15.00	25.20	115.71	1.936
18	15.40	27.10	117.43	1.969
19	15.60	24.70	118.29	1.927
20	16.00	24.40	120.01	1.922
21	16.20	21.50	120.87	1.872
22	16.90	21.70	123.88	1.875
23	17.30	26.00	125.60	1.950
24	18.20	23.30	129.47	1.903
25	18.50	17.80	130.76	1.808
26	19.70	16.00	135.92	1.777
27	21.20	18.80	142.37	1.825
28	23.20	18.20	150.97	1.815
29	24.00	22.20	154.40	1.884
30	24.10	25.00	154.83	1.933
31	25.00	27.10	158.70	1.969
32	25.40	24.00	160.42	1.915
33	25.60	25.20	161.28	1.936
34	26.30	25.30	164.29	1.938
35	27.50	30.30	169.45	2.024
36	27.90	29.00	171.17	2.002
37	28.30	34.80	172.89	2.102
38	29.10	36.10	176.33	2.125
39	29.60	30.00	178.46	2.019
40	30.40	30.70	181.92	2.031
41	30.80	29.50	183.64	2.010
42	31.30	24.70	185.79	1.927
43	31.80	25.30	187.94	1.938
44	32.10	27.20	189.23	1.971
45	33.00	28.20	193.10	1.988
46	34.20	27.50	198.26	1.976
47	36.00	24.00	206.00	1.915
48	37.20	26.10	211.15	1.952
49	38.00	24.80	214.59	1.929
50	39.00	29.80	218.89	2.016
51	39.80	31.20	222.33	2.040
52	40.80	30.00	226.63	2.019
53	41.30	27.20	228.78	1.971
54	41.90	25.80	231.36	1.946
55	42.70	28.80	234.80	1.998
56	43.50	28.00	238.24	1.984
57	43.60	26.80	238.67	1.964
58	44.20	28.80	241.25	1.998
59	44.70	28.00	243.40	1.984
60	45.20	27.30	245.55	1.972
61	46.30	29.20	250.28	2.005
62	47.00	28.50	253.29	1.993
63	47.10	27.60	253.72	1.978
64	47.50	26.90	255.44	1.965
65	48.20	27.70	258.45	1.979
66	48.70	27.00	260.60	1.967
67	49.70	27.20	264.89	1.971
68	50.80	29.20	266.18	2.005
69	50.60	30.40	268.76	2.026
70	51.00	28.00	270.49	1.984
71	51.80	27.00	272.92	1.967
72	52.00	23.50	274.78	1.907
73	52.70	22.30	277.79	1.884
74	53.00	19.20	279.08	1.832
75	53.90	20.80	282.95	1.860
76	54.10	24.20	283.81	1.919
77	55.00	28.00	287.68	1.984
78	55.50	25.30	289.83	1.938
79	56.20	24.20	292.84	1.919
80	56.50	26.00	294.13	1.950
81	56.90	34.00	295.85	2.088
82	57.30	36.00	297.57	2.123
83	58.00	32.40	300.58	2.061
84	58.20	29.30	301.44	2.007
85	59.20	34.30	305.74	2.093
86	60.00	25.00	309.18	1.933
87	60.60	22.40	311.76	1.888
88	61.00	26.00	313.48	1.950
89	61.50	26.40	315.63	1.957
90	61.60	27.70	316.06	1.979
91	62.30	27.30	319.07	1.972
92	62.50	28.00	319.92	1.998
93	63.40	29.50	323.79	2.010
94	64.60	27.50	328.95	1.976
95	65.30	29.00	331.96	2.002
96	66.00	26.50	334.97	1.958
97	66.90	26.80	338.84	1.964
98	67.00	28.10	339.27	1.986
99	68.30	28.60	344.86	1.995
100	69.50	26.00	350.02	1.950

PEACE BOREHOLE OOR-17

J	DIGITIZED DEPTH, X (DIV)	DIGITIZED DENSITY, Y (DIV)	COMPUTED DEPTH (FT)	COMPUTED DENSITY (GM/CC)
101	70.00	22.00	352.17	1.881
102	70.90	24.10	356.04	1.917
103	71.40	24.30	358.19	1.920
104	71.50	23.20	358.62	1.901
105	72.20	22.50	361.63	1.889
106	72.60	24.90	363.35	1.931
107	73.00	24.00	365.07	1.915
108	73.50	27.00	367.22	1.967
109	73.80	24.00	368.51	1.915
110	74.40	26.50	371.09	1.958
111	74.70	23.80	372.38	1.912
112	75.20	25.00	374.53	1.933
113	75.50	20.30	375.81	1.851
114	76.00	18.70	377.96	1.824
115	76.50	20.00	380.11	1.846
116	76.70	25.10	380.97	1.934
117	77.50	24.20	384.41	1.919
118	78.00	21.80	386.56	1.877
119	78.50	25.30	388.71	1.938
120	80.40	29.50	396.88	2.010
121	80.80	26.30	398.60	1.990
122	81.00	26.00	399.46	1.950
123	81.40	25.00	401.18	1.933
124	82.10	25.80	404.19	1.946
125	82.40	28.00	405.48	1.984
126	83.00	25.70	408.06	1.910
127	83.70	25.80	411.07	1.946
128	84.00	23.00	412.36	1.898
129	84.70	22.00	415.37	1.881
130	85.00	16.80	416.66	1.791
131	86.00	19.00	420.96	1.829
132	86.20	22.00	421.82	1.881
133	87.30	24.50	426.55	1.924
134	87.90	24.70	429.13	1.927
135	88.10	28.30	429.99	1.990
136	88.60	29.50	432.13	2.010
137	89.20	27.80	433.85	1.991
138	89.30	21.20	435.14	1.867
139	90.00	19.30	438.15	1.834
140	90.80	26.50	441.59	1.958
141	91.20	25.20	443.31	1.936
142	92.00	28.70	446.75	1.997
143	92.30	28.40	448.04	1.991
144	92.80	29.60	450.19	2.012
145	93.60	26.30	453.63	1.955
146	94.00	25.00	455.35	1.933
147	94.70	26.00	458.36	1.950
148	116.40	26.00	551.65	1.950
149	116.50	32.00	552.08	2.054
150	123.00	32.00	580.03	2.054
151	123.50	33.00	582.18	2.071
152	124.00	31.80	584.33	2.050
153	124.70	31.70	587.34	2.048
154	126.00	33.40	592.93	2.078
155	126.70	31.60	595.94	2.047
156	127.50	32.00	599.37	2.054
157	128.00	34.80	601.52	2.102
158	129.00	35.50	605.82	2.111
159	130.00	33.40	610.12	2.078
160	130.30	32.00	611.41	2.036
161	131.80	27.00	617.86	1.967
162	132.50	28.80	620.01	1.998
163	132.80	28.90	622.16	2.000
164	133.00	32.00	623.02	2.036
165	133.40	29.30	624.74	2.007
166	134.10	29.30	627.75	2.007
167	134.60	32.00	629.90	2.054
168	135.00	31.60	631.62	2.047
169	135.50	32.60	633.77	2.047
170	135.70	32.00	634.63	2.054
171	136.40	29.00	637.64	2.002
172	137.00	27.40	640.22	1.974
173	137.50	29.30	642.37	2.007
174	138.00	29.00	644.52	2.002
175	138.70	30.00	647.53	2.019
176	139.30	33.70	650.11	2.083
177	140.00	32.80	653.11	2.067
178	140.80	32.80	656.55	2.067
179	141.20	34.30	658.27	2.093
180	141.80	32.00	660.85	2.054
181	142.60	31.00	664.29	2.036
182	144.00	35.00	670.31	2.106
183	145.20	30.50	675.47	2.028
184	145.80	32.20	678.05	2.057
185	146.50	31.80	680.20	2.050
186	147.00	34.70	683.21	2.100
187	148.20	29.00	688.37	2.002
188	148.90	30.30	691.38	2.024
189	149.80	30.30	695.25	2.024
190	150.00	31.50	696.11	2.045
191	150.80	32.00	699.55	2.054
192	151.30	29.30	701.70	2.007
193	152.70	28.20	707.72	1.988
194	154.20	31.80	714.16	2.050
196	154.50	34.00	714.59	2.088
196	155.10	34.50	718.03	2.097
197	157.00	29.30	726.20	2.007
198	158.30	34.60	731.79	2.099
199	159.20	29.30	735.66	2.007
200	160.40	33.50	740.82	2.080

TABLE 6-8. -- Endpoints of segments of piecewise linear fits [Eq. (11)] to density profiles from gamma-gamma logging. Table continues on succeeding pages. Data given for boreholes OOR-17, OSR-21, ORT-20, OQT-19, OBZ-4, OCT-5, OAR-2A, OIT-11, OKT-13, and OPZ-18 in OAK crater and KAR-1 in KOA crater.

TABLE 6-8 (Continued)

PEACE BOREHOLE OOR-17

J	DIGITIZED DEPTH, X (DIV)	DIGITIZED DENSITY, Y (DIV)	COMPUTED DEPTH (FT)	COMPUTED DENSITY (GM/CC)
201	162.00	47.30	747.70	1.972
202	162.80	46.40	751.34	2.026
203	163.20	46.20	752.86	2.126
204	164.00	45.60	756.30	2.114
205	164.80	46.70	759.74	2.135
206	165.30	46.00	761.89	2.123
207	166.00	46.00	765.09	2.123
208	166.30	47.00	766.19	2.140
209	166.70	45.70	767.90	2.118
210	167.00	45.80	769.19	2.085
211	168.00	50.40	773.49	2.026
212	168.50	51.30	775.64	2.042
213	169.40	51.30	779.51	2.042
214	169.80	50.00	781.23	2.019
215	170.50	51.00	784.67	2.036
216	171.00	54.00	786.39	2.088
217	171.50	55.00	788.54	2.106
218	172.60	51.10	793.27	2.038
219	173.60	46.70	797.57	2.135
220	174.00	47.40	799.29	2.147
221	174.70	46.30	802.30	2.128
222	175.30	54.00	804.88	2.088
223	175.80	50.20	807.03	2.022
224	176.60	49.00	810.47	2.002
225	177.50	52.70	814.34	2.066
226	179.40	53.80	822.50	2.085
227	180.80	52.80	828.52	2.067
228	181.00	54.30	829.38	2.093
229	181.80	56.00	832.82	2.123
230	182.30	55.80	834.97	2.085
231	183.10	52.20	838.41	2.057
232	184.50	56.40	844.43	2.130
233	185.00	51.70	846.58	2.048
234	186.00	53.00	850.86	2.071
235	186.40	57.80	852.60	2.154
236	187.50	55.50	857.33	2.114
237	188.50	53.50	861.63	2.010
238	189.50	50.00	865.93	2.019
239	189.80	53.00	867.22	2.071
240	190.50	51.60	870.23	2.036
241	191.90	58.00	876.24	2.157
242	193.00	50.30	880.97	2.024
243	194.20	52.80	886.13	2.067
244	195.10	52.00	890.00	2.227
245	196.60	51.70	896.45	2.048
246	198.00	54.60	902.47	2.095
247	199.20	52.30	907.63	2.059
248	199.70	52.30	909.78	2.059
249	201.30	57.00	916.66	2.140
250	202.30	50.30	920.96	2.024
251	202.60	49.80	923.11	2.014
252	203.50	50.80	926.12	2.033
253	205.00	51.70	932.56	2.048
254	205.80	52.30	936.00	2.059
255	206.30	54.20	938.15	2.092
256	207.30	55.40	942.45	2.112
257	207.80	54.10	944.60	2.090
258	208.40	55.70	947.18	2.118
259	208.60	57.40	948.04	2.147
260	209.20	57.90	950.62	2.156
261	209.70	57.00	952.77	2.140
262	209.90	56.00	953.63	2.123
263	210.30	58.00	955.35	2.157
264	211.00	46.20	958.36	2.299
265	211.70	42.50	961.37	2.233
266	212.50	49.50	964.81	2.010
267	213.20	47.80	967.82	1.961
268	214.50	52.40	973.41	2.061
269	215.80	54.40	979.00	2.095
270	217.00	50.00	984.16	2.019
271	217.70	50.10	987.16	2.021
272	218.20	53.60	989.31	2.071
273	219.00	50.00	992.75	2.019
274	219.50	47.50	994.90	1.976
275	220.20	48.80	997.91	1.998
276	220.70	58.00	1000.06	2.157
277	221.40	57.00	1003.07	2.140
278	221.80	55.00	1004.79	2.106
279	222.20	57.50	1006.51	2.149
280	223.00	54.50	1009.95	2.097
281	223.40	45.50	1011.67	1.941
282	224.60	42.30	1016.83	1.886
283	225.30	45.00	1019.84	1.898
284	225.40	48.00	1020.27	1.984
285	226.00	44.70	1022.85	1.927
286	226.60	46.00	1025.43	1.950
287	226.80	42.40	1026.29	1.888
288	227.30	49.00	1028.44	2.002
289	230.40	52.90	1041.76	2.069
290	231.00	50.80	1044.34	2.033
291	231.30	48.60	1045.63	1.995
292	232.00	47.00	1048.64	1.967
293	232.50	48.00	1050.78	1.984
294	233.00	49.70	1052.94	2.014
295	233.70	48.20	1055.95	1.988
296	234.30	48.10	1058.53	1.986
297	235.00	49.50	1061.54	2.010
298	236.20	47.80	1066.70	1.967
299	237.60	47.00	1073.58	1.967
300	239.20	54.00	1079.60	2.088

PEACE BOREHOLE OOR-17

J	DIGITIZED DEPTH, X (DIV)	DIGITIZED DENSITY, Y (DIV)	COMPUTED DEPTH (FT)	COMPUTED DENSITY (GM/CC)
301	240.00	55.70	1083.04	2.118
302	240.70	54.90	1086.05	2.104
303	241.10	53.30	1087.77	2.076
304	242.50	52.00	1091.64	2.071
305	242.20	53.30	1092.50	2.076
306	243.10	53.50	1096.37	2.080
307	243.50	54.90	1098.08	2.104
308	243.80	55.00	1099.37	2.106
309	243.90	56.10	1099.80	2.125
310	244.20	58.10	1101.09	2.159
311	244.60	58.90	1102.81	2.173
312	244.80	60.20	1103.67	2.196
313	245.10	60.60	1104.96	2.202
314	245.50	57.70	1106.68	2.152
315	245.70	56.30	1107.54	2.128
316	246.20	52.70	1109.69	2.066
317	246.50	52.40	1110.98	2.061
318	246.60	52.00	1111.41	2.054
319	246.90	51.90	1112.70	2.052
320	247.10	51.60	1113.56	2.047
321	247.50	51.50	1115.28	2.045
322	247.80	50.30	1116.57	2.024
323	248.00	50.20	1117.43	2.022
324	248.40	52.00	1119.15	2.054
325	249.00	53.90	1121.73	2.087
326	249.10	54.20	1122.16	2.092
327	249.40	55.40	1123.45	2.112
328	249.70	55.60	1124.74	2.116
329	249.90	57.10	1125.60	2.142
330	250.20	57.30	1126.89	2.145
331	250.70	60.70	1129.04	2.204

Y0, B, S:	.00	1.50	57.80	
X0, A, B, C:	30.00	180.20	500.00	116.30

TABLE 6-8 (Continued)

PEACE BOREHOLE DSR-21

J	DIGITIZED DEPTH, X (DIV)	DIGITIZED DENSITY, Y (DIV)	COMPUTED DEPTH (FT)	COMPUTED DENSITY (GM/CC)
1	10.00	54.00	130.68	2.033
2	10.30	55.00	131.85	2.049
3	11.00	49.50	134.59	1.955
4	11.60	43.70	136.94	1.871
5	12.30	39.00	139.69	1.798
6	12.90	41.60	142.03	1.839
7	13.60	49.00	144.78	1.955
8	14.30	49.60	148.30	1.964
9	14.80	51.40	149.47	1.992
10	15.20	51.80	151.04	1.998
11	15.60	54.90	152.61	2.047
12	15.80	54.60	153.39	2.042
13	16.70	56.80	156.92	2.077
14	17.20	50.00	158.87	1.970
15	18.00	39.00	162.01	1.799
16	18.50	41.00	163.96	1.829
17	19.30	21.50	167.10	1.637
18	19.60	43.00	169.06	1.861
19	20.20	42.00	170.62	1.845
20	20.60	26.50	172.97	1.715
21	21.30	41.20	174.93	1.832
22	21.60	40.00	176.10	1.813
23	22.10	42.20	178.04	1.841
24	23.00	42.00	181.59	1.845
25	23.50	47.00	183.55	1.923
26	24.20	40.20	186.29	1.817
27	24.60	41.20	187.85	1.832
28	25.20	39.00	190.20	1.798
29	25.50	42.70	191.38	1.856
30	26.10	42.90	193.73	1.859
31	26.80	49.00	196.47	1.955
32	27.30	48.80	198.43	1.951
33	27.80	47.70	199.60	1.934
34	28.40	46.60	202.73	1.920
35	29.00	49.00	205.06	1.955
36	29.60	48.50	207.43	1.947
37	30.60	50.00	209.00	1.970
38	30.70	51.60	211.74	1.998
39	31.00	50.00	212.92	1.970
40	31.30	45.50	214.09	1.900
41	32.00	43.50	216.83	1.868
42	32.70	46.80	219.57	1.908
43	33.50	20.80	222.71	1.626
44	34.10	19.30	225.06	1.603
45	34.90	20.80	228.19	1.626
46	35.00	22.00	223.58	1.845
47	35.40	22.40	230.15	1.851
48	35.90	25.30	232.11	1.897
49	36.70	26.50	235.02	1.912
50	37.10	26.00	236.80	1.908
51	38.20	25.70	241.11	1.903
52	39.20	25.80	245.03	1.904
53	39.60	20.80	247.39	1.826
54	40.00	18.00	248.16	1.782
55	40.60	17.80	250.51	1.779
56	41.00	22.00	252.08	1.845
57	41.50	47.30	254.04	1.926
58	42.00	24.70	255.99	1.887
59	42.80	21.30	259.13	1.829
60	43.10	23.00	260.30	1.861
61	43.30	23.80	261.08	1.873
62	44.00	21.70	263.83	1.840
63	44.20	21.80	264.61	1.842
64	44.50	23.00	265.78	1.861
65	45.60	23.00	270.09	1.861
66	46.00	20.70	271.66	1.824
67	46.70	24.00	274.40	1.876
68	46.90	24.80	275.18	1.889
69	47.00	29.00	275.57	1.955
70	47.50	30.20	277.53	1.973
71	48.00	29.00	279.49	1.955
72	48.40	28.00	281.06	1.939
73	49.00	20.40	283.41	1.820
74	49.20	19.00	284.19	1.798
75	50.00	20.30	287.32	1.816
76	50.40	27.00	288.89	1.923
77	50.60	28.00	289.67	1.939
78	50.90	26.90	290.85	1.922
79	51.60	26.90	293.59	1.922
80	51.90	24.50	294.76	1.884
81	52.40	24.40	297.50	1.889
82	53.20	28.80	299.85	1.951
83	53.70	28.00	301.81	1.939
84	54.20	20.20	303.77	1.817
85	54.60	19.40	305.34	1.804
86	55.00	20.00	306.90	1.813
87	55.70	25.70	309.64	1.903
88	56.60	20.00	313.17	1.813
89	57.00	20.40	314.74	1.820
90	57.30	23.50	315.91	1.868
91	57.80	25.50	317.87	1.900
92	58.10	26.00	319.04	1.908
93	58.80	23.20	321.78	1.864
94	59.10	24.30	322.96	1.881
95	59.60	24.50	324.92	1.884
96	60.00	23.50	326.48	1.868
97	60.20	19.50	327.27	1.806
98	60.70	16.00	329.22	1.751
99	60.90	15.00	330.01	1.735
100	61.20	15.00	331.18	1.735

PEACE BOREHOLE DSR-21

J	DIGITIZED DEPTH, X (DIV)	DIGITIZED DENSITY, Y (DIV)	COMPUTED DEPTH (FT)	COMPUTED DENSITY (GM/CC)
101	61.90	19.00	333.92	1.798
102	62.10	19.50	334.71	1.806
103	62.60	24.00	336.67	1.876
104	62.80	24.30	337.45	1.881
105	63.50	22.00	340.19	1.845
106	64.00	21.00	342.15	1.829
107	64.30	18.00	343.32	1.782
108	64.60	16.00	344.50	1.751
109	65.00	15.80	346.06	1.748
110	65.80	11.00	349.20	1.672
111	66.20	14.50	350.76	1.727
112	66.70	16.00	352.72	1.751
113	67.10	21.70	354.29	1.840
114	67.70	21.90	356.64	1.843
115	68.00	23.80	357.81	1.873
116	68.40	26.20	359.38	1.911
117	69.00	26.20	361.73	1.911
118	69.20	24.00	362.51	1.876
119	70.00	23.70	365.64	1.871
120	70.20	24.60	366.43	1.886
121	70.70	24.60	368.39	1.886
122	71.00	23.80	369.56	1.873
123	71.20	18.00	370.34	1.782
124	71.40	15.80	371.13	1.748
125	72.00	15.70	373.48	1.746
126	72.70	23.00	376.22	1.861
127	73.00	24.00	377.39	1.876
128	73.40	23.30	378.96	1.865
129	74.10	13.70	381.70	1.715
130	74.50	10.20	383.27	1.660
131	75.00	9.10	385.23	1.643
132	75.40	12.00	386.79	1.688
133	75.80	13.80	388.36	1.716
134	76.10	12.60	389.53	1.697
135	76.50	15.20	391.10	1.738
136	77.30	15.40	394.23	1.741
137	77.40	16.50	394.62	1.759
138	78.00	14.20	396.97	1.723
139	78.40	14.40	398.54	1.726
140	78.70	12.30	399.72	1.693
141	79.10	15.80	401.28	1.748
142	79.50	13.60	402.85	1.713
143	79.90	15.40	404.41	1.741
144	80.50	19.00	406.76	1.798
145	81.00	24.50	408.72	1.884
146	81.60	27.40	411.07	1.929
147	82.10	26.70	413.03	1.918

YOU Q, S:	.00	1.50	63.40	
YOU A, B, C:	30.00	209.00	1.00	.25535467

TABLE 6-8 (Continued)

PEACE BOREHOLE DR1-20

J	DIGITIZED DEPTH, X (DIV)	DIGITIZED DENSITY, Y (DIV)	COMPUTED DEPTH (FT)	COMPUTED DENSITY (GM/CC)
1	2.80	4.70	119.82	1.917
2	5.60	6.90	123.74	1.951
3	4.40	6.70	126.48	1.948
4	4.90	7.30	128.05	1.958
5	5.90	7.30	131.96	1.958
6	6.10	3.10	132.75	1.892
7	6.90	2.70	135.88	1.885
8	7.20	2.00	137.06	1.874
9	7.50	4.70	138.23	1.917
10	8.20	5.30	140.98	1.926
11	9.00	9.80	144.11	1.997
12	9.30	7.30	145.29	1.958
13	10.10	9.80	148.42	1.997
14	10.50	6.30	149.99	1.942
15	11.00	6.20	151.95	1.940
16	11.50	7.00	153.91	1.953
17	12.20	15.00	156.65	2.079
18	12.60	17.20	158.27	2.113
19	13.20	15.00	160.57	2.079
20	14.00	8.00	163.70	1.969
21	14.50	8.00	165.66	1.969
22	15.20	10.90	168.41	2.014
23	15.70	9.50	170.37	1.992
24	16.30	9.50	172.72	1.992
25	16.50	8.30	173.50	1.973
26	17.10	9.50	175.85	1.992
27	17.60	8.30	177.81	1.973
28	17.70	6.80	178.20	1.950
29	18.00	11.60	179.38	2.025
30	18.40	10.00	180.95	2.000
31	19.00	11.80	183.30	2.028
32	19.20	7.20	184.08	1.956
33	20.00	4.80	187.22	1.918
34	20.50	4.90	189.17	1.920
35	21.60	3.70	194.27	1.901
36	21.90	3.20	194.66	1.893
37	22.50	7.00	197.01	1.953
38	23.00	10.00	198.97	2.000
39	23.40	12.10	200.54	2.033
40	23.90	10.00	202.50	2.000
41	24.20	8.30	203.67	1.973
42	24.80	8.30	206.02	1.973
43	25.60	10.20	209.16	2.003
44	26.30	9.50	211.90	1.992
45	26.80	6.30	213.86	1.942
46	26.90	8.00	214.25	1.969
47	27.90	8.70	218.17	1.980
48	28.00	10.00	218.56	2.000
49	28.50	9.70	220.52	1.995
50	29.80	12.00	225.62	2.031
51	30.70	11.00	229.14	2.016
52	31.00	9.80	230.32	1.997
53	31.80	10.20	233.45	2.003
54	32.30	11.50	235.41	2.024
55	33.00	9.20	238.16	1.987
56	34.00	8.20	242.07	1.972
57	34.20	9.10	242.86	1.986
58	35.00	8.60	245.99	1.978
59	35.50	10.90	247.95	2.014
60	36.20	10.50	250.69	2.008
61	36.50	9.90	251.87	1.998
62	37.50	10.80	255.79	2.013
63	38.00	9.00	257.75	1.984
64	38.40	4.50	260.86	1.910
65	39.10	5.00	262.06	1.921
66	39.80	4.30	262.84	1.910
67	40.00	8.00	265.58	1.921
68	41.00	10.00	269.50	2.000
69	41.90	9.30	273.03	1.989
70	42.40	9.90	274.99	1.998
71	43.00	8.50	277.34	1.976
72	43.50	8.40	279.30	1.975
73	44.10	5.80	281.65	1.934
74	44.50	9.70	283.22	1.995
75	45.00	10.50	343.95	2.008
76	45.50	12.00	345.91	2.031
77	46.40	11.50	349.44	2.024
78	47.50	7.00	353.75	1.953
79	47.90	7.00	355.32	1.953
80	48.50	10.00	356.87	2.000
81	48.90	13.50	359.24	2.055
82	49.30	14.10	360.80	2.064
83	49.80	13.10	362.76	2.049
84	50.50	12.90	365.51	2.046
85	50.90	11.50	367.07	2.024
86	51.50	12.50	369.43	2.039
87	52.00	11.60	371.36	2.025
88	52.40	12.60	372.95	2.041
89	53.10	11.80	375.69	2.028
90	53.50	12.70	377.26	2.042
91	54.10	13.20	379.61	2.050
92	54.70	11.80	381.96	2.028
93	55.20	15.00	385.88	2.047
94	55.60	11.70	387.84	2.027
95	56.10	10.30	391.37	2.005
96	56.50	15.00	396.07	2.079
97	56.80	15.80	397.25	2.091
98	57.10	16.30	399.21	2.099
99	57.60	15.60	402.73	2.087
100	57.90	13.00	404.69	2.047

PEACE BOREHOLE DR1-20

J	DIGITIZED DEPTH, X (DIV)	DIGITIZED DENSITY, Y (DIV)	COMPUTED DEPTH (FT)	COMPUTED DENSITY (GM/CC)
101	75.80	11.70	405.87	2.027
102	76.20	11.10	407.43	2.017
103	77.10	12.90	410.96	2.046
104	78.80	11.20	417.62	2.019
105	79.00	10.80	418.41	2.080
106	79.90	6.40	421.93	1.943
107	80.40	8.50	423.89	1.976
108	80.60	10.00	424.68	2.000
109	80.80	10.30	425.46	2.005
110	81.20	9.90	427.03	1.998
111	81.60	3.50	428.59	1.898
112	82.10	2.80	430.55	1.874
113	82.70	5.30	432.90	1.895
114	83.50	7.00	435.26	1.953
115	83.70	8.70	436.82	1.980
116	84.00	7.20	438.00	1.956
117	84.40	6.90	439.57	1.951
118	84.50	5.50	439.96	1.929
119	85.30	4.60	441.92	1.915
120	85.60	10.00	444.27	2.000
121	86.00	11.00	445.84	2.016
122	86.60	9.60	448.19	1.994
123	86.90	9.50	449.36	1.989
124	87.20	7.30	450.54	1.958
125	87.90	9.50	453.28	1.992
126	88.30	8.46	454.85	1.975
127	88.60	9.00	456.02	1.984
128	89.30	.60	458.77	1.852
129	89.80	6.70	460.73	1.948
130	90.10	7.00	461.90	1.953
131	90.60	17.10	464.64	2.112
132	91.40	15.00	467.00	2.047
133	91.70	-12.00	468.17	1.654
134	92.00	-14.20	469.35	1.619
135	93.00	2.00	473.27	1.874
136	93.70	14.80	476.01	2.075
137	94.30	14.70	478.36	2.074
138	94.80	13.80	480.32	2.060
139	95.20	12.50	481.89	2.036
140	95.70	12.40	483.85	2.038
141	96.00	16.00	485.02	2.094
142	96.40	16.30	486.59	2.099
143	96.90	15.80	488.55	2.091
144	97.50	10.50	490.90	2.008
145	98.00	10.40	492.86	2.006
146	98.40	1.40	494.43	1.865
147	98.80	2.20	495.99	1.877
148	99.30	-.80	497.95	1.830
149	100.00	6.40	500.69	1.943
150	100.30	6.00	501.87	1.937
151	100.70	7.30	503.44	1.958
152	101.30	6.50	505.79	1.945
153	101.50	7.50	506.57	1.961
154	102.00	7.70	508.53	1.964
155	102.70	11.40	511.27	2.022
156	103.20	8.40	513.23	1.975
157	104.00	8.40	516.37	1.975
158	104.20	7.30	517.15	1.958
159	104.50	7.00	518.33	1.953
160	105.30	1.60	521.46	1.868
161	106.00	3.30	524.21	1.895
162	106.20	5.10	524.99	1.923
163	106.50	4.50	526.16	1.914
164	106.80	5.00	527.34	1.921
165	107.50	3.50	530.08	1.898
166	107.70	4.50	530.87	1.914
167	108.30	5.20	533.22	1.925
168	108.60	4.70	534.39	1.917
169	109.00	5.60	535.96	1.931
170	109.50	4.50	537.92	1.914
171	109.70	3.60	538.70	1.899
172	109.90	4.40	539.49	1.912
173	110.40	-.30	541.45	1.838
174	110.50	.70	541.84	1.854
175	111.00	.70	543.80	1.854
176	112.00	8.00	547.72	1.969
177	112.30	6.00	548.89	1.937
178	114.50	6.70	549.68	1.948
179	113.00	6.70	551.64	1.948
180	113.40	9.00	553.20	1.984
181	113.60	11.00	553.99	2.016
182	114.10	10.00	555.95	2.000
183	114.90	1.70	559.08	1.869
184	115.20	1.50	560.26	1.866
185	115.80	4.60	562.61	1.915
186	116.10	4.80	563.78	1.918
187	116.40	6.00	564.96	1.937
188	117.00	6.70	567.31	1.948
189	117.30	6.50	568.48	1.945
190	117.70	7.90	570.05	1.967
191	118.00	8.00	571.23	1.969
192	118.30	9.10	572.40	1.986

YO: A: S:	10.00	2.00	63.60	
XO: A: B: C:	30.00	226.40	250.00	63.80

TABLE 6-8 (Continued)

PEACE BOREHOLE DDT-19

J	DIGITIZED DEPTH, X (DIV)	DIGITIZED DENSITY, Y (DIV)	COMPUTED DEPTH (FT)	COMPUTED DENSITY (GM/CC)
1	29.00	55.40	238.57	2.057
2	29.70	55.00	241.32	2.050
3	30.00	56.70	242.50	1.983
4	30.50	30.60	244.47	1.981
5	31.00	28.50	246.43	1.948
6	31.50	30.00	248.40	1.972
7	32.00	28.50	250.34	1.946
8	32.40	29.80	251.93	1.969
9	32.90	29.90	253.90	1.970
10	33.20	32.00	255.08	2.003
11	33.70	33.20	257.04	2.022
12	34.10	35.20	258.61	2.053
13	34.50	35.60	260.19	2.060
14	35.00	35.10	262.15	2.052
15	35.50	30.60	264.12	1.981
16	36.00	27.30	266.08	1.929
17	36.40	27.00	268.44	1.925
18	37.40	41.80	271.59	2.000
19	37.60	32.50	273.16	2.011
20	38.00	34.30	274.94	2.039
21	38.50	34.10	275.91	2.036
22	39.00	35.30	277.87	2.055
23	39.40	33.60	279.45	2.028
24	39.70	32.90	280.63	2.017
25	40.30	28.50	282.98	1.948
26	40.40	30.00	283.38	1.972
27	41.00	30.30	285.74	1.976
28	41.70	34.00	288.49	2.035
29	42.10	33.60	290.06	2.028
30	42.80	35.20	292.81	2.055
31	43.40	33.30	295.17	2.024
32	43.80	34.50	296.74	2.042
33	44.40	35.00	299.10	2.050
34	44.80	37.00	300.67	2.082
35	45.20	34.70	301.46	2.046
36	45.70	33.00	304.21	2.019
37	46.00	32.00	305.39	2.003
38	46.40	35.00	306.96	2.050
39	47.00	35.40	309.32	2.057
40	47.80	34.40	310.50	2.041
41	47.50	33.20	311.28	2.055
42	48.00	32.50	313.25	2.011
43	48.50	32.90	315.21	2.017
44	48.80	34.10	316.39	2.036
45	49.20	37.90	317.96	2.096
46	49.70	37.10	319.93	2.083
47	50.50	32.80	323.07	2.016
48	51.00	33.00	325.04	2.019
49	51.30	35.40	326.22	2.057
50	51.80	36.90	328.18	2.080
51	52.30	35.40	330.15	2.104
52	52.70	34.20	331.72	2.030
53	53.20	31.40	333.69	1.994
54	53.60	28.50	335.26	1.948
55	54.20	32.60	337.62	2.013
56	54.70	30.00	339.58	1.972
57	55.00	29.30	340.76	1.961
58	55.70	26.00	343.51	1.909
59	56.30	29.70	345.87	1.967
60	57.00	30.30	348.62	1.976
61	57.50	32.50	350.59	2.011
62	58.80	34.70	355.71	2.046
63	59.00	34.00	356.48	2.035
64	59.70	30.50	359.23	1.980
65	60.30	29.40	361.59	1.962
66	60.60	29.90	362.77	1.970
67	61.50	12.00	366.31	1.689
68	62.00	12.20	368.27	1.692
69	62.50	20.00	370.24	1.814
70	63.20	26.00	372.99	1.909
71	63.90	31.00	375.74	1.990
72	64.40	27.90	377.71	1.939
73	64.90	33.50	379.67	2.027
74	65.00	35.80	380.07	2.126
75	65.40	41.40	381.64	2.151
76	65.70	40.00	382.82	2.129
77	66.30	39.30	385.18	2.118
78	66.70	40.00	386.75	2.129
79	67.20	41.30	388.71	2.149
80	67.50	41.20	389.89	2.148
81	68.30	40.30	393.04	2.134
82	68.80	38.50	395.00	2.097
83	69.00	38.40	399.72	2.104
84	70.30	38.00	400.90	2.097
85	70.70	34.00	402.47	2.035
86	71.00	32.00	403.65	2.003
87	71.30	32.00	404.83	2.003
88	71.60	28.10	406.79	1.942
89	72.00	32.00	407.58	2.003
90	72.30	32.40	409.54	2.009
91	73.00	33.70	411.51	2.030
92	73.70	30.00	414.26	1.972
93	74.00	31.00	415.44	1.987
94	74.30	31.20	416.62	1.991
95	75.00	34.40	419.37	2.041
96	75.20	33.60	420.16	2.028
97	76.00	33.60	423.30	2.028
98	76.60	33.00	425.66	2.019
99	77.00	33.40	427.23	2.025
100	77.20	35.20	428.02	2.053

PEACE BOREHOLE DDT-19

J	DIGITIZED DEPTH, X (DIV)	DIGITIZED DENSITY, Y (DIV)	COMPUTED DEPTH (FT)	COMPUTED DENSITY (GM/CC)
101	77.90	35.60	430.77	2.060
102	78.40	34.00	432.73	2.035
103	79.00	33.40	435.09	2.025
104	79.50	35.10	437.06	2.052
105	80.50	35.20	440.99	2.053
106	81.00	29.80	442.95	1.969
107	81.80	29.60	446.10	1.965
108	82.50	33.00	446.85	2.019
109	83.00	33.20	450.81	2.022
110	83.70	34.00	453.57	2.035
111	84.30	36.00	455.92	2.066
112	84.90	34.00	458.28	2.035
113	85.20	35.20	459.46	2.053
114	85.60	31.50	461.03	1.995
115	85.90	31.20	462.21	1.991
116	86.00	32.00	462.61	2.003
117	86.80	31.20	465.75	1.991
118	87.10	34.70	466.93	2.046
119	87.60	36.70	468.89	2.077
120	88.10	35.80	470.86	2.063
121	88.70	29.00	473.22	1.956
122	89.00	27.30	474.40	1.929
123	90.00	32.00	478.32	2.003
124	90.40	31.00	479.90	1.987
125	91.00	34.80	482.26	2.047
126	91.70	39.00	485.01	2.113
127	92.00	38.30	486.19	2.102
128	92.80	35.00	487.37	2.050
129	92.80	35.70	488.55	2.030
130	93.00	30.50	490.12	1.980
131	93.40	33.60	491.69	2.028
132	94.00	34.00	494.05	2.035
133	94.50	36.00	496.01	2.066
134	94.90	35.00	497.59	2.050
135	95.10	37.00	498.37	2.082
136	95.60	37.40	500.34	2.088
137	96.30	36.70	503.09	2.077
138	96.70	34.30	504.66	2.039
139	97.20	33.40	506.63	2.025
140	97.50	33.80	507.81	2.031
141	97.80	34.00	508.98	2.035
142	97.90	35.00	509.38	2.050
143	98.70	35.60	512.52	2.060
144	99.00	35.00	513.70	2.050
145	99.40	31.60	515.27	1.997
146	100.00	32.50	517.63	2.011
147	100.30	32.00	518.81	2.003
148	100.80	33.30	520.78	2.024
149	101.30	31.20	522.74	1.991
150	101.60	27.00	523.92	1.925
151	102.00	26.50	525.49	1.917
152	102.30	27.90	526.67	1.939
153	102.70	26.80	528.24	1.921
154	103.00	29.10	529.42	1.958
155	103.80	28.00	532.57	1.940
156	104.00	29.30	533.35	1.961
157	104.40	29.60	534.93	1.965
158	104.90	28.30	536.89	1.945
159	105.60	28.70	539.64	1.951
160	106.00	31.00	541.21	1.987
161	106.60	31.80	543.57	2.000
162	107.30	29.20	546.32	1.959
163	107.70	31.00	547.90	1.987
164	108.20	29.00	549.86	1.956
165	108.90	28.70	552.61	1.951
166	109.40	27.80	554.58	1.937
167	109.90	31.00	556.54	1.987
168	110.00	30.00	556.94	1.972
169	110.70	32.60	559.69	2.013
170	111.00	32.00	560.87	2.003
171	111.20	33.00	561.65	2.019
172	111.60	33.50	563.23	2.027
173	112.10	32.80	565.19	2.016
174	112.80	34.00	567.94	2.035
175	113.00	32.90	568.73	2.017
176	114.00	33.30	572.66	2.024
177	114.50	34.20	573.84	2.038
178	115.00	34.10	576.59	2.036
179	115.80	33.00	579.73	2.019
180	116.20	34.40	581.31	2.041
181	116.90	33.70	584.06	2.030
182	117.20	34.40	585.24	2.041
183	117.60	32.00	586.81	2.003
184	118.60	35.00	588.38	2.050
185	118.60	33.40	590.74	2.025
186	119.10	36.20	592.70	2.069
187	119.80	34.20	595.46	2.038
188	120.40	33.90	597.81	2.033
189	120.90	33.20	599.78	2.022
190	121.50	33.60	602.14	2.028
191	122.00	29.00	604.10	1.956
192	122.40	31.00	605.67	1.987
193	122.80	32.00	607.25	2.003
194	122.90	31.00	607.64	1.987
195	123.50	35.80	610.00	2.050
196	124.00	34.00	611.96	2.035
197	124.30	33.70	613.14	2.061
198	124.80	35.00	615.11	2.050
199	125.30	34.80	617.07	2.047
200	126.00	30.60	619.82	1.972

TABLE 6-8 (Continued)

PEACE BOREHOLE 001-19

J	DIGITIZED DEPTH, X (DIV)	DIGITIZED DENSITY, Y (DIV)	COMPUTED DEPTH (FT)	COMPUTED DENSITY (GM/CC)
201	126.50	28.30	622.97	1.945
202	127.70	33.00	626.51	2.019
203	128.00	33.40	627.68	2.025
204	128.50	32.70	629.65	2.014
205	129.00	32.50	631.62	2.011
206	129.50	35.00	633.58	2.050
207	130.40	34.70	637.12	2.046
208	131.00	33.30	639.48	2.024
209	131.40	33.50	641.05	2.027
210	131.80	33.10	642.62	2.020
211	132.00	33.60	643.41	2.028
212	132.70	33.80	646.16	2.031
213	133.00	35.00	647.34	2.050
214	133.20	34.30	648.12	2.039
215	133.60	34.20	650.48	2.038
216	134.10	33.40	651.66	2.025
217	134.30	31.00	652.45	1.987
218	134.80	32.20	654.41	2.006
219	135.20	30.90	655.98	1.986
220	135.70	33.00	657.95	2.019
221	136.20	30.90	659.91	1.986
222	136.50	32.00	661.09	2.003
223	137.00	32.00	663.06	2.003
224	137.80	36.30	666.20	2.071
225	138.30	39.30	668.17	2.118
226	138.50	38.30	668.95	2.102
227	138.90	38.00	670.53	2.097
228	139.70	35.00	673.67	2.050
229	140.10	34.30	675.24	2.039
230	140.80	35.30	677.99	2.055
231	141.30	34.00	679.96	2.035
232	142.10	28.60	683.10	1.950
233	142.40	30.00	684.28	1.972
234	142.90	30.40	686.25	1.978
235	143.20	33.00	687.43	2.019
236	143.50	34.50	688.61	2.042
237	143.90	33.80	690.18	2.031
238	144.60	35.00	692.93	2.050
239	145.00	34.30	694.50	2.039
240	145.90	33.50	698.04	2.027
241	146.10	34.60	698.83	2.044
242	146.70	33.90	701.18	2.033
243	147.00	32.00	702.36	2.003
244	147.50	31.00	704.33	1.987
245	148.20	32.20	707.08	2.006
246	148.80	34.50	710.22	2.042
247	149.70	34.00	712.98	2.035
248	150.00	31.80	714.15	1.992
249	150.70	29.20	716.91	1.959
250	151.70	35.00	720.84	2.050
251	152.00	36.50	722.02	2.074
252	152.60	36.20	724.37	2.069
253	153.00	35.40	725.94	2.057
254	153.60	36.90	728.30	2.080
255	154.00	35.00	729.88	2.050
256	155.00	34.20	733.81	2.038
257	155.90	35.60	737.34	2.060
258	156.20	34.90	738.52	2.049
259	157.00	35.70	741.67	2.061
260	157.70	34.30	744.42	2.039
261	158.40	33.80	747.17	2.031
262	159.00	36.40	749.53	2.072
263	159.50	35.80	751.49	2.063
264	159.90	36.50	753.07	2.074
265	160.50	34.50	755.42	2.042
266	160.90	35.10	757.00	2.052
267	161.50	32.50	759.36	2.011
268	162.00	33.00	761.32	2.019
269	162.40	32.00	762.89	2.003
270	163.20	28.40	766.04	1.947
271	163.60	28.60	767.61	1.950

Y0, A, S1	.00	1.50	63.60	
X0, A, G, C1	30.00	242.50	1.00	.25442833

PEACE BOREHOLE 002-04

J	DIGITIZED DEPTH, X (DIV)	DIGITIZED DENSITY, Y (DIV)	COMPUTED DEPTH (FT)	COMPUTED DENSITY (GM/CC)
1	46.50	40.00	393.66	2.184
2	47.20	38.50	397.52	2.155
3	47.50	39.60	398.81	2.177
4	48.40	37.00	402.67	2.132
5	49.00	41.00	405.25	2.080
6	49.50	38.30	407.39	2.018
7	50.60	38.40	412.11	2.020
8	51.00	41.40	413.83	2.037
9	51.50	41.30	415.97	2.035
10	51.70	32.40	416.83	2.054
11	55.20	35.20	423.27	2.102
12	54.00	35.20	426.70	2.102
13	55.10	30.50	431.43	2.021
14	55.50	30.90	433.14	2.028
15	56.20	30.10	436.15	2.015
16	57.00	34.50	439.58	2.090
17	59.00	38.50	448.16	2.158
18	59.70	37.70	451.17	2.144
19	60.20	39.00	453.31	2.167
20	61.00	39.00	456.75	2.167
21	61.50	41.10	458.89	2.203
22	62.00	40.00	461.04	2.184
23	62.70	45.00	464.04	2.098
24	63.30	33.70	466.62	2.076
25	63.70	35.00	468.34	2.098
26	64.50	33.80	471.77	2.078
27	65.30	39.00	475.20	2.167
28	66.70	33.70	481.21	2.076
29	67.70	36.00	485.50	2.115
30	68.00	35.50	486.79	2.073
31	68.60	35.00	489.37	2.098
32	69.20	34.00	491.94	2.081
33	69.50	38.00	493.23	2.150
34	70.60	43.00	497.95	2.235
35	72.00	37.90	503.96	2.146
36	72.70	37.30	506.96	2.138
37	73.30	35.00	509.54	2.098
38	74.70	37.60	515.55	2.146
39	75.20	36.00	517.69	2.115
40	76.20	34.70	521.98	2.093
41	78.70	34.80	532.71	2.095
42	79.50	33.00	536.15	2.064
43	80.00	19.00	538.29	1.825
44	80.40	21.60	540.01	1.869
45	81.00	19.00	542.58	1.825
46	81.50	34.60	544.73	2.091
47	82.40	40.00	548.59	2.184
48	83.30	37.30	552.46	2.138
49	83.70	38.10	554.17	2.151
50	84.30	35.50	556.75	2.107
51	85.00	32.00	559.75	2.047
52	85.10	28.50	560.18	1.987
53	85.50	27.50	561.90	1.970
54	86.70	39.00	567.05	2.167
55	87.30	40.00	569.62	2.184
56	88.50	37.50	574.77	2.141
57	90.00	43.00	581.21	2.235
58	91.00	37.70	585.50	2.140
59	91.50	33.50	587.65	2.073
60	92.50	35.30	591.94	2.103
61	92.80	28.30	593.23	2.155
62	94.00	41.00	598.38	2.201
63	95.00	38.00	602.67	2.150
64	95.60	34.70	605.25	2.093
65	96.00	28.20	606.96	1.982
66	96.60	26.50	609.54	1.953
67	97.50	32.50	613.40	2.056
68	98.00	26.00	615.55	1.944
69	98.70	24.70	618.55	1.922
70	99.00	32.00	619.84	2.047
71	99.60	36.20	623.27	2.119
72	100.30	34.50	625.42	2.090
73	101.00	37.40	628.42	2.139
74	101.20	38.00	631.85	2.150
75	102.20	36.50	633.57	2.124
76	102.30	31.80	634.00	2.044
77	103.00	29.50	637.00	2.004
78	104.00	31.00	641.30	2.201
79	105.40	26.90	647.31	1.960
80	106.30	29.40	651.17	2.003
81	107.00	26.00	654.17	1.944
82	107.40	28.00	655.89	1.979
83	108.60	26.30	661.04	1.950
84	108.70	25.00	661.47	1.927
85	109.20	26.00	663.61	1.944
86	109.60	29.50	665.33	1.919
87	110.50	32.60	669.19	2.057
88	111.80	29.50	674.77	2.004
89	112.40	32.50	677.35	2.056
90	113.00	11.30	679.92	1.693
91	113.80	7.60	683.36	1.630
92	115.00	23.40	688.51	1.900
93	115.60	29.60	691.08	2.177
94	116.30	31.00	694.09	2.030
95	117.50	29.30	699.24	2.172
96	118.20	32.80	702.24	2.061
97	119.00	33.40	705.67	2.071
98	119.30	30.00	706.96	2.013
99	119.60	33.40	709.11	2.071
100	120.20	30.00	710.82	2.013

TABLE 6-8 (Continued)

PEACE BOREHOLE 082-04

J	DIGITIZED DEPTH, X (DIV)	DIGITIZED DENSITY, Y (DIV)	COMPUTED DEPTH (FT)	COMPUTED DENSITY (GM/CC)
101	120.60	32.30	712.54	2.052
102	121.00	26.50	714.26	1.953
103	121.50	29.00	716.40	1.996
104	122.30	26.30	719.84	1.944
105	122.80	34.70	721.98	2.093
106	124.50	33.50	724.99	2.073
107	124.00	32.70	727.13	2.025
108	125.00	33.70	731.43	2.076
109	125.50	30.00	733.57	2.013
110	126.40	27.50	737.43	1.970
111	126.90	29.70	739.58	2.008
112	127.50	28.50	742.15	1.987
113	127.60	32.00	743.44	2.047
114	129.00	35.50	748.59	2.107
115	129.60	35.30	752.03	2.103
116	130.40	37.60	754.60	2.143
117	131.00	35.50	757.18	2.107
118	131.50	23.00	759.32	1.893
119	132.50	24.60	763.61	1.930
120	133.00	24.00	765.76	1.910
121	134.00	39.50	770.05	2.175
122	136.30	38.20	779.92	2.153
123	136.50	39.20	780.78	2.170
124	139.90	36.50	795.37	2.124
125	141.10	41.20	800.52	2.204
126	142.20	38.00	805.25	2.150
127	143.10	39.00	809.11	2.167
128	144.50	36.70	815.12	2.127
129	145.30	38.50	818.55	2.158
130	146.50	32.50	823.70	2.056
131	147.50	35.00	827.99	2.098
132	147.60	32.00	828.28	2.047
133	148.20	31.00	831.00	2.030
134	149.40	39.10	836.15	2.168
135	150.70	35.30	841.73	2.103
136	151.10	32.20	843.44	2.050
137	152.00	32.20	847.31	2.050
138	152.40	35.00	849.02	2.098
139	153.00	35.00	851.60	2.098
140	153.50	32.20	853.74	2.050
141	154.40	32.20	857.61	2.050
142	155.00	37.00	860.18	2.132
143	156.00	36.00	864.47	2.159
144	156.40	37.00	866.19	2.132
145	156.90	37.90	868.34	2.148
146	157.50	36.00	870.91	2.115
147	158.40	36.00	874.77	2.115
148	158.50	37.50	875.20	2.141
149	159.20	38.10	878.21	2.151
150	159.90	37.50	881.21	2.141
151	160.30	38.30	882.93	2.155
152	161.80	31.90	889.37	2.045
153	163.00	32.50	894.52	2.056
154	163.10	36.80	894.94	2.129
155	164.80	42.00	902.24	2.218
156	166.20	36.30	908.25	2.121
157	166.90	37.00	911.25	2.132
158	167.20	35.50	912.54	2.107
159	167.80	36.00	915.12	2.115
160	168.20	35.00	916.83	2.098
161	168.50	37.50	918.12	2.141
162	169.00	38.50	920.27	2.158
163	170.00	44.50	924.56	2.261
164	171.30	36.80	930.14	2.129
165	174.50	34.80	943.87	2.095
166	175.40	35.30	947.73	2.103
167	176.00	33.00	950.31	2.064
168	177.00	33.00	954.60	2.064
169	178.50	35.00	961.04	2.098
170	179.40	40.00	964.90	2.184
171	180.10	40.00	967.91	2.184
172	181.20	44.00	972.63	2.252
173	182.80	39.00	979.49	2.167
174	183.60	36.20	983.79	2.153
175	184.60	34.50	987.22	2.095
176	186.30	32.50	994.52	2.056
177	187.00	37.30	997.52	2.158
178	187.60	37.30	1000.09	2.158
179	188.60	35.00	1004.38	2.098
180	189.00	37.50	1006.10	2.141
181	190.00	38.00	1010.40	2.150
182	190.40	39.20	1012.11	2.170
183	191.20	38.00	1015.97	2.150
184	191.70	35.80	1017.69	2.112
185	192.30	36.60	1020.27	2.126
186	193.50	34.40	1025.42	2.088
187	194.60	34.00	1030.14	2.081
188	195.50	36.00	1034.00	2.115
189	196.50	35.50	1038.29	2.107
190	197.60	40.00	1043.01	2.184
191	198.70	31.40	1047.73	2.037
192	199.50	29.30	1051.17	2.001
193	200.00	38.50	1053.31	2.158
194	200.90	40.50	1057.18	4.192
195	201.50	35.40	1059.89	2.105
196	202.20	31.80	1062.76	2.044
197	203.00	31.00	1066.19	2.030
198	206.00	35.60	1079.06	2.109
199	207.60	32.70	1085.93	2.059
200	209.00	34.50	1091.94	2.090

PEACE BOREHOLE 082-04

J	DIGITIZED DEPTH, X (DIV)	DIGITIZED DENSITY, Y (DIV)	COMPUTED DEPTH (FT)	COMPUTED DENSITY (GM/CC)
201	209.70	33.30	1094.94	2.060
202	210.50	33.70	1098.38	2.076
203	210.80	35.20	1099.67	2.102
204	211.50	35.30	1102.67	2.103
205	211.60	36.50	1103.10	2.124
206	213.00	36.40	1109.11	2.122
207	213.30	33.80	1110.40	2.078
208	214.00	31.30	1113.40	2.035
209	214.60	32.50	1115.97	2.056
210	215.70	32.50	1120.70	2.056
211	216.50	31.20	1123.27	2.033
212	217.30	34.20	1127.56	2.085
213	218.00	34.30	1130.57	2.086
214	219.00	33.80	1134.86	2.180
215	220.00	35.00	1139.15	2.440
216	220.50	32.80	1141.30	2.403
217	221.40	32.50	1145.16	2.397
218	222.90	33.00	1151.60	2.167
219	224.00	40.70	1156.32	2.196
220	225.20	44.70	1161.47	2.264
221	227.00	41.30	1169.19	2.548
222	228.50	60.00	1175.63	2.526
223	230.00	34.70	1182.07	2.093
224	232.30	35.00	1191.94	2.098
225	233.50	36.00	1197.09	2.115
226	234.00	34.00	1199.24	2.081
227	234.40	36.00	1200.95	2.115
228	235.00	37.00	1203.53	2.132
229	235.40	41.50	1205.25	2.209
230	236.70	39.00	1210.82	2.167
231	237.50	33.50	1214.26	2.415
232	238.30	35.40	1217.69	2.413
233	239.50	35.00	1222.84	2.098
234	240.50	36.80	1227.13	2.129
235	241.00	40.80	1229.26	2.197
236	241.80	36.30	1232.71	2.115
237	242.00	35.10	1233.57	2.100
238	242.90	27.70	1237.43	1.974
239	243.40	25.80	1239.58	1.941
240	244.10	26.10	1242.58	1.946
241	244.80	25.00	1246.02	1.927
242	245.40	25.20	1248.16	1.931
243	245.70	25.80	1249.45	1.941
244	246.00	26.10	1250.74	1.946
245	246.20	25.80	1251.60	1.941
246	246.30	24.70	1252.03	1.922
247	246.70	24.40	1253.74	1.917
248	246.90	23.30	1254.60	1.898
249	247.20	23.00	1256.32	1.893
250	247.50	23.20	1257.18	1.897
251	247.70	24.40	1258.03	1.917
252	248.40	24.30	1261.04	1.915
253	248.70	26.30	1262.33	1.950
254	249.10	27.70	1264.04	1.974
255	250.10	45.20	1268.34	2.273
256	250.30	46.10	1269.19	2.288
257	250.50	45.50	1270.05	2.278
258	250.90	45.50	1271.77	2.278
259	251.50	36.90	1274.34	2.131
260	252.00	32.70	1276.49	2.059
261	252.20	33.20	1277.35	2.068
262	252.60	33.30	1279.06	2.069
263	252.80	35.10	1279.92	2.100
264	253.80	45.40	1284.22	2.276
265	254.70	36.90	1288.08	2.131
266	255.00	34.10	1289.37	2.083
267	255.30	33.70	1290.65	2.076
268	255.60	34.90	1291.94	2.097
269	256.20	33.20	1294.52	2.066
270	257.00	29.40	1297.95	2.003
271	257.40	30.90	1299.67	2.028
272	258.70	34.30	1305.25	2.086
273	259.10	34.50	1306.96	2.090
274	259.60	32.90	1309.11	2.062
275	260.10	29.10	1311.25	1.997
276	260.30	28.80	1312.11	1.992
277	260.50	29.10	1312.97	1.997
278	260.80	30.30	1314.26	2.018
279	261.00	29.10	1315.12	1.997
280	261.10	28.80	1315.55	1.992
281	261.30	29.00	1316.40	1.996
282	262.00	27.60	1319.41	1.972
283	262.30	29.50	1320.70	2.004
284	263.00	31.50	1323.70	2.038
285	263.40	32.10	1325.42	2.049
286	263.80	31.90	1327.13	2.045
287	264.10	30.40	1328.42	2.020
288	264.60	30.10	1330.57	2.015
289	265.30	30.20	1333.57	2.016
290	265.40	30.40	1334.00	2.020
291	266.00	29.20	1336.58	1.999
292	266.20	29.00	1337.43	1.996
293	266.40	28.40	1338.29	1.985
294	266.60	28.70	1339.15	1.991
295	266.90	28.70	1340.44	1.991
296	267.50	29.30	1343.01	2.001
297	267.90	28.90	1344.73	1.994
298	268.00	29.40	1345.16	2.003
299	268.40	29.40	1346.88	2.003
300	268.80	29.90	1348.59	2.011

TABLE 6-8 (Continued)

PEACE BOREHOLE 082-04

J	DIGITIZED DEPTH, X (DIV)	DIGITIZED DENSITY, Y (DIV)	COMPUTED DEPTH (FT)	COMPUTED DENSITY (GM/CC)
301	269,40	51,40	1351,37	2,037
302	269,50	52,50	1351,68	2,056
303	269,90	53,20	1353,31	2,068
304	270,40	48,70	1355,46	2,162
305	270,60	49,40	1356,32	2,174
306	270,80	49,40	1357,18	2,180
307	271,00	49,20	1358,03	2,170
308	271,50	48,70	1360,18	2,162
309	271,60	47,80	1360,61	2,146
310	271,80	48,60	1361,47	2,160
311	272,00	48,70	1362,33	2,162
312	272,20	48,60	1363,18	2,144
313	272,50	43,40	1364,47	2,242
314	273,20	41,50	1367,48	2,209
315	274,00	44,10	1370,91	2,083
316	274,50	42,60	1373,06	2,057
317	274,90	42,00	1374,77	2,047
318	275,30	42,60	1376,49	2,061
319	276,30	42,00	1380,78	2,047
320	276,40	41,40	1381,21	2,037
321	277,00	41,40	1383,79	2,037
322	277,20	29,20	1384,64	1,499
323	277,50	46,10	1385,93	1,980
324	277,70	46,10	1386,79	1,980
325	278,10	47,30	1388,51	1,967
326	278,30	47,90	1389,37	1,977
327	278,50	50,70	1390,22	2,025
328	279,00	51,10	1392,37	2,032
329	279,20	52,00	1393,23	2,047
330	279,70	51,60	1395,37	2,040
331	280,10	51,10	1397,09	2,032
332	280,60	29,60	1399,24	2,006
333	281,00	29,60	1400,95	2,006
334	281,80	30,30	1404,39	2,018
335	282,80	51,80	1409,39	2,044
336	282,10	52,50	1405,67	2,056
337	282,40	51,80	1406,96	2,044
338	283,00	51,90	1409,54	2,045
339	283,30	50,40	1410,82	2,020
340	283,60	49,70	1412,11	2,008
341	283,80	50,30	1412,97	2,018
342	284,20	29,80	1414,69	2,009
343	284,90	30,20	1417,69	2,016
344	285,10	50,40	1418,55	2,020
345	285,20	50,10	1418,98	2,015
346	285,50	50,40	1420,27	2,020
347	286,00	29,90	1422,41	2,011
348	286,30	50,10	1423,70	2,015
349	286,50	51,80	1424,56	2,044
350	286,90	51,40	1426,28	2,037
351	287,40	51,50	1428,42	2,038
352	288,20	51,40	1431,85	2,037
353	288,50	50,30	1433,14	2,018
354	288,80	29,90	1434,86	2,011
355	289,40	51,40	1437,00	2,037
356	289,70	53,30	1438,29	2,069
357	290,10	53,40	1440,01	2,071
358	290,50	52,60	1441,73	2,057
359	290,80	52,40	1443,01	2,054
360	291,30	54,10	1445,16	2,083
361	291,50	55,10	1446,02	2,100
362	292,20	56,00	1449,02	2,115
363	292,50	55,30	1450,51	2,102
364	292,70	56,00	1451,17	2,115
365	293,00	55,90	1452,46	2,180
366	293,40	56,90	1454,17	2,165
367	293,90	56,90	1456,32	2,165
368	294,10	56,40	1457,18	2,122
369	294,30	55,00	1458,03	2,098
370	294,60	56,30	1459,32	2,121
371	295,10	56,50	1461,47	2,124
372	295,20	57,20	1461,90	2,136
373	295,90	51,00	1464,90	2,030
374	296,50	49,70	1466,62	2,008
375	296,40	49,50	1467,05	2,004
376	296,80	53,80	1468,76	2,078
377	297,20	55,40	1470,48	2,105
378	297,60	55,70	1473,06	2,110
379	298,20	55,70	1474,77	2,110
380	298,50	56,90	1476,06	2,131
381	299,50	54,40	1480,35	2,086
382	299,80	52,30	1481,64	2,052
383	300,20	52,40	1483,36	2,054
384	301,10	51,50	1487,22	2,038
385	301,30	50,40	1488,08	2,020
386	302,50	56,30	1493,23	2,121
387	302,90	54,10	1494,94	2,083
388	303,70	52,00	1498,38	2,047
389	303,90	52,60	1499,24	2,057
390	304,10	53,90	1500,09	2,079
391	304,80	53,90	1503,10	2,079
392	305,20	54,80	1504,82	2,095
393	305,60	54,90	1506,53	2,097
394	306,00	56,30	1508,25	2,131
395	306,50	59,90	1509,54	2,182
396	306,40	59,70	1512,11	2,179
397	307,50	55,50	1514,69	2,107
398	308,00	55,10	1516,83	2,100
399	308,70	57,80	1519,84	2,146

Y0, B, S:		,00	1,50	58,50
X0, A, B, C:	30,00	323,70	570,00	116,50

PEACE BOREHOLE 081-05

J	DIGITIZED DEPTH, X (DIV)	DIGITIZED DENSITY, Y (DIV)	COMPUTED DEPTH (FT)	COMPUTED DENSITY (GM/CC)
1	3,00	45,60	182,40	1,902
2	4,00	39,00	186,34	2,112
3	5,00	39,10	190,27	2,114
4	5,20	48,30	191,06	2,101
5	5,70	40,30	193,03	2,133
6	6,30	40,45	195,39	2,134
7	6,80	45,30	197,36	2,180
8	7,30	40,60	199,33	2,137
9	7,50	42,80	200,12	2,144
10	8,00	40,00	202,09	2,128
11	8,20	41,00	202,87	2,144
12	8,70	41,10	204,84	2,145
13	9,80	40,90	209,17	2,142
14	10,50	47,50	211,93	2,246
15	11,20	48,50	214,68	2,104
16	12,00	31,30	217,83	1,991
17	12,50	52,20	219,80	2,005
18	13,00	50,20	221,77	1,974
19	13,70	52,30	224,53	2,007
20	14,40	58,40	227,29	2,103
21	15,10	59,70	230,04	2,123
22	15,50	58,80	231,61	2,076
23	16,00	57,70	233,58	2,092
24	16,50	56,70	235,55	2,108
25	17,00	55,80	237,52	2,188
26	17,40	44,00	239,09	2,191
27	18,00	49,70	241,46	2,280
28	18,30	45,40	242,64	2,213
29	18,60	48,00	243,82	2,112
30	18,80	53,00	244,61	2,018
31	19,30	20,00	246,57	1,827
32	19,60	17,30	248,54	1,772
33	20,60	43,00	252,48	1,861
34	21,50	30,00	255,24	1,971
35	22,00	51,00	257,20	1,987
36	22,50	54,00	258,59	2,034
37	22,60	53,50	259,57	2,026
38	23,50	57,60	263,11	2,090
39	23,60	56,30	263,50	2,070
40	24,40	44,00	266,65	2,191
41	24,60	46,30	268,23	2,133
42	25,00	41,50	269,01	2,151
43	25,80	54,00	272,16	2,034
44	26,20	55,10	273,74	2,051
45	26,50	53,00	274,92	2,018
46	27,60	52,30	279,25	2,007
47	28,00	46,00	280,83	2,065
48	28,40	55,30	283,19	2,054
49	29,00	57,50	284,76	2,089
50	29,50	56,20	286,73	2,068
51	29,90	56,00	288,31	2,065
52	30,30	53,30	289,88	2,022
53	30,50	52,50	290,67	2,010
54	31,00	53,00	292,64	2,018
55	31,50	51,40	294,61	1,993
56	32,00	53,00	296,57	2,018
57	32,50	50,00	298,54	1,971
58	33,00	53,60	300,51	2,027
59	33,80	56,70	303,66	2,076
60	34,00	56,10	304,45	2,067
61	34,70	59,20	307,20	2,115
62	35,00	58,00	308,39	2,097
63	35,70	61,00	311,14	2,144
64	36,00	56,50	312,32	2,070
65	36,40	57,40	314,68	2,087
66	37,00	54,60	316,26	2,043
67	37,50	54,00	317,44	2,034
68	37,70	54,80	319,01	2,046
69	38,20	61,90	320,98	2,158
70	38,40	60,70	321,77	2,139
71	39,10	60,70	324,53	2,139
72	39,70	53,40	326,89	2,024
73	40,30	55,00	329,25	2,049
74	40,80	56,80	331,22	2,078
75	41,30	60,90	333,19	2,142
76	42,00	58,50	335,94	2,104
77	42,20	59,40	336,73	2,119
78	42,90	59,40	339,49	2,119
79	43,00	60,00	339,88	2,128
80	43,40	57,30	341,46	2,089
81	43,80	59,00	343,03	2,112
82	44,50	57,40	345,80	2,087
83	44,90	62,80	347,36	2,172
84	45,30	58,60	348,94	2,106
85	45,40	60,70	350,90	2,139
86	47,00	56,70	355,63	2,076
87	47,70	56,20	358,39	2,068
88	48,40	60,70	361,14	2,139
89	49,10	59,80	363,90	2,125
90	49,80	54,20	366,65	2,037
91	50,50	54,10	369,41	2,035
92	50,60	55,20	369,80	2,053
93	50,90	54,10	370,98	2,035
94	52,00	54,00	375,31	2,034
95	52,70	56,00	378,07	2,065
96	56,60	52,70	381,61	2,013
97	54,00	54,00	383,19	2,034
98	56,80	54,00	391,06	2,034
99	56,90	54,20	394,61	2,194
100	57,40	26,00	396,57	1,906

TABLE 6-8 (Continued)

PEACE BOREHOLE OCT-05

J	DIGITIZED DEPTH, X (DIV)	DIGITIZED DENSITY, Y (DIV)	COMPUTED DEPTH (FT)	COMPUTED DENSITY (GM/CC)
101	58.00	22.00	398.94	1.845
102	58.50	37.30	402.09	2.086
103	59.50	38.60	404.84	2.106
104	60.00	37.00	406.81	2.081
105	60.50	39.00	408.78	2.112
106	61.10	40.00	411.14	2.128
107	62.20	36.60	415.47	2.075
108	65.20	39.40	419.41	2.119
109	64.70	30.00	425.31	2.285
110	66.00	28.00	430.43	2.348
111	66.40	29.30	432.01	2.274
112	67.30	27.40	435.55	2.264
113	68.00	31.50	438.31	2.308
114	68.80	27.40	441.46	2.244
115	69.60	27.70	445.39	2.249
116	70.00	28.80	446.18	2.266
117	70.40	27.80	447.76	2.250
118	71.20	28.20	450.90	2.257
119	71.60	28.30	452.27	2.337
120	72.60	26.10	456.42	2.381
121	73.00	24.50	457.93	2.336
122	73.30	25.30	459.17	2.368
123	73.80	25.10	461.14	2.365
124	74.30	27.40	463.11	2.401
125	75.00	29.30	465.87	2.431
126	75.70	28.00	468.62	2.411
127	76.00	29.00	469.80	2.426
128	76.50	28.20	471.77	2.414
129	77.00	26.90	473.74	2.456
130	77.50	26.50	475.71	2.387
131	78.20	31.00	478.46	2.301
132	78.40	28.70	479.25	2.265
133	78.60	29.50	480.04	2.277
134	79.30	30.30	482.79	2.290
135	79.90	29.80	485.16	2.282
136	80.50	31.00	487.52	2.301
137	80.80	30.00	488.70	2.285
138	81.40	28.70	491.06	2.202
139	81.90	27.30	493.03	2.164
140	83.00	28.70	497.36	2.265
141	84.00	28.80	501.30	2.266
142	84.40	30.00	502.87	2.285
143	84.90	29.20	504.84	2.272
144	85.20	28.00	506.02	2.254
145	85.60	27.00	507.60	2.238
146	86.10	31.60	509.57	2.313
147	86.50	27.80	511.14	2.329
148	86.70	31.00	511.93	2.301
149	87.00	29.80	513.11	2.297
150	87.80	26.20	516.26	2.225
151	88.20	29.50	517.83	2.277
152	88.60	30.40	519.41	2.291
153	89.20	28.30	521.77	2.258
154	89.40	26.70	522.56	2.233
155	89.90	25.60	524.53	2.216
156	90.20	26.80	525.71	2.235
157	90.80	27.00	528.07	2.238
158	91.00	25.00	528.86	2.206
159	91.40	25.10	530.43	2.208
160	92.00	28.00	532.79	2.254
161	92.50	29.20	534.76	2.272
162	92.80	28.00	535.94	2.254
163	93.30	25.00	537.91	2.206
164	93.50	25.50	538.70	2.214
165	94.10	25.00	541.06	2.206
166	94.60	26.30	543.03	2.227
167	95.00	23.00	544.61	2.175
168	95.50	24.50	546.57	2.199
169	96.30	22.80	549.72	2.172
170	96.70	24.60	551.30	2.203
171	97.30	26.00	553.66	2.222
172	97.80	28.70	555.63	2.263
173	98.40	26.80	557.99	2.235
174	99.00	30.80	560.35	2.297
175	99.50	32.30	562.32	2.321
176	100.00	31.40	564.28	2.307
177	100.30	26.50	565.47	2.230
178	100.80	25.60	567.44	2.219
179	101.50	31.00	570.20	2.301
180	102.00	30.30	572.16	2.290
181	102.70	31.00	574.92	2.301
182	103.40	36.00	577.68	2.379
183	104.30	29.30	581.22	2.274
184	104.80	27.40	583.19	2.244
185	105.70	34.00	586.75	2.348
186	106.00	34.10	587.91	2.349
187	106.60	37.30	590.27	2.400
188	107.00	32.20	591.85	2.319
189	107.70	33.80	594.61	2.345
190	108.00	32.30	595.79	2.321
191	108.50	33.60	597.76	2.341
192	108.90	33.60	599.33	2.341
193	109.20	31.70	600.51	2.312
194	109.70	33.10	602.48	2.334
195	110.30	29.50	604.84	2.277
196	111.10	29.20	607.99	2.272
197	112.00	32.30	611.53	2.321
198	112.70	32.40	614.29	2.323
199	113.30	28.00	616.65	2.254
200	113.60	25.00	617.83	2.206

PEACE BOREHOLE OCT-05

J	DIGITIZED DEPTH, X (DIV)	DIGITIZED DENSITY, Y (DIV)	COMPUTED DEPTH (FT)	COMPUTED DENSITY (GM/CC)
201	114.90	34.00	619.01	2.191
202	114.40	27.00	620.98	2.238
203	115.10	28.90	623.74	2.268
204	116.50	24.80	629.25	2.203
205	117.30	27.00	632.40	2.238
206	17.70	26.60	633.98	2.232
207	118.70	29.00	637.91	2.269
208	119.20	28.00	639.88	2.254
209	119.60	29.00	641.46	2.269
210	120.00	28.30	643.03	2.101
211	120.20	29.70	643.82	2.123
212	120.80	28.40	646.18	2.103
213	121.40	27.50	645.54	2.246
214	121.80	31.00	650.12	2.301
215	122.60	30.60	653.27	2.294
216	123.30	25.40	656.02	2.213
217	123.70	26.20	657.60	2.225
218	125.60	26.10	665.08	2.224
219	126.00	29.30	666.65	2.274
220	127.00	32.70	670.59	2.327
221	127.10	24.50	670.98	2.356
222	128.00	23.70	674.33	2.343
223	128.50	31.50	676.30	2.308
224	129.00	31.60	678.46	2.310
225	129.50	31.00	680.43	2.301
226	130.00	32.80	682.40	2.329
227	130.80	32.10	685.55	2.318
228	131.00	31.00	686.34	2.301
229	131.90	30.00	689.88	2.285
230	132.30	31.00	691.46	2.301
231	133.00	31.00	694.21	2.301
232	133.20	31.70	695.00	2.312
233	133.80	30.80	697.36	2.297
234	135.00	31.40	702.09	2.307
235	135.40	32.00	703.66	2.316
236	136.40	31.90	707.60	2.315
237	137.00	29.20	709.96	2.272
238	137.90	28.30	713.50	2.258
239	138.50	30.40	715.87	2.291
240	139.00	30.50	717.83	2.293
241	139.30	31.20	719.01	2.304
242	140.00	30.40	721.77	2.291
243	140.40	31.70	723.35	2.312
244	140.90	30.80	725.31	2.297
245	141.00	28.00	725.71	2.254
246	141.90	24.70	729.25	2.202
247	142.30	26.50	730.83	2.230
248	143.40	26.00	735.16	2.222
249	144.30	27.20	738.70	2.241
250	145.00	27.00	741.46	2.238
251	145.50	29.60	743.42	2.279
252	145.90	30.10	746.18	2.286
253	146.40	28.00	747.76	2.254
254	147.00	24.60	749.33	2.200
255	147.80	22.70	752.48	2.170
256	148.40	25.40	754.84	2.213
257	149.00	26.80	757.20	2.235
258	149.70	30.50	759.96	2.293
259	150.20	28.70	761.93	2.265
260	150.80	30.00	764.29	2.285
261	151.30	26.00	766.26	2.222
262	152.00	28.50	769.01	2.261
263	152.40	28.00	770.59	2.254
264	153.00	24.00	772.95	2.348
265	153.50	23.80	774.92	2.345
266	153.90	25.00	776.50	2.363
267	154.30	23.00	778.07	2.332
268	154.60	24.00	779.25	2.269
269	155.30	27.00	782.01	2.238
270	156.00	28.00	784.76	2.254
271	156.40	26.30	786.34	2.227
272	157.30	25.20	789.88	2.210
273	157.60	26.70	791.06	2.233
274	158.00	24.30	792.64	2.195
275	158.70	29.00	795.39	2.269
276	159.20	27.60	797.36	2.247
277	159.60	28.90	798.94	2.268
278	160.00	23.00	800.51	2.175
279	160.60	24.00	802.87	2.191
280	161.30	23.30	805.63	2.180
281	162.20	22.70	809.17	2.170
282	162.90	23.90	811.93	2.189
283	163.40	23.20	813.90	2.178
284	163.70	24.70	815.08	2.202
285	164.30	24.90	817.44	2.205
286	165.00	28.40	820.20	2.260
287	165.60	28.30	822.56	2.258
288	165.80	27.60	823.35	2.247
289	166.20	31.20	824.92	2.304
290	166.60	33.20	825.71	2.335
291	167.30	33.20	829.25	2.335
292	167.70	28.30	830.83	2.211
293	168.00	24.60	832.01	2.197
294	168.80	25.20	835.16	2.210
295	169.00	26.80	835.94	2.235
296	169.60	26.10	839.09	2.224
297	170.00	27.30	839.88	2.243
298	170.60	26.30	842.24	2.227
299	171.10	28.40	843.82	2.260
300	171.30	26.80	845.00	2.235

TABLE 6-8 (Continued)

PEACE BOREHOLE OCT-05

J	DIGITIZED DEPTH, X (DIV)	DIGITIZED DENSITY, Y (DIV)	COMPUTED DEPTH (FT)	COMPUTED DENSITY (GM/CC)
501	172.80	47.60	846.94	2.247
502	172.60	49.40	850.12	2.276
503	173.40	50.50	853.27	2.293
504	174.00	46.80	855.63	2.235
505	175.00	46.50	859.57	2.227
506	176.00	47.00	863.50	2.238
507	176.20	48.10	864.29	2.255
508	176.70	47.90	866.26	2.252
509	177.20	46.00	868.23	2.222
510	177.70	44.70	870.20	2.202
511	178.00	45.40	871.38	2.213
512	178.50	45.00	873.35	2.206
513	179.00	42.80	875.31	2.172
514	179.80	45.80	878.46	2.219
515	180.30	49.50	880.43	2.277
516	181.00	41.80	883.19	2.156
517	181.80	38.90	886.34	2.111
518	182.50	43.50	889.08	2.183
519	183.20	41.40	891.85	2.150
520	183.90	41.50	894.61	2.151
521	184.50	43.30	896.97	2.180
522	185.20	42.90	899.72	2.173
523	186.00	43.80	902.87	2.188
524	187.60	45.70	906.01	2.186
525	187.80	43.20	909.96	2.178
526	188.50	42.20	912.72	2.162
527	189.50	48.00	916.65	2.254
528	190.00	49.60	918.62	2.279
529	190.50	47.90	920.59	2.252
530	191.00	42.00	922.56	2.159
531	191.30	40.30	926.10	2.133
532	192.20	43.00	927.28	2.175
533	192.60	41.70	928.86	2.155
534	193.60	40.00	932.79	2.128
535	194.50	39.60	936.34	2.122
536	196.70	41.70	943.03	2.155
537	196.60	41.80	944.61	2.156
538	197.40	46.00	947.76	2.222
539	197.80	51.20	949.33	2.304
540	198.30	53.20	951.30	2.335
541	198.80	51.50	953.27	2.308
542	199.30	46.80	955.24	2.222
543	199.60	44.00	956.42	2.193
544	200.00	45.00	957.99	2.206
545	200.30	48.40	959.17	2.260
546	200.70	49.20	960.75	2.272
547	201.60	47.50	964.29	2.246
548	202.90	42.00	969.41	2.159
549	203.70	37.00	972.56	2.081
550	204.50	38.20	975.71	2.100
551	205.20	42.70	978.46	2.170
552	206.30	44.30	982.79	2.195
553	207.10	46.50	985.94	2.184
554	207.80	47.80	988.70	2.203
555	208.70	42.00	992.24	2.159
556	209.20	41.20	994.21	2.147
557	209.70	42.30	996.18	2.164
558	210.00	39.70	997.36	2.123

YO+ BY S:	.00	1.50	0.70	
XO+ AX BY C:	35.00	288.70	1.00	.254

PEACE BOREHOLE DAM-2A

J	DIGITIZED DEPTH, X (DIV)	DIGITIZED DENSITY, Y (DIV)	COMPUTED DEPTH (FT)	COMPUTED DENSITY (GM/CC)
1	5.80	28.30	141.87	1.948
2	6.60	27.00	145.36	1.927
3	7.10	29.70	146.53	1.970
4	7.90	24.30	149.64	1.884
5	9.00	25.70	153.91	2.065
6	9.80	33.50	156.26	2.030
7	10.00	30.00	157.40	1.975
8	10.80	37.30	160.90	2.090
9	11.20	29.00	162.46	1.959
10	11.80	26.80	164.79	1.924
11	12.60	26.80	167.90	1.924
12	13.00	30.80	169.45	1.987
13	13.40	31.00	171.01	1.991
14	13.70	33.20	172.17	2.025
15	14.00	35.30	173.34	2.059
16	14.30	35.00	174.50	2.054
17	14.90	26.20	176.83	1.915
18	15.20	31.80	178.00	2.003
19	15.70	27.00	179.94	1.927
20	16.00	24.00	181.11	1.880
21	16.50	28.00	183.05	1.785
22	17.00	28.50	184.99	1.793
23	17.40	26.80	186.55	1.924
24	17.60	30.70	187.32	1.986
25	18.00	30.20	188.88	1.978
26	18.20	31.80	189.65	2.003
27	18.90	31.00	192.37	1.991
28	19.20	33.00	193.54	2.022
29	19.90	27.00	196.26	1.927
30	20.10	32.80	197.04	2.019
31	20.40	34.00	198.20	2.038
32	21.60	32.00	200.53	2.006
33	21.60	32.00	202.85	2.006
34	21.80	33.20	203.64	2.025
35	22.60	33.50	206.75	2.030
36	23.20	32.80	209.08	2.019
37	23.50	34.10	210.25	2.040
38	24.10	33.50	212.58	2.030
39	25.10	35.80	216.46	2.066
40	26.00	33.80	219.96	2.035
41	26.80	37.70	223.07	2.097
42	27.30	32.70	225.01	2.017
43	28.50	39.30	228.90	2.122
44	29.00	31.40	231.61	1.997
45	29.20	34.10	232.39	2.040
46	29.60	34.80	233.95	2.051
47	29.90	34.60	235.11	2.047
48	30.10	32.90	235.89	2.100
49	30.80	35.00	238.61	2.054
50	31.00	29.80	239.39	1.965
51	31.50	27.00	241.33	1.927
52	32.00	29.00	243.27	1.959
53	33.40	23.80	248.71	1.877
54	33.80	25.00	250.26	1.896
55	34.00	28.30	251.04	1.948
56	34.40	30.80	252.59	1.975
57	34.50	29.00	252.98	1.959
58	35.00	28.20	254.93	1.948
59	35.30	29.00	256.09	1.959
60	36.00	32.40	258.81	2.013
61	36.40	32.00	260.37	2.006
62	37.00	36.00	262.70	2.070
63	37.70	30.50	265.42	1.983
64	38.10	35.50	266.97	2.062
65	38.50	31.30	268.52	1.995
66	39.00	32.00	270.47	2.006
67	40.00	33.60	274.35	2.190
68	40.40	35.00	275.91	2.180
69	41.40	32.70	279.79	2.017
70	41.50	33.50	280.18	2.030
71	42.20	33.50	282.90	2.030
72	42.50	37.00	284.07	2.085
73	43.50	37.70	287.95	2.097
74	43.80	37.00	289.12	2.085
75	44.20	38.80	290.67	2.114
76	44.80	29.50	293.00	1.967
77	45.50	39.00	295.72	2.117
78	45.80	38.60	296.89	2.111
79	46.30	41.00	298.83	2.149
80	47.00	30.30	301.55	1.979
81	47.80	35.40	304.66	2.060
82	48.30	33.00	306.60	2.022
83	48.50	31.80	307.38	2.003
84	48.70	33.40	308.15	2.028
85	49.00	33.30	309.32	2.027
86	49.20	36.00	310.10	2.070
87	49.60	34.30	312.43	2.043
88	50.10	37.00	313.59	2.085
89	50.40	37.30	314.76	2.090
90	51.00	36.50	317.09	2.078
91	51.60	33.00	320.20	2.022
92	52.30	36.40	322.14	2.076
93	53.00	33.30	324.86	2.027
94	53.80	34.90	326.03	2.038
95	54.10	26.30	329.13	1.911
96	54.50	31.80	331.85	2.003
97	55.00	27.00	332.63	1.927
98	55.90	26.30	334.18	1.916
99	56.00	29.80	336.52	1.972
100	56.40	25.50	338.07	1.903

TABLE 6-8 (Continued)

PEACE BOREHOLE BAR-2A

J	DIGITIZED DEPTH, X (DIV)	DIGITIZED DENSITY, Y (DIV)	COMPUTED DEPTH (FT)	COMPUTED DENSITY (GM/CC)
101	58.40	38.00	345.84	2.101
102	59.00	32.50	348.17	2.014
103	59.50	35.80	350.11	2.065
104	60.00	35.80	352.06	2.066
105	60.20	37.50	352.83	2.093
106	60.40	36.00	353.16	2.070
107	61.00	34.00	355.94	2.038
108	61.50	33.00	357.11	2.022
109	62.00	37.00	359.83	2.085
110	62.40	33.80	361.38	2.035
111	63.00	37.40	363.71	2.092
112	63.60	39.00	366.04	2.117
113	64.30	37.20	368.76	2.089
114	65.00	41.20	371.48	2.152
115	65.40	39.80	373.04	2.130
116	66.00	31.00	375.37	1.993
117	66.30	33.00	376.53	2.022
118	66.40	33.50	376.48	2.030
119	67.00	32.00	380.03	2.006
120	67.70	34.30	381.97	2.043
121	68.10	33.80	383.53	2.036
122	69.00	37.80	387.02	2.098
123	69.50	37.50	388.19	2.093
124	69.90	38.90	390.52	2.116
125	70.30	38.20	392.07	2.112
126	70.80	38.00	393.24	2.101
127	71.00	26.00	395.57	1.911
128	71.70	34.00	397.51	2.038
129	72.50	36.50	400.62	2.080
130	73.30	37.00	403.73	2.085
131	73.90	34.80	406.06	2.051
132	74.20	37.70	407.23	2.097
133	74.80	37.80	409.56	2.098
134	75.40	34.40	411.89	2.044
135	75.60	36.00	412.67	2.070
136	76.30	37.00	415.38	2.085
137	76.70	39.00	416.94	2.117
138	77.50	38.30	420.05	2.106
139	78.00	38.60	421.99	2.127
140	78.70	38.30	424.71	2.106
141	79.10	36.20	426.26	2.073
142	79.80	45.20	428.98	2.215
143	80.30	34.00	430.93	2.038
144	81.10	33.00	433.65	2.188
145	81.40	34.50	435.20	2.046
146	82.00	33.00	437.53	2.022
147	82.30	35.00	438.70	2.054
148	85.00	44.40	441.42	2.203
149	84.00	39.00	445.30	2.117
150	84.50	41.05	447.24	2.149
151	85.10	33.00	449.57	2.022
152	85.70	29.00	451.91	1.959
153	86.00	24.80	453.07	1.880
154	86.50	29.00	455.01	1.958
155	86.80	31.00	456.18	2.101
TOP OF SI	.00	1.50	63.23	
BOT. A. B. C:	30.00	235.50	1.00	.25739647

PEACE BOREHOLE OIT-11

J	DIGITIZED DEPTH, X (DIV)	DIGITIZED DENSITY, Y (DIV)	COMPUTED DEPTH (FT)	COMPUTED DENSITY (GM/CC)
1	1.90	32.00	169.57	2.002
2	3.00	36.60	173.70	2.074
3	3.60	35.20	176.06	2.052
4	4.40	36.70	179.21	2.075
5	4.80	39.10	180.79	2.113
6	5.00	40.30	181.57	2.132
7	5.40	40.00	183.15	2.127
8	5.60	38.50	183.94	2.103
9	5.80	36.20	184.72	2.067
10	6.50	35.40	187.48	2.055
11	6.80	36.00	188.66	2.064
12	7.00	38.60	189.45	2.105
13	7.50	38.20	190.63	2.099
14	7.80	35.00	192.60	2.049
15	8.30	36.80	194.57	2.077
16	8.50	37.00	195.35	2.080
17	9.00	39.00	197.32	2.111
18	9.40	43.40	198.90	2.180
19	10.00	45.00	201.26	2.205
20	10.60	43.90	203.62	2.188
21	11.30	38.00	206.38	2.098
22	12.20	33.00	209.92	2.017
23	12.70	31.40	211.89	1.992
24	13.50	34.00	214.25	2.033
25	13.80	34.20	215.43	2.036
26	13.80	35.00	216.22	2.049
27	14.20	36.00	217.80	2.064
28	14.80	34.30	220.16	2.038
29	15.30	34.50	222.13	2.041
30	16.00	36.30	224.88	2.069
31	17.00	30.00	228.82	1.970
32	17.40	28.70	230.39	1.950
33	18.00	32.60	232.76	2.011
34	18.60	33.50	235.12	2.025
35	19.30	28.30	237.87	1.944
36	20.00	27.00	240.63	1.923
37	20.30	31.00	241.81	1.986
38	20.50	32.00	242.60	2.002
39	21.00	30.40	244.57	1.976
40	21.50	29.00	246.54	1.955
41	22.10	25.80	248.90	1.904
42	22.50	29.40	250.47	1.961
43	23.00	30.30	252.44	1.975
44	23.70	35.00	255.20	2.049
45	24.20	35.20	257.17	2.052
46	25.00	37.30	260.31	2.085
47	25.80	37.20	263.46	2.083
48	26.00	35.60	264.25	2.058
49	26.40	35.20	265.83	2.052
50	26.60	35.80	267.40	2.061
51	27.20	35.00	268.98	2.049
52	28.00	36.30	272.13	2.069
53	28.50	35.00	273.31	2.049
54	28.70	33.10	274.88	2.019
55	28.90	33.50	275.67	2.025
56	29.30	33.50	277.24	2.025
57	29.70	34.30	278.82	2.038
58	30.00	35.40	280.00	2.055
59	30.50	34.40	281.97	2.039
60	30.80	33.00	283.15	2.017
61	31.70	34.20	286.69	2.036
62	32.30	29.50	289.06	1.962
63	32.70	28.30	290.63	1.944
64	33.40	32.50	293.39	2.009
65	33.80	32.80	294.96	2.014
66	34.10	34.70	296.14	2.044
67	34.70	33.00	298.50	2.017
68	34.90	33.20	299.29	2.020
69	35.50	33.20	300.87	2.020
70	35.80	34.60	302.05	2.042
71	36.10	34.50	304.02	2.041
72	36.60	34.90	303.98	2.047
73	37.00	32.80	307.56	2.014
74	37.60	34.00	309.92	2.033
75	38.00	31.80	311.50	1.998
76	38.50	32.20	313.46	2.005
77	39.00	28.70	315.43	1.950
78	39.40	32.00	317.01	2.002
79	39.90	29.30	318.98	1.959
80	40.10	30.50	319.76	1.978
81	40.40	33.90	320.94	2.031
82	40.90	31.30	322.91	1.991
83	42.00	35.00	327.24	2.049
84	42.60	40.00	329.61	2.127
85	43.30	36.40	332.36	2.071
86	43.80	35.30	334.33	2.053
87	44.00	32.00	335.12	2.002
88	45.00	32.60	339.06	2.011
89	45.60	35.40	341.42	2.055
90	46.40	34.00	344.57	2.033
91	46.80	30.50	346.54	1.978
92	47.20	31.30	347.72	1.991
93	48.00	31.30	350.87	1.991
94	48.50	33.50	352.05	2.025
95	49.40	34.20	356.38	2.036
96	50.20	32.00	359.53	2.002
97	50.70	29.60	361.50	1.964
98	51.30	29.70	363.46	1.966
99	51.70	32.50	365.43	2.009
100	52.50	38.50	368.58	2.103

TABLE 6-8 (Continued)

PEASE BOREHOLE GIT-11

J	DIGITIZED DEPTH, X (DIV)	DIGITIZED DENSITY, Y (DIV)	COMPUTED DEPTH (FT)	COMPUTED DENSITY (GM/CC)
101	56.00	39.00	370.55	2.111
102	56.40	37.80	372.13	2.092
103	56.70	39.00	373.31	2.111
104	56.00	38.50	374.49	2.103
105	56.20	35.90	375.28	2.063
106	56.40	36.70	376.06	2.044
107	56.90	36.30	378.03	2.056
108	55.50	36.10	380.39	2.066
109	55.90	37.20	381.97	2.083
110	56.30	38.00	383.54	2.096
111	56.60	35.90	384.72	2.063
112	56.90	37.90	385.91	2.094
113	57.30	38.00	387.48	2.096
114	57.60	35.30	388.66	2.053
115	58.30	33.20	391.42	2.020
116	58.90	35.40	393.78	2.055
117	59.60	39.00	396.54	2.111
118	60.00	38.70	398.11	2.107
119	60.40	37.00	399.69	2.080
120	60.90	35.00	401.65	2.049
121	61.70	36.00	404.80	2.064
122	62.00	37.20	405.98	2.083
123	62.30	36.50	407.17	2.072
124	63.00	32.00	409.92	2.002
125	63.40	32.30	411.50	2.006
126	64.00	35.20	413.86	2.052
127	64.30	36.80	415.04	2.077
128	64.80	35.00	417.01	2.049
129	65.40	36.60	419.37	2.074
130	65.70	35.20	420.55	2.052
131	66.30	36.60	422.91	2.074
132	66.60	36.40	424.09	2.071
133	66.90	35.30	424.88	2.053

Y0, Q, S: .00 1.50 63.80

X0, A, B, C: 30.00 280.00 1.00 .254

PEASE BOREHOLE GRT-13

J	DIGITIZED DEPTH, X (DIV)	DIGITIZED DENSITY, Y (DIV)	COMPUTED DEPTH (FT)	COMPUTED DENSITY (GM/CC)
1	1.80	28.50	180.53	1.947
2	2.00	41.50	181.32	2.150
3	2.20	40.60	182.11	2.136
4	5.00	41.10	185.26	2.144
5	7.60	27.20	203.37	1.926
6	8.70	40.50	207.71	1.978
7	9.50	44.70	210.86	1.887
8	10.20	40.40	213.61	1.976
9	10.60	40.40	215.19	1.976
10	11.00	42.30	216.76	2.006
11	11.90	40.20	220.31	1.973
12	12.30	34.50	221.88	2.038
13	12.80	35.60	223.85	2.058
14	13.40	34.10	226.22	2.034
15	14.00	37.00	228.58	2.080
16	15.00	37.00	232.52	2.080
17	15.60	34.00	234.88	2.033
18	16.50	36.20	238.42	2.067
19	17.50	34.00	242.36	2.033
20	17.80	31.70	243.54	1.997
21	19.00	37.60	248.27	2.089
22	20.20	40.20	253.00	2.130
23	20.90	38.00	255.75	2.111
24	21.60	34.00	258.51	2.033
25	22.50	37.40	262.05	2.086
26	23.80	37.20	267.17	1.926
27	24.60	33.20	270.32	2.020
28	25.00	31.00	271.90	1.986
29	25.50	33.00	273.87	2.017
30	26.00	17.50	275.84	1.774
31	26.80	21.60	278.99	1.842
32	27.50	34.20	281.74	2.036
33	28.30	29.00	284.90	1.955
34	29.60	26.40	290.07	1.914
35	30.00	29.00	291.59	1.955
36	30.40	30.20	293.17	1.973
37	31.20	27.80	296.32	1.936
38	32.00	28.00	299.47	1.939
39	32.10	31.80	299.86	1.998
40	32.80	32.00	302.62	2.002
41	33.00	34.30	303.41	2.038
42	33.50	32.80	305.37	2.014
43	33.90	33.20	306.95	2.020
44	34.50	32.50	309.31	2.009
45	35.00	35.00	311.28	2.049
46	36.00	36.20	315.22	2.067
47	36.50	35.40	317.19	2.055
48	37.20	36.90	319.95	2.078
49	37.90	35.80	322.76	2.061
50	38.40	33.20	324.67	2.020
51	39.30	33.20	328.22	2.020
52	39.50	33.90	329.00	2.031
53	40.10	33.80	331.37	2.030
54	40.70	31.30	333.73	1.991
55	40.90	31.00	334.52	1.986
56	41.10	29.60	335.30	1.964
57	41.80	30.00	338.06	1.970
58	42.40	36.30	340.42	2.069
59	44.20	29.00	347.51	1.955
60	45.00	32.20	350.66	2.005
61	45.60	31.60	353.03	1.995
62	46.20	27.80	355.39	1.936
63	46.70	29.00	357.36	1.955
64	47.50	35.00	360.51	2.049
65	48.00	36.00	362.48	2.064
66	48.10	37.40	362.87	2.086
67	49.10	37.00	366.81	2.080
68	49.90	32.20	369.96	2.005
69	50.60	33.00	371.54	2.017
70	50.90	35.20	373.90	2.052
71	51.10	35.20	374.69	2.052
72	52.10	34.20	378.63	2.036
73	52.50	35.60	380.20	2.058
74	53.00	35.60	382.17	2.058
75	53.10	35.10	382.56	2.050
76	53.20	36.00	382.96	2.064
77	54.00	36.00	386.11	2.064
78	54.20	36.50	386.90	2.072
79	54.70	32.90	388.87	2.016
80	55.20	32.90	390.83	2.016
81	55.50	31.70	392.02	1.997
82	55.80	33.00	393.20	2.017
83	56.10	34.30	394.38	2.038
84	56.50	34.80	395.95	2.045
85	57.00	34.30	397.92	2.038
86	57.50	32.00	399.89	2.002
87	56.40	28.70	403.44	1.903
88	59.40	29.10	407.37	1.956
89	60.00	25.50	409.74	1.900
90	60.90	29.90	413.28	1.890
91	61.50	31.20	415.65	1.989
92	62.00	31.20	417.61	1.989
93	63.10	29.70	421.95	1.966
94	63.80	33.20	424.70	2.020
95	64.10	31.70	425.88	1.997
96	64.50	31.00	427.46	1.986
97	65.00	31.00	429.43	1.986
98	65.20	30.80	430.22	1.983
99	65.80	33.30	432.58	2.022
100	64.50	32.80	435.14	2.014

TABLE 6-8 (Continued)

PEACE BOREHOLE OKT-13

J	DIGITIZED DEPTH, X (DIV)	DIGITIZED DENSITY, Y (DIV)	COMPUTED DEPTH (FT)	COMPUTED DENSITY (GM/CC)
101	66,80	33,30	436,52	2,022
102	67,60	29,30	439,67	1,959
103	68,10	30,50	441,64	1,978
104	69,00	37,00	445,16	2,080
105	69,40	35,20	446,76	2,052
106	70,30	36,00	450,30	2,064
107	70,80	38,60	452,27	2,108
108	71,31	38,00	454,24	2,096
109	72,10	39,60	457,39	2,124
110	73,80	25,50	464,09	1,900
111	74,00	30,00	464,87	1,970
112	75,00	34,00	468,81	2,033
113	75,20	36,20	469,60	2,067
114	75,80	33,80	471,96	2,030
115	76,20	34,20	473,54	2,036
116	76,80	31,50	475,90	1,994
117	77,20	34,80	477,48	2,045
118	77,60	34,80	479,05	2,045
119	78,20	36,00	481,41	2,096
120	79,00	34,00	484,56	2,033
121	79,50	32,00	486,53	2,002
122	80,00	30,70	488,50	1,981
123	80,10	32,00	488,90	2,002
124	80,80	33,50	491,65	2,025
125	81,10	32,80	492,83	2,014
126	81,30	35,90	493,62	2,063
127	82,20	34,20	497,17	2,036
128	82,40	34,60	497,95	2,042
129	83,00	32,00	500,32	2,002
130	83,25	31,80	501,11	1,998
131	83,60	32,00	502,68	2,002
132	84,20	33,00	505,04	2,111
133	85,00	33,50	508,19	2,103
134	85,70	34,10	510,95	2,034
135	86,10	35,20	512,53	2,052
136	86,30	33,00	513,31	2,111
137	86,80	33,50	515,28	2,103
138	87,40	33,70	517,65	2,107
139	88,00	35,50	520,01	2,036
140	88,80	31,60	523,16	1,995
141	90,00	40,50	527,89	2,155
142	90,80	42,10	531,04	2,160
143	91,20	41,90	532,61	2,157
144	91,60	43,50	534,19	2,182
145	93,00	35,00	539,70	2,049
146	94,50	35,00	545,61	2,049
147	95,10	37,60	547,97	2,089
148	95,80	38,00	550,73	2,096
149	96,70	36,70	554,27	2,044
150	97,20	35,30	556,24	2,053
151	98,00	34,30	559,39	2,036
152	98,20	36,90	560,18	2,078
153	99,00	36,30	563,33	2,069
154	99,20	37,70	564,12	2,091
155	100,00	33,70	567,27	2,028
156	100,50	35,00	569,24	2,049
157	101,10	37,40	571,60	2,086
158	101,90	33,80	574,75	2,030
159	102,90	34,00	578,69	2,033
160	103,20	48,00	579,87	2,252
161	104,50	60,00	584,99	2,440
162	106,20	54,40	591,68	2,339
163	106,80	56,40	594,05	2,371
164	107,30	56,10	596,02	2,066
165	107,80	56,70	597,99	2,075
166	108,20	53,60	599,56	2,027
167	108,50	54,80	600,74	2,045
168	109,20	54,80	603,50	2,045
169	109,50	58,40	604,68	2,102
170	110,00	58,80	606,65	2,108
171	110,30	59,80	607,83	2,124
172	111,20	53,40	611,38	2,024
173	112,30	41,70	615,71	2,154
174	113,30	40,70	619,65	2,138
175	113,80	41,70	621,62	2,154
176	114,50	41,70	624,37	2,154
177	115,00	38,50	626,34	2,103
178	116,00	38,00	630,28	2,096
179	117,10	38,70	634,61	2,107
180	117,50	41,30	636,19	2,147
181	118,10	42,30	638,55	2,163
182	119,20	39,00	642,88	2,111
183	119,80	39,90	645,25	2,125
184	120,20	39,00	646,82	2,111
185	120,80	38,60	649,18	2,105
186	121,10	36,70	650,36	2,075
187	121,70	41,00	652,73	2,143
188	122,30	43,80	655,09	2,187
189	123,40	42,90	659,42	2,172
190	124,20	43,10	662,57	2,176
191	125,60	42,00	668,09	2,004
192	126,00	43,80	669,66	2,030
193	126,30	42,70	670,84	2,013
194	127,00	45,20	673,60	2,052
195	128,30	42,80	678,72	2,171
196	129,10	38,20	681,87	2,099
197	130,20	42,80	686,20	2,014
198	130,90	45,00	688,96	2,049
199	131,40	46,80	690,73	2,077
200	132,10	44,10	693,69	2,019

PEACE BOREHOLE OKT-13

J	DIGITIZED DEPTH, X (DIV)	DIGITIZED DENSITY, Y (DIV)	COMPUTED DEPTH (FT)	COMPUTED DENSITY (GM/CC)
201	132,40	45,10	694,87	2,050
202	133,00	45,10	697,23	2,050
203	133,80	49,70	700,38	2,122
204	134,40	46,70	702,74	2,075
205	135,00	46,70	705,11	2,075
206	135,20	45,00	705,89	2,049
207	135,50	45,00	707,08	2,049
208	135,90	47,70	708,65	2,091
209	136,70	47,20	711,80	2,083
210	137,00	50,80	712,98	2,139
211	137,80	51,40	716,13	2,149
212	138,30	49,30	718,10	2,116
213	138,60	49,30	720,07	2,116
214	140,80	52,00	727,95	2,082
215	142,10	52,00	733,07	2,158
216	142,80	51,80	735,82	2,155
217	143,30	48,50	737,79	2,103
218	143,80	50,00	739,76	2,127
219	144,50	51,40	742,52	2,149
220	145,50	45,70	746,46	2,060
221	146,00	46,00	748,43	2,064
222	146,50	45,80	750,40	2,061
223	147,00	48,30	752,37	2,100
224	147,60	48,30	754,73	2,100
225	148,00	51,50	756,30	2,150
226	148,70	51,60	759,06	2,152
227	148,90	52,40	759,85	2,165
228	149,80	48,80	763,79	2,108
229	150,40	49,00	765,76	2,111
230	151,00	48,20	768,12	2,099
231	151,20	48,60	768,91	2,108
232	151,80	45,70	771,27	2,060
233	153,50	54,50	777,96	2,041
234	153,90	55,00	779,54	2,049
235	155,30	51,20	785,05	2,146
236	156,90	45,40	791,35	2,055
237	157,00	46,00	791,75	2,064
238	157,10	46,20	792,14	2,067
239	158,10	50,90	796,08	2,141
240	158,80	50,90	798,84	2,141
241	159,60	48,60	801,99	2,105
242	160,30	48,50	804,74	2,103
243	161,10	53,50	807,89	2,025
244	161,80	53,10	810,65	2,019
245	162,70	57,00	814,20	2,080
246	163,70	57,20	818,13	2,083
247	164,10	50,10	819,71	2,129
248	165,00	48,70	823,25	2,107
249	165,80	51,70	826,40	2,028
250	166,10	51,70	827,59	2,028
251	166,50	52,00	829,16	2,007
252	167,30	55,30	832,31	2,053
253	168,10	48,30	835,46	2,100
254	168,80	48,20	838,22	2,099
255	169,20	49,00	839,79	2,111
256	169,50	48,80	840,98	2,108
257	170,00	48,80	842,95	2,108
258	170,30	47,20	844,13	2,083
259	171,20	46,80	847,67	2,077
260	171,60	48,50	849,25	2,103
261	172,00	47,60	850,82	2,060
262	172,60	50,00	853,18	2,127
263	173,20	48,30	855,55	2,100
264	173,30	48,00	855,94	2,096
265	174,20	49,00	859,49	1,955
266	175,50	50,60	864,61	2,136
267	176,20	53,00	867,36	2,017
268	176,90	51,00	870,12	1,986
269	177,40	47,20	872,09	2,083
270	177,80	45,80	873,66	2,061
271	178,10	48,90	874,84	2,096
272	178,70	43,70	877,21	2,028
273	179,30	45,00	879,57	2,049
274	179,50	44,00	880,36	2,033
275	180,80	45,40	885,48	2,212
276	186,00	45,50	890,20	2,056
277	183,00	47,80	894,14	2,092
278	183,50	45,20	896,11	2,052
279	184,50	44,80	900,05	2,045
280	185,80	45,50	905,17	2,056
281	186,20	47,20	904,74	2,083
282	186,70	46,00	908,71	2,064
283	187,00	43,50	909,90	2,025
284	187,50	43,50	911,86	2,025

YO, B, S:	,00	1,50	63,40	
XO, A, B, C:	29,52	285,70	1,80	,25399

TABLE 6-8 (Continued)

PEACE BOREHOLE DPZ-1B

J	DIGITIZED DEPTH, X (DIV)	DIGITIZED DENSITY, Y (DIV)	COMPUTED DEPTH (FT)	COMPUTED DENSITY (GM/CC)
1	46.00	9.00	389.89	1.984
2	47.00	9.00	393.83	1.984
3	47.40	7.10	395.40	1.954
4	47.90	7.40	397.37	1.959
5	48.40	6.10	399.34	1.939
6	48.90	6.30	401.31	1.942
7	49.30	4.60	402.88	1.915
8	49.90	6.20	405.25	1.940
9	50.30	6.50	406.82	1.945
10	51.00	9.30	409.58	1.989
11	51.50	9.30	411.55	1.989
12	52.00	13.30	413.51	2.052
13	53.30	15.20	418.65	2.082
14	53.60	14.50	419.81	2.071
15	55.10	15.70	425.72	2.090
16	55.30	16.70	426.51	2.105
17	55.80	15.00	428.47	2.079
18	56.00	12.00	429.26	2.031
19	56.30	11.70	430.44	2.027
20	56.80	13.00	432.41	2.047
21	58.00	22.30	437.14	2.193
22	59.00	20.00	441.07	2.157
23	59.20	17.60	441.86	2.119
24	59.50	17.90	443.04	2.124
25	60.80	13.50	446.16	2.052
26	61.50	17.20	450.92	2.113
27	62.00	20.00	452.88	2.157
28	62.30	19.80	454.07	2.154
29	62.70	20.60	455.64	2.167
30	63.90	11.60	460.36	2.025
31	64.30	11.30	461.94	2.020
32	64.50	13.20	462.73	2.050
33	65.20	13.20	465.48	2.050
34	65.40	15.00	466.27	2.079
35	65.90	13.00	468.24	2.047
36	66.60	12.60	471.78	2.041
37	67.10	13.20	472.96	2.050
38	67.50	17.40	474.54	2.116
39	68.00	20.00	476.51	2.157
40	68.60	23.60	478.87	2.214
41	68.70	22.90	479.26	2.203
42	69.30	22.70	481.62	2.200
43	70.00	17.20	484.38	2.113
44	70.40	17.40	485.96	2.116
45	70.90	19.40	487.92	2.148
46	71.20	18.90	489.10	2.140
47	71.30	19.70	490.29	2.153
48	71.60	18.20	490.68	2.129
49	72.10	17.90	492.65	2.124
50	72.20	13.90	493.04	2.061
51	72.80	14.20	495.40	2.066
52	73.00	15.30	496.19	2.083
53	73.20	14.40	496.98	2.069
54	73.60	14.20	498.55	2.066
55	74.30	10.00	501.31	4.000
56	75.00	15.50	504.07	2.086
57	75.50	16.50	506.03	2.102
58	76.20	20.70	508.79	2.168
59	76.70	18.60	510.76	2.135
60	77.10	18.40	512.33	2.132
61	77.60	17.00	514.30	2.110
62	78.20	18.90	516.66	2.140
63	79.50	16.30	521.78	2.099
64	80.10	19.80	524.14	2.154
65	81.10	19.80	528.08	2.154
66	81.30	18.40	528.87	2.132
67	82.10	19.60	532.02	2.151
68	83.00	18.00	535.56	2.126
69	84.50	15.70	541.47	2.090
70	84.90	15.90	543.04	2.093
71	85.40	12.10	545.01	2.033
72	85.80	12.40	546.59	2.038
73	86.30	11.90	548.55	2.030
74	87.00	16.60	551.31	2.104
75	87.20	16.70	552.10	2.105
76	87.60	16.80	553.67	2.138
77	88.20	17.70	556.03	2.121
78	88.90	13.80	558.79	2.060
79	89.10	15.00	559.58	2.079
80	89.40	15.50	560.76	2.083
81	90.20	14.80	563.91	2.075
82	90.50	13.30	565.09	2.052
83	91.00	19.70	567.06	2.153
84	92.00	26.00	570.99	2.252
85	92.60	22.00	573.36	2.189
86	92.90	22.00	574.54	2.189
87	93.50	15.00	576.90	2.047
88	94.10	16.10	579.26	2.096
89	94.30	16.20	580.05	2.097
90	94.90	23.50	582.41	2.212
91	95.20	19.00	583.59	2.142
92	96.20	14.90	587.53	2.077
93	96.80	18.90	589.89	2.140
94	97.80	3.30	593.83	1.892
95	98.30	2.90	595.80	1.888
96	99.20	16.40	599.34	2.101
97	99.90	9.60	602.10	1.994
98	100.20	11.70	603.28	2.027
99	100.90	11.60	606.03	2.025
100	101.20	16.00	607.21	2.094

PEACE BOREHOLE DPZ-1B

J	DIGITIZED DEPTH, Y (DIV)	DIGITIZED DENSITY, Y (DIV)	COMPUTED DEPTH (FT)	COMPUTED DENSITY (GM/CC)
101	102.00	17.50	610.36	2.118
102	102.40	22.00	611.94	2.189
103	103.10	20.80	614.70	2.170
104	103.60	22.20	616.66	2.192
105	104.00	20.40	618.24	2.164
106	104.80	19.60	621.39	2.151
107	105.10	17.00	622.57	2.110
108	105.40	15.50	623.75	2.086
109	106.70	16.00	628.87	2.094
110	107.00	18.00	630.05	2.126
111	107.20	18.20	630.84	2.129
112	108.00	23.30	633.99	2.209
113	108.70	24.70	636.74	2.231
114	109.00	23.00	637.92	2.204
115	109.60	22.00	640.29	2.189
116	110.10	19.30	642.25	2.146
117	111.00	17.00	645.80	2.110
118	111.40	17.90	647.37	2.124
119	112.60	17.00	652.10	2.110
120	113.20	17.70	653.40	2.121
121	113.60	18.20	659.97	2.129
122	115.00	16.80	661.55	2.102
123	115.60	16.20	663.91	2.097
124	115.90	15.20	665.09	2.082
125	117.10	15.60	669.81	2.088
126	118.20	20.10	674.14	2.159
127	119.30	15.90	678.47	2.093
128	119.90	16.30	680.84	2.099
129	120.00	14.00	681.23	2.063
130	121.10	14.70	685.56	2.074
131	121.40	19.20	686.74	2.145
132	122.10	18.00	689.50	2.126
133	123.10	23.30	693.44	2.209
134	123.60	23.30	695.40	2.209
135	123.70	24.20	695.80	2.223
136	124.30	19.30	698.16	2.146
137	124.50	20.20	698.95	2.160
138	125.70	18.90	703.67	2.140
139	126.20	20.90	705.64	2.171
140	126.70	19.50	707.61	2.149
141	127.20	19.50	709.58	2.149
142	127.90	16.80	712.33	2.107
143	129.00	17.10	716.66	2.112
144	129.60	20.00	719.03	2.157
145	130.10	19.20	720.99	2.145
146	130.60	19.60	722.96	2.151
147	131.20	18.70	725.33	2.058
148	132.00	18.70	728.47	2.058
149	132.90	18.10	732.02	2.127
150	133.20	15.80	733.20	2.091
151	133.40	16.20	733.99	2.097
152	134.10	16.20	736.74	2.097
153	134.90	20.00	739.89	2.157
154	135.20	18.90	741.07	2.140
155	135.30	19.10	741.47	2.143
156	136.20	16.70	745.01	2.105
157	136.60	17.80	746.59	2.123
158	136.90	16.70	747.77	2.105
159	137.60	16.40	750.52	2.101
160	138.00	15.00	752.10	2.079
161	138.50	16.70	754.07	2.105
162	139.00	18.90	756.03	2.140
163	139.40	18.90	757.61	2.140
164	139.70	17.50	758.79	2.118
165	140.00	17.50	759.97	2.118
166	140.60	14.10	762.33	2.064
167	141.30	14.10	765.09	2.064
168	141.40	13.40	765.48	2.053
169	141.90	15.20	767.45	2.082
170	142.00	14.60	767.84	2.072
171	142.70	14.10	770.60	2.064
172	143.00	15.50	771.78	2.086
173	143.40	15.70	773.36	2.090
174	143.50	16.60	773.75	2.104
175	144.00	12.30	775.72	2.036
176	144.80	9.20	778.87	1.987
177	145.10	11.20	780.05	2.019
178	145.70	9.90	782.41	1.998
179	146.20	10.90	784.38	2.014
180	146.40	10.80	785.17	2.013
181	146.90	13.00	787.14	2.047
182	147.10	12.20	787.92	2.035
183	147.70	11.90	790.29	2.030
184	148.10	14.00	791.86	2.063
185	149.20	18.00	796.19	2.126
186	150.00	17.50	799.34	2.118
187	150.80	14.70	802.49	2.074
188	151.20	14.70	804.07	2.074
189	151.40	13.50	804.85	2.055
190	152.00	16.20	807.21	2.097
191	152.40	15.50	808.79	2.086
192	153.00	18.00	811.15	2.126
193	153.50	15.20	813.12	2.082
194	154.10	16.00	815.48	2.094
195	154.80	15.50	818.24	2.086
196	155.20	16.90	819.81	2.108
197	156.00	12.20	822.96	2.035
198	156.20	12.20	823.75	2.035
199	156.90	10.00	826.51	2.000
200	157.30	10.00	828.08	2.000

TABLE 6-8 (Continued)

PEACE BOREHOLE DPZ-1B

J	DIGITIZED DEPTH, X (DIV)	DIGITIZED DENSITY, Y (DIV)	COMPUTED DEPTH (FT)	COMPUTED DENSITY (GM/CC)
201	157.40	8.90	830.44	1.983
202	158.40	10.00	832.41	2.000
203	158.70	9.10	833.59	1.986
204	159.20	14.30	835.56	2.068
205	159.60	14.70	837.14	2.074
206	160.00	16.30	838.71	2.099
207	161.00	14.60	842.65	2.072
208	162.00	14.20	846.59	2.066
209	162.60	13.00	848.95	2.047
210	163.50	13.80	852.49	2.060
211	164.00	16.00	854.46	2.094
212	164.30	17.00	855.64	2.110
213	165.80	6.30	861.55	1.942
214	166.40	10.00	863.91	2.000
215	166.80	11.00	865.48	2.016
216	167.20	10.00	867.06	2.000
217	168.00	13.20	870.21	2.050
218	168.20	13.20	870.99	2.050
219	168.40	15.80	871.78	2.091
220	169.10	15.70	874.54	2.090
221	169.60	15.00	876.51	2.079
222	169.80	15.30	877.29	2.083
223	170.20	17.20	878.87	2.113
224	170.60	16.90	880.44	2.108
225	171.00	18.50	882.02	2.134

YO: Q: S:	10.00	2.00	63.60	
XO: A: B: C:	30.00	526.90	1.09	.254

PEACE BOREHOLE KAR-01

J	DIGITIZED DEPTH, X (DIV)	DIGITIZED DENSITY, Y (DIV)	COMPUTED DEPTH (FT)	COMPUTED DENSITY (GM/CC)
1	20.00	26.40	189.93	1.921
2	20.70	16.30	192.74	1.760
3	21.20	26.00	194.75	1.915
4	21.40	60.00	195.55	1.978
5	21.80	27.00	197.16	1.931
6	22.20	10.00	198.76	1.659
7	22.40	1.00	199.57	1.516
8	23.00	7.00	201.98	1.612
9	23.30	9.10	203.18	1.645
10	23.70	7.70	204.79	1.623
11	24.10	10.00	206.40	1.659
12	24.50	17.80	208.00	1.784
13	24.80	16.00	209.21	1.755
14	24.90	15.20	209.61	1.742
15	25.10	15.10	210.41	1.741
16	25.20	14.00	210.82	1.723
17	25.40	16.80	211.62	1.768
18	26.00	10.80	214.03	1.659
19	26.40	2.00	215.64	1.532
20	26.90	3.00	217.65	1.548
21	27.20	13.00	218.85	1.707
22	27.50	25.60	220.06	1.908
23	28.80	4.30	225.28	1.569
24	29.30	10.40	227.29	1.666
25	29.80	10.60	229.30	1.669
26	30.10	17.70	230.50	1.782
27	31.00	1.20	234.12	1.519
28	31.50	4.00	236.13	1.564
29	31.60	3.80	236.53	1.561
30	31.90	5.10	237.73	1.581
31	32.40	8.00	239.74	1.548
32	32.50	.70	240.14	1.511
33	33.20	12.70	242.96	1.703
34	33.40	13.20	243.76	1.711
35	33.70	18.80	244.96	1.800
36	34.20	11.90	246.97	1.690
37	34.60	11.00	248.58	1.675
38	34.90	8.00	249.79	1.628
39	35.60	16.00	252.60	1.755
40	36.00	15.00	254.20	1.739
41	36.60	16.70	256.62	1.766
42	37.00	17.00	258.22	1.771
43	37.30	20.50	259.43	1.827
44	37.70	21.30	261.03	1.840
45	37.90	20.00	261.84	1.819
46	38.20	19.00	263.04	1.803
47	38.30	18.00	263.44	1.787
48	38.70	17.90	265.05	1.785
49	39.40	13.20	267.86	1.711
50	39.70	15.00	269.07	1.739
51	40.10	25.20	270.68	1.902
52	40.60	22.60	272.68	1.860
53	41.00	22.50	274.29	1.859
54	41.20	22.00	275.10	1.851
55	41.60	23.20	276.70	1.870
56	42.10	23.20	278.71	1.870
57	42.30	24.00	279.51	1.883
58	42.70	26.20	281.12	1.918
59	43.50	23.20	284.34	1.870
60	43.80	25.00	285.54	1.899
61	44.30	23.80	287.55	1.880
62	44.70	24.70	289.16	1.894
63	44.90	23.60	289.96	1.876
64	45.20	17.40	291.17	1.778
65	45.80	24.20	293.58	1.886
66	46.70	10.00	297.19	1.659
67	47.30	25.70	299.60	1.910
68	47.50	23.00	300.41	1.867
69	47.60	22.90	300.81	1.865
70	47.70	21.20	301.21	1.838
71	48.20	30.80	303.22	1.991
72	48.30	28.20	303.62	1.950
73	48.40	30.80	304.02	1.991
74	48.80	20.00	305.63	1.819
75	49.20	25.90	307.23	1.913
76	49.80	22.10	309.65	1.852
77	50.10	24.10	310.85	1.884
78	50.50	20.30	312.46	1.824
79	51.10	29.60	314.87	1.972
80	51.50	29.70	316.48	1.974
81	52.00	32.00	318.48	2.010
82	52.20	31.00	319.29	1.994
83	52.80	21.90	321.70	1.849
84	53.60	40.80	324.91	2.151
85	54.10	30.00	326.92	1.978
86	54.50	26.30	328.53	1.919
87	54.90	29.90	330.13	1.977
88	55.50	15.00	332.54	1.739
89	55.80	12.90	333.75	1.706
90	56.40	18.00	336.16	1.787
91	56.70	17.50	337.37	1.811
92	57.10	13.20	338.97	1.711
93	57.80	19.90	341.79	1.817
94	58.80	20.60	345.80	1.829
95	59.00	22.80	346.61	1.864
96	59.40	23.60	348.21	1.876
97	59.80	30.30	349.82	1.983
98	60.50	16.40	352.63	1.762
99	61.20	25.00	355.44	1.899
100	61.60	26.60	357.05	1.924

TABLE 6-8 (Continued)

PEACE BOREHOLE KAR-01

J	DIGITIZED DEPTH, X (DIV)	DIGITIZED DENSITY, Y (DIV)	COMPUTED DEPTH (FT)	COMPUTED DENSITY (GM/CC)
101	67.30	26.60	379.95	1.924
102	68.00	29.70	382.76	1.974
103	68.30	39.00	383.97	2.122
104	69.00	31.80	386.78	2.007
105	69.70	40.00	389.59	2.136
106	70.30	52.30	392.00	2.334
107	70.90	38.10	394.41	2.108
108	71.60	52.60	397.23	2.339
109	72.00	40.00	398.83	2.136
110	72.80	25.00	402.05	1.899
111	73.20	39.00	403.65	2.122
112	73.50	40.60	404.86	2.148
113	74.00	34.00	406.87	2.042
114	74.30	32.70	408.07	2.022
115	75.10	40.00	411.29	2.138
116	76.00	37.00	414.90	2.090
117	76.20	33.20	415.71	2.030
118	77.00	43.00	418.92	2.186
119	77.60	22.20	421.33	1.854
120	78.20	36.50	423.74	2.083
121	78.80	33.40	426.15	2.033
122	79.50	48.00	428.96	2.202
123	80.30	21.70	432.18	1.846
124	80.70	31.30	433.78	1.999
125	81.30	12.20	436.20	1.695
126	82.00	31.00	439.01	1.994
127	82.70	37.00	441.82	2.090
128	83.10	34.50	443.43	2.050
129	83.50	34.60	445.03	2.052
130	84.00	37.00	447.04	2.090
131	84.60	36.10	449.45	2.076
132	85.00	37.60	451.06	2.100
133	85.40	37.00	452.67	2.090
134	86.00	33.50	455.08	2.034
135	86.50	33.50	457.09	2.034
136	86.80	31.80	458.29	2.007
137	87.30	36.00	460.30	2.074
138	87.90	34.10	462.71	2.044
139	88.10	36.70	463.51	2.085
140	88.80	21.00	466.33	1.835
141	89.00	25.00	467.13	1.899
142	89.40	18.00	468.74	1.787
143	90.00	41.00	471.15	2.154
144	90.30	44.00	472.35	2.202
145	90.70	42.00	473.96	2.170
146	91.20	32.00	475.97	2.010
147	91.70	37.00	477.98	2.090
148	92.10	41.50	479.58	2.162
149	92.70	36.30	481.99	2.079
150	93.10	45.00	483.60	2.218
151	93.80	25.00	486.41	1.899
152	94.40	20.30	488.82	1.824
153	94.70	23.20	490.03	1.870
154	95.20	2.00	492.04	1.532
155	96.10	17.20	495.65	1.774
156	96.70	12.40	498.06	1.698
157	97.10	18.70	499.67	1.798
158	97.70	12.00	502.08	1.691
159	98.30	28.20	504.49	1.950
160	98.60	30.50	505.70	1.986
161	99.50	22.00	509.31	1.851
162	100.60	35.00	513.73	2.058
163	101.20	38.90	516.14	2.120
164	101.40	38.40	516.95	2.112
165	101.90	31.40	518.95	2.001
166	102.20	34.50	520.16	2.050
167	102.70	30.00	522.17	1.978
168	103.00	28.30	523.37	1.951
169	103.30	26.00	524.58	1.915
170	103.70	30.00	526.19	1.978
171	104.00	32.50	527.39	2.018
172	104.20	31.30	528.19	1.999
173	104.50	31.10	529.40	1.996
174	105.00	31.30	531.41	1.999
175	105.30	31.10	532.61	1.996
176	105.80	32.00	534.62	2.010
177	106.10	32.10	535.83	2.012
178	106.50	35.00	537.43	2.058
179	107.30	38.00	540.65	2.106
180	107.90	38.00	543.06	2.106
181	108.30	40.00	544.67	2.138
182	108.80	38.60	546.67	2.116
183	108.90	38.50	547.08	2.114
184	109.50	40.70	548.68	2.149
185	110.00	37.20	551.50	2.093
186	110.50	25.10	553.50	1.900
187	111.60	24.70	557.92	1.967
188	112.30	23.70	560.74	1.678
189	113.20	30.00	564.35	1.978
190	113.80	32.90	566.76	2.025
191	114.40	28.80	569.17	1.959
192	115.00	36.90	571.58	2.089
193	115.40	36.00	573.19	2.074
194	115.80	37.60	574.80	2.100
195	116.30	35.00	576.81	2.058
196	117.60	30.80	582.03	1.978
197	118.30	29.40	584.84	1.969
198	119.10	25.80	588.05	1.911
199	120.40	33.70	593.28	2.133
200	121.30	40.60	596.89	2.148

PEACE BOREHOLE KAR-01

J	DIGITIZED DEPTH, X (DIV)	DIGITIZED DENSITY, Y (DIV)	COMPUTED DEPTH (FT)	COMPUTED DENSITY (GM/CC)
201	121.70	40.00	598.50	2.138
202	122.30	45.60	600.91	2.227
203	122.80	42.00	602.92	2.170
204	123.10	34.50	604.12	2.050
205	124.00	34.00	607.74	2.042
206	124.40	35.70	609.35	2.069
207	124.80	36.00	610.95	2.074
208	125.40	37.50	613.36	2.098
209	126.00	36.80	615.77	2.087
210	126.50	37.40	617.78	2.096
211	126.80	37.00	618.99	2.090
212	127.20	37.00	620.60	2.090
213	127.70	36.00	622.60	2.074
214	128.10	36.20	624.21	2.077
215	128.70	32.30	626.62	2.015
216	129.20	33.90	628.63	2.041
217	129.60	32.00	630.24	2.010
218	129.80	31.50	631.04	2.002
219	130.20	32.90	632.65	2.025
220	131.00	31.50	635.86	2.002
221	131.70	33.40	638.67	2.033
222	132.70	31.00	642.69	1.994
223	133.00	32.40	643.90	2.017
224	133.90	32.90	647.51	2.025
225	134.40	30.40	649.52	1.985
226	134.80	31.50	651.13	2.002
227	135.20	34.30	652.74	2.047
228	135.40	34.00	653.54	2.042
229	136.10	34.30	656.35	2.047
230	136.70	32.90	658.76	2.025
231	136.90	33.10	659.57	2.028
232	137.40	32.80	661.57	2.023
233	138.00	34.30	663.98	2.047
234	138.40	34.00	665.59	2.042
235	138.90	35.00	667.60	2.058
236	139.40	35.20	669.61	2.061
237	139.90	36.50	671.62	2.082
238	140.30	36.90	673.22	2.089
239	141.10	34.50	676.44	2.050
240	141.80	37.00	679.25	2.090
241	142.20	37.90	680.86	2.104
242	142.40	37.50	681.66	2.098
243	143.10	33.10	684.47	2.028
244	143.90	33.40	687.69	2.033
245	144.20	34.40	688.89	2.049
246	144.70	32.50	690.90	2.018
247	145.90	32.30	691.70	2.015
248	145.30	34.00	693.31	2.042
249	146.50	36.00	698.13	2.074
250	146.70	37.60	698.94	2.100
251	147.20	38.00	700.94	2.106
252	147.80	37.60	703.36	2.100
253	148.10	35.60	704.56	2.068
254	148.30	35.30	705.36	2.063
255	148.80	38.00	707.37	2.106
256	149.30	38.40	709.38	2.112
257	149.50	39.60	710.18	2.132
258	149.80	39.50	711.39	2.130
259	150.10	39.10	712.60	2.124
260	150.50	40.00	714.20	2.138
261	150.90	39.70	715.81	2.133
262	151.30	37.00	717.42	2.090
263	151.60	36.20	718.62	2.077
264	152.10	37.50	720.63	2.098
265	152.70	36.10	723.04	2.076
266	153.20	39.00	725.05	2.122
267	153.40	39.30	725.85	2.127
268	153.90	39.00	727.86	2.122
269	154.30	39.50	729.47	2.130
270	155.10	37.70	732.68	2.101
271	155.80	39.70	735.49	2.133
272	156.70	36.00	739.11	2.074
273	157.20	36.40	741.12	2.081
274	157.60	35.60	742.73	2.068
275	157.90	35.40	743.93	2.065
276	158.30	37.50	745.54	2.098
277	158.70	38.20	747.15	2.109
278	159.30	35.80	749.56	2.071
279	160.00	37.60	752.37	2.100
280	160.50	37.20	754.38	2.093
281	161.10	38.50	756.79	2.114
282	161.50	38.20	758.39	2.109
283	161.80	37.50	759.60	2.098
284	162.30	37.70	761.61	2.101
285	162.70	36.50	763.22	2.082
286	163.20	39.20	765.22	2.125
287	164.30	33.50	769.64	2.034
288	164.90	33.30	772.05	2.031
289	165.20	32.60	773.26	2.023
290	165.70	34.50	775.27	2.050
291	166.80	38.10	779.69	2.108
292	168.20	36.20	785.31	2.077
293	168.60	34.20	786.92	2.045
294	169.10	36.80	788.93	2.087
295	169.80	37.50	791.74	2.098
296	170.30	36.90	793.75	2.089
297	170.70	38.30	795.35	2.111
298	171.30	38.10	797.77	2.108
299	171.80	38.40	799.77	2.112
300	172.50	37.60	802.59	2.100

TABLE 6-8 (Continued)

PEACE BOREHOLE KAR-01

J	DIGITIZED DEPTH, X (DIV)	DIGITIZED DENSITY, Y (DIV)	COMPUTED DEPTH (FT)	COMPUTED DENSITY (GM/CC)
301	173.30	39.00	805.80	2.122
302	173.60	38.00	807.81	2.106
303	174.10	36.40	809.01	2.049
304	174.70	31.80	811.42	2.007
305	175.40	35.00	814.24	2.058
306	176.00	34.20	816.65	2.045
307	176.20	32.20	817.45	2.014
308	176.50	32.00	818.66	2.010
309	176.90	30.40	820.26	1.985
310	177.50	30.10	822.67	1.980
311	178.00	28.10	824.68	1.948
312	178.70	34.00	827.49	2.042
313	179.20	40.30	829.50	2.143
314	180.10	31.30	833.12	1.999
315	180.60	37.00	835.93	2.090
316	181.00	37.30	836.73	2.095
317	181.30	36.00	837.94	2.074
318	181.80	31.80	839.95	2.007
319	182.30	36.50	841.96	2.082
320	182.90	38.70	844.37	2.117
321	184.10	31.30	849.19	1.999
322	184.70	35.00	851.60	2.058
323	185.30	37.30	854.01	2.095
324	185.70	36.00	855.62	2.074
325	186.00	34.20	856.82	2.045
326	186.30	32.90	858.03	2.025
327	187.30	39.40	862.04	2.128
328	187.80	37.70	864.05	2.101
329	188.20	36.40	865.66	2.112
330	188.50	37.60	866.87	2.100
331	188.90	34.20	868.47	2.045
332	189.50	35.50	870.88	2.066
333	190.00	32.30	872.89	2.015
334	190.50	32.30	874.90	2.015
335	190.60	31.20	875.30	1.998
336	191.20	30.90	877.71	1.993
337	192.00	38.00	880.93	2.106
338	192.60	35.40	883.34	2.065
339	193.20	33.70	885.75	2.037
340	194.20	36.30	889.76	2.111
341	194.50	37.50	890.97	2.098
342	195.10	34.90	893.38	2.042
343	195.70	38.10	895.79	2.108
344	196.10	38.00	897.40	2.106
345	197.00	44.00	901.01	2.202
346	197.30	41.50	902.22	2.162
347	197.80	40.80	904.23	2.151
348	198.00	39.30	905.03	2.127
349	198.60	39.50	907.44	2.130
350	199.20	36.20	909.85	2.109
351	199.50	35.50	911.06	2.066
352	199.90	35.30	912.66	2.063
353	200.40	38.00	914.67	2.106
354	200.60	42.00	915.48	2.170
355	201.00	42.40	917.08	2.176
356	201.50	41.00	918.29	2.154
357	202.00	36.90	921.10	2.089
358	202.40	38.90	922.71	2.120
359	202.90	39.10	924.72	2.124
360	203.90	43.10	928.73	2.187
361	204.00	41.00	929.14	2.154
362	204.60	37.40	931.55	2.096
363	205.10	40.70	933.56	2.149
364	205.70	37.70	935.97	2.101
365	206.10	40.50	937.57	2.146
366	206.80	39.30	940.38	2.127
367	207.20	40.90	941.99	2.152
368	207.40	41.20	942.80	2.157
369	208.10	44.60	945.61	2.211
370	208.80	40.50	948.42	2.146
371	209.00	36.50	949.22	2.082
372	209.50	34.10	951.23	2.044
373	210.60	40.80	955.65	2.151
374	211.40	28.90	958.86	1.961
375	212.20	36.90	962.08	2.089
376	213.50	36.40	967.30	2.081
377	214.00	37.30	969.31	2.095
378	214.70	34.30	972.12	2.047
379	215.50	36.00	975.34	2.074
380	215.90	39.50	976.94	2.130
381	216.50	38.70	979.35	2.117
382	218.20	47.50	986.18	2.258
383	219.00	39.30	989.40	2.127
384	219.30	40.00	990.60	2.138
385	220.40	38.00	995.02	2.106
386	222.30	28.00	1002.66	1.947
387	223.10	36.60	1005.87	2.084
388	223.70	33.00	1008.28	2.026
389	224.00	32.50	1009.48	2.018
390	224.50	40.00	1011.49	2.138
391	225.00	40.60	1013.50	2.148
392	225.40	36.30	1015.11	2.111
393	226.00	30.70	1017.52	1.990
394	226.70	33.50	1020.33	2.034
395	227.10	37.90	1021.94	2.104
396	228.00	34.10	1025.55	2.044
397	228.70	37.00	1028.37	2.090
398	229.20	40.30	1030.38	2.143
399	230.00	32.50	1033.59	2.018
400	230.50	32.40	1035.60	2.017

PEACE BOREHOLE KAR-01

J	DIGITIZED DEPTH, X (DIV)	DIGITIZED DENSITY, Y (DIV)	COMPUTED DEPTH (FT)	COMPUTED DENSITY (GM/CC)
401	230.90	30.00	1037.21	1.978
402	231.00	30.50	1037.61	1.986
403	231.90	30.50	1041.22	1.986
404	232.50	36.00	1043.63	2.074
405	233.00	35.00	1045.64	2.058
406	233.20	33.50	1046.45	2.034
407	233.60	32.90	1048.05	2.025
408	234.30	34.10	1050.86	2.044
409	234.70	32.50	1052.47	2.018
410	235.00	29.50	1053.68	1.970
411	236.00	32.20	1057.69	2.014
412	236.60	32.00	1060.10	2.010
413	237.40	35.10	1063.32	2.060
414	238.20	31.00	1066.53	1.994
415	238.80	32.50	1068.94	2.018
416	239.20	32.40	1070.55	2.017
417	240.00	38.00	1073.76	2.106
418	240.20	43.50	1074.57	2.194
419	240.70	45.70	1076.58	2.229
420	241.00	44.00	1077.78	2.202
421	241.40	41.50	1079.39	2.162
422	241.90	39.40	1081.40	2.128
423	242.20	36.70	1082.60	2.085
424	242.50	36.40	1083.81	2.081
425	243.00	37.50	1085.82	2.098
426	243.30	36.00	1087.02	2.074
427	244.20	34.40	1090.64	2.049
428	244.80	36.70	1093.05	2.085
429	245.10	34.00	1094.25	2.042
430	245.30	31.00	1095.06	1.994
431	245.60	30.10	1096.26	1.980
432	245.90	30.00	1097.47	1.978
433	246.10	29.20	1098.27	1.966
434	246.30	29.00	1099.07	1.963
435	247.00	29.30	1101.89	1.967
436	247.70	37.50	1104.70	2.098
437	248.20	34.30	1106.71	2.047
438	248.50	33.40	1107.91	2.033
439	248.80	29.00	1109.12	1.963
440	249.10	30.10	1110.32	1.980
441	249.60	30.10	1112.33	1.980
442	250.00	33.80	1113.94	2.039
443	250.70	31.00	1116.75	1.994
444	251.20	32.30	1118.76	2.015
445	251.60	32.70	1120.37	2.022
446	252.00	34.80	1121.97	2.055
447	252.50	35.00	1123.98	2.058
448	253.20	29.80	1126.79	1.975
449	254.00	33.50	1130.01	2.034
450	254.60	31.00	1132.42	1.994
451	255.00	31.40	1134.03	2.001
452	255.60	30.00	1136.44	1.978
453	256.00	32.00	1138.04	2.010
454	256.70	32.90	1140.86	2.018
455	257.00	36.00	1142.06	2.074
456	257.20	36.50	1142.86	2.082
457	257.40	36.00	1143.67	2.074
458	258.00	26.00	1146.08	1.915
459	258.50	35.00	1148.09	2.058
460	258.80	37.00	1149.29	2.090
461	259.40	35.00	1150.90	2.058
462	259.70	30.70	1152.91	1.990
463	260.30	34.20	1155.32	2.045
464	261.00	32.40	1158.13	2.017
465	261.30	34.20	1159.34	2.045
466	261.80	33.10	1161.34	2.124
467	262.50	32.90	1164.16	2.025
468	263.00	34.00	1166.17	2.042
469	263.90	31.00	1169.78	1.994
470	264.50	34.10	1172.19	2.044
471	265.00	34.00	1174.20	2.042
472	265.40	33.10	1175.81	2.060
473	265.80	34.50	1177.41	2.050
474	266.40	34.20	1179.82	2.045
475	266.60	33.20	1180.63	2.030
476	267.00	34.40	1182.23	2.057
477	267.40	33.20	1183.84	2.061
478	267.70	36.70	1185.05	2.085

YO, B, S:	.00	1.50	62.70	
XO, A, B, C:	30.00	230.10	875.00	217.80

APPENDIX 6-2

DENSITIES OF "CORAL" AND ITS SOLID COMPONENT AS CONTINUOUS FUNCTIONS OF DEPTH

Data on the composition of coral solids[1] place its density ρ_S in a narrow range of values (2.71 to 2.93 g/cc; see Tremba and Ristvet, 1986). Within that range, however, ρ_S varies erratically over the discrete set of borehole depths for which solid composition has been measured. Hence, in a given borehole, straight-line connections between measured (ρ_S,z)-points embody virtually all the extant information on the continuous change of ρ_S with depth (or altitude) z. At that level of description, we have:

$$\rho_S = [(z-z_m)\rho_S^{m+1} + (z_{m+1}-z)\rho_S^{m}]/(z_{m+1}-z_m) \quad ; m=1,2,\ldots,M \qquad \textbf{Eq. (13)}$$

with (ρ_S^m, z_m) denoting point m of the set measured for a given borehole, and with the points so ordered that depth decreases as m increases.

For the same borehole, let the z_j-points of Eq. (11) also be ordered so that depth decreases as j increases. Now, merge the two sets of z-values, and number different z's of the combined set in the order of decreasing depth (again), obtaining thereby the values z_k (k=1,2,...,K+1). The z-interval between z_k and z_{k+1} (k=1,2,...,K) must then lie entirely within one of the z-intervals on which ρ (the density of coral) has the linear depth-dependence specified by Eq. (11); it must also lie entirely within one of the z-intervals of linear variation of ρ_S (the density of the coral solid) specified by Eq. (13). However, a given z_k-value need not appear among the z_j's of Eq. (11); if not, then, at $z=z_k$, the value of ρ $(=\rho_k)$ is obtained from Eq. (11) for the z_j-interval in which $z=z_k$ falls. Likewise, for a z_k-value not among the z_m's of Eq. (13), we find the z_m-interval in which z_k falls, and use Eq. (13) to compute ρ_S at z_k $(\rho_S=\rho_S^k)$. Eqs. (11) and (13) can then be replaced by the following equivalent relations:

$$\begin{aligned} \rho &= [(z-z_k)\ \rho_{k+1}^- + (z_{k+1}-z)\ \rho_k^+]/(z_{k+1}-z_k) \\ \rho_S &= [(z-z_k)\ \rho_S^{k+1} + (z_{k+1}-z)\ \rho_S]/(z_{k+1}-z_k) \end{aligned} \quad ; k=1,2,\ldots,K \qquad \textbf{Eq. (14)}$$

In accord with Appendix 6-1, $\rho_k^- = \rho_k^+ = \rho_k$ for the γ-γ profiles; for the BHG profiles, $\rho_k^+ = \rho_{k+1}^- = \rho_{k+1/2}$, where $\rho_{k+1/2} = \rho_{j+1/2}$ -- the value of j being set by the requirement that the interval from z_k to z_{k+1} lie on the interval of Table 6-7 from z_j to z_{j+1}.

For each borehole included in the BHG survey, Table 6-9 (located in this Appendix) presents the depths z_k (k=1,2,...,K+1) that mark the endpoints of

---

[1] See footnote 3 on page 6-1 for explanation of use of "coral" in this text.

the depth-intervals on which both ρ and ρ_S are simple linear functions of z [Eq. (14)]. For each depth z_k, the density of either coral or its solid component is also shown (third and fourth columns of table). Where blank spaces appear between two listed values of coral density ρ (called "BHG DENSITY" in tbl. 6-9), those two ρ's are identical; that same value applies everywhere between them. Also, where values of ρ appear, the density ρ_S of coral's solid component does not; the value of ρ_S at that blank spot is given by Eq. (13) with z equal to the depth listed (or to its negative, if z denotes height).

MASS OF SOLID AS A CONTINUOUS FUNCTION OF DEPTH IN A BOREHOLE

Table 6-9 (in this Appendix 6-2) and Eqs. (13) allow ρ and ρ_S to be computed for any depth and borehole covered by the BHG survey. Hence, the mass m_s of coral solid can also be computed from Eq. (5). In fact, given piecewise linear dependence of ρ and ρ_S on z [Eq. (14)], m_s can be expressed in terms of z using only elementary functions. In particular, if z lies between z_k and z_{k+1}, then:

$$m_S = m_S^k + \int_{z_k}^{z} \rho_S \left(\frac{\rho - \rho_L}{\rho_S - \rho_L} \right) dh \quad ; \quad k = 1,2,..,K \qquad \textbf{Eq. (15)}$$

where $m_s^1 = 0$ and

$$m_S^k = m_S^{k-1} + \int_{z_{k-1}}^{z_k} \rho_S \left(\frac{\rho - \rho_L}{\rho_S - \rho_L} \right) dh \quad ; \quad k = 2,3,..,K+1 \qquad \textbf{Eq. (16)}$$

Next, observing that $\rho_S/(\rho_S-\rho_L)=(\rho_S-\rho_L+\rho_L)/(\rho_S-\rho_L)$, we can write Eq. (15) as follows:

$$m_S = m_S^k + \int_{z_k}^{z} [(\rho - \rho_L) + \rho_L \left(\frac{\rho - \rho_L}{\rho_S - \rho_L} \right)] \, dh \qquad \textbf{Eq. (17)}$$

Replacing ρ and ρ_S in Eq. (17) by their linear equivalents in terms of z [Eq. (14)], we obtain

$$m_S = m_S^k + \int_{z_k}^{z} \left\{ a_k + b_k(h-z_k) + \rho_L \left[\frac{a_k + b_k(h-z_k)}{a_k' + b_k'(h-z_k)} \right] \right\} dh \qquad \textbf{Eq. (18)}$$

where

$$a_k = \rho_k - \rho_L, \; b_k = (\rho_{k+1} - \rho_k)/(z_{k+1} - z_k); \; a_k' = \rho_S - \rho_L, \; b_k' = (\rho^{k+1} - \rho_S^k)/(z_{k+1} - z_k) \qquad \textbf{Eq. (19)}$$

The integral of Eq. (17) is readily found as an explicit function of z (Pierce, 1929)

$$m_S = m_S^k + a_k x + b_k x^2 + \rho_L \left[\frac{b_k x}{b'_k} + \frac{(a_k b'_k - a'_k b_k)}{(b'_k)^2} \cdot \ln\left(\frac{a'_k + b'_k x}{a'_k} \right) \right] \qquad \text{Eq. (20)}$$

where $x = z - z_k$.

From Eq. (16), it follows that $m_S = m_S^{k+1}$, when z is set equal to z_{k+1} in Eq. (20); with m_S^{k+1} known, a similar computation then gives m_S^{k+2}, etc. Thus, using the depths and densities of Table 6-9, the m_S^k-values (k=2,...,K+1) can be computed in sequence from Eq. (20). For each borehole of the BHG survey, the resulting values of m_S^2, m_S^3, m_S^{K+1} appear in the seventh column of Table 6-9, starting at the greatest depth logged in that hole. Listed in the sixth column is an approximation to m^k -- $\underline{m}_S$, say -- obtained by setting ρ_S equal to its mid-value $\underline{\rho}_S^k \equiv 1/2(\rho_S^{k+1} + \rho_S^k)$, the mean of ρ_S on the z-interval from z_k to z_{k+1}. Using that value for ρ_S in the integral of Eq. (15), but with ρ still related to z by Eq. (14), we can write

$$m_S \approx \underline{m}_S = \underline{m}_S^k + \frac{\underline{\rho}_S^k}{\underline{\rho}_S^k - \rho_L} \int_{z_k}^{z} (\rho - \rho_L)\, dh = \underline{m}_S^k + (a_k x + b_k x^2)\underline{\rho}_S^k / (\underline{\rho}_S^k - \rho_L) \qquad \text{Eq. (21)}$$

where $\underline{m}_S^1 = 0$, and $\underline{m}_S^{k+1}$ is the value obtained for $\underline{m}_S$ by setting z equal to z_{k+1} in Eq. (21) (or $x = z_{k+1} - z_k$). Replacing the $\underline{\rho}_S^k$ (k=1,2,...,K) of Eq. (21), for all k, by the single value 2.821 g/cc (half the sum of aragonite and calcite densities) yields yet a coarser estimate of m_S, and the approximate values of m_S^k listed in the fifth column of Table 6-9.

Table 6-10 (also located in Appendix 6-2), identical in format and derivation to Table 6-9, differs from Table 6-9 only in that the density profiles on which it rests came from γ-γ logging (not from BHG surveys).

DENSIFICATION: THICKNESS CHANGES AS CONTINUOUS FUNCTIONS OF DEPTH IN CRATER HOLES

Eq. (20) allows us to compute the solid mass per unit cross-section, m_S^a, from the greatest depth logged to the depth at $z=z_a$ in a given borehole. The horizon at z_a in the given borehole -- horizon "a" -- will generally have somewhat different depth in a second borehole[1]. Let $z=z_a^*$ at that horizon in the latter hole, with m_S^{a*} denoting solid mass (per unit cross-section) in the second hole, from the greatest depth logged therein to horizon "a". For any

---

[1] As needed, the depths to a given horizon in different boreholes have been found herein by linear interpolation among the horizon-depths fixed by PEACE Program geologists (see Chapter 7 of the current Report, particularly tbls. 7-2 and 7-4).

depth above "a" in the first borehole, the solid mass between "a" and that depth is equal to $m_S - m_S^a$ ($\equiv \Delta m_S$), where m_S is computed to the depth in question from Eq. (20), using the a_k- and b_k-values for that first borehole. Likewise, in the second borehole, the solid mass from "a" to a given depth above "a" is equal to $m_S - m_S^{a*}$ ($\equiv \Delta m_S^*$), with m_S computed from Eq. (20) using a_k- and b_k-values appropriate to that borehole. For each choice of z in the second hole -- $z=z^*$, say -- Δm_S^* can be computed simply by evaluating the right-hand member of Eq. (20) and subtracting m_S^{a*} from the result. However, in the first hole, finding the value of z at which the solid mass Δm_S above "a" is equal to Δm_S^*, plainly requires equating Δm_S to Δm_S^*. The relation determining z is therefore the following:

$$\Delta m_S^* + m_S^a = m_S^k + a_k x + b_k x^2 + \rho_L \left[\frac{b_k x}{b_k'} + \frac{(a_k b_k' - a_k' b_k)}{(b_k')^2} \ln\left(\frac{a_k' + b_k' x}{a_k'} \right) \right] \qquad \text{Eq. (22)}$$

where $x = z - z_k$.

Eq. (22), which is transcendental, can be solved for x (hence z) by numerical means. Exactly one value of x satisfies it because m_S [Eq. (20)] increases monotonically as depth decreases, and the mass Δm_S^* above horizon "a" in the second borehole is ≥ 0. Solution of Eq. (22) for x is greatly expedited by foreknowledge of m_k (k=1,2,...,K): As k is increased from k=1, it reaches a level at which positive values of $\Delta m_S^* + m_S^a - m_S^k$ turn negative; the root of Eq. (21) must lie on the z_k-interval over which that change of sign occurs. With the root of Eq. (22) so bounded, it can be found easily by search or iteration. Repeating the process for a series of ever-shallower z's gives a set of (z^*,z) pairs for which the solid mass between horizon "a" ($z=z_a^*$) and level z^* in the second hole is equal to that between "a" ($z=z_a$) and level z in the first. The height of the column between z_a and z is $z-z_a$ (or its negative if z denotes depth); $z^*-z_a^*$ gives the corresponding height in the second hole (for equal mass above "a"). If the two holes are actually the same, but with pre- and post-shot density profiles representing the "second" and "first" holes, respectively, then $z-z_a$ and $z^*-z_a^*$ (or their negatives) give the post- and pre-shot thicknesses of a column above "a" that contains the same mass of solid at both times. The change in that column's thickness due to shot-induced changes in density is just $(z^*-z_a^*)-(z-z_a)$ (or its negative).

Under the key assumption given previously on pages 6-7 and 6-8, the pre-shot profiles are found today in control holes -- whence, we do in fact compute (z^*,z) pairs from profiles in different holes. A detail of the calculation (noted previously on pages 6-8 through 6-10) lies in redefining horizon "a" at each successive geologic horizon met along the stepwise march in z^* (from depth toward the sea floor). With z^* referring to the control hole, z is then allowed to shift suddenly to its value, in the crater hole, at a newly encountered geologic horizon. Geologic horizons are thereby strictly retained as Lagrangian surfaces, regardless of departures from the ideal of simple subsidence, or of actual differences between pre-shot density profiles

and control-hole profiles. In addition (see p.6-8 through 6-10), differences in column height are thereby computed from densities in materials that are (as nearly as possible) the same.[1]

Curves of thickness-change vs. depth are plotted as a series of dots when z^* refers to a control hole (jumps in z can then occur, marking shifts to geologic crater-hole horizons). When z^* refers to a crater hole, curves of thickness-change vs. depth are drawn with dashes (jumps in z then mark shifts to geologic horizons in control holes). The mean of a dotted and dashed curve is also drawn, as a continuous line.

As functions of present crater-hole depth, the thickness changes computed from profiles of the BHG survey were presented in preceeding sections (p. 6-7 and 6-8 and 6-8 through 6-10) (see figs. 6-4 through 6-9). Corresponding curves, deduced from γ-γ density profiles, appear on succeeding pages as Figures 6-27 through 6-53.

REFERENCES CITED

See pages 6-35 and 6-36 for references cited in this Appendix.

---

[1] Thickness-change curves were first computed with horizon "a" fixed near Contour D. Except for larger gaps between end-of-data and the sea floor, there are no appreciable differences between those curves and the ones presented in this report -- and no change at all in conclusions drawn from them (conclusions first reached, in fact, with horizon "a" fixed).

BOREHOLE 00R-17

K	PEACE DEPTH (FT)	BHG DENSITY (GM/CC)	DENSITY OF SOLID COMPONENT (GM/CC)	CUMULATIVE SOLID MASS (GM/CM**2) RHO=2.821	RHO=<RHO>	LINEAR SPLINE FOR RHO
0	1000.00		2.8210			
1	1140.81		2.8210			
2	1140.80		2.7262			
3	1134.50		2.7149			
4	1120.50		2.7364			
5	1110.50		2.7303			
6	1102.20		2.7344			
7	1092.60		2.7201			
8	1080.50		2.7242			
9	1065.50		2.7262			
10	1049.70		2.7242			
11	1032.80		2.7303			
12	1015.20		2.7385			
13	1023.40		2.7201			
14	1013.40		2.7140			
15	1002.70		2.7242			
16	993.20		2.7343			
17	990.90		2.8633			
18	975.20		2.8700			
19	962.90		2.7888			
20	939.20		2.8965			
21	921.40		2.9151			
22	912.20		2.8928			
23	891.00	2.013		0.	0.	0.
24	889.20		2.9183	85.	84.	84.
25	870.20		2.9159	944.	966.	966.
26	857.00	2.013		1609.	1579.	1579.
27	857.00	2.018		1609.	1579.	1579.
28	852.60		2.9206	1818.	1784.	1784.
29	840.20		2.9202	2408.	2363.	2363.
30	827.00	2.018		3036.	2978.	2978.
31	827.00	2.036		3036.	2978.	2978.
32	826.20		2.9252	3074.	3016.	3016.
33	812.30		2.9241	3767.	3676.	3676.
34	794.20		2.9186	4628.	4536.	4536.
35	789.00	2.036		4876.	4783.	4783.
36	789.00	1.993		4876.	4783.	4783.
37	785.20		2.9082	5052.	4956.	4956.
38	762.30		2.9206	6114.	5999.	5999.
39	751.50		2.9130	6614.	6490.	6490.
40	747.00	1.993		6823.	6695.	6695.
41	747.00	2.013		6823.	6695.	6695.
42	737.80		2.9183	7256.	7122.	7122.
43	728.70		2.8836	7925.	7779.	7779.
44	718.00	2.013		8432.	8279.	8279.
45	718.00	2.018		8432.	8279.	8279.
46	700.20		2.8948	9040.	8879.	8879.
47	683.00	2.018		9858.	9686.	9686.
48	683.00	2.036		9858.	9686.	9686.
49	666.80		2.8928	10643.	10459.	10459.
50	652.70		2.8768	11326.	11134.	11134.
51	645.00	2.036		11698.	11503.	11503.
52	645.00	1.993		11698.	11503.	11503.
53	628.30		2.8588	12475.	12270.	12270.
54	618.60		2.8610	12922.	12716.	12716.
55	603.00	1.993		13646.	13431.	13431.
56	603.00	1.976		13646.	13431.	13431.
57	602.90		2.8997	13650.	13436.	13436.
58	584.20		2.8543	14411.	14188.	14188.
59	578.50		2.7282	14762.	14541.	14541.
60	560.00	1.976		15604.	15401.	15401.
61	560.00	1.974		15604.	15401.	15401.
62	558.70		2.7242	15663.	15461.	15461.
63	533.60		2.7303	16804.	16625.	16625.
64	528.00	1.974		17059.	16884.	16884.
65	528.00	2.027		17059.	16884.	16884.
66	525.90		2.7364	17160.	16987.	16987.
67	508.20		2.7282	18009.	17852.	17852.
68	505.00	2.027		18163.	18009.	18009.
69	505.00	1.977		18163.	18009.	18009.
70	502.60		2.7282	18272.	18120.	18120.
71	502.20		2.7364	18290.	18139.	18139.
72	491.20		2.7262	18793.	18652.	18652.
73	481.20		2.7242	19253.	19120.	19120.
74	477.00	1.987		19446.	19317.	19317.
75	477.00	1.976		19446.	19317.	19317.
76	470.20		2.7282	19756.	19633.	19633.
77	456.20		2.7241	20393.	20284.	20284.
78	446.00	1.976		20858.	20759.	20759.
79	446.00	1.967		20858.	20759.	20759.
80	441.20		2.7181	21075.	20980.	20980.
81	426.20		2.6777	21751.	21664.	21664.
82	420.40		2.7749	22013.	21926.	21926.
83	417.00	1.967		22166.	22082.	22082.
84	417.00	1.944		22166.	22082.	22082.
85	411.70		2.7262	22400.	22319.	22319.
86	408.70		2.7426	22884.	22812.	22812.
87	388.50		2.6743	23721.	23353.	23353.
88	388.00	1.944		23443.	23375.	23375.
89	388.00	1.951		23443.	23375.	23375.
90	376.20		2.7467	23966.	23902.	23902.
91	363.00	1.951		24552.	24491.	24491.
92	363.00	1.872		24552.	24491.	24491.
93	354.20		2.9136	24909.	24844.	24844.
94	345.00	1.872		25262.	25210.	25210.
95	345.00	1.801		25282.	25210.	25210.
96	344.20		2.9206	25316.	25243.	25243.
97	328.60		2.8565	25970.	25889.	25889.
98	317.00	1.801		26457.	26373.	26373.
99	317.00	2.036		26457.	26373.	26373.
100	297.50		2.7952	27401.	27319.	27319.

BOREHOLE 00R-17

K	PEACE DEPTH (FT)	BHG DENSITY (GM/CC)	DENSITY OF SOLID COMPONENT (GM/CC)	CUMULATIVE SOLID MASS (GM/CM**2) RHO=2.821	RHO=<RHO>	LINEAR SPLINE FOR RHO
101	289.00	2.036		27813.	27734.	27734.
102	289.00	1.882		27813.	27734.	27734.
103	286.20		2.7467	27926.	27851.	27851.
104	275.20		2.8341	28379.	28305.	28305.
105	271.00	1.882		28552.	28477.	28477.
106	271.00	1.993		28552.	28477.	28477.
107	264.80		2.8341	28824.	28749.	28749.
108	255.40		2.8454	29238.	29161.	29161.
109	257.00	1.993		30047.	29965.	29965.
110	257.00	1.947		30047.	29965.	29965.
111	253.70		2.8655	30192.	30109.	30109.
112	228.90		2.8432	30581.	30495.	30495.
113	212.00	1.947		31151.	31062.	31062.
114	207.20		2.8633			
115	192.20		2.8299			
116	186.60		2.8343			
117	177.50		2.8568			
118	164.20		2.8091			
119	157.90		2.8243			
120	151.70		2.8745			
121	143.20		2.8561			
122	128.50		2.8365			
123	124.20		2.9259			
124	113.80		2.9275			
125	107.20		2.9290			
126	86.20		2.9252			
127	66.90		2.9240			
128	56.30		2.9252			
129	56.29		2.8210			
130	.00		2.8210			

BOREHOLE 05R-21

K	PEACE DEPTH (FT)	BHG DENSITY (GM/CC)	DENSITY OF SOLID COMPONENT (GM/CC)	CUMULATIVE SOLID MASS (GM/CM**2) RHO=2.821	RHO=<RHO>	LINEAR SPLINE FOR RHO
0	3800.00		2.8210			
1	432.71		2.8210			
2	432.70		2.8432			
3	424.00	1.906		0.	0.	0.
4	421.50		2.7282	115.	117.	117.
5	411.40		2.8124	560.	567.	567.
6	404.00	1.886		921.	929.	929.
7	404.00	1.922		921.	929.	929.
8	401.60		2.7760	1024.	1033.	1033.
9	384.00	1.922		1780.	1794.	1794.
10	384.00	1.889		1780.	1794.	1794.
11	363.00		2.8387	2649.	2663.	2663.
12	354.80	1.889		3021.	3034.	3034.
13	354.00	1.890		3021.	3034.	3034.
14	346.80		2.8543	3320.	3330.	3330.
15	336.00		2.8588	3767.	3775.	3775.
16	324.00	1.890		4264.	4269.	4269.
17	324.00	1.888		4264.	4269.	4269.
18	320.90		2.8365	4393.	4397.	4397.
19	304.20		2.9476	5083.	5084.	5084.
20	294.00	1.888		5505.	5506.	5506.
21	294.00	1.945		5505.	5506.	5506.
22	291.00		2.7718	5637.	5639.	5639.
23	270.70		2.8124	6531.	6539.	6539.
24	264.00	1.945		6827.	6834.	6834.
25	264.00	1.911		6827.	6834.	6834.
26	260.50		2.8663	6975.	6982.	6982.
27	249.90		2.8508	7426.	7429.	7429.
28	234.00	1.911		8103.	8101.	8101.
29	234.00	1.837		8103.	8101.	8101.
30	218.90		2.8541	8690.	8684.	8684.
31	209.00	1.837		9075.	9066.	9066.
32	209.00	1.895		9075.	9066.	9066.
33	208.70		2.8633	9087.	9078.	9078.
34	190.00		2.8341	9821.	9809.	9809.
35	188.00	1.895		10057.	10044.	10044.
36	188.00	1.920		10057.	10044.	10044.
37	176.00		2.8168	10400.	10387.	10387.
38	159.00	1.920		11129.	11115.	11115.
39	159.00	1.969		11129.	11115.	11115.
40	146.00		2.8409	11729.	11714.	11714.
41	134.00	1.969		12263.	12263.	12263.
42	131.00		2.9066			
43	115.00		2.9298			
44	84.20		2.9290			
45	84.19		2.8210			
46	.00		2.8210			

TABLE 6-9. -- Mass of solid in vertical columns of unit cross-section, from BHG-survey data (continued on next 3 pages).

BOREHOLE OHT-20

K	PEACE DEPTH (FEET)	BHG DENSITY (GM/CC)	DENSITY OF SOLID COMPONENT (GM/CC)	CUMULATIVE SOLID MASS (GM/CM**2) RHO=2.821	RHO=<RHO>	LINEAR SPLINE FOR RHO
0	1800.00		2.8210			
1	591.41		2.8210			
2	591.40		2.8678			
3	581.00	1.929		0.	0.	0.
4	572.40		2.7571	372.	375.	375.
5	551.90		2.7242	1260.	1278.	1278.
6	551.00	1.929		1299.	1318.	1318.
7	537.40		2.7242	1888.	1919.	1919.
8	527.40		2.7241	2321.	2361.	2361.
9	521.00	1.929		2598.	2644.	2644.
10	521.00	1.949		2598.	2644.	2644.
11	511.40		2.7160	3014.	3069.	3069.
12	491.00	1.949		3926.	4000.	4000.
13	491.00	2.009		3926.	4000.	4000.
14	481.60		2.7242	4369.	4453.	4453.
15	471.00	2.009		4868.	4963.	4963.
16	471.00	2.048		4868.	4963.	4963.
17	464.80		2.7201	5172.	5273.	5273.
18	451.00	2.048		5848.	5964.	5964.
19	451.00	2.014		5846.	5964.	5964.
20	442.60		2.7181	6237.	6361.	6361.
21	432.10		2.7190	6745.	6879.	6879.
22	421.00	2.014		7269.	7416.	7416.
23	421.00	2.003		7269.	7416.	7416.
24	416.90		2.7344	7461.	7612.	7612.
25	401.90		2.7196	8164.	8321.	8321.
26	391.00	2.003		8674.	8829.	8829.
27	391.00	1.969		8674.	8829.	8829.
28	387.70		2.8974	8827.	8980.	8980.
29	367.40		2.8341	9764.	9909.	9909.
30	361.00	1.989		10060.	10203.	10203.
31	361.00	1.998		10060.	10203.	10203.
32	351.40		2.9090	10484.	10622.	10622.
33	332.40		2.8882	11324.	11449.	11449.
34	331.00	1.998		11386.	11510.	11510.
35	331.00	1.922		11386.	11510.	11510.
36	313.60		2.7824	12146.	12269.	12269.
37	303.30		2.8233	12576.	12700.	12700.
38	301.00	1.922		12675.	12799.	12799.
39	301.00	1.942		12675.	12799.	12799.
40	283.80		2.8277	13430.	13554.	13554.
41	272.40		2.8565	13931.	14052.	14052.
42	271.00	1.942		13993.	14113.	14113.
43	271.00	1.807		13993.	14113.	14113.
44	256.00	1.807		14554.	14673.	14673.
45	256.00	1.926		14554.	14673.	14673.
46	254.40		2.8341	14625.	14742.	14742.
47	233.60		2.8633	15521.	15635.	15635.
48	226.00	1.926		15849.	15959.	15959.
49	226.00	1.971		15849.	15959.	15959.
50	222.20		2.8951	16021.	16129.	16129.
51	211.40		2.8859	16511.	16612.	16612.
52	211.00	1.971		16529.	16630.	16630.
53	211.00	1.826		16529.	16630.	16630.
54	200.90		2.8856	16916.	17012.	17012.
55	190.40		2.7844	17319.	17414.	17414.
56	186.00	1.826		17488.	17584.	17584.
57	186.00	2.010		17488.	17584.	17584.
58	178.10		2.9090	17861.	17953.	17953.
59	165.90		2.8299	18436.	18523.	18523.
60	161.10		2.9198	18663.	18747.	18747.
61	160.00	2.010		18715.	18798.	18798.
62	160.00	1.848		18715.	18798.	18798.
63	146.60		2.9297	19243.	19316.	19316.
64	136.00	1.848		19661.	19726.	19726.
65	131.90		2.9096			
66	131.89		2.8210			
67	.00		2.8210			

BOREHOLE OHT-19

K	PEACE DEPTH (FEET)	BHG DENSITY (GM/CC)	DENSITY OF SOLID COMPONENT (GM/CC)	CUMULATIVE SOLID MASS (GM/CM**2) RHO=2.821	RHO=<RHO>	LINEAR SPLINE FOR RHO
0	1800.00		2.8210			
1	818.51		2.8210			
2	818.50		2.9096			
3	808.50		2.9151			
4	798.10		2.9042			
5	798.00	1.956		0.	0.	0.
6	783.50		2.9198	647.	635.	635.
7	768.80		2.9257	1311.	1287.	1287.
8	768.00	1.956		1338.	1313.	1313.
9	768.00	2.041		1338.	1313.	1313.
10	759.10		2.9148	1771.	1738.	1738.
11	749.10		2.9113	2257.	2216.	2216.
12	738.00	2.041		2798.	2747.	2747.
13	738.00	2.011		2798.	2747.	2747.
14	729.50		2.9139	3199.	3141.	3141.
15	708.00	2.011		4214.	4139.	4139.
16	708.00	2.018		4214.	4139.	4139.
17	700.10		2.8974	4590.	4509.	4509.
18	678.00	2.018		5641.	5544.	5544.
19	678.00	2.013		5641.	5544.	5544.
20	670.00		2.9066	6020.	5916.	5916.
21	659.50		2.8951	6516.	6405.	6405.
22	648.00	2.013		7061.	6945.	6945.
23	648.00	2.030		7061.	6945.	6945.
24	629.40		2.7242	7956.	7849.	7849.
25	618.00	2.030		8505.	8407.	8407.
26	618.00	2.040		8505.	8407.	8407.
27	598.60		2.8081	9448.	9358.	9358.
28	588.00	2.040		9963.	9873.	9873.
29	588.00	1.951		9963.	9873.	9873.
30	578.50		2.8343	10384.	10294.	10294.
31	558.00	1.951		11294.	11208.	11208.
32	558.00	1.948		11294.	11208.	11208.
33	549.00		2.7221	11691.	11613.	11613.
34	538.90		2.7140	12138.	12069.	12069.
35	528.00	1.948		12620.	12562.	12562.
36	528.00	1.998		12620.	12562.	12562.
37	515.50		2.7140	13202.	13158.	13158.
38	498.00	1.998		14018.	13993.	13993.
39	498.00	2.056		14018.	13993.	13993.
40	483.50		2.7181	14734.	14725.	14725.
41	468.00	2.056		15499.	15493.	15493.
42	468.00	2.046		15499.	15493.	15493.
43	448.00		2.7201	16477.	16474.	16474.
44	433.00	2.046		17211.	17221.	17221.
45	433.00	2.011		17211.	17221.	17221.
46	409.20		2.7995	18335.	18356.	18356.
47	403.00	2.011		18627.	18648.	18648.
48	403.00	2.008		18627.	18648.	18648.
49	393.50		2.8905	19792.	18811.	18811.
50	380.50		2.9040	19687.	19693.	19693.
51	380.00	2.008		19710.	19716.	19716.
52	380.00	1.922		19710.	19716.	19716.
53	358.00	1.922		20656.	20646.	20646.
54	358.00	1.972		20656.	20646.	20646.
55	355.50		2.9020	20769.	20758.	20758.
56	338.70		2.8365	21531.	21513.	21513.
57	328.00	1.972		22016.	21997.	21997.
58	328.00	1.948		22016.	21997.	21997.
59	311.10		2.7973	22763.	22746.	22746.
60	298.00	1.948		23343.	23327.	23327.
61	298.00	1.900		23343.	23327.	23327.
62	296.50		2.8233	23405.	23389.	23389.
63	278.00	1.900		24390.	24371.	24371.
64	278.00	1.906		24390.	24371.	24371.
65	251.90		2.8768	25281.	25254.	25254.
66	238.00	1.906		25867.	25834.	25834.
67	238.00	1.890		25867.	25834.	25834.
68	226.90		2.8700	26327.	26290.	26290.
69	216.30		2.8541	26766.	26725.	26725.
70	208.00	1.890		27110.	27068.	27068.
71	208.00	1.942		27110.	27068.	27068.
72	196.90		2.8059	27598.	27556.	27556.
73	189.80		2.6974	27910.	27866.	27866.
74	178.00	1.942		28428.	28378.	28378.
75	178.00	1.959		28428.	28378.	28378.
76	171.20		2.8387	28726.	28674.	28674.
77	168.00		2.9159	28866.	28813.	28813.
78	163.90		2.9158	29067.	29010.	29010.
79	148.70		2.9213	29711.	29642.	29642.
80	148.00	1.959		29741.	29672.	29672.
81	148.00	1.807		29741.	29672.	29672.
82	138.00	1.807		30116.	30039.	30039.
83	127.80		2.9251			
84	122.90		2.9185			
85	118.00		2.9197			
86	117.99		2.8210			
87	.00		2.8210			

TABLE 6-9 (page 2 of 3 pages). -- Mass of solid in vertical columns of unit cross-section, from BHG-survey data.

BOREHOLE OT6-23

K	PEACL DEPTH (FEET)	BHG DENSITY (GM/CC)	DENSITY OF SOLID COMPONENT (GM/CC)	CUMULATIVE SOLID MASS (GM/CM**2) RHO=2.821	RHO=(RHO)	LINEAR SPLINE FOR RHO
0	1800.00		2.8210			
1	734.00	2.156		0.	0.	0.
2	720.01		2.8210	756.	756.	756.
3	720.00		2.9253	756.	756.	756.
4	689.60		2.8791	2421.	2395.	2395.
5	674.00	2.156		3250.	3214.	3214.
6	674.00	2.072		3250.	3214.	3214.
7	659.60		2.8859	3972.	3927.	3927.
8	629.00	2.072		5006.	4949.	4949.
9	629.00	2.026		5006.	4949.	4949.
10	584.00	2.026		7664.	7615.	7615.
11	584.00	2.117		7664.	7615.	7615.
12	566.50		2.7885	8579.	8543.	8543.
13	549.00	2.117		10017.	10006.	10006.
14	539.00	2.008		10017.	10006.	10006.
15	535.40		2.7447	10186.	10178.	10178.
16	503.50		2.7973	11648.	11695.	11695.
17	494.00	2.008		12156.	12143.	12143.
18	494.00	2.049		12156.	12143.	12143.
19	472.90		2.9136	13195.	13192.	13192.
20	464.00	2.049		13607.	13597.	13597.
21	464.00	2.017		13607.	13597.	13597.
22	440.30		2.8805	14733.	14706.	14706.
23	440.29		2.8210	14733.	14706.	14706.
24	434.00	2.017		15032.	15005.	15005.
25	434.00	2.000		15032.	15005.	15005.
26	404.00	2.000		16433.	16406.	16406.
27	404.00	2.031		16433.	16406.	16406.
28	374.00	2.031		17850.	17823.	17823.
29	374.00	2.037		17850.	17823.	17823.
30	344.00	2.037		19304.	19277.	19277.
31	344.00	2.016		19304.	19277.	19277.
32	314.00	2.018		20751.	20703.	20703.
33	.00		2.8210			

BOREHOLE OPZ-16

K	PEACL DEPTH (FEET)	BHG DENSITY (GM/CC)	DENSITY OF SOLID COMPONENT (GM/CC)	CUMULATIVE SOLID MASS (GM/CM**2) RHO=2.821	RHO=(RHO)	LINEAR SPLINE FOR RHO
0	1800.00		2.8210			
1	1062.00	2.031		0.	0.	0.
2	1052.00	2.031		1445.	1445.	1445.
3	1052.00	1.951		1445.	1445.	1445.
4	1002.00	1.951		2776.	2776.	2776.
5	1002.00	2.052		2776.	2776.	2776.
6	967.00	2.052		4498.	4498.	4498.
7	967.00	2.048		4498.	4498.	4498.
8	937.00	2.048		5967.	5967.	5967.
9	937.00	2.115		5967.	5967.	5967.
10	902.00	2.115		7794.	7794.	7794.
11	902.00	2.107		7794.	7794.	7794.
12	871.51		2.8210	9374.	9374.	9374.
13	871.50		2.9253	9375.	9375.	9375.
14	867.00	2.107		9408.	9603.	9603.
15	867.00	2.031		9408.	9603.	9603.
16	866.80		2.9189	9618.	9613.	9613.
17	852.20		2.9150	10821.	10803.	10803.
18	837.00	2.031		11053.	11022.	11022.
19	837.00	1.951		11053.	11022.	11022.
20	832.50		2.9252	11235.	11200.	11200.
21	823.20		2.9206	11666.	11622.	11622.
22	813.60		2.9183	12091.	12040.	12040.
23	809.00		2.9043	12295.	12240.	12240.
24	807.00	1.951		12364.	12328.	12328.
25	807.00	2.052		12384.	12326.	12326.
26	794.00		2.9183	13023.	12956.	12956.
27	772.00	2.052		14106.	14018.	14018.
28	772.00	2.048		14106.	14018.	14018.
29	766.90		2.9206	14355.	14263.	14263.
30	742.00	2.048		15575.	15463.	15463.
31	742.00	2.115		15575.	15463.	15463.
32	737.70		2.8859	15800.	15684.	15684.
33	719.90		2.7241	16729.	16617.	16617.
34	709.20		2.7303	17288.	17186.	17186.
35	707.00	2.115		17402.	17304.	17304.
36	707.00	2.107		17402.	17304.	17304.
37	672.50		2.7241	19190.	19127.	19127.
38	672.00	2.107		19216.	19154.	19154.
39	672.00	2.122		19216.	19154.	19154.
40	668.50		2.8146	19400.	19340.	19340.
41	651.70		2.7303	20283.	20231.	20231.
42	647.00	2.122		21055.	21019.	21019.
43	647.00	2.107		21055.	21019.	21019.
44	631.60		2.7241	21835.	21804.	21804.
45	616.90		2.7201	22122.	22109.	22109.
46	610.00	2.107		22454.	22448.	22448.
47	610.00	2.139		22454.	22448.	22448.
48	602.50		2.7120	22854.	22857.	22857.
49	595.30		2.7613	23334.	23346.	23346.
50	582.00	2.139		23948.	23959.	23959.
51	582.00	2.191		23948.	23959.	23959.
52	578.90		2.9136	24121.	24130.	24130.
53	558.90		2.8743	25237.	25231.	25231.
54	552.00	2.191		25623.	25612.	25612.
55	552.00	2.086		25623.	25612.	25612.
56	533.10		2.8882	26583.	26561.	26561.
57	522.00	2.086		27147.	27119.	27119.
58	522.00	2.003		27147.	27119.	27119.
59	517.70		2.8633	27349.	27318.	27318.
60	492.00	2.003		28552.	28519.	28519.
61	492.00	2.180		28552.	28519.	28519.
62	491.90		2.8059	28558.	28524.	28524.
63	475.90		2.9090	29404.	29365.	29365.
64	457.00	2.180		30405.	30352.	30352.
65	457.00	1.962		30405.	30352.	30352.
66	452.90		2.8541	30589.	30535.	30535.
67	433.50		2.9166	31459.	31395.	31395.
68	418.90		2.8081	32114.	32045.	32045.
69	393.90		2.9065	33236.	33159.	33159.
70	382.00	1.962		33770.	33686.	33686.
71	382.00	1.997		33770.	33686.	33686.
72	376.40		2.8498	34031.	33945.	33945.
73	361.90		2.8565	34706.	34615.	34615.
74	352.00	1.997		35167.	35072.	35072.
75	352.00	1.956		35167.	35072.	35072.
76	347.40		2.8768	35372.	35275.	35275.
77	331.20		2.8745	36099.	35994.	35994.
78	322.00	1.956		36305.	36396.	36396.
79	322.00	1.957		36305.	36396.	36396.
80	313.90		2.8745	36859.	36746.	36746.
81	294.90		2.8682	37669.	37566.	37566.
82	292.00	1.957		37815.	37691.	37691.
83	292.00	1.807		37815.	37691.	37691.
84	277.90		2.8905	38344.	38212.	38212.
85	266.50		2.8829	38778.	38641.	38641.
86	262.00	1.807		38939.	38800.	38800.
87	262.00	1.812		38939.	38800.	38800.
88	249.90		2.8814	39395.	39251.	39251.
89	233.00		2.8635	40033.	39882.	39882.
90	232.99		2.8210	40033.	39882.	39882.
91	202.00	1.812		40070.	39919.	39919.
92	.00		2.8210			

TABLE 6-9 (page 3 of 3 pages). -- Mass of solid in vertical columns of unit cross-section, from BHG-survey data.

BOREHOLE OOR-17

J	PLACE DEPTH (FT)	G - G DENSITY (GM/CC)	DENSITY OF SOLID COMPONENT (GM/CC)	CUMULATIVE SOLID MASS (GM/CM**2) RHO=2.821	RHO*(RHO)	LINEAR SPLINE FOR RHO
0	1180.00		2.8210			
1	1179.81		2.8210			
2	1179.60		2.7262			
3	1179.39	2.204		0.	0.	0.
4	1179.18	2.145		118.	121.	121.
5	1178.99	2.142		187.	192.	192.
6	1178.85	2.116		233.	238.	238.
7	1178.70		2.7149	240.	245.	245.
8	1178.54	2.112		300.	307.	307.
9	1178.35	2.092		367.	375.	375.
10	1178.14	2.087		389.	397.	397.
11	1177.94	2.204		527.	539.	539.
12	1177.73	2.145		645.	659.	659.
13	1177.60	2.142		714.	730.	730.
14	1177.39	2.116		760.	776.	776.
15	1177.25	2.112		827.	845.	845.
16	1177.10	2.092		894.	912.	912.
17	1176.78	2.087		916.	935.	935.
18	1176.50		2.7364	978.	998.	998.
19	1176.25	2.054		1045.	1066.	1066.
20	1176.03	2.022		1128.	1151.	1151.
21	1175.87	2.024		1169.	1193.	1193.
22	1175.28	2.045		1232.	1257.	1257.
23	1175.56	2.047		1516.	1342.	1342.
24	1175.70	2.052		1358.	1385.	1385.
25	1175.41	2.054		1421.	1450.	1450.
26	1175.25	2.061		1443.	1472.	1472.
27	1175.10		2.7303	1477.	1506.	1506.
28	1174.89	2.066		1507.	1537.	1537.
29	1174.74	2.128		1617.	1649.	1649.
30	1174.68	2.152		1663.	1696.	1696.
31	1174.96	2.202		1756.	1793.	1793.
32	1174.67	2.196		1830.	1867.	1867.
33	1174.81	2.173		1878.	1915.	1915.
34	1174.40		2.7344	1912.	1950.	1950.
35	1174.09	2.159		1972.	2011.	2011.
36	1173.80	2.145		2041.	2081.	2081.
37	1173.67	2.106		2064.	2104.	2104.
38	1173.38	2.104		2130.	2172.	2172.
39	1173.27	2.080		2218.	2262.	2262.
40	1172.80		2.7291	2408.	2456.	2456.
41	1172.50	2.076		2415.	2461.	2461.
42	1172.34	2.071		2456.	2505.	2505.
43	1172.17	2.076		2651.	2704.	2704.
44	1171.85	2.104		2738.	2793.	2793.
45	1171.44	2.118		2895.	2953.	2953.
46	1171.30		2.7242	3026.	3087.	3087.
47	1171.10	2.088		3072.	3134.	3134.
48	1170.98	1.967		3361.	3429.	3429.
49	1170.70	1.981		3674.	3748.	3748.
50	1170.50		2.7262	3729.	3804.	3804.
51	1170.34	2.010		3914.	3993.	3993.
52	1170.23	1.986		4054.	4136.	4136.
53	1170.10	1.988		4173.	4257.	4257.
54	1169.99	2.034		4314.	4401.	4401.
55	1169.79	1.984		4414.	4503.	4503.
56	1169.70		2.7242	4464.	4554.	4554.
57	1169.54	1.967		4512.	4603.	4603.
58	1169.43	1.995		4650.	4744.	4744.
59	1169.34	2.053		4711.	4806.	4806.
60	1169.20		2.7303	4786.	4883.	4883.
61	1169.06	2.069		4838.	4935.	4935.
62	1168.90		2.7385	5161.	5264.	5264.
63	1168.44	2.002		5483.	5592.	5592.
64	1168.29	1.988		5577.	5689.	5689.
65	1168.13	1.950		5614.	5726.	5726.
66	1167.98		2.7201	5681.	5795.	5795.
67	1167.85	1.927		5727.	5842.	5842.
68	1167.67	1.984		5842.	5959.	5959.
69	1167.54	1.898		5861.	5978.	5978.
70	1167.43	1.886		5946.	6106.	6106.
71	1167.30		2.7120	6180.	6254.	6254.
72	1167.17	1.961		6205.	6331.	6331.
73	1167.05	2.097		6287.	6415.	6415.
74	1166.91	2.145		6468.	6599.	6599.
75	1166.79	2.106		6554.	6692.	6692.
76	1166.67	2.140		6649.	6784.	6784.
77	1166.70		2.7242	6669.	6805.	6805.
78	1166.46	2.157		6811.	6950.	6950.
79	1166.31	1.998		6920.	7060.	7060.
80	1166.20	1.970		7058.	7202.	7202.
81	1166.10		2.7343	7137.	7282.	7282.
82	1165.95	2.019		7158.	7304.	7304.
83	1165.90		2.8633	7248.	7393.	7393.
84	1165.81	2.071		7326.	7471.	7471.
85	1165.76	2.021		7432.	7575.	7575.
86	1165.16	2.019		7575.	7717.	7717.
87	1164.90	2.045		7830.	7970.	7970.
88	1164.20		2.8700	8022.	8161.	8161.
89	1163.41	2.061		8112.	8249.	8249.
90	1163.20	1.981		8378.	8515.	8515.
91	1163.01	2.010		8518.	8655.	8655.
92	1162.90		2.7888	8614.	8751.	8751.
93	1161.37	2.235		8699.	8837.	8837.
94	1158.56	2.299		8878.	9017.	9017.
95	1155.35	2.157		9052.	9190.	9190.
96	1153.60	2.128		9143.	9282.	9282.
97	1152.77	2.140		9189.	9327.	9327.
98	1150.66	2.156		9305.	9445.	9445.
99	1148.04	2.147		9444.	9581.	9581.
100	1147.18	2.116		9489.	9626.	9626.

BOREHOLE OOR-17

J	PLACE DEPTH (FT)	G - G DENSITY (GM/CC)	DENSITY OF SOLID COMPONENT (GM/CC)	CUMULATIVE SOLID MASS (GM/CM**2) RHO=2.821	RHO*(RHO)	LINEAR SPLINE FOR RHO
101	944.60	2.090		9623.	9758.	9758.
102	942.45	2.112		9733.	9868.	9868.
103	939.20		2.8965	9901.	10034.	10034.
104	938.15	2.092		9955.	10087.	10087.
105	936.00	2.059		10063.	10193.	10193.
106	932.56	2.048		10233.	10360.	10360.
107	926.12	2.053		10546.	10668.	10668.
108	923.11	2.016		10690.	10810.	10810.
109	921.20		2.8191	10781.	10899.	10899.
110	920.98	2.024		10793.	10911.	10911.
111	916.66	2.140		11010.	11124.	11124.
112	912.20		2.8948	11243.	11353.	11353.
113	909.78	2.059		11564.	11473.	11473.
114	907.60	2.059		11471.	11578.	11578.
115	902.97	2.099		11781.	11834.	11834.
116	896.45	2.048		12033.	12132.	12132.
117	890.00	2.227		12377.	12469.	12469.
118	889.20		2.9183	12423.	12514.	12514.
119	886.15	2.067		12585.	12673.	12673.
120	880.97	2.024		12837.	12921.	12921.
121	876.49	2.157		13079.	13158.	13158.
122	870.23	2.036		13388.	13461.	13461.
123	870.20		2.9159	13389.	13462.	13462.
124	867.22	2.071		13536.	13607.	13607.
125	865.93	2.019		13599.	13668.	13668.
126	861.83	2.010		13803.	13868.	13868.
127	857.36	2.114		14016.	14078.	14078.
128	852.80		2.9206	14267.	14324.	14324.
129	852.80	2.154		14267.	14324.	14324.
130	850.88	2.071		14357.	14412.	14412.
131	846.58	2.048		14570.	14621.	14621.
132	844.43	2.130		14680.	14729.	14729.
133	840.20		2.9252	14888.	14943.	14943.
134	838.41	2.057		14987.	15031.	15031.
135	834.97	2.085		15160.	15199.	15199.
136	832.82	2.125		15271.	15308.	15308.
137	829.38	2.093		15449.	15483.	15483.
138	828.52	2.067		15493.	15526.	15526.
139	826.46		2.9232	15609.	15640.	15640.
140	822.50	2.085		15796.	15823.	15823.
141	814.54	2.066		16207.	16225.	16225.
142	812.50		2.9241	16306.	16323.	16323.
143	810.47	2.002		16394.	16409.	16409.
144	807.06	2.022		16556.	16568.	16568.
145	804.98	2.088		16662.	16672.	16672.
146	802.90	2.128		16796.	16804.	16804.
147	799.29	2.147		16956.	16961.	16961.
148	797.57	2.135		17048.	17051.	17051.
149	794.20		2.9166	17221.	17221.	17221.
150	793.27	2.038		17267.	17266.	17266.
151	788.54	2.106		17504.	17499.	17499.
152	786.59	2.088		17614.	17607.	17607.
153	785.20		2.9062	17674.	17666.	17666.
154	784.67	2.086		17700.	17691.	17691.
155	781.23	2.019		17865.	17853.	17853.
156	779.51	2.042		17948.	17935.	17935.
157	775.64	2.042		18136.	18120.	18120.
158	773.49	2.026		18240.	18222.	18222.
159	769.19	2.085		18452.	18430.	18430.
160	767.90	2.118		18518.	18495.	18495.
161	766.10	2.140		18609.	18585.	18585.
162	764.89	2.123		18678.	18652.	18652.
163	762.30		2.9206	18819.	18786.	18786.
164	761.89	2.123		18836.	18807.	18807.
165	759.74	2.135		18950.	18918.	18918.
166	756.30	2.117		19131.	19096.	19096.
167	752.86	2.126		19312.	19274.	19274.
168	751.50		2.9190	19381.	19342.	19342.
169	751.14	2.046		19399.	19359.	19359.
170	747.70	1.972		19559.	19516.	19516.
171	740.84	2.080		19889.	19840.	19840.
172	737.80		2.9183	20038.	19987.	19987.
173	735.66	2.007		20140.	20087.	20087.
174	731.79	2.099		20331.	20274.	20274.
175	726.20	2.007		20606.	20545.	20545.
176	725.70		2.8836	20725.	20663.	20663.
177	718.06	2.097		21088.	20942.	20942.
178	714.59	2.088		21184.	21115.	21115.
179	714.16	2.050		21205.	21137.	21137.
180	707.72	1.988		21512.	21440.	21440.
181	701.70	2.007		21792.	21716.	21716.
182	700.20		2.8948	21864.	21787.	21787.
183	699.35	2.054		21896.	21818.	21818.
184	696.11	2.045		22065.	21985.	21985.
185	693.25	2.024		22106.	22026.	22026.
186	691.08	2.025		22291.	22208.	22208.
187	688.87	2.002		22434.	22349.	22349.
188	685.41	2.100		22687.	22599.	22599.
189	680.20	2.050		22839.	22748.	22748.
190	678.05	2.057		22945.	22852.	22852.
191	675.47	2.028		23070.	22976.	22976.
192	670.31	2.106		23328.	23230.	23230.
193	666.80		2.8948	23506.	23406.	23406.
194	664.29	2.036		23629.	23527.	23527.
195	660.85	2.054		23797.	23693.	23693.
196	658.47	2.093		23927.	23821.	23821.
197	654.55	2.067		24014.	23907.	23907.
198	653.11	2.067		24185.	24077.	24077.
199	652.70		2.8768	24236.	24087.	24087.
200	650.11	2.083		24357.	24226.	24226.

TABLE 6-10. -- Mass of solid in vertical columns of unit cross-section, from γ-γ survey data. Table continued on succeeding 19 pages.

TABLE 6-10 (Continued)

BOREHOLE 00R-17

J	PLACE DEPTH (FT)	G - G DENSITY (GM/CC)	DENSITY OF SOLID COMPONENT (GM/CC)	CUMULATIVE SOLID MASS (GM/CM**2) RHO=2.821	RHO=(RHO)	LINEAR SPLINE FOR RHO
201	647.59	2.019		24463.	24352.	24352.
202	644.52	2.002		24605.	24492.	24492.
203	642.37	2.007		24706.	24592.	24592.
204	640.22	1.979		24806.	24691.	24691.
205	637.84	2.002		24925.	24809.	24809.
206	634.65	2.054		25069.	24952.	24952.
207	632.77	2.047		25211.	24994.	24994.
208	630.62	2.047		25317.	25098.	25098.
209	628.48	2.054		25301.	25182.	25182.
210	626.50		2.8588	25376.	25259.	25259.
211	624.75	2.007		25404.	25285.	25285.
212	622.74	2.007		25546.	25425.	25425.
213	620.62	2.036		25628.	25507.	25507.
214	622.46	2.000		25669.	25547.	25547.
215	620.01	1.998		25769.	25647.	25647.
216	618.00		2.8610	25834.	25711.	25711.
217	617.08	1.967		25868.	25745.	25745.
218	611.41	2.036		26170.	26043.	26043.
219	610.16	2.078		26233.	26106.	26106.
220	605.06	2.111		26453.	26324.	26324.
221	602.90		2.8997	26605.	26473.	26473.
224	601.52	2.102		26676.	26543.	26543.
223	599.37	2.054		26785.	26650.	26650.
224	595.94	2.047		26953.	26817.	26817.
225	592.96	2.078		27103.	26964.	26964.
226	587.84	2.098		27381.	27240.	27240.
227	586.20		2.8543	27437.	27295.	27295.
228	584.65	2.050		27528.	27387.	27387.
229	582.18	2.071		27635.	27494.	27494.
230	580.05	2.054		27742.	27602.	27602.
231	578.50		2.7282	27817.	27676.	27676.
232	558.70		2.7242	28793.	28673.	28673.
233	552.08	2.058		29119.	29006.	29006.
234	551.65	1.950		29139.	29027.	29027.
235	533.60		2.7303	29938.	29842.	29842.
236	525.90		2.7364	30279.	30190.	30190.
237	508.20		2.7282	31063.	30988.	30988.
238	502.60		2.7282	31312.	31241.	31241.
239	502.20		2.7364	31329.	31259.	31259.
240	491.20		2.7242	31817.	31756.	31756.
241	481.20		2.7252	32259.	32208.	32208.
242	470.20		2.7282	32747.	32705.	32705.
243	458.56	1.950		33271.	33240.	33240.
244	456.20		2.7241	33566.	33537.	33537.
245	455.50	1.933		33903.	33875.	33875.
246	453.63	1.953		33979.	33952.	33952.
247	450.69	2.012		33687.	33614.	33614.
248	448.04	1.991		33727.	33716.	33716.
249	446.75	1.957		33797.	33778.	33778.
250	443.51	1.936		33952.	33936.	33936.
251	441.58	1.958		34028.	34014.	34014.
252	441.20		2.7181	34046.	34031.	34031.
253	438.15	1.834		34172.	34160.	34160.
254	435.19	1.867		34291.	34281.	34281.
255	433.85	1.981		34346.	34337.	34337.
256	432.13	2.010		34426.	34418.	34418.
257	429.99	1.990		34527.	34518.	34518.
258	429.13	1.927		34565.	34557.	34557.
259	426.55	1.924		34676.	34668.	34668.
260	426.20		2.8277	34691.	34683.	34683.
261	421.82	1.881		34875.	34868.	34868.
262	420.56	1.829		34909.	34902.	34902.
263	420.40		2.7759	34931.	34924.	34924.
264	416.66	1.791		35071.	35066.	35066.
265	415.57	1.881		35121.	35116.	35116.
266	412.56	1.898		35246.	35243.	35243.
267	411.78		2.7282	35273.	35272.	35272.
268	411.07	1.846		35301.	35300.	35300.
269	408.06	1.910		35431.	35432.	35432.
270	405.46	1.984		35545.	35548.	35548.
271	404.19	1.946		35603.	35608.	35608.
272	401.18	1.938		35735.	35742.	35742.
273	400.70		2.7446	35756.	35763.	35763.
274	399.46	1.950		35811.	35818.	35818.
275	398.66	1.940		35849.	35858.	35858.
276	396.80	2.010		35930.	35937.	35937.
277	388.71	1.998		36301.	36312.	36312.
278	388.30		2.8283	36318.	36322.	36322.
279	384.26	1.877		36392.	36403.	36403.
280	384.41	1.919		36482.	36493.	36493.
281	380.47	1.934		36630.	36643.	36643.
282	380.11	1.846		36666.	36679.	36679.
283	377.96	1.824		36749.	36763.	36763.
284	376.20		2.7467	36818.	36833.	36833.
285	375.61	1.851		36833.	36848.	36848.
286	374.53	1.933		36887.	36902.	36902.
287	372.58	1.912		36979.	36996.	36996.
288	371.09	1.958		37035.	37053.	37053.
289	368.71	1.915		37148.	37166.	37166.
290	367.22	1.967		37204.	37223.	37223.
291	365.07	1.915		37299.	37317.	37317.
292	363.35	1.941		37373.	37391.	37391.
293	361.93	1.889		37446.	37463.	37463.
294	358.64	1.921		37571.	37587.	37587.
295	358.19	1.920		37589.	37605.	37605.
296	356.04	1.917		37681.	37696.	37696.
297	354.20		2.9136	37759.	37773.	37773.
298	352.17	1.881		37843.	37855.	37855.
299	350.02	1.950		37935.	37945.	37945.
300	344.86	1.995		38169.	38175.	38175.

BOREHOLE 00R-17

J	PLACE DEPTH (FT)	G - G DENSITY (GM/CC)	DENSITY OF SOLID COMPONENT (GM/CC)	CUMULATIVE SOLID MASS (GM/CM**2) RHO=2.821	RHO=(RHO)	LINEAR SPLINE FOR RHO
301	344.20					
302	339.27	1.986				
303	336.84	1.964				
304	334.97	1.958				
305	331.96	2.002				
306	328.95	1.976				
307	326.60					
308	323.79	2.010				
309	319.92	1.998				
310	319.47	1.972				
311	316.06	1.979				
312	313.63	1.957				
313	313.48	1.950				
314	311.76	1.806				
315	309.18	1.953				
316	305.74	2.093				
317	301.44	2.007				
318	300.58	2.061				
319	297.57	2.123				
320	297.20					
321	295.85	2.088				
322	294.13	1.950				
323	292.64	1.919				
324	289.85	1.938				
325	287.68	1.984				
326	286.20					
327	285.81	1.919				
328	282.95	1.860				
329	279.08	1.832				
330	277.77	1.886				
331	275.20					
332	274.78	1.907				
333	273.92	1.967				
334	270.48	1.984				
335	268.36	2.026				
336	266.18	2.005				
337	264.09	1.971				
338	264.00					
339	260.60	1.967				
340	258.45	1.979				
341	255.44	1.965				
342	255.40					
343	253.72	1.978				
344	253.29	1.993				
345	250.28	2.005				
346	248.35	1.972				
347	243.40	1.984				
348	241.45	1.998				
349	238.87	1.964				
350	236.24	1.984				
351	234.80	1.998				
352	233.70					
353	231.56	1.946				
354	228.78	1.971				
355	226.65	2.019				
356	224.90					
357	222.35	2.040				
358	218.89	2.016				
359	214.09	1.929				
360	211.15	1.952				
361	207.20					
362	206.00	1.915				
363	198.28	1.976				
364	193.10	1.988				
365	192.20					
366	189.23	1.971				
367	187.94	1.938				
368	186.30					
369	185.19	1.927				
370	183.64	2.010				
371	181.92	2.031				
372	178.98	2.019				
373	177.30					
374	176.38	2.125				
375	172.87	2.102				
376	171.17	2.002				
377	169.45	2.024				
378	164.29	1.938				
379	164.20					
380	161.26	1.986				
381	160.42	1.915				
382	158.70	1.969				
383	157.90					
384	154.85	1.938				
385	154.40	1.884				
386	151.70					
387	150.97	1.815				
388	148.20					
389	142.57	1.825				
390	135.92	1.777				
391	130.76	1.808				
392	129.47	1.903				
393	128.30					
394	125.60	1.950				
395	124.20					
396	123.88	1.875				
397	120.87	1.872				
398	120.01	1.922				
399	118.49	1.927				
400	117.43	1.969				

BOREHOLE 00R-17

J	PLACE DEPTH (FT)	G - G DENSITY (GM/CC)	DENSITY OF SOLID COMPONENT (GM/CC)	CUMULATIVE SOLID MASS (GM/CM**2) RHO=2.821	RHO=(RHO)	LINEAR SPLINE FOR RHO
			2.9206	38200.	38205.	38205.
				38427.	38429.	38429.
				38447.	38448.	38448.
				38620.	38619.	38619.
				38758.	38755.	38755.
				38897.	38893.	38893.
			2.8565	38913.	38909.	38909.
				39136.	39131.	39131.
				39318.	39312.	39312.
				39357.	39351.	39351.
				39444.	39488.	39488.
				39514.	39507.	39507.
				39609.	39602.	39602.
				39683.	39676.	39676.
				39792.	39785.	39785.
				39955.	39948.	39948.
				40166.	40160.	40160.
				40208.	40202.	40202.
				40361.	40356.	40356.
			2.7952	40365.	40360.	40360.
				40450.	40446.	40446.
				40532.	40528.	40529.
				40588.	40585.	40585.
				40719.	40716.	40716.
				40815.	40814.	40814.
			2.7467	40882.	40882.	40882.
				40987.	40988.	40988.
				41022.	41024.	41024.
				41175.	41178.	41178.
				41226.	41229.	41229.
			2.9241	41334.	41337.	41337.
				41352.	41355.	41355.
				41389.	41392.	41392.
				41546.	41548.	41548.
				41627.	41629.	41629.
				41749.	41751.	41751.
				41808.	41810.	41810.
			2.8541	41813.	41815.	41815.
				42003.	42004.	42004.
				42100.	42102.	42102.
				42237.	42237.	42237.
			2.8454	42239.	42239.	42239.
				42315.	42315.	42315.
				42335.	42335.	42335.
				42475.	42474.	42474.
				42693.	42691.	42691.
				42792.	42789.	42789.
				42891.	42888.	42888.
				43009.	43005.	43005.
				43029.	43024.	43024.
				43188.	43182.	43182.
			2.8655	43239.	43232.	43232.
				43344.	43337.	43337.
				43459.	43451.	43451.
				43559.	43551.	43551.
			2.8432	43642.	43633.	43633.
				43766.	43756.	43756.
				43931.	43921.	43921.
				44126.	44115.	44115.
				44277.	44264.	44264.
			2.8683	44450.	44436.	44436.
				44501.	44487.	44487.
				44843.	44826.	44826.
				45079.	45062.	45062.
			2.8299	45120.	45103.	45103.
				45256.	45238.	45238.
				45313.	45295.	45295.
			2.8343	45385.	45367.	45367.
				45407.	45389.	45389.
				45504.	45485.	45485.
				45586.	45567.	45567.
				45751.	45731.	45731.
			2.8588	45798.	45778.	45778.
				45858.	45838.	45838.
				46038.	46016.	46016.
				46122.	46100.	46100.
				46204.	46182.	46182.
				46440.	46418.	46418.
			2.8681	46444.	46422.	46422.
				46571.	46550.	46550.
				46608.	46587.	46587.
				46684.	46662.	46662.
			2.8233	46720.	46699.	46699.
				46855.	46834.	46834.
				46874.	46852.	46852.
			2.8745	46981.	46958.	46958.
				47010.	46986.	46986.
			2.8541	47305.	47279.	47279.
				47337.	47311.	47311.
				47577.	47550.	47550.
				47766.	47738.	47738.
				47818.	47790.	47790.
			2.8365	47867.	47839.	47839.
				47985.	47955.	47955.
			2.9259	48045.	48014.	48014.
				48058.	48027.	48027.
				48180.	48147.	48147.
				48216.	48182.	48182.
				48290.	48255.	48255.
				48328.	48292.	48292.

TABLE 6-10 (Continued)

BOREHOLE DOR-17

J	PEACE DEPTH (FT)	G - G DENSITY (GM/CC)	DENSITY OF SOLID COMPONENT (GM/CC)	CUMULATIVE SOLID MASS (GM/CM**2) RHO=2.821	RHO=<RHO>	LINEAR SPLINE FOR RHO
401	115.71	1.936		48405.	48367.	48367.
402	114.42	1.946		48461.	48423.	48423.
403	113.80		2.9275	48489.	48449.	48449.
404	111.41	1.919		48592.	48551.	48551.
405	109.03	1.905		48702.	48658.	48658.
406	107.20		2.9290	48771.	48726.	48726.
407	106.29	1.919		48811.	48765.	48765.
408	102.81	1.931		48959.	48911.	48911.
409	97.65	1.894		49179.	49125.	49125.
410	95.08	1.901		49287.	49231.	49231.
411	94.22	1.929		49323.	49267.	49267.
412	90.78	1.950		49479.	49415.	49415.
413	86.20		2.9252	49671.	49608.	49608.
414	85.90	1.874		49766.	49701.	49701.
415	82.61	1.889		49919.	49753.	49753.
416	80.05	1.888		49926.	49857.	49857.
417	78.51	1.898		49997.	49928.	49927.
418	75.73	1.889		50105.	50033.	50033.
419	74.44	1.907		50159.	50086.	50086.
420	72.72	1.905		50231.	50157.	50157.
421	66.90		2.9220			
422	56.50		2.9252			
423	56.29		2.8210			
424	.00		2.8210			

BOREHOLE DOR-21

J	PEACE DEPTH (FT)	G - G DENSITY (GM/CC)	DENSITY OF SOLID COMPONENT (GM/CC)	CUMULATIVE SOLID MASS (GM/CM**2) RHO=2.821	RHO=<RHO>	LINEAR SPLINE FOR RHO
0	1800.00		2.8210			
1	432.71		2.8210			
2	432.70		2.8432			
3	421.50		2.7282			
4	413.65	1.918		0.	0.	0.
5	411.40		2.8124	70.	70.	70.
6	411.07	1.929		84.	85.	85.
7	408.72	1.884		184.	184.	184.
8	406.76	1.798		260.	261.	261.
9	404.41	1.781		344.	345.	345.
10	402.85	1.713		397.	398.	398.
11	401.60		2.7760	439.	441.	441.
12	401.28	1.748		450.	452.	452.
13	399.72	1.693		502.	504.	504.
14	398.59	1.726		540.	543.	543.
15	396.97	1.723		593.	596.	596.
16	394.62	1.759		673.	677.	677.
17	394.23	1.741		687.	691.	691.
18	391.10	1.756		794.	799.	799.
19	389.53	1.697		846.	851.	851.
20	388.06	1.716		885.	890.	890.
21	386.79	1.668		935.	941.	941.
22	385.25	1.693		983.	989.	989.
23	383.27	1.660		1042.	1048.	1048.
24	381.70	1.715		1092.	1098.	1098.
25	376.36	1.865		1192.	1199.	1199.
26	377.59	1.576		1256.	1262.	1262.
27	376.22	1.961		1305.	1310.	1310.
28	373.98	1.746		1406.	1412.	1412.
29	371.13	1.798		1487.	1493.	1493.
30	370.54	1.782		1515.	1521.	1521.
31	369.56	1.873		1545.	1551.	1551.
32	368.39	1.886		1593.	1599.	1599.
33	366.45	1.886		1673.	1680.	1680.
34	365.64	1.871		1705.	1711.	1711.
35	363.00		2.8387	1813.	1819.	1819.
36	362.51	1.876		1833.	1838.	1838.
37	361.73	1.911		1865.	1871.	1871.
38	359.58	1.911		1965.	1970.	1970.
39	357.81	1.873		2030.	2035.	2035.
40	356.64	1.843		2077.	2082.	2082.
41	354.29	1.840		2169.	2173.	2173.
42	352.72	1.751		2227.	2231.	2231.
43	350.76	1.727		2294.	2297.	2297.
44	349.20	1.672		2344.	2348.	2348.
45	346.80		2.8543	2422.	2425.	2425.
46	346.06	1.748		2447.	2450.	2450.
47	344.50	1.751		2502.	2504.	2504.
48	343.56	1.782		2543.	2545.	2545.
49	342.15	1.829		2587.	2589.	2589.
50	340.19	1.845		2663.	2664.	2664.
51	337.45	1.861		2773.	2774.	2774.
52	336.67	1.876		2805.	2805.	2805.
53	336.00		2.8588	2832.	2832.	2832.
54	334.71	1.806		2862.	2881.	2881.
55	333.92	1.798		2911.	2910.	2910.
56	331.18	1.755		3003.	3007.	3007.
57	330.01	1.755		3048.	3047.	3047.
58	329.22	1.751		3075.	3074.	3074.
59	327.27	1.806		3146.	3144.	3144.
60	326.48	1.868		3177.	3174.	3174.
61	324.92	1.864		3240.	3238.	3238.
62	322.96	1.881		3321.	3318.	3318.
63	321.78	1.864		3369.	3365.	3365.
64	320.90		2.8355	3404.	3401.	3401.
65	319.04	1.908		3482.	3478.	3478.
66	317.87	1.900		3531.	3527.	3527.
67	315.91	1.868		3612.	3608.	3608.
68	314.74	1.820		3659.	3653.	3653.
69	313.17	1.813		3717.	3713.	3713.
70	309.64	1.903		3858.	3853.	3853.
71	306.90	1.813		3967.	3962.	3962.
72	305.34	1.804		4026.	4020.	4020.
73	304.20		2.8476	4069.	4063.	4063.
74	303.77	1.817		4085.	4079.	4079.
75	301.61	1.939		4165.	4158.	4158.
76	299.85	1.951		4251.	4245.	4245.
77	297.50	1.889		4352.	4345.	4345.
78	296.76	1.804		4465.	4459.	4459.
79	293.59	1.922		4514.	4509.	4509.
80	291.00		2.7718	4626.	4621.	4621.
81	290.85	1.922		4632.	4627.	4627.
82	289.67	1.959		4683.	4679.	4679.
83	288.89	1.923		4717.	4713.	4713.
84	287.52	1.818		4780.	4777.	4777.
85	284.19	1.798		4898.	4896.	4896.
86	283.41	1.820		4927.	4925.	4925.
87	281.06	1.939		5024.	5022.	5022.
88	279.49	1.955		5093.	5092.	5092.
89	277.53	1.873		5181.	5180.	5180.
90	275.57	1.935		5269.	5269.	5269.
91	275.18	1.889		5286.	5285.	5285.
92	274.40	1.876		5318.	5318.	5318.
93	271.64	1.824		5426.	5426.	5426.
94	270.70		2.8124	5463.	5464.	5464.
95	270.09	1.861		5488.	5488.	5488.
96	265.78	1.861		5660.	5660.	5660.
97	264.61	1.842		5706.	5706.	5706.
98	263.83	1.840		5737.	5737.	5737.
99	261.48	1.873		5846.	5845.	5845.
100	260.50		2.8633	5870.	5869.	5869.

TABLE 6-10 (Continued)

BOREHOLE USR-21

J	PLACE DEPTH (FT)	G - G DENSITY (GM/CC)	DENSITY OF SOLID COMPONENT (GM/CC)	CUMULATIVE SOLID MASS (GM/CM**2) RHO=2.821	RHO=(PHO)	LINEAR SPLINE FOR PHO
101	260,50	1,861		5878.	5877.	5877.
102	259,15	1,829		5924.	5922.	5922.
103	255,97	1,887		6043.	6046.	6046.
104	254,09	1,928		6132.	6129.	6129.
105	252,08	1,845		6213.	6209.	6209.
106	250,51	1,779		6272.	6267.	6267.
107	249,90		2,8588	6294.	6289.	6289.
108	245,18	1,782		6457.	6352.	6352.
109	247,58	1,826		6386.	6381.	6381.
110	245,05	1,904		6480.	6475.	6475.
111	241,11	1,903		6645.	6638.	6638.
112	236,80	1,908		6827.	6819.	6819.
113	236,02	1,312		6860.	6852.	6852.
114	232,11	1,897		7025.	7015.	7015.
115	230,15	1,851		7105.	7095.	7095.
116	228,58	1,845		7166.	7156.	7156.
117	228,19	1,826		7182.	7171.	7171.
118	225,06	1,603		7300.	7289.	7289.
119	222,71	1,826		7389.	7377.	7377.
120	219,57	1,908		7515.	7502.	7502.
121	218,90		2,8521	7544.	7531.	7531.
122	216,85	1,868		7629.	7615.	7615.
123	214,09	1,900		7741.	7727.	7727.
124	212,92	1,970		7793.	7778.	7778.
125	211,74	1,998		7847.	7831.	7831.
126	209,00	1,970		7972.	7956.	7956.
127	208,20		2,8633	7986.	7970.	7970.
128	207,46	1,947		8043.	8026.	8026.
129	205,08	1,955		8147.	8129.	8129.
130	202,73	1,920		8249.	8231.	8231.
131	199,60	1,934		8385.	8366.	8366.
132	196,43	1,951		8436.	8417.	8417.
133	196,47	1,955		8523.	8504.	8504.
134	193,73	1,859		8639.	8619.	8619.
135	191,88	1,856		8733.	8713.	8713.
136	190,20	1,798		8778.	8758.	8758.
137	190,00		2,8341	8786.	8765.	8765.
138	187,85	1,832		8867.	8846.	8846.
139	186,25	1,817		8927.	8906.	8906.
140	185,55	1,923		9058.	9017.	9017.
141	183,59	1,845		9118.	9098.	9098.
142	178,06	1,691		9244.	9223.	9223.
143	176,10	1,813		9312.	9291.	9291.
144	176,00		2,8368	9316.	9295.	9295.
145	174,95	1,832		9367.	9346.	9346.
146	172,97	1,915		9437.	9416.	9416.
147	170,62	1,849		9533.	9512.	9512.
148	169,06	1,861		9595.	9574.	9574.
149	167,10	1,831		9672.	9651.	9651.
150	165,96	1,829		9794.	9773.	9773.
151	162,01	1,798		9868.	9846.	9846.
152	158,47	1,970		9996.	9975.	9975.
153	156,52	2,077		10090.	10069.	10069.
154	153,69	2,042		10265.	10243.	10243.
155	152,61	2,047		10303.	10281.	10281.
156	151,04	1,998		10378.	10356.	10356.
157	149,47	1,992		10451.	10428.	10428.
158	148,30	1,964		10504.	10482.	10482.
159	146,00		2,8409	10607.	10584.	10584.
160	144,78	1,955		10662.	10639.	10639.
161	142,03	1,839		10776.	10752.	10752.
162	139,66	1,790		10866.	10841.	10841.
163	136,99	1,871		10972.	10946.	10946.
164	134,59	1,955		11072.	11045.	11045.
165	131,80	2,049		11200.	11171.	11171.
166	131,00		2,9066	11242.	11212.	11212.
167	130,48	2,053		11257.	11227.	11227.
168	115,00		2,9298			
169	84,20		2,9290			
170	84,19		2,8210			
171	,00		2,8210			

BOREHOLE OKT-20

J	PLACE DEPTH (FT)	G - G DENSITY (GM/CC)	DENSITY OF SOLID COMPONENT (GM/CC)	CUMULATIVE SOLID MASS (GM/CM**2) RHO=2.821	RHO=(PHO)	LINEAR SPLINE FOR PHO
0	1800,00		2,8210			
1	591,41		2,8210			
2	591,40		2,8676			
3	572,40	1,986		0.	0.	0.
4	572,40		2,7571	0.	0.	0.
5	571,22	1,989		54.	54.	54.
6	570,05	1,987		107.	108.	108.
7	568,48	1,985		177.	179.	179.
8	567,31	1,948		228.	232.	232.
9	564,96	1,937		332.	337.	337.
10	563,78	1,918		383.	388.	388.
11	562,61	1,915		433.	439.	439.
12	560,26	1,866		530.	539.	539.
13	559,08	1,869		578.	587.	587.
14	555,95	2,000		719.	726.	726.
15	553,99	2,016		807.	820.	820.
16	553,40	1,984		843.	857.	857.
17	551,90		2,7292	902.	917.	917.
18	551,64	1,998		914.	929.	929.
19	549,68	1,948		1001.	1018.	1018.
20	548,89	1,937		1035.	1053.	1053.
21	547,72	1,969		1087.	1106.	1106.
22	545,80	1,859		1254.	1276.	1276.
23	543,84	1,854		1331.	1355.	1355.
24	541,45	1,838		1347.	1371.	1371.
25	539,49	1,912		1426.	1452.	1452.
26	538,20	1,899		1460.	1486.	1486.
27	537,42	1,914		1493.	1520.	1520.
28	537,40		2,7282	1515.	1543.	1543.
29	535,96	1,931		1577.	1606.	1606.
30	534,59	1,917		1644.	1675.	1675.
31	533,22	1,925		1695.	1726.	1726.
32	530,87	1,914		1795.	1829.	1829.
33	530,08	1,898		1828.	1863.	1863.
34	527,40		2,7241	1942.	1979.	1979.
35	527,24	1,921		1945.	1981.	1981.
36	526,16	1,914		1995.	2033.	2033.
37	524,99	1,923		2045.	2084.	2084.
38	524,21	1,855		2078.	2118.	2118.
39	521,96	1,868		2191.	2233.	2233.
40	518,83	1,953		2324.	2369.	2369.
41	517,15	1,958		2376.	2422.	2422.
42	516,37	1,975		2412.	2458.	2458.
43	513,23	1,975		2554.	2604.	2604.
44	511,60		2,7160	2630.	2682.	2682.
45	511,47	2,022		2646.	2697.	2697.
46	508,34	1,964		2773.	2827.	2827.
47	506,37	1,961		2861.	2917.	2917.
48	505,79	1,945		2895.	2953.	2953.
49	503,44	1,958		3000.	3060.	3060.
50	501,87	1,937		3069.	3130.	3130.
51	500,69	1,945		3121.	3183.	3183.
52	497,95	1,950		3234.	3299.	3299.
53	495,99	1,877		3312.	3378.	3378.
54	494,43	1,865		3375.	3443.	3443.
55	492,86	2,006		3443.	3513.	3513.
56	490,90	2,008		3536.	3607.	3607.
57	488,55	2,091		3651.	3725.	3725.
58	486,59	2,099		3751.	3827.	3827.
59	485,02	2,094		3832.	3909.	3909.
60	483,85	2,038		3890.	3969.	3969.
61	481,89	2,036		3985.	4066.	4066.
62	481,60		2,7292	3999.	4080.	4080.
63	480,32	2,060		4062.	4145.	4145.
64	478,36	2,074		4160.	4244.	4244.
65	476,01	2,075		4278.	4365.	4365.
66	474,27	1,874		4403.	4492.	4492.
67	469,33	1,619		4538.	4631.	4631.
68	468,17	1,654		4573.	4666.	4666.
69	467,00	2,047		4619.	4714.	4714.
70	464,80		2,7201	4730.	4827.	4827.
71	464,64	2,112		4736.	4835.	4835.
72	461,98	1,955		4870.	4970.	4970.
73	460,73	1,948		4923.	5023.	5023.
74	458,77	1,852		5005.	5107.	5107.
75	456,82	1,964		5122.	5227.	5227.
76	454,85	1,975		5176.	5282.	5282.
77	453,28	1,992		5248.	5355.	5355.
78	450,54	1,958		5373.	5483.	5483.
79	449,36	1,969		5426.	5538.	5538.
80	448,19	1,994		5480.	5593.	5593.
81	445,84	2,016		5591.	5706.	5706.
82	444,27	2,000		5664.	5781.	5781.
83	442,80		2,7181	5731.	5849.	5849.
84	441,92	1,915		5769.	5889.	5889.
85	439,96	1,929		5854.	5975.	5975.
86	439,57	1,951		5871.	5992.	5992.
87	438,00	1,956		5941.	6064.	6064.
88	436,82	1,980		5994.	6118.	6118.
89	435,26	1,953		6064.	6190.	6190.
90	432,90	1,895		6166.	6294.	6294.
91	432,10		2,7140	6199.	6328.	6328.
92	430,53	1,874		6262.	6393.	6393.
93	428,09	1,898		6365.	6475.	6475.
94	427,03	1,998		6412.	6546.	6546.
95	425,46	2,005		6486.	6621.	6621.
96	424,68	2,000		6522.	6658.	6658.
97	423,89	1,976		6559.	6695.	6695.
98	421,93	1,943		6646.	6785.	6785.
99	418,41	2,000		6806.	6948.	6948.
100	417,62	2,019		6843.	6985.	6985.

TABLE 6-10 (Continued)

BOREHOLE ORT-20

J	PEACL DEPTH DIFF	G - G DENSITY (GM/CC)	DENSITY OF SOLID COMPONENT (GM/CC)	CUMULATIVE SOLID MASS (GM/CM**2) RHO=2.821	RHO*(RHO)	LINEAR SPLINE FOR RHO
101	416.90		2.7344	6678.	7020.	7020.
102	410.96	2.046		7164.	7312.	7312.
103	407.46	2.017		7334.	7483.	7483.
104	405.87	2.027		7409.	7559.	7559.
105	404.69	2.047		7466.	7616.	7616.
106	402.73	2.057		7563.	7712.	7712.
107	401.90		2.8146	7604.	7754.	7754.
108	399.21	2.099		7740.	7890.	7890.
109	397.20	2.091		7841.	7990.	7990.
110	396.07	2.079		7901.	8050.	8050.
111	391.57	2.005		8130.	8277.	8277.
112	387.84	2.067		8297.	8442.	8442.
113	387.70		2.8974	8304.	8449.	8449.
114	385.88	2.047		8392.	8536.	8536.
115	381.96	2.028		8582.	8723.	8723.
116	379.61	2.050		8696.	8836.	8836.
117	377.26	2.042		8811.	8950.	8950.
118	375.69	2.028		8887.	9026.	9026.
119	372.92	2.041		9020.	9157.	9157.
120	371.38	2.025		9095.	9233.	9233.
121	369.43	2.039		9190.	9327.	9327.
122	367.40		2.8341	9287.	9424.	9424.
123	367.07	2.029		9303.	9440.	9440.
124	365.51	2.046		9379.	9515.	9515.
125	362.76	2.049		9513.	9649.	9649.
126	360.80	2.069		9610.	9745.	9745.
127	359.24	2.055		9685.	9822.	9822.
128	356.84	2.000		9801.	9934.	9934.
129	355.52	1.953		9872.	10004.	10004.
130	353.75	1.956		9962.	10073.	10073.
131	351.40		2.9050	10088.	10178.	10178.
132	349.44	2.029		10140.	10268.	10268.
133	345.91	2.031		10310.	10435.	10435.
134	343.95	2.008		10403.	10527.	10527.
135	342.40		2.8882	10946.	11062.	11062.
136	313.60		2.7849	11842.	11955.	11955.
137	306.60		2.8233	12309.	12424.	12424.
138	283.80		2.8277	13217.	13331.	13331.
139	283.22	1.995		13244.	13358.	13358.
140	281.65	1.994		13314.	13429.	13429.
141	279.30	1.975		13419.	13533.	13533.
142	277.34	1.976		13508.	13622.	13622.
143	274.99	1.996		13617.	13730.	13730.
144	273.05	1.989		13708.	13820.	13820.
145	272.48		2.8365	13737.	13849.	13849.
146	269.50	2.000		13871.	13983.	13983.
147	265.58	1.921		14047.	14157.	14157.
148	263.84	1.910		14164.	14274.	14274.
149	262.08	1.921		14198.	14307.	14307.
150	260.88	1.910		14268.	14377.	14377.
151	257.15	1.984		14386.	14495.	14495.
152	255.19	2.013		14477.	14586.	14586.
153	254.90		2.8391	14493.	14601.	14601.
154	251.81	1.998		14662.	14770.	14770.
155	250.64	2.008		14717.	14824.	14824.
156	247.95	2.019		14846.	14953.	14953.
157	245.99	1.978		14937.	15044.	15044.
158	242.86	1.986		15081.	15187.	15187.
159	242.07	1.972		15117.	15223.	15223.
160	238.16	1.987		15296.	15401.	15401.
161	235.41	2.024		15425.	15529.	15529.
162	235.40		2.8633	15511.	15614.	15614.
163	233.45	2.003		15617.	15721.	15721.
164	230.32	1.997		15764.	15766.	15766.
165	229.14	2.016		15719.	15820.	15820.
166	225.62	2.031		15868.	15967.	15967.
167	222.20		2.8951	16030.	16147.	16147.
168	220.52	1.995		16127.	16225.	16225.
169	218.54	2.000		16220.	16315.	16315.
170	218.17	1.980		16238.	16333.	16333.
171	214.65	1.969		16416.	16508.	16508.
172	213.86	1.942		16434.	16526.	16526.
173	211.90	1.992		16522.	16613.	16613.
174	211.40		2.8859	16545.	16636.	16636.
175	209.16	2.003		16650.	16739.	16739.
176	206.02	1.973		16795.	16882.	16882.
177	203.67	1.973		16901.	16987.	16987.
178	202.50	2.000		16956.	17041.	17041.
179	200.90		2.8836	17031.	17115.	17115.
180	200.54	2.043		17049.	17133.	17133.
181	198.97	2.000		17123.	17206.	17206.
182	197.01	1.953		17212.	17295.	17295.
183	194.66	1.694		17313.	17396.	17396.
184	194.27	1.901		17330.	17412.	17412.
185	190.90		2.7624	17493.	17577.	17577.
186	189.17	1.920		17546.	17629.	17629.
187	187.24	1.918		17630.	17713.	17713.
188	184.08	1.956		17767.	17850.	17850.
189	183.60	2.028		17803.	17886.	17886.
190	180.95	2.000		17914.	17997.	17997.
191	179.08	2.025		17989.	18070.	18070.
192	178.20	1.950		18043.	18123.	18123.
193	178.10		2.9090	18047.	18128.	18128.
194	177.81	1.973		18060.	18140.	18140.
195	175.85	1.992		18150.	18229.	18229.
196	173.50	1.973		18258.	18335.	18335.
197	172.72	1.992		18294.	18371.	18371.
198	170.67	1.992		18403.	18479.	18479.
199	168.41	2.014		18495.	18570.	18570.
200	165.90		2.8229	18611.	18686.	18686.

BOREHOLE ORT-20

J	PEACL DEPTH DIFF	G - G DENSITY (GM/CC)	DENSITY OF SOLID COMPONENT (GM/CC)	CUMULATIVE SOLID MASS (GM/CM**2) RHO=2.821	RHO*(RHO)	LINEAR SPLINE FOR RHO
201	165.66	1.949		18622.	18697.	18697.
202	163.70	1.969		18710.	18785.	18785.
203	161.10		2.9198	18834.	18906.	18906.
204	160.57	2.079		18860.	18932.	18932.
205	158.26	2.113		18981.	19050.	19050.
206	156.65	2.079		19061.	19129.	19129.
207	155.91	1.953		19191.	19257.	19257.
208	151.75	1.940		19278.	19342.	19342.
209	149.99	1.942		19364.	19426.	19426.
210	148.42	1.997		19435.	19495.	19495.
211	146.60		2.9297	19518.	19577.	19577.
212	145.29	1.958		19577.	19635.	19635.
213	144.11	1.997		19631.	19688.	19688.
214	140.98	1.926		19772.	19826.	19826.
215	138.29	1.917		19889.	19941.	19941.
216	137.06	1.874		19938.	19989.	19989.
217	135.88	1.885		19987.	20037.	20037.
218	132.75	1.892		20116.	20164.	20164.
219	131.96	1.959		20150.	20197.	20197.
220	131.90		2.9096	20153.	20200.	20200.
221	131.89		2.8210	20153.	20200.	20200.
222	128.05	1.958		20325.	20372.	20372.
223	126.48	1.948		20395.	20442.	20442.
224	123.74	1.951		20516.	20563.	20563.
225	119.84	1.917		20687.	20734.	20734.
226	.00		2.8210			

TABLE 6-10 (Continued)

BOREHOLE OBT-19

J	PLACE DEPTH (FT)	G - G DENSITY (GM/CC)	DENSITY OF SOLID COMPONENT (GM/CC)	CUMULATIVE SOLID MASS (GM/CM**2) RHO=2.821	RHO=<RHO>	LINEAR SPLINE FOR RHO
0	1800.00		2.8210			
1	838.51		2.8210			
2	818.50		2.9096			
3	808.50		2.9151			
4	798.10		2.9042			
5	788.50		2.9198			
6	778.60		2.9287			
7	767.61	1.950		0.	0.	0.
8	766.64	1.947		70.	68.	68.
9	762.89	2.003		213.	209.	209.
10	761.92	2.019		287.	281.	281.
11	759.56	2.021		380.	373.	373.
12	759.10		2.9128	392.	385.	385.
13	757.00	2.052		494.	485.	485.
14	755.42	2.042		571.	560.	560.
15	753.07	2.074		687.	675.	675.
16	751.49	2.063		766.	752.	752.
17	749.53	2.072		864.	848.	848.
18	749.10		2.9113	885.	870.	870.
19	747.17	2.031		980.	962.	962.
20	744.42	2.039		1113.	1093.	1093.
21	741.67	2.061		1248.	1226.	1226.
22	738.52	2.049		1403.	1378.	1378.
23	737.54	2.060		1461.	1435.	1435.
24	733.81	2.038		1635.	1606.	1606.
25	729.88	2.050		1827.	1794.	1794.
26	729.50		2.9159	1845.	1812.	1812.
27	726.30	2.080		1905.	1871.	1871.
28	725.93	2.057		2023.	1987.	1987.
29	724.37	2.069		2101.	2063.	2063.
30	722.02	2.074		2219.	2180.	2180.
31	720.84	2.059		2278.	2237.	2237.
32	716.91	1.959		2462.	2418.	2418.
33	714.15	1.992		2586.	2542.	2542.
34	712.98	2.035		2643.	2597.	2597.
35	710.22	2.042		2777.	2728.	2728.
36	707.08	2.006		2927.	2876.	2876.
37	704.33	1.987		3055.	3002.	3002.
38	702.86	2.003		3147.	3092.	3092.
39	701.18	2.033		3203.	3147.	3147.
40	700.10		2.8974	3255.	3199.	3199.
41	698.86	2.044		3317.	3260.	3260.
42	698.04	2.027		3355.	3298.	3298.
43	694.50	2.034		3526.	3466.	3466.
44	692.93	2.050		3603.	3541.	3541.
45	690.18	2.031		3737.	3673.	3673.
46	688.61	2.042		3813.	3748.	3748.
47	687.43	2.019		3870.	3804.	3804.
48	686.25	1.978		3925.	3858.	3858.
49	684.28	1.972		4014.	3946.	3946.
50	683.10	1.950		4067.	3998.	3998.
51	679.96	2.035		4215.	4142.	4142.
52	677.99	2.055		4309.	4236.	4236.
53	675.24	2.029		4443.	4369.	4369.
54	673.67	2.050		4520.	4444.	4444.
55	670.53	2.097		4678.	4600.	4600.
56	670.00		2.9066	4705.	4626.	4626.
57	668.95	2.102		4759.	4679.	4679.
58	668.17	2.118		4800.	4719.	4719.
59	666.20	2.071		4901.	4818.	4818.
60	663.06	2.003		5053.	4968.	4968.
61	661.09	2.003		5148.	5059.	5059.
62	659.91	1.986		5200.	5113.	5113.
63	659.50		2.8991	5219.	5132.	5132.
64	657.95	2.019		5292.	5204.	5204.
65	655.98	1.966		5384.	5295.	5295.
66	654.41	2.006		5457.	5367.	5367.
67	652.45	1.967		5548.	5458.	5458.
68	651.66	2.025		5585.	5495.	5495.
69	650.48	2.038		5642.	5551.	5551.
70	648.32	2.039		5757.	5665.	5665.
71	647.34	2.050		5795.	5704.	5704.
72	646.16	2.031		5852.	5761.	5761.
73	645.41	2.028		5885.	5894.	5894.
74	642.62	2.020		6022.	5931.	5931.
75	641.05	2.027		6098.	6007.	6007.
76	639.48	2.024		6173.	6083.	6083.
77	637.12	2.036		6287.	6198.	6198.
78	635.55	2.050		6360.	6374.	6374.
79	631.62	2.211		6545.	6470.	6470.
80	629.65	2.014		6648.	6564.	6564.
81	629.40		2.7292	6660.	6577.	6577.
82	627.84	2.024		6741.	6660.	6660.
83	626.01	2.019		6798.	6717.	6717.
84	624.97	1.945		6960.	6882.	6882.
85	619.92	1.972		7100.	7025.	7025.
86	617.07	2.047		7230.	7157.	7157.
87	615.11	2.030		7327.	7254.	7254.
88	613.14	2.061		7424.	7352.	7352.
89	611.96	2.035		7481.	7411.	7411.
90	610.00	2.050		7577.	7508.	7508.
91	607.64	1.987		7689.	7621.	7621.
92	607.25	2.003		7708.	7639.	7639.
93	605.67	1.987		7781.	7713.	7713.
94	604.10	1.956		7852.	7784.	7784.
95	602.14	2.028		7943.	7876.	7876.
96	599.78	2.022		8056.	7989.	7989.
97	598.60		2.8881	8112.	8046.	8046.
98	597.81	2.033		8150.	8084.	8084.
99	595.46	2.038		8264.	8198.	8198.
100	592.70	2.069		8400.	8334.	8334.

BOREHOLE OBT-19

J	PLACE DEPTH (FT)	G - G DENSITY (GM/CC)	DENSITY OF SOLID COMPONENT (GM/CC)	CUMULATIVE SOLID MASS (GM/CM**2) RHO=2.821	RHO=<RHO>	LINEAR SPLINE FOR RHO
101	590.74	2.025		8496.	8430.	8430.
102	588.69	2.050		8611.	8545.	8545.
103	586.81	2.003		8686.	8620.	8620.
104	585.24	2.041		8761.	8695.	8695.
105	584.06	2.030		8818.	8752.	8752.
106	581.31	2.041		8951.	8885.	8885.
107	579.13	2.019		9027.	8961.	8961.
108	578.50		2.8843	9066.	9019.	9019.
109	576.59	2.036		9178.	9111.	9111.
110	573.84	2.038		9311.	9245.	9245.
111	572.66	2.024		9368.	9301.	9301.
112	568.73	2.017		9555.	9489.	9489.
113	567.94	2.035		9593.	9527.	9527.
114	565.19	2.016		9725.	9660.	9660.
115	563.23	2.027		9819.	9755.	9755.
116	561.65	2.019		9894.	9830.	9830.
117	560.87	2.003		9931.	9868.	9868.
118	559.59	2.013		9986.	9924.	9924.
119	556.94	1.972		10114.	10053.	10053.
120	556.54	1.987		10132.	10071.	10071.
121	554.58	1.937		10220.	10161.	10161.
122	552.61	1.951		10307.	10249.	10249.
123	549.86	1.956		10429.	10374.	10374.
124	549.00		2.7221	10468.	10413.	10413.
125	547.90	1.987		10518.	10465.	10465.
126	546.52	1.959		10589.	10538.	10538.
127	543.57	2.000		10715.	10666.	10666.
128	541.21	1.987		10825.	10778.	10778.
129	539.64	1.951		10896.	10851.	10851.
130	538.90		2.7140	10929.	10885.	10885.
131	536.69	1.945		11017.	10975.	10975.
132	534.95	1.965		11105.	11065.	11065.
133	533.35	1.961		11176.	11137.	11137.
134	532.57	1.940		11210.	11173.	11173.
135	529.62	1.958		11350.	11315.	11315.
136	528.24	1.921		11401.	11368.	11368.
137	526.67	1.939		11469.	11438.	11438.
138	525.49	1.917		11520.	11490.	11490.
139	523.92	1.925		11588.	11559.	11559.
140	522.74	1.991		11640.	11613.	11613.
141	520.78	2.024		11733.	11707.	11707.
142	518.81	2.003		11826.	11803.	11803.
143	517.63	2.011		11881.	11859.	11859.
144	515.50		2.7140	11981.	11962.	11962.
145	515.27	1.997		11992.	11973.	11973.
146	513.70	2.050		12067.	12049.	12049.
147	512.52	2.060		12125.	12109.	12109.
148	509.58	2.050		12280.	12268.	12268.
149	508.98	2.035		12300.	12287.	12287.
150	507.81	2.031		12357.	12346.	12346.
151	506.63	2.025		12413.	12404.	12404.
152	504.66	2.039		12508.	12501.	12501.
153	503.09	2.027		12586.	12580.	12580.
154	500.54	2.088		12725.	12723.	12723.
155	498.37	2.082		12825.	12825.	12825.
156	497.59	2.050		12864.	12865.	12865.
157	496.01	2.066		12942.	12944.	12944.
158	494.05	2.035		13036.	13043.	13043.
159	491.69	2.028		13152.	13159.	13159.
160	490.12	1.980		13226.	13235.	13235.
161	488.55	2.050		13300.	13310.	13310.
162	487.37	2.050		13357.	13369.	13369.
163	486.19	2.102		13416.	13429.	13429.
164	485.01	2.113		13477.	13492.	13492.
165	483.50		2.7181	13555.	13571.	13571.
166	482.46	2.047		13616.	13634.	13634.
167	479.90	1.987		13729.	13748.	13748.
168	478.33	2.003		13802.	13822.	13822.
169	476.40	1.929		13879.	14000.	14000.
170	473.22	1.986		14031.	14051.	14051.
171	470.86	2.063		14142.	14162.	14162.
172	468.89	2.077		14240.	14260.	14260.
173	468.08		2.8882	14285.	14304.	14304.
174	466.93	2.046		14336.	14356.	14356.
175	465.75	1.991		14394.	14411.	14411.
176	462.61	2.003		14540.	14557.	14557.
177	462.21	1.991		14558.	14575.	14575.
178	461.03	1.995		14613.	14629.	14629.
179	459.96	2.053		14688.	14705.	14705.
180	458.28	2.035		14746.	14762.	14762.
181	455.94	2.066		14862.	14879.	14879.
182	453.57	2.035		14977.	14996.	14996.
183	450.81	2.022		15110.	15130.	15130.
184	448.85	2.019		15203.	15225.	15225.
185	448.00		2.7201	15243.	15266.	15266.
186	446.10	1.965		15331.	15355.	15355.
187	442.95	1.969		15473.	15500.	15500.
188	440.99	2.053		15565.	15594.	15594.
189	437.06	2.052		15759.	15791.	15791.
190	435.09	2.025		15854.	15888.	15888.
191	432.76	2.035		15968.	16003.	16003.
192	430.77	2.060		16064.	16101.	16101.
193	428.82	2.053		16200.	16239.	16239.
194	427.26	2.025		16236.	16277.	16277.
195	425.66	2.019		16313.	16353.	16353.
196	423.50	2.028		16426.	16467.	16467.
197	420.16	2.028		16577.	16620.	16620.
198	419.37	2.041		16615.	16658.	16658.
199	416.62	1.991		16746.	16790.	16790.
200	415.44	1.987		16800.	16845.	16845.

TABLE 6-10 (Continued)

BOREHOLE DDT-19

J	PEACL DEPTH (FT)	G - G DENSITY (GM/CC)	DENSITY OF SOLID COMPONENT (GM/CC)	CUMULATIVE SOLID MASS (GM/CM**2) RHO=2.821	RHO=(RHO)	LINEAR SPLINE FOR RHO
201	414.26	1.972		16856.	16899.	16899.
202	411.31	2.030		16983.	17026.	17026.
203	409.34	2.009		17076.	17122.	17122.
204	409.20		2.7995	17092.	17139.	17139.
205	407.38	2.003		17169.	17215.	17215.
206	406.79	1.942		17204.	17251.	17251.
207	404.86	2.003		17293.	17340.	17340.
208	403.85	2.003		17349.	17395.	17395.
209	402.47	2.045		17405.	17450.	17450.
210	400.90	2.097		17483.	17528.	17528.
211	399.72	2.104		17544.	17588.	17588.
212	399.50		2.8905	17555.	17599.	17599.
213	395.00	2.097		17767.	17808.	17808.
214	393.04	2.134		17890.	17929.	17929.
215	389.89	2.148		18056.	18094.	18094.
216	388.71	2.149		18121.	18157.	18157.
217	386.75	2.129		18226.	18260.	18260.
218	385.18	2.118		18309.	18342.	18342.
219	382.82	2.129		18433.	18464.	18464.
220	381.64	2.151		18496.	18526.	18526.
221	380.50		2.9040	18556.	18586.	18586.
222	380.07	2.126		18579.	18608.	18608.
223	378.67	2.027		18649.	18678.	18678.
224	377.71	1.959		18689.	18717.	18717.
225	375.74	1.880		18770.	18796.	18796.
226	372.99	1.909		18882.	18906.	18906.
227	370.24	1.814		18992.	19014.	19014.
228	368.27	1.892		19060.	19082.	19082.
229	366.91	1.849		19123.	19144.	19144.
230	362.77	1.970		19259.	19278.	19278.
231	361.59	1.962		19312.	19330.	19330.
232	359.23	1.980		19419.	19435.	19435.
233	356.48	2.035		19549.	19563.	19563.
234	355.50		2.9020	19595.	19609.	19609.
235	353.73	2.046		19682.	19694.	19694.
236	350.59	2.011		19834.	19843.	19843.
237	348.62	1.976		19925.	19934.	19934.
238	345.87	1.967		20050.	20057.	20057.
239	343.51	1.909		20153.	20159.	20159.
240	340.76	1.961		20273.	20279.	20279.
241	337.98	1.972		20326.	20332.	20332.
242	336.70		2.8365	20366.	20372.	20372.
243	337.62	2.013		20417.	20422.	20422.
244	333.26	1.946		20525.	20530.	20530.
245	333.69	1.994		20596.	20601.	20601.
246	331.72	2.038		20689.	20694.	20694.
247	330.15	2.104		20768.	20773.	20773.
248	328.18	2.080		20868.	20873.	20873.
249	326.22	2.064		20967.	20972.	20972.
250	325.04	2.019		21024.	21029.	21029.
251	323.07	2.016		21118.	21123.	21123.
252	319.98	2.083		21272.	21277.	21277.
253	317.96	2.096		21372.	21378.	21378.
254	316.69	2.036		21451.	21456.	21456.
255	315.21	2.017		21507.	21513.	21513.
256	313.25	2.011		21600.	21607.	21607.
257	311.28	2.053		21695.	21702.	21702.
258	311.10		2.7973	21704.	21711.	21711.
259	310.50	2.041		21735.	21741.	21741.
260	309.52	2.057		21791.	21799.	21799.
261	306.96	2.050		21907.	21915.	21915.
262	305.39	2.083		21983.	21991.	21991.
263	304.21	2.019		22039.	22047.	22047.
264	301.46	2.046		22171.	22180.	22180.
265	300.67	2.082		22210.	22219.	22219.
266	299.10	2.050		22289.	22297.	22297.
267	298.72	2.042		22404.	22413.	22413.
268	296.50		2.8233	22416.	22424.	22424.
269	295.17	2.024		22480.	22488.	22488.
270	292.81	2.055		22595.	22603.	22603.
271	290.06	2.028		22729.	22737.	22737.
272	288.49	2.035		22804.	22812.	22812.
273	285.74	1.976		22934.	22941.	22941.
274	283.58	1.972		23041.	23048.	23048.
275	282.98	1.948		23058.	23065.	23065.
276	280.62	2.017		23167.	23173.	23173.
277	279.45	2.028		23223.	23229.	23229.
278	277.87	2.055		23299.	23305.	23305.
279	275.91	2.036		23395.	23401.	23401.
280	273.94	2.059		23491.	23496.	23496.
281	273.16	2.011		23528.	23533.	23533.
282	271.59	2.000		23602.	23607.	23607.
283	268.44	1.925		23743.	23747.	23747.
284	266.08	1.929		23845.	23848.	23848.
285	264.12	1.981		23933.	23935.	23935.
286	262.15	2.052		24026.	24027.	24027.
287	260.19	2.060		24123.	24124.	24124.
288	258.61	2.053		24201.	24201.	24201.
289	257.04	2.022		24277.	24276.	24276.
290	255.08	2.003		24370.	24368.	24368.
291	253.90	1.970		24424.	24422.	24422.
292	251.93	1.969		24513.	24510.	24510.
293	251.90		2.9268	24515.	24511.	24511.
294	250.36	1.948		24584.	24579.	24579.
295	248.40	1.972		24672.	24666.	24666.
296	246.93	1.948		24760.	24753.	24753.
297	244.97	1.981		24848.	24841.	24841.
298	243.00	1.983		24938.	24930.	24930.
299	241.34	1.950		24988.	24985.	24985.
300	238.97	2.057		25180.	25120.	25120.

BOREHOLE DDT-19

J	PEACL DEPTH (FT)	G - G DENSITY (GM/CC)	DENSITY OF SOLID COMPONENT (GM/CC)	CUMULATIVE SOLID MASS (GM/CM**2) RHO=2.821	RHO=(RHO)	LINEAR SPLINE FOR RHO
301	226.90		2.9700			
302	216.30		2.8541			
303	196.90		2.8059			
304	189.80		2.8974			
305	171.20		2.8387			
306	168.00		2.9159			
307	163.40		2.9133			
308	148.70		2.9213			
309	123.60		2.9291			
310	122.90		2.9135			
311	118.00		2.9197			
312	117.99		2.8210			
313	.00		2.8210			

TABLE 6-10 (Continued)

BOREHOLE OBZ-04

J	PEACL DEPTH (FT)	G + G DENSITY (GM/CC)	DENSITY OF SOLID COMPONENT (GM/CC)	CUMULATIVE SOLID MASS (GM/CM**2) RHO=2.821	RHO=(RHO)	LINEAR SPLINE FOR RHO
0	1800.00		2.8210			
1	1795.81		2.8210			
2	1795.80		2.7242			
3	1785.10		2.7140			
4	1783.30		2.7201			
5	1778.30		2.7242			
6	1775.90		2.7241			
7	1765.20		2.7181			
8	1734.80		2.7241			
9	1698.90		2.7140			
10	1694.80		2.7140			
11	1693.50		2.7140			
12	1650.90		2.7241			
13	1635.50		2.7140			
14	1626.10		2.7140			
15	1616.10		2.7140			
16	1610.70		2.7242			
17	1589.50		2.7140			
18	1519.84	2.146		0.	0.	0.
19	1516.83	2.100		156.	161.	161.
20	1514.59	2.107		269.	274.	274.
21	1512.11	2.179		407.	415.	415.
22	1509.54	2.182		549.	560.	560.
23	1508.20	2.131		619.	631.	631.
24	1506.33	2.097		708.	723.	723.
25	1504.82	2.095		796.	813.	813.
26	1503.10	2.079		884.	902.	902.
27	1500.09	2.079		1035.	1056.	1056.
28	1499.29	2.057		1078.	1100.	1100.
29	1498.58	2.047		1121.	1143.	1143.
30	1494.94	2.083		1292.	1318.	1318.
31	1493.23	2.121		1380.	1408.	1408.
32	1488.40		2.7303	1623.	1655.	1655.
33	1488.08	2.020		1638.	1671.	1671.
34	1487.22	2.038		1679.	1713.	1713.
35	1485.36	2.054		1868.	1905.	1905.
36	1481.69	2.052		1953.	1991.	1991.
37	1480.85	2.048		2017.	2057.	2057.
38	1476.08	2.131		2240.	2284.	2284.
39	1474.77	2.110		2307.	2353.	2353.
40	1473.08	2.110		2397.	2444.	2444.
41	1470.48	2.105		2530.	2580.	2580.
42	1468.76	2.078		2618.	2670.	2670.
43	1467.05	2.004		2701.	2755.	2755.
44	1466.62	2.008		2722.	2775.	2775.
45	1464.90	2.030		2803.	2859.	2859.
46	1461.90	2.136		2956.	3014.	3014.
47	1461.87	2.124		2978.	3037.	3037.
48	1459.54	2.121		3091.	3152.	3152.
49	1458.08	2.098		3158.	3220.	3220.
50	1457.18	2.122		3202.	3266.	3266.
51	1456.52	2.165		3248.	3312.	3312.
52	1454.17	2.165		3366.	3432.	3432.
53	1452.46	2.180		3460.	3528.	3528.
54	1451.17	2.115		3529.	3599.	3599.
55	1450.31	2.103		3574.	3644.	3644.
56	1449.02	2.115		3641.	3712.	3712.
57	1446.62	2.130		3766.	3871.	3871.
58	1445.16	2.083		3840.	3916.	3916.
59	1443.01	2.054		3948.	4025.	4025.
60	1441.73	2.057		4011.	4090.	4090.
61	1440.01	2.071		4096.	4177.	4177.
62	1438.49	2.069		4182.	4265.	4265.
63	1437.00	2.037		4246.	4329.	4329.
64	1434.86	2.011		4348.	4434.	4434.
65	1433.14	2.018		4430.	4517.	4517.
66	1431.85	2.037		4492.	4580.	4580.
67	1428.92	2.038		4636.	4750.	4750.
68	1426.28	2.037		4762.	4856.	4856.
69	1424.56	2.044		4846.	4941.	4941.
70	1423.70	2.015		4887.	4983.	4983.
71	1422.40	2.011		4948.	5046.	5046.
72	1420.27	2.020		5050.	5149.	5149.
73	1418.98	2.015		5111.	5212.	5212.
74	1418.30	2.020		5131.	5233.	5233.
75	1417.69	2.016		5172.	5274.	5274.
76	1414.69	2.009		5314.	5419.	5419.
77	1412.97	2.018		5395.	5502.	5502.
78	1412.11	2.008		5436.	5544.	5544.
79	1410.82	2.020		5497.	5606.	5606.
80	1409.54	2.045		5559.	5669.	5669.
81	1406.98	2.044		5685.	5797.	5797.
82	1405.67	2.056		5748.	5862.	5862.
83	1404.69	2.014		5811.	5926.	5926.
84	1404.69	2.018		5811.	5926.	5926.
85	1400.95	2.006		5994.	6092.	6092.
86	1399.24	2.005		6054.	6174.	6174.
87	1397.20		2.7262	6151.	6273.	6273.
88	1397.07	2.032		6156.	6278.	6278.
89	1395.37	2.040		6240.	6363.	6363.
90	1393.23	2.047		6344.	6470.	6470.
91	1392.37	2.042		6386.	6513.	6513.
92	1390.22	2.025		6484.	6618.	6618.
93	1389.37	1.977		6529.	6659.	6659.
94	1388.51	1.967		6568.	6699.	6699.
95	1386.79	1.980		6646.	6778.	6778.
96	1385.93	1.980		6685.	6818.	6818.
97	1384.64	1.999		6745.	6879.	6879.
98	1383.79	2.037		6786.	6921.	6921.
99	1381.21	2.037		6910.	7049.	7049.
100	1380.78	2.047		6931.	7070.	7070.

BOREHOLE OBZ-04

J	PEACL DEPTH (FT)	G + G DENSITY (GM/CC)	DENSITY OF SOLID COMPONENT (GM/CC)	CUMULATIVE SOLID MASS (GM/CM**2) RHO=2.821	RHO=(RHO)	LINEAR SPLINE FOR RHO
101	1379.20		2.7140	7009.	7149.	7149.
102	1376.44	2.061		7143.	7286.	7286.
103	1374.77	2.047		7221.	7373.	7373.
104	1373.06	2.057		7312.	7459.	7459.
105	1370.92	2.083		7419.	7569.	7569.
106	1367.48	2.209		7604.	7758.	7758.
107	1364.47	2.294		7776.	7934.	7934.
108	1363.18	2.194		7850.	8010.	8010.
109	1362.99	2.162		7897.	8058.	8058.
110	1361.47	2.160		7944.	8106.	8106.
111	1360.61	2.146		7990.	8153.	8153.
112	1360.18	2.167		8014.	8177.	8177.
113	1358.05	2.170		8131.	8297.	8297.
114	1357.18	2.160		8178.	8345.	8345.
115	1356.52	2.174		8225.	8394.	8394.
116	1355.96	2.162		8272.	8442.	8442.
117	1355.31	2.065		8384.	8556.	8556.
118	1351.80	2.056		8470.	8644.	8644.
119	1351.17	2.037		8491.	8665.	8665.
120	1348.59	2.011		8614.	8791.	8791.
121	1346.88	2.008		8694.	8874.	8874.
122	1345.36	2.003		8775.	8956.	8956.
123	1344.78	1.994		8795.	8976.	8976.
124	1343.01	2.001		8875.	9058.	9058.
125	1340.49	1.991		8992.	9181.	9181.
126	1339.15	1.991		9054.	9242.	9242.
127	1338.29	1.985		9094.	9282.	9282.
128	1337.49	1.996		9133.	9323.	9323.
129	1336.38	1.999		9173.	9364.	9364.
130	1334.00	2.020		9295.	9488.	9488.
131	1333.07	2.016		9315.	9509.	9509.
132	1330.67	2.015		9458.	9654.	9654.
133	1328.42	2.020		9560.	9759.	9759.
134	1327.13	2.045		9622.	9822.	9822.
135	1325.42	2.049		9706.	9908.	9908.
136	1323.70	2.038		9790.	9994.	9994.
137	1320.70	2.004		9933.	10141.	10141.
138	1319.41	1.972		9992.	10201.	10201.
139	1316.80	1.996		10130.	10343.	10343.
140	1315.55	1.992		10170.	10383.	10383.
141	1315.12	1.997		10190.	10404.	10404.
142	1314.25	2.018		10230.	10445.	10445.
143	1312.97	1.997		10291.	10507.	10507.
144	1312.11	1.992		10331.	10548.	10548.
145	1311.25	1.997		10371.	10589.	10589.
146	1309.11	2.062		10474.	10694.	10694.
147	1306.46	2.090		10582.	10805.	10805.
148	1305.25	2.056		10669.	10894.	10894.
149	1299.67	2.028		10945.	11177.	11177.
150	1297.95	2.003		11027.	11260.	11260.
151	1294.54	2.008		11193.	11430.	11430.
152	1291.94	2.007		11323.	11563.	11563.
153	1290.65	2.026		11384.	11630.	11630.
154	1289.37	2.083		11454.	11697.	11697.
155	1288.08	2.131		11520.	11765.	11765.
156	1284.42	2.276		11736.	11988.	11988.
157	1279.92	2.100		11977.	12233.	12233.
158	1278.06	2.069		12021.	12277.	12277.
159	1277.20	2.068		12107.	12365.	12365.
160	1276.49	2.059		12149.	12409.	12409.
161	1274.34	2.131		12259.	12521.	12521.
162	1271.77	2.278		12405.	12670.	12670.
163	1270.05	2.278		12508.	12775.	12775.
164	1269.19	2.288		12559.	12828.	12828.
165	1268.34	2.273		12611.	12881.	12881.
166	1264.04	1.974		12837.	13112.	13112.
167	1262.33	1.950		12914.	13191.	13191.
168	1261.04	1.915		12970.	13248.	13248.
169	1258.05	1.917		13098.	13379.	13379.
170	1257.18	1.897		13134.	13417.	13417.
171	1256.32	1.893		13170.	13453.	13453.
172	1254.60	1.898		13242.	13526.	13526.
173	1253.74	1.917		13278.	13564.	13564.
174	1252.03	1.922		13351.	13639.	13639.
175	1251.60	1.941		13370.	13658.	13658.
176	1250.74	1.946		13408.	13697.	13697.
177	1249.45	1.941		13465.	13755.	13755.
178	1248.16	1.951		13521.	13812.	13812.
179	1246.04	1.927		13614.	13907.	13907.
180	1242.58	1.946		13764.	14061.	14061.
181	1239.98	1.941		13896.	14196.	14196.
182	1237.40	1.974		13992.	14294.	14294.
183	1236.57	2.100		14179.	14485.	14485.
184	1232.71	2.115		14223.	14531.	14531.
185	1229.48	2.197		14409.	14721.	14721.
186	1228.10		2.7140	14419.	14732.	14732.
187	1227.13	2.129		14526.	14841.	14841.
188	1222.84	2.098		14750.	15070.	15070.
189	1217.69	2.413		15054.	15380.	15380.
190	1214.26	2.415		15262.	15614.	15614.
191	1210.82	2.167		15490.	15827.	15827.
192	1208.25	2.209		15801.	16144.	16144.
193	1205.53	2.162		15895.	16240.	16240.
194	1200.90	2.115		16030.	16379.	16379.
195	1199.24	2.081		16119.	16469.	16469.
196	1197.09	2.115		16229.	16582.	16582.
197	1191.94	2.096		16496.	16854.	16854.
198	1189.40		2.7242	16626.	16987.	16987.
199	1182.07	2.093		17002.	17371.	17371.
200	1175.65	2.526		17398.	17775.	17775.

TABLE 6-10 (Continued)

BOREHOLE DBZ-04

J	PLACE DEPTH (FT)	G - G DENSITY (GM/CC)	DENSITY OF SOLID COMPONENT (GM/CC)	CUMULATIVE SOLID MASS (GM/CM**2) RHO=2.821	RHO=(RHO)	LINEAR SPLINE FOR RHO
201	1169.19	2.548		17864.	18251.	18251.
202	1161.47	2.264		18375.	18773.	18773.
203	1156.32	2.196		18672.	19077.	19077.
204	1151.80	2.167		18933.	19344.	19344.
205	1145.16	2.397		19321.	19740.	19740.
206	1141.30	2.403		19575.	20000.	20000.
207	1139.15	2.440		19719.	20147.	20147.
208	1134.86	2.180		19983.	20417.	20417.
209	1130.57	2.086		20210.	20650.	20650.
210	1127.56	2.085		20363.	20806.	20806.
211	1123.27	2.043		20576.	21024.	21024.
212	1121.60		2.7120	20657.	21107.	21107.
213	1121.59		2.8210	20657.	21107.	21107.
214	1120.70	2.056		20701.	21151.	21151.
215	1115.97	2.056		20934.	21384.	21384.
216	1113.40	2.035		21060.	21510.	21516.
217	1110.40	2.018		21209.	21658.	21658.
218	1109.11	2.172		21275.	21725.	21725.
219	1103.10	2.124		21581.	22041.	22041.
220	1102.67	2.103		21613.	22063.	22063.
221	1099.67	2.102		21768.	22218.	22218.
222	1098.38	2.076		21834.	22284.	22284.
223	1094.94	2.069		22006.	22456.	22456.
224	1091.94	2.090		22158.	22608.	22608.
225	1085.93	2.059		22460.	22910.	22910.
226	1079.06	2.109		22808.	23258.	23258.
227	1066.19	2.030		23452.	23902.	23902.
228	1062.76	2.044		23618.	24068.	24068.
229	1058.89	2.105		23812.	24262.	24262.
230	1057.18	2.192		23903.	24355.	24355.
231	1053.31	2.158		24118.	24567.	24567.
232	1051.17	2.001		24226.	24676.	24676.
233	1047.75	2.037		24389.	24839.	24839.
234	1046.01	2.184		24435.	25085.	25085.
235	1038.29	2.107		24868.	25338.	25338.
236	1034.00	2.115		25111.	25561.	25561.
237	1030.14	2.081		25310.	25760.	25760.
238	1025.42	2.088		25549.	25999.	25999.
239	1020.27	2.126		25816.	26266.	26266.
240	1017.69	2.112		25951.	26401.	26401.
241	1015.97	2.150		26042.	26492.	26492.
242	1012.11	2.170		26252.	26702.	26702.
243	1010.40	2.150		26345.	26795.	26795.
244	1006.10	2.141		26575.	27025.	27025.
245	1004.39	2.098		26665.	27115.	27115.
246	1000.09	2.138		26890.	27340.	27340.
247	997.52	2.138		27027.	27477.	27477.
248	994.52	2.056		27182.	27631.	27631.
249	987.66	2.095		27548.	27998.	27998.
250	983.79	2.153		27729.	28179.	28179.
251	979.99	2.167		27962.	28412.	28412.
252	972.63	2.252		28352.	28802.	28802.
253	967.91	2.184		28622.	29072.	29072.
254	964.48	2.184		28786.	29238.	29238.
255	961.04	2.098		28995.	29445.	29445.
256	954.60	2.064		29320.	29770.	29770.
257	950.31	2.064		29534.	29984.	29984.
258	947.73	2.103		29665.	30114.	30114.
259	943.87	2.095		29863.	30313.	30313.
260	930.14	2.129		30578.	31028.	31028.
261	924.56	2.261		30891.	31341.	31341.
262	920.27	2.158		31134.	31584.	31584.
263	918.12	2.141		31250.	31700.	31700.
264	914.85	2.098		31417.	31767.	31767.
265	910.12	2.115		31406.	31856.	31856.
266	912.54	2.107		31540.	31990.	31990.
267	911.25	2.132		31608.	32058.	32058.
268	908.25	2.121		31766.	32216.	32216.
269	902.24	2.218		32095.	32545.	32545.
270	894.94	2.129		32497.	32947.	32947.
271	891.54	2.056		32519.	32968.	32968.
272	889.87	2.043		32772.	33221.	33221.
273	882.98	2.155		33103.	33553.	33553.
274	881.21	2.141		33195.	33645.	33645.
275	878.21	2.151		33357.	33806.	33806.
276	875.20	2.141		33516.	33968.	33968.
277	874.77	2.115		33541.	33990.	33990.
278	870.91	2.115		33742.	34192.	34192.
279	868.34	2.148		33879.	34329.	34329.
280	866.19	2.152		33992.	34443.	34443.
281	864.47	2.150		34085.	34535.	34535.
282	860.18	2.132		34314.	34764.	34764.
283	857.61	2.050		34446.	34896.	34896.
284	855.04	2.050		34636.	35086.	35086.
285	851.60	2.098		34744.	35193.	35193.
286	849.02	2.098		34876.	35326.	35326.
287	847.31	2.050		34962.	35412.	35412.
288	845.44	2.050		35152.	35602.	35602.
289	841.13	2.103		35288.	35688.	35688.
290	836.15	2.168		35535.	35985.	35985.
291	831.00	2.030		35800.	36250.	36250.
292	829.28	2.047		35883.	36333.	36333.
293	827.99	2.098		35948.	36398.	36398.
294	825.70	2.056		36164.	36614.	36614.
295	818.55	2.158		36431.	36881.	36881.
296	815.12	2.127		36615.	37065.	37065.
297	809.11	2.167		36938.	37388.	37388.
298	805.25	2.150		37147.	37597.	37597.
299	800.52	2.204		37408.	37858.	37858.
300	795.37	2.124		37689.	38139.	38139.

BOREHOLE DBZ-04

J	PLACE DEPTH (FT)	G - G DENSITY (GM/CC)	DENSITY OF SOLID COMPONENT (GM/CC)	CUMULATIVE SOLID MASS (GM/CM**2) RHO=2.821	RHO=(RHO)	LINEAR SPLINE FOR RHO
301	780.78	2.170		38473.	38923.	38923.
302	779.42	2.158		38520.	38969.	38969.
303	778.05	2.175		38588.	39038.	39038.
304	765.76	1.910		39267.	39717.	39717.
305	763.61	1.750		39350.	39800.	39800.
306	759.32	1.845		39514.	39964.	39964.
307	757.18	2.107		39614.	40064.	40064.
308	754.60	2.143		39750.	40199.	40199.
309	752.03	2.103		39885.	40335.	40335.
310	748.59	2.107		40063.	40512.	40512.
311	743.44	2.047		40322.	40772.	40772.
312	742.15	1.987		40383.	40833.	40833.
313	739.58	2.008		40503.	40953.	40953.
314	737.45	1.970		40602.	41052.	41052.
315	735.37	2.013		40781.	41231.	41231.
316	731.45	2.076		40986.	41336.	41336.
317	727.13	2.025		41097.	41546.	41546.
318	724.99	2.073		41202.	41652.	41652.
319	721.98	2.093		41384.	41804.	41804.
320	719.84	1.984		41458.	41908.	41908.
321	716.40	1.996		41617.	42067.	42067.
322	714.26	1.955		41714.	42164.	42164.
323	712.54	2.052		41795.	42245.	42245.
324	710.82	2.013		41878.	42327.	42327.
325	709.11	2.071		41961.	42411.	42411.
326	706.96	2.013		42066.	42516.	42516.
327	705.67	2.071		42128.	42578.	42578.
328	702.23	2.061		42300.	42749.	42749.
329	699.25	2.172		42457.	42906.	42906.
330	694.09	2.030		42722.	43172.	43172.
331	691.08	2.177		42877.	43327.	43327.
332	688.01	1.900		43002.	43452.	43452.
333	683.36	1.530		43185.	43635.	43635.
334	679.92	1.695		43289.	43739.	43739.
335	677.35	2.036		43394.	43844.	43844.
336	674.77	2.004		43518.	43968.	43968.
337	669.19	2.057		43787.	44237.	44237.
338	665.53	1.919		43965.	44415.	44415.
339	663.61	1.944		44040.	44489.	44489.
340	661.47	1.927		44133.	44583.	44583.
341	661.04	1.950		44152.	44602.	44602.
342	655.89	1.979		44384.	44833.	44833.
343	654.17	1.944		44461.	44910.	44910.
344	651.17	2.003		44597.	45047.	45047.
345	647.31	1.960		44774.	45224.	45224.
346	641.30	2.201		45078.	45528.	45528.
347	637.00	2.004		45299.	45749.	45749.
348	634.00	2.044		45443.	45893.	45893.
349	633.57	2.124		45465.	45915.	45915.
350	631.85	2.150		45556.	46006.	46006.
351	628.42	2.139		45740.	46190.	46190.
352	625.42	2.090		45897.	46347.	46347.
353	623.27	2.119		46008.	46458.	46458.
354	619.84	2.047		46182.	46632.	46632.
355	618.35	1.922		46241.	46691.	46691.
356	615.35	1.944		46372.	46822.	46822.
357	613.40	2.056		46472.	46922.	46922.
358	609.54	1.903		46653.	47103.	47103.
359	606.96	1.982		46769.	47219.	47219.
360	605.25	2.093		46853.	47302.	47302.
361	602.67	2.150		46988.	47438.	47438.
362	598.36	2.201		47224.	47674.	47674.
363	593.25	2.155		47508.	47958.	47958.
364	591.94	2.103		47577.	48026.	48026.
365	587.85	2.073		47795.	48245.	48245.
366	585.50	2.144		47906.	48356.	48356.
367	581.41	2.245		48146.	48596.	48596.
368	574.77	2.141		48504.	48954.	48954.
369	569.62	2.184		48785.	49235.	49235.
370	567.05	2.167		48927.	49377.	49377.
371	561.90	1.970		49184.	49634.	49634.
372	560.16	1.987		49262.	49712.	49712.
373	559.75	2.047		49283.	49733.	49733.
374	556.75	2.107		49434.	49884.	49884.
375	554.17	2.151		49570.	50020.	50020.
376	552.46	2.138		49662.	50112.	50112.
377	548.59	2.184		49872.	50322.	50322.
378	546.75	2.091		50078.	50528.	50528.
379	542.56	1.825		50174.	50624.	50624.
380	540.01	1.869		50276.	50725.	50725.
381	538.49	1.825		50343.	50793.	50793.
382	536.15	2.064		50438.	50888.	50888.
383	532.71	2.095		50611.	51061.	51061.
384	529.98	2.093		51160.	51610.	51610.
385	527.69	2.115		51382.	51832.	51832.
386	525.55	2.146		51496.	51946.	51946.
387	509.54	2.098		51812.	52262.	52261.
388	506.96	2.138		51946.	52396.	52396.
389	503.96	2.188		52107.	52557.	52557.
390	497.95	2.235		52443.	52893.	52893.
391	493.45	2.150		52707.	53157.	53157.
392	491.94	2.081		52774.	53224.	53224.
393	489.37	2.098		52905.	53355.	53355.
394	486.79	2.073		53036.	53486.	53486.
395	485.50	2.115		53102.	53552.	53552.
396	481.21	2.076		53322.	53772.	53772.
397	475.20	2.167		53636.	54087.	54087.
398	471.77	2.078		53818.	54268.	54268.
399	468.34	2.098		53993.	54443.	54443.
400	466.62	2.076		54089.	54539.	54539.

TABLE 6-10 (Continued)

BOREHOLE 082-04

J	PLACE DEPTH (FT)	G - G DENSITY (GM/CC)	DENSITY OF SOLID COMPONENT (GM/CC)	CUMULATIVE SOLID MASS (GM/CM**2) RHO=2.821	RHO=(RHO)	LINEAR SPLINE FOR RHO
401	464.04	2.098		54211.	54661.	54661.
402	461.04	2.184		54372.	54822.	54822.
403	458.89	2.203		54492.	54942.	54942.
404	456.75	2.167		54611.	55061.	55061.
405	453.31	2.167		54799.	55248.	55248.
406	451.17	2.144		54915.	55365.	55365.
407	448.16	2.158		55077.	55527.	55527.
408	445.08	2.090		55229.	54978.	55978.
409	436.15	2.015		55697.	56147.	56147.
410	433.14	2.028		55841.	56291.	56291.
411	431.93	2.021		55925.	56373.	56373.
412	426.70	2.102		56157.	56607.	56607.
413	423.27	2.102		56334.	56784.	56784.
414	416.83	2.054		56659.	57109.	57109.
415	415.97	2.035		56701.	57151.	57151.
416	413.83	2.047		56805.	57255.	57255.
417	412.11	2.020		56887.	57337.	57337.
418	407.39	2.018		57112.	57562.	57562.
419	405.25	2.030		57215.	57665.	57665.
420	402.67	2.142		57345.	57795.	57795.
421	398.81	2.177		57534.	58004.	58004.
422	397.32	2.155		57624.	58074.	58074.
423	393.66	2.184		57836.	58286.	58286.
424	.00		2.8210			

BOREHOLE 001-05

J	PLACE DEPTH (FT)	G - G DENSITY (GM/CC)	DENSITY OF SOLID COMPONENT (GM/CC)	CUMULATIVE SOLID MASS (GM/CM**2) RHO=2.821	RHO=(RHO)	LINEAR SPLINE FOR RHO
0	1000.00		2.8210			
1	997.36	2.128		0.	0.	0.
2	996.18	2.164		63.	63.	63.
3	994.21	2.147		170.	170.	170.
4	992.24	2.159		276.	276.	276.
5	988.70	2.095		463.	463.	463.
6	985.74	2.109		605.	605.	605.
7	982.79	2.195		774.	774.	774.
8	978.46	2.173		1015.	1015.	1015.
9	975.71	2.100		1161.	1161.	1161.
10	972.56	2.081		1322.	1322.	1322.
11	969.41	2.159		1487.	1487.	1487.
12	964.29	2.246		1776.	1776.	1776.
13	960.75	2.272		1985.	1985.	1985.
14	959.17	2.260		2079.	2079.	2079.
15	957.99	2.206		2147.	2147.	2147.
16	956.42	2.191		2235.	2235.	2235.
17	955.24	2.222		2302.	2302.	2302.
18	953.27	2.308		2419.	2419.	2419.
19	951.50	2.335		2541.	2541.	2541.
20	949.53	2.304		2663.	2663.	2663.
21	947.76	2.222		2757.	2757.	2757.
22	944.61	2.156		2932.	2932.	2932.
23	943.03	2.155		3018.	3018.	3018.
24	936.69	2.122		3374.	3374.	3374.
25	932.74	2.128		3561.	3561.	3561.
26	928.86	2.155		3771.	3771.	3771.
27	927.28	2.175		3857.	3857.	3857.
28	926.10	2.133		3921.	3921.	3921.
29	922.56	2.159		4111.	4111.	4111.
30	920.59	2.252		4223.	4223.	4223.
31	918.62	2.279		4340.	4340.	4340.
32	916.65	2.254		4457.	4457.	4457.
33	912.72	2.162		4680.	4680.	4680.
34	909.96	2.178		4831.	4831.	4831.
35	906.81	2.186		5005.	5005.	5005.
36	902.87	2.188		5224.	5224.	5224.
37	899.72	2.173		5399.	5399.	5399.
38	896.97	2.180		5551.	5551.	5551.
39	894.81	2.151		5680.	5680.	5680.
40	891.85	2.150		5828.	5828.	5828.
41	889.09	2.185		5979.	5979.	5979.
42	886.64	2.111		6127.	6127.	6127.
43	883.19	2.156		6294.	6294.	6294.
44	880.43	2.277		6451.	6451.	6451.
45	878.46	2.219		6567.	6567.	6567.
46	875.31	2.172		6743.	6743.	6743.
47	873.35	2.206		6853.	6853.	6853.
48	871.58	2.213		6965.	6965.	6965.
49	870.40	2.202		7032.	7032.	7032.
50	868.23	2.222		7143.	7143.	7143.
51	866.26	2.252		7258.	7258.	7258.
52	864.29	2.255		7374.	7374.	7374.
53	863.50	2.238		7420.	7420.	7420.
54	859.37	2.227		7647.	7647.	7647.
55	855.63	2.235		7875.	7875.	7875.
56	853.27	2.293		8015.	8015.	8015.
57	850.12	2.276		8205.	8205.	8205.
58	848.94	2.247		8274.	8274.	8274.
59	845.00	2.235		8504.	8504.	8504.
60	843.82	2.260		8573.	8573.	8573.
61	842.44	2.227		8665.	8665.	8665.
62	839.88	2.243		8802.	8802.	8802.
63	838.09	2.224		8847.	8847.	8847.
64	835.94	2.235		9029.	9029.	9029.
65	835.16	2.210		9074.	9074.	9074.
66	832.01	2.197		9252.	9252.	9252.
67	830.83	2.211		9318.	9318.	9318.
68	829.25	2.335		9412.	9412.	9412.
69	825.71	2.335		9635.	9635.	9635.
70	824.92	2.304		9684.	9684.	9684.
71	823.35	2.247		9778.	9778.	9778.
72	822.96	2.258		9824.	9824.	9824.
73	820.20	2.260		9964.	9964.	9964.
74	817.44	2.205		10123.	10123.	10123.
75	815.08	2.202		10256.	10256.	10256.
76	813.90	2.178		10322.	10322.	10322.
77	811.93	2.189		10431.	10431.	10431.
78	809.17	2.170		10584.	10584.	10584.
79	805.63	2.180		10779.	10779.	10779.
80	802.87	2.191		10932.	10932.	10932.
81	800.51	2.175		11063.	11063.	11063.
82	798.94	2.268		11153.	11153.	11153.
83	797.36	2.247		11246.	11246.	11246.
84	795.39	2.269		11362.	11362.	11362.
85	792.64	2.195		11522.	11522.	11522.
86	791.06	2.233		11612.	11612.	11612.
87	789.88	2.210		11679.	11679.	11679.
88	786.34	2.227		11882.	11882.	11882.
89	784.76	2.254		11973.	11973.	11973.
90	782.01	2.238		12134.	12134.	12134.
91	779.25	2.269		12297.	12297.	12297.
92	778.07	2.332		12369.	12369.	12369.
93	776.50	2.363		12468.	12468.	12468.
94	774.92	2.345		12569.	12569.	12569.
95	772.95	2.348		12693.	12693.	12693.
96	770.59	2.254		12837.	12837.	12837.
97	769.01	2.261		12930.	12930.	12930.
98	766.26	2.222		13091.	13091.	13091.
99	764.29	2.285		13207.	13207.	13207.
100	761.96	2.265		13348.	13348.	13348.

TABLE 6-10 (Continued)

BOREHOLE 021-05

J	PEACL DEPTH (FT)	G - G DENSITY (GM/CC)	DENSITY OF SOLID COMPONENT (GM/CC)	CUMULATIVE SOLID MASS (GM/CM**2) RHO=2.821	RHO=<PHO>	LINEAR SPLINE FOR RHO
101	759,46	2,293		13466.	13466.	13466.
102	757,20	2,255		13630.	13630.	13630.
103	754,84	2,213		13765.	13765.	13765.
104	752,48	2,170		13897.	13897.	13897.
105	749,53	2,200		14072.	14072.	14072.
106	747,76	2,254		14163.	14163.	14163.
107	746,18	2,286		14257.	14257.	14257.
108	743,82	2,279		14423.	14423.	14423.
109	741,46	2,268		14539.	14539.	14539.
110	738,70	2,281		14698.	14698.	14698.
111	735,16	2,222		14904.	14904.	14904.
112	730,83	2,230		15153.	15153.	15153.
113	729,25	2,202		15243.	15243.	15243.
114	725,71	2,254		15447.	15447.	15447.
115	725,61	2,297		15471.	15471.	15471.
116	725,35	2,312		15591.	15591.	15591.
117	721,77	2,291		15687.	15687.	15687.
118	719,01	2,304		15855.	15855.	15855.
119	717,85	2,293		15927.	15927.	15927.
120	715,87	2,291		16047.	16047.	16047.
121	713,50	2,258		16188.	16188.	16188.
122	709,96	2,272		16399.	16399.	16399.
123	707,60	2,315		16542.	16542.	16542.
124	703,66	2,316		16785.	16785.	16785.
125	702,09	2,307		16882.	16882.	16882.
126	697,36	2,297		17171.	17171.	17171.
127	695,00	2,312		17316.	17316.	17316.
128	694,21	2,301		17364.	17364.	17364.
129	691,96	2,301		17533.	17533.	17533.
130	689,60	2,285		17628.	17628.	17628.
131	686,64	2,301		17843.	17843.	17843.
132	685,05	2,318		17892.	17892.	17892.
133	682,40	2,329		18088.	18088.	18088.
134	680,43	2,301		18209.	18209.	18209.
135	678,46	2,310		18330.	18330.	18330.
136	676,50	2,308		18451.	18451.	18451.
137	674,53	2,345		18574.	18574.	18574.
138	670,98	2,356		18798.	18798.	18798.
139	670,59	2,327		18823.	18823.	18823.
140	666,65	2,274		19064.	19064.	19064.
141	665,08	2,224		19156.	19156.	19156.
142	657,60	2,225		19586.	19586.	19586.
143	656,02	2,213		19676.	19676.	19676.
144	653,27	2,294		19838.	19838.	19838.
145	650,12	2,301		20030.	20030.	20030.
146	648,54	2,246		20124.	20124.	20124.
147	646,18	2,103		20254.	20254.	20254.
148	643,82	2,123		20377.	20377.	20377.
149	643,03	2,101		20418.	20418.	20418.
150	641,46	2,269		20505.	20505.	20505.
151	639,88	2,254		20599.	20599.	20599.
152	637,91	2,269		20715.	20715.	20715.
153	635,94	2,232		20946.	20946.	20946.
154	632,80	2,238		21037.	21037.	21037.
155	629,25	2,203		21218.	21218.	21218.
156	625,74	2,268		21537.	21537.	21537.
157	620,98	2,258		21699.	21699.	21699.
158	619,01	2,191		21811.	21811.	21811.
159	617,83	2,206		21878.	21878.	21878.
160	616,65	2,254		21946.	21946.	21946.
161	614,29	2,323		22089.	22089.	22089.
162	611,54	2,321		22260.	22260.	22260.
163	607,99	2,272		22476.	22476.	22476.
164	604,85	2,277		22664.	22664.	22664.
165	602,48	2,334		22809.	22809.	22809.
166	600,51	2,312		22931.	22931.	22931.
167	599,33	2,341		23005.	23005.	23005.
168	597,76	2,341		23104.	23104.	23104.
169	595,79	2,321		23227.	23227.	23227.
170	594,61	2,345		23301.	23301.	23301.
171	591,85	2,319		23474.	23474.	23474.
172	590,27	2,400		23574.	23574.	23574.
173	587,91	2,349		23727.	23727.	23727.
174	586,73	2,348		23802.	23802.	23802.
175	583,19	2,244		24017.	24017.	24017.
176	581,22	2,274		24134.	24134.	24134.
177	577,68	2,379		24355.	24355.	24355.
178	574,92	2,301		24528.	24528.	24528.
179	572,16	2,290		24696.	24696.	24696.
180	570,20	2,301		24815.	24815.	24815.
181	567,44	2,219		24978.	24978.	24978.
182	565,47	2,250		25092.	25092.	25092.
183	564,29	2,307		25162.	25162.	25162.
184	562,32	2,321		25283.	25283.	25283.
185	560,35	2,297		25404.	25404.	25404.
186	557,99	2,235		25545.	25545.	25545.
187	555,63	2,245		25683.	25683.	25683.
188	553,66	2,222		25798.	25798.	25798.
189	551,30	2,203		25933.	25933.	25933.
190	549,72	2,172		26020.	26020.	26020.
191	546,57	2,199		26195.	26195.	26195.
192	544,61	2,175		26305.	26305.	26305.
193	543,03	2,227		26393.	26393.	26393.
194	541,06	2,206		26506.	26506.	26506.
195	538,70	2,214		26640.	26640.	26640.
196	537,91	2,206		26684.	26684.	26684.
197	535,94	2,254		26798.	26798.	26798.
198	534,76	2,272		26868.	26868.	26868.
199	532,79	2,254		26985.	26985.	26985.
200	530,43	2,208		27121.	27121.	27121.

BOREHOLE 021-05

J	PEACL DEPTH (FT)	G - G DENSITY (GM/CC)	DENSITY OF SOLID COMPONENT (GM/CC)	CUMULATIVE SOLID MASS (GM/CM**2) RHO=2.821	RHO=<PHO>	LINEAR SPLINE FOR PHO
201	528,86	2,206		27210.	27210.	27210.
202	526,07	2,238		27255.	27255.	27255.
203	525,71	2,235		27393.	27393.	27393.
204	524,53	2,216		27460.	27460.	27460.
205	522,96	2,233		27573.	27573.	27573.
206	521,77	2,258		27619.	27619.	27619.
207	519,41	2,291		27761.	27761.	27761.
208	517,85	2,277		27856.	27856.	27856.
209	516,26	2,265		27948.	27948.	27948.
210	513,11	2,297		28135.	28135.	28135.
211	511,93	2,301		28207.	28207.	28207.
212	511,14	2,329		28255.	28255.	28255.
213	509,57	2,313		28353.	28353.	28353.
214	507,60	2,238		28471.	28471.	28471.
215	506,02	2,254		28563.	28563.	28563.
216	504,84	2,272		28633.	28633.	28633.
217	502,87	2,265		28751.	28751.	28751.
218	501,68	2,266		28846.	28846.	28846.
219	497,36	2,265		29079.	29079.	29079.
220	493,03	2,164		29326.	29326.	29326.
221	491,06	2,202		29435.	29435.	29435.
222	488,70	2,285		29573.	29573.	29573.
223	487,52	2,301		29645.	29645.	29645.
224	485,16	2,282		29788.	29788.	29788.
225	482,79	2,290		29931.	29931.	29931.
226	480,81	2,277		30047.	30047.	30047.
227	479,23	2,265		30144.	30144.	30144.
228	478,46	2,301		30191.	30191.	30191.
229	475,71	2,387		30365.	30365.	30365.
230	475,74	2,456		30497.	30497.	30497.
231	471,77	2,414		30630.	30630.	30630.
232	469,80	2,426		30761.	30761.	30761.
233	468,62	2,411		30840.	30840.	30840.
234	465,67	2,431		31024.	31024.	31024.
235	463,11	2,401		31208.	31208.	31208.
236	461,14	2,365		31336.	31336.	31336.
237	459,17	2,368		31462.	31462.	31462.
238	457,99	2,356		31538.	31538.	31538.
239	456,82	2,381		31639.	31639.	31639.
240	455,27	2,337		31840.	31840.	31840.
241	450,90	2,257		31984.	31984.	31984.
242	447,76	2,250		32169.	32169.	32169.
243	446,18	2,266		32262.	32262.	32262.
244	445,39	2,249		32309.	32309.	32309.
245	441,96	2,244		32539.	32539.	32539.
246	438,81	2,308		32728.	32728.	32728.
247	435,65	2,244		32893.	32893.	32893.
248	432,01	2,274		33102.	33102.	33102.
249	430,43	2,348		33199.	33199.	33199.
250	425,31	2,285		33516.	33516.	33516.
251	419,41	2,119		33848.	33848.	33848.
252	415,47	2,075		34050.	34050.	34050.
253	411,14	2,128		34274.	34274.	34274.
254	408,78	2,112		34398.	34398.	34398.
255	406,81	2,081		34499.	34499.	34499.
256	404,84	2,106		34599.	34599.	34599.
257	402,09	2,086		34741.	34741.	34741.
258	398,94	1,845		34882.	34882.	34882.
259	396,57	1,908		34979.	34979.	34979.
260	394,61	2,194		35076.	35076.	35076.
261	391,06	2,034		35260.	35260.	35260.
262	388,19	2,034		35641.	35641.	35641.
263	381,61	2,013		35716.	35716.	35716.
264	378,07	2,065		35888.	35888.	35888.
265	375,91	2,084		36023.	36023.	36023.
266	370,98	2,055		36233.	36233.	36233.
267	369,80	2,053		36290.	36290.	36290.
268	369,41	2,035		36310.	36310.	36310.
269	366,65	2,057		36443.	36443.	36443.
270	363,90	2,165		36582.	36582.	36582.
271	361,14	2,139		36729.	36729.	36729.
272	358,39	2,068		36871.	36871.	36871.
273	355,63	2,076		37009.	37009.	37009.
274	350,90	2,139		37254.	37254.	37254.
275	348,94	2,106		37358.	37358.	37358.
276	347,36	2,172		37442.	37442.	37442.
277	345,00	2,087		37566.	37566.	37566.
278	343,03	2,112		37668.	37668.	37668.
279	341,46	2,089		37749.	37749.	37749.
280	339,88	2,128		37831.	37831.	37831.
281	339,49	2,139		37851.	37851.	37851.
282	336,73	2,119		37996.	37996.	37996.
283	335,94	2,104		38037.	38037.	38037.
284	333,19	2,142		38182.	38182.	38182.
285	331,22	2,078		38284.	38284.	38284.
286	329,25	2,049		38382.	38382.	38382.
287	326,89	2,024		38496.	38496.	38496.
288	324,53	2,139		38616.	38616.	38616.
289	321,77	2,139		38763.	38763.	38763.
290	320,98	2,156		38805.	38805.	38805.
291	319,01	2,046		38907.	38907.	38907.
292	317,44	2,034		38983.	38983.	38983.
293	316,26	2,043		39041.	39041.	39041.
294	314,68	2,067		39119.	39119.	39119.
295	312,32	2,070		39236.	39238.	39238.
296	311,14	2,144		39299.	39299.	39299.
297	308,39	2,097		39444.	39444.	39444.
298	307,20	2,115		39505.	39505.	39505.
299	304,45	2,067		39646.	39646.	39646.
300	303,66	2,076		39685.	39685.	39685.

TABLE 6-10 (Continued)

BOREHOLE OCT-05

J	PLACE DEPTH D(FT)	G - G DENSITY (GM/CC)	DENSITY OF SOLID COMPONENT (GM/CC)	CUMULATIVE SOLID MASS (GM/CM**2) RHO=2.821	RHO=F(RHO)	LINEAR SPLINE FOR RHO
301	300.51	2.027		39840.	39840.	39840.
302	298.49	1.971		39932.	39932.	39932.
303	296.57	2.018		40023.	40023.	40023.
304	294.61	1.993		40114.	40114.	40114.
305	292.64	2.018		40206.	40206.	40206.
306	290.67	2.010		40302.	40302.	40302.
307	288.68	2.023		40339.	40339.	40339.
308	286.71	2.065		40416.	40416.	40416.
309	284.75	2.068		40494.	40494.	40494.
310	284.76	2.069		40594.	40594.	40594.
311	280.19	2.054		40673.	40673.	40673.
312	280.85	2.065		40790.	40790.	40790.
313	279.25	2.007		40866.	40866.	40866.
314	274.92	2.018		41071.	41071.	41071.
315	273.74	2.051		41128.	41128.	41128.
316	272.16	2.034		41205.	41205.	41205.
317	269.01	2.151		41366.	41366.	41366.
318	268.23	2.135		41408.	41408.	41408.
319	266.65	2.191		41493.	41493.	41493.
320	263.50	2.070		41660.	41660.	41660.
321	263.11	2.090		41680.	41680.	41680.
322	259.57	2.026		41855.	41855.	41855.
323	258.59	2.034		41912.	41912.	41912.
324	257.40	1.987		41968.	41968.	41968.
325	255.42	1.971		42058.	42058.	42058.
326	252.48	1.861		42175.	42175.	42175.
327	248.54	1.772		42325.	42325.	42325.
328	246.57	1.827		42398.	42398.	42398.
329	244.61	2.018		42482.	42482.	42482.
330	243.82	2.112		42522.	42522.	42522.
331	242.64	2.213		42586.	42586.	42586.
332	241.46	2.260		42655.	42655.	42655.
333	239.09	2.191		42792.	42792.	42792.
334	237.52	2.185		42880.	42880.	42880.
335	235.55	2.106		42986.	42986.	42986.
336	233.58	2.092		43087.	43087.	43087.
337	231.61	2.078		43187.	43187.	43187.
338	230.04	2.123		43268.	43268.	43268.
339	227.28	2.103		43411.	43411.	43411.
340	225.33	2.007		43547.	43547.	43547.
341	221.77	1.974		43675.	43675.	43675.
342	219.80	2.005		43766.	43766.	43766.
343	217.85	1.991		43858.	43858.	43858.
344	214.68	2.104		44012.	44012.	44012.
345	211.93	2.246		44164.	44164.	44164.
346	209.17	2.142		44318.	44318.	44318.
347	204.84	2.145		44550.	44550.	44550.
348	202.87	2.144		44655.	44655.	44655.
349	202.09	2.126		44697.	44697.	44697.
350	200.12	2.144		44802.	44802.	44802.
351	199.93	2.137		44844.	44844.	44844.
352	197.96	2.180		44951.	44951.	44951.
353	195.59	2.134		45048.	45051.	45048.
354	193.03	2.133		45163.	45183.	45183.
355	191.06	2.101		45266.	45286.	45286.
356	190.27	2.114		45327.	45327.	45327.
357	186.34	2.112		45532.	45532.	45532.
358	182.40	1.902		45717.	45717.	45717.
359	.00		2.8210			

BOREHOLE OAR-2A

J	PLACE DEPTH D(FT)	G - G DENSITY (GM/CC)	DENSITY OF SOLID COMPONENT (GM/CC)	CUMULATIVE SOLID MASS (GM/CM**2) RHO=2.821	RHO=F(RHO)	LINEAR SPLINE FOR RHO
1	1000.00		2.8210			
2	993.51		2.8210			
3	993.50		2.7303			
4	984.00		2.7201			
5	964.90		2.7140			
6	962.40		2.7303			
7	954.90		2.7262			
8	944.20		2.7181			
9	933.50		2.9159			
10	924.20		2.8016			
11	915.90		2.8958			
12	903.90		2.8904			
13	895.80		2.8851			
14	886.80		2.9034			
15	877.00		2.8973			
16	864.40		2.9160			
17	855.60		2.9182			
18	844.00		2.9143			
19	835.80		2.9058			
20	824.30		2.9167			
21	812.80		2.9198			
22	801.50		2.9237			
23	792.50		2.9159			
24	783.60		2.9244			
25	774.40		2.9269			
26	764.80		2.9253			
27	756.70		2.9182			
28	744.40		2.9183			
29	734.50		2.9253			
30	724.90		2.9258			
31	715.90		2.9090			
32	706.50		2.8882			
33	694.60		2.9113			
34	684.00		2.8974			
35	675.10		2.8859			
36	663.20		2.8589			
37	648.60		2.9090			
38	642.20		2.9066			
39	635.50		2.9090			
40	622.70		2.9159			
41	610.90		2.9043			
42	600.50		2.8836			
43	590.50		2.8498			
44	581.20		2.8610			
45	570.90		2.7544			
46	566.50		2.7343			
47	564.00		2.7221			
48	554.00		2.7140			
49	541.40		2.7140			
50	530.40		2.7613			
51	519.60		2.7739			
52	517.10		2.7950			
53	517.00		2.7932			
54	512.10		2.8168			
55	510.20		2.7845			
56	502.10		2.8293			
57	490.10		2.7343			
58	480.50		2.7140			
59	470.70		4.7241			
60	457.60		2.8454			
61	456.10	2.101		0.	0.	0.
62	455.01	1.959		56.	56.	56.
63	453.07	1.880		139.	140.	140.
64	451.91	1.959		189.	190.	190.
65	449.97	2.022		297.	299.	299.
66	448.48		2.7242	355.	358.	358.
67	447.49	2.149		415.	420.	420.
68	445.30	2.117		519.	525.	525.
69	441.80		2.7181	708.	719.	719.
70	441.42	2.203		730.	741.	741.
71	439.10		2.7447	853.	867.	867.
72	438.70	2.054		873.	887.	887.
73	437.53	2.022		930.	945.	945.
74	435.20	2.046		1043.	1060.	1060.
75	434.30		2.7120	1088.	1107.	1107.
76	433.65	2.180		1124.	1143.	1143.
77	430.95	2.038		1265.	1287.	1287.
78	430.90		2.7323	1266.	1288.	1288.
79	429.90		2.7467	1317.	1340.	1340.
80	428.48	2.215		1367.	1391.	1391.
81	426.26	2.073		1513.	1539.	1539.
82	424.73	2.106		1592.	1619.	1619.
83	421.99	2.327		1734.	1763.	1763.
84	420.80		2.7634	1797.	1826.	1826.
85	420.05	2.106		1836.	1866.	1866.
86	418.00		2.7385	1942.	1974.	1974.
87	417.70		2.7364	1958.	1990.	1990.
88	416.94	2.117		1998.	2030.	2030.
89	415.38	2.085		2078.	2112.	2112.
90	412.67	2.070		2215.	2250.	2250.
91	411.89	2.044		2253.	2289.	2289.
92	410.40		2.8016	2317.	2353.	2353.
93	409.56	2.098		2370.	2406.	2406.
94	408.20		2.9043	2440.	2475.	2475.
95	407.23	2.097		2490.	2524.	2524.
96	406.06	2.051		2548.	2582.	2582.
97	403.73	2.085		2665.	2696.	2696.
98	400.62	2.030		2816.	2848.	2848.
99	397.51	2.038		2969.	2995.	2995.
100	395.57	1.911		3057.	3082.	3082.
	393.40		2.9066	3158.	3182.	3182.

TABLE 6-10 (Continued)

BOREHOLE DAH-2A

J	PLACE DEPTH (FT)	G - G DENSITY (GM/CC)	DENSITY OF SOLID COMPONENT (GM/CC)	CUMULATIVE SOLID MASS (GM/CM**2) RHO=2.821	RHO=<RHO>	LINEAR SPLINE FOR RHO
101	393.24	2.101		3167.	3190.	3190.
102	392.10		2.8255	3226.	3248.	3248.
103	392.07	2.112		3227.	3250.	3250.
104	390.52	2.116		3308.	3331.	3331.
105	388.50		2.8974	3417.	3434.	3434.
106	388.19	2.093		3428.	3450.	3450.
107	387.02	2.098		3488.	3509.	3509.
108	383.90		2.8974	3645.	3663.	3663.
109	383.58	2.036		3663.	3681.	3681.
110	381.97	2.043		3738.	3755.	3755.
111	380.60	2.006		3831.	3847.	3847.
112	378.48	2.030		3905.	3920.	3920.
113	376.38	2.022		3998.	4012.	4012.
114	375.47	1.991		4053.	4066.	4066.
115	373.80		2.8768	4129.	4141.	4141.
116	373.04	2.140		4169.	4180.	4180.
117	371.48	2.152		4252.	4262.	4262.
118	368.76	2.069		4394.	4404.	4404.
119	366.04	2.117		4535.	4544.	4544.
120	363.71	2.092		4655.	4665.	4665.
121	361.38	2.035		4771.	4781.	4781.
122	361.20		2.7866	4780.	4790.	4790.
123	360.00		2.8565	4839.	4850.	4850.
124	359.83	2.085		4848.	4859.	4859.
125	357.20		2.8700	4978.	4987.	4987.
126	357.11	2.022		4982.	4991.	4991.
127	355.94	2.038		5038.	5047.	5047.
128	355.30		2.7760	5060.	5069.	5069.
129	355.16	2.070		5077.	5086.	5086.
130	352.83	2.093		5195.	5205.	5205.
131	352.06	2.066		5234.	5244.	5244.
132	350.11	2.066		5331.	5342.	5342.
133	348.17	2.014		5425.	5437.	5437.
134	346.60		2.8124	5502.	5513.	5513.
135	345.89	2.101		5540.	5552.	5552.
136	338.07	1.903		5904.	5913.	5913.
137	337.80		2.9043	5916.	5924.	5924.
138	336.52	1.972		5972.	5980.	5980.
139	334.18	1.916		6075.	6082.	6082.
140	333.90		2.7866	6087.	6095.	6095.
141	332.63	1.927		6141.	6150.	6150.
142	331.85	2.003		6176.	6185.	6185.
143	329.13	1.911		6298.	6306.	6306.
144	326.03	2.039		6439.	6446.	6446.
145	325.00		2.8602	6489.	6495.	6495.
146	324.86	2.027		6496.	6502.	6502.
147	322.24	2.076		6629.	6634.	6634.
148	320.20	2.022		6725.	6728.	6728.
149	317.09	2.078		6877.	6879.	6879.
150	315.40		2.8610	6963.	6964.	6964.
151	314.76	2.098		6996.	6997.	6997.
152	313.59	2.085		7055.	7056.	7056.
153	312.43	2.043		7113.	7113.	7113.
154	310.11	2.070		7228.	7228.	7228.
155	309.32	2.027		7266.	7265.	7265.
156	308.15	2.028		7322.	7321.	7321.
157	307.58	2.003		7359.	7357.	7357.
158	306.60	2.022		7396.	7394.	7394.
159	305.80		2.8768	7435.	7432.	7432.
160	305.60		2.8146	7446.	7441.	7441.
161	304.66	2.060		7491.	7488.	7488.
162	301.35	1.979		7635.	7635.	7635.
163	298.83	2.149		7774.	7770.	7770.
164	298.60		2.8588	7786.	7782.	7782.
165	296.89	2.111		7877.	7872.	7872.
166	295.72	2.117		7938.	7933.	7933.
167	294.00		2.7803	8024.	8020.	8020.
168	293.00	1.967		8070.	8066.	8066.
169	291.50		2.8498	8141.	8137.	8137.
170	290.67	2.114		8183.	8179.	8179.
171	289.12	2.085		8263.	8259.	8259.
172	287.95	2.097		8323.	8318.	8318.
173	287.50		2.8321	8346.	8341.	8341.
174	284.07	2.085		8521.	8516.	8516.
175	282.90	2.030		8578.	8574.	8574.
176	280.18	2.050		8710.	8704.	8704.
177	279.79	2.017		8728.	8723.	8723.
178	275.91	2.180		8928.	8922.	8922.
179	274.35	2.190		9015.	9008.	9008.
180	270.47	2.006		9214.	9208.	9208.
181	268.52	1.955		9305.	9298.	9298.
182	267.80		2.8341	9335.	9332.	9332.
183	266.97	2.062		9380.	9373.	9373.
184	265.44	1.983		9454.	9447.	9447.
185	262.70	2.070		9584.	9579.	9579.
186	260.37	2.006		9697.	9693.	9693.
187	259.40		2.7291	9743.	9740.	9740.
188	258.81	2.013		9771.	9768.	9768.
189	256.09	1.959		9896.	9896.	9896.
190	254.95	1.946		9948.	9948.	9948.
191	252.98	1.959		10034.	10036.	10036.
192	252.59	1.975		10051.	10054.	10054.
193	251.04	1.948		10121.	10124.	10124.
194	250.46	1.896		10155.	10158.	10158.
195	248.71	1.877		10219.	10222.	10222.
196	243.27	1.959		10451.	10456.	10456.
197	241.36	1.927		10537.	10541.	10541.
198	240.50		2.8343	10573.	10577.	10577.
199	239.59	1.965		10622.	10627.	10627.
200	238.61	2.054		10659.	10663.	10663.

BOREHOLE DAP-2A

J	PLACE DEPTH (FT)	G - G DENSITY (GM/CC)	DENSITY OF SOLID COMPONENT (GM/CC)	CUMULATIVE SOLID MASS (GM/CM**2) RHO=2.821	RHO=<RHO>	LINEAR SPLINE FOR RHO
201	235.89	2.100		10796.	10800.	10800.
202	235.11	2.047		10835.	10839.	10839.
203	233.95	2.051		10692.	10896.	10896.
204	232.69	2.040		10968.	10972.	10972.
205	231.61	1.997		11005.	11009.	11009.
206	228.90	2.122		11140.	11144.	11144.
207	225.30		2.8168	11320.	11324.	11324.
208	225.01	2.017		11334.	11338.	11338.
209	223.07	2.097		11430.	11434.	11434.
210	219.96	2.035		11585.	11589.	11589.
211	216.46	2.066		11757.	11760.	11760.
212	212.58	2.030		11947.	11950.	11950.
213	211.50		2.8476	11999.	12002.	12002.
214	210.25	2.040		12060.	12062.	12062.
215	209.08	2.019		12116.	12118.	12118.
216	206.75	2.030		12228.	12230.	12230.
217	203.64	2.025		12377.	12380.	12380.
218	202.86	2.006		12414.	12417.	12417.
219	201.20		2.7613	12492.	12496.	12496.
220	200.54	2.006		12523.	12528.	12528.
221	198.20	2.038		12635.	12640.	12640.
222	197.04	2.019		12691.	12697.	12697.
223	196.26	1.927		12726.	12732.	12732.
224	193.54	2.022		12850.	12857.	12857.
225	192.37	1.991		12904.	12912.	12912.
226	189.65	2.003		13031.	13038.	13038.
227	188.88	1.978		13067.	13074.	13074.
228	187.32	1.986		13138.	13145.	13145.
229	186.55	1.924		13173.	13180.	13180.
230	186.30		2.8454	13183.	13190.	13190.
231	186.20		2.8498	13187.	13194.	13194.
232	184.99	1.793		13235.	13241.	13241.
233	183.05	1.785		13306.	13312.	13312.
234	181.11	1.880		13381.	13387.	13387.
235	179.94	1.927		13430.	13436.	13436.
236	178.00	2.003		13510.	13523.	13523.
237	176.86	1.915		13570.	13575.	13575.
238	174.50	2.054		13677.	13682.	13682.
239	173.90		2.8255	13706.	13712.	13712.
240	173.64	2.059		13734.	13739.	13739.
241	172.90		2.8498	13756.	13761.	13761.
242	172.60		2.8791	13770.	13775.	13775.
243	172.17	2.025		13791.	13796.	13796.
244	171.01	1.991		13846.	13850.	13850.
245	169.45	1.967		13918.	13921.	13921.
246	167.90	1.924		13987.	13989.	13989.
247	164.79	1.924		14121.	14121.	14121.
248	162.46	1.959		14223.	14222.	14222.
249	160.90	2.090		14298.	14295.	14295.
250	157.60	1.975		14448.	14443.	14443.
251	156.24	2.030		14520.	14515.	14515.
252	153.91	2.065		14634.	14627.	14627.
253	152.20		2.9090	14717.	14708.	14708.
254	150.60		2.9136	14788.	14778.	14778.
255	149.64	1.884		14829.	14818.	14818.
256	148.53	1.970		14963.	14950.	14950.
257	145.56	1.927		15015.	15001.	15001.
258	145.10		2.8997	15026.	15012.	15012.
259	144.50		2.8498	15052.	15038.	15038.
260	141.87	1.948		15168.	15153.	15153.
261	139.40		2.8498			
262	138.90		2.8387			
263	135.99		2.8468			
264	134.60		2.8948			
265	130.60		2.9275			
266	120.20		2.9341			
267	110.70		2.9283			
268	110.69		2.8210			
269	.00		2.8210			

TABLE 6-10 (Continued)

BOREHOLE DIT-11

J	PEALL DEPTH (FT)	G - G DENSITY (GM/CC)	DENSITY OF SOLID COMPONENT (GM/CC)	CUMULATIVE SOLID MASS (GM/CM**2) RHO=2.821	RHO=<RHO>	LINEAR SPLINE FOR RHO
1	1800.00		2.8210			
2	424.80	2.053		0.	0.	0.
3	424.09	2.071		39.	39.	39.
4	422.91	2.078		98.	98.	98.
5	420.99	2.059		216.	216.	216.
6	419.37	2.074		274.	274.	274.
7	417.01	2.049		392.	392.	392.
8	415.04	2.077		489.	489.	489.
9	413.86	2.052		548.	548.	548.
10	411.50	2.006		662.	662.	662.
11	409.92	2.002		736.	736.	736.
12	407.17	2.074		869.	869.	869.
13	405.98	2.083		929.	929.	929.
14	404.80	2.064		988.	988.	988.
15	401.65	2.049		1144.	1144.	1144.
16	399.69	2.080		1242.	1242.	1242.
17	398.11	2.107		1322.	1322.	1322.
18	396.54	2.111		1401.	1401.	1401.
19	393.78	2.055		1544.	1544.	1544.
20	391.42	2.020		1658.	1658.	1658.
21	388.66	2.053		1792.	1792.	1792.
22	387.48	2.096		1851.	1851.	1851.
23	385.91	2.094		1932.	1932.	1932.
24	384.72	2.065		1991.	1991.	1991.
25	383.54	2.096		2051.	2051.	2051.
26	381.97	2.083		2131.	2131.	2131.
27	380.39	2.066		2210.	2210.	2210.
28	378.13	2.069		2328.	2328.	2328.
29	376.06	2.044		2426.	2426.	2426.
30	375.28	2.061		2466.	2466.	2466.
31	374.49	2.103		2504.	2504.	2504.
32	373.31	2.111		2565.	2565.	2565.
33	372.13	2.092		2626.	2626.	2626.
34	370.55	2.111		2708.	2708.	2708.
35	368.58	2.103		2810.	2810.	2810.
36	365.43	2.009		2965.	2965.	2965.
37	363.86	1.946		3038.	3038.	3038.
38	361.50	1.964		3144.	3144.	3144.
39	359.53	2.002		3234.	3234.	3234.
40	356.68	2.036		3384.	3384.	3384.
41	352.95	2.025		3593.	3593.	3593.
42	350.87	1.991		3649.	3649.	3649.
43	347.72	1.991		3794.	3794.	3794.
44	346.54	1.978		3848.	3848.	3848.
45	344.57	2.033		3941.	3941.	3941.
46	341.42	2.055		4095.	4095.	4095.
47	339.06	2.011		4209.	4209.	4209.
48	335.12	2.002		4394.	4394.	4394.
49	334.33	2.053		4431.	4431.	4431.
50	332.96	2.071		4529.	4529.	4529.
51	329.81	2.147		4671.	4671.	4671.
52	327.44	2.049		4791.	4791.	4791.
53	322.91	1.991		4997.	4997.	4997.
54	320.94	2.031		5090.	5090.	5090.
55	319.76	1.978		5146.	5146.	5146.
56	318.98	1.959		5181.	5181.	5181.
57	317.01	2.002		5272.	5272.	5272.
58	315.43	1.950		5343.	5343.	5343.
59	313.86	2.005		5433.	5433.	5433.
60	311.50	1.998		5525.	5525.	5525.
61	309.92	2.033		5600.	5600.	5600.
62	307.56	2.019		5713.	5713.	5713.
63	305.98	2.047		5789.	5789.	5789.
64	304.02	2.041		5885.	5885.	5885.
65	302.05	2.042		5981.	5981.	5981.
66	301.87	2.020		6037.	6037.	6037.
67	299.29	2.020		6118.	6118.	6118.
68	298.50	2.017		6150.	6150.	6150.
69	296.14	2.044		6264.	6264.	6264.
70	294.96	2.019		6321.	6321.	6321.
71	293.39	2.009		6395.	6395.	6395.
72	290.63	1.944		6521.	6521.	6521.
73	289.06	1.962		6591.	6591.	6591.
74	286.69	2.036		6701.	6701.	6701.
75	285.12	2.017		6871.	6871.	6871.
76	283.97	2.039		6928.	6928.	6928.
77	280.00	2.005		7024.	7024.	7024.
78	278.82	2.038		7082.	7082.	7082.
79	277.24	2.025		7158.	7158.	7158.
80	275.67	2.025		7233.	7233.	7233.
81	274.88	2.019		7271.	7271.	7271.
82	273.31	2.049		7347.	7347.	7347.
83	272.13	2.069		7405.	7405.	7405.
84	268.98	2.049		7561.	7561.	7561.
85	267.40	2.061		7639.	7639.	7639.
86	265.83	2.052		7717.	7717.	7717.
87	264.25	2.058		7794.	7794.	7794.
88	263.46	2.083		7834.	7834.	7834.
89	260.31	2.085		7993.	7993.	7993.
90	257.17	2.052		8151.	8151.	8151.
91	255.20	2.049		8247.	8247.	8247.
92	252.44	1.975		8378.	8378.	8378.
93	250.47	1.961		8466.	8466.	8466.
94	248.90	1.904		8535.	8535.	8535.
95	246.54	1.955		8637.	8637.	8637.
96	244.57	1.976		8726.	8726.	8726.
97	242.60	2.002		8817.	8817.	8817.
98	241.81	1.986		8853.	8853.	8853.
99	240.63	1.923		8906.	8906.	8906.
100	237.87	1.944		9026.	9026.	9026.
101	235.14	2.025		9153.	9153.	9153.

BOREHOLE DIT-11

J	PEACE DEPTH (FT)	G - G DENSITY (GM/CC)	DENSITY OF SOLID COMPONENT (GM/CC)	CUMULATIVE SOLID MASS (GM/CM**2) RHO=2.821	RHO=<RHO>	LINEAR SPLINE FOR RHO
101	232.76	2.011		9265.	9265.	9265.
102	230.59	1.950		9373.	9373.	9373.
103	228.82	1.970		9448.	9448.	9448.
104	224.88	2.069		9631.	9631.	9631.
105	222.18	2.041		9767.	9767.	9767.
106	220.16	2.038		9863.	9863.	9863.
107	217.80	2.064		9979.	9979.	9979.
108	216.22	2.049		10056.	10056.	10056.
109	215.43	2.036		10095.	10095.	10095.
110	214.25	2.033		10152.	10152.	10152.
111	211.89	1.992		10264.	10264.	10264.
112	209.92	2.017		10356.	10356.	10356.
113	206.38	2.096		10531.	10531.	10531.
114	203.62	2.188		10678.	10678.	10678.
115	201.26	2.205		10811.	10811.	10811.
116	198.90	2.180		10943.	10943.	10943.
117	197.32	2.111		11028.	11028.	11028.
118	195.35	2.080		11129.	11129.	11129.
119	194.57	2.077		11168.	11168.	11168.
120	192.60	2.049		11266.	11266.	11266.
121	190.63	2.099		11365.	11365.	11365.
122	189.45	2.105		11426.	11426.	11426.
123	188.66	2.064		11466.	11466.	11466.
124	187.48	2.055		11524.	11524.	11524.
125	184.72	2.067		11661.	11661.	11661.
126	183.94	2.105		11701.	11701.	11701.
127	183.15	2.127		11742.	11742.	11742.
128	181.97	2.152		11825.	11825.	11825.
129	180.79	2.113		11867.	11867.	11867.
130	179.21	2.075		11947.	11947.	11947.
131	176.06	2.052		12104.	12104.	12104.
132	173.70	2.074		12222.	12222.	12222.
133	169.37	2.002		12432.	12432.	12432.
134	.00		2.8210			

TABLE 6-10 (Continued)

BOREHOLE OKT-13

J	PEACL DEPTH DIFT)	G - G DENSITY (GM/CC)	DENSITY OF SOLID COMPONENT (GM/CC)	CUMULATIVE SOLID MASS (GM/CM**2) RHO=2.821	RHO=<RHO>	LINEAR SPLINE FOR RHO
0	1800.00		2.8210			
1	911.66	2.025		0.	0.	0.
2	909.90	2.025		94.	94.	94.
3	908.71	2.064		152.	152.	152.
4	906.74	2.083		251.	251.	251.
5	905.17	2.056		330.	330.	330.
6	900.05	2.045		581.	581.	581.
7	896.11	2.052		774.	774.	774.
8	894.14	2.052		873.	873.	873.
9	890.20	2.056		1071.	1071.	1071.
10	885.48	2.212		1322.	1322.	1322.
11	880.56	2.033		1591.	1591.	1591.
12	879.57	2.049		1629.	1629.	1629.
13	877.61	2.028		1744.	1744.	1744.
14	874.84	2.096		1861.	1861.	1861.
15	873.66	2.061		1921.	1921.	1921.
16	872.09	2.083		2000.	2000.	2000.
17	870.11	1.986		2095.	2095.	2095.
18	867.36	2.017		2224.	2224.	2224.
19	864.61	2.136		2363.	2363.	2363.
20	859.49	1.955		2613.	2613.	2613.
21	855.94	2.096		2783.	2783.	2783.
22	853.55	2.100		2803.	2803.	2803.
23	853.15	2.127		2926.	2926.	2926.
24	850.82	2.080		3048.	3048.	3048.
25	849.25	2.103		3129.	3129.	3129.
26	847.67	2.077		3209.	3209.	3209.
27	844.13	2.043		3388.	3388.	3388.
28	842.95	2.108		3449.	3449.	3449.
29	840.98	2.108		3551.	3551.	3551.
30	839.79	2.111		3612.	3612.	3612.
31	838.22	2.099		3694.	3694.	3694.
32	835.46	2.100		3836.	3836.	3836.
33	832.91	2.053		3995.	3995.	3995.
34	829.16	2.002		4146.	4146.	4146.
35	827.59	2.028		4220.	4220.	4220.
36	826.40	2.026		4277.	4277.	4277.
37	823.25	2.107		4435.	4435.	4435.
38	819.71	2.129		4620.	4620.	4620.
39	818.13	2.083		4702.	4702.	4702.
40	814.20	2.060		4901.	4901.	4901.
41	810.65	2.019		5075.	5075.	5075.
42	807.87	2.025		5206.	5206.	5206.
43	804.74	2.103		5363.	5363.	5363.
44	801.99	2.105		5506.	5506.	5506.
45	798.84	2.141		5671.	5671.	5671.
46	796.08	2.141		5819.	5819.	5819.
47	792.14	2.067		6022.	6022.	6022.
48	791.75	2.064		6042.	6042.	6042.
49	791.35	2.055		6061.	6061.	6061.
50	785.05	2.146		6386.	6386.	6386.
51	779.54	2.049		6669.	6669.	6669.
52	777.96	2.041		6746.	6746.	6746.
53	771.27	2.060		7075.	7075.	7075.
54	768.91	2.108		7194.	7194.	7194.
55	768.12	2.099		7235.	7235.	7235.
56	765.76	2.111		7357.	7357.	7357.
57	763.79	2.108		7460.	7460.	7460.
58	759.85	2.165		7669.	7669.	7669.
59	759.06	2.152		7712.	7712.	7712.
60	756.50	2.150		7861.	7861.	7861.
61	754.73	2.100		7944.	7944.	7944.
62	752.37	2.100		8065.	8065.	8065.
63	750.40	2.061		8165.	8165.	8165.
64	748.43	2.064		8263.	8263.	8263.
65	746.46	2.060		8361.	8361.	8361.
66	742.52	2.149		8564.	8564.	8564.
67	739.76	2.127		8711.	8711.	8711.
68	737.79	2.103		8814.	8814.	8814.
69	735.82	2.155		8918.	8918.	8918.
70	733.07	2.158		9067.	9067.	9067.
71	727.93	2.002		9326.	9326.	9326.
72	720.07	2.116		9716.	9716.	9716.
73	718.10	2.116		9819.	9819.	9819.
74	716.13	2.149		9923.	9923.	9923.
75	712.98	2.139		10092.	10092.	10092.
76	711.80	2.083		10154.	10154.	10154.
77	708.65	2.031		10314.	10314.	10314.
78	707.08	2.049		10393.	10393.	10393.
79	705.89	2.049		10451.	10451.	10451.
80	705.11	2.075		10490.	10490.	10490.
81	702.74	2.075		10609.	10609.	10609.
82	700.38	2.122		10730.	10730.	10730.
83	697.43	2.050		10890.	10890.	10890.
84	694.87	2.050		11006.	11006.	11006.
85	693.69	2.019		11063.	11063.	11063.
86	690.93	2.077		11198.	11198.	11198.
87	688.96	2.049		11296.	11296.	11296.
88	686.20	2.014		11429.	11429.	11429.
89	681.87	2.099		11643.	11643.	11643.
90	678.72	2.171		11811.	11811.	11811.
91	675.96	2.052		12077.	12077.	12077.
92	670.84	2.013		12210.	12210.	12210.
93	669.66	2.030		12266.	12266.	12266.
94	668.09	2.002		12341.	12341.	12341.
95	662.97	2.176		12622.	12622.	12622.
96	659.42	2.172		12795.	12795.	12795.
97	655.99	2.187		13035.	13035.	13035.
98	652.74	2.148		13164.	13164.	13164.
99	650.38	2.075		13286.	13286.	13286.
100	649.18	2.105		13347.	13347.	13347.

BOREHOLE OKT-13

J	PEACL DEPTH DIFT)	G - G DENSITY (GM/CC)	DENSITY OF SOLID COMPONENT (GM/CC)	CUMULATIVE SOLID MASS (GM/CM**2) RHO=2.821	RHO=<RHO>	LINEAR SPLINE FOR RHO
101	646.84	2.111		13469.	13469.	13469.
102	645.25	2.125		13552.	13552.	13552.
103	642.88	2.111		13675.	13675.	13675.
104	638.55	2.163		13906.	13906.	13906.
105	636.19	2.147		14034.	14034.	14034.
106	634.61	2.107		14117.	14117.	14117.
107	630.28	2.096		14340.	14340.	14340.
108	626.34	2.103		14543.	14543.	14543.
109	624.37	2.154		14647.	14647.	14647.
110	621.82	2.154		14796.	14796.	14796.
111	619.85	2.138		14902.	14902.	14902.
112	615.71	2.154		15113.	15113.	15113.
113	611.38	2.024		15334.	15334.	15334.
114	607.83	2.124		15512.	15512.	15512.
115	606.65	2.108		15574.	15574.	15574.
116	604.68	2.102		15675.	15675.	15675.
117	603.50	2.045		15735.	15735.	15735.
118	600.74	2.045		15869.	15869.	15869.
119	598.58	2.027		15927.	15927.	15927.
120	597.99	2.075		16004.	16004.	16004.
121	596.02	2.066		16103.	16103.	16103.
122	594.05	2.071		16201.	16201.	16201.
123	591.68	2.039		16318.	16318.	16318.
124	589.99	2.440		16707.	16707.	16707.
125	579.87	2.252		17031.	17031.	17031.
126	576.69	2.033		17094.	17094.	17094.
127	574.73	2.030		17284.	17284.	17284.
128	571.60	2.086		17440.	17440.	17440.
129	569.24	2.049		17558.	17558.	17558.
130	567.27	2.028		17653.	17653.	17653.
131	564.14	2.091		17810.	17810.	17810.
132	563.35	2.069		17849.	17849.	17849.
133	560.18	2.078		18008.	18008.	18008.
134	559.39	2.038		18047.	18047.	18047.
135	556.24	2.055		18201.	18201.	18201.
136	554.27	2.044		18297.	18297.	18297.
137	550.73	2.196		18474.	18474.	18474.
138	547.97	2.064		18615.	18615.	18615.
139	545.61	2.049		18734.	18734.	18734.
140	539.70	2.049		19023.	19023.	19023.
141	534.19	2.182		19311.	19311.	19311.
142	532.61	2.157		19397.	19397.	19397.
143	531.04	2.160		19483.	19483.	19483.
144	527.89	2.135		19652.	19652.	19652.
145	525.16	1.995		19888.	19888.	19888.
146	520.01	2.056		20039.	20039.	20039.
147	517.65	2.107		20158.	20158.	20158.
148	515.28	2.103		20280.	20280.	20280.
149	513.31	2.111		20382.	20382.	20382.
150	512.53	2.032		20422.	20422.	20422.
151	510.95	2.038		20499.	20499.	20499.
152	508.19	2.103		20637.	20637.	20637.
153	505.04	2.111		20800.	20800.	20800.
154	502.68	2.002		20917.	20917.	20917.
155	501.11	1.998		20991.	20991.	20991.
156	500.32	2.002		21027.	21027.	21027.
157	497.95	2.042		21140.	21140.	21140.
158	497.17	2.036		21178.	21178.	21178.
159	493.62	2.063		21352.	21352.	21352.
160	492.83	2.014		21390.	21390.	21390.
161	491.65	2.025		21447.	21447.	21447.
162	488.30	2.002		21577.	21577.	21577.
163	486.50	1.981		21595.	21595.	21595.
164	486.53	2.002		21687.	21687.	21687.
165	484.56	2.033		21780.	21780.	21780.
166	481.91	2.096		21937.	21937.	21937.
167	479.05	2.045		22055.	22055.	22055.
168	477.48	2.045		22132.	22132.	22132.
169	475.90	1.994		22207.	22207.	22207.
170	473.54	2.656		22319.	22319.	22319.
171	471.96	2.030		22395.	22395.	22395.
172	469.60	2.067		22511.	22511.	22511.
173	468.81	2.033		22550.	22550.	22550.
174	454.87	1.970		22734.	22734.	22734.
175	464.09	1.900		22768.	22768.	22768.
176	457.59	2.124		23085.	23085.	23085.
177	454.24	2.096		23249.	23249.	23249.
178	452.67	2.108		23350.	23350.	23350.
179	450.50	2.064		23450.	23450.	23450.
180	446.76	2.052		23626.	23626.	23626.
181	445.18	2.000		23704.	23704.	23704.
182	442.64	1.978		23875.	23875.	23875.
183	439.47	1.959		23964.	23964.	23964.
184	436.52	2.022		24109.	24109.	24109.
185	435.34	2.014		24165.	24165.	24165.
186	432.38	2.022		24297.	24297.	24297.
187	430.22	1.983		24407.	24407.	24407.
188	429.43	1.985		24443.	24443.	24443.
189	427.46	1.986		24534.	24534.	24534.
190	425.88	1.997		24607.	24607.	24607.
191	424.70	2.029		24663.	24663.	24663.
192	421.95	1.966		24790.	24790.	24790.
193	417.61	1.989		24988.	24988.	24988.
194	415.65	1.985		25079.	25079.	25079.
195	413.28	1.890		25182.	25182.	25182.
196	409.74	1.900		25330.	25330.	25330.
197	407.37	1.956		25432.	25432.	25432.
198	403.44	1.603		25603.	25603.	25603.
199	395.89	2.002		25760.	25760.	25760.
200	397.92	2.038		25854.	25854.	25854.

TABLE 6-10 (Continued)

BOREHOLE OKT-13

J	PLACE DEPTH (FT)	G - G DENSITY (GM/CC)	DENSITY OF SOLID COMPONENT (GM/CC)	CUMULATIVE SOLID MASS (GM/CM**2) RHO*2.821	RHO*(RMO)	LINEAR SPLINE FOR RHO
201	395.95	2.045		25950.	25950.	25950.
202	394.90	2.038		26027.	26027.	26027.
203	393.89	2.017		26083.	26083.	26083.
204	392.82	1.997		26139.	26139.	26139.
205	391.83	2.016		26194.	26194.	26194.
206	390.87	2.016		26288.	26288.	26288.
207	389.90	2.072		26384.	26384.	26384.
208	388.11	2.064		26423.	26423.	26423.
209	387.96	2.064		26580.	26580.	26580.
210	387.56	2.050		26600.	26600.	26600.
211	387.17	2.056		26619.	26619.	26619.
212	386.20	2.058		26716.	26716.	26716.
213	378.65	2.036		26794.	26794.	26794.
214	374.69	2.052		26986.	26986.	26986.
215	373.90	2.052		27024.	27024.	27024.
216	371.54	2.017		27139.	27139.	27139.
217	369.96	2.095		27213.	27213.	27213.
218	366.81	2.080		27367.	27367.	27367.
219	362.87	2.086		27566.	27566.	27566.
220	362.46	2.064		27586.	27586.	27586.
221	360.51	2.049		27683.	27683.	27683.
222	357.96	1.955		27831.	27831.	27831.
223	355.99	1.936		27917.	27917.	27917.
224	353.03	1.995		28029.	28029.	28029.
225	350.06	2.005		28134.	28134.	28134.
226	347.51	1.955		28278.	28278.	28278.
227	340.42	2.069		28613.	28613.	28613.
228	338.06	1.970		28726.	28726.	28726.
229	335.80	1.964		28850.	28850.	28850.
230	334.52	1.986		28886.	28886.	28886.
231	333.73	1.991		28922.	28922.	28922.
232	331.37	2.030		29034.	29034.	29034.
233	329.00	2.031		29148.	29148.	29148.
234	328.22	2.020		29185.	29185.	29185.
235	324.67	2.020		29354.	29354.	29354.
236	322.70	2.061		29450.	29450.	29450.
237	319.75	2.078		29588.	29588.	29588.
238	317.19	2.055		29726.	29726.	29726.
239	315.22	2.067		29823.	29823.	29823.
240	311.28	2.049		30010.	30010.	30010.
241	309.31	2.009		30113.	30113.	30113.
242	306.95	2.020		30225.	30225.	30225.
243	305.37	2.014		30300.	30300.	30300.
244	303.41	2.038		30394.	30394.	30394.
245	302.62	2.002		30432.	30432.	30432.
246	299.56	1.958		30560.	30560.	30560.
247	299.47	1.939		30578.	30578.	30578.
248	296.32	1.936		30716.	30716.	30716.
249	293.17	1.973		30856.	30856.	30856.
250	291.59	1.955		30927.	30927.	30927.
251	290.02	1.914		30996.	30996.	30996.
252	284.90	1.955		31219.	31219.	31219.
253	281.74	2.036		31365.	31365.	31365.
254	278.99	1.842		31486.	31486.	31486.
255	275.84	1.774		31604.	31604.	31604.
256	273.87	2.017		31646.	31646.	31646.
257	271.90	1.986		31778.	31778.	31778.
258	270.32	2.020		31852.	31852.	31852.
259	267.17	1.426		31995.	31995.	31995.
260	262.05	2.086		32236.	32236.	32236.
261	258.91	2.053		32411.	32411.	32411.
262	255.75	2.111		32549.	32549.	32549.
263	253.00	2.130		32694.	32694.	32694.
264	248.47	2.089		32940.	32940.	32940.
265	243.94	1.997		33170.	33170.	33170.
266	242.36	2.033		33226.	33226.	33226.
267	238.92	2.067		33419.	33419.	33419.
268	234.88	2.033		33593.	33593.	33593.
269	232.52	2.060		33710.	33710.	33710.
270	230.58	2.080		33909.	33909.	33909.
271	226.44	2.034		34026.	34026.	34026.
272	223.85	2.058		34142.	34142.	34142.
273	221.88	2.038		34238.	34238.	34238.
274	220.31	1.973		34312.	34312.	34312.
275	216.76	2.006		34476.	34476.	34476.
276	215.19	1.976		34549.	34549.	34549.
277	213.61	1.976		34620.	34620.	34620.
278	210.86	1.867		34740.	34740.	34740.
279	207.71	1.976		34877.	34877.	34877.
280	205.57	1.926		35070.	35070.	35070.
281	185.26	2.144		35946.	35946.	35946.
282	182.11	2.156		36114.	36114.	36114.
283	181.52	2.150		36157.	36157.	36157.
284	180.56	1.947		36195.	36195.	36195.
285	.00		2.8210			

BOREHOLE OPZ-18

J	PLACE DEPTH (FT)	G - G DENSITY (GM/CC)	DENSITY OF SOLID COMPONENT (GM/CC)	CUMULATIVE SOLID MASS (GM/CM**2) RHO*2.821	RHO*(RMO)	LINEAR SPLINE FOR RHO
0	1800.00		2.8210			
1	1045.01	2.134		0.	0.	0.
2	1043.94	2.108		83.	83.	83.
3	1041.86	2.113		165.	165.	165.
4	1040.29	2.083		246.	246.	246.
5	1039.30	2.079		285.	285.	285.
6	1037.36	2.090		385.	385.	385.
7	1034.77	2.091		526.	526.	526.
8	1033.99	2.050		565.	565.	565.
9	1033.29	2.050		604.	604.	604.
10	1030.05	2.000		755.	755.	755.
11	1028.47	2.016		829.	829.	829.
12	1026.90	2.000		903.	903.	903.
13	1024.54	1.942		1010.	1010.	1010.
14	1018.68	2.110		1293.	1293.	1293.
15	1017.45	2.094		1354.	1354.	1354.
16	1015.98	2.060		1453.	1453.	1453.
17	1011.94	2.047		1628.	1628.	1628.
18	1009.58	2.066		1744.	1744.	1744.
19	1005.64	2.072		1941.	1941.	1941.
20	1001.70	2.059		2141.	2141.	2141.
21	1000.15	2.074		2221.	2221.	2221.
22	998.35	2.068		2300.	2300.	2300.
23	996.59	1.986		2395.	2395.	2395.
24	995.40	2.010		2450.	2450.	2450.
25	993.44	1.986		2541.	2541.	2541.
26	991.07	2.000		2650.	2650.	2650.
27	989.50	2.000		2723.	2723.	2723.
28	986.74	2.035		2854.	2854.	2854.
29	985.96	2.035		2893.	2893.	2893.
30	982.81	2.108		3050.	3050.	3050.
31	981.43	2.086		3131.	3131.	3131.
32	978.47	2.094		3272.	3272.	3272.
33	976.11	2.082		3392.	3392.	3392.
34	974.15	2.126		3494.	3494.	3494.
35	971.78	2.086		3616.	3616.	3616.
36	970.21	2.097		3697.	3697.	3697.
37	967.84	2.035		3816.	3816.	3816.
38	967.06	2.074		3855.	3855.	3855.
39	965.48	2.074		3934.	3934.	3934.
40	962.33	2.118		4095.	4095.	4095.
41	959.18	2.126		4261.	4261.	4261.
42	954.85	2.063		4483.	4483.	4483.
43	953.28	2.030		4560.	4560.	4560.
44	950.92	2.035		4674.	4674.	4674.
45	950.13	2.047		4712.	4712.	4712.
46	948.16	2.013		4807.	4807.	4807.
47	947.37	2.014		4844.	4844.	4844.
48	945.40	1.998		4936.	4936.	4936.
49	943.04	2.019		5048.	5048.	5048.
50	941.86	1.987		5103.	5103.	5103.
51	938.71	2.036		5252.	5252.	5252.
52	936.74	2.104		5350.	5350.	5350.
53	936.35	2.090		5371.	5371.	5371.
54	934.77	2.086		5451.	5451.	5451.
55	933.59	2.064		5510.	5510.	5510.
56	930.84	2.072		5648.	5648.	5648.
57	930.44	2.082		5668.	5668.	5668.
58	928.47	2.053		5766.	5766.	5766.
59	926.08	2.064		5786.	5786.	5786.
60	925.69	2.064		5923.	5923.	5923.
61	922.96	2.118		6043.	6043.	6043.
62	921.78	2.118		6105.	6105.	6105.
63	920.60	2.140		6168.	6168.	6168.
64	919.03	2.140		6252.	6252.	6252.
65	917.46	2.105		6355.	6355.	6355.
66	915.09	2.079		6456.	6456.	6456.
67	913.51	2.101		6536.	6536.	6536.
68	910.76	2.105		6678.	6678.	6678.
69	909.58	2.123		6740.	6740.	6740.
70	906.00	2.145		6822.	6822.	6822.
71	904.45	2.143		7009.	7009.	7009.
72	904.07	2.140		7030.	7030.	7030.
73	902.88	2.157		7093.	7093.	7093.
74	899.73	2.097		7260.	7260.	7260.
75	896.98	2.097		7401.	7401.	7401.
76	896.19	2.091		7441.	7441.	7441.
77	895.01	2.127		7503.	7503.	7503.
78	891.47	2.058		7684.	7684.	7684.
79	888.32	2.058		7840.	7840.	7840.
80	885.96	2.151		7962.	7962.	7962.
81	883.99	2.145		8068.	8068.	8068.
82	882.02	2.154		8173.	8173.	8173.
83	880.44	2.108		8255.	8255.	8255.
84	878.87	2.113		8337.	8337.	8337.
85	877.29	2.085		8418.	8418.	8418.
86	876.51	2.079		8458.	8458.	8458.
87	874.54	2.090		8558.	8558.	8558.
88	871.78	2.091		8699.	8699.	8699.
89	871.01		2.8210	8712.	8712.	8712.
90	871.50		2.9253	8713.	8713.	8713.
91	870.99	2.050		8738.	8737.	8737.
92	870.21	2.050		8777.	8775.	8775.
93	867.06	2.000		8926.	8923.	8923.
94	866.80		2.9159	8940.	8935.	8935.
95	865.48	2.016		9002.	8996.	8996.
96	863.91	2.000		9076.	9069.	9069.
97	861.55	1.942		9183.	9174.	9174.
98	855.64	2.110		9466.	9452.	9452.
99	854.46	2.094		9527.	9512.	9512.
100	852.49	2.060		9626.	9609.	9609.

TABLE 6-10 (Continued)

BOREHOLE DP2-18

J	PLACE DEPTH (FT)	G - G DENSITY (GM/CC)	DENSITY OF SOLID COMPONENT (GM/CC)	CUMULATIVE SOLID MASS (GM/CM**2) RHO=2.821	RHO=<RHO>	LINEAR SPLINE FOR RHO
101	852,20		2,9130	9640.	9623.	5623.
102	848,95	2,047		9801.	9780.	9780.
103	846,59	2,066		9917.	9895.	9895.
104	842,65	2,072		10114.	10068.	10068.
105	838,71	2,099		10314.	102 4.	10244.
106	837,14	2,074		10394.	10363.	10363.
107	835,56	2,068		10473.	10440.	10440.
108	833,59	1,986		10568.	10533.	10533.
109	832,90		2,9252	10600.	10564.	10564.
110	832,41	2,000		10622.	10586.	10586.
111	830,44	1,985		10715.	10676.	10676.
112	828,08	2,000		10823.	10783.	10783.
113	826,51	2,000		10896.	10855.	10855.
114	824,75	2,035		11027.	10983.	10983.
115	823,20		2,9206	11054.	11010.	11010.
116	822,96	2,035		11065.	11021.	11021.
117	819,81	2,108		11223.	11176.	11176.
118	818,24	2,086		11304.	11255.	11255.
119	817,45	2,094		11345.	11393.	11393.
120	813,89		2,9183	11541.	11487.	11487.
121	813,12	2,082		11565.	11511.	11511.
122	811,15	2,126		11667.	11611.	11611.
123	809,00		2,9043	11778.	11721.	11721.
124	808,79	2,086		11789.	11731.	11731.
125	807,21	2,097		11869.	11810.	11810.
126	804,85	2,055		11988.	11927.	11927.
127	804,07	2,074		12028.	11966.	11966.
128	802,49	2,074		12107.	12044.	12044.
129	799,54	2,118		12268.	12202.	12202.
130	796,19	2,126		12434.	12365.	12365.
131	794,00		2,9183	12547.	12476.	12476.
132	791,86	2,063		12655.	12582.	12582.
133	790,29	2,050		12732.	12658.	12658.
134	787,92	2,055		12846.	12770.	12770.
135	787,14	2,047		12885.	12807.	12807.
136	785,17	2,013		12979.	12900.	12900.
137	784,38	2,014		13017.	12937.	12937.
138	782,41	1,995		13109.	13028.	13028.
139	780,05	2,019		13221.	13137.	13137.
140	778,87	1,967		13276.	13191.	13191.
141	775,72	2,026		13425.	13337.	13337.
142	773,75	2,104		13523.	13434.	13434.
143	773,36	2,090		13543.	13454.	13454.
144	771,78	2,066		13624.	13532.	13532.
145	770,60	2,064		13683.	13591.	13591.
146	767,84	2,072		13821.	13726.	13726.
147	767,45	2,082		13841.	13745.	13745.
148	766,90		2,9206	13868.	13772.	13772.
149	765,48	2,053		13939.	13842.	13842.
150	765,09	2,064		13958.	13861.	13861.
151	762,93	2,064		14096.	13995.	13995.
152	759,97	2,118		14216.	14114.	14114.
153	758,79	2,118		14278.	14175.	14175.
154	757,61	2,140		14340.	14236.	14236.
155	756,03	2,140		14425.	14319.	14319.
156	754,07	2,105		14520.	14420.	14420.
157	752,10	2,079		14629.	14519.	14519.
158	750,52	2,101		14709.	14598.	14598.
159	747,77	2,105		14851.	14739.	14739.
160	746,59	2,123		14913.	14799.	14799.
161	745,01	2,105		14995.	14880.	14880.
162	741,87	2,118		15181.	15064.	15064.
163	741,07	2,140		15202.	15085.	15085.
164	739,89	2,157		15266.	15148.	15148.
165	737,70		2,8859	15383.	15263.	15263.
166	736,72	2,097		15432.	15312.	15312.
167	733,99	2,097		15574.	15452.	15452.
168	733,20	2,091		15614.	15492.	15492.
169	732,02	2,127		15675.	15553.	15553.
170	728,47	2,058		15857.	15735.	15735.
171	725,53	2,058		16013.	15892.	15892.
172	722,96	2,151		16135.	16015.	16015.
173	720,99	2,145		16241.	16123.	16123.
174	719,80		2,7241	16299.	16183.	16183.
175	719,03	2,157		16347.	16231.	16231.
176	716,66	2,112		16472.	16359.	16359.
177	712,53	2,107		16647.	16589.	16589.
178	709,38	2,149		16843.	16737.	16737.
179	709,20		2,7303	16863.	16758.	16758.
180	707,61	2,149		16949.	16845.	16845.
181	705,64	2,171		17056.	16954.	16954.
182	703,67	2,140		17162.	17063.	17063.
183	698,93	2,160		17417.	17323.	17323.
184	698,16	2,146		17459.	17366.	17366.
185	695,80	2,223		17591.	17500.	17500.
186	695,40	2,209		17613.	17523.	17523.
187	693,44	2,209		17725.	17637.	17637.
188	689,50	2,126		17940.	17856.	17856.
189	686,74	2,145		18087.	18006.	18006.
190	685,56	2,074		18148.	18068.	18068.
191	681,23	2,063		18364.	18289.	18289.
192	680,84	2,099		18384.	18310.	18310.
193	678,47	2,093		18505.	18433.	18433.
194	674,14	2,159		18734.	18666.	18666.
195	672,50		2,7221	18822.	18756.	18756.
196	669,81	2,088		18961.	18898.	18898.
197	668,50		2,8146	19026.	18965.	18965.
198	665,09	2,082		19201.	19139.	19139.
199	663,91	2,097		19262.	19199.	19199.
200	661,53	2,102		19383.	19322.	19322.

BOREHOLE DP2-18

J	PLACE DEPTH (FT)	G - G DENSITY (GM/CC)	DENSITY OF SOLID COMPONENT (GM/CC)	CUMULATIVE SOLID MASS (GM/CM**2) RHO=2.821	RHO=<RHO>	LINEAR SPLINE FOR RHO
201	659,97	2,129		19465.	19405.	19405.
202	658,40	2,121		19548.	19489.	19489.
203	652,10	2,110		19877.	19823.	19823.
204	651,70		2,7303	19898.	19844.	19844.
205	647,37	2,124		20124.	20075.	20075.
206	645,80	2,110		20207.	20159.	20159.
207	642,65	2,146		20394.	20349.	20349.
208	640,29	2,189		20502.	20459.	20459.
209	637,92	2,204		20634.	20595.	20595.
210	636,74	2,231		20702.	20663.	20663.
211	633,99	2,209		20859.	20824.	20824.
212	631,60		2,7221	20991.	20959.	20959.
213	630,84	2,129		21032.	21001.	21001.
214	630,05	2,126		21073.	21043.	21043.
215	626,87	2,094		21135.	21106.	21106.
216	625,75	2,086		21196.	21372.	21372.
217	622,57	2,110		21457.	21434.	21434.
218	621,39	2,151		21519.	21498.	21498.
219	618,24	2,164		21690.	21673.	21673.
220	616,66	2,192		21777.	21762.	21762.
221	616,40		2,7201	21792.	21777.	21777.
222	614,70	2,170		21886.	21873.	21873.
223	611,94	2,189		22038.	22029.	22029.
224	610,36	2,118		22123.	22116.	22116.
225	607,21	2,094		22286.	22282.	22282.
226	606,03	2,045		22345.	22342.	22342.
227	603,68	2,027		22477.	22477.	22477.
228	602,50		2,7140	22514.	22515.	22515.
229	602,10	1,994		22533.	22534.	22534.
230	599,34	2,101		22668.	22672.	22672.
231	595,80	1,888		22832.	22840.	22840.
232	593,85	1,892		22914.	22922.	22922.
233	593,50		2,7613	22928.	22936.	22936.
234	589,69	2,140		23101.	23111.	23111.
235	587,35	2,077		23223.	23234.	23234.
236	585,59	2,142		23428.	23437.	23437.
237	582,81	2,212		23493.	23502.	23502.
238	580,05	2,097		23621.	23628.	23628.
239	579,26	2,096		23661.	23667.	23667.
240	578,90		2,9156	23680.	23686.	23686.
241	576,90	2,047		23779.	23784.	23784.
242	574,54	2,189		23903.	23905.	23905.
243	573,36	2,189		23969.	23970.	23970.
244	570,99	2,252		24104.	24103.	24103.
245	567,06	2,153		24326.	24322.	24322.
246	565,09	2,052		24428.	24422.	24422.
247	563,91	2,075		24486.	24480.	24480.
248	560,76	2,063		24645.	24638.	24638.
249	559,38	2,079		24705.	24697.	24697.
250	556,99		2,8743	24739.	24730.	24730.
251	556,79	2,060		24744.	24736.	24736.
252	556,03	2,141		24885.	24875.	24875.
253	553,67	2,138		25010.	24998.	24998.
254	552,10	2,105		25093.	25080.	25080.
255	551,31	2,104		25133.	25121.	25121.
256	548,95	2,050		25271.	25257.	25257.
257	546,59	2,038		25366.	25351.	25351.
258	545,01	2,033		25442.	25426.	25426.
259	543,04	2,053		25540.	25523.	25523.
260	541,47	2,090		25621.	25602.	25602.
261	539,56	2,124		25727.	25904.	25904.
262	533,10		2,8882	26058.	26038.	26038.
263	532,04	2,151		26116.	26091.	26091.
264	528,87	2,132		26284.	26257.	26257.
265	528,08	2,154		26326.	26299.	26299.
266	524,13	2,154		26539.	26509.	26509.
267	521,78	2,099		26664.	26633.	26633.
268	517,70		2,8653	26877.	26844.	26844.
269	516,66	2,140		26932.	26899.	26899.
270	514,30	2,110		27056.	27022.	27022.
271	512,55	2,132		27160.	27125.	27125.
272	510,76	2,135		27243.	27208.	27208.
273	508,79	2,168		27350.	27314.	27314.
274	506,03	2,102		27496.	27460.	27460.
275	504,07	2,086		27597.	27560.	27560.
276	501,51	2,000		27731.	27694.	27694.
277	498,55	2,066		27864.	27827.	27827.
278	496,98	2,069		27943.	27906.	27906.
279	496,19	2,093		27983.	27946.	27946.
280	495,40	2,066		28022.	27985.	27985.
281	493,04	2,061		28140.	28103.	28103.
282	492,65	2,124		28160.	28123.	28123.
283	491,90		2,8079	28199.	28163.	28163.
284	490,68	2,129		28264.	28227.	28227.
285	490,29	2,153		28285.	28248.	28248.
286	489,10	2,140		28348.	28312.	28312.
287	487,92	2,148		28411.	28375.	28375.
288	485,96	2,116		28516.	28479.	28479.
289	484,38	2,113		28598.	28561.	28561.
290	481,62	2,200		28747.	28709.	28709.
291	479,26	2,203		28880.	28840.	28840.
292	478,87	2,214		28903.	28862.	28862.
293	476,51	2,157		29034.	28992.	28992.
294	475,72		2,9050	29067.	29024.	29024.
295	474,54	2,116		29139.	29095.	29095.
296	472,96	2,050		29219.	29173.	29173.
297	471,78	2,041		29274.	29230.	29230.
298	468,24	2,047		29443.	29401.	29401.
299	466,47	2,079		29547.	29497.	29497.
300	465,28	2,050		29586.	29536.	29536.

TABLE 6-10 (Continued)

BOREHOLE OF2-18

J	PEACL DEPTH (FT)	G - G DENSITY (GM/CC)	DENSITY OF SOLID COMPONENT (GM/CC)	CUMULATIVE SOLID MASS (GM/CM**2) RHO=2.821	RHO=<RHO>	LINEAR SPLINE FOR RHO
301	462,73	2,050		29722.	29670.	29670.
302	461,99	2,020		29760.	29707.	29707.
303	460,26	2,025		29835.	29782.	29782.
304	458,64	2,167		30077.	30022.	30022.
305	456,01	2,194		30163.	30107.	30107.
306	452,90		2,8591	30226.	30170.	30170.
307	452,86	2,187		30227.	30171.	30171.
308	450,92	2,118		30332.	30275.	30275.
309	448,16	2,052		30471.	30413.	30413.
310	443,84	2,124		30732.	30671.	30671.
311	441,66	2,119		30794.	30732.	30732.
312	441,07	2,157		30836.	30774.	30774.
313	437,14	2,195		31053.	30987.	30987.
314	433,50		2,9166	31246.	31177.	31177.
315	432,91	2,047		31300.	31231.	31231.
316	430,94	2,027		31396.	31325.	31325.
317	429,26	2,031		31453.	31381.	31381.
318	428,97	2,079		31491.	31419.	31419.
319	426,51	2,105		31592.	31519.	31519.
320	425,72	2,090		31632.	31559.	31559.
321	419,81	2,071		31931.	31856.	31856.
322	418,90		2,8081	31977.	31902.	31902.
323	418,65	2,082		31990.	31916.	31916.
324	413,51	2,052		32046.	32171.	32171.
325	411,55	1,989		32340.	32265.	32265.
326	409,58	1,984		32431.	32355.	32355.
327	406,82	1,995		32555.	32479.	32479.
328	405,25	1,990		32624.	32548.	32548.
329	402,88	1,915		32726.	32649.	32649.
330	401,31	1,942		32794.	32716.	32716.
331	399,34	1,959		32881.	32802.	32802.
332	397,37	1,959		32968.	32888.	32888.
333	395,40	1,954		33056.	32974.	32974.
334	393,90		2,9065	33124.	33041.	33041.
335	393,83	1,988		33127.	33044.	33044.
336	389,69	1,984		33308.	33222.	33222.
337	376,40		2,8498			
338	361,90		2,8565			
339	347,40		2,8768			
340	331,10		2,8745			
341	313,90		2,8745			
342	294,90		2,8882			
343	277,90		2,8905			
344	266,60		2,8839			
345	249,90		2,8814			
346	233,00		2,8633			
347	232,99		2,8210			
348	,00		2,8210			

BOREHOLE KAP-01

J	PEACL DEPTH (FT)	G - G DENSITY (GM/CC)	DENSITY OF SOLID COMPONENT (GM/CC)	CUMULATIVE SOLID MASS (GM/CM**2) RHO=2.821	RHO=<RHO>	LINEAR SPLINE FOR RHO
0	1800,00		2,8210			
1	1185,05	2,085		0.	0.	0.
2	1183,84	2,061		61.	61.	61.
3	1182,63	2,057		140.	140.	140.
4	1180,63	2,030		218.	218.	218.
5	1179,82	2,045		257.	257.	257.
6	1177,91	2,050		375.	375.	375.
7	1175,81	2,060		455.	455.	455.
8	1174,20	2,042		534.	534.	534.
9	1172,19	2,044		632.	632.	632.
10	1169,78	1,994		746.	746.	746.
11	1166,17	2,042		918.	918.	918.
12	1164,16	2,025		1015.	1015.	1015.
13	1162,54	2,124		1157.	1157.	1157.
14	1159,54	2,045		1259.	1259.	1259.
15	1158,13	2,017		1317.	1317.	1317.
16	1155,62	2,045		1452.	1452.	1452.
17	1152,91	1,990		1567.	1567.	1567.
18	1150,90	2,038		1663.	1663.	1663.
19	1149,29	2,090		1744.	1744.	1744.
20	1148,09	2,058		1804.	1804.	1804.
21	1146,08	1,915		1897.	1897.	1897.
22	1143,67	2,074		2009.	2009.	2009.
23	1142,86	2,082		2049.	2049.	2049.
24	1142,06	2,074		2090.	2090.	2090.
25	1140,66	2,018		2149.	2149.	2149.
26	1138,04	2,010		2282.	2282.	2282.
27	1136,44	1,978		2357.	2357.	2357.
28	1134,03	2,001		2468.	2468.	2468.
29	1132,42	1,994		2543.	2543.	2543.
30	1130,01	2,034		2657.	2657.	2657.
31	1126,79	1,975		2808.	2808.	2808.
32	1125,98	2,058		2941.	2941.	2941.
33	1121,97	2,055		3041.	3041.	3041.
34	1120,37	2,622		3119.	3119.	3119.
35	1119,76	2,015		3195.	3195.	3195.
36	1116,75	1,994		3289.	3289.	3289.
37	1115,94	2,039		3423.	3423.	3423.
38	1112,53	1,980		3499.	3499.	3499.
39	1110,52	1,980		3591.	3591.	3591.
40	1109,12	1,963		3645.	3645.	3645.
41	1107,91	2,033		3701.	3701.	3701.
42	1106,71	2,047		3760.	3760.	3760.
43	1104,70	2,098		3861.	3861.	3861.
44	1101,89	1,967		3996.	3996.	3996.
45	1099,07	1,965		4123.	4123.	4123.
46	1098,27	1,966		4159.	4159.	4159.
47	1097,47	1,978		4196.	4196.	4196.
48	1096,26	1,980		4251.	4251.	4251.
49	1095,06	1,994		4306.	4306.	4306.
50	1094,25	2,042		4345.	4345.	4345.
51	1093,05	2,065		4404.	4404.	4404.
52	1090,64	2,049		4525.	4525.	4525.
53	1087,02	2,074		4704.	4704.	4704.
54	1085,82	2,098		4765.	4765.	4765.
55	1083,81	2,081		4868.	4868.	4868.
56	1082,60	2,085		4929.	4929.	4929.
57	1081,40	2,128		4991.	4991.	4991.
58	1079,39	2,162		5099.	5099.	5099.
59	1077,78	2,202		5188.	5188.	5188.
60	1076,58	2,229		5257.	5257.	5257.
61	1074,97	2,194		5371.	5371.	5371.
62	1073,76	2,106		5414.	5414.	5414.
63	1070,55	2,017		5574.	5574.	5574.
64	1068,94	2,018		5650.	5650.	5650.
65	1066,53	1,994		5763.	5763.	5763.
66	1063,32	2,060		5918.	5918.	5918.
67	1060,10	2,030		6073.	6073.	6073.
68	1057,69	2,014		6187.	6187.	6187.
69	1055,68	1,970		6373.	6373.	6373.
70	1052,47	2,018		6429.	6429.	6429.
71	1050,86	2,044		6507.	6507.	6507.
72	1048,45	2,025		6643.	6643.	6643.
73	1046,45	2,034		6720.	6720.	6720.
74	1045,64	2,058		6759.	6759.	6759.
75	1043,63	2,074		6859.	6859.	6859.
76	1041,22	1,986		6975.	6975.	6975.
77	1037,61	1,986		7142.	7142.	7142.
78	1037,41	1,978		7160.	7160.	7160.
79	1035,60	2,017		7235.	7235.	7235.
80	1033,59	2,018		7331.	7331.	7331.
81	1030,38	2,143		7493.	7493.	7493.
82	1028,37	2,090		7598.	7598.	7598.
83	1025,55	2,044		7738.	7738.	7738.
84	1021,94	2,104		7920.	7920.	7920.
85	1020,33	2,034		8001.	8001.	8001.
86	1017,52	1,990		8133.	8133.	8133.
87	1015,11	2,111		8252.	8252.	8252.
88	1013,50	2,148		8337.	8337.	8337.
89	1011,49	2,138		8444.	8444.	8444.
90	1009,48	2,018		8546.	8546.	8546.
91	1008,28	2,026		8603.	8603.	8603.
92	1005,87	2,084		8722.	8722.	8722.
93	1002,66	1,947		8875.	8875.	8875.
94	995,02	2,106		9241.	9241.	9241.
95	990,60	2,138		9473.	9473.	9473.
96	989,40	2,127		9537.	9537.	9537.
97	986,18	2,258		9716.	9716.	9716.
98	979,35	2,117		10096.	10096.	10096.
99	976,74	2,130		10223.	10223.	10223.
100	975,34	2,074		10306.	10306.	10306.

TABLE 6-10 (Continued)

BOREHOLE KAR-01

J	PEACE DEPTH (FT)	G-G DENSITY (GM/CC)	DENSITY OF SOLID COMPONENT (GM/CC)	CUMULATIVE SOLID MASS (GM/CM**2) RHO=2.821	RHO=(RHO)	LINEAR SPLINE FOR RHO
101	972.12	2.047		10466.	10466.	10466.
102	969.31	2.095		10606.	10606.	10606.
103	967.50	2.081		10709.	10709.	10709.
104	962.08	2.089		10974.	10974.	10974.
105	958.86	1.961		11128.	11128.	11128.
106	955.65	2.151		11286.	11286.	11286.
107	951.43	2.044		11513.	11513.	11513.
108	949.72	2.362		11613.	11613.	11613.
109	946.52	2.146		11655.	11655.	11655.
110	945.61	2.211		11810.	11810.	11810.
111	942.80	2.157		11966.	11966.	11966.
112	941.99	2.152		12010.	12010.	12010.
113	940.38	2.127		12096.	12096.	12096.
114	937.57	2.146		12245.	12245.	12245.
115	935.97	2.101		12330.	12330.	12330.
116	933.56	2.149		12457.	12457.	12457.
117	931.35	2.096		12563.	12563.	12563.
118	929.14	2.154		12690.	12690.	12690.
119	926.73	2.187		12712.	12712.	12712.
120	924.72	2.124		12929.	12929.	12929.
121	922.71	2.120		13035.	13035.	13035.
122	921.10	2.089		13118.	13118.	13118.
123	918.29	2.154		13265.	13265.	13265.
124	917.08	2.176		13331.	13331.	13331.
125	915.48	2.110		13419.	13419.	13419.
126	914.67	2.106		13462.	13462.	13462.
127	912.66	2.063		13564.	13564.	13564.
128	911.06	2.066		13644.	13644.	13644.
129	909.85	2.109		13706.	13706.	13706.
130	907.44	2.130		13832.	13832.	13832.
131	905.83	2.127		13959.	13959.	13959.
132	904.63	2.151		14002.	14002.	14002.
133	902.22	2.162		14111.	14111.	14111.
134	901.01	2.202		14178.	14178.	14178.
135	897.40	2.106		14373.	14373.	14373.
136	895.79	2.108		14456.	14456.	14456.
137	893.38	2.042		14578.	14578.	14578.
138	890.97	2.098		14698.	14698.	14698.
139	889.76	2.111		14761.	14761.	14761.
140	885.75	2.037		14963.	14963.	14963.
141	883.34	2.065		15081.	15081.	15081.
142	880.93	2.106		15203.	15203.	15203.
143	877.71	1.995		15361.	15361.	15361.
144	875.30	1.998		15473.	15473.	15473.
145	874.90	2.015		15492.	15492.	15492.
146	872.89	2.015		15587.	15587.	15587.
147	870.88	2.066		15685.	15685.	15685.
148	868.47	2.045		15804.	15804.	15804.
149	866.87	2.100		15885.	15885.	15885.
150	865.66	2.112		15947.	15947.	15947.
151	864.05	2.101		16030.	16030.	16030.
152	862.04	2.128		16135.	16135.	16135.
153	858.03	2.025		16337.	16337.	16337.
154	856.82	2.045		16396.	16396.	16396.
155	855.62	2.074		16455.	16455.	16455.
156	854.01	2.095		16537.	16537.	16537.
157	851.60	2.058		16658.	16658.	16658.
158	849.19	1.999		16774.	16774.	16774.
159	844.37	2.117		17013.	17013.	17013.
160	841.96	2.042		17137.	17137.	17137.
161	839.95	2.087		17235.	17235.	17235.
162	837.94	2.074		17333.	17333.	17333.
163	836.73	2.095		17394.	17394.	17394.
164	835.93	2.090		17435.	17435.	17435.
165	833.12	1.999		17572.	17572.	17572.
166	829.50	2.145		17753.	17753.	17753.
167	827.49	2.042		17856.	17856.	17856.
168	824.68	1.948		17987.	17987.	17987.
169	822.67	1.980		18077.	18077.	18077.
170	820.26	1.905		18188.	18188.	18188.
171	818.66	2.010		18262.	18262.	18262.
172	817.45	2.014		18319.	18319.	18319.
173	816.65	2.045		18358.	18358.	18358.
174	814.24	2.058		18477.	18477.	18477.
175	811.82	2.007		18612.	18612.	18612.
176	809.81	2.049		18728.	18728.	18728.
177	807.81	2.106		18789.	18789.	18789.
178	805.80	2.122		18894.	18894.	18894.
179	802.59	2.100		19061.	19061.	19061.
180	799.77	2.112		19206.	19206.	19206.
181	797.77	2.108		19311.	19311.	19311.
182	795.36	2.111		19436.	19436.	19436.
183	793.75	2.089		19519.	19519.	19519.
184	791.74	2.098		19621.	19621.	19621.
185	788.53	2.087		19765.	19765.	19765.
186	786.92	2.045		19865.	19865.	19865.
187	785.31	2.777		19945.	19945.	19945.
188	779.89	2.108		20233.	20233.	20233.
189	775.27	2.050		20456.	20456.	20456.
190	773.26	2.023		20553.	20553.	20553.
191	772.05	2.851		20611.	20611.	20611.
192	769.64	2.034		20727.	20727.	20727.
193	765.42	2.125		20950.	20950.	20950.
194	763.42	2.082		21054.	21054.	21054.
195	761.81	2.101		21136.	21136.	21136.
196	759.80	2.098		21240.	21240.	21240.
197	758.39	2.109		21302.	21302.	21302.
198	756.79	2.114		21386.	21386.	21386.
199	754.98	2.093		21510.	21510.	21510.
200	752.97	2.100		21613.	21613.	21613.

BOREHOLE KAR-01

J	PEACE DEPTH (FT)	G-G DENSITY (GM/CC)	DENSITY OF SOLID COMPONENT (GM/CC)	CUMULATIVE SOLID MASS (GM/CM**2) RHO=2.821	RHO=(RHO)	LINEAR SPLINE FOR RHO
201	749.56	2.071		21756.	21756.	21756.
202	747.15	2.109		21879.	21879.	21879.
203	745.34	2.098		21962.	21962.	21962.
204	743.93	2.065		22043.	22043.	22043.
205	742.73	2.088		22103.	22103.	22103.
206	741.12	2.081		22184.	22184.	22184.
207	739.11	2.074		22285.	22285.	22285.
208	735.49	2.153		22472.	22472.	22472.
209	732.68	2.161		22619.	22619.	22619.
210	729.47	2.130		22787.	22787.	22787.
211	727.86	2.122		22872.	22872.	22872.
212	725.85	2.127		22978.	22978.	22978.
213	723.05	2.122		23020.	23020.	23020.
214	721.04	2.076		23123.	23123.	23123.
215	720.03	2.098		23246.	23246.	23246.
216	718.62	2.077		23348.	23348.	23348.
217	717.42	2.090		23409.	23409.	23409.
218	715.81	2.133		23493.	23493.	23493.
219	714.20	2.138		23576.	23576.	23576.
220	712.60	2.124		23663.	23663.	23663.
221	711.39	2.130		23727.	23727.	23727.
222	710.18	2.152		23791.	23791.	23791.
223	709.38	2.112		23833.	23833.	23833.
224	707.37	2.106		23937.	23937.	23937.
225	705.36	2.063		24039.	24039.	24039.
226	704.56	2.068		24079.	24079.	24079.
227	703.36	2.100		24140.	24140.	24140.
228	700.95	2.106		24265.	24265.	24265.
229	698.94	2.100		24368.	24368.	24368.
230	698.13	2.074		24409.	24409.	24409.
231	693.91	2.042		24648.	24648.	24648.
232	691.70	2.015		24725.	24725.	24725.
233	690.90	2.018		24763.	24763.	24763.
234	688.89	2.049		24860.	24860.	24860.
235	687.69	2.033		24919.	24919.	24919.
236	684.87	2.028		25074.	25074.	25074.
237	681.86	2.058		25213.	25213.	25213.
238	680.86	2.104		25255.	25255.	25255.
239	679.25	2.090		25337.	25337.	25337.
240	676.44	2.050		25478.	25478.	25478.
241	673.22	2.069		25639.	25639.	25639.
242	671.62	2.082		25721.	25721.	25721.
243	669.61	2.061		25821.	25821.	25821.
244	667.60	2.058		25921.	25921.	25921.
245	665.59	2.042		26019.	26019.	26019.
246	663.98	2.047		26098.	26098.	26098.
247	661.97	2.025		26215.	26215.	26215.
248	659.97	2.028		26311.	26311.	26311.
249	658.76	2.025		26389.	26389.	26389.
250	656.35	2.047		26466.	26466.	26466.
251	654.34	2.042		26603.	26603.	26603.
252	652.74	2.047		26643.	26643.	26643.
253	651.13	2.002		26720.	26720.	26720.
254	649.52	1.985		26794.	26794.	26794.
255	647.91	2.025		26888.	26888.	26888.
256	645.90	2.017		27061.	27061.	27061.
257	642.89	1.994		27117.	27117.	27117.
258	638.67	2.033		27308.	27308.	27308.
259	635.86	2.002		27441.	27441.	27441.
260	632.65	2.026		27593.	27593.	27593.
261	631.04	2.002		27670.	27670.	27670.
262	630.24	2.010		27707.	27707.	27707.
263	628.63	2.041		27784.	27784.	27784.
264	626.62	2.015		27881.	27881.	27881.
265	624.41	2.077		27999.	27999.	27999.
266	622.60	2.074		28080.	28080.	28080.
267	620.60	2.090		28181.	28181.	28181.
268	618.99	2.090		28263.	28263.	28263.
269	617.78	2.096		28325.	28325.	28325.
270	615.77	2.087		28427.	28427.	28427.
271	613.56	2.098		28551.	28551.	28551.
272	610.95	2.074		28673.	28673.	28673.
273	609.35	2.069		28754.	28754.	28754.
274	607.74	2.042		28833.	28833.	28833.
275	604.12	2.050		29010.	29010.	29010.
276	602.92	2.170		29073.	29073.	29073.
277	600.91	2.227		29185.	29185.	29185.
278	598.50	2.138		29319.	29319.	29319.
279	596.89	2.148		29405.	29405.	29405.
280	595.28	2.143		29596.	29596.	29596.
281	588.05	1.911		29848.	29848.	29848.
282	584.85	1.969		29989.	29989.	29989.
283	582.04	1.978		30116.	30116.	30116.
284	576.81	2.058		30365.	30365.	30365.
285	574.80	2.100		30466.	30466.	30466.
286	573.19	2.074		30548.	30548.	30548.
287	571.58	2.089		30629.	30629.	30629.
288	569.17	1.959		30745.	30745.	30745.
289	566.76	2.025		30856.	30856.	30856.
290	564.35	1.978		30969.	30969.	30969.
291	560.74	1.878		31125.	31125.	31125.
292	557.92	1.967		31246.	31246.	31246.
293	555.50	1.900		31339.	31339.	31339.
294	551.30	2.093		31532.	31532.	31532.
295	548.68	2.149		31680.	31680.	31680.
296	547.08	2.114		31765.	31765.	31765.
297	544.67	2.116		31786.	31786.	31786.
298	544.67	2.138		31892.	31892.	31892.
299	543.06	2.106		31976.	31976.	31976.
300	540.65	2.105		32101.	32101.	32101.

TABLE 6-10 (Continued)

BOREHOLE WAP-01

J	PEACE DEPTH (FT)	G - G DENSITY (GM/CC)	DENSITY OF SOLID COMPONENT (GM/CC)	CUMULATIVE SOLID MASS (GM/CM**2) RHO=2.821	RHO=(RHO)	LINEAR SPLINE FOR RHO
301	547.46	2.058		32264.	32264.	32264.
302	545.83	2.012		32342.	32342.	32342.
303	534.82	2.010		32389.	32389.	32389.
304	532.61	1.996		32493.	32493.	32493.
305	531.41	1.999		32549.	32549.	32549.
306	529.40	1.996		32642.	32642.	32642.
307	528.19	1.999		32699.	32699.	32699.
308	527.39	2.038		32736.	32736.	32736.
309	526.19	1.978		32793.	32793.	32793.
310	524.58	1.915		32863.	32863.	32863.
311	523.37	1.951		32916.	32916.	32916.
312	522.17	1.978		32970.	32970.	32970.
313	520.16	2.050		33065.	33065.	33065.
314	518.95	2.001		33123.	33123.	33123.
315	516.93	2.112		33222.	33222.	33222.
316	514.12	2.120		33264.	33264.	33264.
317	513.73	2.058		33387.	33387.	33387.
318	509.51	1.851		33584.	33584.	33584.
319	505.70	1.926		33739.	33739.	33739.
320	504.49	1.950		33793.	33793.	33793.
321	502.08	1.691		33885.	33885.	33885.
322	499.67	1.796		33968.	33968.	33968.
323	498.06	1.698		34024.	34024.	34024.
324	495.65	1.774		34106.	34106.	34106.
325	492.04	1.832		34215.	34215.	34215.
326	490.03	1.670		34280.	34280.	34280.
327	488.42	1.824		34327.	34327.	34327.
328	486.41	1.899		34424.	34424.	34424.
329	483.80	2.218		34563.	34563.	34563.
330	481.99	2.079		34649.	34649.	34649.
331	479.58	2.162		34776.	34776.	34776.
332	477.96	2.090		34861.	34861.	34861.
333	475.97	2.010		34959.	34959.	34959.
334	473.96	2.170		35062.	35062.	35062.
335	472.35	2.202		35151.	35151.	35151.
336	471.15	2.154		35218.	35218.	35218.
337	468.74	1.787		35327.	35327.	35327.
338	467.13	1.899		35390.	35390.	35390.
339	466.33	1.855		35422.	35422.	35422.
340	465.51	2.085		35548.	35548.	35548.
341	462.71	2.044		35588.	35588.	35588.
342	460.30	2.074		35707.	35707.	35707.
343	458.29	2.007		35805.	35805.	35805.
344	457.09	2.034		35863.	35863.	35863.
345	455.08	2.034		35950.	35950.	35950.
346	452.67	2.090		36079.	36079.	36079.
347	451.06	2.100		36162.	36162.	36162.
348	449.45	2.076		36244.	36244.	36244.
349	447.04	2.090		36366.	36366.	36366.
350	445.03	2.052		36466.	36466.	36466.
351	443.43	2.050		36545.	36545.	36545.
352	441.82	2.090		36626.	36626.	36626.
353	439.01	1.994		36763.	36763.	36763.
354	436.40	1.695		36873.	36873.	36873.
355	433.78	1.999		36968.	36968.	36968.
356	432.18	1.896		37037.	37037.	37037.
357	428.96	2.202		37191.	37191.	37191.
358	426.15	2.038		37336.	37336.	37336.
359	423.74	2.082		37457.	37457.	37457.
360	421.33	1.854		37566.	37566.	37566.
361	418.92	2.186		37681.	37681.	37681.
362	415.71	2.030		37848.	37848.	37848.
363	414.90	2.040		37887.	37887.	37887.
364	411.29	2.138		38076.	38076.	38076.
365	408.07	2.022		38238.	38238.	38238.
366	406.87	2.042		38296.	38296.	38296.
367	404.86	2.146		38399.	38399.	38399.
368	403.65	2.122		38463.	38463.	38463.
369	402.05	1.899		38539.	38539.	38539.
370	398.83	2.138		38692.	38692.	38692.
371	397.23	2.339		38786.	38786.	38786.
372	394.41	2.106		38947.	38947.	38947.
373	392.00	2.334		39085.	39085.	39085.
374	389.59	2.138		39225.	39225.	39225.
375	386.78	2.007		39366.	39366.	39366.
376	383.97	2.122		39506.	39506.	39506.
377	382.76	1.974		39565.	39565.	39565.
378	379.95	1.924		39689.	39689.	39689.
379	377.03	1.924		40676.	40676.	40676.
380	375.44	1.899		40744.	40744.	40744.
381	372.63	1.762		40852.	40852.	40852.
382	369.82	1.985		40967.	40967.	40967.
383	368.21	1.876		41036.	41036.	41036.
384	366.61	1.864		41101.	41101.	41101.
385	365.80	1.829		41133.	41133.	41133.
386	361.79	1.817		41286.	41286.	41286.
387	358.97	1.711		41386.	41386.	41386.
388	357.37	1.811		41443.	41443.	41443.
389	356.16	1.787		41487.	41487.	41487.
390	353.75	1.706		41571.	41571.	41571.
391	352.54	1.739		41611.	41611.	41611.
392	350.13	1.977		41707.	41707.	41707.
393	348.53	1.919		41778.	41778.	41778.
394	346.92	1.972		41849.	41849.	41849.
395	344.91	2.151		41949.	41949.	41949.
396	341.70	1.849		42099.	42099.	42099.
397	339.49	1.944		42203.	42203.	42203.
398	337.48	2.010		42241.	42241.	42241.
399	336.48	1.974		42334.	42334.	42334.
400	334.87	1.972		42407.	42407.	42407.

BOREHOLE WAP-01

J	PEACE DEPTH (FT)	G - G DENSITY (GM/CC)	DENSITY OF SOLID COMPONENT (GM/CC)	CUMULATIVE SOLID MASS (GM/CM**2) RHO=2.821	RHO=(RHO)	LINEAR SPLINE FOR RHO
401	312.46	1.624		42507.	42507.	42507.
402	310.85	1.884		42571.	42571.	42571.
403	309.65	1.852		42620.	42620.	42620.
404	307.25	1.913		42719.	42719.	42719.
405	305.05	1.819		42784.	42784.	42784.
406	304.02	1.791		42851.	42851.	42851.
407	303.62	1.950		42870.	42870.	42870.
408	303.22	1.991		42888.	42888.	42888.
409	301.21	1.838		42973.	42973.	42973.
410	300.81	1.965		42989.	42989.	42989.
411	300.41	1.867		43005.	43005.	43005.
412	299.60	1.910		43039.	43039.	43039.
413	297.19	1.659		43126.	43126.	43126.
414	293.38	1.886		43256.	43256.	43256.
415	291.17	1.778		43349.	43349.	43349.
416	289.96	1.676		43395.	43395.	43395.
417	289.16	1.694		43429.	43429.	43429.
418	287.55	1.880		43495.	43495.	43495.
419	285.34	1.899		43578.	43578.	43578.
420	284.54	1.870		43628.	43628.	43628.
421	281.12	1.918		43761.	43761.	43761.
422	279.51	1.883		43829.	43829.	43829.
423	278.71	1.870		43862.	43862.	43862.
424	276.70	1.870		43943.	43943.	43943.
425	275.10	1.851		44007.	44007.	44007.
426	274.29	1.859		44039.	44039.	44039.
427	272.68	1.860		44103.	44103.	44103.
428	270.88	1.902		44186.	44186.	44186.
429	269.07	1.739		44247.	44247.	44247.
430	267.86	1.711		44287.	44287.	44287.
431	265.05	1.785		44385.	44385.	44385.
432	263.44	1.787		44443.	44443.	44443.
433	263.04	1.803		44458.	44458.	44458.
434	261.03	1.819		44504.	44504.	44504.
435	261.03	1.840		44535.	44535.	44535.
436	259.43	1.827		44597.	44597.	44597.
437	258.22	1.771		44641.	44641.	44641.
438	256.62	1.766		44699.	44699.	44699.
439	254.20	1.759		44783.	44783.	44783.
440	252.60	1.755		44838.	44838.	44838.
441	249.79	1.626		44928.	44928.	44928.
442	248.58	1.675		44964.	44964.	44964.
443	246.97	1.690		45015.	45015.	45015.
444	244.96	1.800		45084.	45084.	45084.
445	243.76	1.711		45126.	45126.	45126.
446	242.96	1.705		45153.	45153.	45153.
447	240.14	1.511		45231.	45231.	45231.
448	239.74	1.548		45241.	45241.	45241.
449	237.73	1.581		45293.	45293.	45293.
450	236.93	1.561		45324.	45324.	45324.
451	236.13	1.564		45335.	45335.	45335.
452	234.12	1.519		45384.	45384.	45384.
453	230.50	1.762		45493.	45493.	45493.
454	229.30	1.669		45533.	45533.	45533.
455	227.29	1.666		45595.	45595.	45595.
456	225.68	1.569		45652.	45652.	45652.
457	220.06	1.908		45831.	45831.	45831.
458	218.85	1.707		45876.	45876.	45876.
459	217.65	1.548		45911.	45911.	45911.
460	215.64	1.532		45960.	45960.	45960.
461	214.03	1.659		46004.	46004.	46004.
462	211.62	1.768		46084.	46084.	46084.
463	210.82	1.723		46111.	46111.	46111.
464	210.41	1.741		46125.	46125.	46125.
465	209.61	1.742		46153.	46153.	46153.
466	209.21	1.755		46167.	46167.	46167.
467	208.00	1.784		46210.	46210.	46210.
468	206.40	1.659		46263.	46263.	46263.
469	204.79	1.623		46311.	46311.	46311.
470	203.18	1.645		46358.	46358.	46358.
471	201.98	1.612		46392.	46392.	46392.
472	199.57	1.516		46455.	46455.	46455.
473	198.76	1.659		46476.	46476.	46476.
474	197.16	1.931		46536.	46536.	46536.
475	195.55	1.978		46607.	46607.	46607.
476	194.75	1.915		46643.	46643.	46643.
477	192.74	1.760		46721.	46721.	46721.
478	189.93	1.921		46831.	46831.	46831.
479	.00		2.8210			

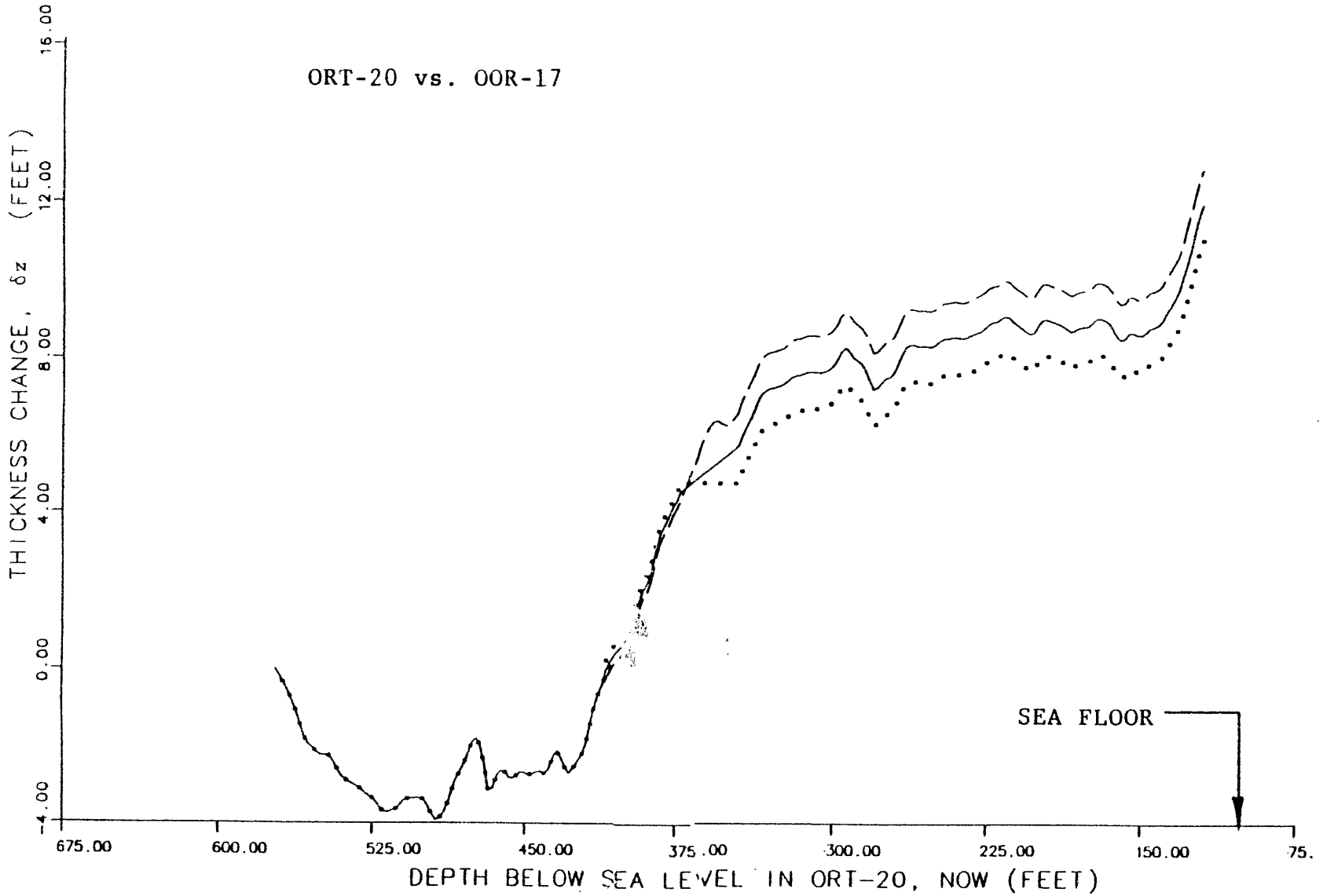

FIGURE 6-27. -- Change in rock thickness from γ-γ densities, assuming simple subsidence. Borehole ORT-20 vs. OOR-17.

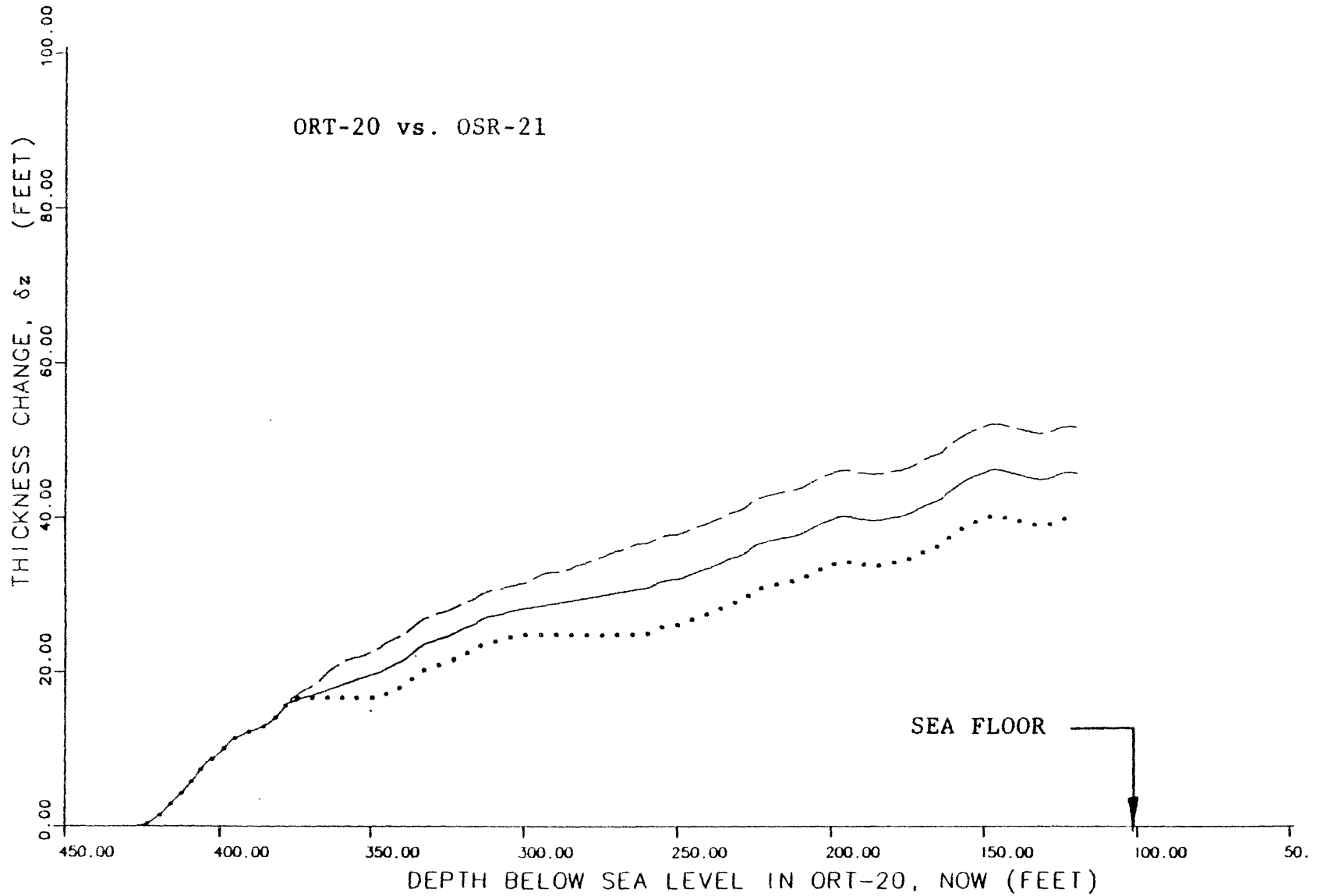

FIGURE 6-28. -- Change in rock thickness from γ-γ densities, assuming simple subsidence. Borehole ORT-20 vs. OSR-21.

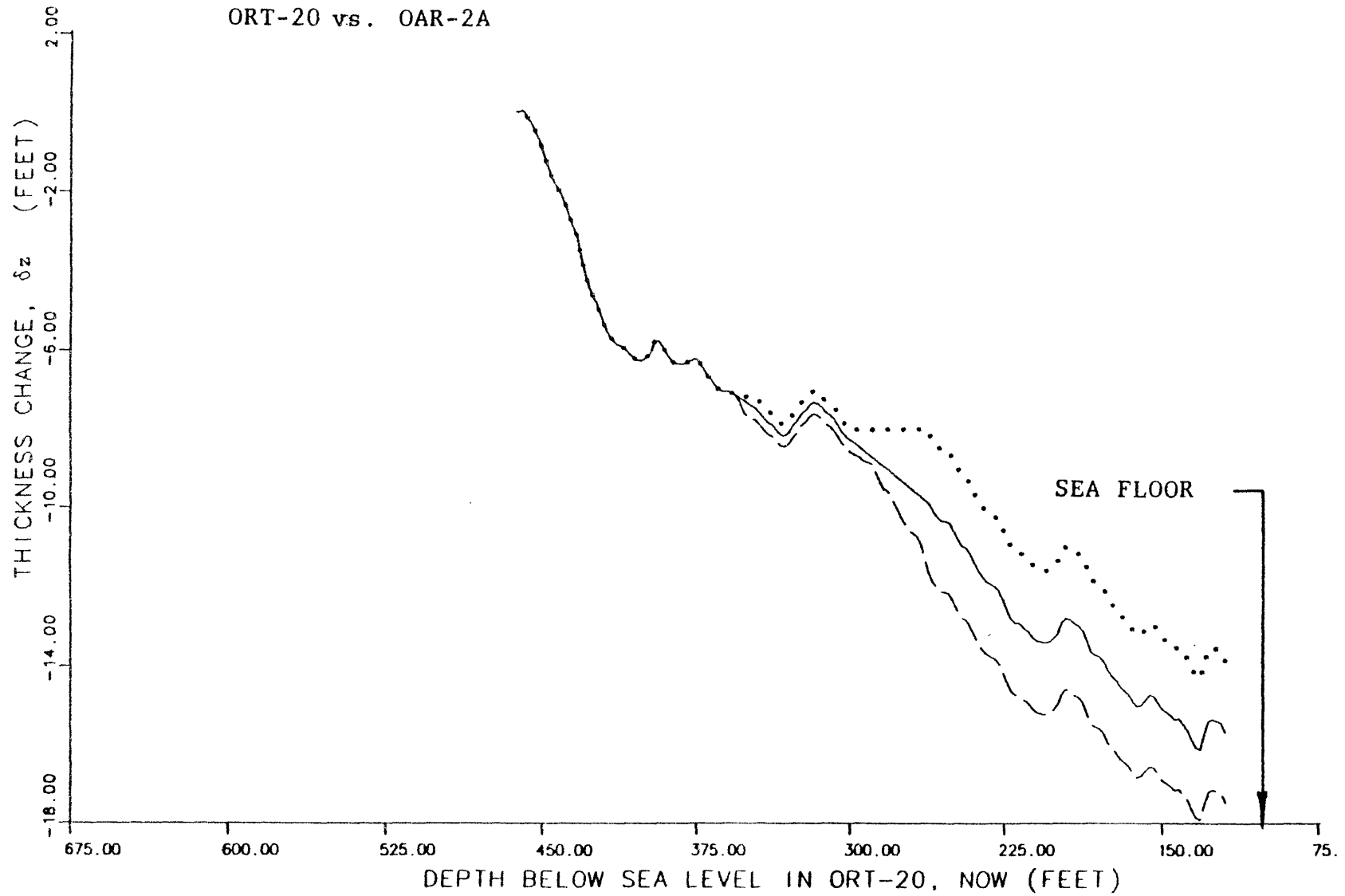

FIGURE 6-29. -- Change in rock thickness from γ-γ densities, assuming simple subsidence. Borehole ORT-20 vs. OAR-2A.

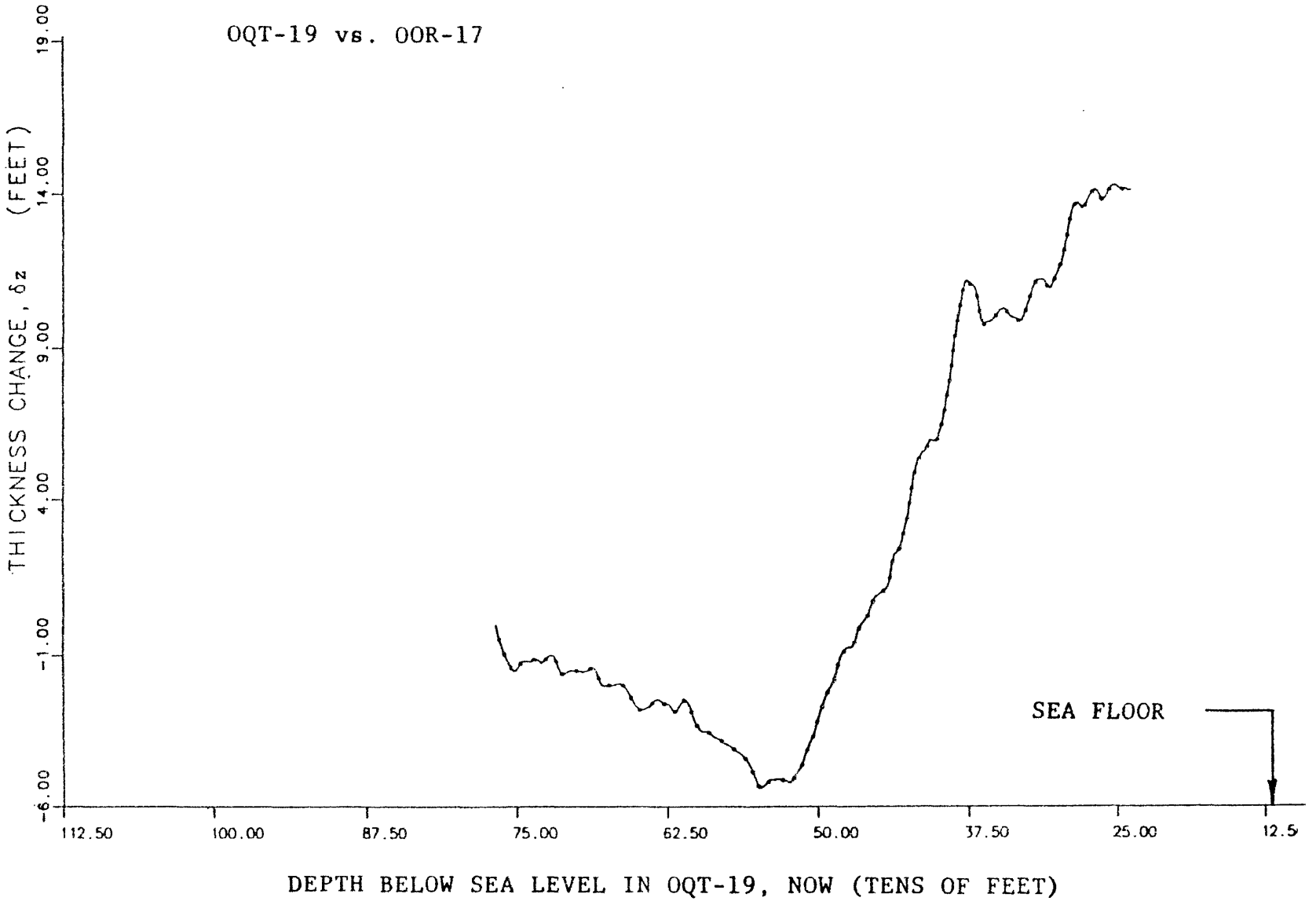

FIGURE 6-30. -- Change in rock thickness from γ-γ densities, assuming simple subsidence. Borehole OQT-19 vs. OOR-17.

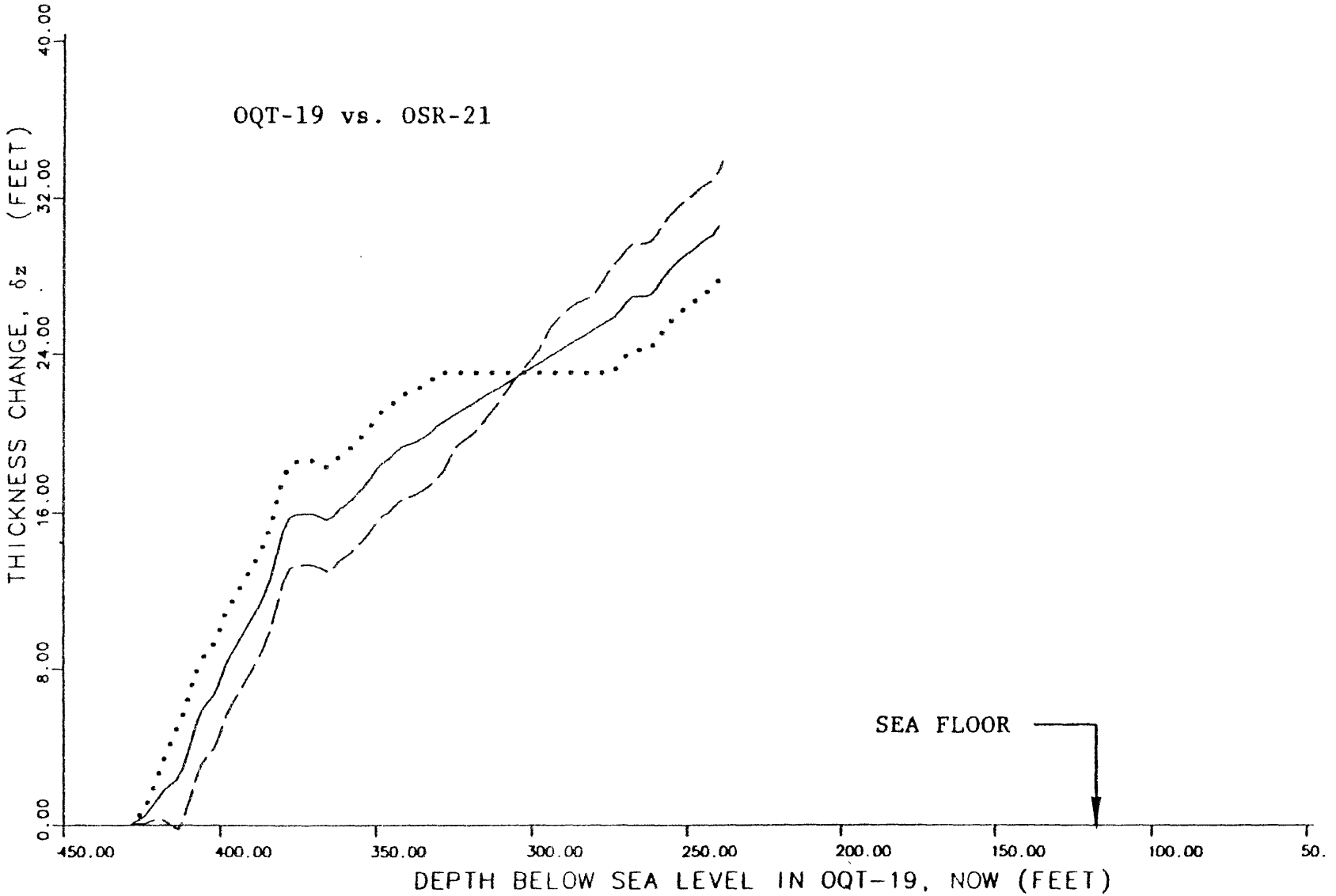

FIGURE 6-31. -- Change in rock thickness from γ-γ densities, assuming simple subsidence. Borehole OQT-19 vs. OSR-21.

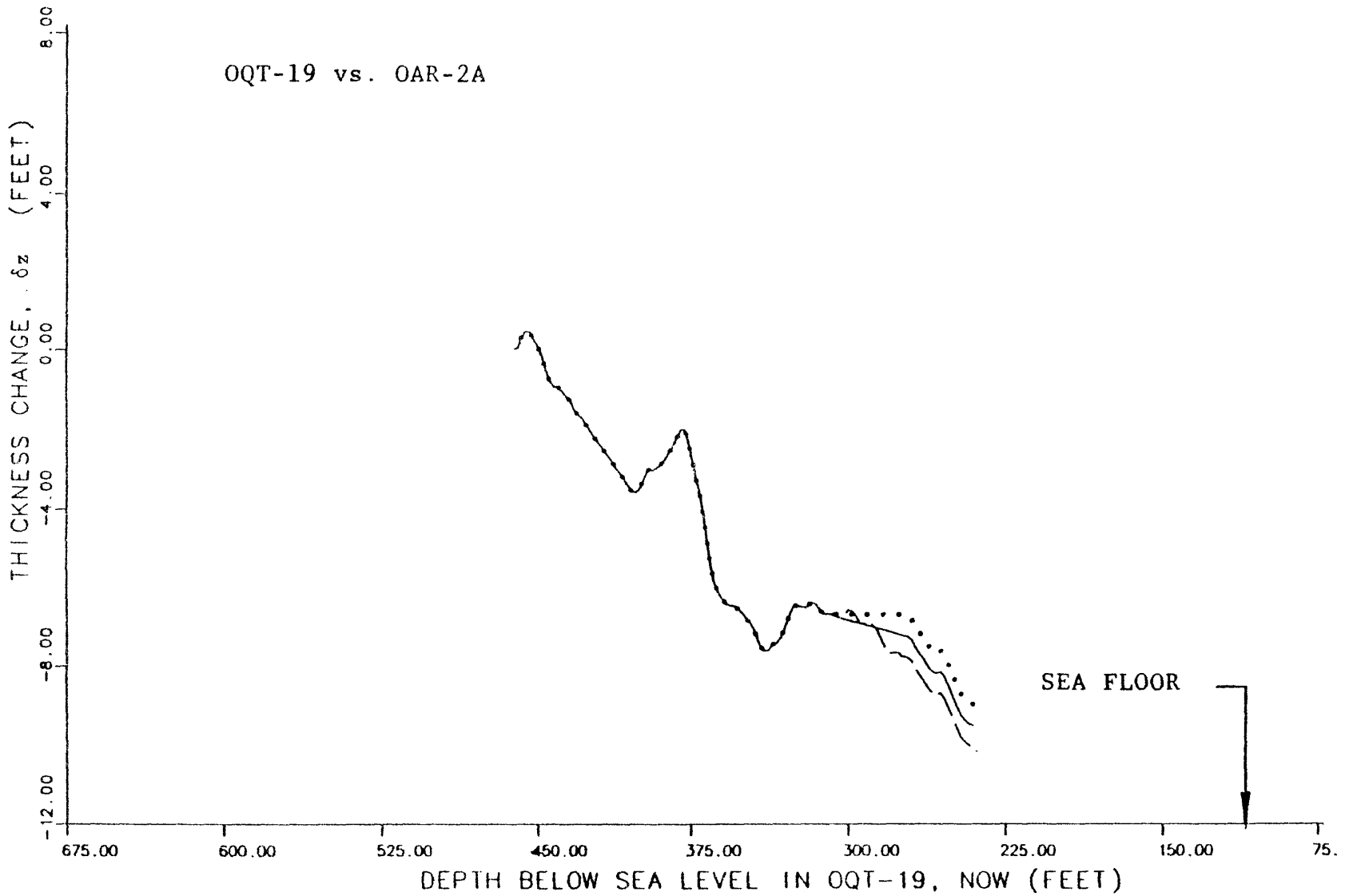

FIGURE 6-32. -- Change in rock thickness from γ-γ densities, assuming simple subsidence. Borehole OQT-19 vs. OAR-2A.

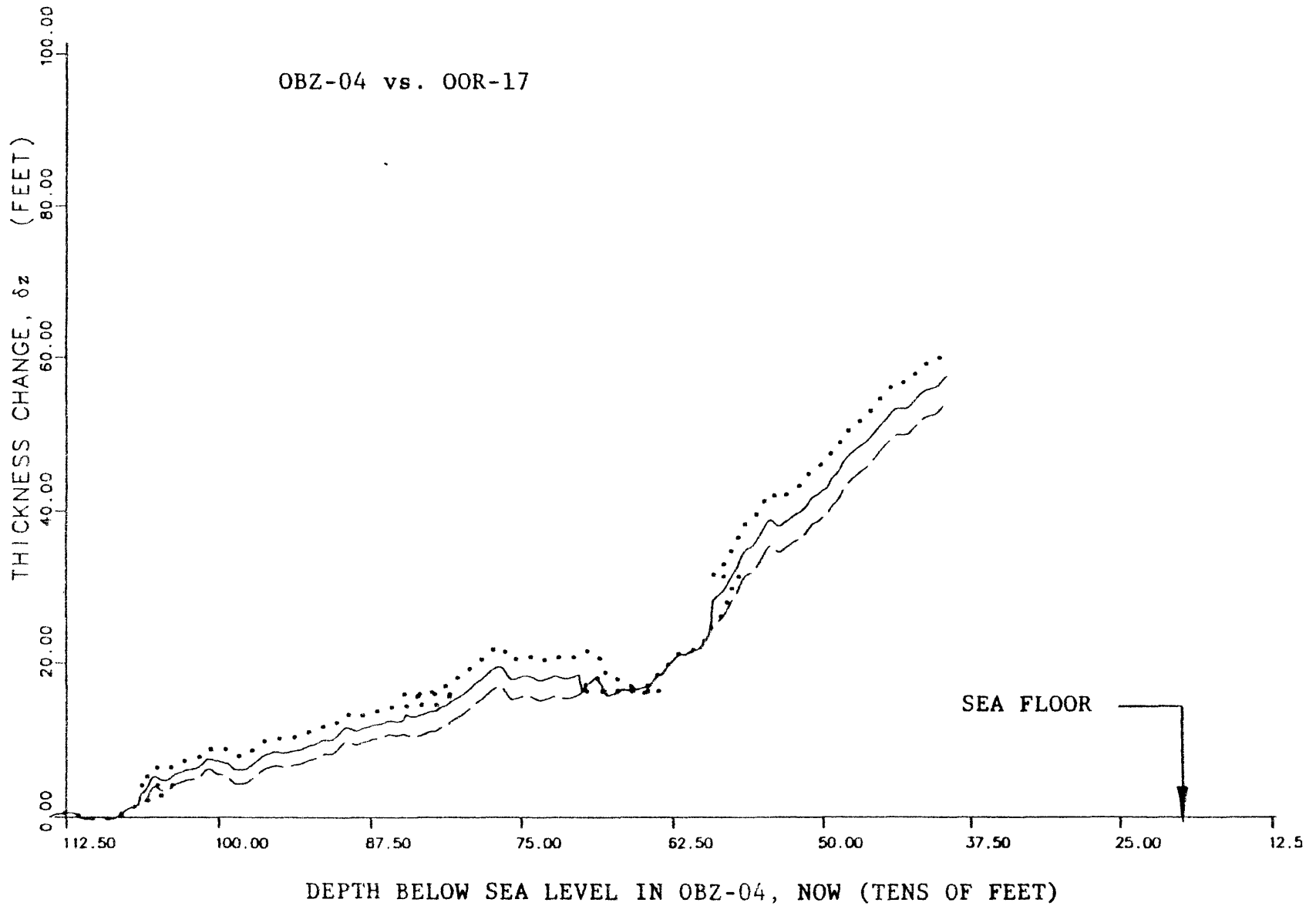

FIGURE 6-33. -- Change in rock thickness from γ-γ densities, assuming simple subsidence. Borehole OBZ-04 vs. OOR-17.

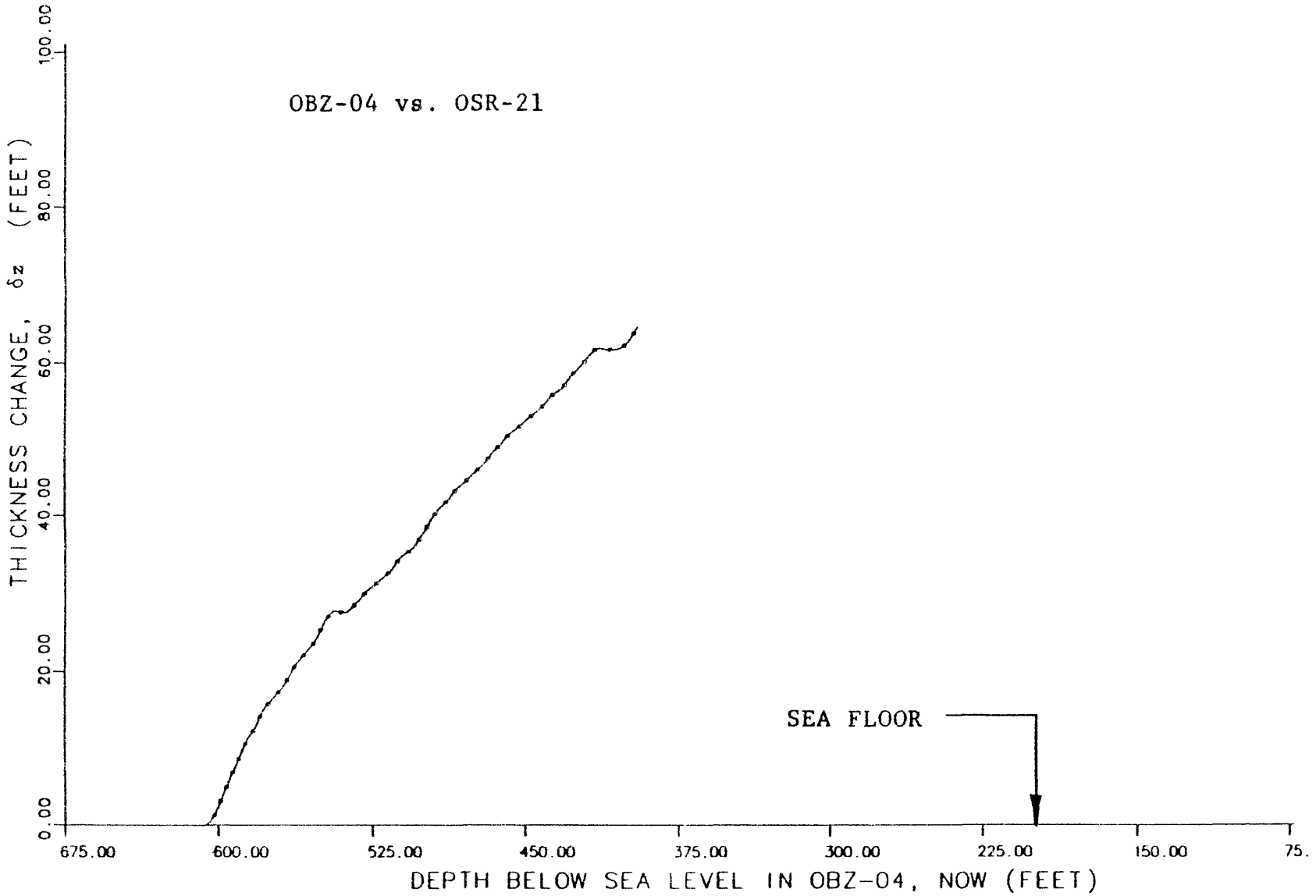

FIGURE 6-34. -- Change in rock thickness from γ-γ densities, assuming simple subsidence. Borehole OBZ-04 vs. OSR-21.

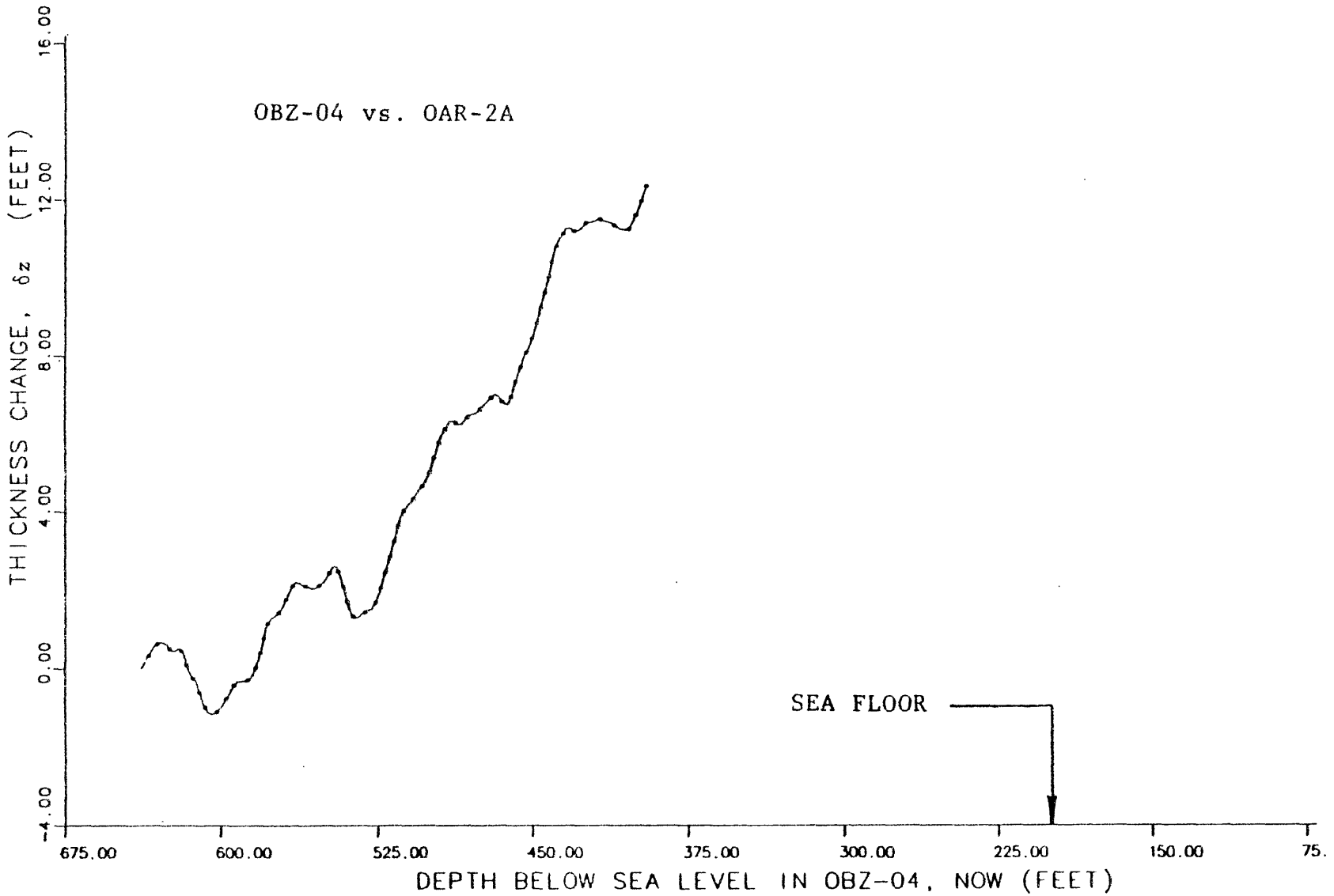

FIGURE 6-35. -- Change in rock thickness from γ-γ densities, assuming simple subsidence. Borehole OBZ-04 vs. OAR-2A.

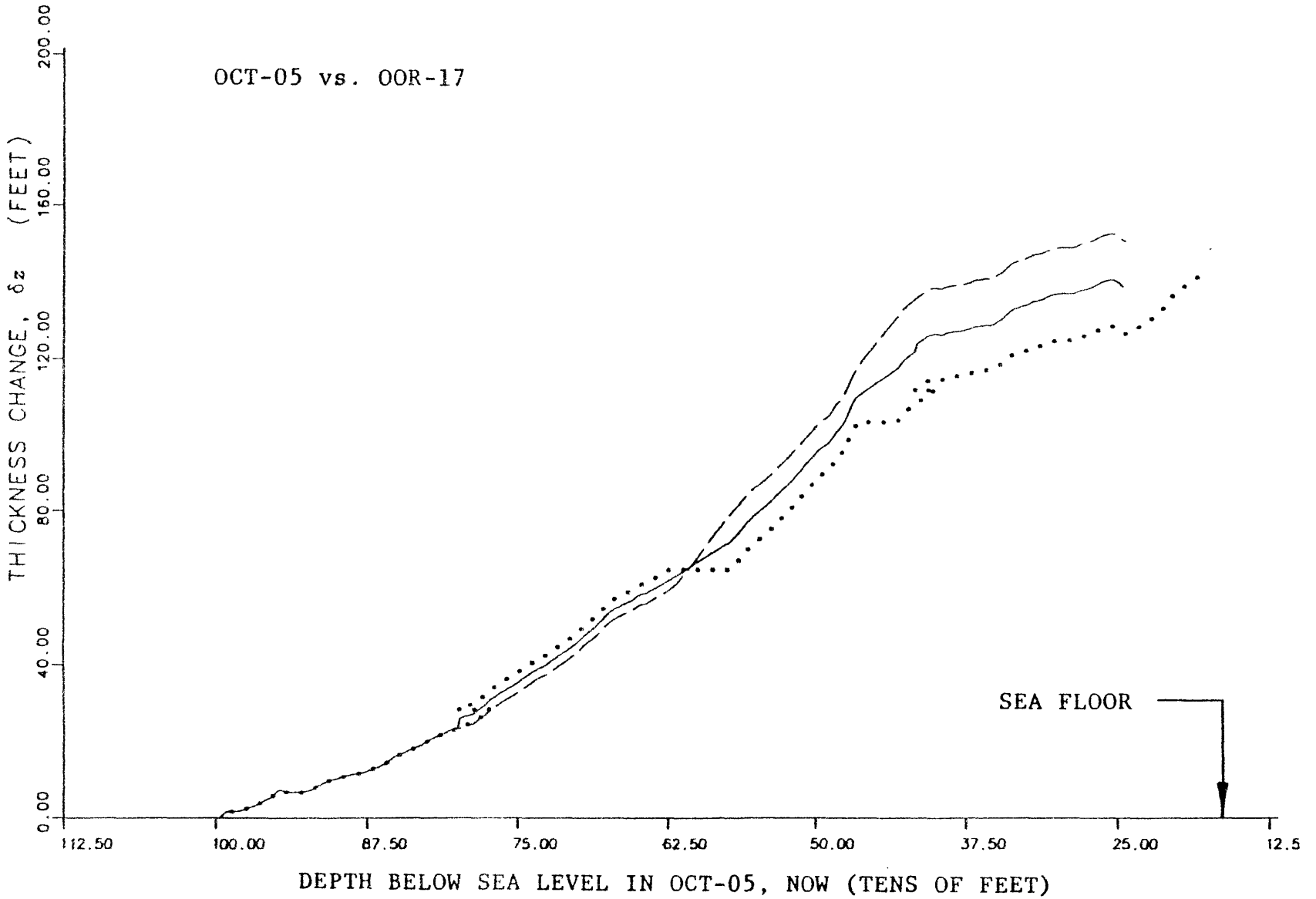

FIGURE 6-36. -- Change in rock thickness from γ-γ densities, assuming simple subsidence. Borehole OCT-05 vs. OOR-17.

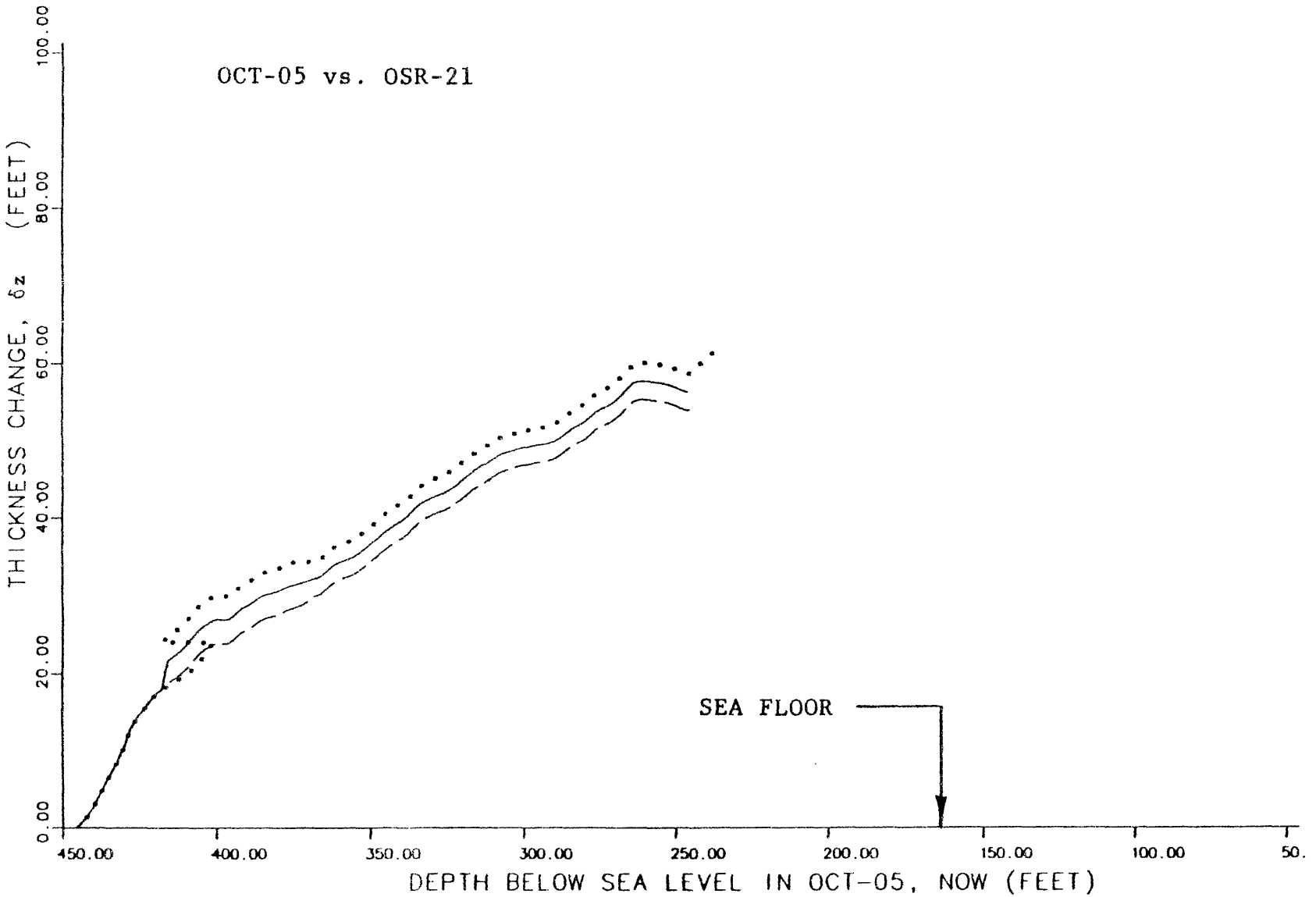

FIGURE 6-37. -- Change in rock thickness from γ-γ densities, assuming simple subsidence. Borehole OCT-05 vs. OSR-21.

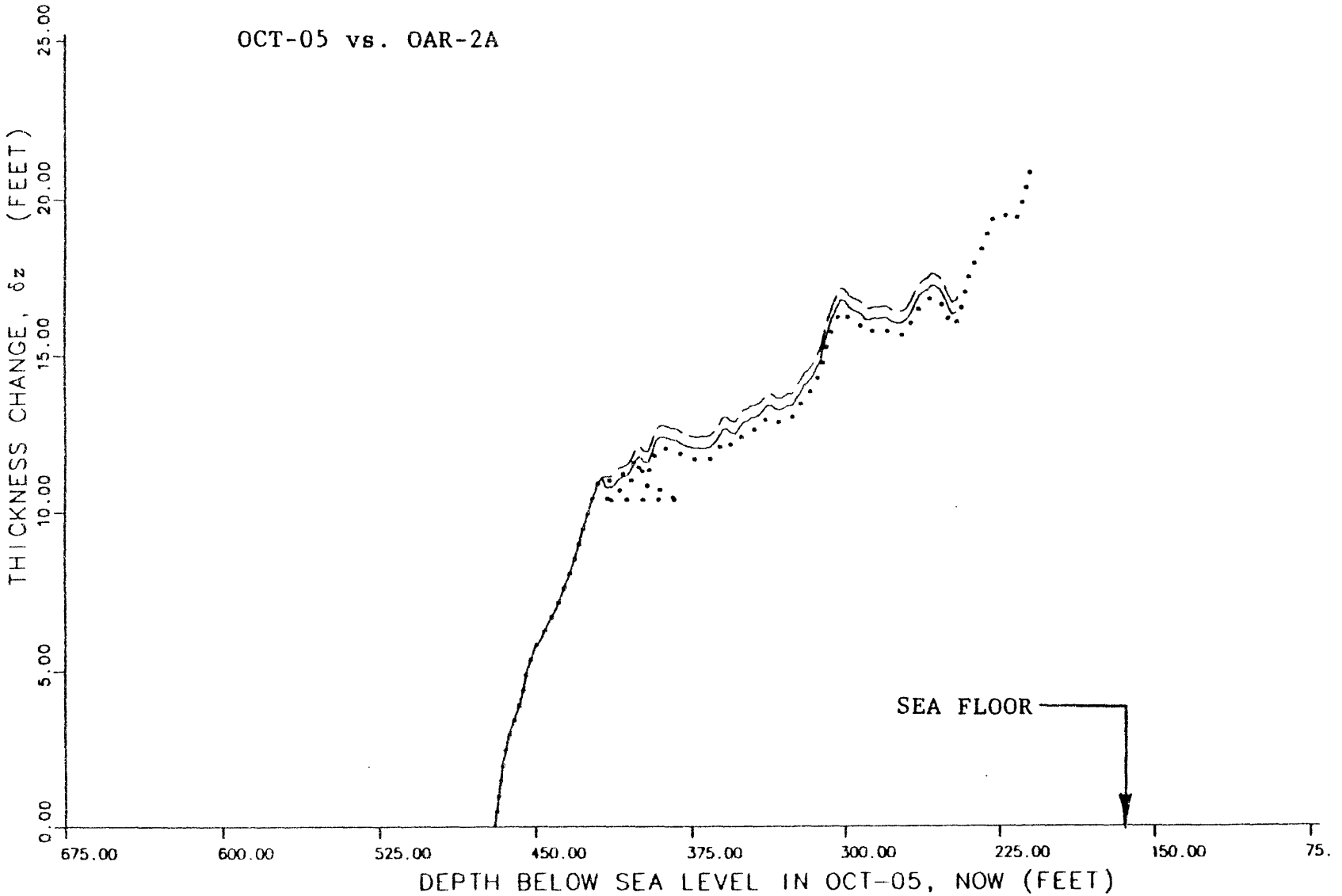

FIGURE 6-38. -- Change in rock thickness from γ-γ densities, assuming simple subsidence. Borehole OCT-05 vs. OAR-2A.

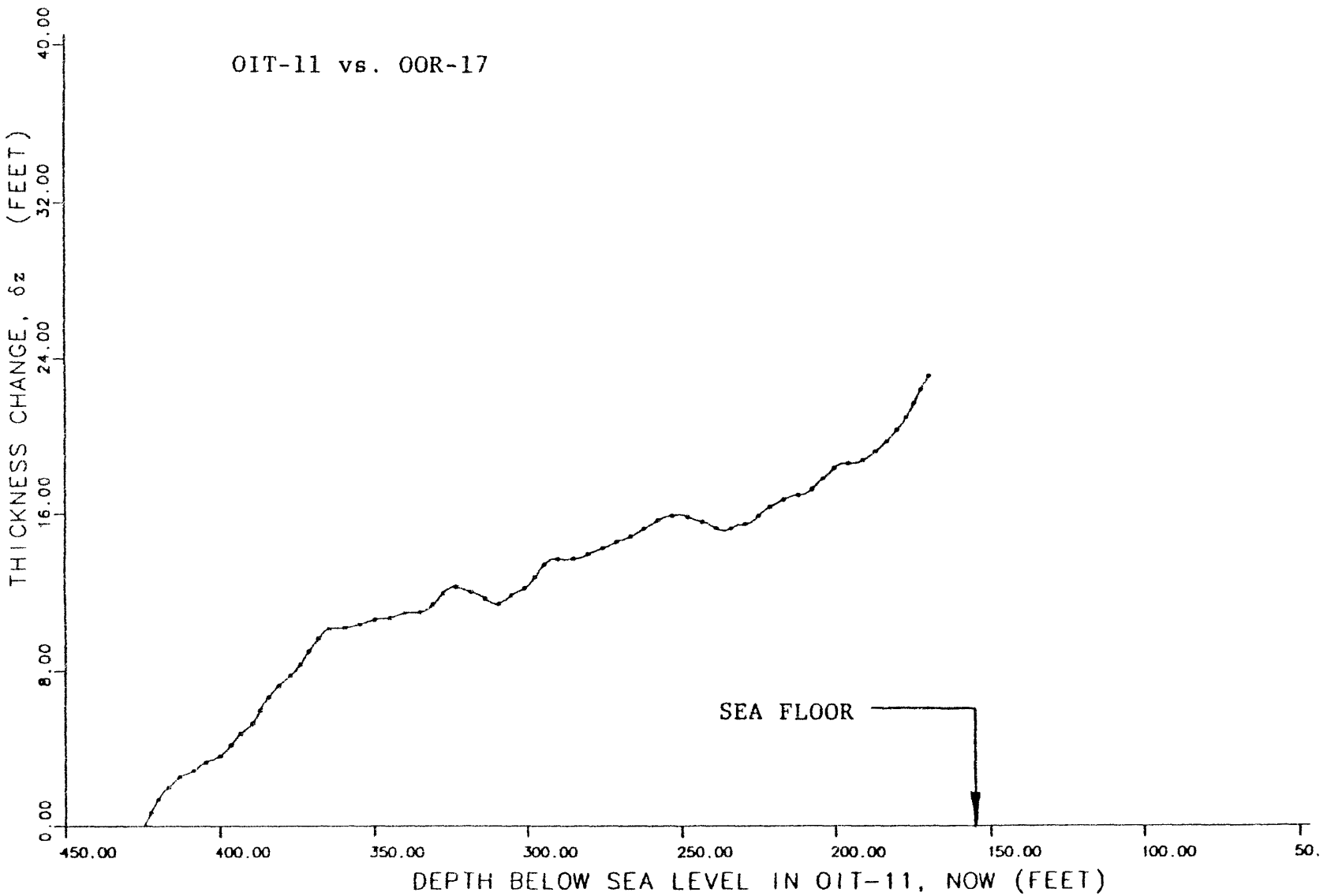

FIGURE 6-39. -- Change in rock thickness from γ-γ densities, assuming simple subsidence. Borehole OIT-11 vs. OOR-17.

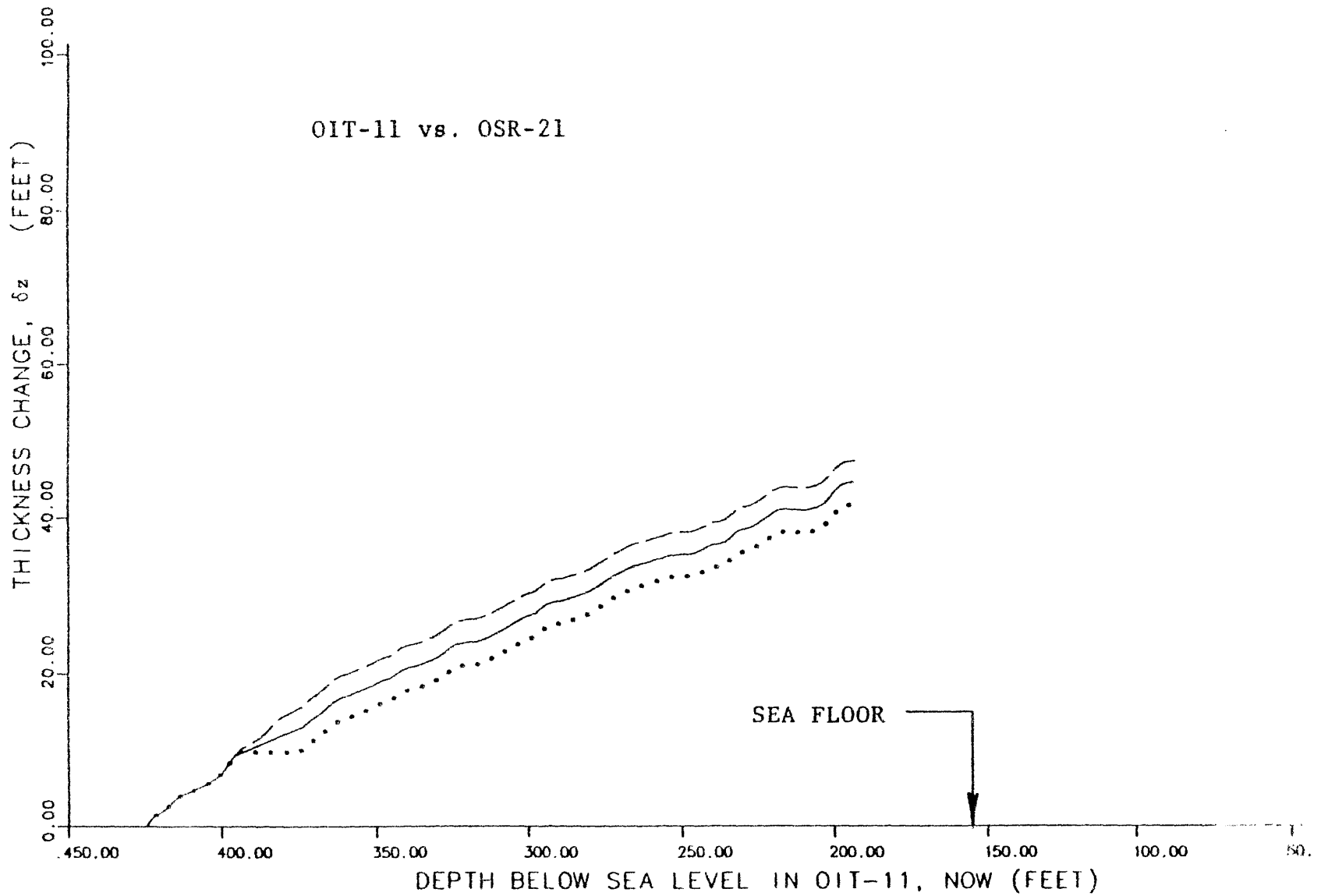

FIGURE 6-40. -- Change in rock thickness from γ-γ densities, assuming simple subsidence. Borehole OIT-11 vs. OSR-21.

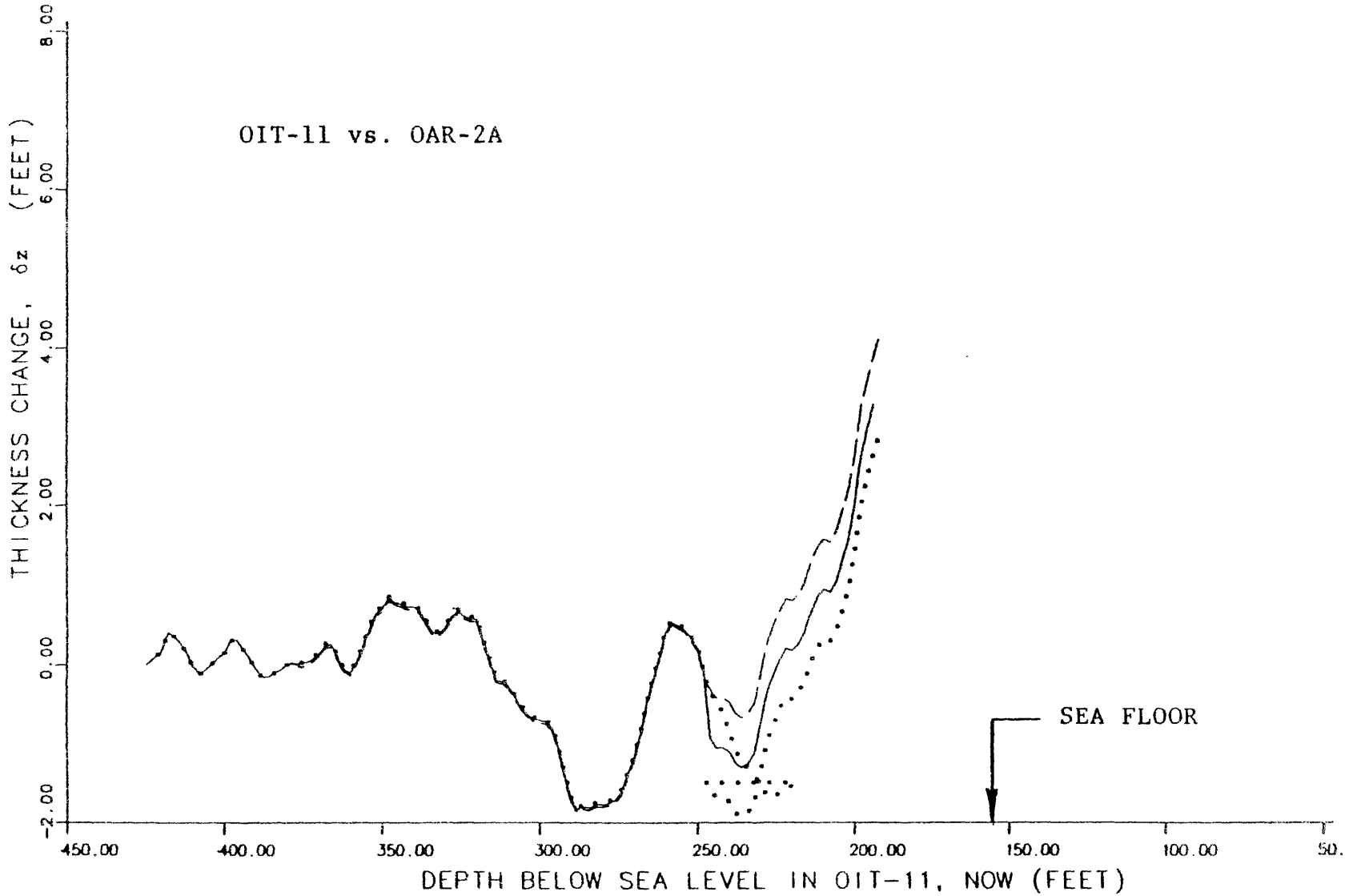

FIGURE 6-41. -- Change in rock thickness from γ-γ densities, assuming simple subsidence. Borehole OIT-11 vs. OAR-2A.

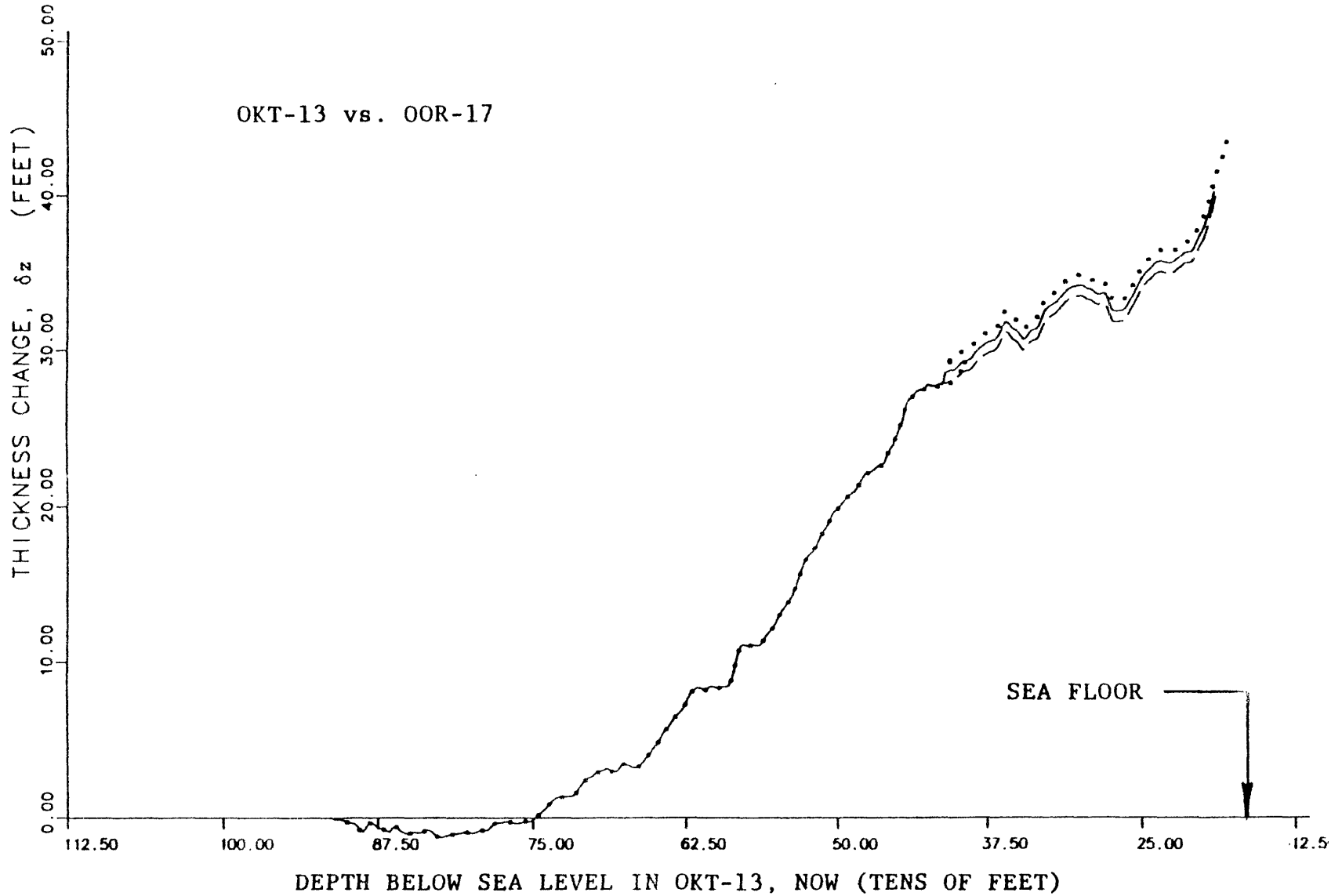

FIGURE 6-42. -- Change in rock thickness from γ-γ densities, assuming simple subsidence. Borehole OKT-13 vs. OOR-17.

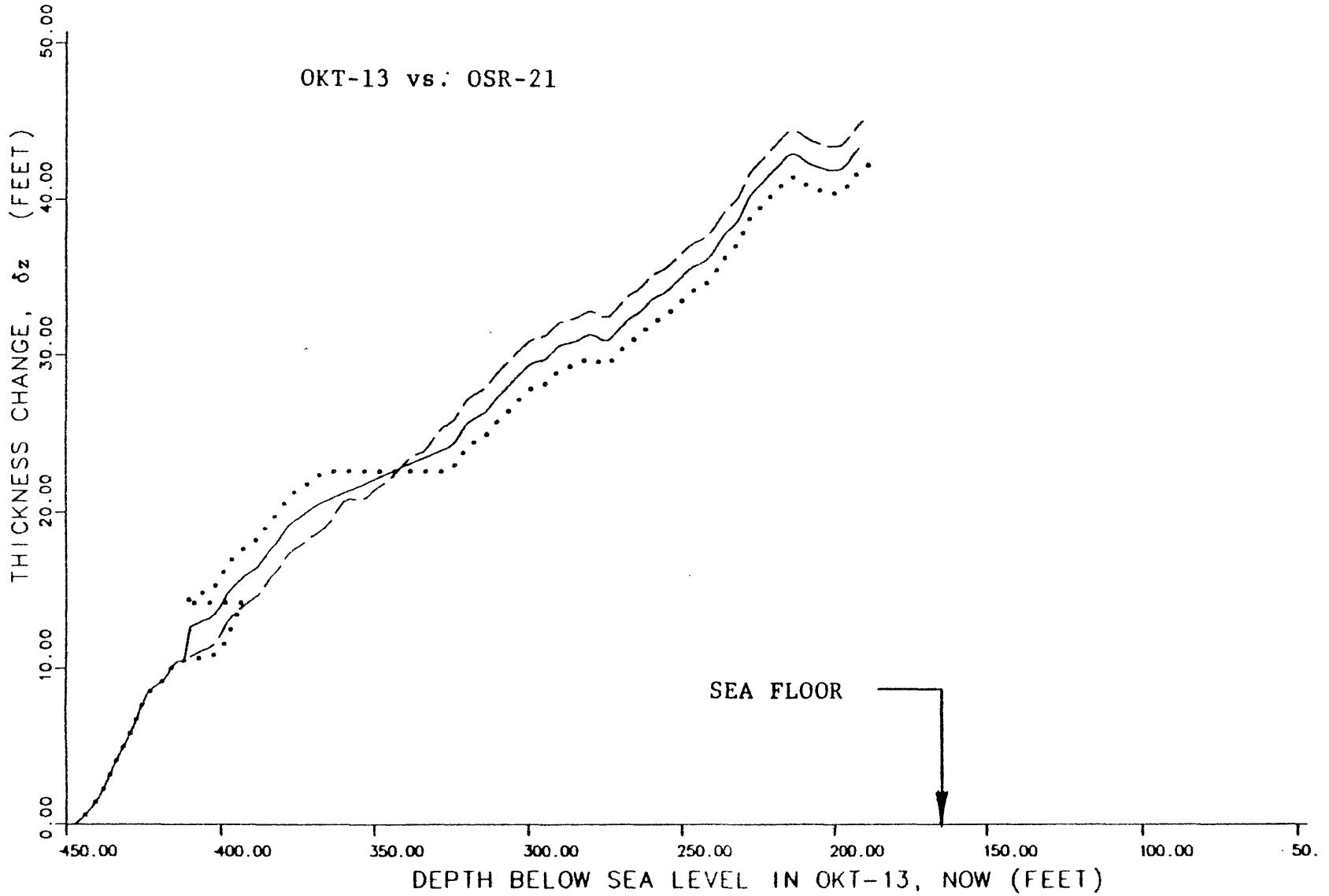

FIGURE 6-43. -- Change in rock thickness from γ-γ densities, assuming simple subsidence. Borehole OKT-13 vs. OSR-21.

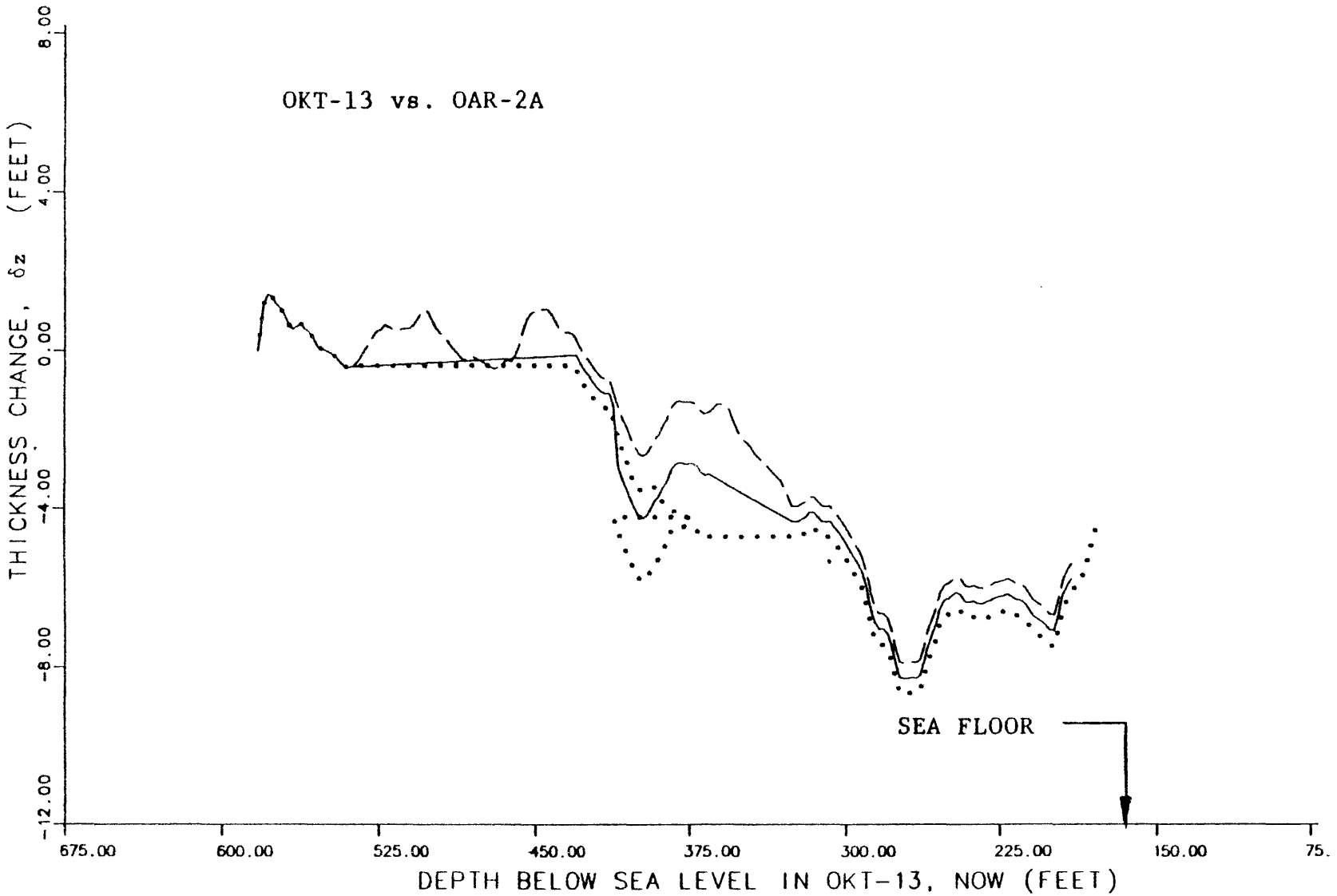

FIGURE 6-44. -- Change in rock thickness from γ-γ densities, assuming simple subsidence. Borehole OKT-13 vs. OAR-2A.

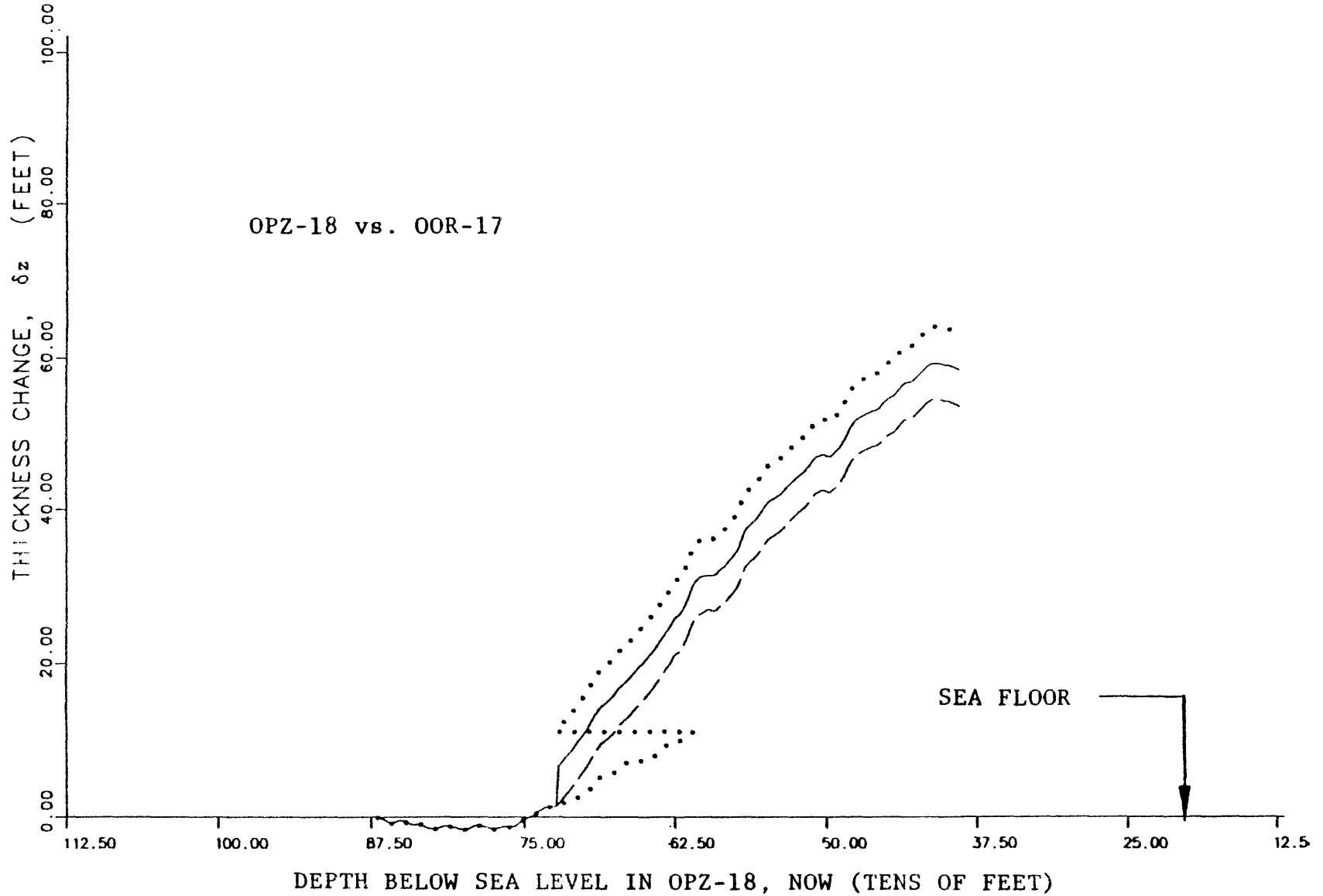

FIGURE 6-45. -- Change in rock thickness from γ-γ densities, assuming simple subsidence. Borehole OPZ-18 vs. OOR-17.

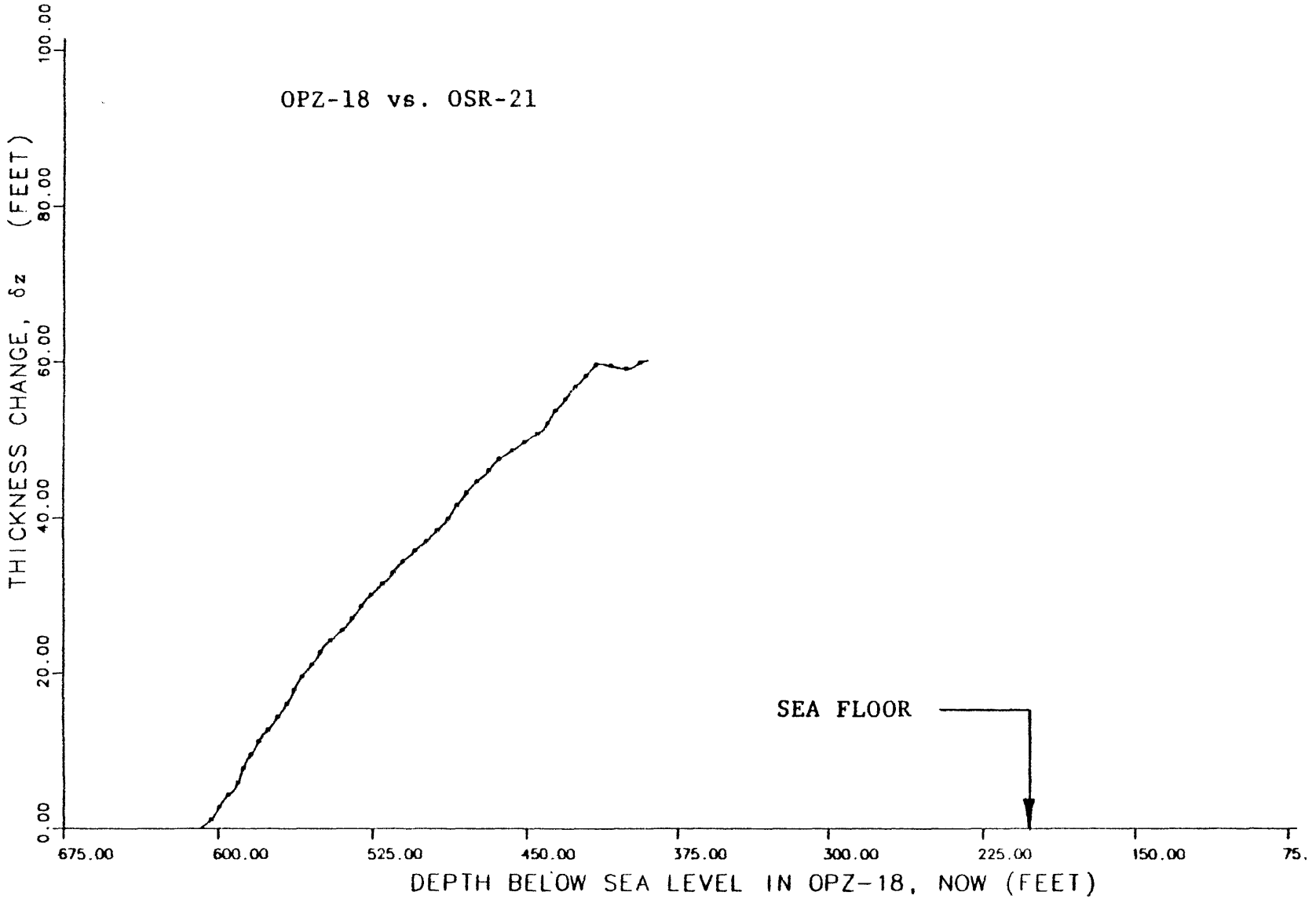

FIGURE 6-46. -- Change in rock thickness from γ-γ densities, assuming simple subsidence. Borehole OPZ-18 vs. OSR-21.

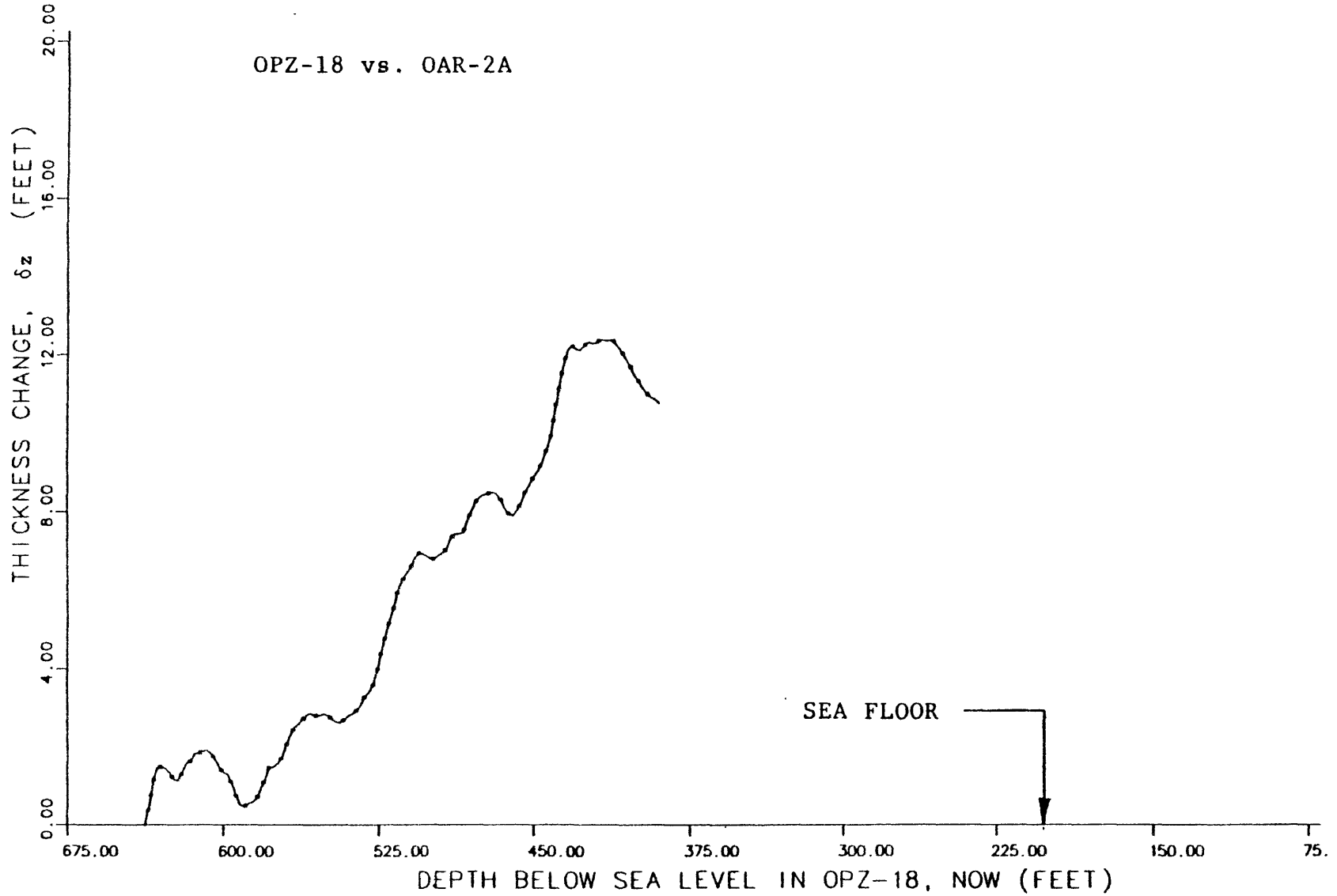

FIGURE 6-47. -- Change in rock thickness from γ-γ densities, assuming simple subsidence. Borehole OPZ-18 vs. OAR-2A.

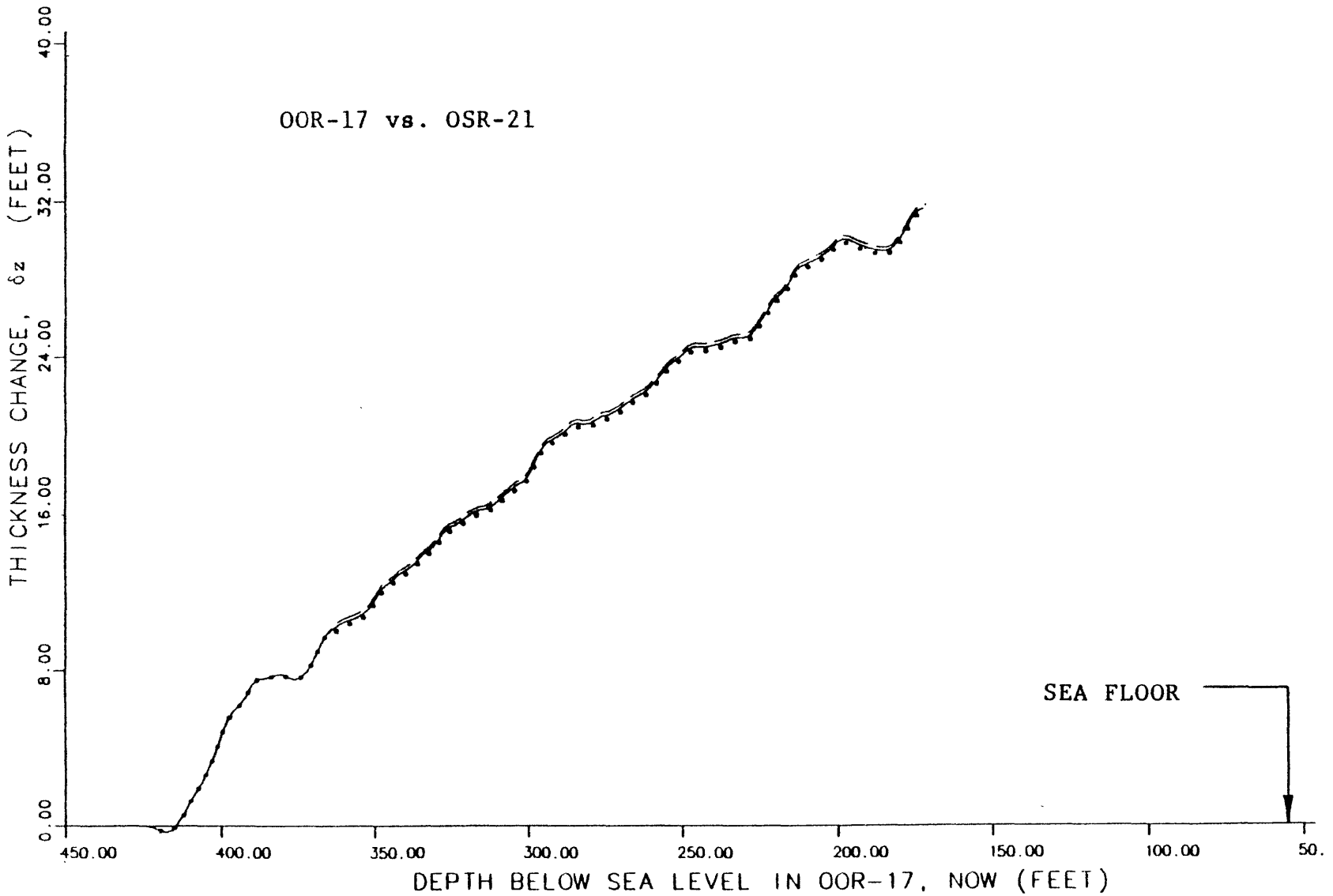

FIGURE 6-48. -- Change in rock thickness from γ-γ densities, assuming simple subsidence. Borehole OOR-17 vs. OSR-21.

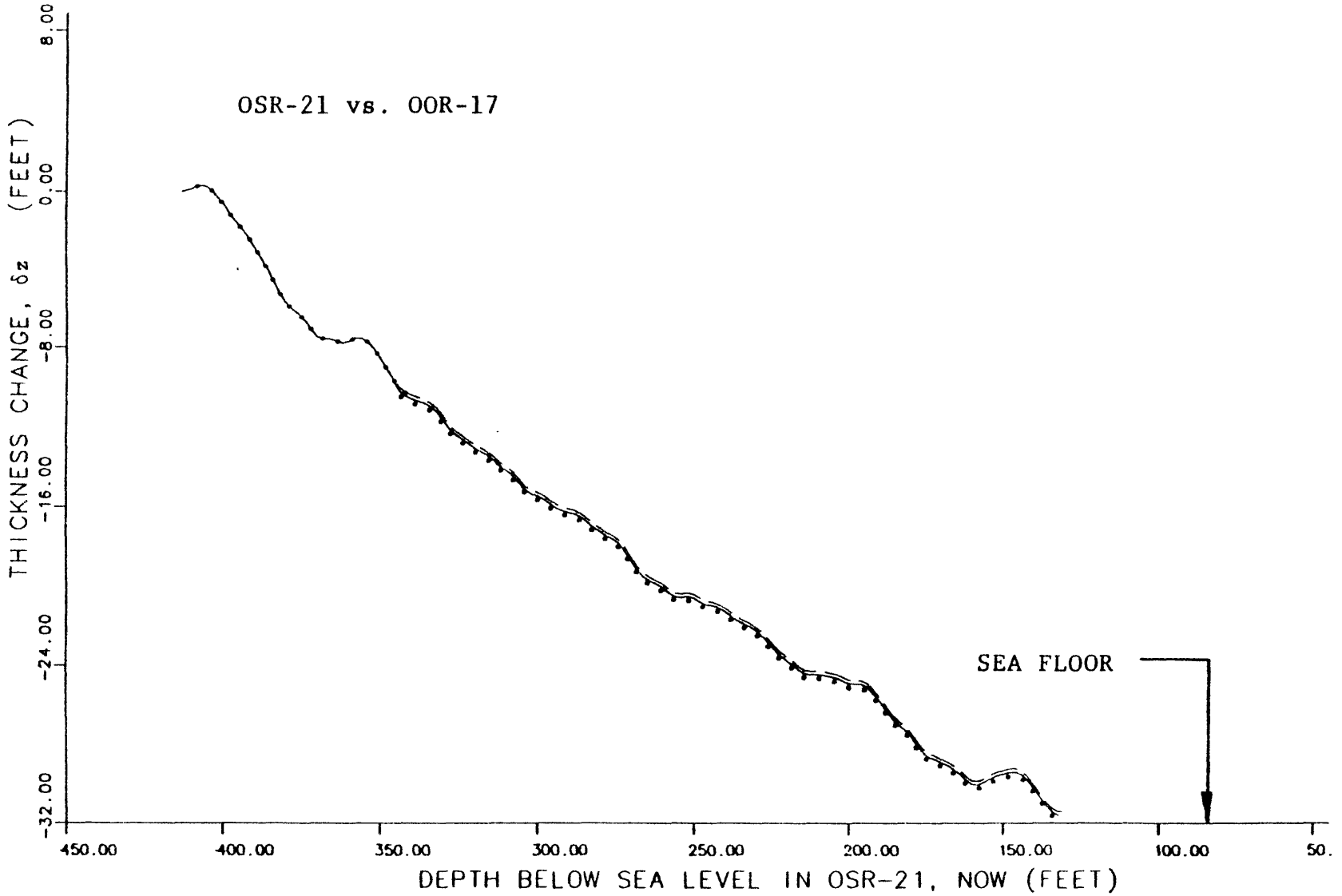

FIGURE 6-49. -- Change in rock thickness from γ-γ densities, assuming simple subsidence. Borehole OSR-21 vs. OOR-17.

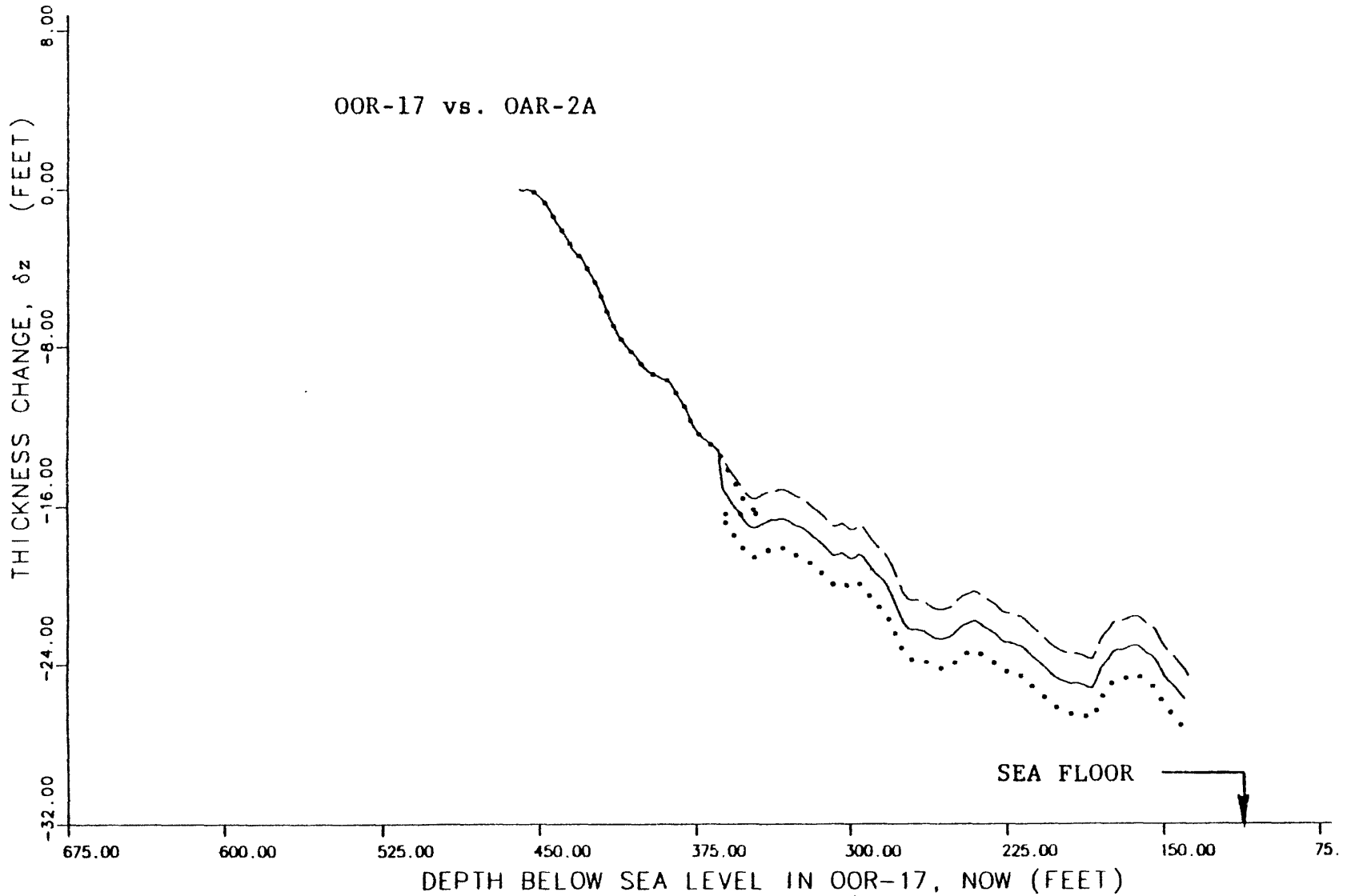

FIGURE 6-50. -- Change in rock thickness from γ-γ densities, assuming simple subsidence. Borehole OOR-17 vs. OAR-2A.

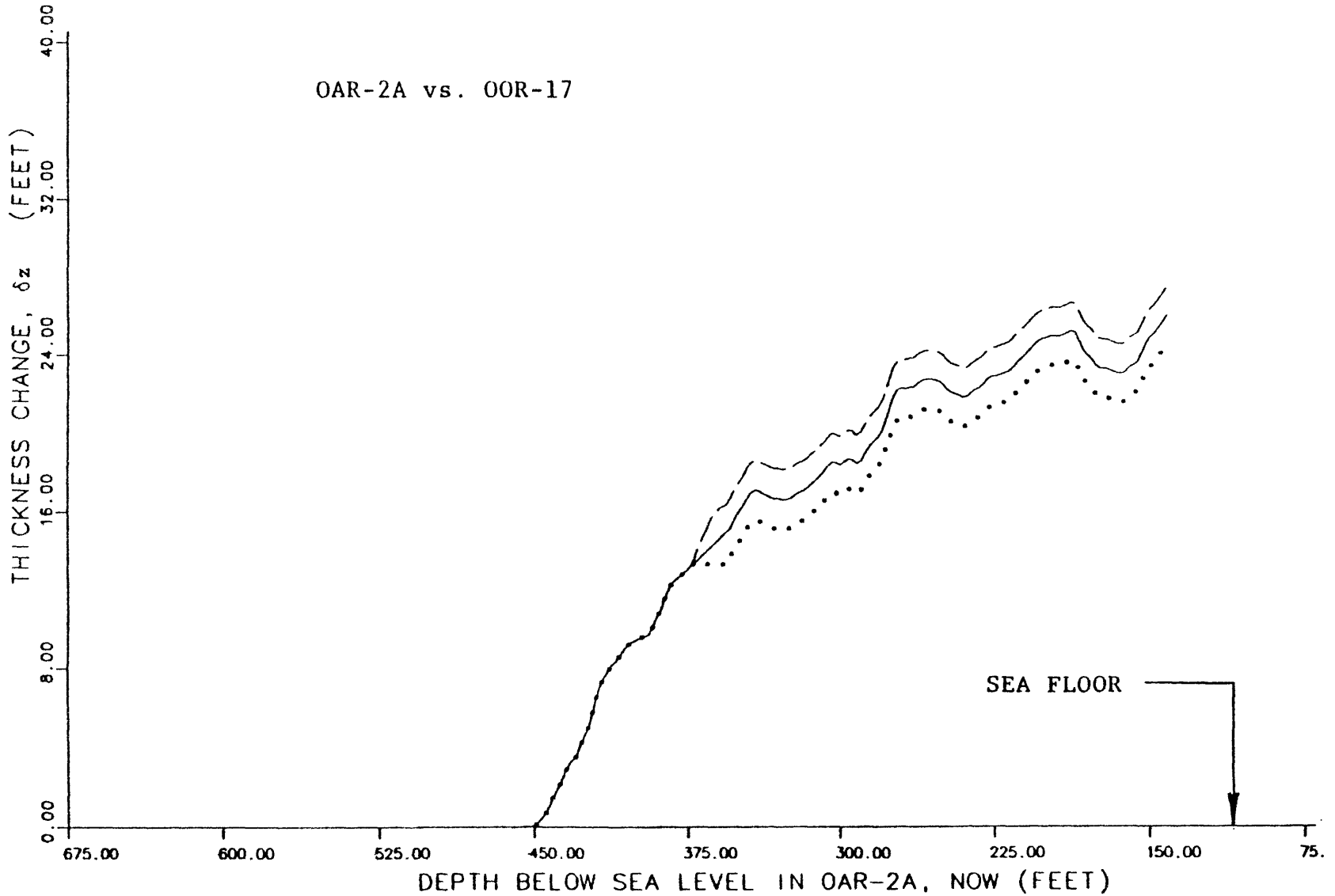

FIGURE 6-51. -- Change in rock thickness from γ-γ densities, assuming simple subsidence. Borehole OAR-2A vs. OOR-17.

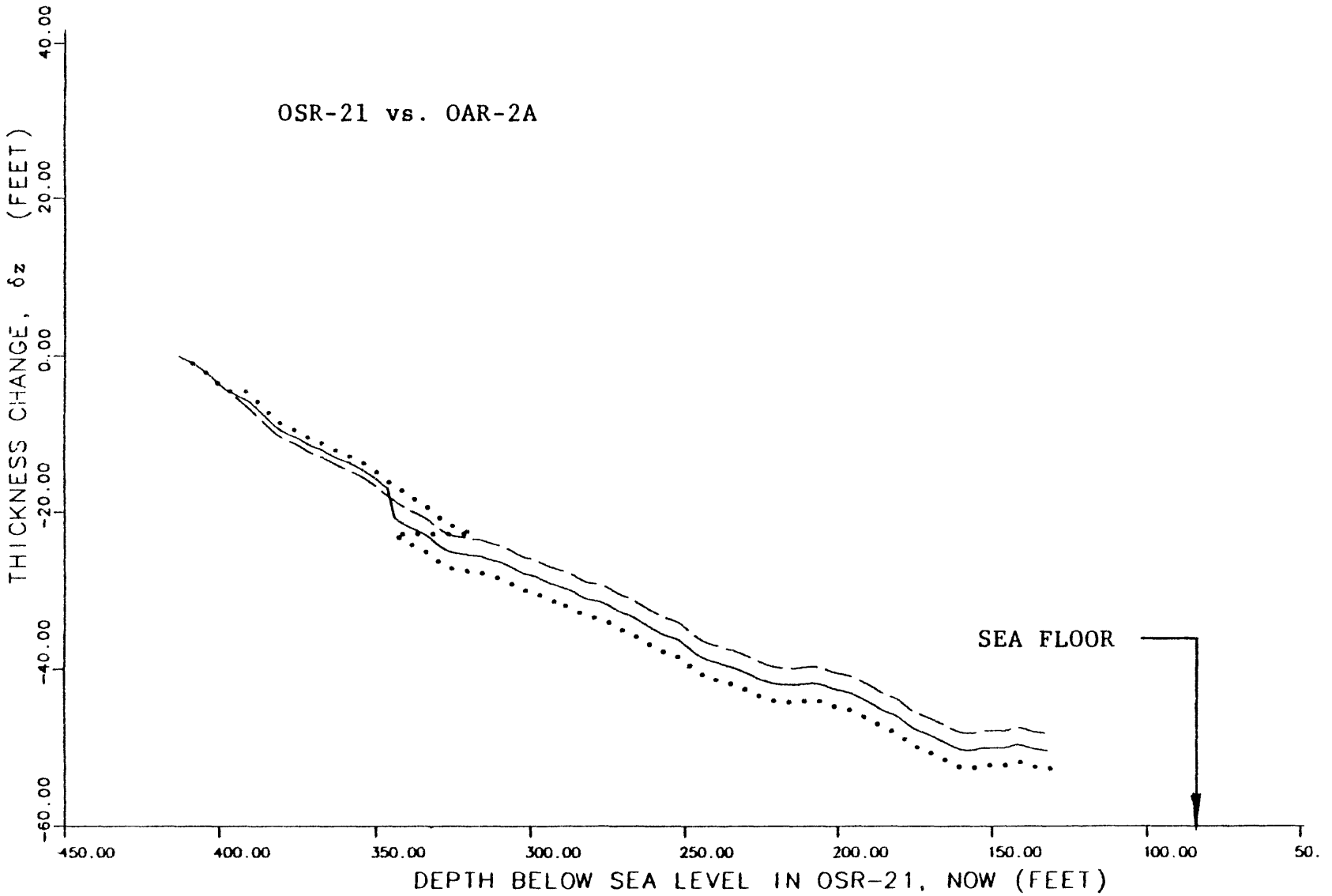

FIGURE 6-52. -- Change in rock thickness from γ-γ densities, assuming simple subsidence. Borehole OSR-21 vs. OAR-2A.

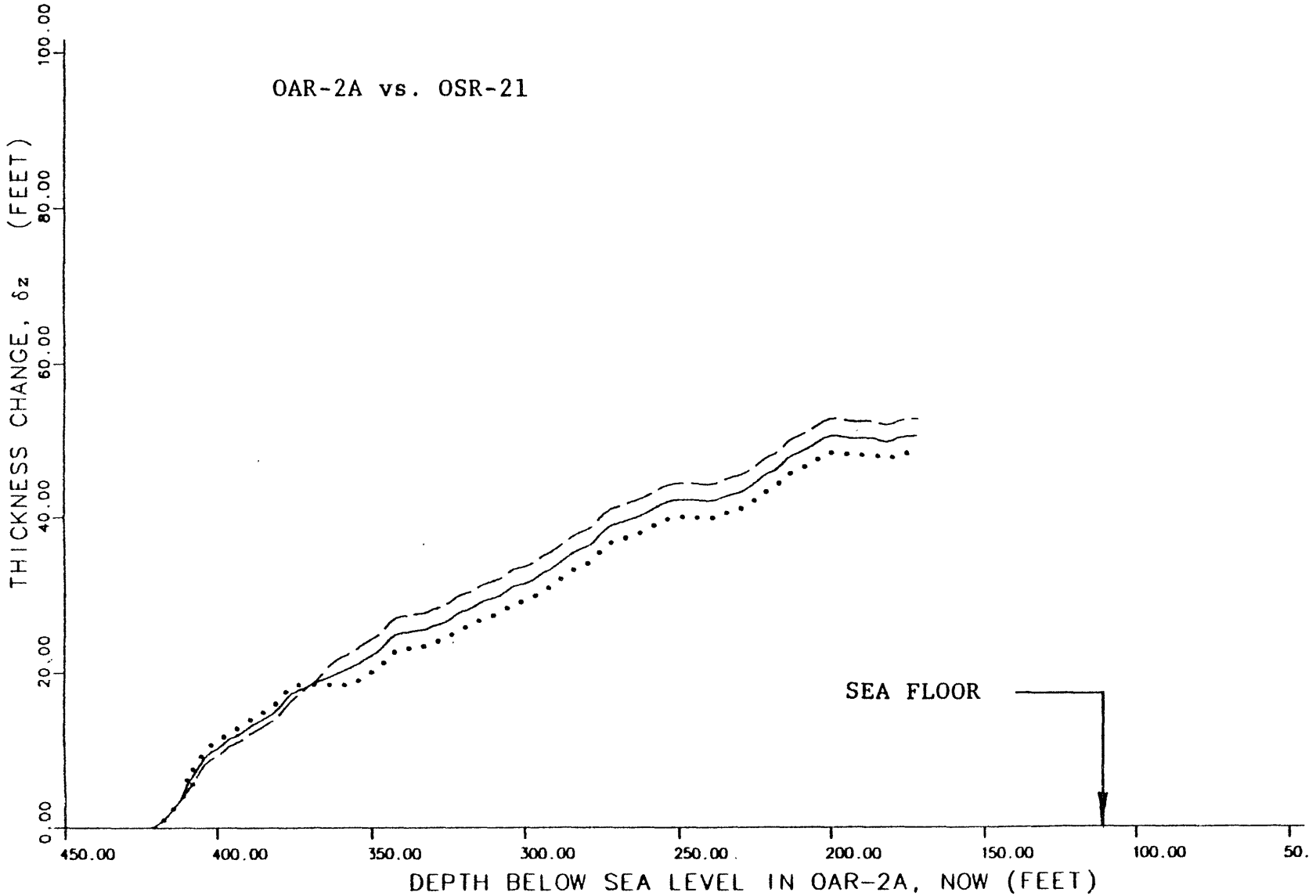

FIGURE 6-53. -- Change in rock thickness from γ-γ densities, assuming simple subsidence. Borehole OAR-2A vs. OSR-21.

CHAPTER 7:
INTEGRATION OF MATERIAL-PROPERTY UNITS, GRAVIMETRY, AND ADDITIONAL STUDIES OF OAK AND KOA CRATERS

By

Bruce R. Wardlaw[1]

INTRODUCTION

Preliminary interpretations of the geology of the OAK and KOA crater areas and of the craters themselves are presented in Wardlaw and Henry (1986a, 1986b). Since those reports, additional information was developed from analyses of borehole gravimetry, paleontologic mixing, thinning, and distribution of shocked calcite, most of which are presented in previous Chapters of the current Open-File Report. These new data require modification of the geologic interpretation of OAK and KOA craters. This Chapter incorporates these new salient data and presents a more comprehensive interpretation than that given by Wardlaw and Henry (1986b). Depths to a few horizons or zones have been reinterpreted, and all pertinent data are presented herein in corrected form as tables. These data supercede all previous information.

The most convenient way to relate the geology to crater phenomenology is to develop geologic material-property units that match the general material-property models for OAK and KOA craters. The geologic framework is reviewed briefly before presentation of the new geologic material-property units (MPs). These units will be used throughout this text in deference to previously used geologic schemes such as the sedimentary packages (SPs) of Wardlaw and Henry (1986a).

PRE-EVENT GEOLOGY OF OAK AND KOA CRATERS

The general stratigraphic sequence of Enewetak Atoll is punctuated by a series of discontinuities within the carbonate sedimentary rock column, of which nine are identified as major disconformities in the upper 1,200 ft (Wardlaw and Henry, 1986a). These major disconformities represent significant exposure and cementation surfaces over most of the atoll. Generally, pervasive cementation is confined to the reef margin (fig. 7-1a), but extends for a considerable distance beneath the lagoon beneath disconformities 5, 8, and 9 (fig. 7-2). Data from the EXPOE Project (Couch and others, 1975), which presents data from shallow boreholes drilled on islands on the reef tract, indicate that the geology is generally similar throughout the reef tract (fig. 7-1c), although the width of the cemented reef margin narrows on the leeward side of the atoll. Cementation also appears to generally decrease in areal distribution in the sequence from disconformity 5 (Pliocene) to disconformity 1

---

1 Branch of Paleontology and Stratigraphy,
U.S. Geological Survey, Reston, VA 22092.

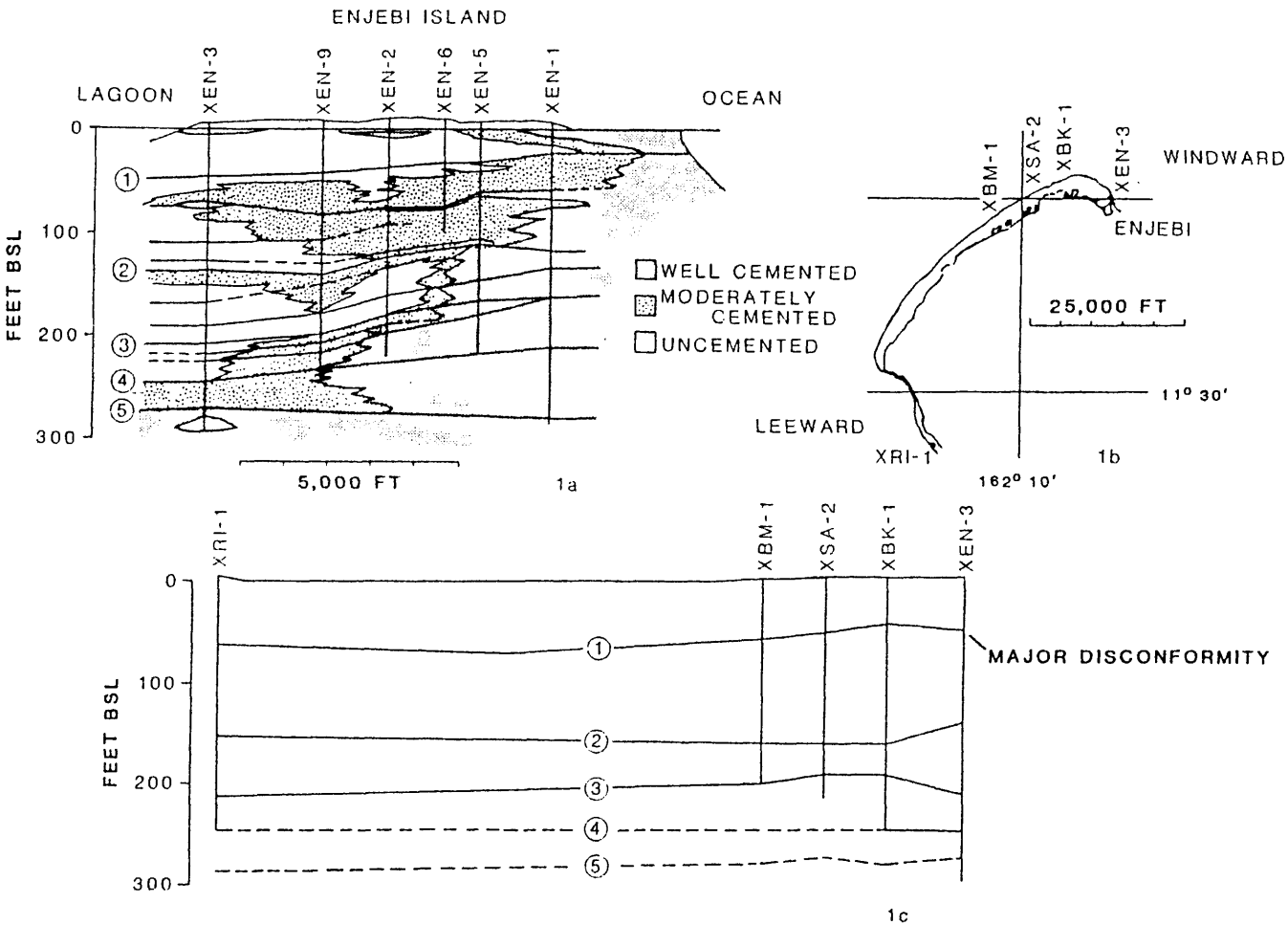

FIGURE 7-1. -- (1a) Distribution of cemented zones in shallow subsurface in transect on Enjebi Island from reef to lagoon from EXPOE cores (modified from Ristvet and others, 1978). (1b) Location of boreholes for 1c. (1c) Relationship of major disconformities (1-5) in shallow subsurface on northern and western portion of Enewetak Atoll.

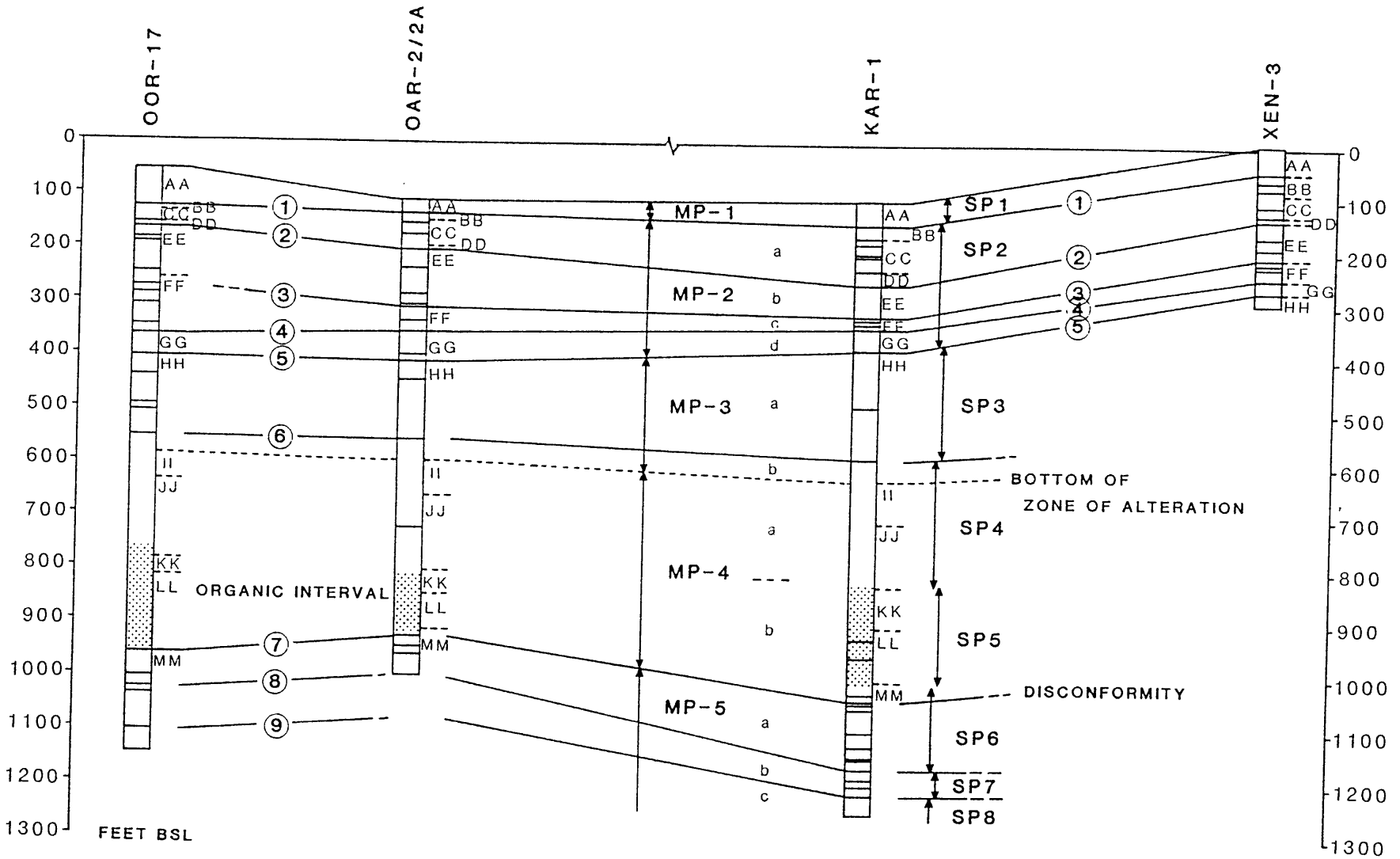

FIGURE 7-2. -- Relationship of discontinuities (shown in columns), major disconformities (1-9), biostratigraphic zones (AA-MM), material property units (MP-1 to MP-5), and sedimentary packages (SP1 to SP8) in reference boreholes. Highly organic zone (SP5) is stippled in columns.

(Pleistocene) as represented in the cross section of Figure 7-1a. From disconformity 1 to the present surface, the area of cementation has increased (fig. 7-1a).

The major disconformities (Wardlaw and Henry, 1986a) and the biostratigraphic zones, based on the distribution of microfossils presented by Cronin, Brouwers, and others (1986), generally correlate readily from borehole to borehole and extend throughout the area of investigation (fig. 7-2). The sedimentary packages (SP) delimited by these disconformities (Wardlaw and Henry, 1986a) and the geologically defined material-property units (MP) proposed herein also are shown on Figure 7-2. The consistency and trends of the disconformities, the SP and MP units, and biostratigraphic zones allow reasonable prediction of pre-shot ground-zero geology for both OAK and KOA. The relationship of discontinuities, cementation zones, and general sediment type for the PEACE Program reference boreholes and the models of ground-zero geology for both OAK and KOA are shown in Figure 7-3. Excellent seismic-reflection profiles (Grow and others, 1986) allow mapping of key surfaces in the undisturbed areas away from the craters, and, combined with the pre-shot geologic models, allow mapping of the probable distribution of these surfaces in a pre-shot configuration below the crater (Wardlaw and Henry, 1986b). Figure 7-4 shows the probable pre-shot surfaces at the top of the Pleistocene (disconformity 1) and at the top of the Pliocene (disconformity 5) in the KOA and OAK areas.

The most convenient way to summarize the geology for crater considerations is in material-property (MP) units. These are units delimited by major geologic horizons that best fit the material model (viz, the geologically defined units that best conform to the mechanical properties important to cratering). Differences between the sedimentary packages (SP) and material-property units are minor (see below) but include, for example, the pervasively cemented zone that includes SP3 and the upper part of SP4 is represented as a single unit (MP-3), although it is divided by a major disconformity (6) that represents a significant exposure surface and geologic gap.

The upper 1,200 feet of sedimentary section at Enewetak is divided into five material-property units (fig. 7-3), as follows:

MP-1 (Holocene, Sedimentary Package 1). -- Aragonitic sediments, from the surface to disconformity 1.

MP-2 (Pleistocene, SP 2). -- Aragonitic sediments with thin calcitic limestones, from disconformity 1 to 5. This unit is subdivided by disconformities 2, 3, and 4.

MP-3 (Upper Pliocene, SP 3 and part of SP 4). -- Cemented interval of vuggy, calcitic limestone and aragonitic or calcitic sands, from disconformity 5 to the base of the alteration zone (see Wardlaw and Henry, 1986b, p. 25 for discussion of alteration zone). This unit is subdivided by disconformity 6.

MP-4 (Upper Miocene-Pliocene, part of SP 4, all of SP 5). -- Aragonitic sands, from base of the alteration zone to disconformity 7. High organic content and high activity on the natural gamma logs identifies a lower subunit.

MP-5 (Miocene, SP 6, SP 7, and SP 8). -- Calcitic sands and limestones, limestone variably developed, from disconformity 7 to bottom of boreholes. This unit is subdivided by disconformities 8 and 9.

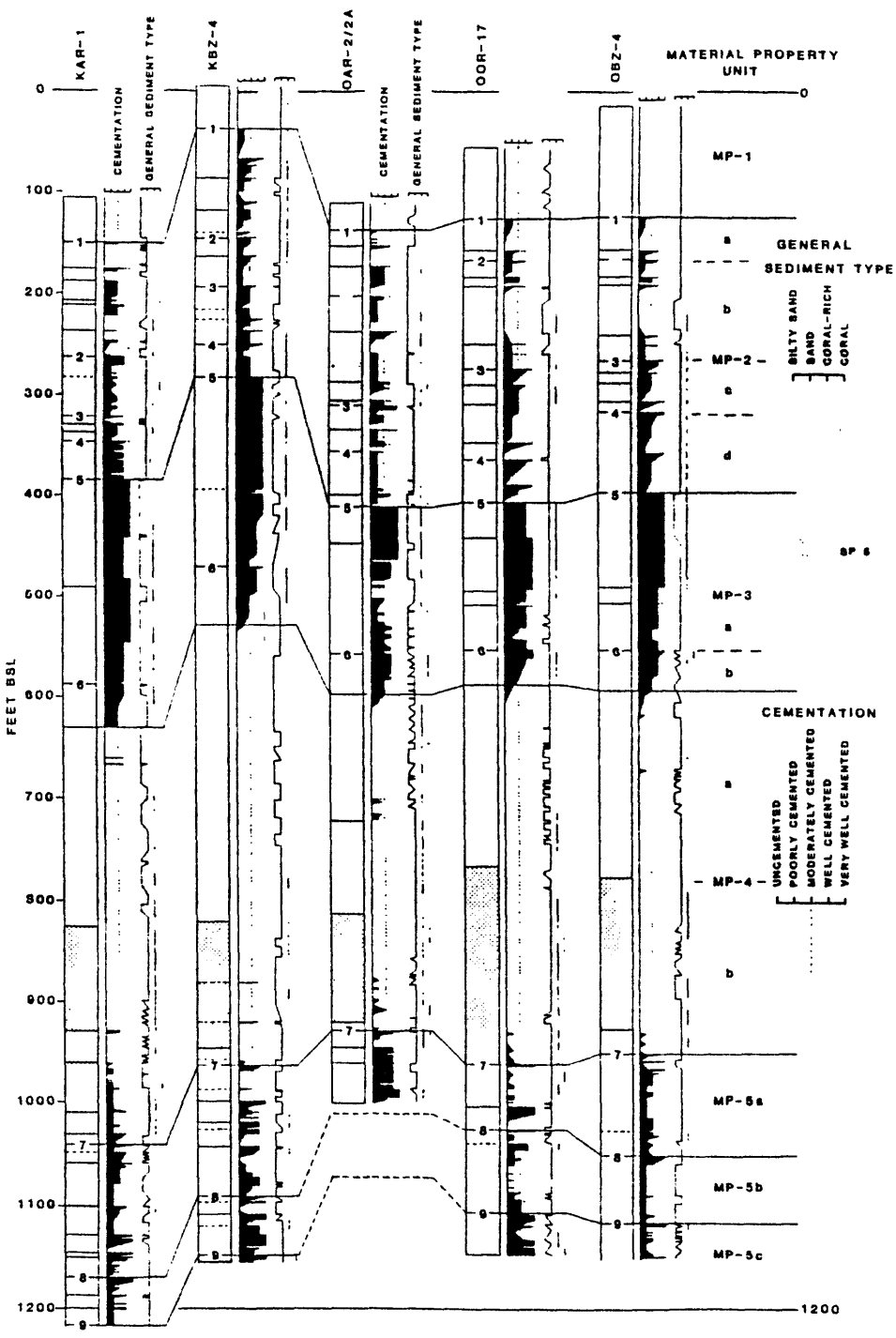

FIGURE 7-3. -- Characterization of cementation and general sediment type and relationship to material property units for reference boreholes and models for ground-zero geology. Discontinuities as lines in columns, major disconformities numbered in columns.

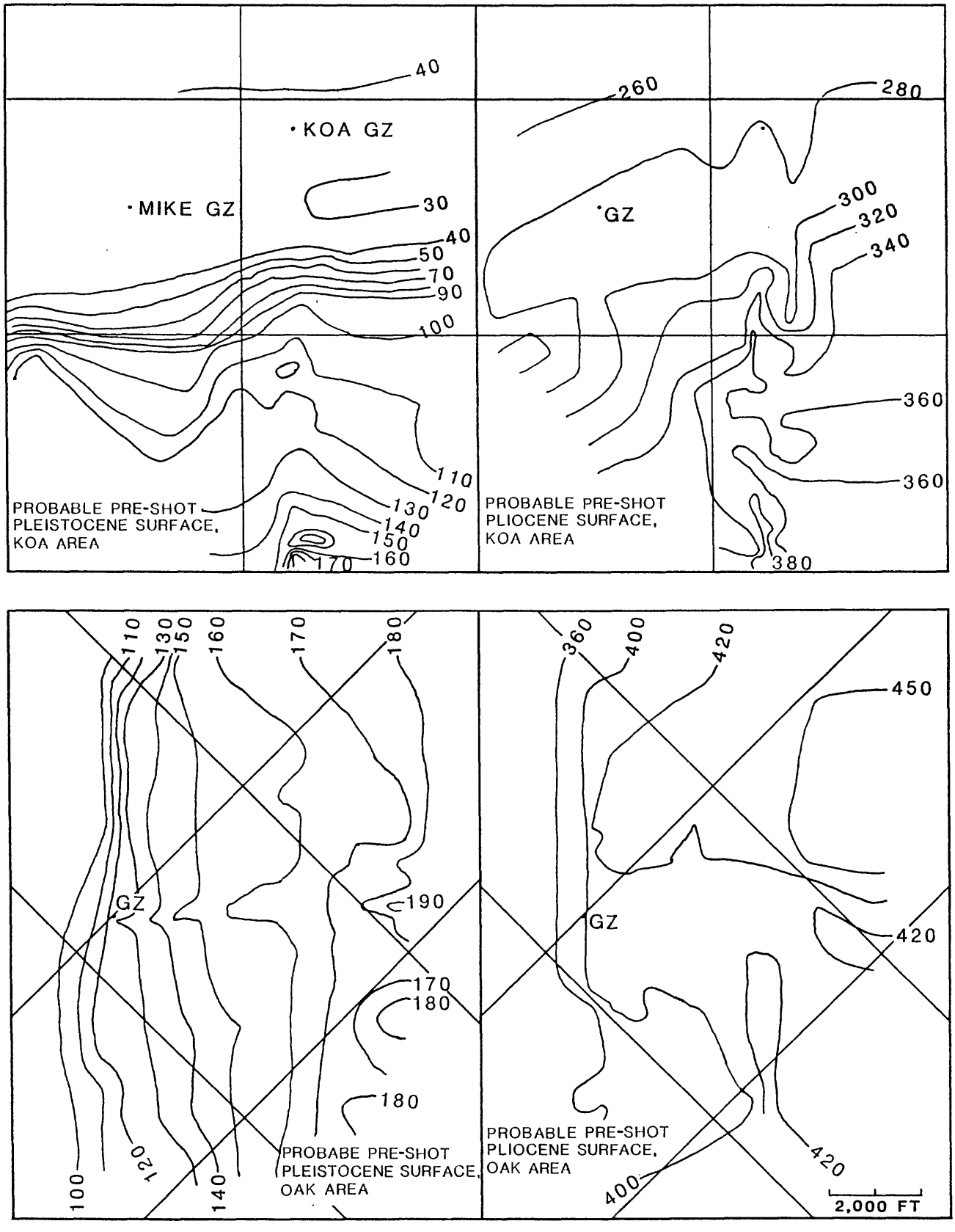

FIGURE 7-4. -- Probable pre-shot surfaces for the Pleistocene (Disconformity 1) and Pliocene (Disconformity 5) in the KOA and OAK areas. Contours in feet.

The pre-event subsurface geology in the KOA and OAK areas differs in three significant ways (fig. 7-5):

(1). MP-2d is more consistently well-cemented in the KOA area.

(2). MP-3 (the upper, well-cemented unit) is thicker (246 ft vs 197 ft) and shallower (top at 282 ft vs 395 ft bsl[1]) in the KOA area.

(3). MP-3 is homogeneous throughout the crater area at KOA. At OAK, this unit changes from a cemented limestone with calcitic sands beneath the reef tract to cemented limestone with aragonitic sands beneath the lagoon, and the cemented intervals appear to decrease in thickness lagoonward (contrast OAR-2/2A to OOR-17; see fig. 7-3).

In addition, the pre-event ground surfaces in OAK and KOA areas differ significantly. KOA is represented by a nearly flat shallow surface on a broad reef tract, whereas OAK is represented by a narrow, shallow reef tract, relatively steep slope, and a flat, deep lagoon bottom.

POST-EVENT GEOLOGY OF OAK AND KOA CRATERS

The excavational craters were modified profoundly by a set of processes that included shock-induced liquefaction and consolidation, subsequent flow and piping of liquefied materials from depth (both laterally and toward and/or to the surface), consequent subsidence of the region adjacent to and beneath the excavational craters, and major and repeated failures of the sidewalls of the initial and subsequent craters.

Crater Zones

OAK and KOA craters can be characterized in the subsurface by geologic, paleontologic, and seismic-reflection crater zones that, in turn, can be related to crater-event history.

Traditional crater terminology does not always adequately apply to the Enewetak craters studied; many subsurface features within the carbonate rock and sediment virtually were undescribed. Thus, limited new terminology was introduced by Wardlaw and Henry (1986b), and a few additional terms are introduced in the current Chapter (designated by an asterisk, *).

Geologic Crater Zones

1. Zone of sonic degradation (ZSD): the stratigraphic interval in which sonic velocities are depressed below expected velocities. Normal or (more correctly) pre-event sonic velocities are determined from the sonic signature of reference boreholes. On the multichannel-seismic profiles, the ZSD appears as a "fuzzy" area in which seismic reflectors are not coherent and are surrounded by an area where

---

[1] Below sea level is abbreviated bsl throughout this Volume.

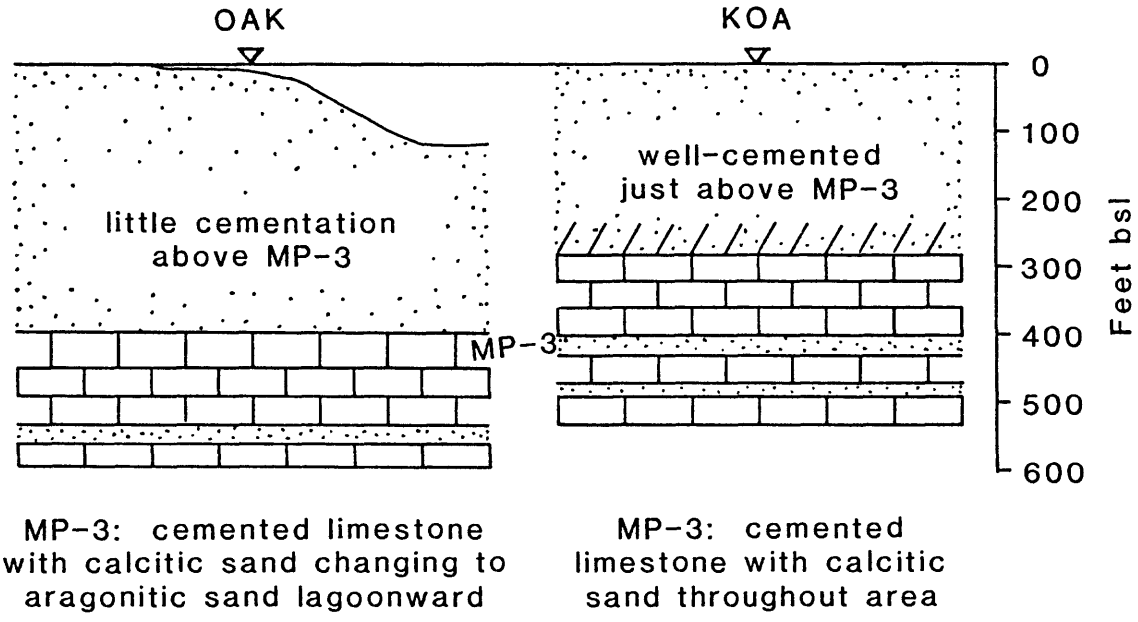

FIGURE 7-5. -- Comparison of pre-shot ground surface and subsurface geology for the OAK and KOA areas.

coherent reflectors are present but downturned. The ZSD represents units of rock and sediment that are fractured or shattered, mixed, and/or otherwise disturbed significantly enough to retard the sonic velocities relative to what they were before the nuclear events occurred. All geologic crater zones lie within the ZSD (fig. 7-6).

2. Geologic crater: the subsurface expression of the crater defined by the ZSD. The geologic crater zones encountered in the central crater are as follows:

3. Alpha 1 ($\alpha 1$): Mud. Late-stage, fine-grained sediments with abundant brown, piped material in OAK.

4. Alpha 2 ($\alpha 2$): Graded sand (distal) and slumps (proximal). Late-stage slope-failure and sand-turbidite flow deposits containing abundant brown, piped material. (Proximal means near material source; distal means far from the material source).

5. Beta 1a ($\beta 1_a$): Graded Rubble. (*) This zone contains proximal rubble and distal sand (as in OPZ-18) with granules of rubblized material. The zone is transitional from the rubble below and slumps above and contains abundant brown, piped material near the top in the central crater area. Both Alpha 2 and Beta 1a show high gamma-ray activity (see fig. 7-17).

6. Beta 1s* ($\beta 1_s$): Hiatus sand. (*) Highly shocked, uppermost unit (MP-1, Holocene) sediments.

7. Beta 1b ($\beta 1_b$): Collapse rubble. (*) Thick rubble bed with sparse brown piped material within the zone in the central crater area. Both zones Beta 1a and Beta 1b are less distinct in the central-most part of the crater, and Beta 1s is missing in the same area because of mixing primarily due to late-stage piping.

8. Beta 2 ($\beta 2$): Transition sand. Pulverized sand within the transition paleontologic zone (see below). It has a limited lateral extent. The sand grains show fractured surfaces but no internal microfracturing.

9. Beta 3 ($\beta 3$): Rubble floatstone. Rubble in which no paleontologic mixing can be shown.

10. Gamma (γ): Fractured and displaced rock and sediment.

11. Delta: (δ) Fractured but undisplaced rock and sediment.

The base of the zone of sonic degradation:

12. Epsilon (ε): In-place, relatively unfractured stratigraphic section; outside and beneath the geologic crater.

The geologic crater zones in the debris blanket are as follows:

13. Beta 1a* ($\beta 1_a$*): Graded sand and rubble *. This zone is found only in boreholes OHT-10 and OJT-12 and may be related to a large collapse and debris flow that breached the debris blanket and flowed into the

lagoon (as seen on the OAK enhanced sea-floor image, Folger and others, 1986).

14. Beta 1b* ($\beta 1_b$*), or Beta (β) undifferentiated: Rubble. Debris with no brown piped material.

15. Disturbed zone: This zone represents slightly altered stratigraphy with no apparent discontinuities.

16. Delta (δ) and Epsilon (ε): Relatively unaffected stratigraphy.

The depths to various crater zones for the transition and ground-zero boreholes for both OAK and KOA craters are given in Table 7-2, and graphically displayed in fence diagrams in Figures 7-7 to 7-10. Interpretations of geologic crater zones on seismic reflection profiles through ground-zero for both OAK and KOA crater (from Wardlaw and Henry, 1986b) are shown in Figures 7-11 and 7-12.

Paleontologic Crater Zones

The paleontologic crater zones for the **central crater** follow. The depths to various paleontologic crater zones for both OAK and KOA craters are given in Table 7-3.

1. Mixed: Fossils from various biostratigraphic zones are mixed together. This zone can be crudely divided into three subzones:
   a. Very mixed with material from mostly upper biostratigraphic zones and piped material from deeper zones.
   b. Mixed material from most of MP-1 and MP-2 plus piped material that decreases in degree of mixing downward.
   c. Mixed material from mostly lower biostratigraphic zones of crater and sparse piped material.

These zones were developed for KOA crater (Wardlaw and Henry, 1986b) and are applicable to OAK with minor modification. In OAK, an additional zone, represented by the "hiatus sand" (Beta 1s), occurs between paleontologic subzones b and c in the lateral part of the crater. This unit consists predominantly of Holocene (near-surface) material and shows little mixing.

2. Transition: Transitional paleontology from mixed to unmixed.

3. Unmixed: Paleontology in normal succession showing no mixing of materials from different biostratigraphic zones.

The paleontologic crater zones for **debris blanket** are:

4. Mixed, undifferentiated: generally like unit 1b within the crater, but without piped material.

5. Transition: as above.

6. Disturbed Zone: unmixed, but sparse faunas.

7. Unmixed: as above.

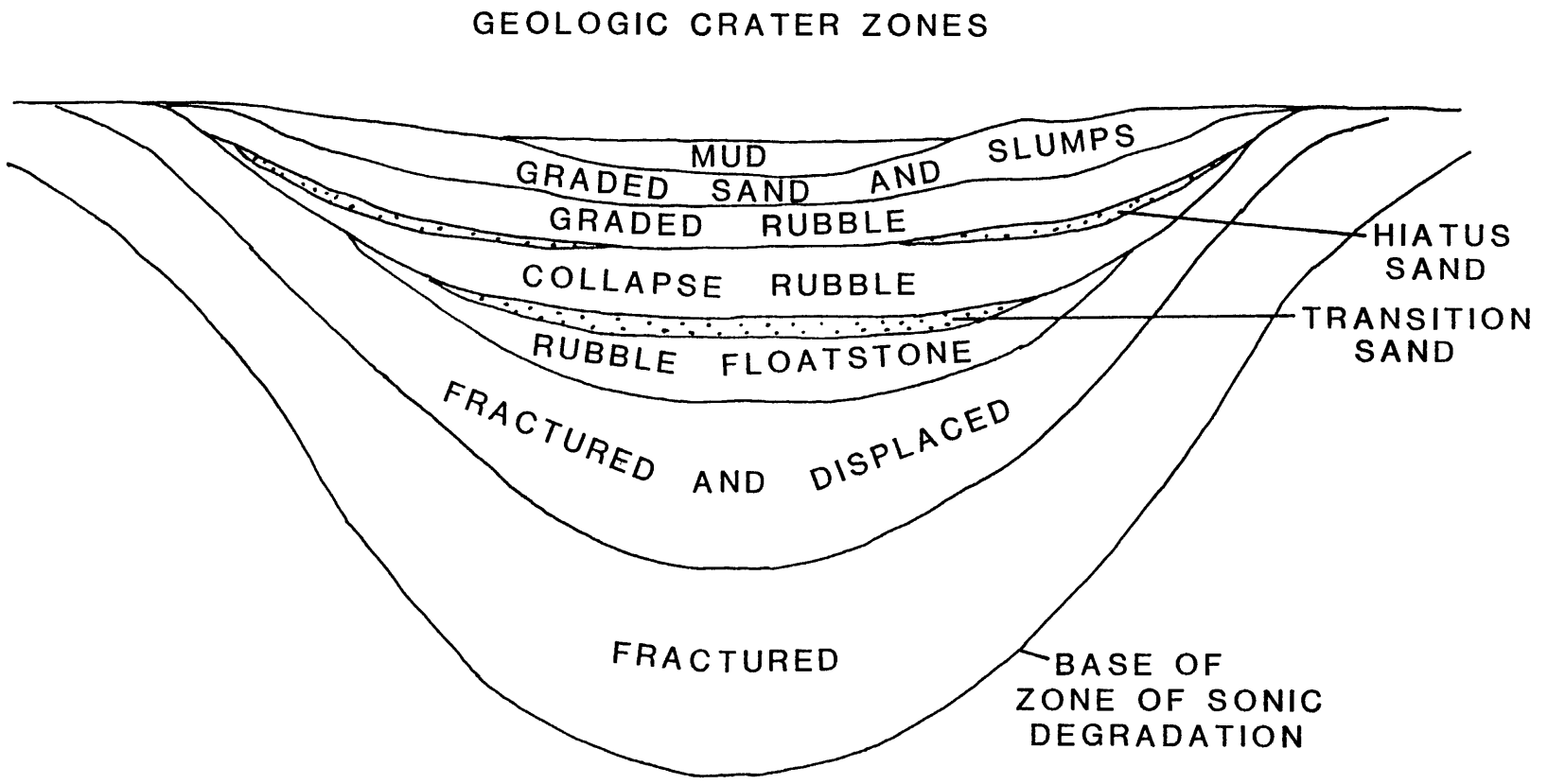

FIGURE 7-6. -- Geologic crater model.

TABLE 7-1. -- Relationship of geologic and paleontologic zones in the crater and debris blanket modified from Wardlaw and Henry (1986b). The hiatus sand { } is present only in the outer crater of OAK.

[PALEONTOLOGIC ZONES]	[GEOLOGIC ZONES]
CENTRAL CRATER	
MIXED a--Very mixed with mostly upper biostratigraphic zones and piped material	ALPHA 1 ($\alpha 1$) Mud ALPHA 2 ($\alpha 2$) Graded sand (distal) and slumps (proximal)
b--Mixed material from most units 1 and 2 and piped material, generally decreasing in mixing downward	BETA 1a ($\beta 1_a$) Graded rubble
{Unmixed upper biostratigraphic zone} c--Mixed material from mostly lower biostratigraphic zones and sparse piped material	{BETA 1s ($\beta 1_s$) Hiatus Sand} BETA 1b ($\beta 1_b$) Collapse rubble
TRANSITION	BETA 2 ($\beta 2$) Transition sand
UNMIXED	BETA 3 ($\beta 3$) Rubble floatstone GAMMA (γ) Fractured, displaced DELTA (δ) Fractured, relatively undisplaced EPSILON (ε) Relatively unfractured, in place
DEBRIS BLANKET	
MIXED (undifferentiated) TRANSITION	DEBRIS (BETA) BETA 1a ($\beta 1_a$) Graded sand and rubble BETA 1b ($\beta 1_b$) Rubble
DISTURBED	DISTURBED
UNMIXED	DELTA (δ) Fractured, relatively undisplaced EPSILON (ε) Relatively unfractured, in place

TABLE 7-2. -- Depth (ft bsl) to tops of the crater zones in OAK and KOA boreholes. ZSD = Zone of Sonic Degradation. Boreholes listed in order of increasing distance from ground-zero.

OAK AND KOA GEOLOGIC CRATER ZONES

ZONE ç	OBZ-4	OPZ-18	OCT-5	OTG-23	OUT-24	OKT-13	OFT-8	OIT-11
Alpha 1	198.7	201.9	163.7	-	-	164.7	130.8	155.0
Alpha 2	229.2	-	164.6	164.0	147.0	165.3	131.1	
Beta 1a	271.7	246.5	174.1	174.0	249.2	177.0	139.4	155.1
Beta 1s	-	-	244.1	219.0	278.6	190.8	152.9	-
Beta 1b	309.1	337.2	310.7	235 ?	288.0	207.0	175.4	
Beta 2	394.9	377.0	-	-	-	-	-	-
Beta 3	415.1	412.3						
Gamma	564.2	522.4	346.3	314.0	332.0	227.3	204.1	171.7
ZSD	1138.7	1082.4	863.7	842.0	830.0	831.7	639.6	697.0

ZONE ç	OET-7	OQT-19	OHT-10	OJT-12	ODT-6	ONT-16	ORT-20	OMT-15
Alpha 1	-	-	-	-	-	-	-	-
Alpha 2	106.9	-	-	-	-	-	-	-
Beta 1a	132.3	-	137.3	143.8	87.4	-	-	-
Beta 1s	-	-	-	-	-	-	-	-
Beta 1b		-	145.2	155.0	-	135.1	-	110.9
Beta 2	-	-	-	-	-	-	-	-
Beta 3			[191.1]	[164.7]	-	[148.0]	-	[119.8]
Gamma	156.3	117.5	286.8	238.0	91.9	176.7	101.4	139.4
ZSD	505.1	413.3	587.1	387.0	311.6	242.7	239.0	223.0

[ ] denotes disturbed zone

ZONE ç	OLT-14	ç	KBZ-4	KCT-5	KFT-8	KDT-6	KET-7
Alpha 1	-	ç	109.1	-	-	-	-
Alpha 2	-	ç	137.3	98.9	77.8	56.2	-
Beta 1a	139.7	ç	167.7	120.0	96.5	79.9	-
Beta 1s	-	ç	-	154.5	-	-	-
Beta 1b	-	ç	238.5	156.1	106.0		-
Beta 2	-	ç	247.2	242.5	-	-	-
Beta 3	-	ç	266.2	259.9	-	-	-
Gamma	147.2	ç	316.2	274.3	153.8	110.1	51.1
ZSD	154.2	ç	1101.1	869.2	590.4	410.0	318.2
		ç					

TABLE 7-3. -- Paleontologic crater zones and relation to the transition sand in OAK and KOA boreholes. Depths in ft below sea floor (ft bsf) are compatible with the footages presented in the paleontologic studies (Cronin, Brouwers, and others, 1986; Brouwers, Cronin, and Gibson, 1986; and Cronin and Gibson, 1987), which are consistently in feet below sea floor (bsf).

	KBZ-4	KCT-5	KFT-8	KDT-6
KOA CRATER				
Mixed Zone	0-137.5	0-140.1	0-28.5	0-43.6
Transition Zone	137.5-142	140.1-155.2	28.5-99.3	43.6-58.5
Transition Sands	138.1-157.1	143.6-161.0	---	---

	OBZ-4	OPZ-18	OCT-5	OKT-13
OAK CRATER				
Mixed Zone	0-180	0-174	0-149	0-55
Transition Zone	180-220	174-211	149-187	55-68
Transition Sands	196.2-216.4	175.1-210.4	---	---

	OFT-8	ODT-6
Mixed Zone	0-64	1.8-4.4
Transition Zone	64-74	---
Transition Sands	---	---

	OHT-10	OJT-12	ONT-16	OMT-15	OLT-14
OAK CRATER DEBRIS BLANKET					
Mixed Zone	0-54	0-20.9	0-12.9	0-8.9	0-7.5
Transition Zone	54-76	20.9-67	12.9-14.7	8.9-15.5	---
Disturbed Zone	76-149.5	67-94.2	14.7-41.6	15.5-28.5	---

Seismic Crater Zones

Grow, Lee, and others (1986) interpreted four subcrater seismic zones from the multichannel seismic-reflection records. They are, from top to bottom: (1) transparent zone, (2) zone of intense fracturing/depression, (3) zone of moderate fracturing/depression; and, 4, zone of minor fracturing/depression. The zone of minor fracturing/depression has not been defined in terms of depth. The seismic zones are compared to geologic craters zones in Table 7-4.

The transparent zone corresponds to the crater fill and the transition sand (where present). In OAK, reefward of SGZ, the base of the transparent zone is difficult to interpret because some large-scale slumps (crater fill) from the reef tract are not completely transparent seismically. The bottom of the zone of intense fracturing/depression falls within gamma, the zone of fracturing and displacement in KOA, and very near the bottom of the rubble zone in OAK. The bottom of the zone of moderate fracturing/depression appears to fall close to the gamma/delta transition or that change from fractured/displaced to fractured/in place material. The delta zone appears to be equivalent to the zone of minor fraturing/depression.

TABLE 7-4. -- Comparison of subcrater seismic zones to selected geologic crater zone boundaries for OAK and KOA craters.

SEISMIC ZONE	GEOLOGIC CRATER ZONE
KOA	
Bottom of Transparent Zone 262 ft bsl	Bottom of Transition Sand 266.2 ft bsl
Bottom of Zone of Intense Fracturing/Depression 460 ft bsl	Bottom of Rubble 316.2 ft bsl
Bottom of Zone of Moderate Fracturing/Depression 755 ft bsl	Bottom of ZSD 1101.1 ft bsl
OAK	
Bottom of Transparent Zone 361 ft bsl	Bottom of Transition Sand 377.0 ft bsl
Bottom of Zone of Intense Fracturing/Depression 590 ft bsl	Bottom of Rubble 564.2 ft bsl
Bottom of Zone of Moderate Fracturing/Depression 918 ft bsl	Bottom of ZSD 1138.7 ft bsl

CRATER FEATURES

Crater Material in the Lagoon

Muddy sediments in the northwestern portion of the lagoon (see fig. 7-13) are derived partly from crater material. Observations leading to this conclusion (Wardlaw and Henry, 1986b) include:

(1). An anomalously high amount of low-Mg calcite in the sediments probably indicates mixing from diagenetically altered subsurface units.

(2). The sediments have an anomalously high content of clay-size material, probably indicating crater-derived material. Normal lagoon sediments do not contain appreciable quantities of naturally produced clay-sized carbonate.

(3). The sediments have measurable radioactivity, probably from the device-derived Cesium-137 (Ristvet and Tremba, 1986).

Thus, a substantial part of the mud in the northwestern portion of the lagoon (fig. 7-13) was derived from pulverization of sediment and rock particles by the nuclear detonations during the excavation of the craters. A considerable volume of fine-grained material was moved from the crater areas to the lagoon, although the volume of this lost material or proportion derived from each of the forty-one nuclear events other than OAK or KOA cannot be estimated.

Breach Deposit in the Lagoon

The enhanced sea-floor image of OAK crater displays a large flow deposit out into the lagoon (fig. 7-14). This feature extends out beyond the limits of the apparent crater, thus it, too, represents loss of material to the lagoon. This feature was not observed until after the field operations, so it was not sampled. The thickness or volume of the deposit is unknown. The deposit appears to represent a breach in the debris blanket through the "channel" (Peterson and Henny, Ch. 5 of this report, p. 5-15) and flow of material out onto the lagoon floor.

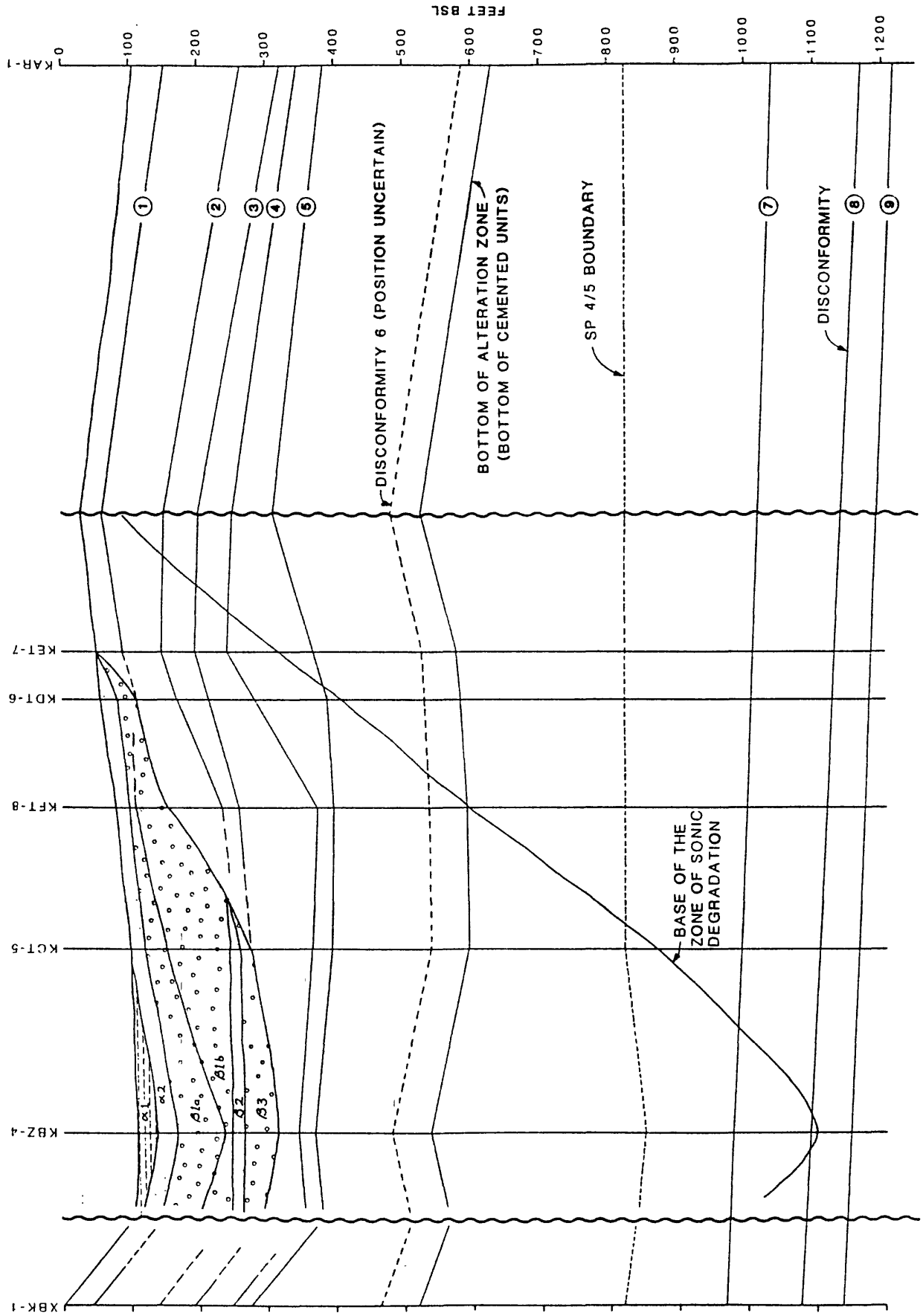

FIGURE 7-7. -- Fence diagram of KOA boreholes showing relationship of crater and geologic horizons. Scale is vertically exaggerated 2:1. Squiggly lines represent breaks to shorten the diagram.

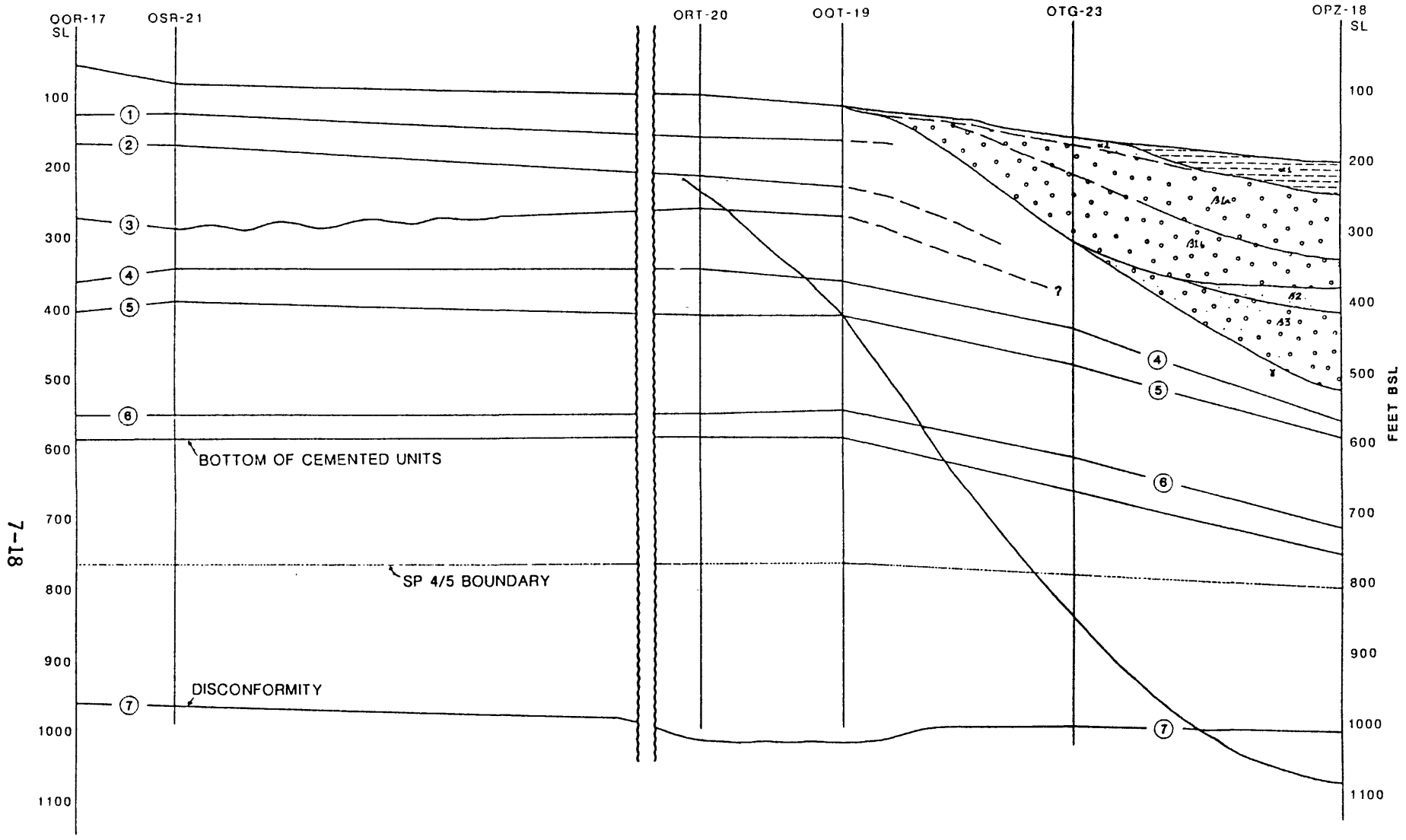

FIGURE 7-8. -- Fence diagram of OAK boreholes OOR-17 to OPZ-18 showing relationship of crater and geologic horizons. Double squiggly lines represent breaks and change in vertical exaggeration from 2:1 on right side to 4:1 on left side.

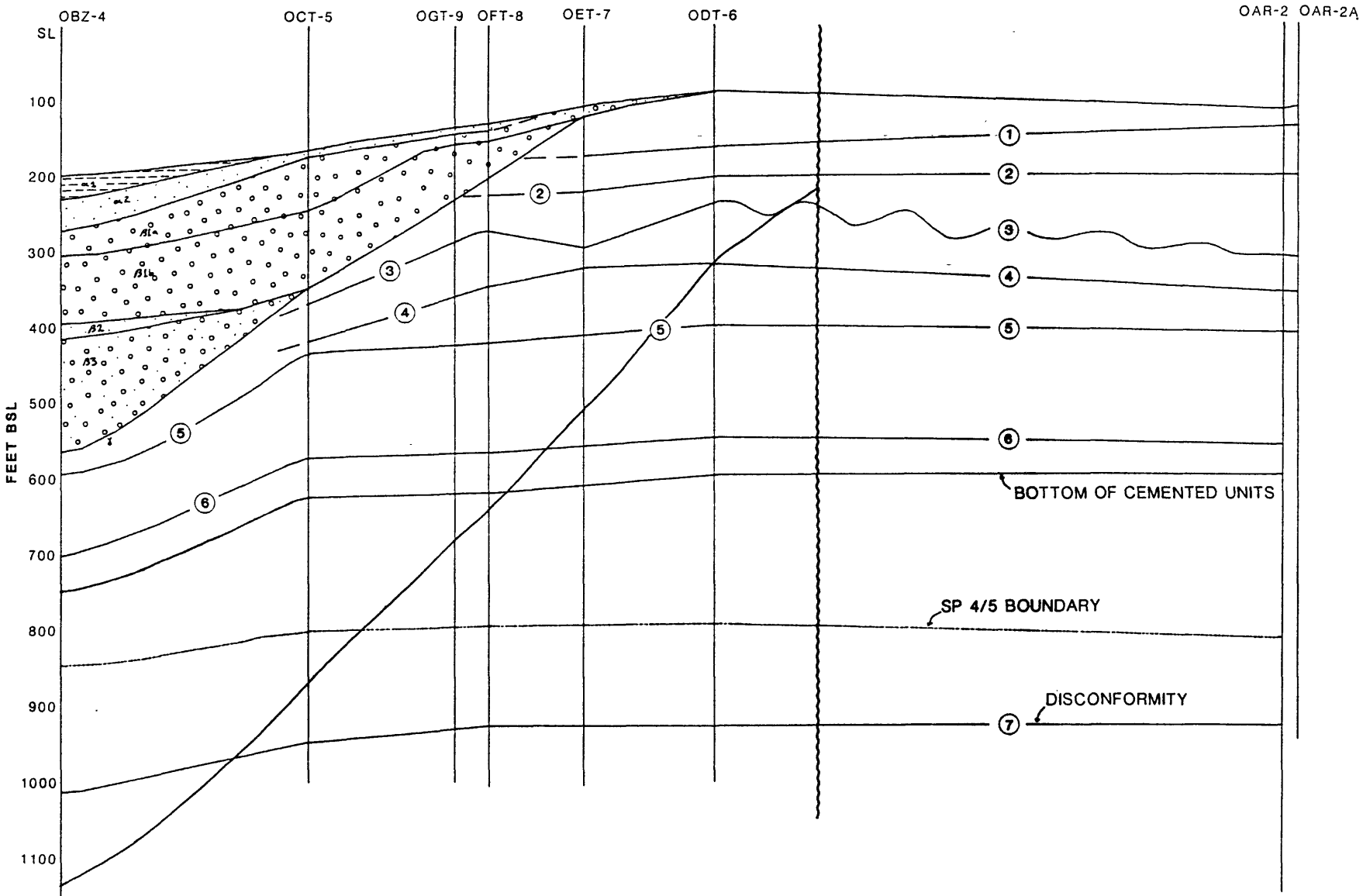

FIGURE 7-9. -- Fence diagram of OAK boreholes OBZ-4 to OAR-2/2A showing relationship of crater and geologic horizons. Scale is vertically exaggerated 2:1 to right of the squiggly line and 4:1 to the left of the line.

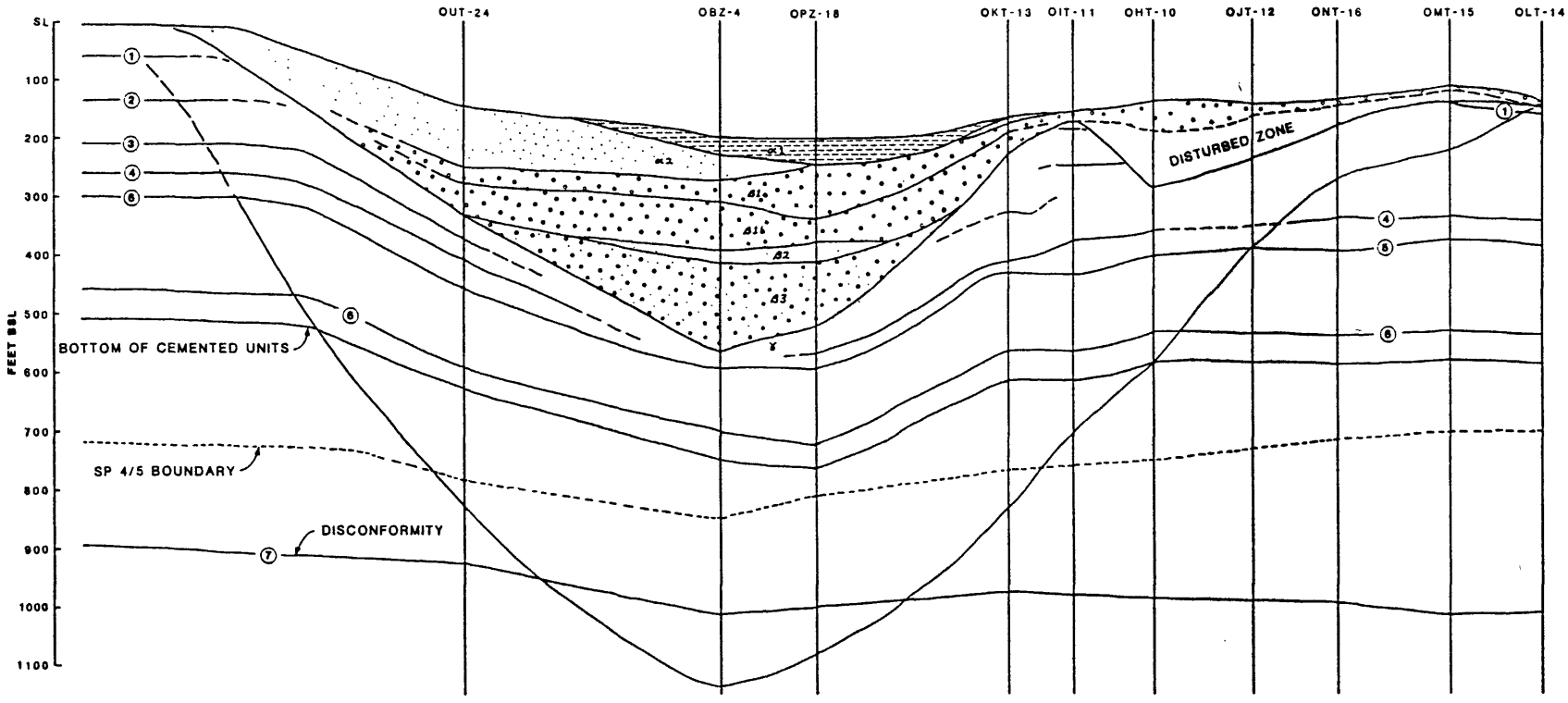

FIGURE 7-10. -- Fence diagram of OAK boreholes from reef tract to OLT-14 showing relationship of crater and geologic horizons. Scale is vertically exaggerated 2:1.

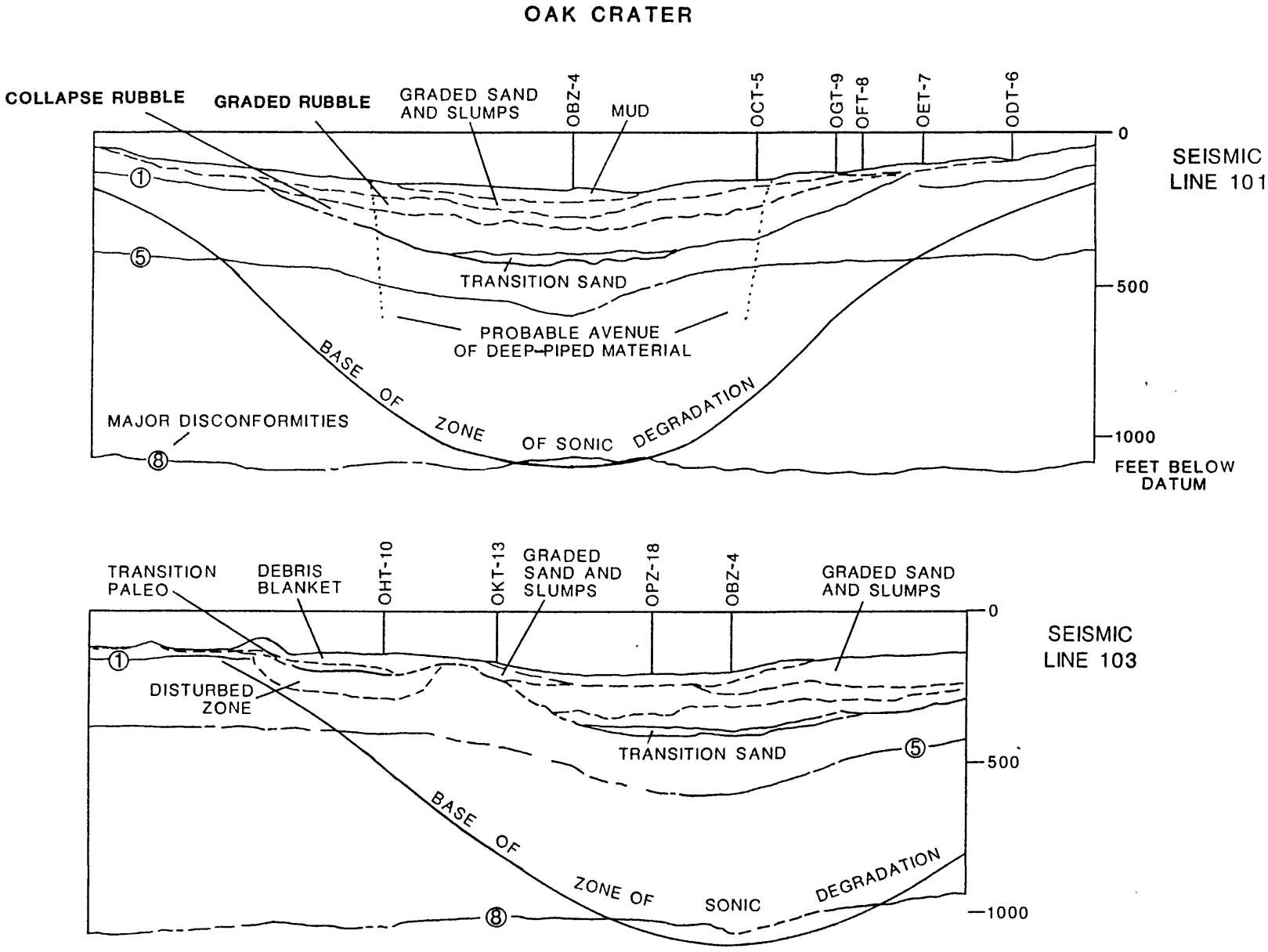

FIGURE 7-11. -- Geologic interpretation of multichannel seismic lines 101 and 103 in proximity of OAK crater (from Wardlaw and Henry, 1986b). Location of lines shown in Grow, Lee, and others (1986).

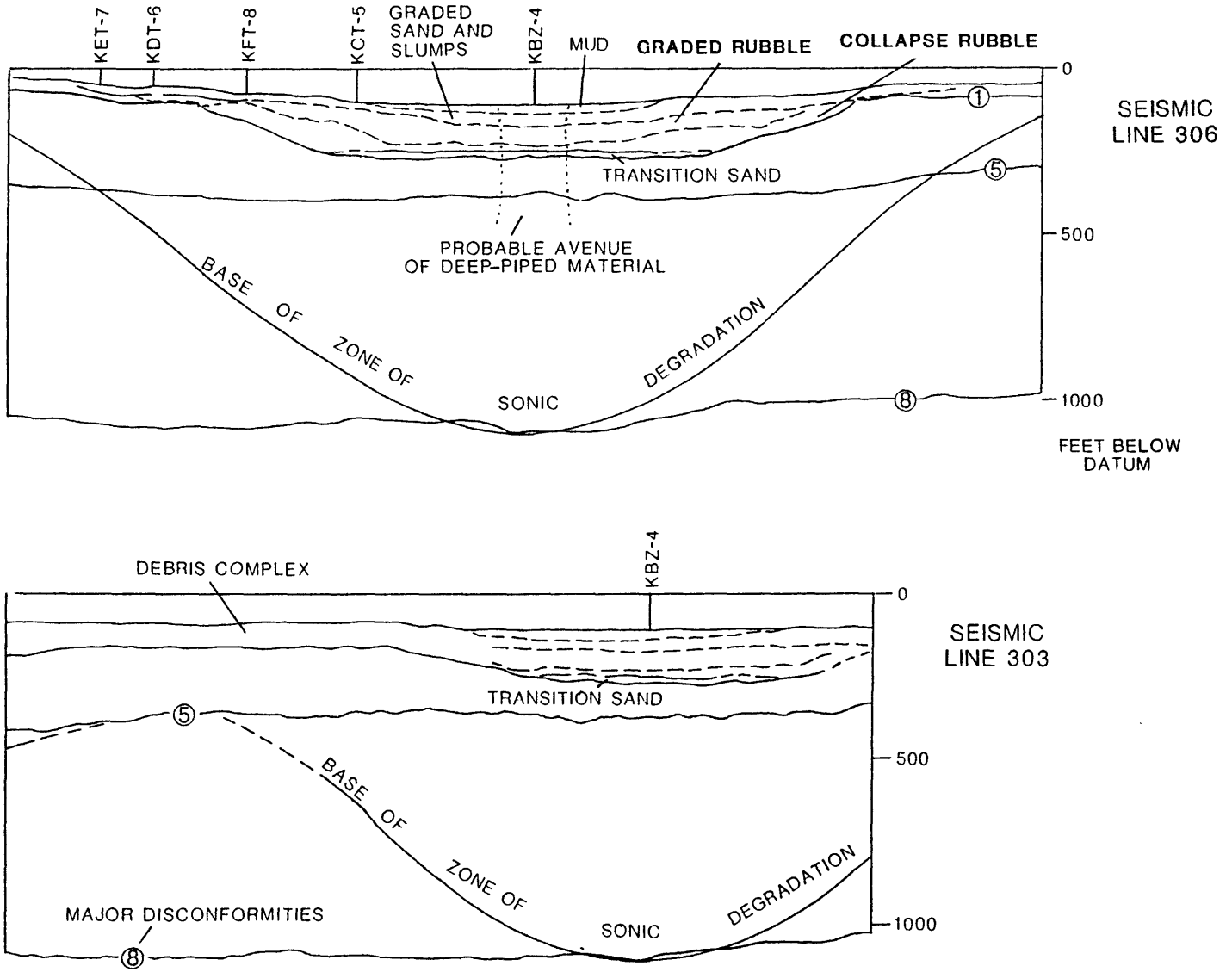

FIGURE 7-12. -- Geologic interpretation of multichannel seismic lines 303 and 306 in proximity of KOA crater (from Wardlaw and Henry, 1986b). Location of lines shown in Grow, Lee, and others (1986).

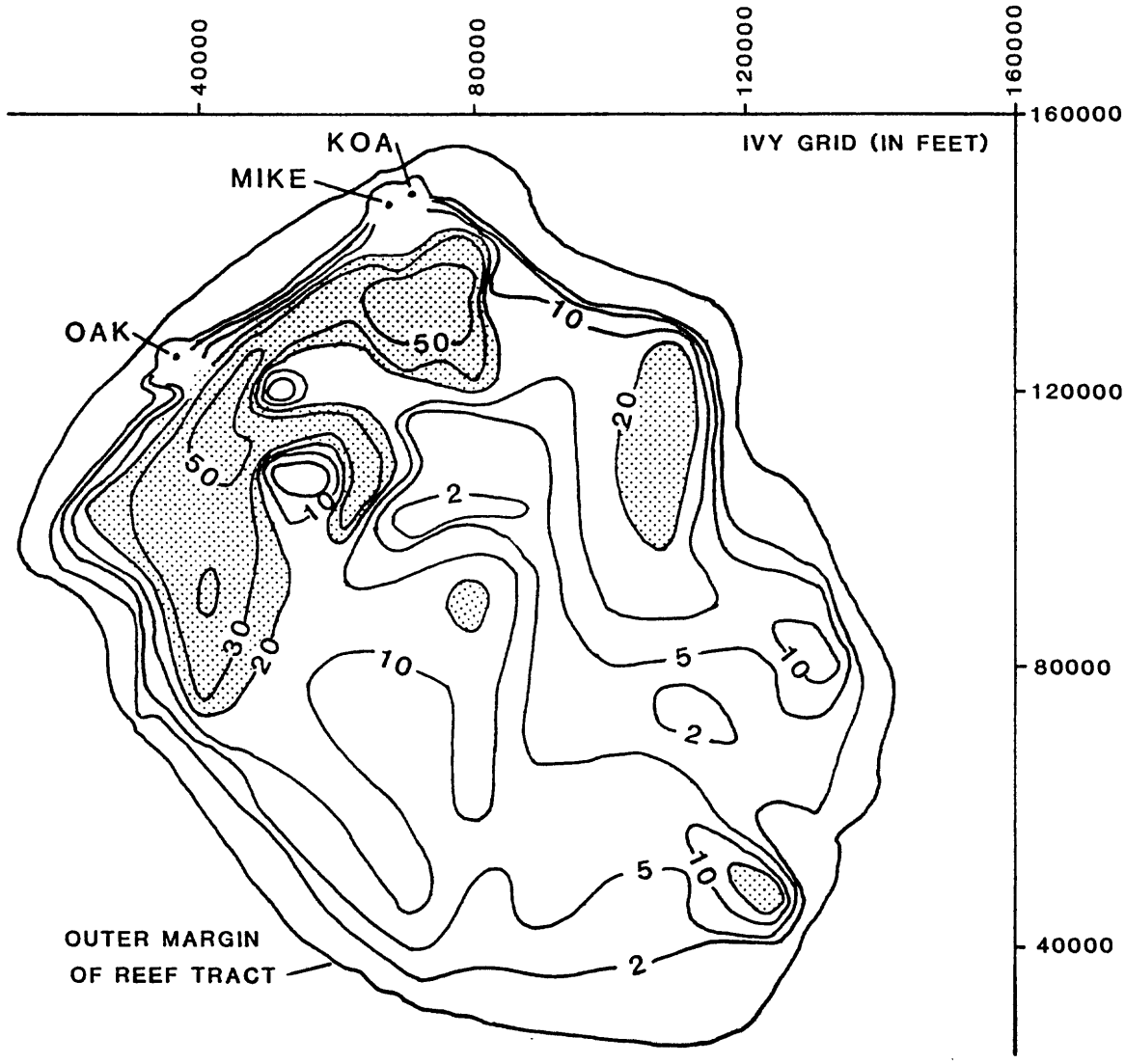

FIGURE 7-13. -- Weight percent mud in bottom sediments of lagoon. Sediments in excess of 10 percent mud are probably indicative of blast-derived mud contribution.

Piping

Brown-stained, organic-rich sediments from MP-4 were piped to the surface in substantial quantities. Several sand mounds (Halley and others, 1986) or "sand volcanoes", covered with moderate-brown, coarse-grained detritus are common on the terraces of OAK crater. This material commonly contains granule- and small-pebble-sized particles (2-64 mm) and may sparsely contain small cobble-sized materials (64-256 mm). The sand volcanoes observed are generally less than 10 ft high, are round to elongate, and are 16-33 ft across and up to 100 ft long. The eight volcanoes documented by Halley and others (1986a) are plotted on the enhanced sea-floor image (fig. 7-14). Similar features that are probably sand volcanoes are also shown. The volcanoes appear to exist in several clusters or swarms on the terraces of OAK crater. No sand volcanoes were observed in the KOA area; however, most surficial features have been obscured by extensive slumping and recent sedimentation (Folger and others, 1986).

Several thin sand dikes filled with brown-stained sediments, confirmed by paleontologic analysis to be from MP-4, were penetrated by the boreholes. These were inclined at a high angle to the borehole under the central crater region and terraces of OAK. Dikes were observed in boreholes OPZ-18 at 667.8 - 668.5 ft, OKT-13 at 615.0 to 615.2 ft, OTG-23 at 472.3 to 473.2 ft, and OFT-8 at 291.1 to 291.9 ft (all depths bsl; see Henry, Wardlaw, and others, 1986). No dikes were observed in the KOA boreholes.

Paleontologic Mixing

The distribution of mixed materials from different biostratigraphic zones within the geologic crater is complicated, but each fossil is a clue to unraveling the history of formation of crater-fill deposits. In addition to the general three to four mixed zones presented in the previous section, both KOA and OAK have an overprint of hydraulic sorting in the central region due to post-deposition upward flow of piped material from strata below the excavational crater. In KBZ-4, the piped material shows hydraulic sorting of various fossil groups (see Brouwers, Cronin, and Gibson, 1986). In OBZ-4 and OPZ-18, the faunas are depleted and represented by sparse piped material in the lower part of the crater fill (fig. 7-15; and Cronin and Gibson, 1987), thought to indicate preferential removal of contained faunas by hydraulic flow and scant deposition of MP-4 faunas.

The mixing within the crater is displayed in Figure 7-16 for OAK and Figure 7-17 for KOA The biostratigraphic zones represented are defined in the reference boreholes in sequence of superposition and with increasing depth are: surficial (S), AA, BB, CC, DD, EE, FF, and GG. Piped material from depth designated as "piped" in the figures is represented by biostratigraphic zones II, JJ, KK, LL, and MM. Because the KOA event excavated down to the DD/EE zone boundary, most EE and all FF material in the crater-fill indicates shallow piping. Because the OAK event excavated down to a point within EE, possibly some EE and all FF and GG material in the crater-fill represents shallow piping. Each crater will be briefly discussed from bottom up (or as they filled).

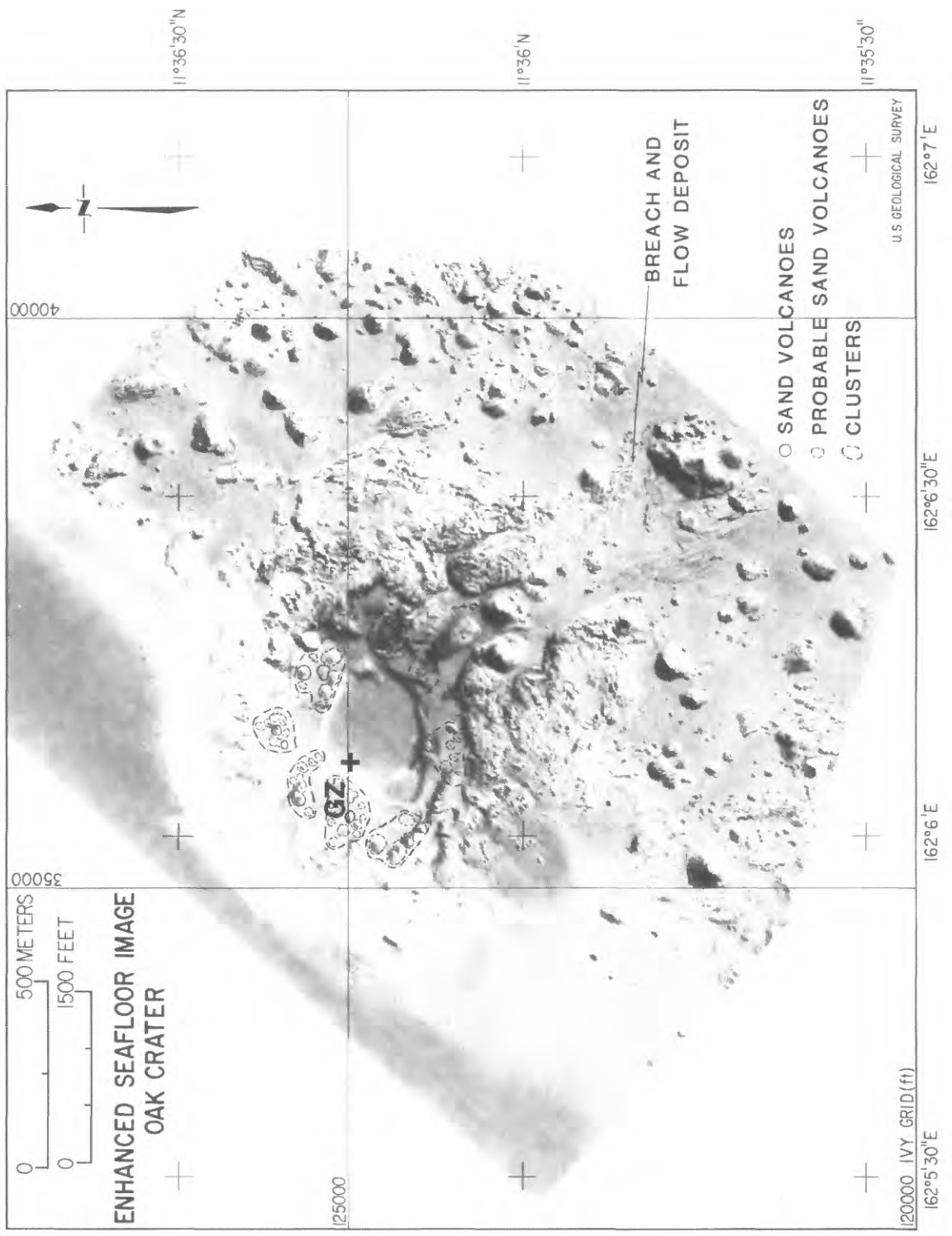

FIGURE 7-14. -- Distribution of observed (solid circles) and probable (dashed circles) sand volcanoes shown in clusters on enhanced sea-floor image of OAK crater and location of breach and flow deposit in lagoon.

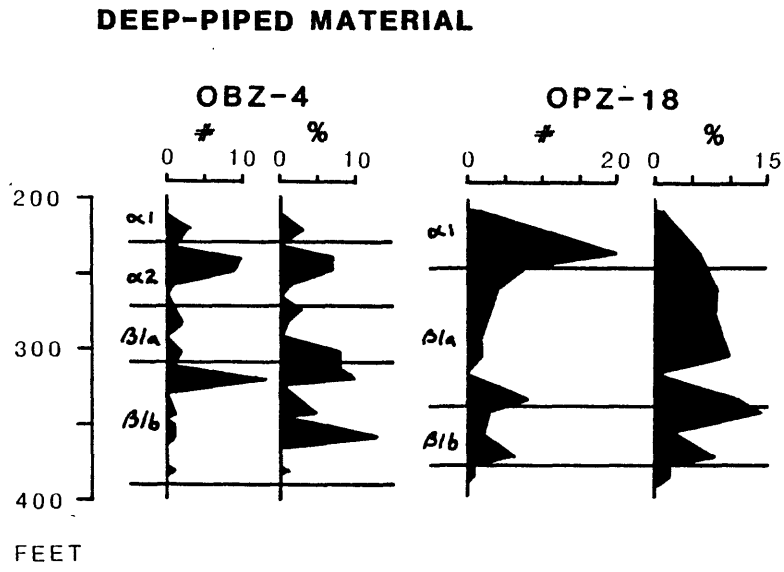

FIGURE 7-15. -- Number of specimens (#) from MP-4 and MP-5 (minor) and percent (%) of total ostracodes picked in crater zones in boreholes OBZ-4 and OPZ-18.

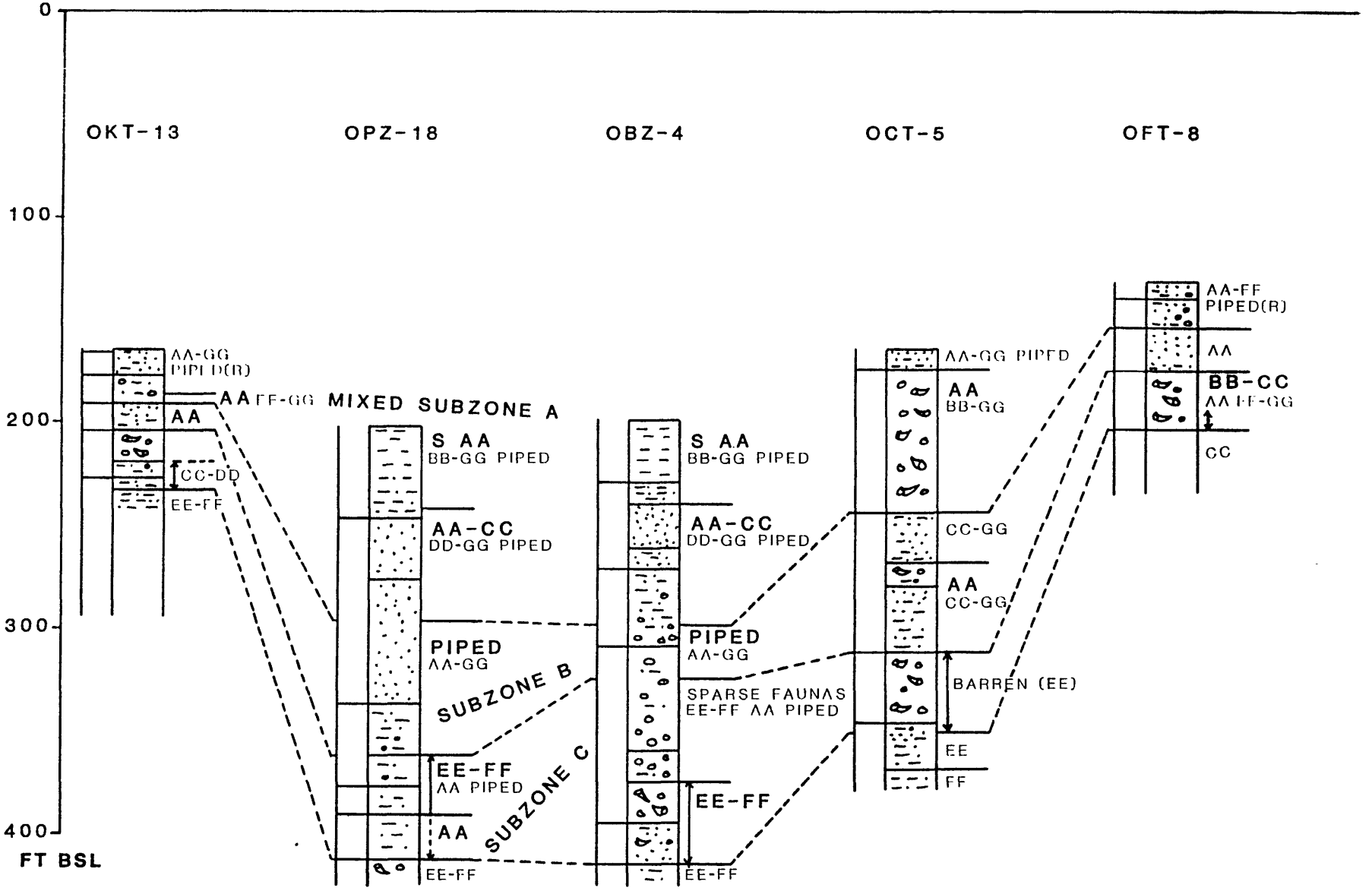

FIGURE 7-16. -- Paleontologic mixing in the mixed zone of OAK crater. Only boreholes with detailed analyses shown. Lithic symbols the same as Figure 7-19. Bold letters indicate abundant material from that particular biostratigraphic zone.

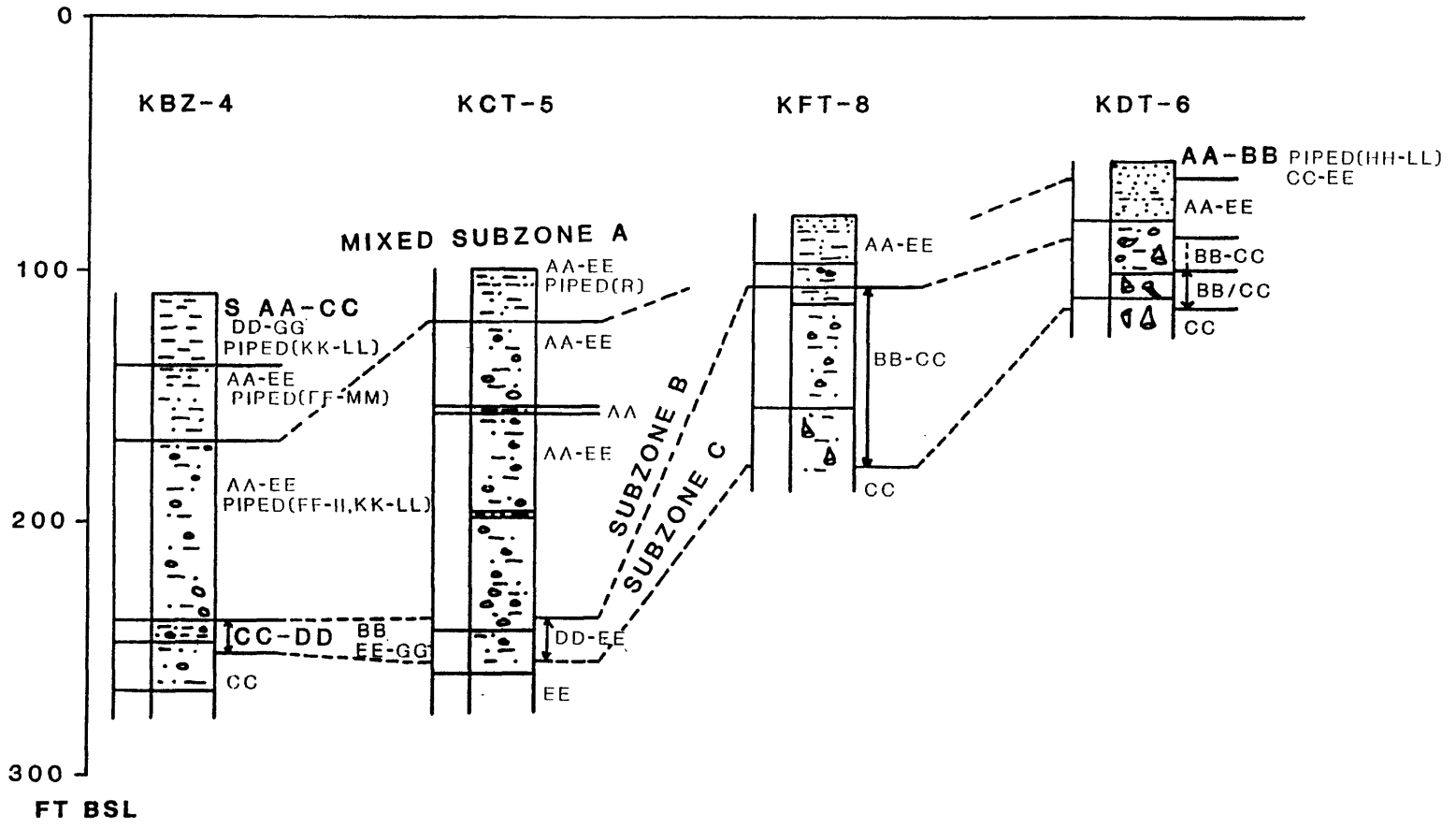

FIGURE 7-17. -- Paleontologic mixing in the mixed zone of KOA crater. Lithic symbols the same as Figure 7-19. Bold letters indicate abundant material from that particular biostratigraphic zone.

OAK Crater.

The lower mixed subzone (C, figs. 7-15 and 7-16) and the transition zone coincide for much of OAK crater (this is because of the limits of resolution, similarity of taxa in the zones, and gradational nature of these zones). This zone contains undifferentiated EE-FF material with sparse AA and deep-piped material in the central crater and of slightly mixed material from progressively stratigraphically higher zones outward to OFT-8 where it contains mostly BB-CC material.

The middle mixed subzone (B) represents a maximum of mixing of material in the central-crater area with components from zones AA-GG mixed with abundant deep-piped material in the upper part of Beta 1b and the lower part of Beta 1a. Laterally, this interval is represented by the "hiatus" sand (Beta 1s) which consists largely of AA material on top of Beta 1b. This situation is complicated at OCT-5 by an apparent local slump that covers and possibly involves the "hiatus" sand (fig. 7-16).

The upper mixed subzone (A) can be divided into two parts in the central-crater area and the inner terraces (OCT-5). In the central-crater area, the lower part consists of common AA-CC material and deep-piped and sparse DD-GG material, and the upper part consists of abundant surficial and AA components with common BB-GG and deep-piped material. Under the inner terraces (OCT-5), the upper mixed subzone consists of a lower part with abundant AA and common BB-GG material (no deep-piped material) and a upper part that is highly mixed with AA-GG and deep-piped material. Laterally, the upper mixed subzone commonly consists of very mixed AA-GG material decreasing outward to AA-FF material with sparse deep-piped material at its top. At OKT-13, the base of the upper mixed subzone (which coincides with the base of Beta 1a) is mixed with material from the underlying unit, the "hiatus" sand (Beta 1s).

Deep-piped material from MP-4 is mixed throughout the crater-fill in both OBZ-4 and OPZ-18, suggesting that the central crater bowl served as the common avenue for venting of MP-4 material. Although sand volcanoes are common on the terraces, mixing of deep-piped material from MP-4 is restricted to surface or near-surface deposits, suggesting that the volcanoes are a late-stage feature and did not represent the more common avenue of venting. Venting under the terraces probably did not take place until significant concentric fracture zones opened sufficiently in the subsiding crater to serve as conduits.

Shallow-piped material is that material in the crater-fill from shallow biostratigraphic zones that remained completely below the excavational crater. In OAK, this material is represented by components of biostratigraphic zones FF-GG. Shallow-piped material is common in the upper mixed subzone throughout the crater-fill, common in the middle mixed subzone, and sparse in the lower mixed subzone in the central crater.

KOA Crater.

The lower mixed subzone (C, fig. 7-17) and the transition zone coincide in most of KOA crater (for the same reasons as in OAK) and consist of CC-DD material with sparse BB and EE-GG material at KBZ-4, of DD-EE material at KCT-5, and of BB-CC material at KFT-8 and KDT-6.

The middle mixed subzone (B) consists of AA-EE material throughout the crater-fill. In addition, at KBZ-4, this zone contains deep-piped material that indicates hydraulic sorting in Beta 1a with FF-II ostracodes and KK-LL foraminifers, and a normal distribution of deep-piped FF-MM ostracodes and foraminifers in Alpha 2. A very thin, muddy "hiatus" sand may be preserved in KCT-5 within the middle of this unit.

The upper mixed subzone (A) is confined to Alpha zones. At KBZ-4, it is dominated by surficial (S) and AA-CC material with sparse DD-GG and deep-piped (KK-LL) material. At KCT-5, it consists of microfossils from AA-EE with very sparse deep-piped material. At KFT-8, the upper mixed subzone cannot be differentiated from the middle mixed subzone, and the whole interval consists of AA-EE material. At KDT-6, it is dominated by AA-BB with CC-EE and deep-piped (HH-LL) material.

Deep-piped material from MP-4 is mixed with other material throughout most of the crater-fill in KBZ-4. It is only found in surficial deposits in the transition boreholes. This suggests that the central bowl in KOA, which is now obscured by pervasive slumping, served as the common avenue for venting deep material from MP-4 just like in OAK.

In KOA, shallow-piped material is represented by components of biostratigraphic zones EE-GG, predominantly EE. The KOA crater-fill material shows much more pervasive shallow piping than in OAK. This shallow piping obscures some of the mixing subzones and yields fairly common mixed faunas of AA-EE. The pervasiveness of the mixing also implies that shallow piping occurred over a broad area. In addition, the paucity of samples and boreholes and a less rigorous study of the KOA material gives less definition of the mixing in KOA.

Estimates of Volume of Piped Material.

The volume of deep-piped material can be estimated with the techniques developed for the detailed paleontologic analysis of the OAK crater by Cronin and Gibson (Ch. 3 of this Report). Deep-piped material occurs only near the surface outside the central bowl and is essentially negligible in quantity. If all grain sizes behaved as those between 63 through 850 μ (the size range from which ostracodes are extracted) and if sedimentary particles of different shapes and densities (minor, all CaCO3) behave the same as ostracode valves and carapaces, then the detailed percentages of piped ostracodes reflect the entire sedimentary assemblage (Cronin and Gibson, Ch. 3 of this report). A conservative volume estimate based on these data is 4.83 million cubic feet (5.1 % of the total volume of central bowl to a depth of 149 ft with a radius of 450 ft from GZ).

A semiquantitative approach also can be attempted for estimating the shallow-piped material in OAK. Shallow-piped material is identified as those ostracodes that characterize the FF/GG zones, those zones that remained completely below the excavational crater. Shallow-piped material is similar in distribution to deep-piped material within the central bowl, it occurs throughout the crater fill. Because of the general low abundance of FF/GG zone indicators, any patterns in the distribution within the crater-fill is difficult to discern. The crater bowl probably was an avenue for shallow

piping, and the piping probably obscures any patterns of distribution in a manner similar to that for deep-piped material. Ostracodes that characterize the FF/GG zones are typically sparse, averaging 0.4 percent in the faunas above the FF/GG zones in the reference boreholes. They average a sparing 7.5 percent in the faunas of the zones that they characterize in the reference boreholes. These ostracodes average 3.3 percent in the central crater-fill faunas. This implies a whopping 41 percent of the central crater-fill material may have been derived from the FF/GG zones. A volume estimate based on these data is 45.62 million cubic feet of shallow-piped material within the central bowl. However, unlike deep-piped material, shallow-piped material is distributed in significant quantities in Beta 1a and Alpha zones outside the central bowl, suggesting a much larger volume than that estimated for the central bowl was piped.

Paleontologic Model of Crater-Fill.

The paleontologic zonation of the crater-fill can be summarized into a simple model that is applicable to both craters studied. It is extremely relevant for constraints on timing of processes of crater-filling. It is presented in Figure 7-18. The zone of shallow-piped material coincides with that of the deep-piped material through mixed subzones B and C in the central crater but encompasses all of mixed subzone A throughout the crater. The zones of piped material indicate the relative timing of arrival of material to the surface. Shallow-piped material first arrived to the surface after the deposition of the hiatus sand (Beta 1s), which probably resulted from wash-back. Deep-piped material first arrived to the surface after the deposition of the graded rubble (Beta 1a), during deposition of Alpha.

The zone of piped material from depth has a strong overprint of mixing and hydraulic sorting in the central bowl, especially in mixed subzone B, where abundant deep-piped material was deposited. The central bowl served as the probable avenue for venting of the deep-piped material. Shallow-piped material also appears to have vented, in part, through the central region. However, shallow piping appears to have occurred throughout the crater wings which implies venting throughout the crater region.

Injection

Holocene sediment (from MP-1) appears at an anomalous depth in borehole OPZ-18 within the transition sand (390.6 to 410.0 ft bsl) and in thin dikes below the transition sand (434.5 to 435.2 ft bsl, and questionably at 415 ft). This appears to be injection of near-surface material at the base of the excavational crater.

Gamma Activity

In Enewetak boreholes, elevated gamma activity appears to reflect the following: (1) the presence of device-produced radionuclides; (2) the presence of brown-stained, organic-rich sediments from MP-4; and (3) various other factors. For example, a gamma peak of the third type occurs within muddy sediments overlying a discontinuity in OIT-11 (fig. 7-19). It appears that other peaks of the third type also can be related to thick zones of "tea-brown" (organically stained) micrite cement.

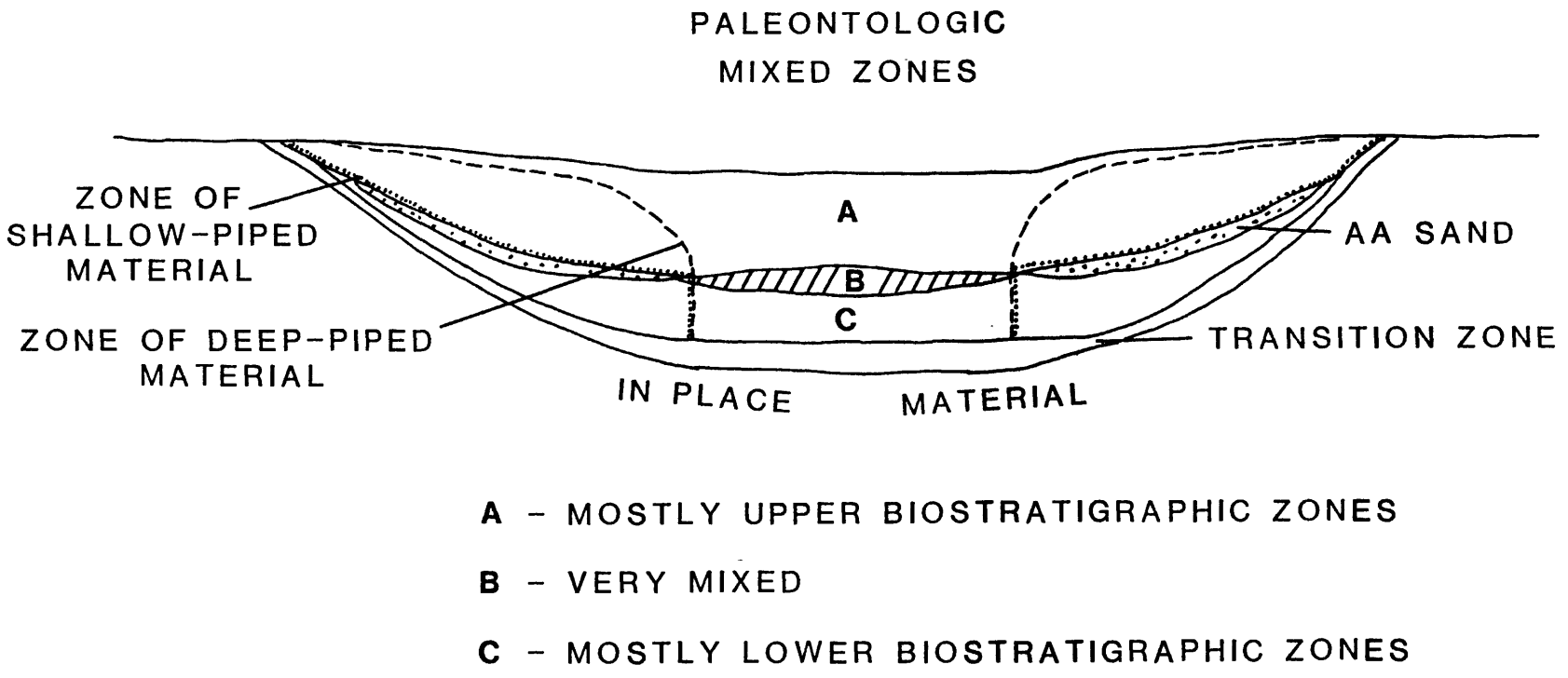

FIGURE 7-18. -- Paleontologic model of the crater-fill and the paleontologic mixed zones.

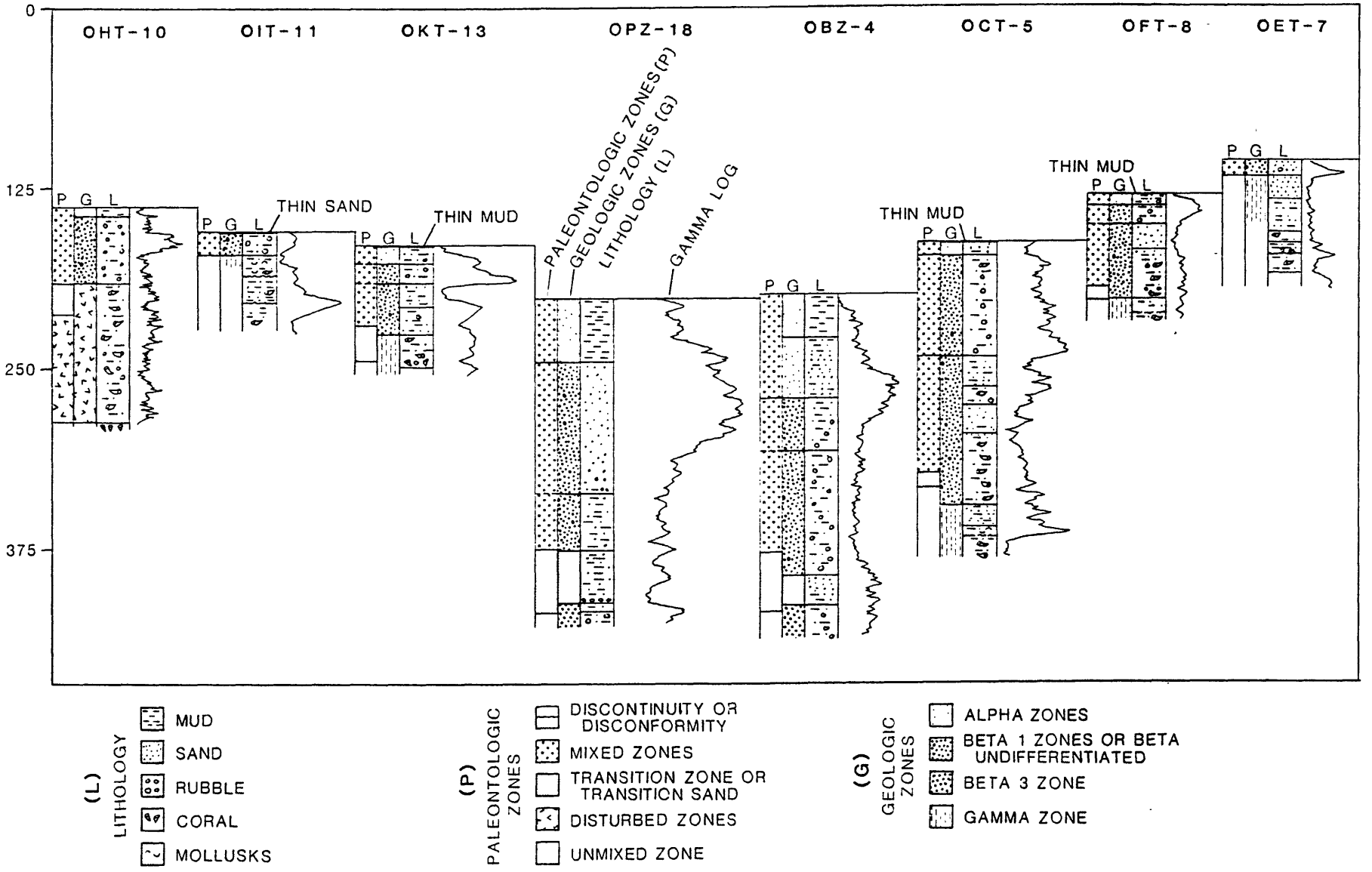

FIGURE 7-19.--Borehole lithology (L), geologic (G) and paleontologic (P) crater zones, and gamma-ray logs for selected boreholes, OAK crater. Location of boreholes shown on Figure 7-20.

Cesium-137 levels coincide directly to the gamma activity in the Alpha, Beta-1, and Beta-2 crater zones (Ristvet and Tremba, 1986). Furthermore, the gamma activity of the brown-stained, organic-rich sediments is caused largely by naturally occurring isotopes of thorium and uranium. These radionuclides were not observed within the Alpha, Beta-1, and Beta-2 crater zones.

Naturally occurring thorium and uranium isotopes were detected in borehole OIT-11 and probably account for the "other" peak (third type) in gamma activity noted above. Similarly, in borehole OHT-10, a small peak in the gamma activity probably reflects naturally occurring thorium and uranium (fig. 7-19).

Figures 7-19 and 7-20 compare the gamma log, paleontologic and geologic crater zones, and general lithologies for KOA and OAK crater areas. Only boreholes on transects with full geologic sampling and open-hole gamma logs were utilized for this comparison. Essentially, the gamma logs confirm the general trends in radionuclide abundance (Ristvet and Tremba, 1986; and fig. 7-21). The Beta-2 / Beta-3 boundary (where present) and the Beta-1 / Gamma boundary (where present) appear to represent the demarcation between occurrence and absence of device-produced radionuclides. Naturally occurring radionuclides appear to reflect the presence of deep-piped material in the Beta-3 crater zone. Device-produced radionuclides are most abundant within the bottom of Alpha-2 (graded sands) and top of Beta-1a (graded rubble) in OBZ-4 and OPZ-18, respectively. In KBZ-4, they are most abundant at the base of Alpha-1 and at the top of Alpha-2. In KCT-5, there is only a trace of radionuclides (device-produced and natural). In borehole OCT-5, device-produced radionuclides are most abundant within the lower part of the Beta-1a crater zone. In OKT-13, device-produced radionuclides show two peaks, one within Beta-1a and the other (larger) near the base of Beta 1b.

Distribution of Radionuclides

The distribution of radionuclides within OAK crater is shown in Figure 7-21 (Ristvet and Tremba, 1986). In OBZ-4, the device- produced radionuclide (Cesium-137) is common in Alpha 1, Alpha 2, and Beta 1a, with peak abundance in Alpha 2. Most of the crater-fill in OPZ-18 consists of muddier sediments than OBZ-4 and consequently contains higher concentrations of Cesium-137. In OPZ-18, radionuclides are common to Alpha 1, Beta 1a, Beta 1b, and Beta 2; the Beta 2 occurrences represent the injected material. Peak abundance is in the upper part of Beta 1a. A moderate amount of cesium is found in OKT-13 below and above the "hiatus" sand (Beta 1s), in Beta 1b, and in Beta 1a and Alpha, respectively.

Radionuclides are sparse in KOA crater and only common within KBZ-4. Here, they mimic the gamma-ray profile (fig. 7-20), with peak abundance in Alpha 1 and a trace at the base of Beta 1b and top of Beta 2.

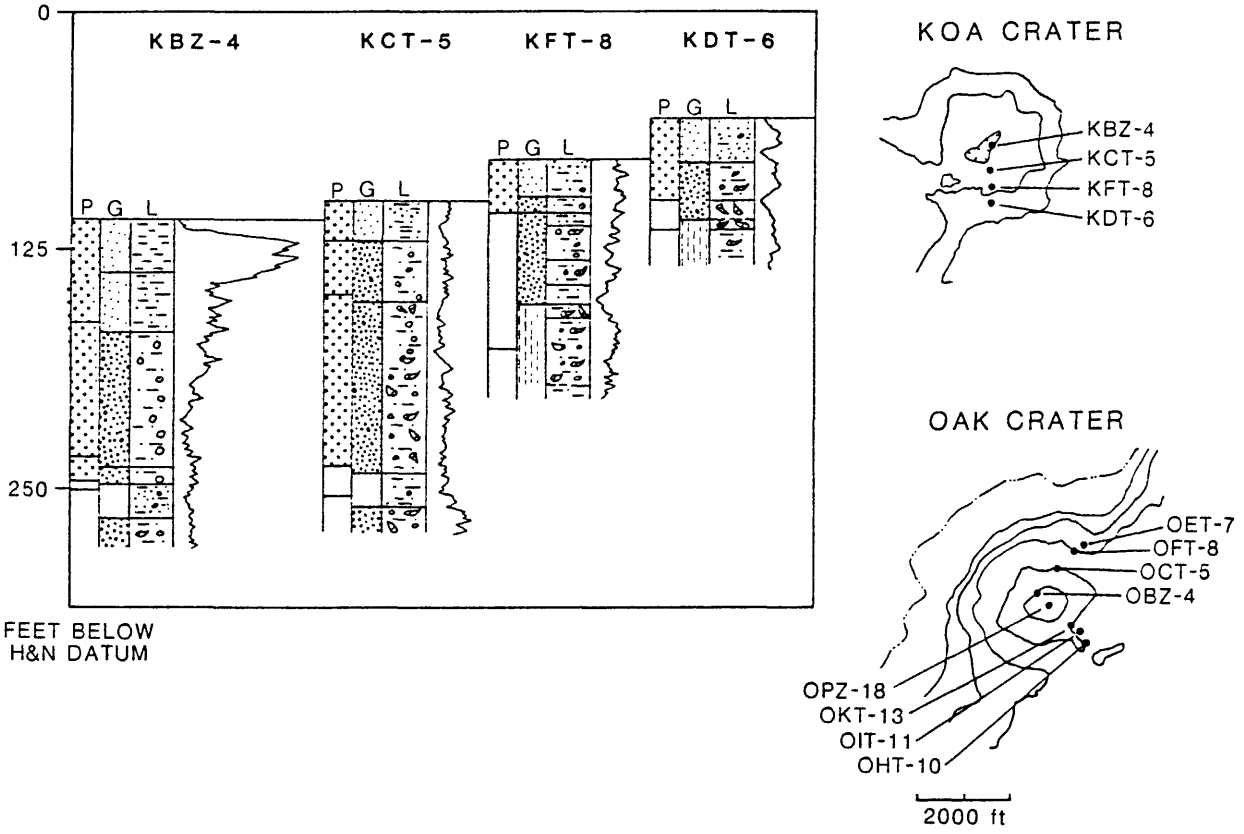

FIGURE 7-20. -- Borehole lithology (L), geologic (G) and paleontologic (P) crater zones, and gamma-ray logs for selected boreholes, KOA crater, and index maps for the KOA and OAK craters. Symbols the same as Figure 7-19.

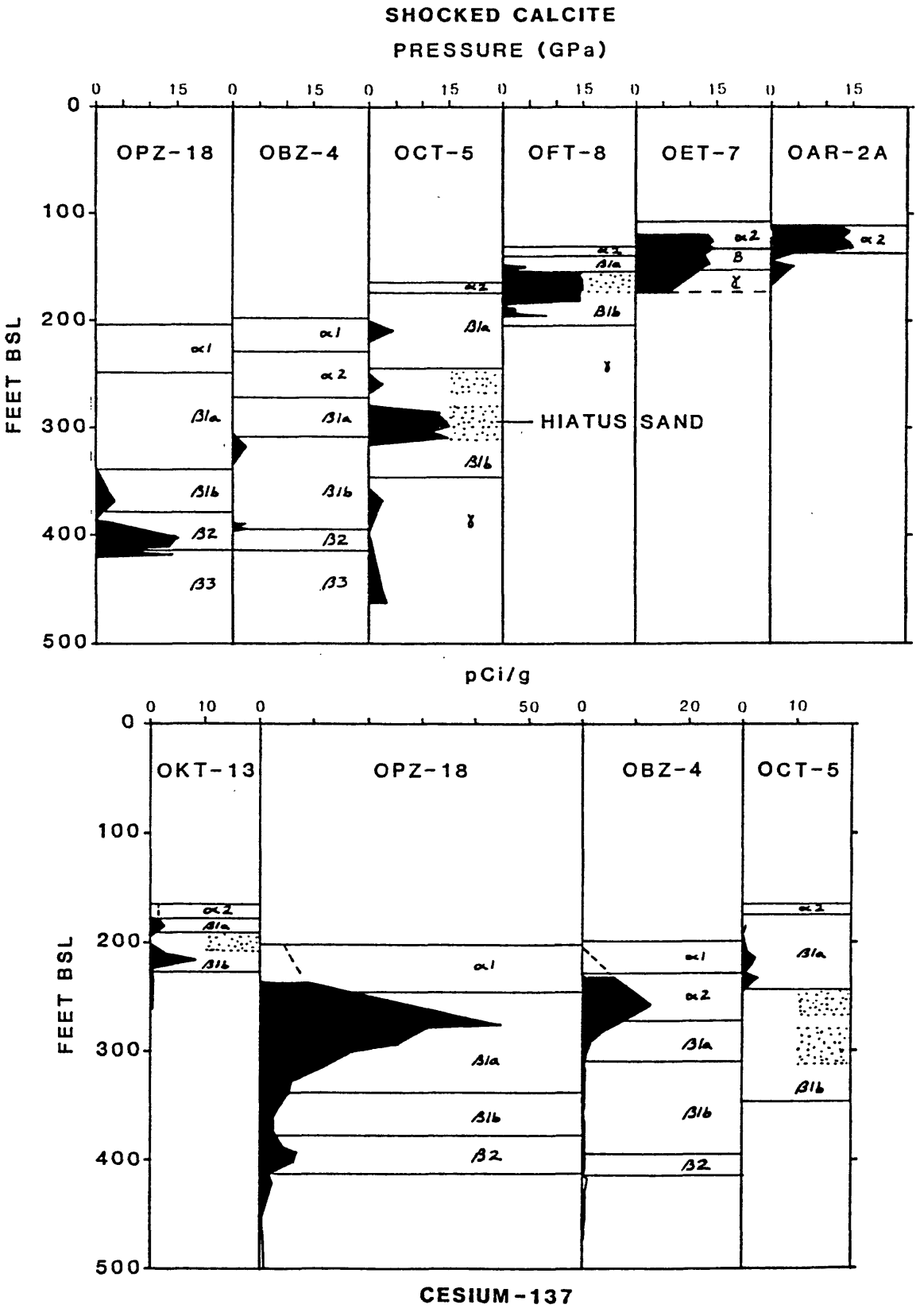

FIGURE 7-21. -- Distribution of shocked calcite and Cesium-137 and relationship to crater zones in boreholes analyzed in OAK crater.

Distribution of Shocked Calcite

The distribution of shocked calcite is shown in Figure 7-21 (Polansky and Ahrens, Ch. 4 of this report). Only sparse, possibly moderately shocked calcite is present in the central crater area within Beta 1b. Highly shocked calcite is found within the injected material in OPZ-18. Under the terraces, possibly moderately shocked calcite is found in Beta 1a, Beta 1b, and Gamma with highly shocked calcite in the "hiatus" sand, Beta 1s. Outside the limits of crater-derived rubble (Beta zone), highly shocked calcite occurs in Alpha 2 and Beta in OET-7 and in Alpha 2 in OAR-2A. The material in OAR-2A represents post-event deposition of shocked calcite away from the crater, probably by the sweeping away of fine-grained ejecta from the reef tract by currents and redeposition of it in the area of OAR-2A. The material in OET-7 in graded sands (Alpha 2) seems to represent post-event deposition like that in OAR-2A. The material in OET-7 in the undifferentiated rubble apparently represents buried ejecta.

Depression and Uplift of Structural Surfaces

The surface at the top of the Pleistocene in both the OAK and KOA areas shows a pattern of central removal and lateral depression on the net-change (delta) figures (figs. 7-22A and 7-23A, respectively) derived from the pre- and post-shot surface contour maps (figs. 7-4 and 7-24). In addition, in the OAK area, two lateral depression troughs are developed along the pre-shot slope from reef to lagoon. Also, the Pleistocene surface appears to be irregularly disrupted or preserved beneath the debris blanket (dashed lines, fig. 7-22A) and irregularly uplifted near the margins of the debris blanket. The maximum current depression observed in OAK is 63 ft and in KOA is 53 ft. The maximum uplift in OAK is 14 ft. No strata in KOA are currently uplifted.

The surface at the top of the Pliocene in the OAK area (fig. 7-22B) shows central concentric depression slightly skewed toward the reef and a broad region of shallow uplift beneath both the debris blanket and the lagoon. The maximum depression is 193 ft beneath GZ. The maximum uplift appears to be about 21 ft. The Pliocene surface in the KOA area certainly was influenced by detonation of the MIKE device (fig. 7-23B). KOA shows a complicated pattern of depression with maximum depression on the lateral wings away from GZ. The pattern of depression from MIKE crater area would suggest that the area in the proximity of KOA GZ experienced 0 to 10 ft depression and the entire region from KOA GZ to MIKE experienced progressively greater depression toward MIKE. This possibly influenced the apparent lateral extension in depression roughly perpendicular to the line from KOA ground-zero to MIKE ground-zero.

COMPARISON OF OAK AND KOA CRATERS

The following comparisons and contrasts can be made between KOA and OAK craters:

(1). The base of the zone of sonic degradation (ZSD) is similar in both craters -- 1,139 ft bsl for OAK ground-zero (GZ) and 1,101 ft bsl for KOA GZ. The ZSD appears to form a narrower cone at KOA

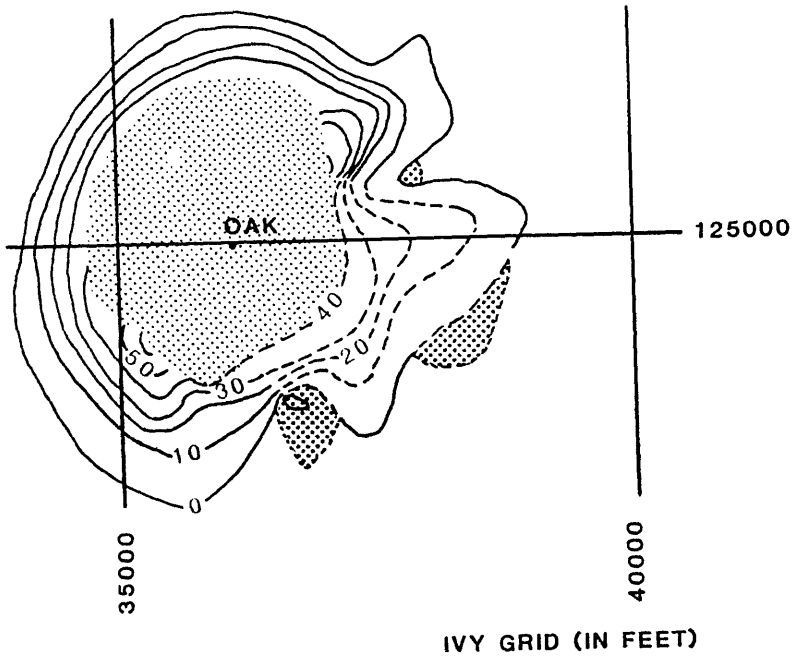

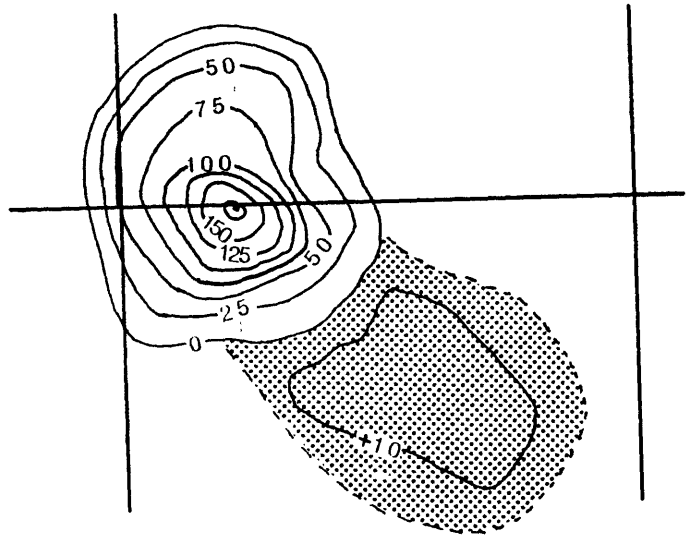

FIGURE 7-22. -- Maximum depression/uplift of Pleistocene and Pliocene surfaces, OAK crater. Pleistocene surface is projected beneath debris blanket, where it is disrupted but probably remains as several isolated outliers such as encountered in OIT-11. Surface is lightly stippled where removed, heavily stippled where uplifted.

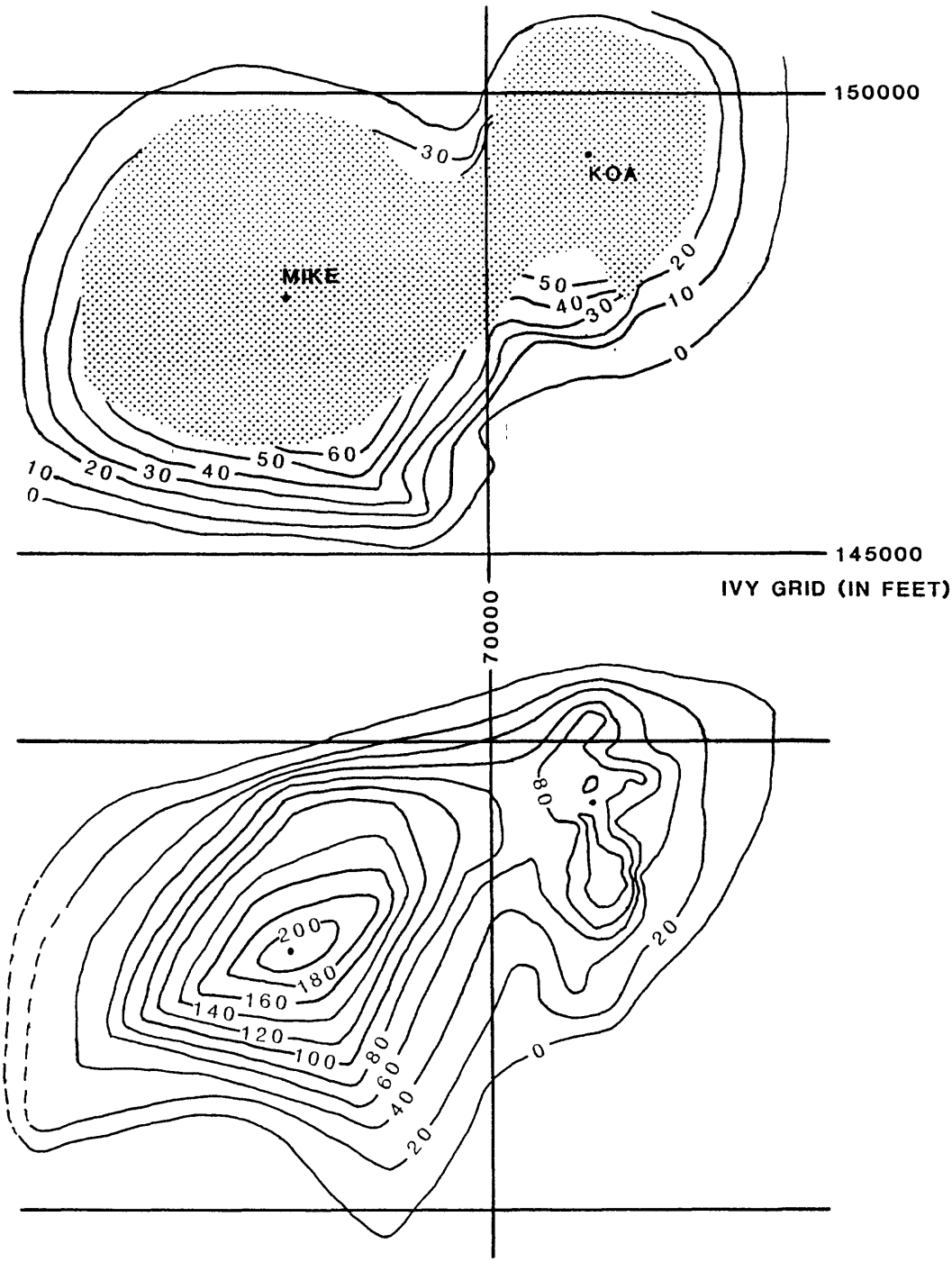

FIGURE 7-23. -- Maximum depression of Pleistocene and Pliocene surfaces, KOA crater. Surface is lightly stippled where removed.

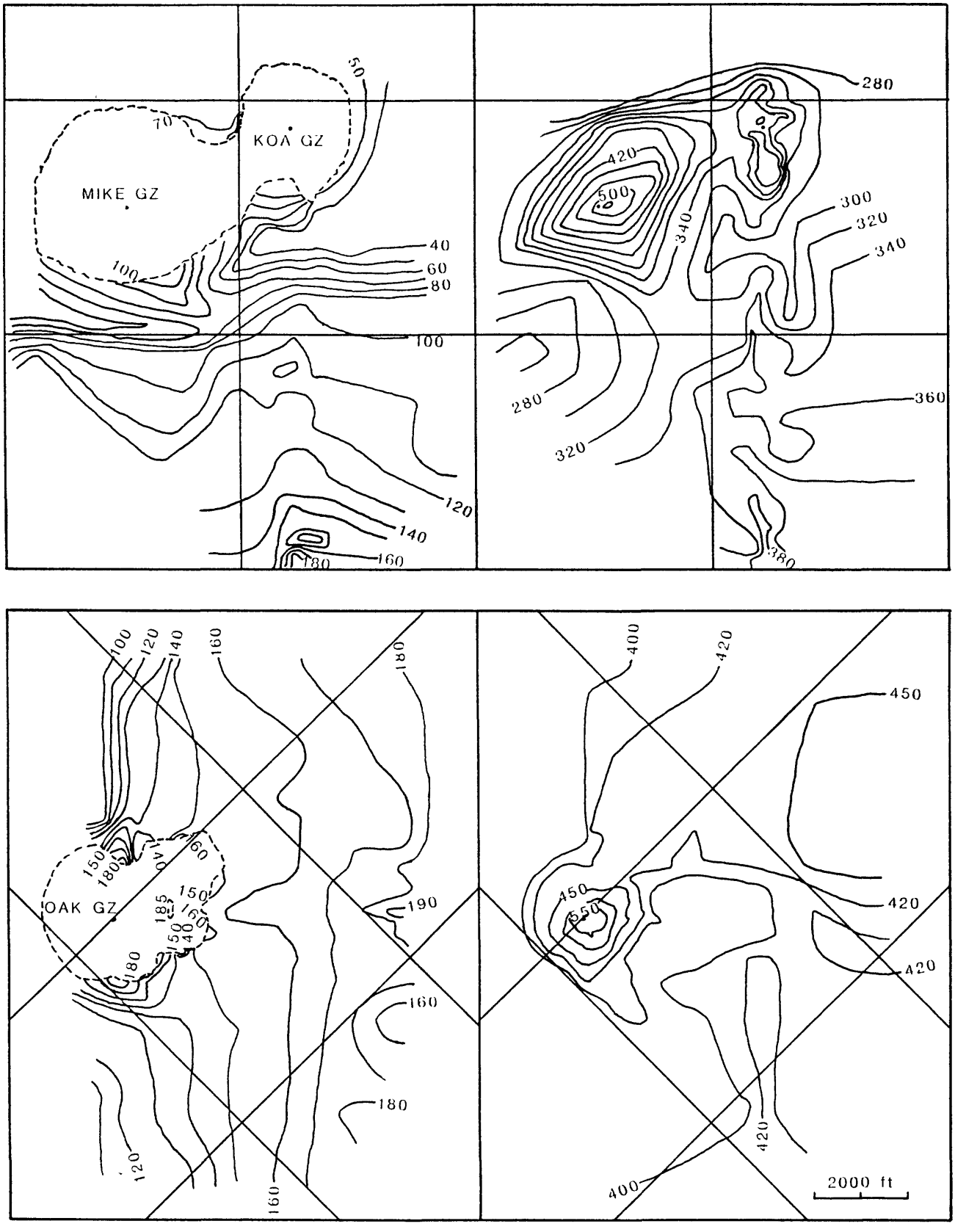

FIGURE 7-24. -- Present-day (post-shot) location of Pleistocene and Pliocene surfaces, KOA and OAK craters. Contours in ft below H&N datum (bsl).

(2). MP-3, the significantly cemented and altered zone, was probably 246 ft thick with the top at 280 ft bsl at KOA GZ and 183 ft thick with the top at 400 ft bsl at OAK GZ.

(3). MP-3 is depressed approximately 193 ft at OAK GZ and approximately 89 ft at KOA GZ. MP-3 shows depression and fracture at OAK and, in addition, at KOA, shows apparent rebound in the central part of the crater.

(4). At ground-zero, the Alpha zone (mud and graded sand) is comparable between KOA and OAK; however, the Beta zone (rubble) is twice as thick at OAK. In particular, Beta 3 (rubble floatstone) is much thinner at KOA. The total lateral extent of the Beta zone is nearly the same at both craters.

(5). The transition sand (Beta 2) is more extensive in KOA than OAK, with an average diameter of approximately 918 ft at KOA and 816 ft at OAK. The transition sand is more elongate oval at KOA than at OAK.

(6). The collapse rubble (Beta 1b) is similar in both craters, although thicker in OAK. The Beta 1b zone thins toward the lagoon at OAK and thins toward MIKE crater at KOA.

(7). The hiatus sand (Beta 1s) is much less extensive at KOA, presumably due to thinner and shorter-term deposition and to more extensive destruction by late-stage collapse.

(8). The graded rubble (Beta 1a) is similar in both craters. The rubble becomes thicker and muddier in the direction of the lagoon at OAK (i.e., toward its distal margin) and in the direction of MIKE crater in KOA For all intent and purpose, for the KOA event, MIKE served as a "lagoon" similar to the natural lagoon off OAK, but much smaller in extent.

(9). The graded sands (Alpha 2) are similar in both craters. This zone is common throughout the KOA crater but absent near the bathymetric center (OPZ-18) of OAK crater.

(10). Mud (Alpha 1) occupies the central region of both craters.

(11). A debris blanket is extensive on the lagoon side of OAK; only two possible debris mounds of limited distribution exist on the MIKE-side of KOA.

(12). Deep-piped material is common only in Alpha 2 in KOA and probably vented in a limited area at the central crater. Deep-piped material is common to Alpha 1, Alpha 2, and Beta 1a in OAK and probably vented in an extensive area of the central crater and terraces.

(13). Shallow-piped material is common to Alpha and Beta 1a zones throughout the crater wings and found in all zones in the central crater in both craters. In KOA, it is represented by EE-GG material in the central

crater and EE material in the crater wings. In OAK, it is represented by FF/GG material throughout the crater.

(14). KOA crater is characterized by late-time sedimentation exceeding subsidence. OAK crater, in contrast, is characterized by late-time subsidence exceeding sedimentation.

(15). Device-produced radionuclides appear to be mostly limited to the Beta 2 and overlying zones in the craters. Radionuclides were detectable only in KBZ-4 for the KOA crater. In OAK crater, peak abundance of device-produced radionuclides progressively moves down in the crater zones away from GZ. For example, the peak abundance is in Alpha 2 in OBZ-4, at the top of Beta 1a in OPZ-18, at the bottom of Beta 1a at OCT-5, and at the bottom of Beta 1b at OKT-13.

GEOLOGIC CRATER MODEL FOR OAK AND KOA

The transition sand (Beta 2) represents the remnants of the base of the excavational crater. It is characterized by sand-sized material that is formed by fracture and pulverization, by its transitional nature from mixed paleontology to unmixed paleontology within it, and by its containing injection dikes and debris. That shocked calcite is not common within the transition sand is due to two factors: (1) the sampling technique used in which granule- and larger-sized clasts were predominantly sampled (Polansky and Ahrens, 1987, Ch. 4 of this report), and (2) the relatively low shock pressures that probably existed in this region at formation (< 15 kilobars).

The rubble floatstone (Beta 3), beneath the base of the excavational crater (Beta 2), may represent fracture and disruption of sediment and rock caused by the maximum growth of the transient crater.

The collapse rubble (Beta 1b) represents crater-sidewall and partial flap collapse. This zone reflects paleontologic mixing of zones near the base of the excavational crater. The asymmetric crater at OAK demonstrates partial sidewall and flap collapse and movement down the resulting slope away from the transient crater to form the majority of the debris blanket. The part of the flap involved in craterward collapse is that closest to the sidewall which would represent paleontologic zones contained in the sidewall itself. That the paleontologic mixing seems to reflect mixing of material from zones near the base of the crater suggests that most of this unit was deposited rapidly as a single, major, crater-wide collapse feature. This major collapse appears to have destroyed the lateral part of the excavational crater base and its sidewalls. The highly mixed material in the central crater bowl represents a variety of depositional modes that may include wash-back and piping of sufficient magnitude to keep the central bowl "boiling" (continuously mixing). This part of the unit was deposited contemporaneously with the "hiatus" sand (Beta 1s) which represents wash-back and a brief period of quasi-stabilization of the crater and deposition of post-event sediments. The "hiatus" sand is well sorted and contains the highest concentration of shocked calcite indicating deposition from wash-back and fall-back, but, curiously, contains no radionuclides. At OAK and KOA craters, the occurrences of radionuclides are spotty. The decades that have transpired since the event have allowed many radionuclides to dissipate (Ristvet and Tremba, 1986). The

remaining commonly detectable radionuclide is Cesium-137. It is associated with muddy sediments (McMurtry and others, 1985; Wardlaw and Henry, 1986b) and may have been preferentially deposited with muds, and, therefore, would not be common in well-sorted sands. Cesium-137 is involved in progressively younger and muddier deposits in the crater-fill toward ground-zero. Its absence in the "hiatus" sand probably indicates the winnowing out of silt and finer grains during the wash-back / fall-back process.

The graded rubble (Beta 1a) represents deposition probably caused by several major slumps. This indicates that subsidence significantly destabilized the existing crater margins and resulted in collapse. One such collapse in OAK appears to have originated on the reef side. Material from this collapse flowed through the crater and breached the debris blanket, leaving deposits on top of the debris blanket (OHT-10, OJT-12), and flowed out into the lagoon, as seen in the enhanced sea-floor image of OAK (fig. 7-14).

The graded sands and slumps (Alpha 2) represent late-stage, local collapse and deposition of the expanding and subsiding crater margins.

Late-stage mud (Alpha 1) represents post-event, low-energy deposition within the central crater. The differences in Alpha 1 and distal Alpha 2 sands are slight, as shown by the sediment analysis by Melzer and Patti (written communication, 1987).

The idealized distribution of these crater units is shown for a symmetric crater (KOA, fig. 7-25A) and for a asymmetric crater (OAK, fig. 7-25B). The gradational units beneath the transition sand that represent gradually less-stressed sediment and rock within the significantly fractured zone of sonic degradation are also shown.

Thinning Analysis

This analysis simply compares the pre-shot model of inferred horizon location to the measured post-shot position. The comparison of positions is shown in Figures 7-26 to 7-29 and Tables 7-5 and 7-7. The analysis is displayed graphically in Figures 7-30 and 7-31 and tabulated in Tables 7-6 and 7-8. The upper correlation line in Figures 7-30 and 7-31 correlates the pre-shot model to the probable original stratigraphic depth now preserved beneath crater-fill (where present).

Stratigraphic Density Profile

The analysis of the borehole gravity surveys (Beyer, Ristvet, and Oberste-Lehn, 1986; and Beyer, Ch. 2 of this report) provide valuable information about bulk density of the strata in the vicinity of OAK crater. By averaging the borehole-gravimetry results within stratigraphic units, the density change can be compared directly with inferred stratigraphic thinning or thickening for areas where borehole gravity surveys were taken. Figure 7-32 and Table 7-9 relate the gravimetry results to the stratigraphic units. MP-2a appears anomalously dense in the reference sections. The average of MP units 2a-c in the reference sections is utilized to compensate for this anomalous density, especially to compare to crater-fill material in the analysis.

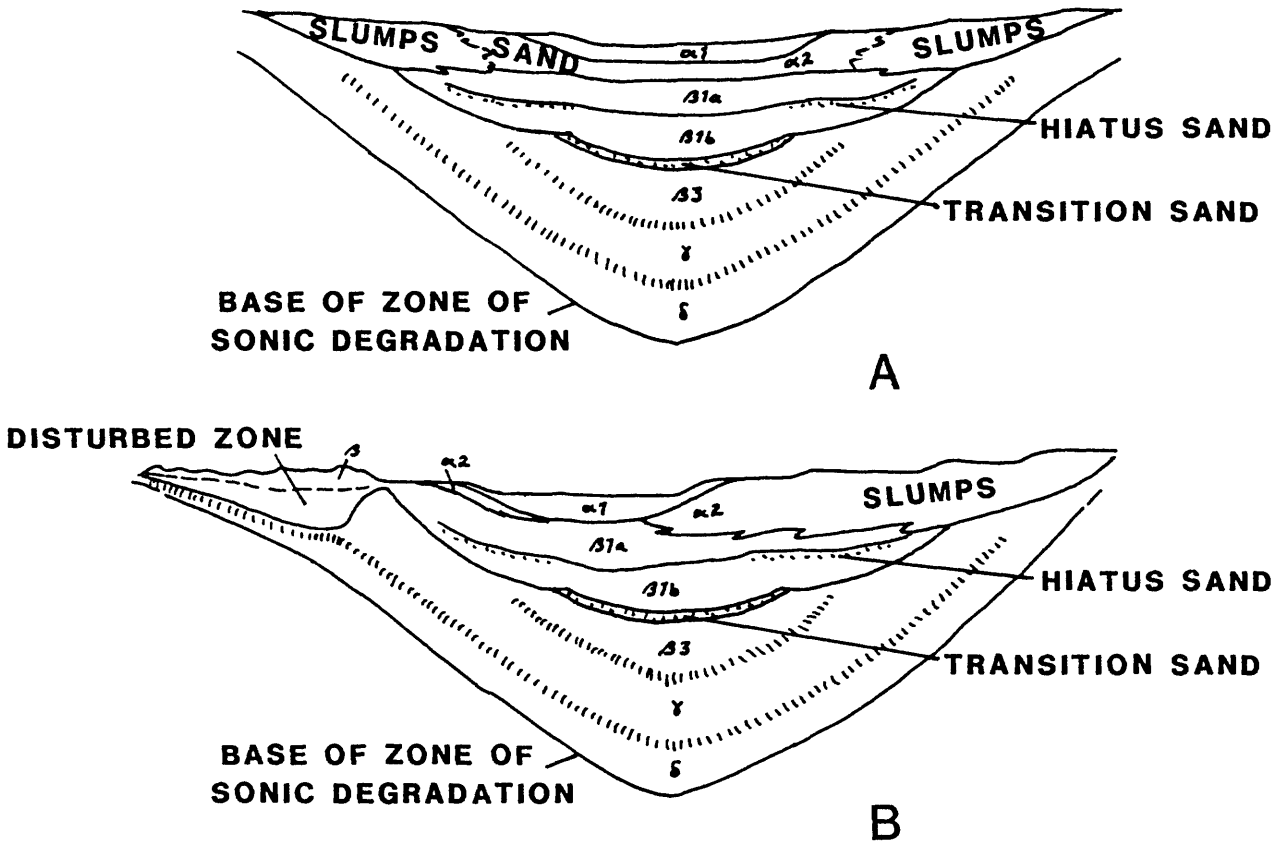

FIGURE 7-25. -- Idealized model of geologic crater for a symmetric crater (A) and an asymmetric crater developed on a significant slope (B).

TABLE 7-5. -- Depth (ft bsl) to MP unit boundaries, pre- and post-shot, OAK crater. Boreholes listed in order of increasing distance from ground zero.

UNIT	OBZ-4		OPZ-18		OCT-5		OTG-23		OUT-24	
1	14	-	47	-	16.5	-	45	-	2	-
2a	123	-	128	-	115	-	128	-	106	-
2b	165	-	166	-	155	-	168	-	145	-
2c	265	-	275	-	255	368.4	253	?	225	373.0
2d	315	-	363	568.9	305	417.9	327	434.0	276	407.0
3a	395	593.0	410	593.0	387	432.7	409	484.0	355	457.1
3b	544	701.2	555	723.5	534	572.2	544	610.0	490	592.0
4a	592	747.3	600	761.9	585	623.7	594	669.0	528	630.0
4b	775	847.7	765	809.9	785	799.7	766	787.0	784	784.0
5a	950	1013.8	956	1000.0	945	944.6	1000	1000.4	925	925.0
5b	1050	1065.1	1050	1063.0	-	-	-	-	1025	1025.0
5c	1115	1114.6	1114	1114.0	-	-	-	-	-	-

UNIT	OKT-13		OFT-8		OIT-11		OET-7		OQT-19	
1	102	-	16	-	122	-	18	-	46	-
2a	141	-	115	204.1	147	185.4	118	173.4	129	168.0
2b	170	232.9	155	223.3	209	247.4	167	220.6	195	233.9
2c	275	326.6	230	272.0	-	-	279	294.7	240	274.7
2d	362	411.6	305	344.6	345	375.0	305	320.4	330	365.3
3a	410	431.3	390	419.8	405	434.8	395	410.0	406	413.3
3b	547	564.0	535	565.0	545	562.0	540	555.0	548	548.3
4a	598	614.7	589	618.0	591	608.0	595	610.0	588	587.5
4b	766	765.8	794	794.0	758	758.0	793	793.0	767	766.5
5a	975	974.5	925	925.0	980	980.0	925	925.0	1020	1020.1
5b	1037	1036.5	-	-	-	-	-	-	-	-
5c	-	-	-	-	-	-	-	-	-	-

UNIT	OHT-10		OJT-12		ODT-6		ONT-16		ORT-20	
1	124	-	115	-	20	-	132	-	70	-
2a	152	-	149	-	116	161.5	149	-	130.5	160.6
2b	212	213.3	216	238.0	160	201.3	219	238.6	187	216.2
2c	-	-	-	-	231	231.3	-	-	243	262.7
2d	361	360.8	350	350.0	315	315.0	338	337.8	327	346.7
3a	419	403.4	405	390.3	397	397.0	407	395.2	405	411.7
3b	547	531.4	547	531.0	546	546.0	550	537.9	552	552.0
4a	600	584.0	600	584.0	594	594.0	600	588.0	586	586.4
4b	751	751.1	732	732.0	792	792.0	715	715.0	767	767.0
5a	987	987.3	991	991.0	925	925.0	994	993.8	1014	1013.5
5b	-	-	-	-	-	-	-	-	-	-
5c	-	-	-	-	-	-	-	-	-	-

(TABLE 7-5 continued on next page.)

TABLE 7-5. (continued from preceeding page.)

UNIT	OMT-15		OLT-14	
1	142	-	132	-
2a	153	140.8	158	159.4
2b	225	225.0	227	227.0
2c	-	-	-	-
2d	335	334.6	341	341.1
3a	395	373.9	399	383.8
3b	551	529.7	550	534.6
4a	600	579.0	600	585.0
4b	702	701.9	700	700.0
5a	1014	1013.5	1010	1010.2

Distance of boreholes from surface ground-zero, in feet:

OBZ-4	7
OPZ-18	335
OCT-5	658
OTG-23	804
OUT-24	858
OKT-13	989
OFT-8	1129
OIT-11	1206
OET-7	1375
OQT-19	1444
OHT-10	1462
OJT-12	1696
ODT-6	1715
ONT-16	1827
ORT-20	1846
OMT-15	2204
OLT-14	2754

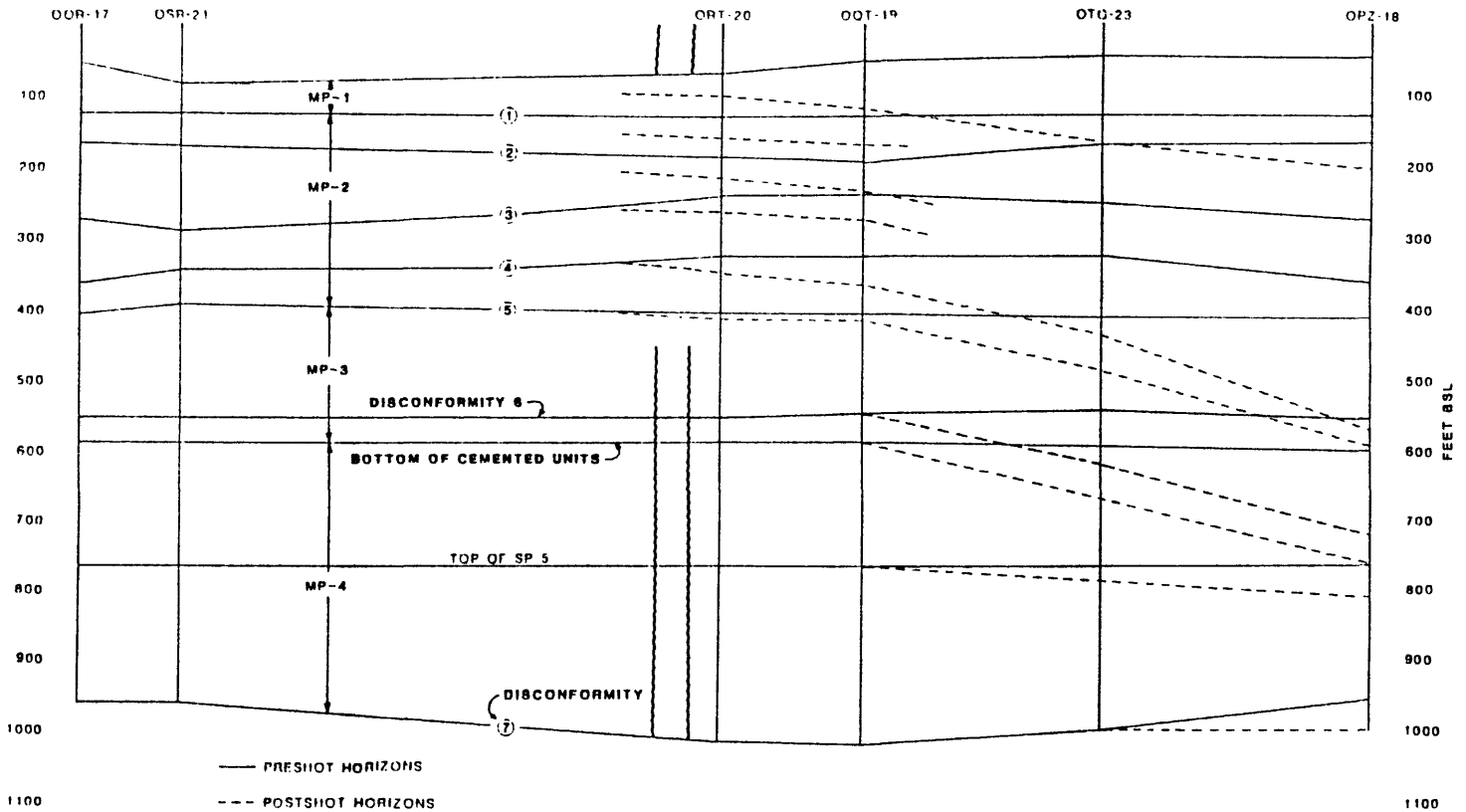

FIGURE 7-26. -- Horizon location in fence diagram from boreholes OOR-17 to OPZ-18. Pre-shot location as a solid line except for unit MP-4a/4b boundary which is short dashes. Dashed line represents post-shot location where different from pre-shot location. Squiggles, breaks, and scale as in Figure 7-8.

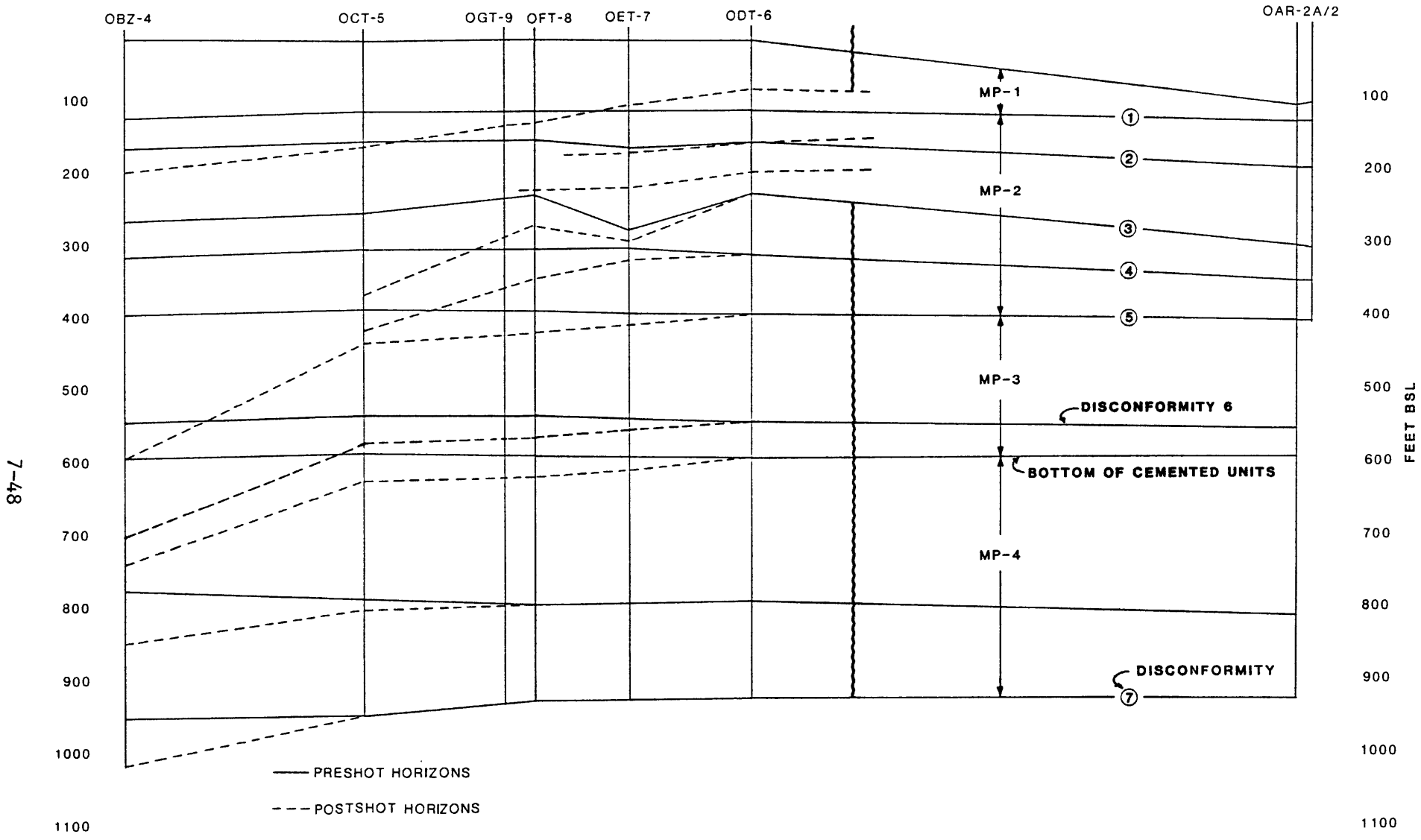

FIGURE 7-27. -- Horizon location in fence diagram from boreholes OBZ-4 to OAR-2/2A as in Figure 7-26. Squiggles, breaks, and scale as in Figure 7-9.

boreholes OOR-17 and OSR-21. Density and porosity changes over the large intervals shown in Figures 2-16 and 2-19 are summarized in Table 2-9.

Many more types of comparisons are possible but are beyond the intent of this paper, which is to provide accurate representative density data and calculated porosity values for atoll materials at the six surveyed boreholes and to present a general density model of the crater.

SUMMARY

Borehole gravity surveys were conducted at OAK crater to obtain accurate large-volume estimates of in situ bulk-density and total porosity of atoll materials beneath and beyond the crater. Reliable density and porosity measurements of undisturbed atoll materials provide important geologic information about these young, loosely consolidated back-reef sediments, and predictions of pre-event material-property conditions for nuclear event calculations. Accurate measurements of differences between the density and porosity of undisturbed atoll materials and the sediment and rock involved in the excavational and apparent OAK craters are crucial to understanding the cratering phenomena at OAK and the mechanics of large crater formation.

Six boreholes were drilled and successfully logged with a borehole gravity meter along a 6,000-foot southwest transect from the bathymetric center of OAK crater (fig. 2-2). Gravity measurements were made in these cased boreholes, generally at spacings of 20 to 35 ft. To obtain reference values for the density and porosity of undisturbed reef-forming material for comparison with material disturbed by cratering processes, gravity surveys were conducted in boreholes OSR-21 and OOR-17, separated by 562 ft, and located approximately 5,500 and 6,050 ft south-southwest of the bathymetric center of OAK crater. Possible densification caused by suspected subsidence on the crater flank just outside the excavational crater was investigated by gravity surveys made in boreholes OQT-19 and ORT-20. These boreholes were separated laterally by 404 ft, and located approximately 1,400 and 1,800 ft south-southwest of the bathymetric center of OAK crater. Gravity surveys were made in borehole OPZ-18 at the bathymetric center of OAK crater, and in OTG-23 located 759 ft south-southwest of OPZ-18 to measure densification beneath the excavational crater and the density of fill within the excavational crater.

The ability of BHG surveys to determine subtle density differences between reef materials located at different locations inside and outside OAK crater depends crucially on the precision of field measurements. Consequently, great effort was devoted to insure that requisite precisions were achieved (Beyer, Ristvet, and Oberste-Lehn, 1986). Repeated measurements show that the precision of BHG densities averages about .01 g/cm3, which is fully adequate for the purposes of the OAK study (fig. 2-3).

BHG measurements permit examination of large volumes of material surrounding the borehole, which means that larger-scale, more distant, lateral density changes are sensed, along with smaller-scale, local density changes that occur within tens to a few hundred feet of the borehole. To obtain BHG density and porosity of atoll materials immediately surrounding each borehole, corrections were calculated and applied for: (1) submarine topography out to a distance of 103 statute miles using bathymetric charts of various scales

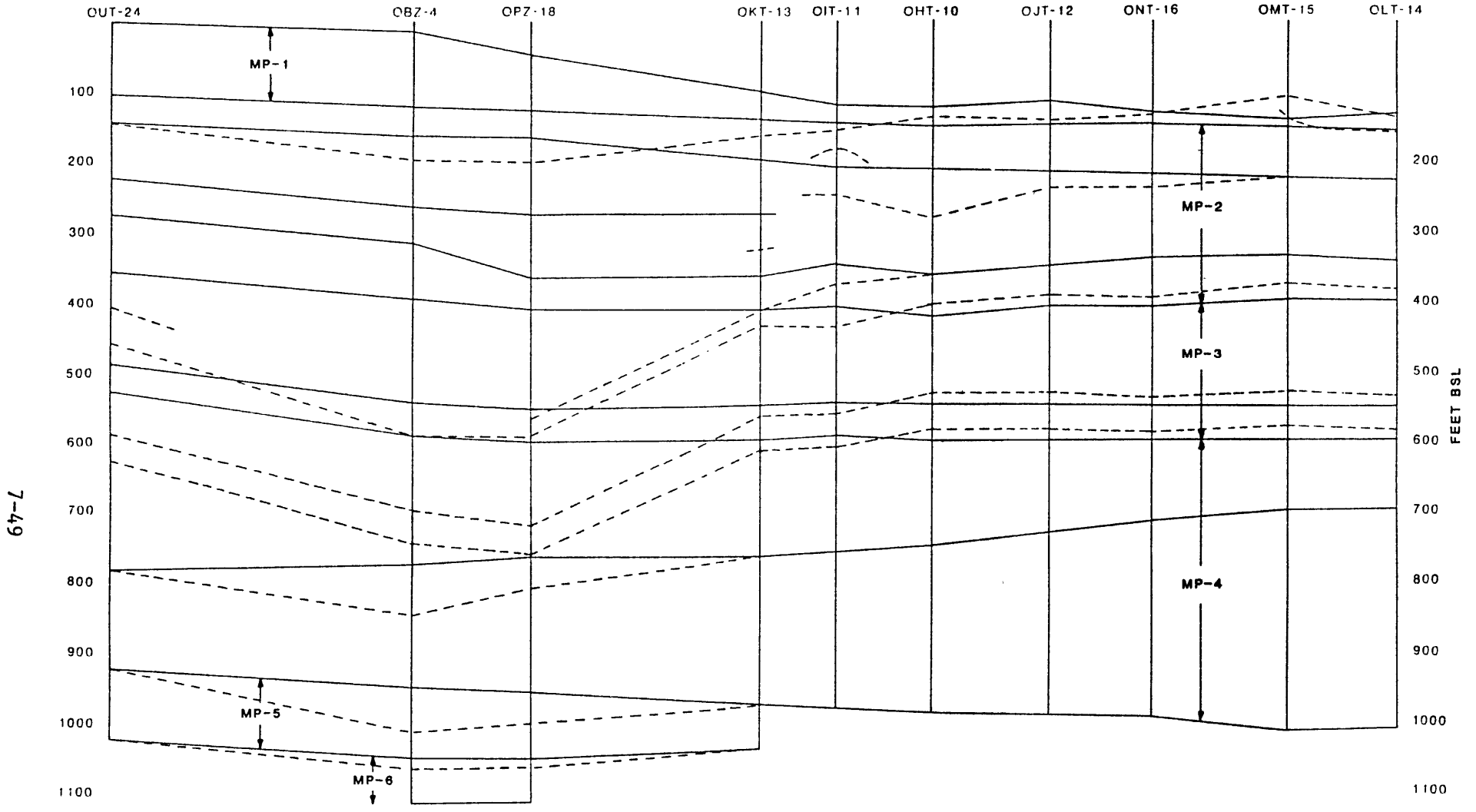

FIGURE 7-28. -- Horizon location in fence diagram from boreholes OUT-24 to OLT-14 as in Figure 7-26. Scale is vertically exaggerated 2:1.

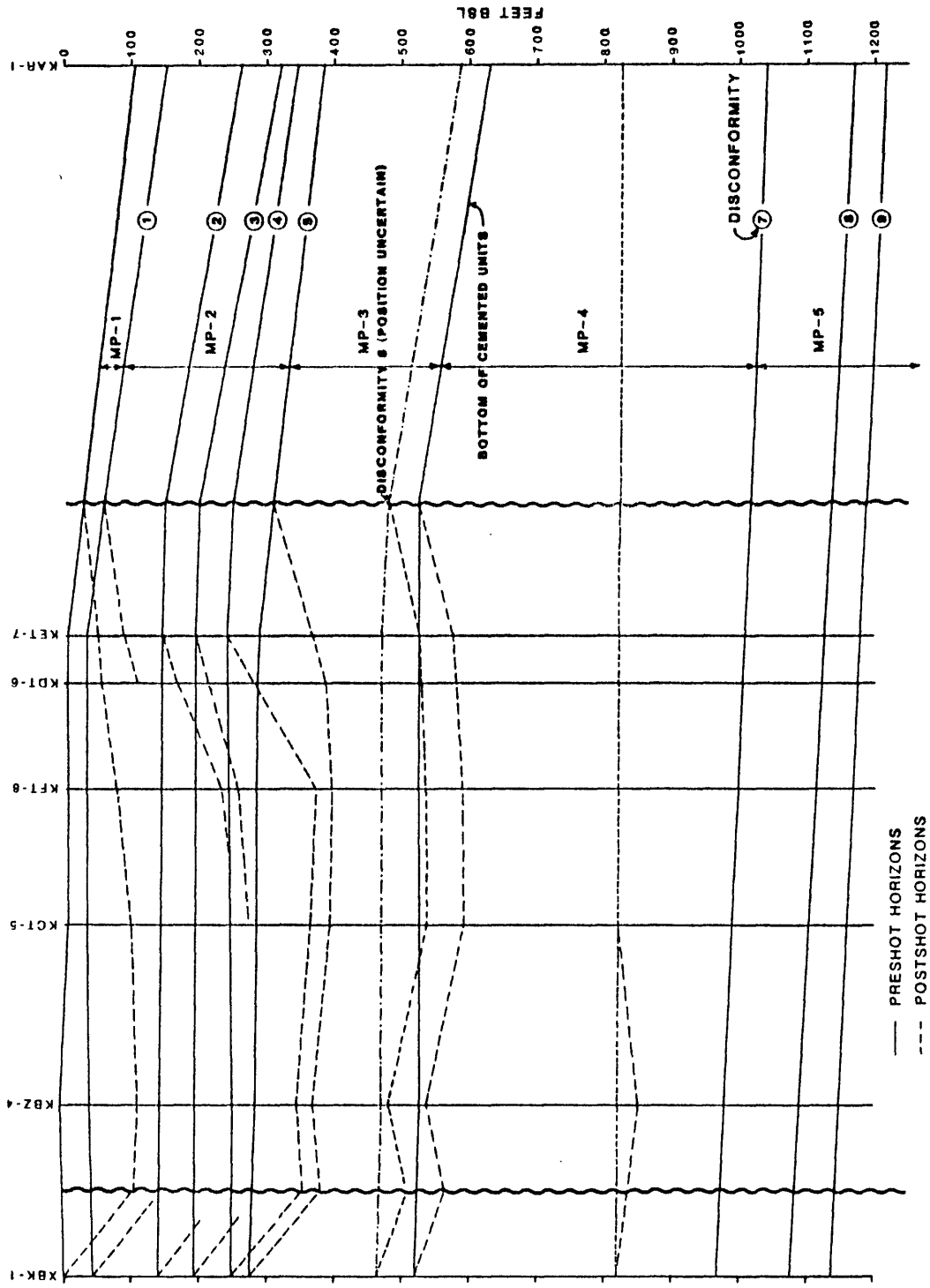

FIGURE 7-29. -- Horizon location in fence diagram from boreholes XBK-1a to KET-7 as in Figure 7-26. Squiggles, breaks, and scale as in Figure 7-7.

TABLE 7-6. -- Thinning/thickening analysis (in percent) of MP units beneath OAK crater. * = percent removed, where removal has occurred lower number indicates thinning in remaining sediments; + = percent thickened; averages indicated by brackets are weighted.

UNIT	OBZ-4		OPZ-18		OCT-5		OTG-23		OUT-24		OKT-13	
1*	100		100		100		100		100		100	
1	-		-		-		-		-		-	
2*	28		17		40		26		28		11	
2a	-		-		-		-		-		-	
2b	-	02	-	08	-	47	-	19	-	30	11	15
2c	-		-		01		-		33		02	
2d	-		49		69		39		37		59	
3a	27	22	10	11	05	04	00	00	00	00	03	02
3b	04		15		00		00		00		01	
4a	45	26	71	33	12	11	31	18	40	26	10	05
4b	05		00		09		09		00		00	
5a	49	39	33	28	00		00		00		00	
5b	23		20		00		00		00		00	

UNIT	OFT-8		OIT-11		OET-7		OQT-19		ODT-6		ORT-20	
1*	100		40		14		23		10		00	
1	-		09		37		21		14		02	
2*	00		00		00		00		00		00	
2a	52		00		04		00		10		02	
2b	35	22	06	03	34	15	09	11	68	16	17	09
2c	03				01		00		00		00	
2d	12		00		00		37		00		17	
3a	00	00	09	07	00	00	05	04	00	00	05	04
3b	00		00		00		00		00		00	
4a	14	09	10	04	09	05	00		00		00	
4b	00		00		00		00		00		00	
5a	00		00		00		00		00		00	
5b	00		00		00		00		00		00	

UNIT	OHT-10		OJT-12		ONT-16		OMT-15		OLT-14	
1*	100		100		100		89		53	
1	-		-		-		-		-	
2*	09		14		02		00		00	
2a	-		-		-		+17		02	
2b	-	13	16	18	17	13	00	10	00	07
2c										
2d	27		27		17		35		18	
3a	00		00		00		00		00	
3b	00		00		00		00		00	
4a	+11	+04	+12	+04	+10	+03	+21	+05	+15	+04
4b	00		00		00		00		00	
5a	00		00		00		00		00	
5b	00		00		00		00		00	

TABLE 7-7. -- Depths (ft bsl) to MP unit boundaries, pre- and post-shot, KOA crater. Boreholes listed in order of increasing distance from ground-zero.

UNIT	KBZ-4		KCT-5		KFT-8		KDT-6		KET-7	
1	+7	-	7	-	6	-	5	-	5	-
2a	37	-	35	-	33	-	33	-	32	-
2b	145	(247.2)	146	(242.5)	146	233.1	147	166.8	148	148.0
2c	193	287.0	195	274.3	195	257.4	195	215.0	195	195.0
2d	250	344.0	246	365.4	244	372.0	243	282.0	242	242.0
3a	282	368.6	285	392.9	285	395.6	286	382.0	288	368.0
3b	470	480.7	470	-	470	-	470	-	470	-
4a	528	539.0	526	593.0	525	590.0	525	581.0	525	575.0
4b	820	848.1	820	820.0	820	820.0	820	820.0	820	820.0
5a	979	979.0	996	996.0	999	999.0	1005	1005.0	1008	1008.0
5b	1090	1089.6	-	-	-	-	-	-	-	-
5c	1147	1147.3	-	-	-	-	-	-	-	-

Distance of boreholes from ground-zero, in feet:

KBZ-4	12
KCT-5	645
KFT-8	870
KDT-6	1182
KET-7	1326

TABLE 7-8. -- Thinning/thickening analysis (in percent) of MP units beneath KOA crater, symbols as in Table 7-6.

UNIT	KBZ-4		KCT-5		KFT-8		KDT-6		KET-7	
1*	100		100		100		100		00	
1	-		-		-		-		+110	
2*	44		55		17		00		00	
2a	-		-		-		49		50	
2b	18	12	+64	+08	49	+16	00	+07	00	+08
2c	00		+78		+133		+39		00	
2d	24		30		57		+132		+173	
3a	41	31		17		19		17		13
3b	00									
4a	+05	03	23	15	23	14	19	12	17	11
4b	18		00		00		00		00	
5a	00		00		00		00		00	
5b	00		00		00		00		00	

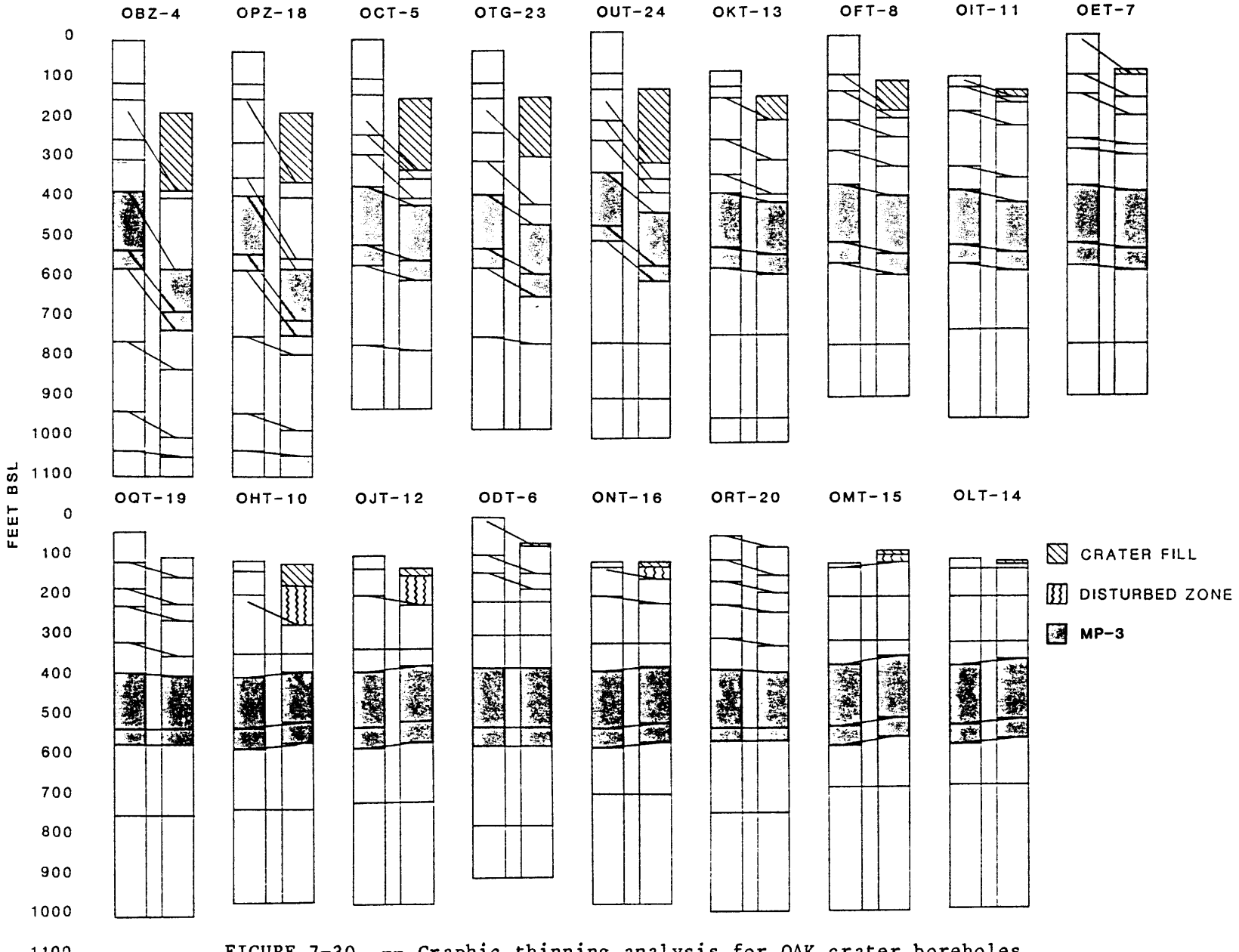

FIGURE 7-30. -- Graphic thinning analysis for OAK crater boreholes. Correlation lines connect pre- and post-shot position of major horizons including stratigraphic base of crater-fill.

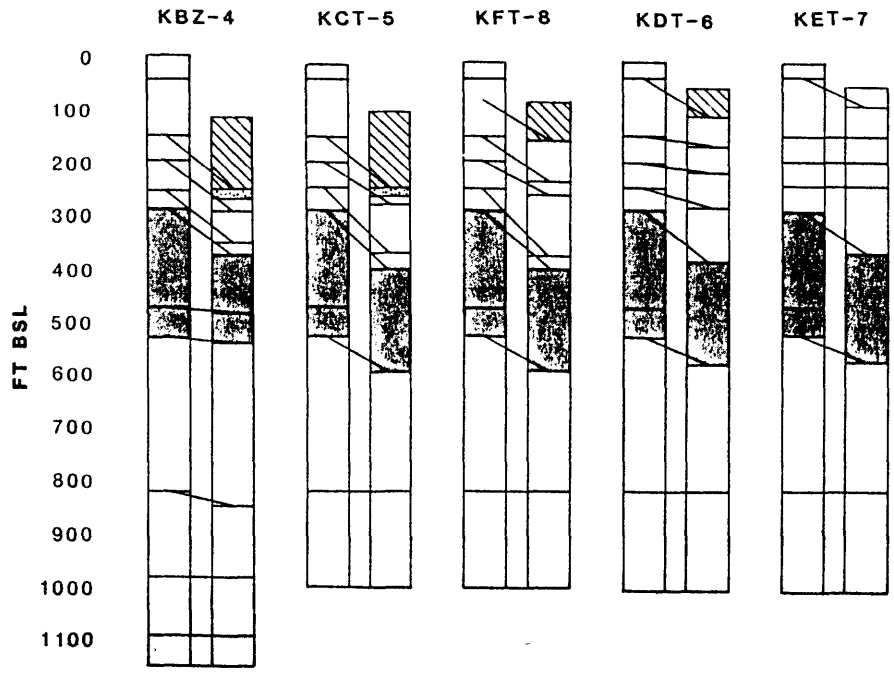

FIGURE 7-31. -- Graphic thinning analysis for KOA crater boreholes as in Figure 7-30.

TABLE 7-9. -- Stratigraphic bulk density analysis. Values in gm/cc. Change from bulk density model (the composite reference sections) is indicated in parenthesis.

AVERAGE DENSITIES FOR STRATIGRAPHIC MATERIAL PROPERTY UNITS AND CRATER ZONES						
	MODEL	ORT-20	OQT-19	OTG-23	OPZ-18	
					1.812(-.06*)	α
					1.876(-.02*)	$\beta 1_a$
1	--	1.855	1.895	--	1.982(+.03*)	$\beta 1_b$
2a	1.965	1.923(-.02)	1.921(-.02)	--	1.967(+.03*)	$\beta 2$
2b	1.908	1.918(+.01)	1.904(-)	--	2.027(+.06*)	$\beta 3$
2c	1.919	1.923(-)	1.942(+.01)	2.017(+.05)	2.124(+.11)	2c
2d	1.920	1.985(+.03)	1.982(+.03)	2.030(+.06)	2.167(+.13)	2d
3a	1.978	1.985(-)	2.018(+.02)	2.052(+.04)	2.116(+.07)	3a
3b	1.976	--	1.950(-.01)	2.063(+.04)	2.080(+.05)	3b
4a	2.011	--	2.025(+.01)	2.150(+.07)	2.045(+.02)	4a
4b	--	--	1.959	--	1.993(+.02)	4b

The model is the average value for units in the reference boreholes OOR-17 and OSR-21, asterisk (*) indicates the difference in bulk density from average value value of normal sediments (2a-c) which is 1.919, OQT-19 is used for model density value of unit 4b.

α = Alpha $\beta 1_a$ = Beta 1a $\beta 1_b$ = Beta 1b

$\beta 2$ = Beta 2 $\beta 3_a$ = Beta 3a

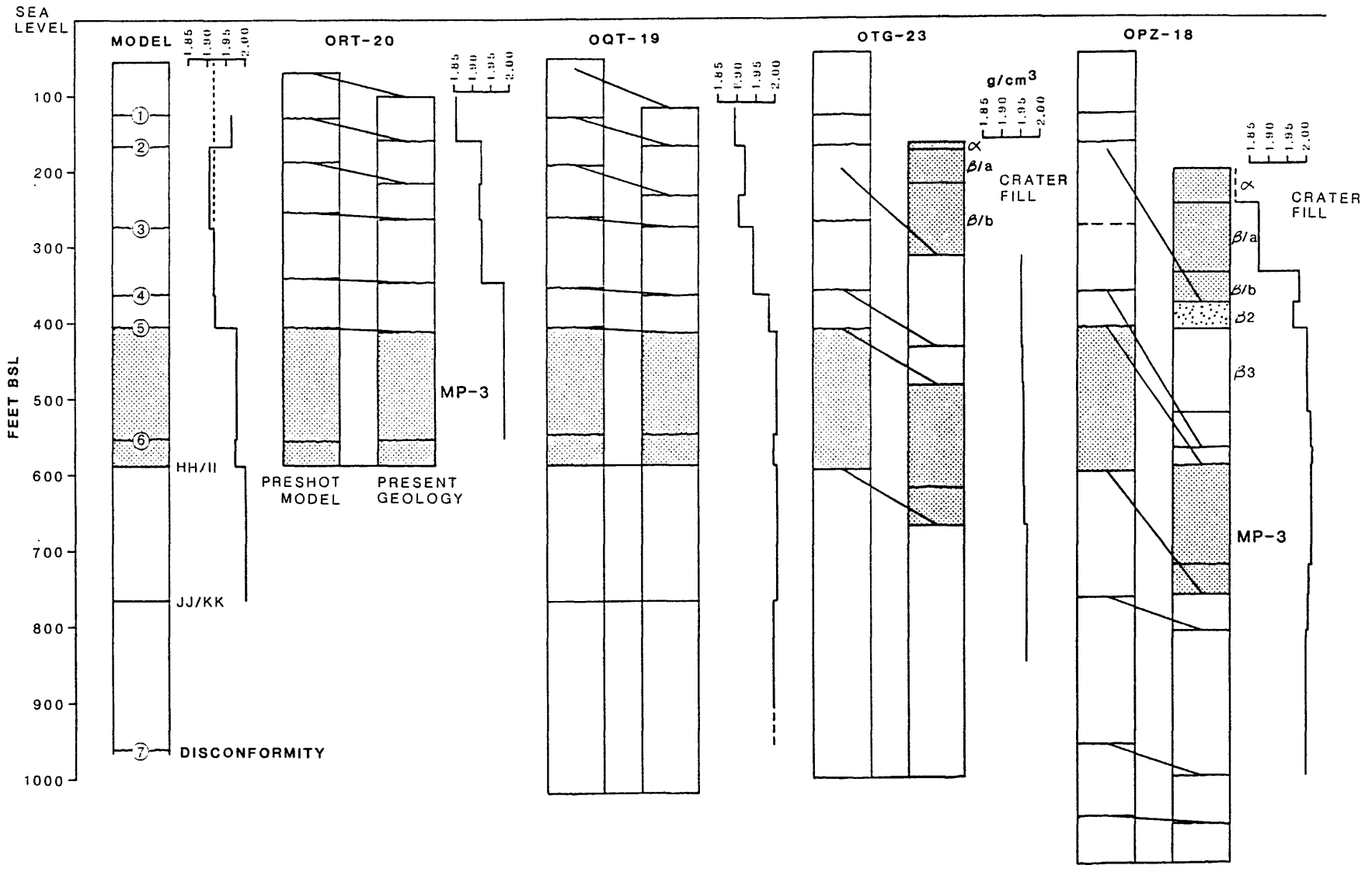

FIGURE 7-32. -- Stratigraphic density profile based on borehole gravimetry.

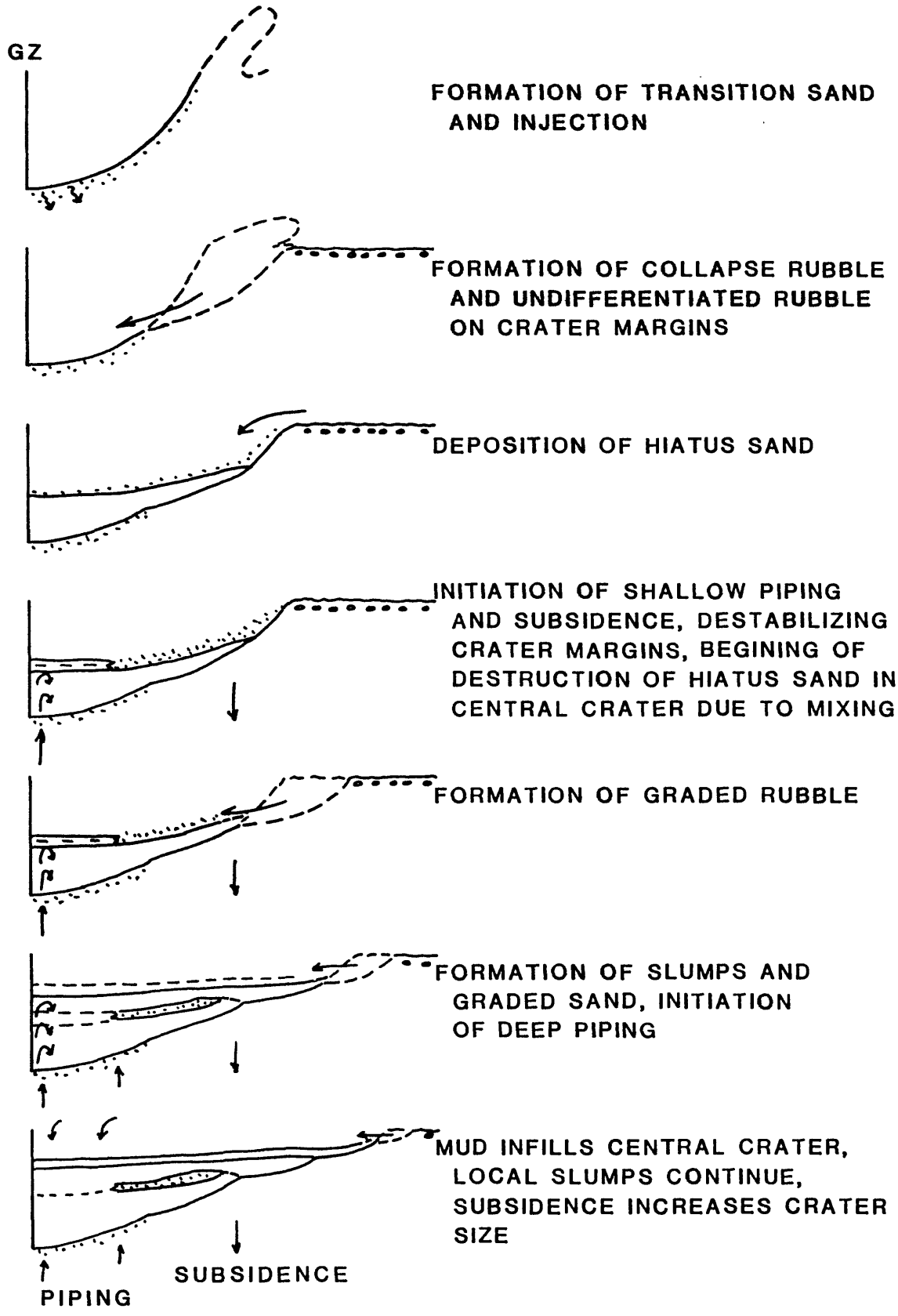

FIGURE 7-33. -- Idealized succession of major depositional events to form geologic crater. No horizontal scale is implied.

General Densification and Flow Patterns

OAK Crater.

The density values measured for the crater zones Alpha and Beta in OAK (OPZ-18) are compared to the average value of normal (undisturbed) sediments in MP-2(a-c). The author feels that the average value for MP-2a through MP-2c also adequately characterizes the upper sediments that were not measured by gamma-gamma density or borehole gravimetry (MP-1 and part of MP-2a). Material in the upper crater zones (Alpha and Beta 1a) in OAK appear to be less dense than normal sediments. Beta 1b and Beta 2 appear to be slightly more dense than normal sediments. Beta 3 has significant densification. Beneath the rubble zone (Beta), the rock and sediment occur in normal stratigraphic order, and density and thinning can be compared directly to the reference sections.

MP-2c (OPZ-18 and OTG-23) immediately subjacent to the Beta zone is moderately densified. Thinning of this unit cannot be calculated because the top of the unit is not preserved in either borehole. However, the significant densification in OPZ-18 suggests this unit behaved similar to the underlying unit, MP-2d in the area of that borehole.

MP-2d under the central crater area shows the most significant densification. However, densification cannot account entirely for the roughly 50 percent thinning of the unit over a wide area.

Densification within MP-3 accounts for most of the thinning observed within that unit except beneath the central crater. Beneath the central crater, collapse of vugs could compensate for considerable volume loss (thinning) with little observed density increase.

MP-4a shows essentially no densification under the central crater area and at least 40 percent thinning over a wide area. MP-4a and MP-4b are differentiated by organic concentration. It is probable that both units flowed and mixed obscuring their relationship in a manner so that the organics identifying MP-4b occur higher than predicted, and thinning in MP-4a is exaggerated (especially in OPZ-18). Nevertheless, the whole unit, MP-4, experienced 20 percent thinning over a wide area that is not accounted for by densification.

If the geologic pre-shot models are correct, than the stratigraphic units that show thinning is excess of that explained by densification must have been partially removed by flow. Two units under the central crater area that indicate significant flow are MP-2d and MP-4a. Material from these units previously has been shown to have been piped (vertical flow) to the surface. Material from MP-4 is involved in the majority of deep piping, but the estimated volume of that material preserved in the crater fill only accounts for a small amount of material that flowed.

It appears most of the volume lost is accounted by lateral flow. Two lines of evidence support this: (1) The density increase detected in MP-4 at the base of OTG-23 suggests lateral densification presumably from lateral

flow, and (2) The uplifted MP-3 over much of the lagoon (refer to fig. 7-21) appears to be caused by thickening of MP-4. This bulging or bulking of MP-4 clearly is visible in all the seismic-reflection survey profiles that run through the lagoon opposite the crater.

Piping (vertical flow) is clearly a post-dynamic phenomenon. The units that appear to have experienced lateral flow, also were involved with late-stage piping. These units in OAK appear to be MP-2c over a limited extent (because it was excavated in the central portion of the crater) and MP-2d, MP-4a, and MP-4b (over a wider extent). Deep piping appears to have been vented initially through the central part of the crater and subsequently through concentric fracture zones developed farther laterally (due to subsidence) represented by the piped mounds or volcanoes preserved on the terraces today. Shallow piping appears to be a more widespread phenomena over the crater area, though it too was, at least partially, vented through the central part of the crater as evidenced by the presence of shallow-piped material in all central crater zones.

KOA Crater.

By comparison with OAK crater, KOA experienced much more shallow lateral and vertical flow within its units. Thinning and bulking (thickening) is observed in MP-2b, MP-2c, and MP-2d. The thinning appears in increasing area in each lower unit and, therefore, the thickening occurs farther from ground-zero with depth. MP-3 appears more thinned than in OAK and may have experienced flow. MP-4 appears to have thinned and flowed. However, the thinning in MP-4 is complicated in its area of distribution; represented by central rebound and perhaps channeled vertical flow through the central uplift. Shallow piping appears to have been pervasive and is indicated by the common EE material in much of the mixed zone. Venting of some of the shallow-piped material in the areas of KBZ-4 and KCT-5 is suggested by the deeper mixing of this shallow-piped material in the crater fill of these boreholes.

Relative Timing of Depositional Events

The idealized succession of depositional events is shown in Figure 7-33.

For purpose of discussion, the following stages of crater development, referred to as craters, are defined:

(1). Maximum transient crater. That crater formed when the outgoing velocity vector is zero, prior to rebound. The formation of the Beta 3 rubble beneath the excavational crater is thought to represent the maximum transient-crater growth.

(2). Terminal transient crater. That crater formed at the end of the transient-crater phase, following rebound.

(3). Collapse crater. That crater formed at the end of the formation of the rubble from the collapse of the sidewall/flap (early stage collapse, Beta 1b).

(4). Initial slump crater. That crater formed at the end of the formation of late-stage collapse rubble (Beta 1a).

(5). Apparent crater. That crater observed today, determined by extrapolation of post-shot measurements to the land or water surface at shot time (B. L. Ristvet, personal communication). This crater also has been referred to as the subsidence crater.

For OAK crater, in chronologic order from oldest to youngest, the sequence of depositional events is:

(1). Formation of transition sand (Beta 2) at base of transient crater, dynamic lateral flow of subsurface units, air-blast deformation.

(2). Collapse of excavational-crater wall/rim destroying lateral extent of transition sand and forming collapse rubble (Beta 1b); formation of collapse crater; initiation of liquefied (post-dynamic) flow, especially in MP-2c, MP-2d, MP-4a, and MP-4b; and initiation of subsidence.

(3). Penecontemporaneous formation of undifferentiated rubble zone external of collapse crater by partial flap collapse in addition to prior air-blast deformation.

(4). Penecontemporaneous formation of debris blanket by probable partial failure and movement of the excavational-crater wall/rim lagoonward.

(5). Infilling of at least part of remaining crater bowl (collapse crater) by wash- and/or fall-back initiating deposition of "hiatus" sand (Beta 1s); and initiation of winnowing (removal in water suspension) of fine-grained sediments.

(6). Continuation of deposition of "hiatus" sand over outer crater and contemporaneous initiation of shallow piping in the central crater; continued liquefied lateral flow and subsidence; continued winnowing.

(7). A sequence of crater-margin collapses to form graded rubble (Beta 1a). One collapse (slump) resulted in a flow large enough to cross the crater, breach the debris blanket, and flow into the lagoon. Subsidence, piping, liquefied lateral flow, and winnowing continued. Shallow-piped material reached the surface throughout the crater before or during initiation of Beta 1a deposition.

(8). Margin slumping and graded-sand (turbidite) deposition (Alpha 2); subsidence, piping, liquefied lateral flow, and winnowing continued. Deep-piped material reached the surface at the beginning of Alpha 2 deposition.

(9). Late-time partial infilling of central part of the crater with mud (Alpha 1); subsidence, piping, and lateral flow continuing but progressively less. Mud deposition has continued to present. Local slumping, sand deposition, and winnowing has continued along the reef margin mainly as a consequence of natural geologic processes.

Because the OAK crater developed on a slope, the bathymetric center of the crater moved downslope at the end of early-stage collapse (generally shown as an apparent, progressively lagoonward migration of the low point of successive crater-fill units in fig. 7-25B).

For KOA crater, the events (from oldest to youngest) are:

(1). Same as in OAK.

(2). Same as in OAK; liquefied lateral flow especially in MP-2b, MP-2c,MP-2d, MP-4a, and MP-4b.

(3). Penecontemporaneous formation of debris mounds by partial MIKE-ward collapse and movement of crater wall/rim.

(4). Same as in OAK, resulting in the much-thickened section at KET-7.

(5). Same as in OAK.

(6). Possible deposition of a thin "hiatus" sand over outer crater (this was mostly destroyed by subsequent collapse); initiation of shallow piping; and continued liquefied lateral flow and subsidence.

(7). A sequence of crater-margin collapse to form graded rubble; subsidence, shallow piping, and liquefied lateral flow continued.

(8). Margin slumping and graded-sand (turbidite-flow) deposition (Alpha 2) and piping in the central part of the crater; continued but reduced subsidence and lateral flow. Deep-piped material reached the surface at the initiation of Alpha 2 deposition.

(9). Late-time infilling of central part of the crater with mud (Alpha 1); localized slumping and sand deposition around most of crater (except near MIKE). Subsidence has lessened markedly. Deep piping has discontinued before deposition of mud (Alpha 1).

VOLUME PROBLEMS

Beyer (Ch. 2 of this report) and Trulio (Ch. 6) demonstrate that densification can only account for 8 to 15 percent of the subsidence measured in the crater wings of OAK. Yet OAK appears to be substantially a subsidence crater. Peterson and Henny (Ch. 5) show substantial late-time subsidence (post two months post-shot) by comparing the 1958 H&N post-shot map with the 1984 USGS bathymetric map. Peterson and Henny estimate an apparent (conservative) volume increase of the crater of 231 million cubic ft or 25 percent of the apparent crater volume. Piping clearly demonstrates the existence of a long-term unstable liquefied mass at depth beneath the crater.

Piping is <u>one</u> avenue by which this liquefied mass could achieve stability. It <u>is</u> the expression of liquefied flow vertically. Dikes, lagoon uplift, and densification of MP-4 laterally all demonstrate lateral flow.

Evidence for Piping and Lateral Flow

Piping is not an hypothesis but a process the results of which are observed in both OAK and KOA craters.

Surface. -- Sand volcanoes are present on the terraces of OAK crater (fig. 7-14). Their presence on the terraces indicates that deep piping persisted after the majority of Alpha deposition (slumps and sand turbidity flows) and that flow (at least vertical) is a very long-term process.

Crater-Fill. -- The volume of piped material is estimated for the crater-fill of the central bowl of OAK. Deep-piped material (biostratigraphic zones II-MM) is 4.83 million cubic ft. Shallow-piped material (biostratigraphic zones FF-GG) is 45.62 million cubic ft. Deep-piped material is only surficial outside the central bowl (i.e., on the terraces). Shallow-piped material is throughout the crater-fill above the hiatus sand (Beta 1s), so an appreciable additional volume exists but has not been calculated (further paleontologic study is needed for these estimates). Shallow piping reached the crater surface after deposition of the hiatus sand. Deep piping reached the crater surface after deposition of the graded rubble (Beta 1b). This is true for both OAK and KOA craters and suggests that shallow piping reached the surface on the order of minutes, deep piping on the order of hours, and both persisted for days. In OAK, deep- and shallow-piped material is present in the late-stage mud (Alpha 1) deposits suggesting very long-term deposition (many months). In KOA, only shallow-piped material is present in the late-stage mud (Alpha 1) deposits. Deep-piped material is present in the graded sands (Alpha 2) suggesting an ending of deep-piping at the initiation of Alpha 1 deposition in KOA (approximately 1-2 months). If the liquefied material mass exhibits vertical flow for days, why is lateral flow constrained to the dynamic phase of crater development? Material from MP-4 (deep-piped) would have an effective seal by MP-3 in most places except in the proximity of large fractures and vents. The material was depressed under the central crater and the sealed avenue of flow would be up along the lower surface of MP-3.

Subsurface. -- Unit MP-4 shows densification away from the central crater. Borehole gravimetry shows a substantial increase in density in MP-4 in OQT-23 for that part that was measured (refer to tbl. 7-9). Gamma-gamma density shows a similar substantial increase in density throughout MP-4 in OKT-13. The H&N post-shot bathymetry (Peterson and Henny, Ch. 5 of this report) shows a rise in the lagoon sea-floor depth that exceeds the thickness of the debris measured in several boreholes. This indicates uplift of the surface. As previously mentioned, MP-3 shows uplift throughout the lagoon (refer to fig. 7-22). Both these lines of evidence suggest significant lateral flow of MP-4, densifying the material laterally and uplifting the overlying sediment and rock over much of the lagoon. It appears that calculations down to the line of zero net displacement (contour D, Trulio, Ch. 6 of this report) do not adequately encompass all significant subsurface crater phenomena because much appears to happen below this line.

Loss of Material from the Crater. -- In OAK, large ejecta or debris is found entirely within the apparent crater. Halley and others (1986b) demonstrated several clasts (unspecified size, but generally cobble-sized or larger material collected by submersible) to be debris. Debris rays were observed along the reef tract, generally all within the apparent crater. The debris blanket is within the apparent crater. Where did all the material go to form the apparent crater?

Debris is indicated outside the apparent crater in three places:

(1). In the breach and turbidite flow deposit (fig. 7-14) deposition of an unknown volume of debris is inferred from the enhanced sea-floor image.

(2). At OAR-2A, the upper 25 ft of sediment (mostly sand) contains highly shocked material, probably ejecta swept from the reef tract and deposited at this site. This thickness could represent a substantial amount of material deposited along the toe of the slope from reef to lagoon on both the northeast and southwest sides of the crater.

(3). In mud in the lagoon, clay-sized material is common in samples from throughout the northeastern part of the lagoon (Wardlaw and Henry, 1986b). It is probably mostly blast-derived and represents a substantial volume of fine-grained ejecta and material from the craters. Post-shot photographs show mud-ladened plumes into the ocean and lagoon far beyond the apparent crater, suggesting this loss was not trivial.

The uplifted area in the lagoon near OAK (fig. 7-22) suggests that a considerable volume of material from MP-4 moved outside the apparent crater in the subsurface. If a 5-7 percent density increase accompanied this thickening it would account for an appreciable amount of the apparent crater.

SUMMARY

OAK and KOA craters are similar. They exhibit the same geologic crater zonation. The zone of sonic degradation that defines the geologic crater is very similar for both craters. OAK and KOA differ in type of device, in coupling, and in depth and radius of the various stages of crater development that are not within the scope of this paper. The KOA area was preconditioned by MIKE and possibly other devices. It contains a better, thicker cemented interval (MP-3) at shallower depths than OAK. These two factors contributed strongly to the major differences between KOA and OAK. KOA is a crater that developed early and had far less late-stage modification, as indicated by its lack of late-stage piping and diminished late-stage subsidence. OAK, on the other hand, is a crater most of which developed later and had significant late-stage subsidence and piping. It appears that as much as 66 percent of the apparent crater volume of OAK may be due to subsidence. In contrast, only about 20 percent of KOA may be due to subsidence.

Piping requires a liquefied material mass at depth. Piping lasted for months at both craters. Subsidence lasted for months at both craters. The prolonged existence of a liquefied material mass at depth is related causally to prolonged subsidence.

REFERENCES CITED

Beyer, L. A., Ristvet, B. L., and Oberste-Lehn, D., 1986, Chapter 8: Preliminary density and porosity data and field techniques of borehole gravity surveys, OAK crater, in, Henry, T. W., and Wardlaw, B. R., eds., Pacific Enewetak Atoll Crater Exploration (PEACE) Program, Enewetak Atoll, Republic of the Marshall Islands; Part 3: Stratigraphic analysis and other geologic and geophysical studies in vicinity of OAK and KOA craters: U.S. Geological Survey Open-File Report 86-555, 28 p.

Beyer, L. A., 1987, Chapter 2: Analysis of borehole gravity surveys at OAK crater, in, Henry, T. W., and Wardlaw, B. R., eds., Pacific Enewetak Crater Exploration (PEACE) Program, Enewetak Atoll, Republic of the Marshall Islands; Part 4: Additional studies of OAK and KOA craters, U.S. Geological Survey Open-File Report 87-xxx.

Brouwers, E. M., Cronin, T. M., and Gibson, T. G., 1986, Chapter 11: Additional paleontologic studies, OAK and KOA craters, in, Henry, T. W., and Wardlaw, eds., Pacific Enewetak Atoll Crater Exploration (PEACE) Program, Enewetak Atoll, Republic of the Marshall Islands; Part 3: Stratigraphic analysis and other geologic and geophysical studies in vicinity of KOA and OAK craters: U.S. Geological Survey Open-File Report 86-555, 18 p.

Couch, R. F., Jr., Fetzer, J. A., Goter, E. R., Ristvet, B. L., Tremba, E. L., Walter, D. R., and Wenland, V. P., 1975, Drilling operations on Eniwetok Atoll during Project EXPOE: Air Force Weapons Laboratory Technical Report AFWL-TR-75-216, Kirtland Air Force Base, New Mexico, 270 p.

Cronin, T. M., Brouwers, E. M., Bybell, L. M., Edwards, L. E., Gibson, T. G., Margerum, R., and Poore, R. Zoro, 1986, Pacific Enewetak Crater Exploration (PEACE) Program, Enewetak Atoll, Republic of the Marshall Islands; Part 2: Paleontology and biostratigraphy application to OAK and KOA craters, U.S. Geological Survey Open-File Report 86-159, 39 p.

Cronin, T. M., and Gibson, T. G., 1987, Chapter 3: Paleontologic evidence for sedimentary mixing at OAK crater, Enewetak Atoll, in, Henry, T. W., and Wardlaw, B. R., eds., Pacific Enewetak Crater Exploration (PEACE) Program, Enewetak Atoll, Republic of the Marshall Islands; Part 4: Additional studies of OAK and KOA craters, U.S. Geological Survey Open-File Report 87-665.

Folger, D. W., Robb, J. M., Hampson, J. C., Davis, P. A., Bridges, P. M., and Roddy, D. J., 1986, Sidescan-sonar survey of OAK and KOA craters, in, Folger, D. W., ed., Sea-floor observations and subbottom seismic characteristics of OAK and KOA craters, Enewetak Atoll, Marshall Islands: U.S. Geological Survey Bulletin 1678, 18 p.

Grow, J. A., Lee, M. W., Miller, J. J., Agena, W. F., Hampson, J. C., Foster, D. S., and Woellner, R. A., 1986, Multichannel seismic-reflection survey of KOA and OAK craters, in, Folger, D. W., ed., Sea-floor observations and subbottom seismic characteristics of OAK and KOA craters, Enewetak Atoll, Marshall Islands: U.S. Geological Survey Bulletin 1678, 46 p.

Halley, R. B., Slater, R. A., Shinn, E. A., Folger, D. W., Hudson, J. H., Kindinger, J. L., and Roddy, D. J., 1986a, Observations of OAK and KOA craters from the submersible, in, Folger, D. W., ed., Sea-floor observations and subbottom seismic characteristics of OAK and KOA craters, Enewetak Atoll, Marshall Islands: U.S. Geological Survey Bulletin 1678, 32 p.

Halley, R. B., Major, R. P., Ludwig, K. R., Peterman, Z. L., and Matthews, R. K., 1986b, Preliminary analyses of OAK debris samples, in, Folger, D. W., ed., Sea-floor observations and subbottom seismic characteristics of OAK and KOA craters, Enewetak Atoll, Marshall Islands: U.S. Geological Survey Bulletin 1678, 11 p.

McMurtry, G. M., Schneider, R. C., Colin, P. K., Buddemeier, R. W., and Suchanek, R. H., 1985, Redistribution of fallout radionuclides in Enewetak Atoll lagoon sediments by calianassid bioturbation: Nature, v. 313, no. 6004, p. 674-677.

Peterson, J. L., and Henny, R. W., 1987, Chapter 5: Bathymetric studies of OAK crater, in, Henry, T. W., and Wardlaw, B. R., eds., Pacific Enewetak Crater Exploration (PEACE) Program, Enewetak Atoll, Republic of the Marshall Islands; Part 4: Additional studies of OAK and KOA craters: U.S. Geological Survey Open-File Report 87-665.

Polanskey, Carol, and Ahrens, T. J., 1987, Chapter 4: Shock history of PEACE samples, in, Henry, T. W., and Wardlaw, B. R., eds., Pacific Enewetak Crater Exploration (PEACE) Program, Enewetak Atoll, Republic of the Marshall Islands; Part 4: Additional studies of OAK and KOA craters: U.S. Geological Survey Open-File Report 87-665.

Ristvet, B. L., Tremba, E. L., Couch, R. F., Jr., Fetzer, J. A., Goter, E. R., Walter, D. R., and Wendland, V. P., 1978, Geologic and geophysical investigations of the Eniwetok nuclear craters: Air Force Weapons Laboratory Technical Report AFWL-TR-77-242, 300 p.

Ristvet, B. L., and Tremba, E. L., 1986, Chapter 12: Radiation chemistry of the subsurface of OAK and KOA craters, in, Henry, T. W., and Wardlaw, B.R., eds., Pacific Enewetak Atoll Crater Exploration (PEACE) Program, Enewetak Atoll, Republic of the Marshall Islands; Part 3: Stratigraphic analysis and other geologic and geophysical studies in vicinity of OAK and KOA craters: U.S. Geological Survey Open-File Report 86-555, 15 p.

Trulio, J. G., 1987, Chapter 6: Constraints on densification and piping in the OAK event, in, Henry, T. W., and Wardlaw, B. R., eds., Pacific Enewetak Crater Exploration (PEACE) Program, Enewetak Atoll, Republic of the Marshall Islands; Part 4: Additional studies of OAK and KOA craters: U.S. Geological Survey Open-File Report 87-665.

Wardlaw, B. R., and Henry, T. W., 1986a, Chapter 2: Physical stratigraphic framework, in, Henry, T. W., and Wardlaw, B. R., eds., Pacific Enewetak Atoll Crater Exploration (PEACE) Program, Enewetak Atoll, Republic of the Marshall Islands; Part 3: Stratigraphic analysis and other geologic and geophysical studies in vicinity of OAK and KOA craters: U.S. Geological Survey Open-File Report 86-555, 36 p.

Wardlaw, B. R., and Henry, T. W., 1986b, Chapter 14: Geological interpretation of OAK and KOA craters, in, Henry, T. W., and Wardlaw, B. R., eds., Pacific Enewetak Atoll Crater Exploration (PEACE) Program, Enewetak Atoll, Republic of the Marshall Islands; Part 3: Stratigraphic analysis and other geologic and geophysical studies in vicinity of OAK and KOA craters: U.S. Geological Survey Open-File Report 86-555, 39 p.

****